

FEBRUARY 15, 1987

# **Analytical** **CHEMISTRY**

**Dating  
Techniques in  
Archaeology  
and  
Paleoanthropology  
317 A**





## Introducing the Basic Balances from METTLER. When all you need is the weight.

### The new METTLER J Series

When all you need is the weight, METTLER's new J Series delivers results as only METTLER can. They're built in the METTLER tradition – but brought to you at a new low price, because we took out applications features you may never need. It's designed for users who only need a basic balance, but demand the performance of a METTLER.

Built with METTLER quality. Backed by METTLER service. Bringing confidence to your work. It's an extra balance to increase productivity in your laboratory. It's a back-up balance to help you through a heavy workload. Or it's an easy-to-use electronic balance for the classroom. It's METTLER's basic balance. The J Series – seven new precision balances with capacities from



310 g to 6000 g, readabilities from 0.001 g to 0.1 g, and one new analytical with a 110 g capacity, readability to 0.1 mg. For complete information and a copy of our J Series brochure call 1-800-METTLER, in New Jersey (609) 448-3000 or write Mettler Instrument Corporation, Box 71, Hightstown, NJ 08520.

We understand.  
Precisely.

**METTLER**

CIRCLE 95 ON READER SERVICE CARD



# Monoclonal Antibody-Based Technology for Chemical Analysis



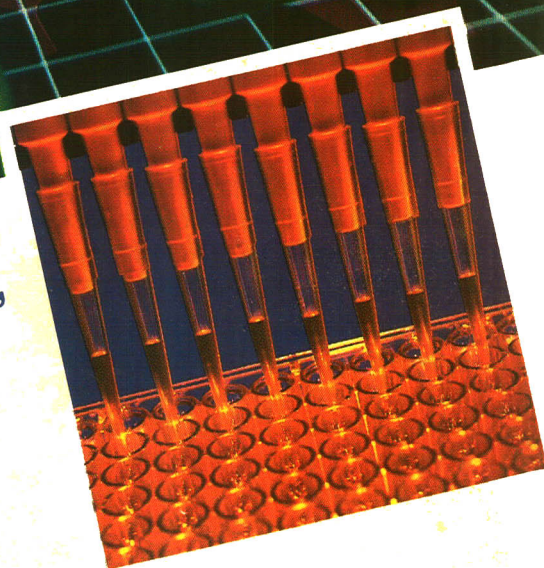
Monoclonal antibodies bind with molecules of the target chemical.

**In industries faced with difficult, time-consuming, and expensive analytical procedures, immunoassays offer a convenient alternative.**

Westinghouse Bio-Analytic Systems Company is using the new hybridoma technology to produce monoclonal antibodies that bind to specific organic chemicals. This advanced technology incorporates these monoclonal antibodies in quantitative immunoassays for chemical analysis.

Immunoassays are simple to perform yet provide for chemical analysis that is sensitive, specific, and reproducible. Detecting and quantifying organic compounds with this system is rapid, cost-effective and accurate. It's as easy to use in the field as it is in the laboratory.

CIRCLE 174 ON READER SERVICE CARD



**See us at the Pittsburgh Analytical Conference,  
March 9-13, Atlantic City, NJ**



Westinghouse Bio-Analytic Systems Company  
Waltz Mill Site  
Madison, PA 15663





## Been waiting long for your samples to dissolve?

Your brand new AA sits idle while you dissolve samples by techniques that haven't changed in a century. Doing acid digestions over a hot plate is tedious, hazardous, time consuming . . . and totally unnecessary!

The CEM Microwave Digestion System reduces AA/ICP sample preparation time from hours to just minutes without generating clouds of acid fumes. The system uses closed vessels of PFA Teflon® which are specially designed for safety at high pressure. The CEM Microwave Digestion System holds a carousel of 12 such vessels. Each vessel has a control valve which opens if excess pressure builds up. These closed vessels allow the acids used for sample digestion to reach temperatures well above their normal boiling point.

Dramatic reductions in sample preparation time are achieved by a combination of rapid microwave heating and elevated digestion temperature. The Microwave Digestion System can be programmed to automatically carry out a digestion in various stages. This frees the operator to attend to other duties while the digestion is taking place.

The CEM system is ideal for sample digestions in nitric, hydrochloric and hydrofluoric acids. It puts you on the cutting edge of laboratory technology with maximum safety, ease of use, lower blanks and reduced acid usage.

And it's a system that drastically cuts the time you spend waiting for dissolutions.

If you'd like more information, or if you want to talk to us about your application, call us now at 800/334-6317. (In NC, call 704/821-7015.)



**CEM**

P. O. Box 200  
Matthews, NC 28106





ANCHAM  
 59(4) 299A-358A/545-688 (1987)  
 ISSN 0003 2700

**Registered in U.S. Patent and Trademark Office;  
 Copyright 1987 by the American Chemical Society**

ANALYTICAL CHEMISTRY (ISSN 0003-2700) is published semimonthly by the American Chemical Society at 1155 16th St., N.W., Washington, D.C. 20036. Editorial offices are located at the same ACS address (202-872-4600; TDD 202-872-8733). Second-class postage paid at Washington, D.C., and additional mailing offices. Postmaster: Send address changes to ANALYTICAL CHEMISTRY Membership & Subscription Services, P.O. Box 3337, Columbus, Ohio 43210.

**Claims for missing numbers** will not be allowed if loss was due to failure of notice of change of address to be received in the time specified; if claim is dated (a) North America: more than 90 days beyond issue date, (b) all other foreign: more than one year beyond issue date, or if the reason given is "missing from files."

**Copyright Permission:** An individual may make a single reprographic copy of an article in this publication for personal use. Reprographic copying beyond that permitted by Section 107 or 108 of the U.S. Copyright Law is allowed, provided that the appropriate per-copy fee is paid through the Copyright Clearance Center, Inc., 27 Congress St., Salem, Mass. 01970. For reprint permission, write Copyright Administrator, B&J Division, ACS, 1155 16th St., N.W., Washington, D.C. 20036.

**Registered names and trademarks, etc.,** used in this publication, even without specific indication thereof, are not to be considered unprotected by law.

**Advertising Management:** Centcom, Ltd., 500 Post Rd. East, Westport, Conn. 06880 (203-226-7131)

**1987 subscription rates include air delivery outside the U.S., Canada, and Mexico**

	1 yr	2 yr
<b>Members</b>		
Domestic	\$ 25	\$ 42
Canada and Mexico	50	92
Europe	77	146
All Other Countries	104	200
<b>Nonmembers</b>		
Domestic	37	62
Canada and Mexico	62	112
Europe	127	231
All Other Countries	154	285

Three-year and other rates contact: Membership & Subscription Services, ACS, P.O. Box 3337, Columbus, Ohio 43210 (614-421-3776).

**Subscription orders by phone** may be charged to Visa, MasterCard, Barclay card, Access, or American Express. Call toll free at (800) 424-6747 from anywhere in the continental United States; from Washington, D.C., call 872-8065. Mail orders for new and renewal subscriptions should be sent with payment to the Business Management Division, ACS, P.O. Box 57136, West End Station, Washington, D.C. 20037.

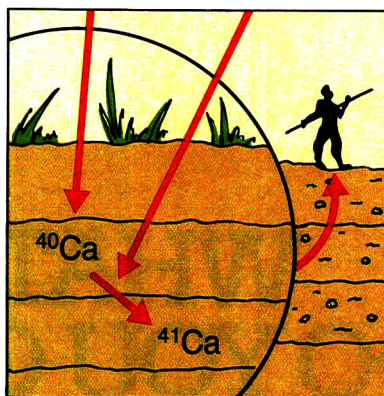
**Subscription service inquiries and changes of address** (Include both old and new addresses with ZIP code and *recent mailing label*) should be directed to the ACS Columbus address noted above. Please allow six weeks for change of address to become effective.

**ACS membership information:** Bebe Olsen, Washington address.

**Single issues**, current year, \$5.00 except review issue and LabGuide, \$10.00; **back issues and volumes and microform editions** available by single volume or back issue collection. For information or to order, call (800) 424-6747 or write the Sales Department at the Washington address.

**Nonmembers rates in Japan:** Rates above do not apply to nonmember subscribers in Japan, who must enter subscription orders with Maruzen Company Ltd., 3-10 Nihonbashi 2-chome, Chuo-ku, Tokyo, 103, Japan. Tel: (03) 272-7211.

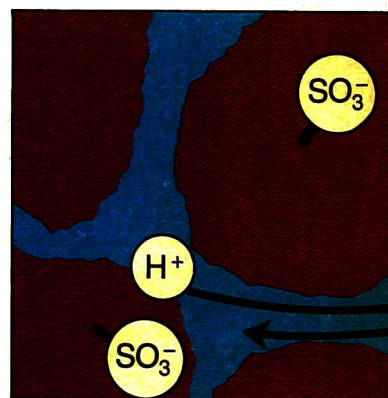
# Analytical CHEMISTRY



## REPORT

317 A

**On the cover: Dating techniques.** Archaeologists have an increasing array of physical dating methods at their disposal. R. E. Taylor of the University of California discusses available techniques, recent advances in radiocarbon dating, and current developments in radiocalcium dating



## INSTRUMENTATION

335 A

**Ion chromatography.** James Fritz of Iowa State University discusses the principles of ion exchange, different types of ion chromatographic systems, instrumentation, sample pretreatment, and applications

## BRIEFS

306 A

## NEWS

315 A

**Hirschfeld honored:** A university fellowship competition and an annual award for research in near-IR spectroscopy are both established to honor the late Tomas Hirschfeld. ▶ **Nominations are sought** for the EAS Award for Outstanding Achievements in the Fields of Analytical Chemistry

## FOCUS

347 A

**Electroanalytical chemistry** is entering an exciting era that will see gas- and solid-phase electrochemistry, electrochemical resolution on the order of Angstroms, and electrochemical expert systems, among other developments

## NEW PRODUCTS & MANUFACTURERS' LITERATURE

352 A

## AUTHOR INDEX

545

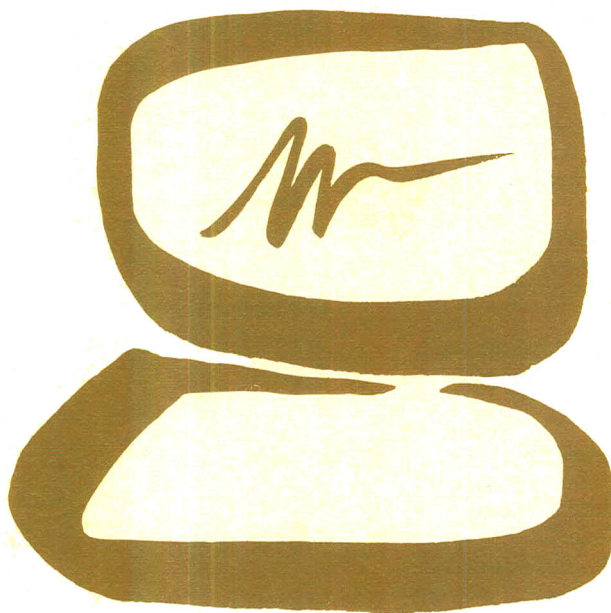
ห้องสมุดกรมวิทยาศาสตร์บริการ  
 ก.ค. 2530



**WHAT  
DO YOU GET  
WHEN YOU CROSS  
CHROMATOGRAPHY  
WITH A PERSONAL  
COMPUTER?**

Booth 723/836 at the Pittsburgh Conference.





**BECKMAN**

CIRCLE 17 ON READER SERVICE CARD



## Reverse-Phase High-Performance Liquid Chromatography/ Nuclear Magnetic Resonance Spectrometry in Protonated Solvents 546

An analgesic mixture is separated in 50:50 H<sub>2</sub>O–acetonitrile, and a phenol mixture is separated in 20:80 H<sub>2</sub>O–methanol. The effects of solvent gradients on the NMR signal are examined for H<sub>2</sub>O–acetonitrile and H<sub>2</sub>O–methanol at pH 7 and 4.4.

David A. Laude, Jr., and C. L. Wilkins\*, Department of Chemistry, University of California, Riverside, Calif. 92521  
*Anal. Chem.*, 59 (1987)

## Compositional and Solid-State Nuclear Magnetic Resonance Study of Humic and Fulvic Acid Fractions of Soil Organic Matter 551

The technique is evaluated by relaxation and spin-counting experiments and elemental constraint calculations. Spin-counting experiments demonstrate that less than 50% of the carbon in three of the fractions is observed.

Michael A. Wilson\* and Anthony M. Vassallo, CSIRO Division of Fossil Fuels, P.O. Box 136, North Ryde, New South Wales 2113, Australia, and E. Michael Perdue\* and J. Helmut Reuter, School of Geophysical Sciences, Georgia Institute of Technology, Atlanta, Ga. 30332  
*Anal. Chem.*, 59 (1987)

## Structural Analysis of Geochemical Samples by Solid-State Nuclear Magnetic Resonance Spectrometry. Role of Paramagnetic Material 558

Spin-counting experiments on coal tars and a fulvic acid show that almost all of the sample carbon is observed in both solution and solid-state NMR spectra.

Anthony M. Vassallo\*, Michael A. Wilson, and Philip J. Collin, CSIRO Division of Fossil Fuels, P.O. Box 136, North Ryde, New South Wales, Australia, and J. Malcolm Oades and Angela G. Waters, Department of Soil Science, Waite Agricultural Research Institute, University of Adelaide, Glen Osmond, South Australia, Australia, and Ronald L. Malcolm, U.S. Geological Survey, Denver Federal Center, Denver, Colo. 80225  
*Anal. Chem.*, 59 (1987)

## Organic-Soluble Lanthanide Nuclear Magnetic Resonance Shift Reagents for Sulfonium and Isothiouonium Salts 562

The species [Ln(fod)<sub>4</sub>]<sup>−</sup>, formed in solution from Ln(fod)<sub>3</sub> and M(fod) (M = Ag or K), is an effective shift reagent for organic salts. The reagents can be used in solvents such as chloroform and benzene.

Thomas J. Wenzel\* and Joseph Zaia, Department of Chemistry, Bates College, Lewiston, Me. 04240  
*Anal. Chem.*, 59 (1987)

## Supersonic Jet Spectroscopy with a Capillary Gas Chromatographic Inlet 567

A jet nozzle is reported that is based on sheath flow gas dynamic focusing that enriches the central core of the jet with analyte to provide better overlap with the incident laser beam. A detection limit of 50 pg is achieved for naphthalene.

Steven W. Stiller and Murray V. Johnston\*, Department of Chemistry and Biochemistry, and Cooperative Institute for Research in Environmental Sciences, Campus Box 215, University of Colorado, Boulder, Colo. 80309-0215  
*Anal. Chem.*, 59 (1987)

## Fluorescence Spectra and Lifetimes of Several Fluorophores Immobilized on Nonionic Resins for Use in Fiber-Optic Sensors 572

Fiber-optic-based instrumentation demonstrates that fluorescence lifetimes and emission spectra of four fluorophores change upon binding to XAD-2 and XAD-4 resins.

Wayde A. Wyatt, Greg E. Poirier, Frank V. Bright, and Gary M. Hieftje\*, Department of Chemistry, Indiana University, Bloomington, Ind. 47405  
*Anal. Chem.*, 59 (1987)

## Identification of Mixture Components in Organic Waste Materials by Carbon-13 Nuclear Magnetic Resonance 576

An algorithm combining the analysis of quantitative <sup>13</sup>C NMR data with a reverse library search procedure is used to identify unknown compounds above the 0.5% level in waste solvent mixtures.

David A. Laude, Jr., and Charles L. Wilkins\*, Department of Chemistry, University of California, Riverside, Riverside, Calif. 92521  
*Anal. Chem.*, 59 (1987)

## Fluorometric Determination of Hydrogen Peroxide in Groundwater 582

Standard addition calibration corrects for natural background fluorescence and non-ideal reaction stoichiometry. The detection limit, defined as the blank plus three standard deviations, ranges from 3.6 to 44.6 nM.

Thomas R. Holm\*, Gregory K. George, and Michael J. Barcelona, State Water Survey Division, Illinois Department of Energy and Natural Resources, 2204 Griffith Drive, Champaign, Ill. 61820  
*Anal. Chem.*, 59 (1987)

## Specificity of the Ion Exchange/Atomic Absorption Method for Free Copper(II) Species Determination in Natural Waters 586

The ion exchange-AA method is more sensitive for Cu<sup>2+</sup> than the ion-selective electrode method. Accurate values of Cu<sup>2+</sup> concentration are obtained by both methods in the presence of anionic copper–ligand complexes.

Jamal A. Sweileh, Dale Lucyk, Byron Kratochvil\*, and Frederick F. Cantwell\*, Department of Chemistry, University of Alberta, Edmonton, Alberta, Canada T6G 2G2  
*Anal. Chem.*, 59 (1987)

\* Corresponding author



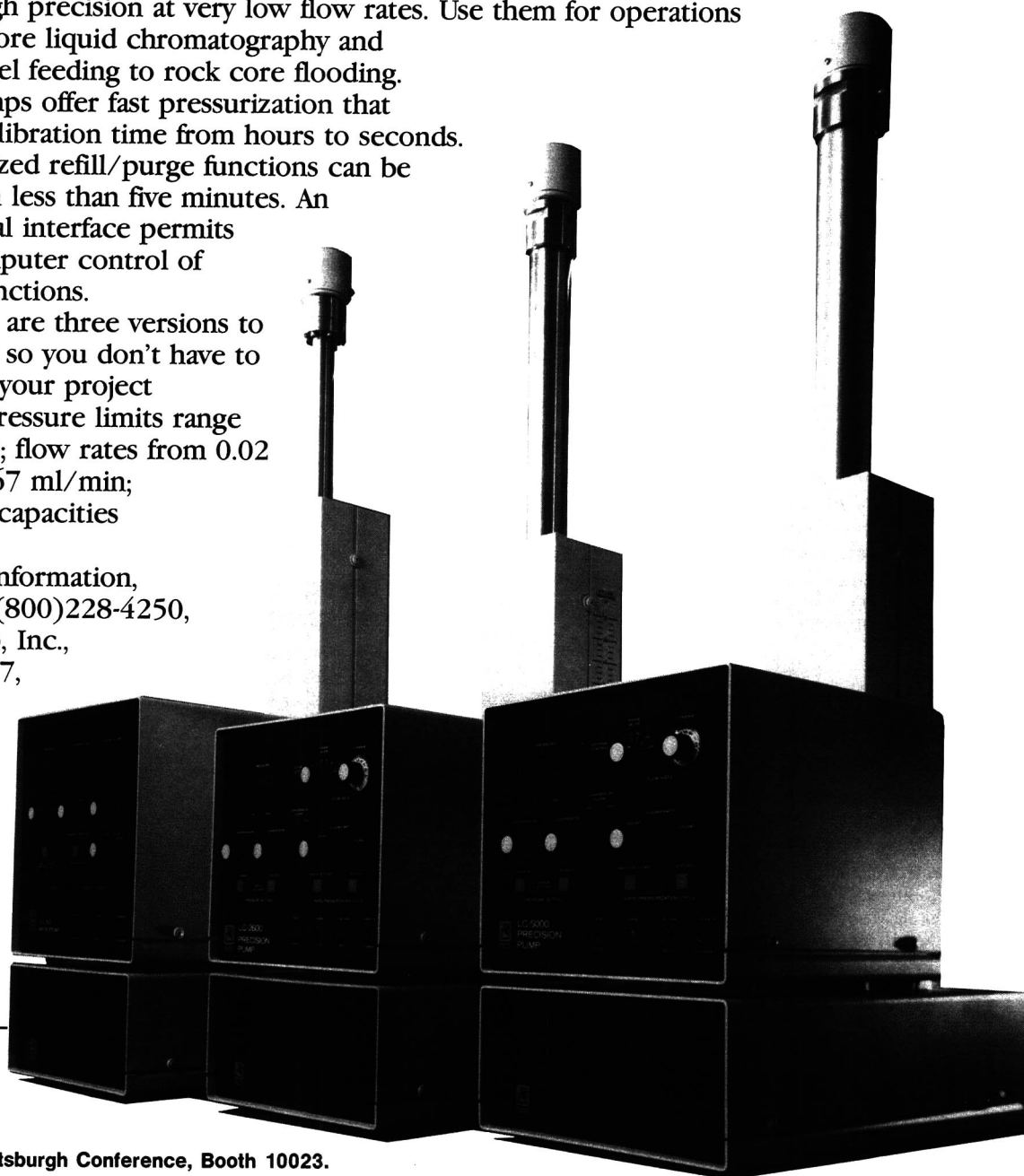
# New syringe pumps give precision flow at micro rates

Because Isco syringe pumps feature high calibration accuracy and no detectable flow noise or pulsation, they'll outperform any reciprocating pump for high precision at very low flow rates. Use them for operations from microbore liquid chromatography and reaction vessel feeding to rock core flooding.

These pumps offer fast pressurization that reduces equilibration time from hours to seconds. Their motorized refill/purge functions can be completed in less than five minutes. An optional serial interface permits external computer control of key pump functions.

Now there are three versions to choose from, so you don't have to compromise your project conditions. Pressure limits range to 10,000 psi; flow rates from 0.02  $\mu\text{l}/\text{min}$  to 6.67 ml/min; and cylinder capacities to 500 ml.

For more information, call toll free (800)228-4250, or write: Isco, Inc., P.O. Box 5347, Lincoln, NE 68505.



See us at The Pittsburgh Conference, Booth 10023.

CIRCLE 72 ON READER SERVICE CARD



## Direct Atomic Emission Determination of Some Trace Metals in Solid Powder Samples with a Magnetically Tailored Capacitive Discharge Plasma 593

Relative errors in the 5–10% range are obtained when a magnetic field of a few kilogauss is used to alter the properties of an electrically vaporized thin film plasma.

David Albers and Richard Sacks\*, Department of Chemistry, University of Michigan, Ann Arbor, Mich. 48109

*Anal. Chem.*, 59 (1987)

## Membrane Interface for Selective Introduction of Volatile Compounds Directly into the Ionization Chamber of a Mass Spectrometer 597

A silicone-based polymer hollow-fiber membrane is used to transport aqueous solutions through the ion volume of a mass spectrometer where permeation occurs selectively and mass spectra of fermentation broths can be recorded continuously.

M. E. Bier and R. G. Cooks\*, Department of Chemistry, Purdue University, West Lafayette, Ind. 47907

*Anal. Chem.*, 59 (1987)

## Electron Capture Negative Ion Chemical Ionization Mass Spectrometry of Derivatized Chlorophenols and Chloroanilines 601

Hammett linear free energy relationships are used to predict the stability of molecular anions, the direction of fragmentation pathways, and the usefulness of a given derivative for analytical purposes using selective ion monitoring.

Thomas M. Trainor\* and Paul Vouros, Barnett Institute of Chemical Analysis and Department of Chemistry, Northeastern University, Boston, Mass. 02115

*Anal. Chem.*, 59 (1987)

## Application of Isotope Dilution Inductively Coupled Plasma Mass Spectrometry to the Analysis of Marine Sediments 610

Eleven trace elements in the marine sediment reference materials MESS-1 and BCSS-1 are determined. The precision of replicate analyses is better than that achieved by alternative calibration strategies in ICP-MS.

J. W. McLaren\*, Diane Beauchemin, and S. S. Berman, Analytical Chemistry Section, Division of Chemistry, National Research Council of Canada, Ottawa, Ontario, Canada K1A 0R9

*Anal. Chem.*, 59 (1987)

## Determination of Sites of Incorporation of Oxygen-18 Atoms in Maduramicin $\alpha$ by Fast Atom Bombardment Mass Spectrometry 614

Five  $^{18}\text{O}$  atoms are found in the biosynthesized maduramicin  $\alpha$  structure. The exact location of these five  $^{18}\text{O}$  atoms is determined from fragmentation patterns.

Ted T. Chang\*, Chemical Research Division, American Cyanamid Company, Stamford, Conn. 06904, and Hwei-Ru Tsou and Marshall M. Siegel, Medical Research Division, American Cyanamid Company, Pearl River, N.Y. 10965

*Anal. Chem.*, 59 (1987)

## Comprehensive Trace Level Determination of Organotin Compounds in Environmental Samples Using High-Resolution Gas Chromatography with Flame Photometric Detection 617

Butyltins and other organotin compounds are determined via extraction, ethylation, and capillary GC analysis with specific detection and mass spectrometric confirmation.

Markus D. Müller, Swiss Federal Research Station, CH-8820 Wädenswil, Switzerland

*Anal. Chem.*, 59 (1987)

## Determination of Alkaline-Earth Metals in Samples Containing a Large Excess of Alkali by Ion Chromatography 624

Alkali metal interferants are removed prior to detection via an automated heart-cutting method. Area response is linear in the range of 10–120 mg/L for  $\text{Mg}^{2+}$  and 20–200 mg/L for  $\text{Ca}^{2+}$ .

Dennis Jenke, Travenol Laboratories, Inc., 6301 Lincoln Avenue, Morton Grove, Ill. 60053

*Anal. Chem.*, 59 (1987)

## Fluorescence Properties of Metal Complexes of 8-Hydroxyquinoline-5-sulfonic Acid and Chromatographic Applications 629

Seventy-eight metal species are examined, and subpicomole detection limits are obtained for Cd, Mg, and Zn. The optimum pH, determined by ligand ionization versus hydroxo complex formation, lies between 5 and 8.

Krystyna Soroka, Rathnapala S. Vithanage, Denise A. Phillips, Brian Walker, and Purnendu K. Dasgupta\*, Department of Chemistry and Biochemistry, Texas Tech University, Lubbock, Tex. 79409-4260

*Anal. Chem.*, 59 (1987)

## Artifacts Arising from the Improper Preparation and Use of Nonaqueous Ion Exchange Resins 636

The effect of inadequate conditioning of nonaqueous macroreticular ion exchange resins and the consequential contamination of the acid and base fractions separated on them are described and physicochemically evaluated.

Michael G. Strachan and R. B. Johns\*, Department of Organic Chemistry, University of Melbourne, Parkville, Victoria 3052, Australia

*Anal. Chem.*, 59 (1987)

## On-Line Supercritical Fluid Extraction–Capillary Gas Chromatography 640

The supercritical fluid extract is decompressed through a restrictor to deposit and concentrate the analytes at the inlet of a standard capillary GC column for subsequent analysis.

Bob W. Wright\*, Stephen R. Frye, Dennis G. McMinn, and Richard D. Smith, Chemical Methods and Separations Group, Chemical Sciences Department, Pacific Northwest Laboratory, Richland, Wash. 99352

*Anal. Chem.*, 59 (1987)

## Theory and Experimental Verification of Catalytic Determinations by Continuous Addition of Catalyst to a Reference Solution 645

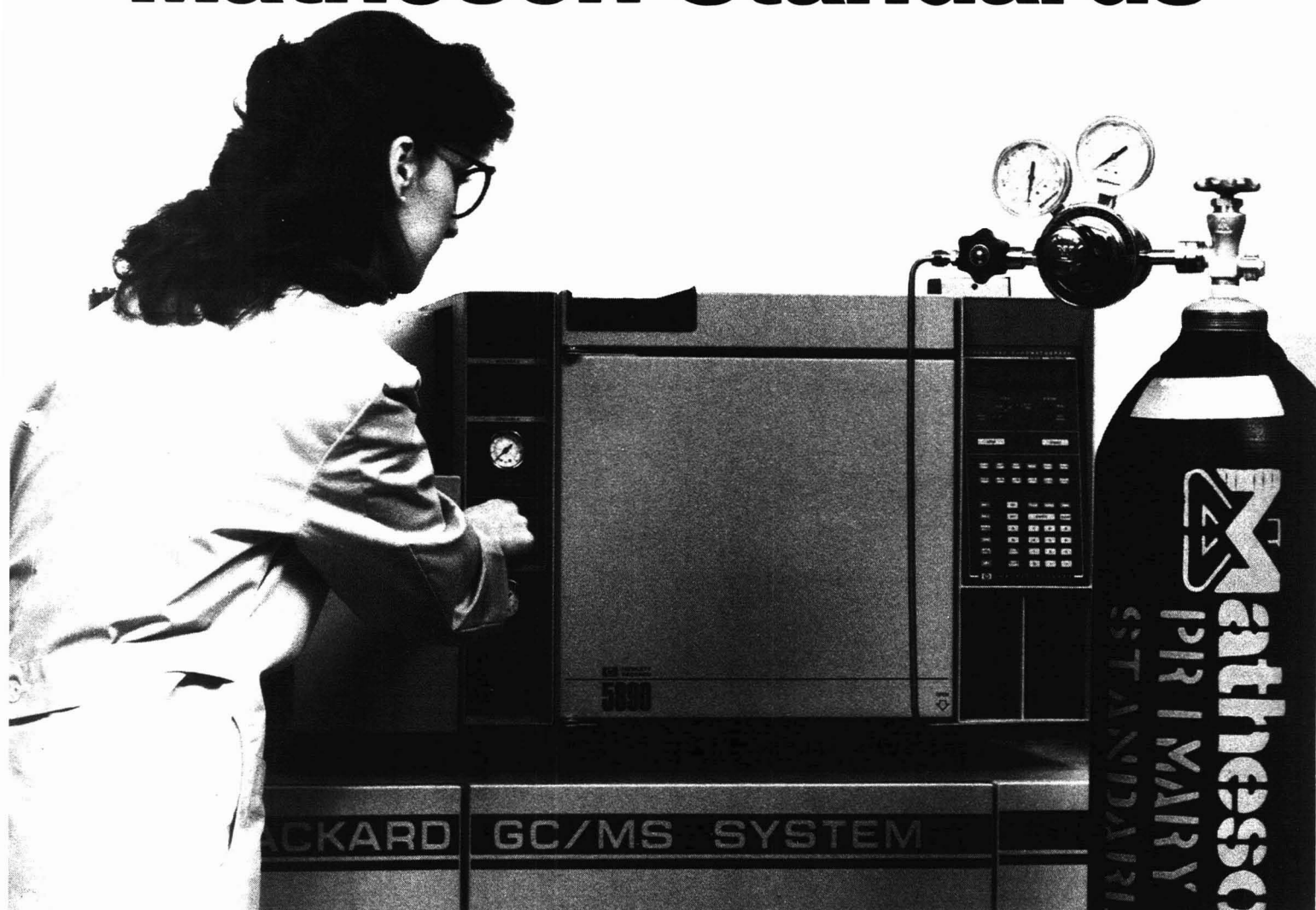
A method of catalytic determination using two different approaches (comparative and pseudostoiichiometric) is reported. Theoretical equations are derived, and experimental assessment is made by examining the behavior of the iodide-catalyzed  $\text{Ce(IV)}\text{--As(III)}$  reaction.

Guillermo López-Cueto\* and A. F. Cueto-Rejón, Department of Analytical Chemistry, University of Alicante, 03080 Alicante, Spain

*Anal. Chem.*, 59 (1987)



# Move Up to Matheson Standards



**Accurate gas chromatography is dependent upon your technique, your equipment, and your gases. A skilled gas chromatographer can enhance the accuracy of his results by using Matheson products exclusively. Three special products are of utmost importance.**

#### **Primary Standard Calibration Mixtures**

The heart of your work centers around your calibration standards. Consider Matheson's Primary Standards to improve your results. The accuracy of these mixtures usually exceeds that of most analytical instruments. Matheson Primary Standards are prepared on high load, high sensitivity analytical balances. Each gas component is carefully quality controlled before being weighed into the

cylinder. Only weights traceable to the National Bureau of Standards are used. These mixtures give the highest degree of accuracy, precision and confidence. Move up today! Insist on Matheson Primary Standards.

#### **Carrier Gases**

The same exacting quality you get in Matheson Primary Standard Calibration Mixtures is also available in Matheson's carrier gases. No slipping in quality control here. Each Matheson UHP, Zero Gas, Ultra Zero Gas, and, of course, Matheson Purity Gas is guaranteed to be exactly what the label says. Nothing more, nothing less. Improve your GC operation today with the right carrier gas from Matheson.

#### **Gas Handling Systems**

Don't jeopardize the integrity of your gases with gas handling equipment of inferior quality. Matheson has

the right piece of equipment for every job. From regulators that don't outgas impurities, to filters for protecting delicate valves, to flowmeters that measure precisely, Matheson equipment is the standard.

**When your work requires the best, don't settle for less than Matheson Standards.**

From pharmaceuticals to petroleum, from laser technology to aerospace, when only the best will do, do what so many experienced scientists do, move up to Matheson Standards.

For more information, contact Matheson, at (201) 867-4100, or circle the Reader Service Number below.

**Matheson®**  
**Gas Products**  
World Leader in Specialty Gases & Equipment  
30 Seaview Drive, Secaucus, NJ 07094

CIRCLE 100 ON READER SERVICE CARD

ห้องสมุดกรมวิทยาศาสตร์บริการ



# WHEATON Rotary Evaporators and Accessories

## Microprocessor Controlled Rotary Evaporators with New and Unique Instruments for Temperature and Vacuum Control

### ROTARY EVAPORATORS

- Preprogram and display RPM, bath temperature, vapor temperature, and operating time
- Safety features provide automatic shutdown in the event of instrument malfunction

### COOL ACE LOW TEMPERATURE CIRCULATING BATHS

- Compact, easy to operate bath for external circulation
- Cooling temperature range 0° to 15°C with a circulating rate of 40 liters/min

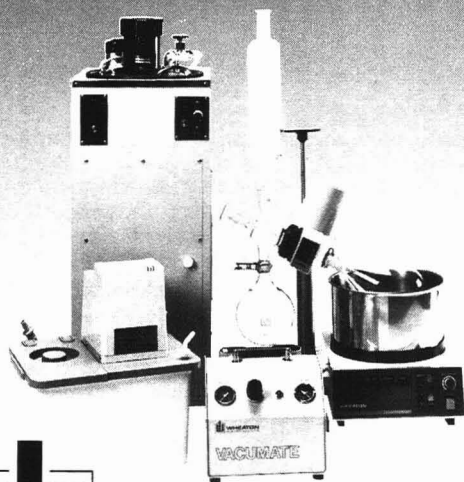
### A3S ASPIRATOR

- Conserve water. Create uniform vacuum to reduce vapor pressure without water tap hookups
- Compact, safe, and easy to operate, the A3S can perform two independent aspirations simultaneously

### VACUMATE™

- Nonelectric explosion resistant vacuum pump ideal for distilling volatile solvents
- Whisper quiet operation with no moving parts

For more information call 609/825-1400 or write:



**WHEATON**  
INSTRUMENTS

1301 N. Tenth Street, Millville, NJ 08332  
609/825-1400, Ext. 3089

Marking a Century of Service 1888-1988

## BRIEFS

### Time-Warping Algorithm Applied to Chromatographic Peak Matching Gas Chromatography/Fourier Transform Infrared/ Mass Spectrometry 649

A time-warping algorithm is used to eliminate the time axis stretch and squeeze in chromatograms so that the peaks can be matched.

Ching Po Wang and Thomas L. Isenhour\*, Department of Chemistry, University of North Carolina, Chapel Hill, N.C. 27514

*Anal. Chem.*, 59 (1987)

### Problems of Smoothing and Differentiation of Data by Least-Squares Procedures and Possible Solutions 654

Smoothing and differentiation of experimental data sometimes necessitates least-squares polynomial fitting of a large number of data points at a time rather than 3, 5, or 7 points with repetition of the procedure for several iterations.

Arshad Khan, Chemistry Department, The Pennsylvania State University, DuBois, Pa. 15801

*Anal. Chem.*, 59 (1987)

### Rigorous Convergence Algorithm for Fitting a Monoexponential Function with a Background Term Using the Least-Squares Method 658

A numerically stable algorithm is developed for analyzing data containing a single exponential function with a background term using the Newton-Raphson method inside an interval located by the Fibonacci order search.

Željko Jeričević, Douglas M. Benson, Joseph Bryan, and Louis C. Smith\*, Department of Medicine and Department of Cell Biology, Baylor College of Medicine, Houston, Tex. 77030

*Anal. Chem.*, 59 (1987)

### Rapid Anodic Stripping Analysis with Ultramicroelectrodes 662

The properties of ultramicroelectrodes enable the determination of heavy metals without the deoxygenation of samples. The detection limit is  $\sim 5 \times 10^{-9}$  M for a 10-s preconcentration time.

Andrzej S. Baranski, Department of Chemistry, University of Saskatchewan, Saskatoon, Saskatchewan, Canada S7N 0W0

*Anal. Chem.*, 59 (1987)

### Electrochemical Determination of Sulfur Dioxide in Air Samples in a Closed-Loop Flow Injection System 666

SO<sub>2</sub>(g) is determined in the 0.3 to 14.0 ppm (v/v) range with RSDs of  $\sim 3\%$  (11 replicas) at a rate of 25 samples per hour.

Angel Ríos, M. D. Luque de Castro, and Miguel Valcárcel\*, Departamento de Química Analítica, Facultad de Ciencias, Universidad de Córdoba, Córdoba, Spain, and Horacio A. Mottola\*, Department of Chemistry, Oklahoma State University, Stillwater, Okla. 74078-0447

*Anal. Chem.*, 59 (1987)

### Characterization of Electrode Heterogeneity with Electrogenerated Chemiluminescence 670

ECL images are magnified and recorded photographically to show the location, size, and geometry of individual active regions.

Royce C. Engstrom\*, Kirk W. Johnson, and Scott DesJarlais, Department of Chemistry, University of South Dakota, Vermillion, S.D. 57069

*Anal. Chem.*, 59 (1987)

CIRCLE 176 ON READER SERVICE CARD



## Unconventional by design.

While conventional mass spectrometers have sought to improve performance with refinements to existing designs, Nicolet has pioneered a totally new technology: Fourier transform mass spectrometry (FTMS).

### Time vs. space spectrometry

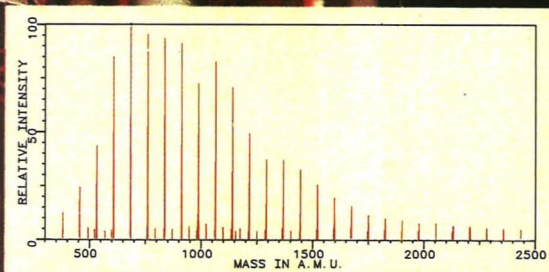
The Nicolet FTMS-2000 separates ion formation, reaction, and detection in time rather than separating ions in space like conventional quadrupole and magnetic sector instruments. This enables relatively simple hardware to perform extremely sophisticated experiments.

### Ion storage

Since ions are stored and non-destructively detected within the FTMS-2000 analyzer, multiple experiments such as chemical ionization, negative ion detection, and multistage mass spectrometry (MS/MS) can be performed without additional analyzers and without associated additional expense. All ions are detected simultaneously, making the FTMS-2000 ideal for use with pulsed techniques such as laser desorption/laser ionization and photo dissociation.

*Positive ion LD/FTMS spectrum of poly (p-phenylene) synthesized from benzene by the Kovacic method.*

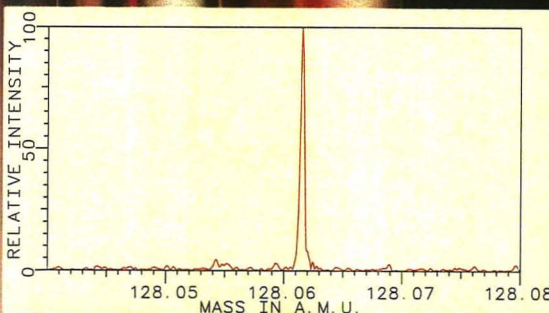
Sample provided courtesy of P. Kovacic, U. of Wisconsin — Milwaukee. Data obtained by C.E. Brown, Medical College of Wisconsin.



### Ultra-high resolution and accurate mass measurement

The patented Nicolet FTMS analyzer has extremely high resolving power and accurate mass measuring capabilities, and accommodates conventional inlet techniques such as capillary-column GC/MS and direct probe introduction.

*High-resolution capillary-column gas chromatography mass spectrum of naphthalene. Resolution of 340,000 (FWHH) at 128 a.m.u.*



**See us at Pittsburgh Conference 1987,  
Booth 8045. Or for more information on the  
FTMS-2000 contact:**

## Nicolet

Nicolet Analytical Instruments  
5225-1 Verona Road P.O. Box 4508  
Madison, Wisconsin 53711  
608/271-3333 / Telex: 910-286-2736  
CIRCLE 110 ON READER SERVICE CARD

FTMS-2000 dual-region cell



# GAS FACTS

published periodically  
for analytical chemists

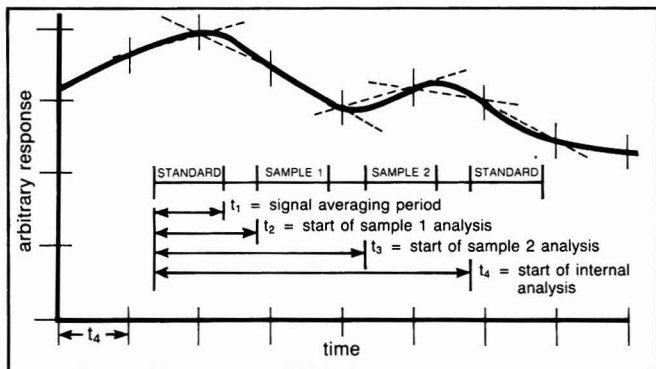
## Compensation by computer for instrument drift

Instrument drifts of the order of 0.5%/hr can pose problems when making very accurate and precise measurements. To control drift to better than 0.1% over a 10 hr period, Scott has developed a unique computer

linear approximations between responses of the introduced standard. The algorithm used to calculate sample response is based on determining response of the standard,  $R_{ix}$ , at the time of analysis of a sample:

$$R_{ix} = R_{i1} + [R_{i1} - R_{i2}] [t_x]/[t_4]$$

$R_{i1}$  is initial response of the standard,  $R_{i2}$  is response of the standard after time  $t_4$ , and  $t_x$  is time elapsed between  $R_{i1}$  and  $R_{ix}$ . For linear response instruments,



controlled system. In it, signal-to-noise ratio is enhanced by digital filtering and signal averaging, and drift is compensated by introducing a standard on a pre-established time basis (ea 10 min) and tracking its response. The computer maintains records of time and responses for both standard and sample.

A few assumptions underlie the program. One is that "zero" drift is negligible in comparison to span drift which is derived by successive

a new slope,  $M_x$ , can be calculated from  $M_x = [y - b]/[R_{ix}]$  where  $y$  is standard concentration and  $b$  is initial intercept. Sample concentration at  $t_x$  can then be calculated. Scott has used this technique to monitor the stability of gases such as CO and H<sub>2</sub>S over time frames of more than a year. Ask for more information.

INFORMATION HOTLINE:  
800-331-4953  
8:00AM-5:00PM Eastern time  
In PA: 215-766-8861

**Scott**  
Specialty Gases

Fremont, CA • Houston, TX •  
Plumsteadville, PA • Troy, MI •  
Longmont, CO • Wakefield, MA •  
San Bernardino, CA • South Plainfield, NJ



123A

CIRCLE 152 ON READER SERVICE CARD

## BRIEFS

### Dielectric Characterization of Binary Solvents Containing Acetonitrile

674

Nonlinear regression functions are established for 10 acetonitrile cosolvent pairs, and the factors determining the deviations from ideal dielectric behavior for the mixtures are identified.

Orland W. Kolling, Chemistry Department, Southwestern College, Winfield, Kan. 67156  
*Anal. Chem.*, 59 (1987)

### Correspondence

#### Characterization of a Microinjector for Capillary Zone Electrophoresis

678

Ross A. Wallingford and Andrew G. Ewing\*, Department of Chemistry, The Pennsylvania State University, University Park, Pa. 16802  
*Anal. Chem.*, 59 (1987)

#### Application of a Modulated Magnetic Field to a Flame Photometric Detection Burner in the Detection of Phosphorus

681

Nobuko I. Wakayama\*, Hisakazu Nozoye, and Ichiro Ogasawara, National Chemical Laboratory for Industry, Tsukuba Research Center, Yatabe, Ibaraki 305, Japan  
*Anal. Chem.*, 59 (1987)

### Aids for Analytical Chemists

#### Purge Gas Enhancement of Peak Resolution in Differential Scanning Calorimetry

684

Guang-Way Jang, Ranjana Segal, and Krishnan Rajeshwar\*, Department of Chemistry, The University of Texas at Arlington, Arlington, Tex. 76019-0065  
*Anal. Chem.*, 59 (1987)

#### Automated Ion-Exchange Column System for Biological Sample Fractionation

687

Y. T. Kim and Christiaan Glerum\*, Ontario Tree Improvement and Forest Biomass Institute, Ontario Ministry of Natural Resources, Maple, Ontario, Canada L0J 1E0

*Anal. Chem.*, 59 (1987)

#### Correction. Elemental Characterization of the National Bureau of Standards Milk Powder Standard Reference Material by Instrumental and Radiochemical Neutron Activation Analysis

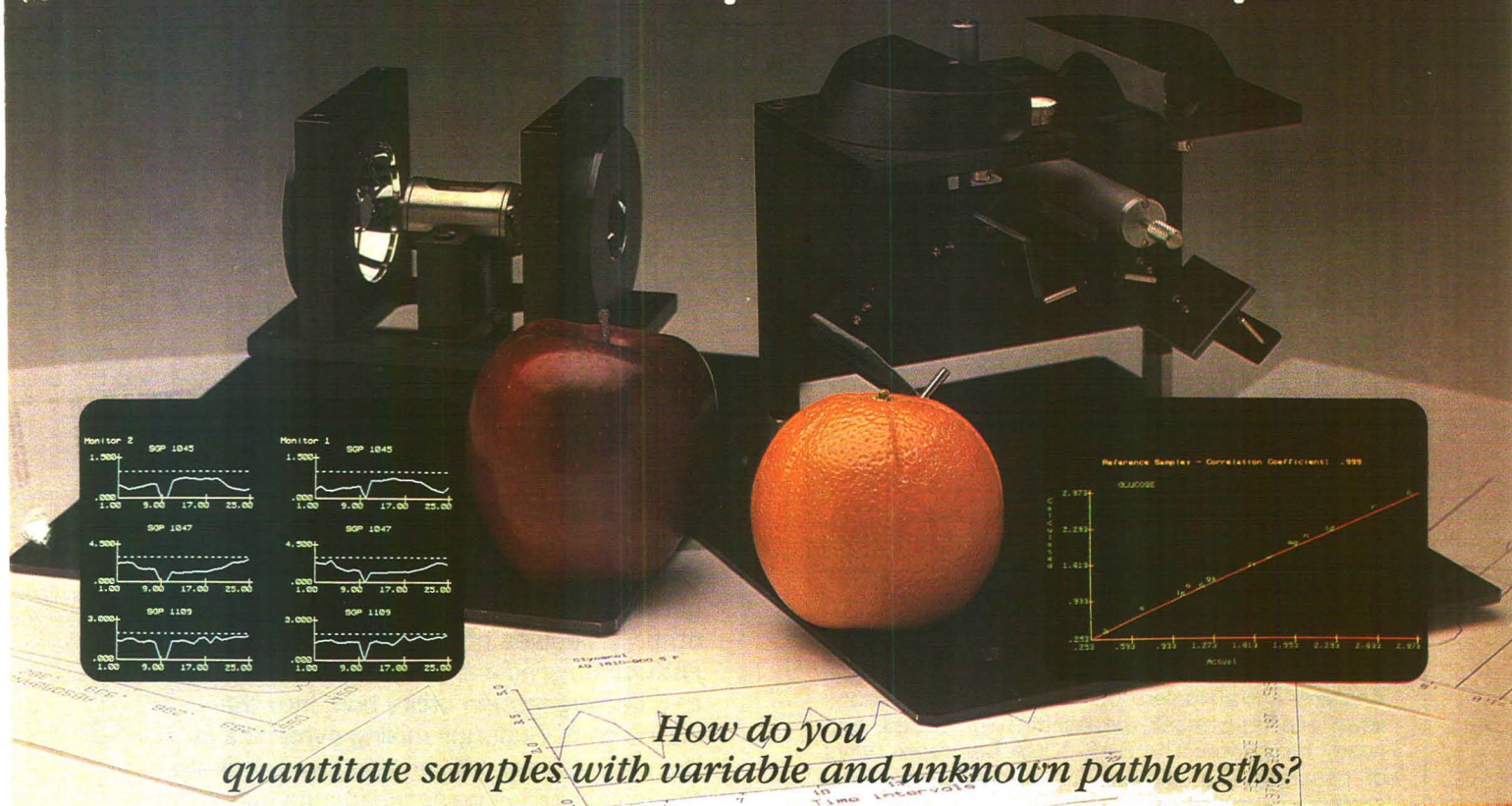
688

Robert R. Greenberg, Center for Analytical Chemistry, National Bureau of Standards, Gaithersburg, Md. 20899

*Anal. Chem.*, 59 (1987)



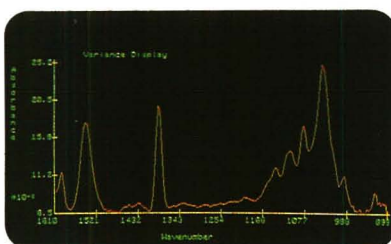
# Finally, an FT-IR quantification package for real-world analytical chemistry.



*How do you  
quantitate samples with variable and unknown pathlengths?*

Nicolet's new Partial Least Squares (PLS) QUANT™ package makes quantitative analysis of your "apples and oranges" easy, and more importantly, extremely accurate. PLS QUANT is based on today's most advanced chemometric quantification algorithm; whereby spectral regions rather than discrete absorption bands are utilized to analyze quantitative data. This greatly simplifies the method set up procedure by eliminating the need to correlate spectral features with individual components.

PLS operates on all Nicolet FT-IR spectrometer systems and is the ideal program for samples with fixed, variable, known or indeterminant pathlengths. The indeterminant pathlength approach is a unique PLS method used for capillary films, molded polymer films, KBr disks and other samples



*PLS Variogram™ indicates the areas of high spectral activity which can be used for the calibration procedure.*



*Nicolet low-cost 5DXC FT-IR with Autosampler analyzes up to eighty QC samples automatically.*

whose thickness cannot be accurately measured.

Since its introduction, Nicolet PLS QUANT has been used to successfully analyze a diverse range of QC samples including: seven components in a commercial detergent; epoxy compounds in prepolymers; terpolymer compositions as cast films; additives in lubrication greases; and powdered analgesic mixtures.

PLS QUANT is completely menu-driven with spreadsheet style entry of all calibration and analysis information. A total of eleven components can be analyzed *simultaneously* with a maximum of twenty-four reference and validation samples used during the calibration. Streamlined for today's high-throughput laboratories, PLS QUANT provides the quantitative information you need — simply, quickly, accurately.

*Send for our PLS QUANT™ Technical Report and Application Notes.*



**Nicolet**

CIRCLE 111 ON READER SERVICE CARD

Nicolet Analytical Instruments 5225-1 Verona Rd. / P.O. Box 4508 / Madison, WI 53711 / 608/271-3333 / Telex: 910-286-2736

See us at Pittsburgh Conference 1987, Booth 7044.



# Driving Lessons Included!



What do the new BAS-100A Electrochemical Analyzer and an Italian sports car have in common? Both are fast, sleek, powerful, fully loaded, and ready for action! The BAS-100A has more ways of reaching the answer to an electroanalytical problem than any other "vehicle" on the road, and it makes the going fun!

New programs and system architecture facilitate the techniques of chronoamperometry, hydrodynamic voltammetry, hydrodynamic modulation voltammetry, hydrodynamic amperometry, AC impedance, and many other pulse and D.C. waveforms. The BAS-100A features improved  $iR$  compensation and expanded data handling and storage. New "micro" voltammetric electrodes can now be accommodated! An external computer (the BASpc™) develops methods files for transfer to the BAS-100A and further massages collected data.

Give us a call for a test drive.

P.S. One big difference: you can buy four BAS-100A Analyzers with all the options for the price of one Ferrari, and you won't get a ticket for speeding.



**BAS**

Bioanalytical  
Systems, Inc

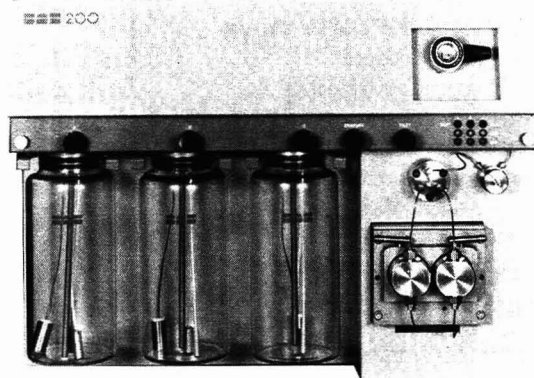
2701 Kent Ave  
West Lafayette  
Indiana 47906

Telex: 276141  
(317) 463-4527

# Excerpts from the history of absolute statements:

*"Man will never walk on the moon"*  
*"It's impossible for the Titanic to sink!"*  
*"The earth is flat!"*  
*"Ternary gradient LCEC can't be done"*

Oops! another absolute bites the dust! The BAS 200 makes gradient elution with multi-channel electrochemical detection a viable option for determinations of amino acids and other molecules of varying polarity. Even **reductive** gradient-LCEC is a breeze, thanks to a deoxygenation utility built into the instrument. Superior mixing dynamics in the BAS solvent delivery system eliminate the high baseline noise which can sabotage gradient-elution LCEC with minimum distortion of gradient profiles. Single or 4-channel variable wavelength UV/VIS detection provide still more options.



Ternary gradient LCEC/LCUV is only one of 20 great ideas built into the BAS 200 Problem Solver.

**BAS**

Bioanalytical  
Systems, Inc

2701 Kent Ave  
West Lafayette  
Indiana 47906

Telex: 276141  
(317) 463-4527

CIRCLE 18 ON READER SERVICE CARD

CIRCLE 19 ON READER SERVICE CARD



## Hirschfeld Fellowship and Award

A university fellowship competition at the University of Washington's Center for Process Analytical Chemistry (CPAC) and an annual award program sponsored by Technicon Industrial Systems have been established to honor the late Tomas Hirschfeld of Lawrence Livermore National Laboratory.

CPAC's new Hirschfeld/CPAC Fellowship involves a competition that is intended to attract outstanding students to the study of process analytical chemistry at the university. The fellowship will provide a two-year stipend that will permit the competition winner to work in an interdisciplinary, industrially oriented research environment, to attend conferences, and to make short- and long-term visits to sponsoring companies. According to CPAC, "Hirschfeld's unique insights, enthusiastic lectures, and creative inventions will continue to inspire scientists and students here and abroad for a long time to come." For more information and fellowship applications, contact Deborah Illman, CPAC, Dept. of Chemistry, Mail Stop BG-10, University of Washington, Seattle, Wash. 98195 (206-545-2326).

In addition, the first in Technicon's new series of Tomas B. Hirschfeld Awards will be presented to a deserving graduate student working in the field of near-infrared analysis (NIRA) at a 1987 Pittsburgh Conference symposium honoring Hirschfeld. According to Technicon, "NIRA was of particular interest to Dr. Hirschfeld, and he contributed substantially to this field. His interaction with students was quite remarkable. Despite his great depth of knowledge, he never intimidated those who came to him with questions. Indeed, he could spark interest by tossing out so many new ideas in a single conversation that a student's problem would become one of selection rather than compilation. It is appropriate, then, that his many thoughts on NIRA be perpetuated in an annual award to a graduate student involved with research in this area of spectroscopy." Additional information on the award is available from Donald A. Burns, Technicon Instruments Corp., 511 Benedict Ave., Tarrytown, N.Y. 10591.

## EAS Award Nominations

Nominations are sought for the 1988 Eastern Analytical Symposium Award for Outstanding Achievements in the Fields of Analytical Chemistry. The award, consisting of a plaque and a \$1000 stipend, will be presented at a special EAS symposium October 3-8, 1988, in New York.

Established in 1986, the award recognizes an individual who has helped shape the field of analytical chemistry. The 1986 winner was George H. Morrison, Editor of ANALYTICAL CHEMISTRY.

A nominating letter, including the nominee's specific accomplishments and a biographical sketch, should be submitted by July 1, 1987, to Robert Weinberger, EAS Awards Committee, Kratos Division of ABI Analytical, 170 Williams Dr., Ramsey, N.J. 07446.

## For Your Information

**International Business Machines Corp. (IBM)** announced on January 8 that it is **closing down its IBM Instruments subsidiary** (Danbury, Conn.). In conjunction with the closing, IBM also has sold its interests in Bruker and Spectrospin, which manufactured some of the instruments sold under the IBM Instruments label. Bruker will continue to market and distribute its own products. New orders for IBM Instruments' products will be accepted through April 13, based on availability. IBM will honor existing warranty obligations and maintenance agreements. IBM's National Service Division will assume responsibility for service, supplies, and parts, which will be available for a minimum of five years. All IBM Instruments employees will be offered other positions within the company.

Nicolet Instrument Corp. and Digital Equipment Corp. recently signed an agreement involving **cooperative marketing of Digital computers and software and Nicolet analytical instruments**. The agreement will enhance the integration of Nicolet instruments, including FT-IR and FT-MS spectrometers, with Digital's computing, communications, and information management systems.

A new **National Bureau of Standards report on quality assurance (QA)** contains abstracts of 160 papers selected as source materials for starting new QA programs and improving existing ones, and as general guides in producing reliable analytical chemistry measurements. The report was assembled by John K. Taylor, who recently retired after 57 years at NBS. "A Collection of Abstracts of Selected Publications Related to Quality Assurance of Chemical Measurements" (publication NBSIR 86-3352, order by PB # 87-106423) is available for \$11.95 prepaid from the National Technical Information Service, Springfield, Va. 22161.

A more rapid, more accurate, and less expensive **technique for measuring uranium concentrations**, particularly in urine bioassays, is the subject of a U.S. patent (no. 4,599,512) that has been awarded to Bruce A. Bushaw of Battelle Pacific Northwest Laboratories and assigned to the U.S. Department of Energy. A device based on the technique is being manufactured and marketed under the brand name Kinetic Phosphorescence Analyzer by Chemchek Instruments of Richland, Wash. The technique involves absorption of laser light and subsequent wavelength-shifted emission by uranium species present in a sample.

The National Committee for Clinical Laboratory Standards has published "**Evaluation of the Linearity of Quantitative Analytical Methods; Proposed Guideline**" (document EP6-P). The purpose of the guideline is to provide analytical chemists with a procedure for evaluating whether an instrument or method meets the manufacturer's linearity specifications. The document is available for \$15 (\$20 overseas) prepaid from NCCLS, 771 E. Lancaster Ave., Villanova, Pa. 19085 (215-525-2435).



# FLUORESCENCE

CIRCLE 1  
ON READER SERVICE CARD

## Fluorimet Filter Fluorometers

The Fluorimet series meets the need for a low-cost, sensitive and stable instrument for routine determinations. Fluorimets

can be equipped with a complete range of analytical accessories, including flow cells for liquid chromatography.



# FLUORESCENCE



## Nova-3

The Nova-3 scanning spectrofluorometer offers the highest standards of convenience, precision and versatility for routine analysis or research at a price substantially below the cost of any other

comparable instrument. Virtually every aspect of operation is controlled by a built-in microcomputer, giving the Nova-3 capabilities that equal or exceed those of far more expensive units.

CIRCLE 2  
ON READER SERVICE CARD

# FLUORESCENCE

CIRCLE 3  
ON READER SERVICE CARD

## FLUOROLOG-2

From UV to IR, our FLUOROLOG-2 line is the ultimate in research spectrofluorometric systems. All FLUOROLOG-2 systems are controlled by our new PC-based DM3000 series of spectroscopy

computers, which give the analyst unparalleled control and data manipulation capabilities via user-friendly, menu-driven software. And combining a FLUOROLOG-2 with the unique SPEX IM-1 real-time digital image-

processing system makes it possible to apply the sensitivity and selectivity of fluorescence to detecting and characterizing complex molecules within the field of the system's microscope.



# FLUORESCENCE

SPEX Industries, long a world leader in advanced research spectrofluorometers, now offers the most complete line of fluorometric instrumentation available anywhere—from inexpensive analytical filter fluorometers to the most sophisticated microspectrofluorometric imaging systems.



INDUSTRIES, INC. 3880 PARK AVE. EDISON, N.J. 08820 201-549-7144 TELEX: 178341

# Dating Techniques in Archaeology and Paleoanthropology



---

## R. E. Taylor

Department of Anthropology  
Institute of Geophysics and Planetary  
Physics  
University of California, Riverside  
Riverside, Calif. 92521

---

Archaeologists are specialists in the study of the surviving material remains that reflect the past behavior of a group of bipedal primates known as the *Hominidae*. Paleoanthropologists examine archaeological as well as paleontological, geological, and paleoecological data in an effort to understand the factors responsible for the origin and early biocultural evolution of the *Hominidae*, or hominids. Archaeologists and paleoanthropologists currently have at their disposal an impressive array of physical dating methods developed by colleagues in the physical sciences. These techniques permit students of hominid biological and cultural evolution to have increasing confidence that the evidence of past hominid morphology and behavior is being placed in the correct chronological order. Because physical scientists have developed various chronometric and analytical methods applicable to archaeological materials, many issues that were extremely difficult for prehistorians to address only a few decades ago are now being actively pursued.

Our species, *Homo sapiens sapiens*

(anatomically modern *Homo sapiens*), is the only living representative of the *Hominidae*—all earlier forms have become extinct. What traditionally has been identified as the earliest group of hominid species, the *Australopithecus*, made its appearance certainly more than 3.6 million, and perhaps as many as 5.5 million years ago in eastern and

---

## REPORT

---

southern Africa. *Homo habilis*, an African hominid whose fossils are found in association with clearly recognized stone tools, first appeared in the fossil record about 2 million years ago. The first hominids found outside Africa were members of genus *Homo* but of another species (*erectus*) and were distributed throughout many parts of the Old World (Eurasia and Africa) by 0.7–1.2 million years ago. Early or archaic forms of *Homo sapiens* have been assigned ages in excess of 100,000 years. Between about 100,000 and 35,000 years ago, a rather diverse population of premodern hominids known as *Homo sapiens neanderthalensis* occupied many regions in western Eurasia. Anatomically modern *Homo sapiens* were hunting and collecting in almost all parts of the Old World (including parts of Australasia) by at least 30,000

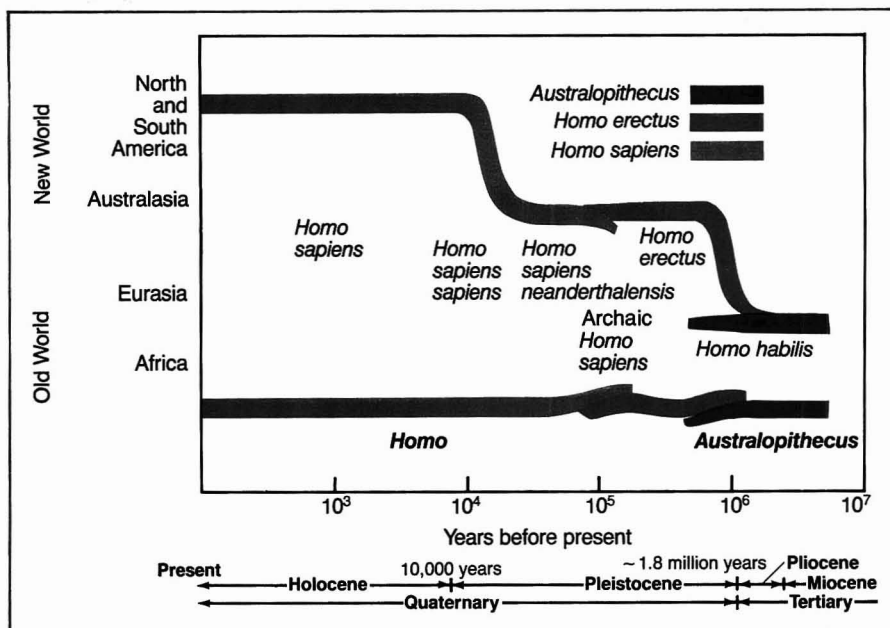
years ago. Although there are tentative reports suggesting human presence as early as 30,000–40,000 years ago in the Western Hemisphere, the current best evidence indicates that the ancestors of most of the Native American populations (misnamed by Europeans as “Indians”) arrived by way of eastern Siberia and Alaska not much before about 13,000–15,000 years ago (1, 2).

The specific age estimates cited above and illustrated in Figure 1 are based largely on data obtained from the application of various physical dating methods developed primarily by chemists and physicists over the last 40 years (3, 4). Prior to this, prehistorians could obtain accurate chronometric (“real”-time) estimates for their materials only in northern Europe and in the southwestern portion of the United States. Varve chronologies (counting and comparing the sequences of annual sedimentary layers in periglacial lakes) have provided important chronometric controls for the last 10,000 years in Scandinavia. In the southwestern United States, dendrochronology (tree ring dating) has provided temporal data for the last two millennia (5). Unfortunately, both methods have been useful only in circumscribed regional contexts, and sometimes there have been severe problems in associating datable materials with specific archaeological contexts. In addition, the age ranges for these techniques have been very limited.

Before the introduction of modern physical dating methods, prehistorians generally were forced to use temporal incrementing schemes that were extremely difficult to calibrate in terms of any chronometric scale. Local and regional stratigraphic and seriation approaches, the development of local and regional artifact complexes (hopefully having temporal significance), and attempts to correlate climatic or even astronomical processes with human fossil or cultural data were all pressed into service in the late 19th and early 20th centuries in an attempt to develop chronologically meaningful frameworks for the hominid record.

Over the last three to four decades, largely due to the development of a variety of physical dating methods by physicists and chemists, there has been what can legitimately be termed a revolution in the ability to assign age estimates to a wide spectrum of archaeological and human skeletal remains. This development represents one of the major advances of modern archaeology and paleoanthropology and vividly illustrates the interdisciplinary character of this field. Because physical dating specialists have become increasingly responsible for reconstructing temporal relationships, prehistorians and paleoanthropologists have





**Figure 1.** Outline of temporal framework for major hominid paleontological and biological groupings and their geographical extent over the last five million years.

increasingly turned their attention to identifying and understanding the mechanisms responsible for the evolution of hominid social and cultural systems. As an example of the type of issues currently being addressed, some paleoanthropologists are questioning the traditional view that hominid biocultural evolution over the last few million years has occurred as the result of small, cumulative, gradual alterations in morphology and behavior. Could it be that there have been long periods of relative stability and little change, punctuated with relatively short intervals characterized by rapid, major change?

Temporally speaking, the interest of prehistorians is focused almost entirely on the most recent geological sub-era of the Cenozoic: the Quaternary (also known by some geologists as the Pleistocene or Anthropogene). Most of this time interval is taken up by the Pleistocene epoch—ca.  $1.8 \times 10^6$  to  $1 \times 10^4$  years ago. The post-Pleistocene—the last 10,000 years—is known as the Holocene, or Recent. Most of the critical biocultural processes that characterize our species occurred during the Pleistocene, particularly the dramatic increase in brain size and organization that provides the physical basis on which our symbol manipulating and language abilities are based.

The classic divisions of the Pleistocene were developed in the middle- and late-19th century, particularly for western Europe. They were based largely on reconstructions by geologists of the sequence of glacial and interglacial periods—the so-called Ice Age successions—during which massive continental glaciers periodically expanded and contracted in the northern por-

tions of Europe and North America. Major worldwide sea level variations associated with the waxing and waning of these glaciers also provided an important calibration scheme, as have the recent biostratigraphic successions identified in deep sea cores, the oxygen isotope climatic stages, and the paleomagnetic reversal time scale for the early Pleistocene and earlier periods. The value of these more recently developed temporal indicators has been greatly enhanced because specific age estimates provided by isotopic dating

methods can be associated with the stages and relative time scales from classic geological sections as well as geomagnetic polarity, biostratigraphic, and oxygen isotope data.

#### Quaternary physical dating methods

Table I lists the major operational and experimental Quaternary physical dating methods that have been applied to archaeological and paleoanthropological materials. One of the major problems confronting those concerned with Quaternary geochronology is the fact that the hominid record, on a relative basis, is extremely compressed at the recent end of the geological time scale. This means that the most useful techniques must be able to assign age estimates with rather close temporal tolerances. In Table I, techniques listed as *operational* are those that have achieved a consensus among specialists that the age estimates provided are generally reliable when used in an appropriate and critical manner. *Experimental* methods lack such a consensus; however, each experimental method listed here may hold future promise pending the resolution of certain problems.

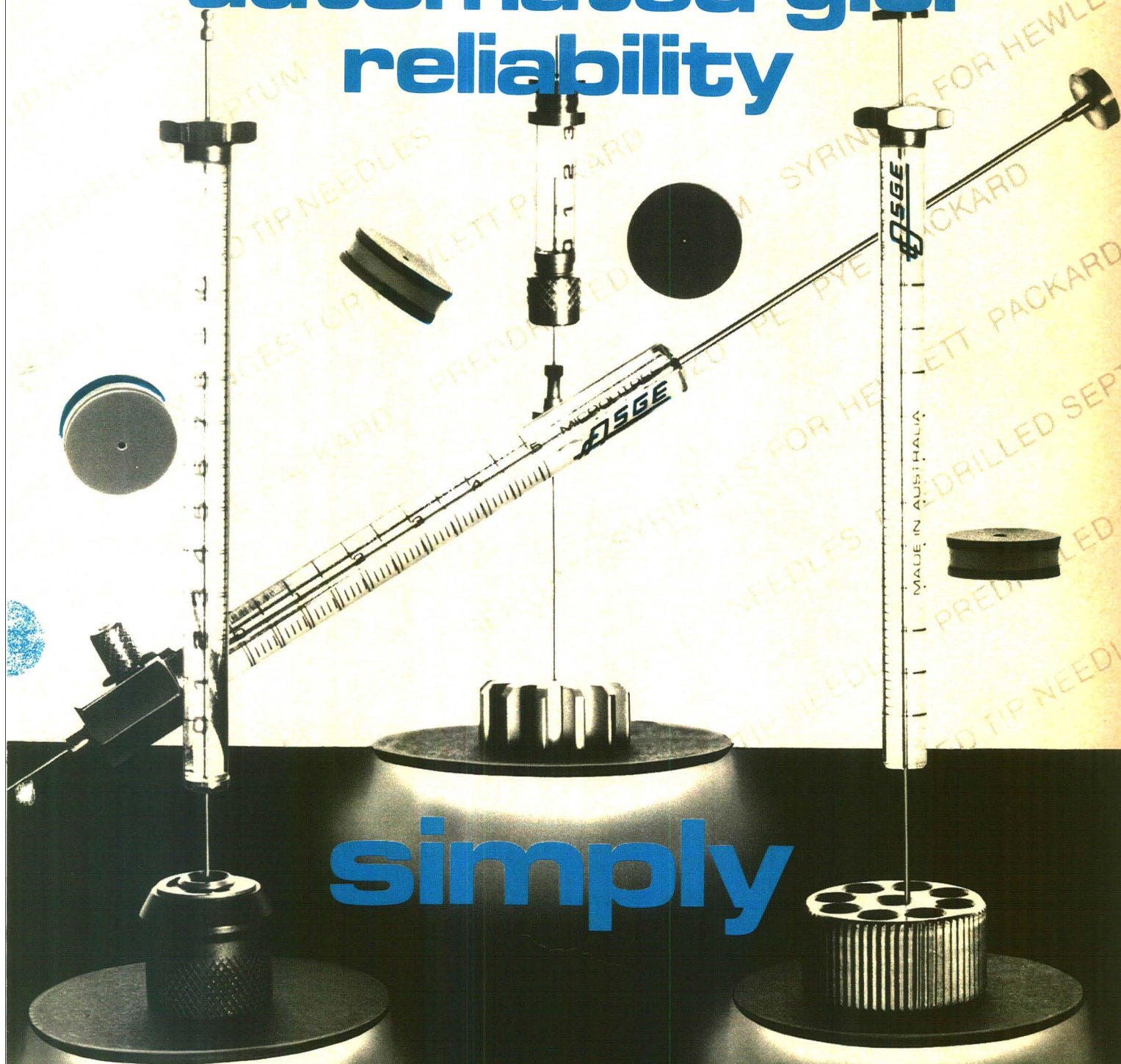
An obvious distinction noted in Table I is whether a dating method provides time placement or relative placement. *Time placement* techniques potentially can yield temporal incrementation that can be converted into "real-time" units (i.e., years), whereas *relative placement* techniques can be used to infer only serial or sequential relationships (i.e., whether one sample is

**Table I. Major Quaternary physical dating methods**

Status	Type	Basis	Method
Operational	Time placement	Radiometric	Radiocarbon (6)
			Potassium-argon (7)
			Fission track (8)
			Uranium series (9)
			Thermoluminescence (10)
			Varve (11)
	Relative placement	Geological	Archaeomagnetism-paleomagnetism (12, 13)
		Geophysical	Dendrochronology (5)
		Biological	Obsidian hydration (14, 15)
		Chemical	FUN (fluorine, uranium, nitrogen) (16)
Experimental	Time placement	Radiometric	Radiocalcium (17)
			Electron spin resonance (18)
			Alpha-particle recoil (19)
	Time and relative placement	Chemical	Obsidian hydration (14, 15)
			Amino acid racemization (20, 21)
			Ion transport mechanisms [Cation ratio (22) Fluorine-nitrogen profile (23, 24)]



# how do you improve automated g.c. reliability



## simply

Using SGE precision state of the art syringe systems.  
Domed tip needles for extended septum life and reduced loading on autosampler mechanisms. SGE's predrilled PTFE coated triple layer septum provide system inertness and eliminates septum coring.

Replaceable needles in case of mechanical failure.

Sizes from 0.5 ul to 10 ul.

Contact your nearest SGE Office for details.



OFFICES: SGE AUSTRALIA - 7 Argent Place, Ringwood, Victoria, 3134. Telex: 33930. Telephone: (03) 874 6333.  
SGE USA - 2007 Kramer Lane, Austin, Texas 78758, U.S.A. Telex: 9108741358. Telephone: (512) 837 7190.  
SGE UNITED KINGDOM - 1 Potters Lane, Kiln Farm, Milton Keynes, MK11 3LA. Telex: 825017. Telephone: (0908) 56 8844.  
SGE FRANCE - 10 Rue Henri Janin, F94190, Villeneuve St. Georges, France. Telex: F201901 SGE. Telephone: 1/382 29 43.  
SGE GERMANY - Fichtenweg 15, D-1608 Weiterstadt 1, Germany. Telex: 419518. Telephone: (6150) 40662.

CIRCLE 151 ON READER SERVICE CARD



similar in age or older or younger than another). The basis of the difference between time and relative placement methods lies largely in the physical or chemical time-sensitive mechanism employed. Time placement methods use fixed-rate processes such as nuclear decay to increment time. Relative placement methods employ variable-rate processes such as chemical reactions to provide age estimates. In some cases, attempts are made to calibrate variable-rate processes with some type of fixed-rate method and then employ a calibrated-variable rate for time placement purposes.

As an example, a calibration approach has been employed in the amino acid racemization method of dating Quaternary bone samples. Radiocarbon data were used to assign a rate constant for the racemization of aspartic acid in bones from a particular temperature regime. It was originally assumed that time and temperature would be the only principal variables in producing the observed D/L ratios (20). Unfortunately, factors in addition to effective environmental temperature have been found to significantly influence D/L ratios in bone, and initial assignment of ages based on D/L aspartic acid ratios in bone has been extensively revised (21). In some instances, a method could be operational for relative placement purposes, but it might be considered as experimental for most time placement applications. This is the current situation with most applications of the obsidian hydration method (14, 15). Physical dating methods can also be catalogued in terms of the physical or chemical basis on which the incrementing phenomenon is based. The best known and most successfully employed operational time placement methods employ nuclear decay schemes.

Both dating specialists and archaeologists continuously remind themselves that each dating technique, whether it is time or relative placement, operates within the framework of a specific set of contextual and geochemical-geophysical assumptions and constraints. The accuracy of the age estimates provided by any dating scheme is directly tied to the degree to which each assumption is fulfilled for each sample or geochemical-geophysical environment. In critically evaluating ages assigned to a sample by a given dating method, an investigator must be aware of both implicit and explicit assumptions on which each method rests. In addition, each method can be characterized by its geographic or environmental restrictions, age range, relevant sample types, and time zero process.

A number of techniques can be employed only within specific geographic regions defined in terms of some envi-

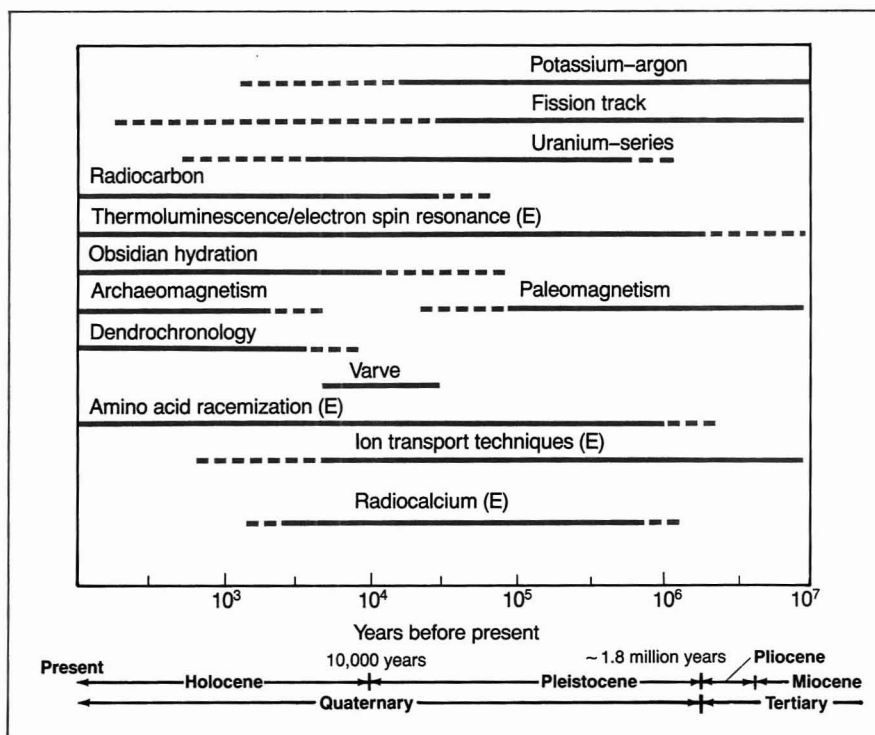
ronmental variable. Dendrochronology, for example, employs patterns in the widths of annual tree ring structures as unique signatures for different time intervals (5). Tree ring width patterns are influenced by a number of regionally focused environmental parameters, including temperature. A standardized "master" tree ring series must be established for each geographic-macroclimatic zone. The same restrictions apply to any technique sensitive to environmental temperature fluctuations such as obsidian hydration and, as previously mentioned, amino acid racemization. Other methods rely on rate structures that are highly temperature-dependent and are influenced by other biogeochemical factors that limit the types of samples that can be routinely used to infer either relative or chronometric age.

Each method also exhibits a characteristic age range over which the technique can be appropriately applied. Figure 2 illustrates these temporal ranges with the experimental methods identified by the (E) designation. For methods employing radioactive decay mechanisms, the age range is primarily governed by the decay rate and geochemical characteristics of the relevant isotope(s), as well as the sensitivity of the existing instrumentation. For time placement methods, standard or conventional maximum and minimum ages can be assigned as well as expanded limits possible involving particular samples and experimental approaches.

The extended or expanded limits of each technique are indicated in Figure 2 by a dotted line. In the case of the  $^{14}\text{C}$  method, for example, the typical maximum ages that can be measured are in the range of 30,000–50,000 years, depending on the amount of sample available and the counting systems employed. By employing relatively large sample sizes, isotopic enrichment, or special experimental configurations, the maximum figure can be extended to as much as 70,000 years.

In some cases, previously established limits can be adjusted with the introduction of new or improved methods of measurement or analysis. For example, the introduction of accelerator mass spectrometry (AMS) to measure  $^{14}\text{C}$  concentrations offers the potential to extend the dating range for this method. In the case of the potassium-argon method as applied to Quaternary samples, the restrictions involve *minimum* ages that can be reliably measured. This value can vary depending on the mineralogy of a sample. There are variations in the degree to which a particular mineral retains the radiogenic argon produced by the decay of the potassium, as well as the degree to which the effects of modern  $^{40}\text{Ar}$  contamination can be excluded along with several other factors (7).

The types of sample material that can be employed for different methods are highly variable. Radiocarbon dating, obviously, can be applied only to carbon-containing samples. Potassi-



**Figure 2.** Temporal range for major Quaternary physical dating methods. Solid line indicates routine capability.

Dotted line indicates extended capabilities under special experimental conditions. E designation indicates experimental technique.



# SIEMENS

## SRS 303...the uncompromised step in x-ray spectrometry

As part of its ongoing commitment to analytical methods and product improvements, Siemens has gone the distance in perfecting x-ray spectrometry. The result:

- ... extends the elemental range all the way down to boron.
- ... includes a new rhodium anode x-ray tube that permits the use of one tube over the full range of the periodic table without compromising performance
- ... introduces a compact size, specifically designed for operator convenience, and space saving
- ... utilizes an integrated x-ray generator that incorporates the latest medium frequency technology

We tie it all together with our most newly developed **next generation** of qualitative and quantitative x-ray fluorescence software.

What does all this mean to you? Simply, expanded analytical and applications capabilities in elemental analysis...unparalleled reliability in your analysis... maximum uptime... optimum ease of use.

Siemens SRS 303...its performance is uncompromising...and we can prove it. For more information write or call:

Siemens AG, Analytical Systems E 689, D 7500 Karlsruhe 21, P.O. Box 21 1262, Federal Republic of Germany. Tel: (0721) 595-4295, Telex: 7825569 Sie D.

Siemens Energy & Automation, Inc., Analytical Systems, One Computer Drive, P.O. Box 5477, Cherry Hill, NJ 08034, (609) 424-9210.

See us at the Pittsburgh Conference Booth #456-465.

CIRCLE 150 ON READER SERVICE CARD

# SRS 303





um-argon measurements can be applied to rock—or, more optimally, to specific mineral constituents of rock samples—laid down during volcanic episodes. For most dating methods, there is generally a range in the desirability of specific sample types—from the optimum sample material to those that generally are not satisfactory except under special conditions. In many cases, extensive pretreatment methods have been developed to reduce contamination to acceptable levels or to isolate an optimum sample fraction. A final consideration for each method relates to the requirement that some physical or chemical mechanism effectively “reset” or “zero” the phenomenon used for temporal incrementation. This mechanism defines the “time zero” point for each technique. For the radiocarbon method, for example, the temporal zero point for terrestrial materials is the death of an organism and, it is hoped, the total isolation of carbon in a sample from active exchange with the modern carbon reservoir from which it originated. In the potassium-argon (7), fission track (8), and thermoluminescence (10) methods, it is typically the most recent episode of heating above a critical temperature that results in the essential elimination or major reduction of the previously acquired radiation damage effects.

The remainder of this discussion will focus briefly on recent advances in the best known Quaternary dating method, radiocarbon ( $^{14}\text{C}$ ), and on current developments in a recently proposed experimental dating method, radiocalcium ( $^{41}\text{Ca}$ ). The  $^{41}\text{Ca}$  technique is an isotopic method that holds the promise of extending the age range for the dating of calcium-containing terrestrial methods (e.g., bone) to as much as 800,000 to 1 million years. The ability to provide direct age estimates for bone and teeth in this age range would be particularly important because these samples are recovered from many archaeological sites, and the period from about 40,000 to about 1 million years currently lacks an operational dating method that can be applied to such materials.

#### Advances in radiocarbon dating

The most widely used and best known late Quaternary physical dating method is the radiocarbon technique (6). The basis of the method can be simply illustrated in terms of the production, distribution, and decay of  $^{14}\text{C}$  (Figure 3). The natural production of  $^{14}\text{C}$  is a secondary effect of cosmic ray bombardment in the upper atmosphere. Following production, it is rapidly oxidized to form  $^{14}\text{CO}_2$ . In this form,  $^{14}\text{C}$  is initially distributed throughout the

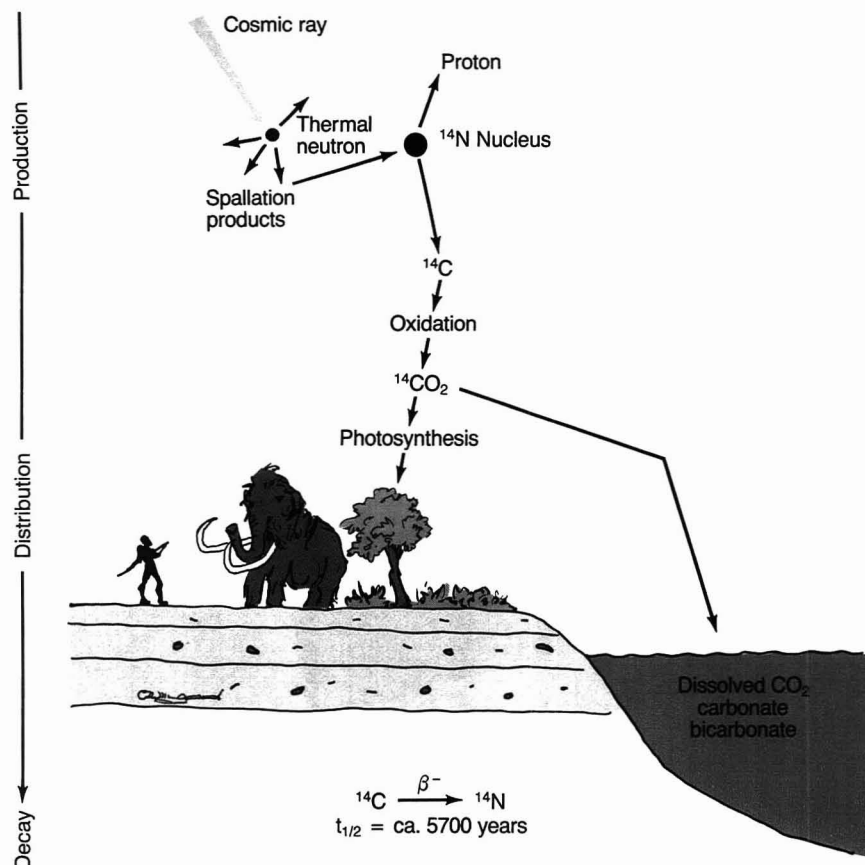
earth's atmosphere. Most of it is subsequently absorbed in the oceans, and a small percentage becomes part of the terrestrial biosphere. Metabolic processes maintain the  $^{14}\text{C}$  content of most living terrestrial organisms in equilibrium with atmospheric  $^{14}\text{C}$ . Once metabolic processes cease—as when an animal or plant dies—the amount of  $^{14}\text{C}$  will begin to decrease by decay at a rate measured by the  $^{14}\text{C}$  half-life. The radiocarbon age of a sample can then be inferred by a measurement of its residual  $^{14}\text{C}$  content. Developed immediately following World War II at the University of Chicago by Willard F. Libby and his co-workers James R. Arnold and Ernest C. Anderson, the method has now provided more than 100,000 age estimates on a wide range of organic materials. The largest percentage of  $^{14}\text{C}$  determinations has been on materials of archaeological interest. Libby was awarded the 1960 Nobel Prize in chemistry for the development of the technique.

There is a general consensus that the impact of the  $^{14}\text{C}$  method on the conduct of prehistoric archaeological studies over the last four decades has been profound. Its influence in archaeology has been likened to the effect of the discovery of periodicity of elements in chemistry. One senior British archaeologist has even ranked the 20th century



## How to enter your data into 1-2-3 with both hands



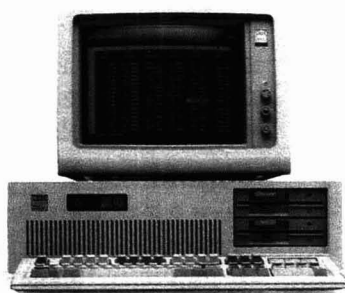


**Figure 3.** Basis of radiocarbon method: production, distribution, and decay of  $^{14}\text{C}$ .  
(Adapted with permission from Reference 6.)

discovery of the  $^{14}\text{C}$  dating method with the discovery of the antiquity of the human species in the 19th century (25). Radiocarbon age estimates currently provide the central core of the late Pleistocene and Holocene prehistoric time scales for most areas of the world.

A number of improvements in  $^{14}\text{C}$  technology have permitted a range of studies examining minor and major anomalies in  $^{14}\text{C}$  age estimates. In the 1970s and early 1980s, a major effort was expended on the calibration of the middle and late Holocene  $^{14}\text{C}$  time scale, primarily as a result of precise  $^{14}\text{C}$  measurements on several long series of dendrochronologically dated wood samples. During the last five years, however, clearly the most important development in  $^{14}\text{C}$  research has been the ability to measure natural  $^{14}\text{C}$  concentrations in samples by direct counting using AMS. During the previous 30 years,  $^{14}\text{C}$  measurements could be obtained only by decay counting. This approach inferred the concentration of  $^{14}\text{C}$  in a sample by monitoring its beta activity. An important stimulus that led to the development of AMS counting for  $^{14}\text{C}$  was the recognition that although there are approximately  $5.9 \times 10^{10}$  atoms of  $^{14}\text{C}$  in one gram of modern carbon, on the average over a 1-min period less than 14 of them will

tied behind your back.



For years, to get data from measurement hardware into Lotus® 1-2-3® you had to do it manually, or write your own program. Both very labor intensive. Lotus Measure™ is here to change all that. It's the first software that seamlessly moves data from measurement hardware directly into 1-2-3 in real time, for immediate display, analysis and storage.

Measure was designed to work as part of 1-2-3, so you'll recognize the familiar 1-2-3 interface. You can even run Measure from 1-2-3 macros.

Measure works with over 8,000 kinds of instruments, in hundreds of applications, managing intelligent instruments over the IEEE-488 or RS-232-C interface bus, or handling A/D boards directly.

Call 1-800-345-1043 to buy your copy of Lotus Measure and ask for product #VD-1666.

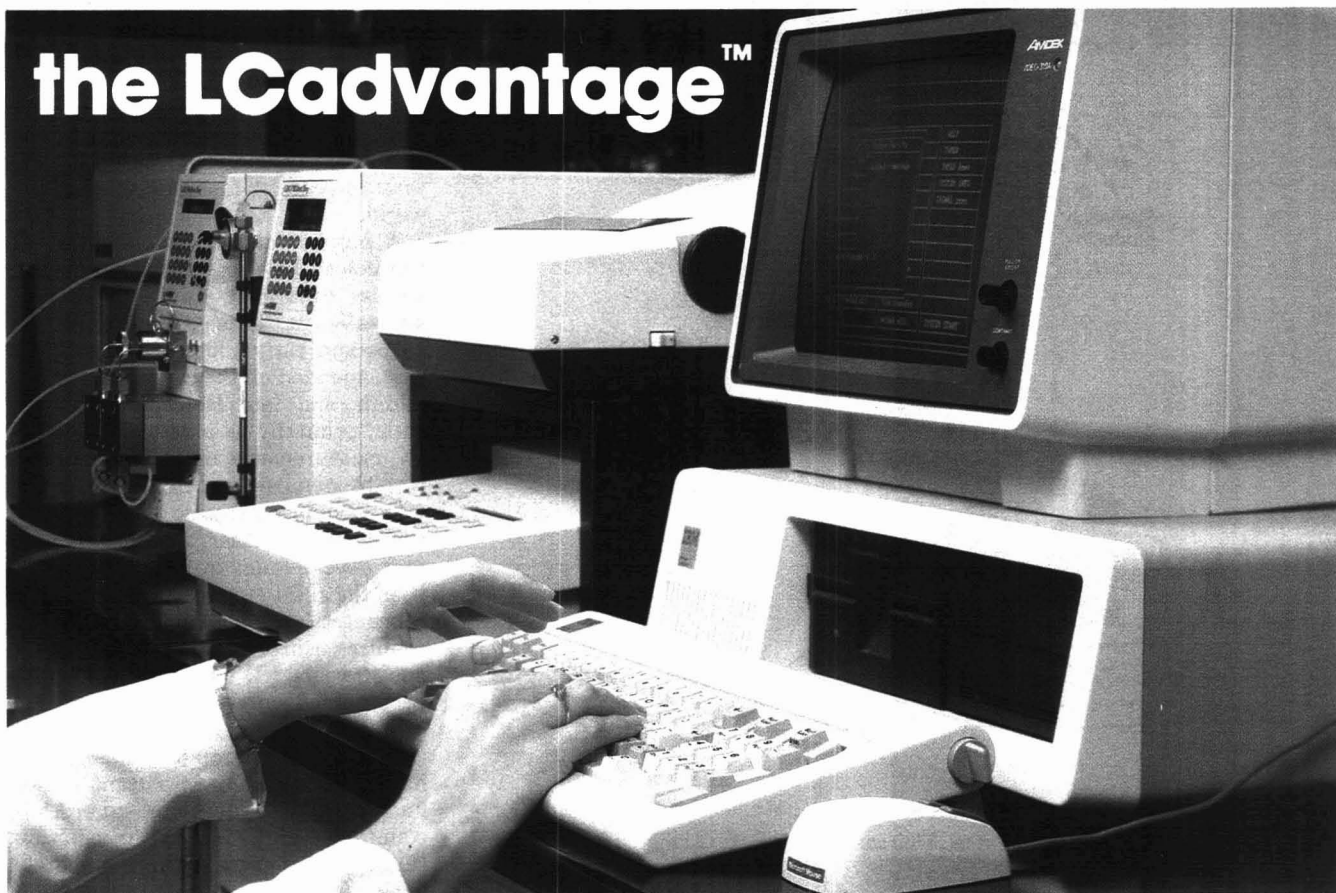
To order the complete Measure demo package for a \$10 cost that's refundable with purchase, call and ask for demo #VD-1674. Or, for more information ask for brochure #VD-1740.



**Lotus Measure™**



# the LCadvantage™



## Programmable Liquid Chromatography

from



**MILTON ROY**  
LDC DIVISION



### *Introducing the Series 4000 System with LCadvantage™ Software.*

Now you can link Milton Roy's quality instruments to your IBM PC and enjoy all the advantages of easier HPLC. The LCadvantage™ software provides a user-friendly interface with Milton Roy's Series 4000 programmable instruments, allowing complete system monitoring and control as well as method and data file storage on the PC's hard disk.

The Series 4000 System consists of the microprocessor controlled CM4000 Ternary Gradient Pump, SM4000 Programmable Wavelength Detector, and the CI-10B Computing Intergrator. The built-in intelligence of these instruments frees the PC from pump control and data col-

lection during separations allowing it to run other applications, create and edit the next method to be used, or process previously stored chromatographic data.

With Milton Roy's Series 4000 equipment you have maximum flexibility in your system configuration from a complete PC-controlled system to individual instruments running separately, without sacrificing instrument performance.

For over 50 years Milton Roy has dedicated its technical and engineering resources to providing quality products for the analytical market. The Series 4000 Programmable LC is a direct result of that commitment.



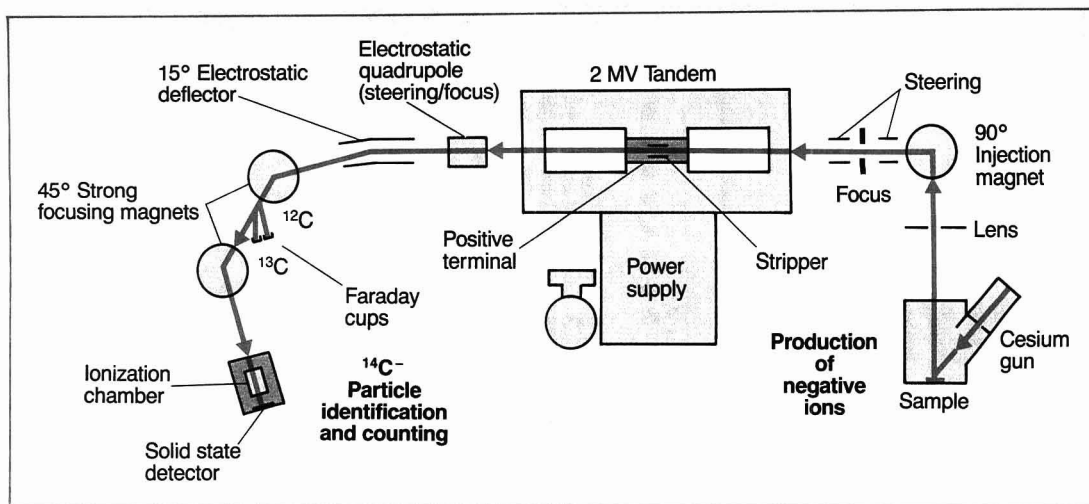
**MILTON ROY**

*Call 1-800-LDC-HPLC today for more information.*

LDC Division, P.O. Box 10235, Riviera Beach, Florida 33404 Toll-free: 800-LDC-HPLC, In Florida: (305) 844-5241 Telex: 441098  
UNITED KINGDOM, Milton Roy, Milton Roy House, Diamond Way, Stone Business Park, Stone, Staffordshire, ST 15 0HH, England Tel: (0785) 813542 Telex: 36623  
FRANCE, Milton Roy S.A., 15 rue Guyton de Morveau, Paris 75013, France Telephone: (1) 45 88 28 00 Telex: 205331  
FEDERAL REPUBLIC OF GERMANY, Milton Roy (Deutschland) GMBH, Jahnstrasse 22-24, 6467 Hasselroth 2, FRG, Telephone: 06055-3355 Telex: 4184357  
JAPAN, Milton Roy K.K., Takanawa Dai-ichi Building 21-41, Takanawa 2-Chome, Minato-Ku, Tokyo 108, Japan Telephone: (03) 473-3181 Telex: 242-4296

See us at Pittcon '87 — Booth Nos. 1041-2040. CIRCLE 91 ON READER SERVICE CARD





**Figure 4.** Simplified schematic of AMS system at University of Arizona (Tucson).

decay. It was recognized that significantly higher efficiencies of atom-by-atom detection such as that employed in mass spectrometers would allow the use of much smaller samples—down to the milligram and even micrograms of carbon range as compared to the grams of carbon typically required with most conventional decay counting systems. For archaeologists, there was also the existing potential of extending the maximum  $^{14}\text{C}$  range beyond the 40,000–70,000-year limit currently practical to as much as 100,000 years with significantly reduced sample size requirements (26).

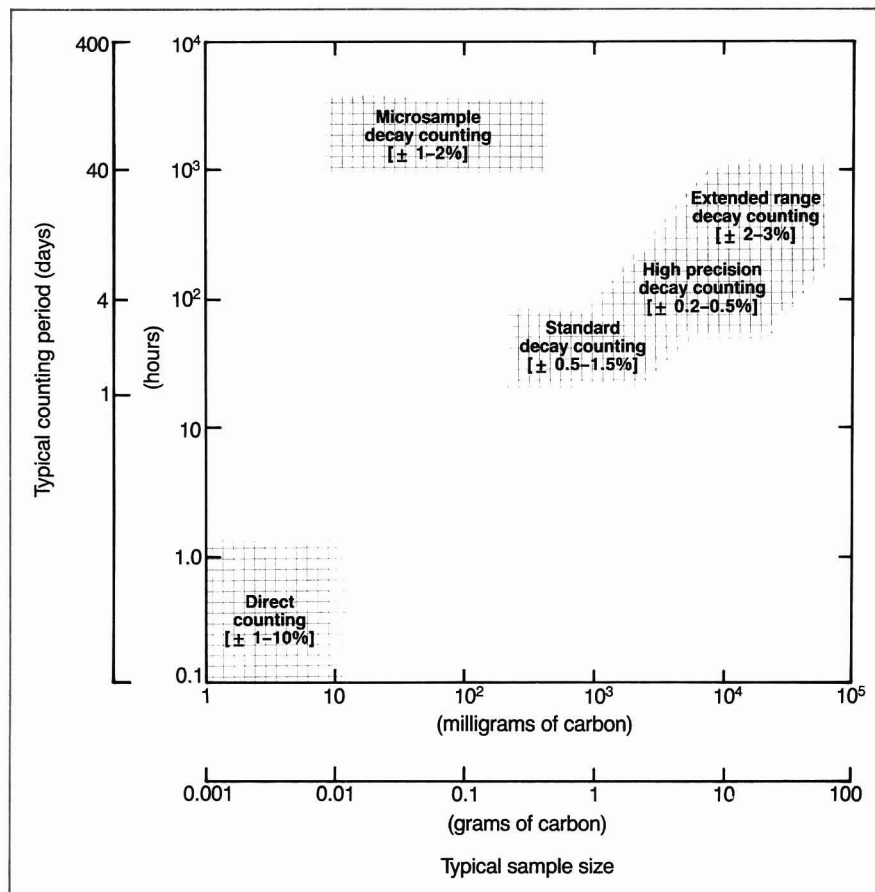
Attempts to make direct counting measurements using a conventional mass spectrometer failed in practical application because  $^{14}\text{C}$  was masked by stable ions with similar charge-to-mass ratios in the mass spectrum. Successful direct counting of  $^{14}\text{C}$  was finally accomplished in the late 1970s by accelerating sample atoms in the form of ions to higher energies in particle accelerators. For energies to the order of 0.5 MeV per nucleon, ions of the same mass and energy but differing nuclear charge (e.g.,  $^{14}\text{C}$  and  $^{14}\text{N}$ ) can be distinguished by measuring the total energy of each ion and its rate of energy loss. Two types of particle accelerators have been employed in direct  $^{14}\text{C}$  measurements: cyclotrons and electrostatic accelerators.

Figure 4 represents a simplified schematic drawing of the beam line arrangement for one type of particle accelerator being used to obtain AMS  $^{14}\text{C}$  measurements. This diagram represents the AMS system currently operating at the University of Arizona (Tucson). Similar instruments are being used at the Research Laboratory for Archaeology and the History of Art at Oxford University and at several other research centers. More than 30 AMS laboratories around the world are now using a variety of accelerator configurations to measure not only  $^{14}\text{C}$  but also a number of other relatively long-

lived cosmogenic isotopes. Figure 5 illustrates the impact of AMS analysis on both the sample sizes required and on the amount of counting time required for various types of decay counting systems as opposed to the new AMS approach.

Some significant data have already been generated as a result of AMS-based  $^{14}\text{C}$  age estimates obtained on samples too small for conventional decay counting. For example, a suite of AMS  $^{14}\text{C}$  values have been obtained on organic extracts from bone samples de-

rived from human skeletons from various sites in the Western Hemisphere (27) and, in one case, from an artifact fabricated from bone (28). These bone samples had previously been assigned ages in the range of about 20,000–70,000 years on the basis of previous decay counting  $^{14}\text{C}$  analysis, the application of other dating techniques such as the amino acid racemization method, or geological criteria. These age assignments—particularly those in excess of about 30,000 years—were highly controversial because, among other



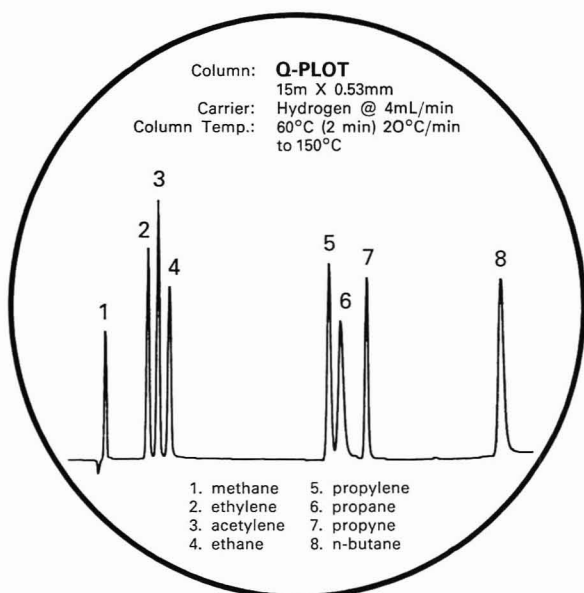
**Figure 5.** Relationship between sample size and typical counting periods for different types of instrumentation employed to measure  $^{14}\text{C}$ .

(Adapted with permission from Reference 6.)



# NEW!

## FROM J&W SCIENTIFIC POROUS POLYMER OPEN TUBULAR COLUMNS



- Baseline Resolution of All Three C<sub>2</sub> Isomers @ 60°C
- Easy-to-Use Megabore Column
  - High Capacity AND High Speed Analysis
- Polymers Synthesized In-House by J&W Scientific

LEARN MORE:  
Attend Paper #575 at the  
Pittsburgh Conference or Request  
a Free Product Bulletin.

## J&W SCIENTIFIC

SPECIALIZING IN HIGH RESOLUTION CHROMATOGRAPHY  
91 BLUE RAVINE ROAD, FOLSOM, CA 95630

Orders: (916) 985-7890  
Write for FREE Technical Information

CIRCLE 81 ON READER SERVICE CARD

Pipetting?  
Single-Shot Microliter  
Dispensing?

Try the  
all-new  
**FMI**  
micro  $\pi$ -petter!



It provides a simple, low-cost means of dispensing very small amounts of fluids for applications such as pipetting, reagent preparation, syringing, precision sampling, repetitive and volumetric dispensing. The variable displacement, valveless RR piston design makes it possible to dispense volumes of 2 to 100  $\mu$ L per shot with incremental adjustment of less than 0.5  $\mu$ L. PiP units are also reversible for aspirating fluids or back flushing the system.

A simple, sealed pushbutton hand/foot pendant switch makes a momentary contact for one dispense per push when the mode switch is in the down (Singles) position, or it may be held down for purging or reagent rinsing when the mode switch is in the up (Repeat) position. Using a combination of forward and reverse modes makes dilutions especially easy. Wetted surfaces of ceramic and fluorocarbon provide for maximum chemical compatibility. A three-speed 110 VAC 60 Hz synchronous motor provides three shot velocities to meet your fluid and vessel requirements.

Two standard models are available at a price of \$450 each  
F.O.B. FMI: Model PiPOCKC—0 to 50  $\mu$ L;  
Model PiP1CKC—0 to 100  $\mu$ L.



**FLUID METERING, INC.**

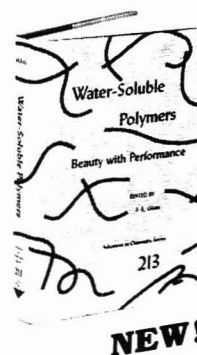
29 ORCHARD STREET, OYSTER BAY, N.Y. 11771 • (516) 922-6050

See us at the Pittsburgh Conference Booths 922/924.

CIRCLE 49 ON READER SERVICE CARD

## Water-Soluble Polymers Beauty with Performance

J.E. Glass, Editor  
North Dakota State  
University



**NEW!**

Brings together the diverse experience of those working with and using water-soluble polymers. Gives a detailed description of important advances in inversion emulsion polymerization of synthetic water-soluble monomers. Reports on the tremendous increase in research and the state-of-the-art in fundamental concepts and application performance of water-soluble polymers. Looks at the solution properties of some important carbohydrate polymers and examines recent developments in the characterization of water-soluble polymers by chromatographic and NMR techniques

### CONTENTS

Water Solubility in Carbohydrate Polymers • Use of Aqueous Size-Exclusion Chromatography • Dilute Solution Properties in Pectin • <sup>13</sup>C-NMR Characterization of Structural Features • Adsorption and Its Influence on Application Properties • Viscosities of Hydrophobically Modified HEC • Polymeric Flocculents in Wastewater Treatment • Metal-Activated Redox Initiation • Role in Oil Well Drillings Muds • Use as Shale Stabilizers in Drilling Fluids • Filtration Control of Bentonite Muds • Use as Aqueous Drilling Fluids Additives • Characterization of Metal Cross-linked Polymer Gels • Polymer Flow Through Porous Media • Polymer-Augmented Waterflooding • Surface Viscoelasticity and Foam Stability • Cellulose Ethers and Coatings Performance • Grafting Reactions of HEC • Associative Thickeners and Coatings Performance • Behavior of Associative Thickeners in Latex Systems • Influence on Rheology of Pigmented Latex Coatings • Rheology of Epoxy-Acrylic Graft Copolymers • Poly(2-ethyl-2-oxazoline)

Advances in Chemistry  
Series No. 213  
444 pages (1986)  
Clothbound  
LC 86-3534  
ISBN 0-8412-0931-6  
US & Canada \$89.95  
Export \$107.95

Order From:  
American Chemical Society  
Distribution Office Dept. 21  
1155 Sixteenth Street, N.W.  
Washington, DC 20036  
or CALL TOLL FREE  
800-424-6747  
and use your credit card!

Developed from a symposium sponsored by the  
Division of Polymeric Materials Science and  
Engineering of the American Chemical Society







# ATTENTION: MATERIALS DEVELOPERS

**IF** you work with—

- ◆ Films
- ◆ Fibers
- ◆ Foams
- ◆ Composites, or
- ◆ Elastomers

**AND** you have Problems with—

- ◆ Characterization,
- ◆ Product or process performance

**BUT** can't solve them easily...

The **best solution** has arrived from Rheometrics, the company whose name stands for quality, accuracy and leadership in materials measurement worldwide.

The **Rheometrics Solids Analyzer (RSA II)** is the newest, most versatile and cost effective solids test instrument available. See it at the Pittsburgh Conference (Booth No. 222-224).

The **RSA II** is the latest example of how Rheometrics provides the best approach to solving materials problems: we tell you what's wrong and how to fix it.

No ifs, ands or buts.

---

## Rheometrics®

### Europe

#### Rheometrics Europe GmbH

Hahnstrasse 70  
D-6000 Frankfurt 71  
West Germany  
Phone (069) 6 66 68 36  
Telex 411577 rheo d  
Telefax (069) 6 66 2007

### Far East

#### Rheometrics Far East Ltd.

1-7-6-Higashigotanda,  
Shinagawa-Ku, Tokyo 141  
Japan  
Phone 03-447-8681  
Telefax 03-447-9237

Rheometrics manufactures a complete line of rheological and impact testing instruments for research, product development, quality control and process control. Rheometrics instruments are used widely in evaluating materials such as thermoplastics, thermosets, elastomers, fluids and suspensions.

### U.S.A.

Corporate Headquarters

#### Rheometrics, Inc.

One Possumtown Road  
Piscataway, NJ 08854  
Phone (201) 560-8550  
Telex 219107 RHEO UR  
Telefax (201) 560-7451  
Service (201) 560-8990

CIRCLE 141 ON READER SERVICE CARD



both temporal coverage and the types of samples that can be directly employed. The use of the K/Ar method and inferences from the paleomagnetic record combined with lithostratigraphic and biostratigraphic analysis have resulted in the establishment of basic chronological structures for the hominid record in the early Quaternary, especially for important sites in eastern Africa. For the late Quaternary—and particularly the most recent 30,000–50,000 years—chronological frameworks are also reasonably complete in broad outline for many areas of the world, largely because this period represents the current practical time span that can be documented by the  $^{14}\text{C}$  method. Thus, although many problems remain, reasonably specific chronological frameworks exist for the hominid biological and cultural evolutionary record for both the Early Pleistocene and the terminal Pleistocene–Holocene. In contrast, the dating frameworks for the period centered on the Middle Pleistocene, about 730,000–125,000 years ago, are generally imprecise and ambiguous. Consequently, the vast majority of well-dated archaeological sites or paleoanthropological localities are older than one million years or younger than about 50,000 years.

In 1979, Grant Raisbeck and Françoise Yiou proposed using a relatively long-lived (ca. 100,000 years) isotope of calcium,  $^{41}\text{Ca}$ , as the basis of a method to infer age for Quaternary bone and other calcium-containing samples (17). (Yoshio Yamaguchi had previously suggested the use of  $^{41}\text{Ca}$  for dating in 1963 [30].) Like  $^{14}\text{C}$ ,  $^{41}\text{Ca}$  is produced by cosmic-ray neutron secondaries. As illustrated in Figure 6, however, the bulk of the radiocalcium is not made in the atmosphere as is the case with  $^{14}\text{C}$ , but primarily in the upper meter of the soil profile by neutron capture on  $^{40}\text{Ca}$ . Following production,  $^{41}\text{Ca}$  would be mixed with the other naturally occurring calcium isotopes into the soil matrix through natural bioturbation processes and groundwater action. Calcium would be taken up into plant tissue in the form of  $\text{Ca}^{2+}$  through ion absorption into the root system. Radiocalcium, like all of the other isotopes of calcium, would also be incorporated into bone mineral.

A  $^{41}\text{Ca}/^{40}\text{Ca}$  equilibrium ratio would be maintained in living organisms by exchange and metabolic processes. In contrast to  $^{14}\text{C}$  dating, in which the death of an animal or plant and the isolation of a sample from one of the carbon reservoirs constitutes the  $t=0$  event (zero B. P. on the  $^{14}\text{C}$  time scale), the  $t=0$  event in the projected  $^{41}\text{Ca}$  method would be the shielding of a sample from the effects of neutron irradiation, for example, by the placement of a sample at a depth in excess of

about three meters of soil or rock overburden either through burial or placement in a cave-rock shelter environment. Age inferences would be based on the measurement of the residual  $^{41}\text{Ca}$  with respect to the stable Ca isotopes. The decay of  $^{41}\text{Ca}$  to  $^{41}\text{K}$  takes place by electron capture and an emission of a neutrino. Until the development of AMS counting technology, it was not practical to pursue research on natural level  $^{41}\text{Ca}$  measurements, primarily due to its expected extremely low terrestrial concentrations. The ratio of  $^{41}\text{Ca}$  to  $^{40}\text{Ca}$  was expected to lie in the range of  $10^{-14}$  to  $10^{-15}$ . For comparison, the  $^{14}\text{C}/^{12}\text{C}$  ratio in modern carbon is about  $10^{-12}$ .

From a technological point of view, the  $^{41}\text{Ca}$  method, in many respects, currently stands at the same point in its development as the  $^{14}\text{C}$  method did in the fall of 1945. The favored mode of production for  $^{41}\text{Ca}$  had been known for some time (thermal neutrons on  $^{14}\text{N}$ ) and, based on this fact and several other considerations, a dating model had been formulated. In 1945, however, the half-life of  $^{14}\text{C}$  was still somewhat uncertain, and natural levels could only be measured after enrichment. Currently, the half-life figure of  $^{41}\text{Ca}$  is known only to about 10%–20%. The first direct measurement of the natural terrestrial concentration of  $^{41}\text{Ca}$  was carried out in April 1986 at the Argonne National Laboratory using the ATLAS linac accelerator system following the enrichment of  $^{41}\text{Ca}$  at the Oak Ridge National Laboratory using a Calutron isotope separator. The value obtained for  $^{41}\text{Ca}/\text{Ca}$  was  $2.0 \pm 0.4 \times 10^{-14}$  (31). Studies are currently underway to determine if the  $^{41}\text{Ca}$  method has the potential to provide a practical means of determining accurate age estimates for Pleistocene bone and other calcium-bearing samples.

### Conclusion

The core issues of contemporary paleoanthropological and prehistoric archaeological studies revolve around the nature and causes of the evolution of hominid behavior over the last few million years as reflected primarily in the physical residue of that behavior. Evolution, of course, means change over time. It is precisely the ability to document and deal with human behavior within an extended temporal framework that allows prehistorians to make their unique contribution by focusing on the nature and causes of the evolution of social and cultural systems within our species and our biological antecedents.

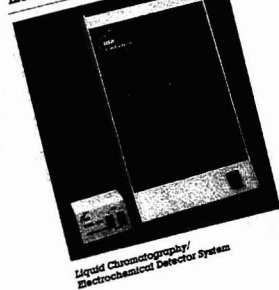
Contemporary prehistorians have come to have at their disposal an increasing array of physical dating methods developed by colleagues in the physical sciences. Because of the in-

## From I Through Z,

Just Some of the Compounds  
You Can Measure At  
Low Picogram Levels

Imipramine	Phenolamines
Indole	Phylloquinone (Vitamin K)
Indole-3-Acetaldehyde	Phytostigmine
Indoleacetic Acid	Triclinic Acid
Indolepyruvic Acid	Polychlorinated Phenols
Isonine	Primidone
Isonit	Prochlorperazine
Iso-Homovanillic Acid	Propyl Gallate
Isoxanthine	Propylparaben
Iso-VMA	Protocatechuic Acid
Isoxypine	Protryptamine
Kynurenic Acid	Proxidine
L-Dopa	Pteroylglutamic Acid
Leu-enkephalin	Pyridoxine (Vitamin B <sub>6</sub> )
Melatonin	Pyridoxal
Mefenoxone	Quinaldic Acid
3-Mercaptopurine (Pencicillamine)	Quinolinic Acid
Metoprolol	Risperine (Methyl Risperine)
Met-enkephalin	Ritodrine
Methionine	Salicylic Acid
Methotrexate	Serotonin (5-HT)
3-Methoxy-4-Hydroxyphenylglycol	(5-Hydroxytryptamine)
3-Methoxy-4-Hydroxyphenylglycol Sulfate	Serotonin Sulfate
3-Methoxyindoleacetic Acid	Sinapic Acid
3-Methoxymethylidopa	Somatostatin
3-Methoxyphenylethylamine	Salbutamol
3-MT (3-Methoxytyramine)	Stellazine
3-Methyl-4-Hydroxyphenyl Glycol	Substance P
5-Methoxytryptamine	Sulindac
Methyl Risperate (Risperone)	Synephrine
Methylparaben	T (Thiodiuronine)
MHPG, MHPG Sulfate	T (Thyroxine)
Morphine	Tetraline
N-Methylphenylephrine	Thapsigargin
N-Methylhistamine	Thimerosal
N-Methylserotonin	Thymine
N-Methyltyrophen	Thyroxine (T <sub>4</sub> )
N-Methyltyramine	Tocopherol (Vitamin E)
Naloxone	Trichloroperazine
NE (Norepinephrine)	Triproline
Neurolept	2,4,5-Trihydroxybenzoic Acid
Neurotensin	(Gallic Acid)
Nicotinamide	Triptamine
Nicotine	Triptophan
Nicotinic Acid	Synamine
Nitrofurantoin	Tyrosine
Nitrofurantoin (NE)	Uracil
Normetazepine	Uric Acid
Normorphine	Vanillic Acid
Octopamine	Vanillylmandelic Acid
Octylphenol	Vanillic Acid
P-OH Phenylacetic Acid	Vasopressin
Parabens	Vitamin
Per-	

### The Coulochem Electrochemical Detector



Prove it for yourself. Call today for a demonstration of the Coulochem in your laboratory.



ESA, Inc.  
45 Wiggins Avenue  
Bedford, Massachusetts 01730  
(617)275-0100

CIRCLE 41 ON READER SERVICE CARD



# Laboratory Chemical Clean-Up, Packaging & Disposal



**1** Inventory and screening



**2** On-site testing and fingerprinting



**3** Computerized identification - classification



**4** D.O.T. "Lab-Pack" packaging of compatible materials



**5** Environmentally secure packaging and transportation

This exclusive system is a self-designed and constantly updated computerized turnkey program. Experienced environmental chemists are fully equipped for on-site chemical inventory, fingerprinting and classification. Packaging and transport of chemicals to disposal facilities are in

compliance with all EPA and DOT regulations.

A wide assortment of laboratory and small quantity chemicals are efficiently identified, packaged and disposed of within one safe full service program.



a subsidiary of environmental systems company

22077 Mound Rd., P.O. Box 1208, Warren, Michigan 48091 • (313) 758-0400 • MI 1-800-482-4484 • US 1-800-482-4482  
Chicago Sales Office: 15 Spinning Wheel Rd., Suite 327, Hinsdale, Illinois 60521 • (312) 323-0410

CIRCLE 60 ON READER SERVICE CARD

creased confidence in the accuracy of the chronological frameworks provided by these techniques, questions and issues heretofore not considered by archaeologists and paleoanthropologists can now be critically addressed. These questions and issues involve much-broadened concerns with the very complex environmental, technological, and ecological factors that have directly and indirectly affected the evolution of our kind of primate.

The search for new dating techniques and refinements of existing methods continues to be actively pursued. The ultimate goal and justification for these studies and for all other archaeological research is the same—to recover the evidence that will permit a scientific understanding of what made *Homo sapiens* the way he or she is.

### Acknowledgments

The research of the UCR Radiocarbon Laboratory is supported by the National Science Foundation (Anthropology Program), with additional funds supplied by UCR Chancellor Theodore L. Huller. Information and comments by Erik Trinkaus, University of New Mexico, dealing with dating of hominid forms have been very helpful and are much appreciated. I am deeply indebted to Roy Middleton, University of Pennsylvania, for calling my attention to Reference 30. This is contribution 86/21 of the Institute of Geophysics and Planetary Physics, University of California, Riverside.

### References

- (1) Cartmill, M.; Pilbeam, D.; Isaac, G. *Am. Sci.* 1986, 74, 410–20.
- (2) Trinkhaus, E. University of New Mexico, personal communication, 1986.
- (3) Curtis, G. H. *Philosophical Transactions of the Royal Society*. (London) 1981, 292B, 7–20.
- (4) Faure, E. *Principles of Isotope Geology*; Wiley: New York, 1977.
- (5) Baillie, M.G.L. *Tree-Ring Dating and Archaeology*; Croom Helm: London, 1982.
- (6) Taylor, R. E. *Radiocarbon Dating: An Archaeological Perspective*; Academic Press: New York, 1987.
- (7) Hall, C. M.; York, D. In *Quaternary Dating Methods*; Mahaney, W. C., Ed.; Elsevier: Amsterdam, 1984, pp. 33–52.
- (8) Fleischer, R. L.; Price, P. B.; Walker, R. M. *Nuclear Tracks in Solids*; University of California Press: Berkeley, 1975.
- (9) Schwarcz, H. P. *Archaeometry* 1980, 22, 3–24.
- (10) Aitken, M. J. *Thermoluminescence Dating*; Academic Press: London, 1985.
- (11) Wenner, C. *Stockholm Contributions in Geology*. 1968, 18, 75–97.
- (12) Tarling, D. H. In *Archaeological Geology*; Rapp, G.; Gifford, J. A., Eds.; Yale University Press: New Haven, 1985, pp. 237–64.
- (13) Cox, F., Ed.; *Plate Tectonics and Geomagnetic Reversals*; W. H. Freeman: San Francisco, 1973.
- (14) Trembour, F.; Friedman, I. In *Quaternary Dating Methods*; Mahaney, W. C., Ed.; Elsevier: Amsterdam, 1984, pp. 141–52.
- (15) Michels, J. W.; Tsong, I.S.T.; Smith, G. A. *Archaeometry*. 1983, 25, 107–17.
- (16) Knight, B.; Lauder, I. *Hum. Bio.* 1969, 41, 323–41.
- (17) Raisbeck, G. M.; Yiou, F. *Nature*. 1979, 277, 42–44.
- (18) Ikeya, M.; Miki, T. *ESR Dating and Dosimetry*; Ionics Publishing Co., Ltd.: Tokyo, 1985.
- (19) Wolfman, D.; Rolniak, T. M. *Archaeo-Physika*. 1979, 10, 512–21.
- (20) Bada, J. L. *Annual Review of Earth and Planetary Science*. 1985, 13, 241–68.
- (21) Ennis, P.; Noltmann, E. A.; Hare, P. E.; Slota, P. J.; Payen, L. A.; Prior, C. A.; Taylor, R. E. *Radiocarbon*. 1986, 28, 539–46.
- (22) Dorn, R. I.; Bamforth, D. B.; Cahill, T. A.; Dohrenwend, J. C.; Turrin, B. D.; Donahue, D. J.; Jull, A.J.T.; Long, A.; Macko, M. E.; Weil, E. B.; Whitley, D. S.; Zabel, T. H. *Science*. 1986, 231, 830–33.
- (23) Taylor, R. E. In *Peopling of the New World*; Ericson, J. E.; Taylor, R. E.; Berger, R., Eds.; Ballena Press: Los Altos, 1982, pp. 285–98.
- (24) Taylor, R. E. In *Bruder, S. J.; Archaeological Investigations at the Hedgpeeth Hills Petroglyph Site*; Museum of Northern Arizona: Flagstaff, 1983, pp. 289–302.
- (25) Daniel, G. *The Origins and Growth of Archaeology*; Crowell: New York, 1967.
- (26) Taylor, R. E.; Donahue, D. J.; Zabel, T. H.; Damon, P. E.; Jull, A.J.T. In *Archaeological Chemistry-III*; Lambert, J. B., Ed.; American Chemical Society: Washington, D.C., 1984, pp. 333–56.
- (27) Taylor, R. E.; Payen, L. A.; Prior, C. A.; Slota, P. J., Jr.; Gillespie, R.; Gowlett, J.A.J.; Hedges, R.E.B.; Jull, A.J.T.; Zabel, T. H.; Donahue, D. J.; Berger, R. *American Antiquity*. 1985, 50, 136–40.
- (28) Nelson, D. E.; Morlan, R. E.; Vogel, J. S.; Southon, J. R.; Harington, C. R. *Science*. 1986, 232, 749–51.
- (29) Wendorf, F.; Schild, R.; Close, A. E.; Donahue, D. J.; Jull, A.J.T.; Zabel, T. J.; Wieckowska, H.; Kobusiewicz, M.; Issawi, B.; el Hadidi, N. *Science*. 1979, 205, 1341–47.
- (30) Yamaguchi, Y. *Progress of Theoretical Physics*. 1963, 29, 567.
- (31) Henning, W.; Kutshera, W. Argonne National Laboratory, personal communication, 1986.



R. E. Taylor received his Ph. D. in anthropology with an emphasis on archaeology and archaeometry (physical science applications in archaeology) from the University of California, Los Angeles (UCLA). While a graduate student at UCLA, he served as a research assistant in the isotope laboratory established by the late Willard F. Libby. Dr. Taylor is currently professor of anthropology and director of the Radiocarbon Laboratory, Institute of Geophysics and Planetary Physics, University of California, Riverside.

## Detect Picogram Levels

### With the Coulochem® Multi-Electrode Coulometric Electrochemical Detector

The Coulochem provides the highest selectivity, stability, and sensitivity for the detection of thousands of neurochemical, biochemical, and pharmaceutical compounds. Consider the Coulochem Detector's:

- High selectivity—interference-free measurement of compounds of interest through use of multiple electrodes.
- High stability—unique cell design provides rapid equilibration, fast set up, and superior reproducibility.
- High sensitivity—reaction with 100% of the sample as a result of unique coulometric design.



Prove it for yourself. Call today for a demonstration of the Coulochem in your laboratory.



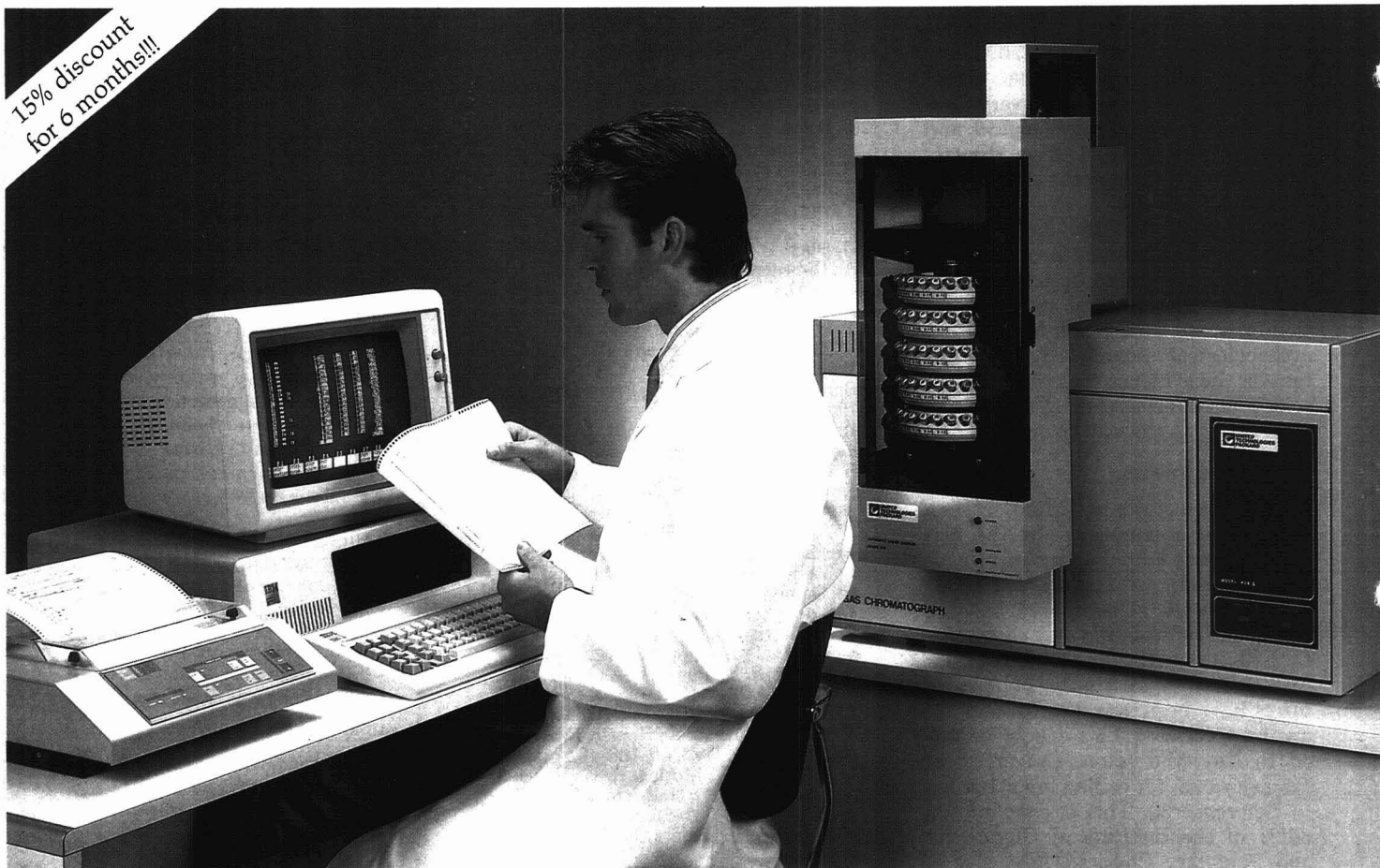
ESA, Inc.  
45 Wiggins Avenue  
Bedford, Massachusetts 01730  
(617)275-0100

CIRCLE 42 ON READER SERVICE CARD



# Packard makes total GC automation affordable!

15% discount  
for 6 months!!!



## Ready-to-go, push-button GC packages

These trouble-free packages take you from sampling all the way to reporting at the touch of a button. Each is a complete, user-friendly system offering optimized GC control, excellent data acquisition, integration and reporting. Furthermore, they can be simply and quickly expanded to four-channel data stations accommodating Packard and other GCs.

### 1: High performance Station

The first Station comprises a high performance satellite GC, Packard Control and Integration system (PCI) with advanced GC control and data processing software, and a high resolution printer/plotter. The satellite is available in a variety of single packed/capillary configurations. A full range of accessories such as automatic samplers is available.

### 2: High capacity/high performance Station

The second Station is similar, but also includes the new Model 910 Automatic Liquid Sampler. This sampler accepts 110 samples in five sample trays, each of which can be linked to a different GC method. This is a truly reliable high throughput system, ideal for multi-user environments, with advanced features normally only found on systems costing much more.

### Now you get even more value for your money!

Packard is currently offering extremely attractive deals on both these GC Stations. Like all Packard GC Stations they already offer a unique combination of performance, capabilities and price. But now, for a six month period you can enjoy a 15% discount on their usual list price... Total gas chromatography automation at affordable prices.

**Ask for the detailed brochures... or even a quote (remember this offer only lasts six months!)**



**CHROMPACK —  
— PACKARD**

Pittsburgh Conference booths 644, 646, 648.

CHROMPACK, INC.

1130 Route 202, Raritan, NJ 08869

CHROMPACK, INC.

2200 Warrenville Road, Downers Grove, IL 60515

Tel: 800-526-3687 or NJ 201-722-8930

CIRCLE 27 ON READER SERVICE CARD



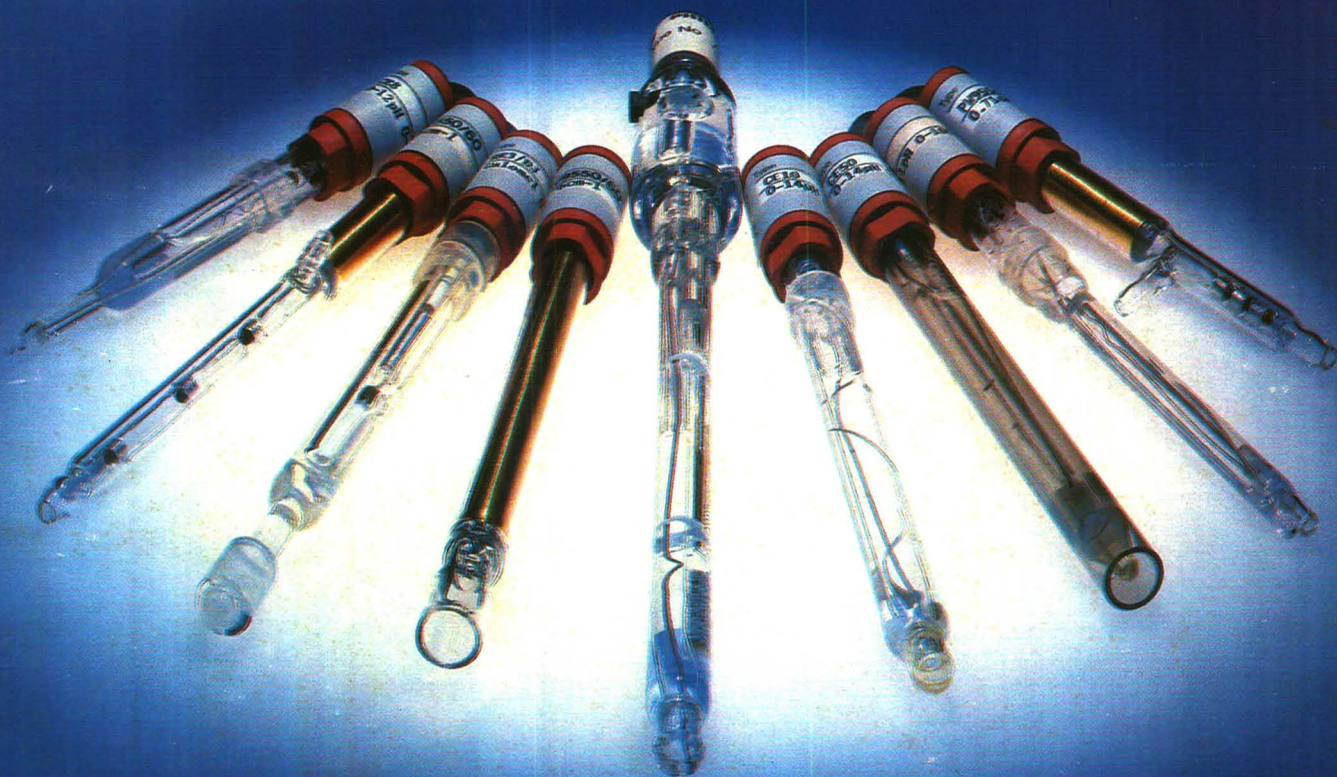
# From TV to pH

The same expertise in glass technology and electronics that perfected colour TV tubes has now advanced the state of the art in pH and conductivity measurement.

In the new range from Philips the selection of electrodes and cells is very impressive. So is the backing of a comprehensive range of complementary meters. For use in lab or field, their sophisticated features even include PC compatibility.

And when you need help with a specialised application who better to ask? After all, who else can offer the special advice and manufacturing facilities of Philips?

Contact us now for our new colour brochure.



Pye Unicam Limited • York Street Cambridge Great Britain CB1 2PX • Tel (0223) 358866 Telex 817331

## Philips Analytical — the quality of experience



Scientific &  
Analytical Equipment

# PHILIPS

CIRCLE 130 ON READER SERVICE CARD

EC07



# What in the world isn't chemical — and how do you keep up with it all?

You keep current with developments by subscribing to the timely, authoritative, comprehensive journals published by the American Chemical Society.

*Langmuir*  
*Analytical Chemistry*  
*Chemical & Engineering News*  
*CHEMTECH*  
*Environmental Science and Technology*  
*Accounts of Chemical Research*  
*Biochemistry*  
*Chemical Reviews*  
*Industrial & Engineering Chemistry*  
*—Process Design and Development*  
*Industrial & Engineering Chemistry*  
*—Product R&D*  
*Industrial and Engineering Chemistry*  
*—Fundamentals*  
*Inorganic Chemistry*  
*Journal of Agricultural & Food Chemistry*  
*Journal of the American Chemical Society*  
*Journal of Chemical & Engineering Data*  
*Journal of Chemical Information and*  
*Computer Sciences*  
*Macromolecules*  
*Journal of Medicinal Chemistry*  
*The Journal of Organic Chemistry*  
*Organometallics*  
*The Journal of Physical Chemistry*  
*ACS Single Article Announcement*  
*Journal of Physical and Chemical Reference Data*

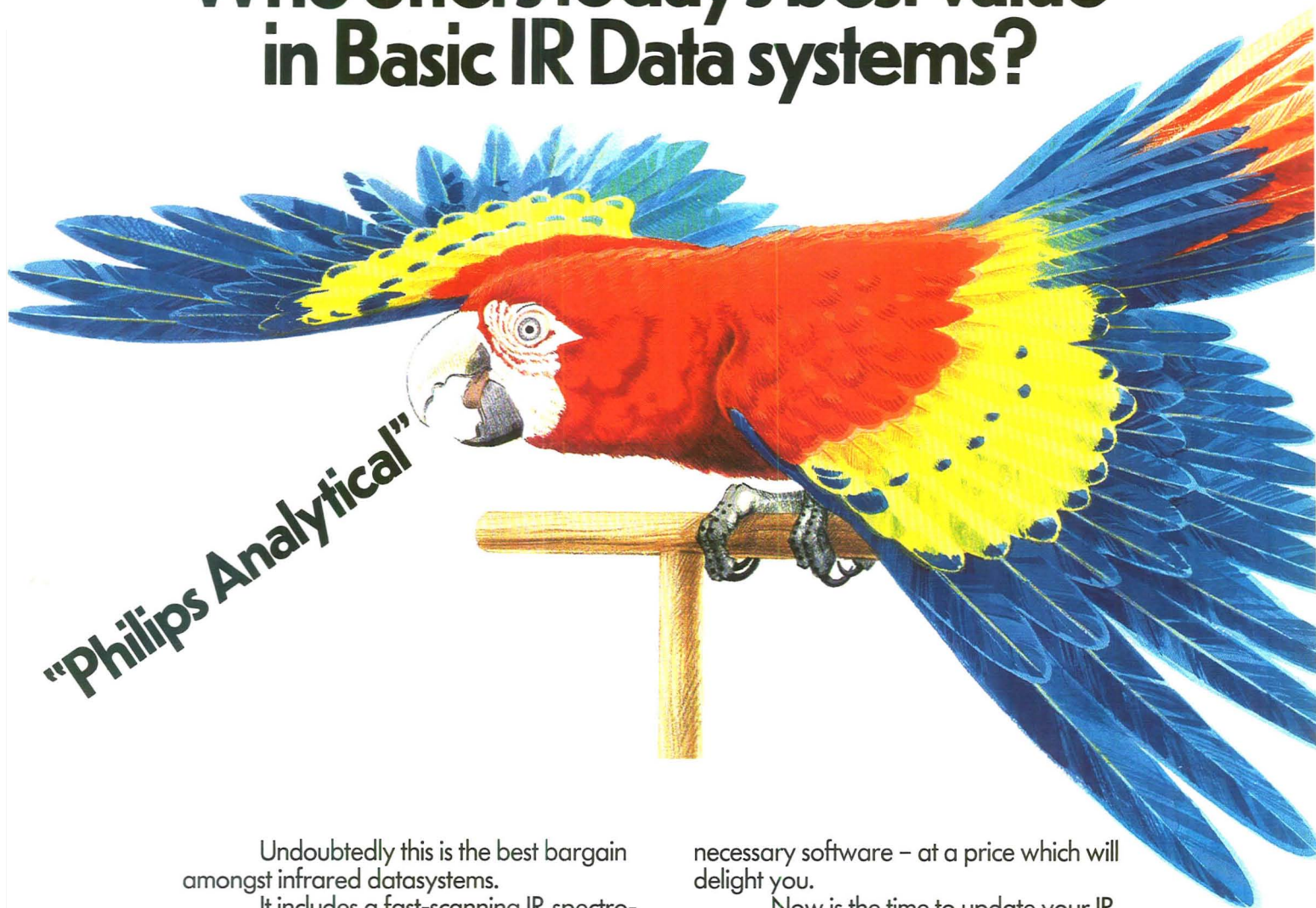


TOLL FREE: U.S. New Orders Only (800) 424-6747  
Cable Address: JIECHEM — Telex: 440159 ACSP UI or 892582 ACSPUBS

AMERICAN CHEMICAL SOCIETY PUBLICATIONS  
1155 Sixteenth Street, N.W., Washington, D.C. 20036 U.S.A.



# Who offers today's best value in Basic IR Data systems?



**"Philips Analytical"**

Undoubtedly this is the best bargain amongst infrared datasystems.

It includes a fast-scanning IR spectrophotometer, linked to an IBM data station, with all the

necessary software – at a price which will delight you.

Now is the time to update your IR capabilities. For your budget's sake. Post the coupon, or write for a brochure.



PU9700



## Unbeatably-priced new BIRD.

**Bigger ideas for better analysis.**



**Scientific and  
Analytical Equipment**

# PHILIPS

CIRCLE 130 ON READER SERVICE CARD

To Pye Unicam Ltd, Cambridge CB1 2PX, Great Britain.  
Please send me details of the PU9700.

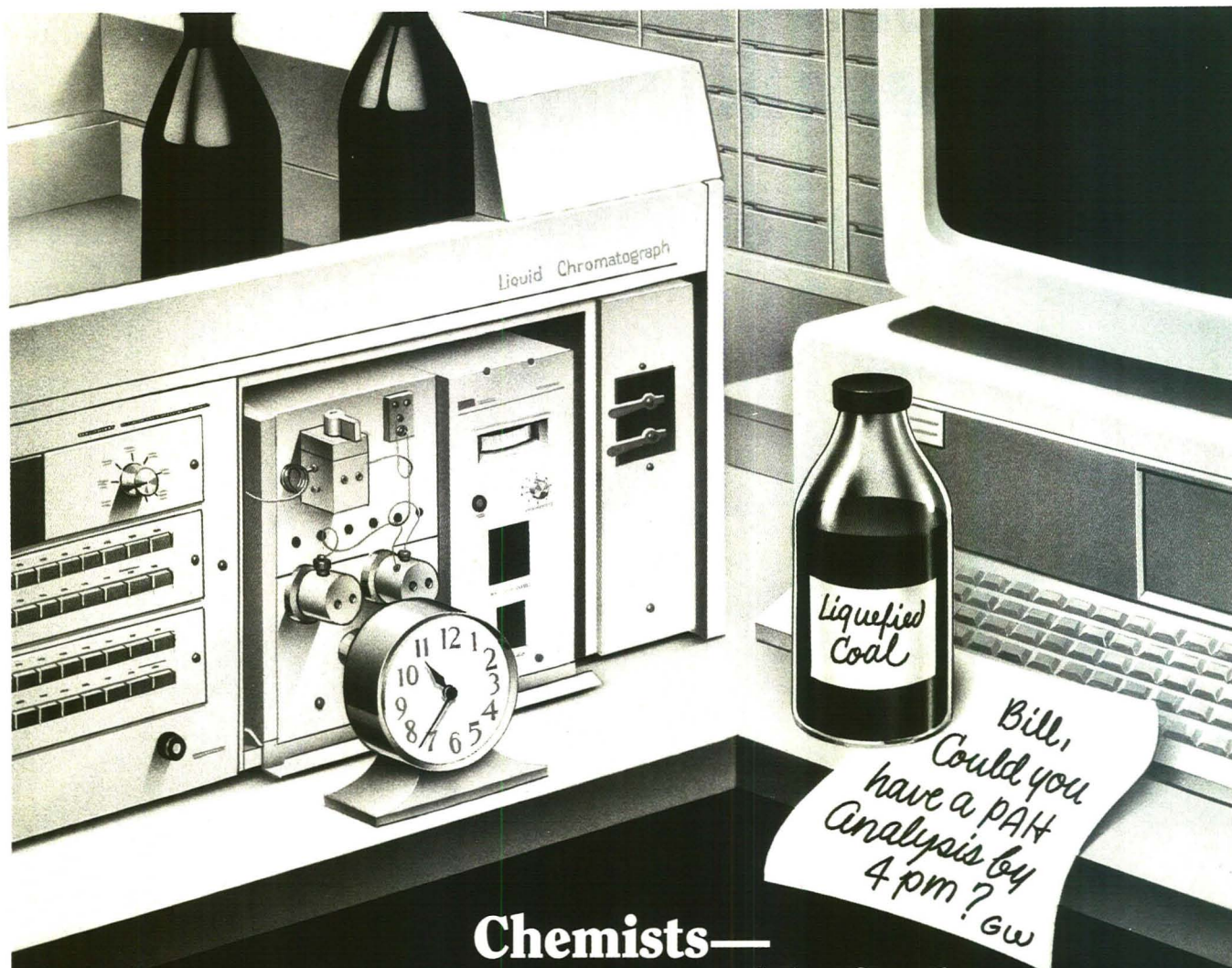
Name

Address

Tel.

DS 11





**Chemists—  
How can you quickly find  
an analytical procedure  
to solve this problem?**

**Search CHEMICAL JOURNALS ONLINE.**

**CHEMICAL JOURNALS ONLINE** is the new powerful information search system that permits you to quickly search over 45,000 journal articles and display:

- Experimental Procedures • Experimental Data
- Preparation Techniques • New Chemical Names • Synthesis Information
- **PLUS CROSSOVER CAPABILITIES WITH CAS ONLINE**

As part of STN, International, **CHEMICAL JOURNALS ONLINE** provides you with the unique ability to instantaneously cross over from **CAS ONLINE** to the full-text of appropriate journals.

**CHEMICAL JOURNALS ONLINE** is not only precise in its searching but also cost effective. In minutes you can save yourself days of tedious work.

**CHEMICAL JOURNALS ONLINE** contains:

- The American Chemical Society's 18 primary journals with over 45,000 articles dating back to 1982.
- A learning file for training and teaching purposes for one low connect hour charge.
- John Wiley & Son's Polymer Journals Online dating back to 1984. (Available Summer 1987)
- Other publisher's journals in the future.

To put **CHEMICAL JOURNALS ONLINE** to work for you, call an American Chemical Society sales representative today at 800-424-6747. The call is free.

Or write, Sales Office, American Chemical Society, 1155 Sixteenth Street, N.W., Washington, D.C. 20036.

Your Research  
Is Not Complete  
Until You Search

**CHEMICAL JOURNALS  
ONLINE**



# Philips Analytical turns fast scanning with brilliant graphics



into child's play.

Whether UV expert or absolute beginner, irrespective of your application, the remarkable new PU8700 Series will provide you with high quality, no compromise answers in seconds.

You will enjoy the experience

so much, you will positively look forward to your next analytical problem.

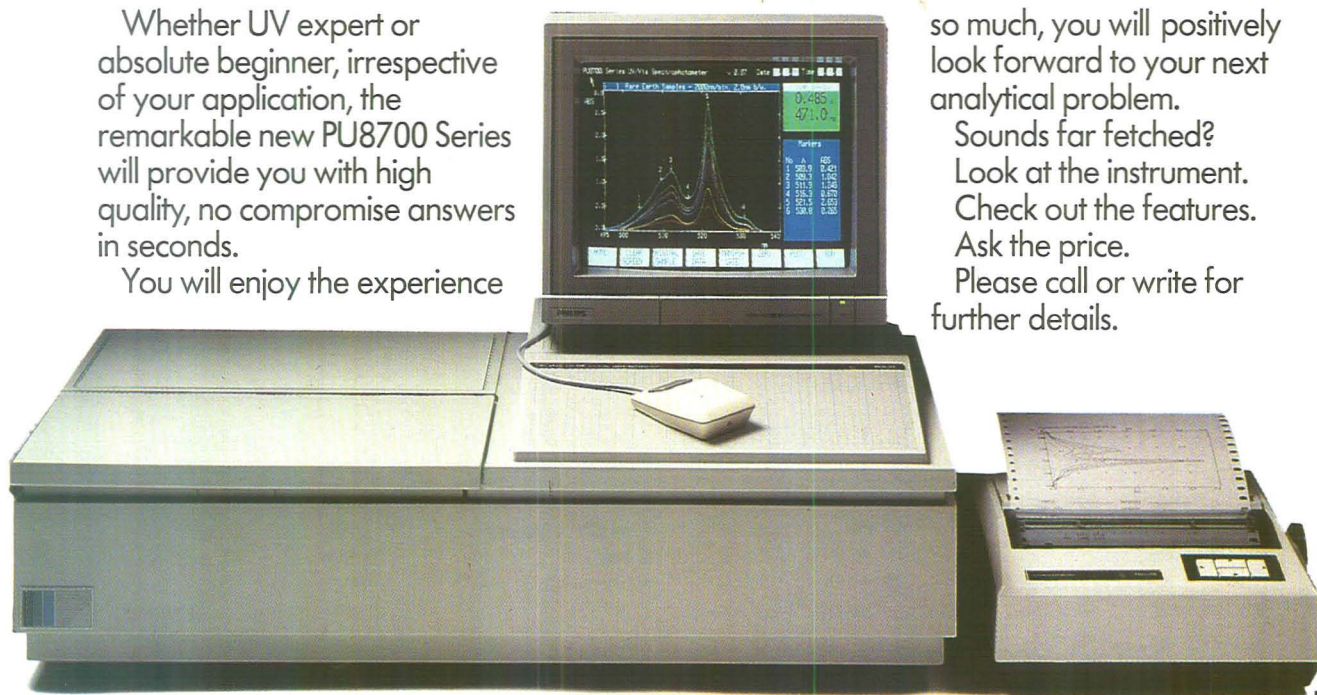
Sounds far fetched?

Look at the instrument.

Check out the features.

Ask the price.

Please call or write for further details.



PU8700

## New, low cost UV/Vis scanners.

### Bigger ideas for better analysis.

Pye Unicam Ltd York Street Cambridge Great Britain CB1 2PX Telephone (0223) 358866 Telex 817331

UV18



Scientific and  
Analytical Equipment

CIRCLE 132 ON READER SERVICE CARD

## PHILIPS



# Introducing the new twice-monthly

Quality  
Research and  
News In Your  
Hands Twice  
as Fast

## **Analytical** CHEMISTRY

Don't miss a single issue! The new, more timely ANALYTICAL CHEMISTRY, contains the same vital information in the field of measurement science. Twenty-four issues a year put the best in ANALYTICAL CHEMISTRY in your hands more often. You'll continue to find the same fine research articles, reports, special departments like Focus and A/C Interface, and the Annual Reviews and LabGuide issues.

### There's never been a better time to subscribe

Call now and you can get your own subscription to the new twice monthly ANALYTICAL CHEMISTRY—including its sought-after annual "Application Reviews" and "LabGuide" issues.

#### SPECIAL RATES

Member*	1 Year	2 Years Save 15%	Nonmember	1 Year	2 Years Save 15%
U.S.	\$ 25	\$ 42	U.S.	\$ 37	\$ 62
Canada & Mexico	\$ 50	\$ 92	Canada & Mexico	\$ 62	\$112
Europe**	\$ 77	\$146	Europe**	\$127	\$231
All Other Countries**	\$104	\$200	All Other Countries**	\$154	\$285

\*Member rates are for personal use only.

\*\*Air service delivery included.

## Call toll free: 800-424-6747

Or write: American Chemical Society, Marketing Communications Department,  
1155 Sixteenth Street NW, Washington, D.C. 20036

This publication is available on microfilm, microfiche, and electronically through  
Chemical Journals Online on STN International.



# Philips Analytical. The buzz word in liquid chromatography systems.



PHILIPS ANALYTICAL ARE HOLDING ONE-DAY HPLC SEMINARS IN LOW-DISPERSION LC & METHOD VALIDATION DURING THE PERIOD 27 JAN TO FEB 25 '87 IN VARIOUS UK LOCATIONS. CALL LINDA DOGGETT ON EXT 308 FOR DETAILS.

PU 4100 is the new fully integrated liquid chromatography system from Philips Analytical. The totally innovative design introduces new standards of performance to the analytical laboratory, whilst also offering the ability to be upgraded to cover the demands of tomorrow's world.

PU 4100 is available with isocratic, binary or quaternary solvent mixing, so that whatever your application, there is an instrument to match your requirements. The UV/Visible detector with true dual beam optics combines exceptional stability with low noise. An intuitive user interface with

clear prompts allows methods to be built up, stored and edited in a simple straightforward manner, while individual parameters may be rapidly changed with a minimum number of keystrokes.

PU 4100 really is liquid chromatography made eazzzzzzzzzy!



## LC made eazzzzzzzy

LC12

### Bigger ideas for better analysis.

Pye Unicam Ltd York Street Cambridge Great Britain CB1 2PX Telephone (0223) 358866 Telex 817331



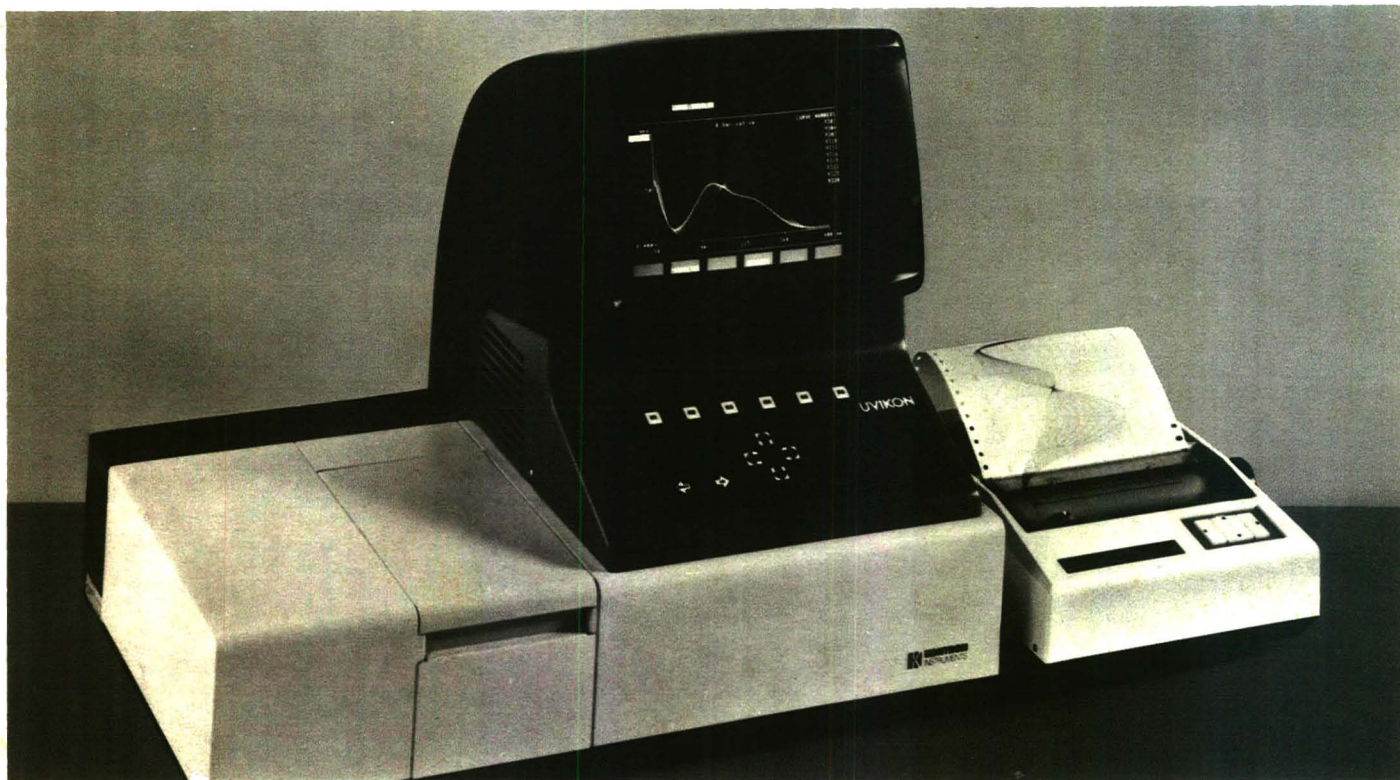
Scientific and Analytical Equipment

# PHILIPS

CIRCLE 133 ON READER SERVICE CARD



# UVIKON®860



## Leading Scientists Rely On The UVIKON®860 UV/VIS Spectrophotometer

### Higher Sensitivity

The symmetrical double beam optical system uses only six reflecting surfaces, for maximum energy throughput, providing ultimate performance with real samples. Your benefit is a **higher signal to noise ratio** and therefore correspondingly **higher sensitivity**.

### Best Reproducibility

The optical base is machined within a tolerance of 0.001%, we add a microprocessor controlled wavelength drive to obtain a wavelength reproducibility of 0.02 nm. Your benefit: best reproducibility, being especially important to **obtain the same results** if a measurement is made **on the slope of a peak** or **on top of a very sharp peak**.

### Signal Resolution 0.000001 ABS

The fully digitized signal processing calculates the absorbance with an unmatched resolution. Your benefit: **small changes in ABS are accurately determined**.

### Curve Memory Software

All spectral and time drive curve data are put automatically into the **large battery-buffered memory**. You make the decision how to handle the data after the measurement.

### Absorbance versus Concentration

Calibration curves are computed either by linear regression, quadratic fit or linear interpolation using up to 12 standards. **Recalculation** of the calibration curve **can be done at any time** without the need to measure the standards again. The calibration data can be stored in the large memory for later use.

### Enzyme Kinetics

The Uvikon 860 lets you control all the parameters, such as the incubation time, the number of data points and time interval. The slope is calculated and displayed along with the activity and the statistical data. **Post assay recalculation is possible** narrowing the range of measured points.

SEE US  
AT PITTSBURGH CONFERENCE  
BOOTH 230

**UVIKON®860 – Performance, Quality, Reliability  
at an Affordable Price**

**Your partner in science and health**



*For further information please contact your local Kontron Company*

Austria (Vienna)	(0222) 692531	Japan (Tokyo)	(03) 2634801
France (Montigny le Br.)	(1) 30438152	Scandinavia (Stockholm)	(46) 8979700
West Germany (Munich)	(08165) 6060	Spain (Madrid)	(01) 7291155
Great Britain (Watford)	(0923) 45991	Switzerland (Zurich)	(01) 4354111
Italy (Milan)	(02) 50721	USA (Everett, Mass.)	(617) 3896400

KONTRON INSTRUMENTS Inc., 9 Plymouth Street, Everett, Massachusetts 02149, USA. Telephone (617) 389-6400, (800) 343-3297, TWX 6817432

International Business Management:

KONTRON INSTRUMENTS AG, Bernerstrasse Süd 169, 8010 Zurich/Switzerland, Telephone (01) 435 4111, Telex 822 191

CIRCLE 85 ON READER SERVICE CARD



# Ion Chromatography

**James S. Fritz**

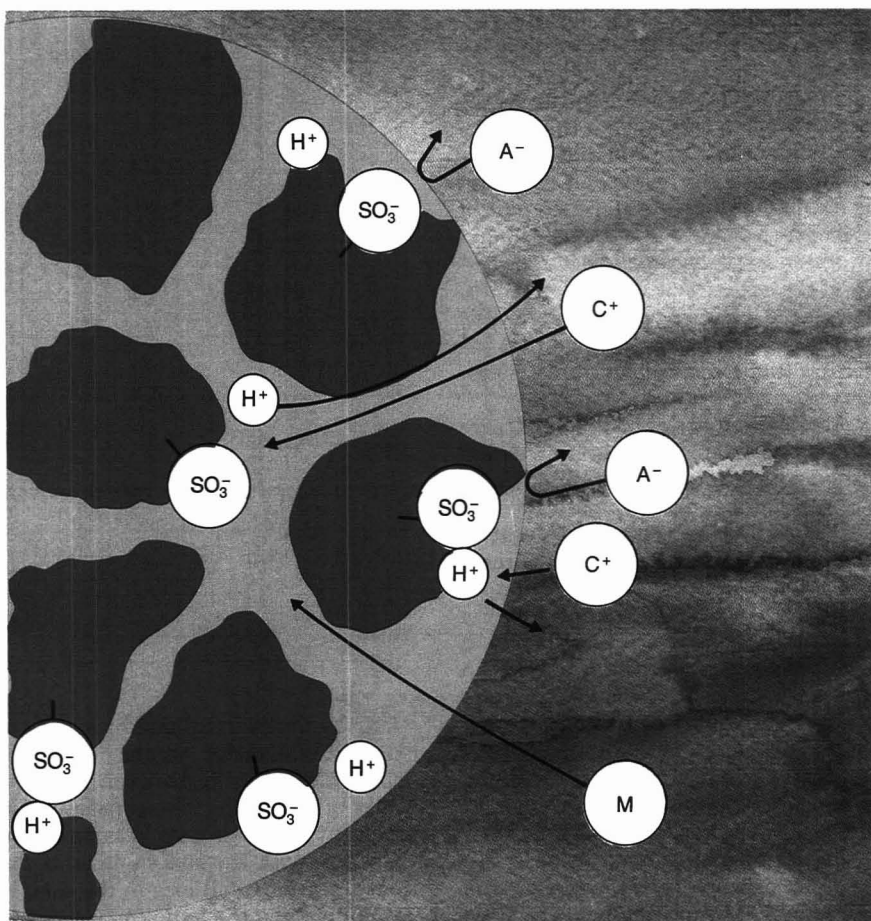
Department of Chemistry and Ames  
Laboratory  
U.S. Department of Energy  
Iowa State University  
Ames, Iowa 50011

Remember the woman in the television commercial when she found out they were taking away her favorite washing detergent? Her reaction might seem mild compared to that of an analyst if you took away her (or his) ion chromatographic setup. There are other detergents, but how can you determine low concentrations of anions without using ion chromatography? At least that is how chemists seem to feel, judging from the growing popularity of ion chromatography.

Ion chromatography makes it possible to separate and measure low concentrations of up to 8 or 10 different anions in a single chromatographic run that takes only a few minutes. The method also works well for cations. Alkali metal ions, ammonium, magnesium, calcium, strontium, and a growing list of other metal cations and amine cations can also be rapidly separated and determined in aqueous samples. Ion chromatography is cost-efficient because the equipment is relatively inexpensive, and several ions can be determined in each chromatogram. Although modern ion chromatography is only about 10 years old, it is now being used routinely in a growing number of industries. Many scientific and environmental studies, such as the analysis of a large number of rainwater samples, might not have been feasible before the advent of ion chromatography.

The name *ion chromatography* refers to any modern and efficient method of separating and determining ions. Most of the samples now analyzed by ion chromatography contain inorganic or hydrophilic organic anions and cations. The most common mode of separation is that of ion exchange chromatography, anions being separated on an anion exchange column and cations on a cation exchange column.

Ion exchange chromatography has



**Figure 1.** Schematic drawing showing cation exchange ( $C^+$  and  $H^+$ ), exclusion of anions ( $A^-$ ) by a cation exchange resin, and the ability of neutral molecules ( $M$ ) to enter and leave the resin.

Magenta areas represent polymer; blue areas represent water.

been used for many years to separate various organic and inorganic ions. The classical methods, however, were often slow and required the collection and analysis of numerous fractions to delineate the chromatogram. Modern chromatographic methods are much faster and more efficient. An automatic detector is always used and the entire chromatogram is recorded. It is this newer type of ion separation that bears the name ion chromatography.

## Principles of ion exchange

**Resins and the exchange process.** Polymeric ion exchange resins are clas-

sified either as *microporous* or *macroporous*. On contact with an aqueous solution, both kinds take up a considerable amount of water into the resin bead. This is partly attributable to the presence of highly polar functional groups in the resin: sulfonate groups for a cation exchange resin and quaternary ammonium groups for an anion exchange resin. Microporous resins swell and form a gel when hydrated and shrink again if the resin becomes dehydrated. Macroporous resins tend to be more highly cross-linked with a large number of hard polymeric microspheres in each bead. Between these



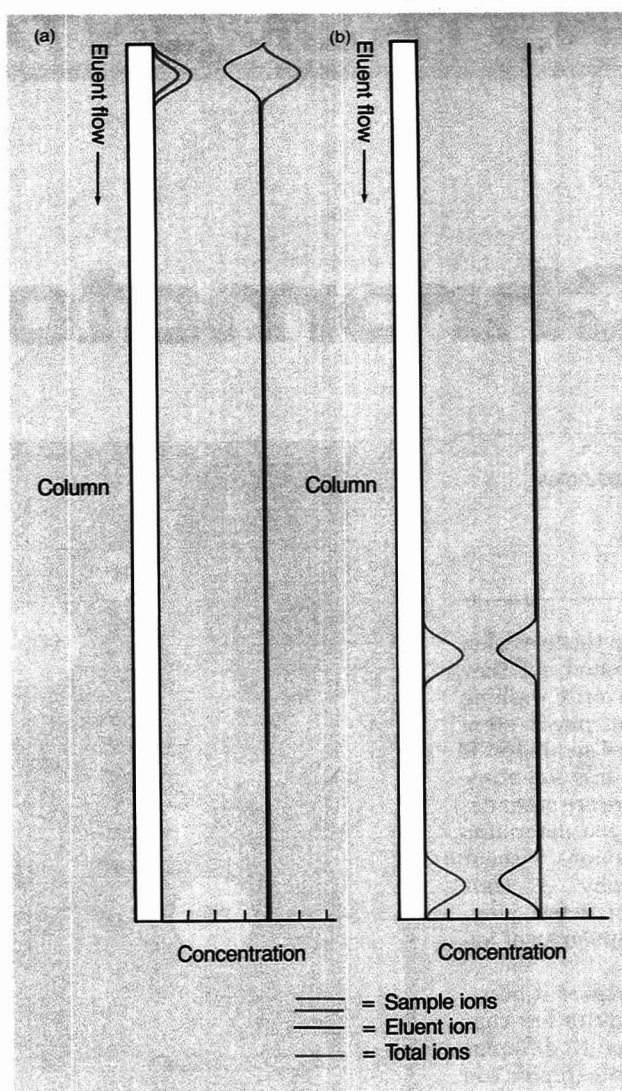
microspheres are many pores and channels that fill up with water when the resin is in contact with an aqueous solution. Macroporous ion exchange resins generally undergo much less swelling and shrinking than do microporous resins.

Figure 1 shows the main features of a cation exchange resin. In reality, there are many more microspheres, channels, and sulfonate groups than can be shown in a drawing of this kind. The  $\text{-SO}_3^-$  groups are chemically attached to benzene rings of the polymer and have little, if any, ability to move. The  $\text{H}^+$  counter ions, however, are electrostatically attracted to the negative sulfonate groups but are free to move about in the water-filled pores and channels inside the resin. Ion exchange occurs when a cation from the outside solution enters the resin and a hydrogen ion leaves the resin. This exchange is not limited to the outermost part of the resin; exchange also occurs with hydrogen ions that are well inside the resin. If the exchanging cation happens to have a  $2^+$  charge, two hydrogen ions leave the resin for each cation that enters, so that electrical neutrality is preserved.

Anions from the outside solution are prevented from entering the cation exchange resin by the "wall" of fixed  $\text{-SO}_3^-$  groups. As depicted by the curved arrows in Figure 1, the negative charges of the sulfonated groups repel the solution anions. Hydrophilic molecular species in the sample solution are not affected by this sulfonate anion barrier and can enter and leave the ion exchange beads. Molecules that are more hydrophobic can also enter the aqueous channels of the resin, but they tend to be retained inside the resin by the van der Waals forces of the polymer (especially the benzene rings).

The interior of anion exchange resin beads is also hydrated. Cations from the sample solution are excluded from the resin by the positive charges on the fixed quaternary ammonium groups, but anions from the outside solution can readily exchange with the mobile anions of the resin. Hydrophilic bases and other molecular species can enter and leave the aqueous channels and pores of the resin.

**Chromatography.** Analytical ion exchange chromatography is basically a simple process. A cation exchange column is used to separate sample cations, and an anion exchange column is used to separate anions. The eluent, which is a dilute solution containing cations and anions, is pumped through the column to replace virtually all of the exchangeable ions in the column with the eluent cation or anion and to establish a constant signal from the detector. Then a small volume of a sample is injected, and the sample ions are taken



**Figure 2.** Schematic representation of ion concentrations in ion exchange chromatography.

(a) Sample injection; (b) elution.

up by the resin column by exchange with an equivalent number of eluent ions. This process is depicted schematically in Figure 2a. The concentration of eluent ions decreases because of ion exchange with the sample ions. If the concentration of all ions in the sample is greater than the ionic concentration of the eluent, the total ionic concentration at the top of the column will increase. This creates a ripple that moves down the column and gives a positive peak as it passes through a conductivity detector. If the sample is less concentrated than the eluent, a negative peak is obtained.

After injection the eluent ions, which continue to be pumped through the column, compete with the sample ions for the exchange sites of the resin and cause the sample ions to move down the column. Owing to differing affinities for the resin exchange sites, the sample ions move at different rates and are eventually separated (Figure 2b). The detector senses when sample ions are passing through the cell and gives a signal that is proportional to their concentration.

Figure 2b shows that the total ion

concentration in the column is constant during the elution step, but the exchange reaction reduces the eluent ion concentration in the column zones where there is a sample ion. This means that a spectrophotometric or other selective detector can be set to detect the sample ions either directly or indirectly by measuring the decrease in eluent ion concentration.

### **Ion chromatography systems**

**Suppressed anion and cation chromatography.** Modern ion chromatography actually began with a paper published in 1975 by Small, Stevens, and Bauman (1). They used a conductivity detector (which is a universal detector for ions) in conjunction with an ion exchange separator column and a second suppressor column. The function of the suppressor column is to greatly reduce the background conductivity by an ion exchange reaction with the eluent. The suppressor column also increases the sensitivity with which sample ions can be detected.

In suppressed ion chromatography, anions are separated on an anion exchange column that contains an anion



exchange resin of low exchange capacity. A dilute solution of a base, such as sodium carbonate-sodium bicarbonate, is used as the eluent. Immediately following the anion exchange column is a cation exchange suppressor unit that converts the eluent to carbonic acid and the counter ion of sample anions from sodium to hydrogen. A conductivity detector is used, and the background conductance from the carbonic acid is low. The anion, and especially the  $H^+$  counter ion, however, are highly conducting provided that the acid form of the anion is ionized to a reasonable extent.

In the earlier instruments, the suppressor unit was a cation exchange column of high capacity that had to be regenerated periodically. Now a membrane unit made of a sulfonated polymer serves as the suppressor unit (2). Eluent and sample ions exchange with hydrogen ions in the membrane as follows:

Eluent:



Sample ion:



A dilute sulfuric acid solution flows continuously around the outside of the membrane. This solution replaces sodium ions in the membrane with hydrogen ions from the sulfuric acid, thus regenerating the membrane.

This system gives excellent separations for a variety of anions. For example, samples containing parts-per-million concentrations of fluoride, chloride, nitrite, phosphate, bromide, nitrate, and sulfate can be completely separated within a few minutes. Anions of weak acids, however, cannot be detected with this system unless a method of detection other than conductivity is used; moreover, this suppression system requires the use of a basic eluent.

A similar system can provide good separations of a number of cations. For cation separations, the separator column contains a cation exchange material, and the suppressor unit is a hydroxyl anion exchanger. The eluent cation typically is  $H^+$  or phenylenediammonium  $[Ph(NH_3)_2^{2+}]$  and is converted by the suppressor unit to  $H_2O$  or  $Ph(NH_2)_2$ , respectively.

Suppressed ion chromatography has been patented; commercial instruments for this type of chromatography are sold exclusively by Dionex Corporation (Sunnyvale, Calif.).

**Single-column anion and cation chromatography.** Researchers at Iowa State University have shown that ion chromatographic analyses of anions and cations can be performed without the use of a suppressor unit if the ion exchange resin used in the separation

column has a sufficiently low exchange capacity and if a very dilute eluent is used (3-5). For separation of anions, the resin must have an exchange capacity between about 0.005 meq/g and 0.10 meq/g. Typical eluents are  $1.0 \times 10^{-4}$  to  $4.0 \times 10^{-4}$  M solutions of sodium or potassium salts of benzoic acid, hydroxybenzoic acid, or phthalic acid. These eluents are sufficiently dilute that the background conductivity is quite low. Most sample anions have a higher equivalent conductance than that of the eluent anion and can therefore be detected even when present in concentrations in the low parts-per-million range. A dilute solution of any of several carboxylic acids also makes an effective eluent (6). With a conductivity detector, the detection limit of most anions is improved by a factor of almost 10 when a carboxylic acid instead of a salt is used as the eluent.

For the separation of cations, a cation exchange column of low capacity is used in conjunction with either a conductivity detector or another type of detector. With a conductivity detector, a dilute solution of nitric acid is typically used for separation of monovalent cations, and a solution of an ethylenediammonium salt is used for separation of divalent cations. Because both of these eluents are more highly conducting than the sample cations, the sample peaks are negative relative to the background (decreasing conductivity). The difference in equivalent conductance between the eluent and sample cations is quite large, and the detection sensitivity is very good, particularly with the acidic eluent. Figure 3 shows a separation of all of the alkali metal ions plus the ammonium ion. In essence, this chromatogram is displayed upside down because the peaks are in the negative direction.

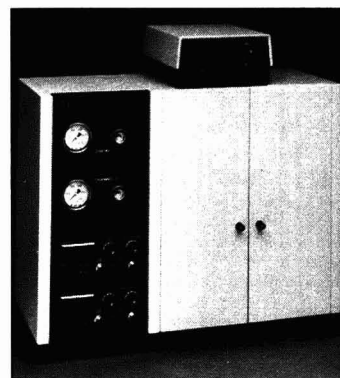
Many of the divalent metal cations have also been separated by single-column ion chromatography (SCIC) (also called nonsuppressed ion chromatography) with conductivity detection. Magnesium(II) and the alkaline earth cations can be separated nicely using an ethylenediammonium salt eluent. The separation can be extended to include several of the divalent transition metal cations by using a weakly complexing eluent such as ethylenediammonium tartrate (7). Still better selectivity is possible by adding a complexing reagent such as ethylenediaminetetraacetic acid (EDTA) or sulfosalicylate to the sample to strongly complex ions such as iron(III) and aluminum(III) (8).

Equipment for SCIC is manufactured by Wescan Instruments and Waters Associates in the United States, by Toyo Soda in Japan, and by several small companies in Europe. Some of the equipment manufactured and sold

## WESCAN

### ION CHROMATOGRAPHY CATALOG

Your **FREE** 1987 Ion Chromatography catalog, which has 15% more new products and column application information, is just a phone call away.  
1-800-642-4667



Stay on your Path To Excellence  
with Wescan

To get your **FREE**

Ion  
Chromatography  
Catalog:

Call 1-800-642-4667

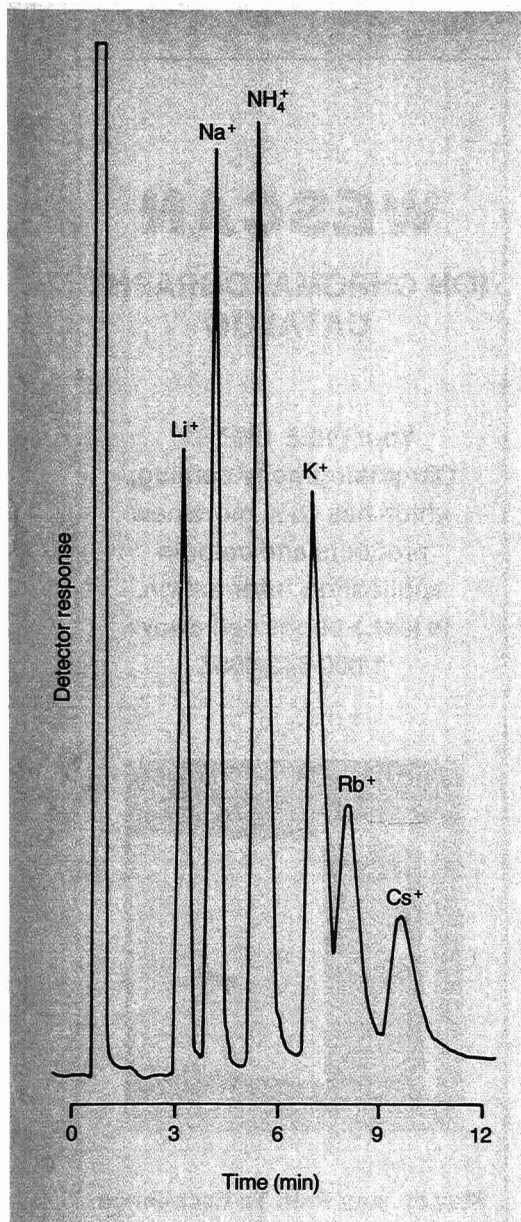
Or Write

**WESCAN INSTRUMENTS, INC.**

2051 Waukegan Road  
Deerfield, Illinois 60015

CIRCLE 173 ON READER SERVICE CARD





**Figure 3.** Separation of alkali metal cations and ammonium cation on a low-capacity cation exchange column using a conductivity detector.

Eluent was 1.0 mM nitric acid. Column was 350 X 2.0 mm packed with 0.059 meq/g cation exchange resin.

by Dionex is actually for SCIC with various detectors.

#### **Ion pair chromatography**

This type of ion chromatography goes by a number of other names including *paired-ion chromatography*, *mobile-phase ion chromatography*, and *ion interaction chromatography* (9). It has the advantage of using the same highly efficient reversed-phase columns that are used in ordinary liquid chromatography (LC). In ion pair chromatography the eluent contains an ionic modifier, which acts as a movable ion exchange site that can be sorbed by the column packing either alone or as an ion pair with a sample ion. Sodium oc-

tanedisulfonate might be a suitable modifier for the separation of cations and a quaternary ammonium salt for the separation of anions. The sample ion is pushed down the column by a competing ion of the same charge (positive or negative) in the eluent. Ion pair chromatography is much like ion exchange chromatography except that the modifier must be renewed continuously by incorporation in the eluent.

Sometimes an organic solvent, acid-base buffer, or complexing reagent is also incorporated in the eluent. A conductivity, spectrophotometric, electrochemical, or possibly a refractive index detector can be used. Owing to the high efficiency of modern LC columns, exceptionally good separations have been obtained in many instances. For example, a complete separation of rare earths has been obtained in less than 10 min on a  $C_{18}$  column using a programmed concentration of  $\alpha$ -hydroxyisobutyric acid in the eluent with sodium octanesulfonate as the modifier (10).

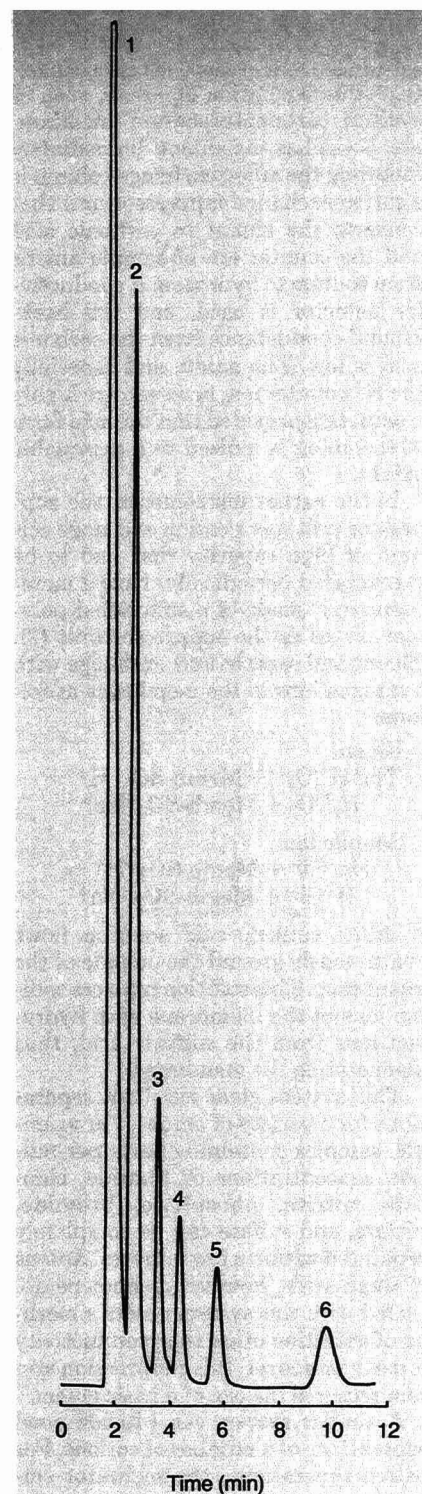
#### **Ion exclusion chromatography**

Strictly speaking, this is not a form of ion chromatography because molecular species rather than ions are separated. An ion exchange column, however, is generally used for the separation, so the two forms of chromatography are related. In addition, ion exclusion chromatography is an excellent way to separate molecular substances from larger amounts of ionic material in the sample.

The separation of  $C_1$ - $C_5$  alkyl carboxylic acids from strong inorganic acids illustrates this type of separation (11). The separation is done on a high-performance cation exchange column in the  $H^+$  form. Ionic material is rejected by the resin and passes through the column at the same rate as the eluent. Carboxylic acids are molecular rather than ionic, and they partition between the occluded liquid inside the resin and the aqueous eluent. Van der Waals interactions between the polymeric resin and the sample acids also play a role in the retention. Ionization of the carboxylic acids is repressed by the high concentration of  $H^+$  within the resin beads and by a low concentration of benzoic or succinic acid in the aqueous eluent.

A typical chromatogram for this separation is shown in Figure 4. The eluent was 0.5 mM benzoic acid in 95% water-5% acetonitrile, and a conductivity detector was used. The sample acids were 1.0 mM each, and a 100- $\mu$ L sample was injected.

Ion exclusion chromatography is also useful for determining weak inorganic acids such as carbon dioxide (carbonic acid), HF, and  $HPO_2$ . Salts of weak acids can also be determined because they are converted to the correspond-



**Figure 4.** Separation of acids by ion exclusion chromatography with a conductivity detector.

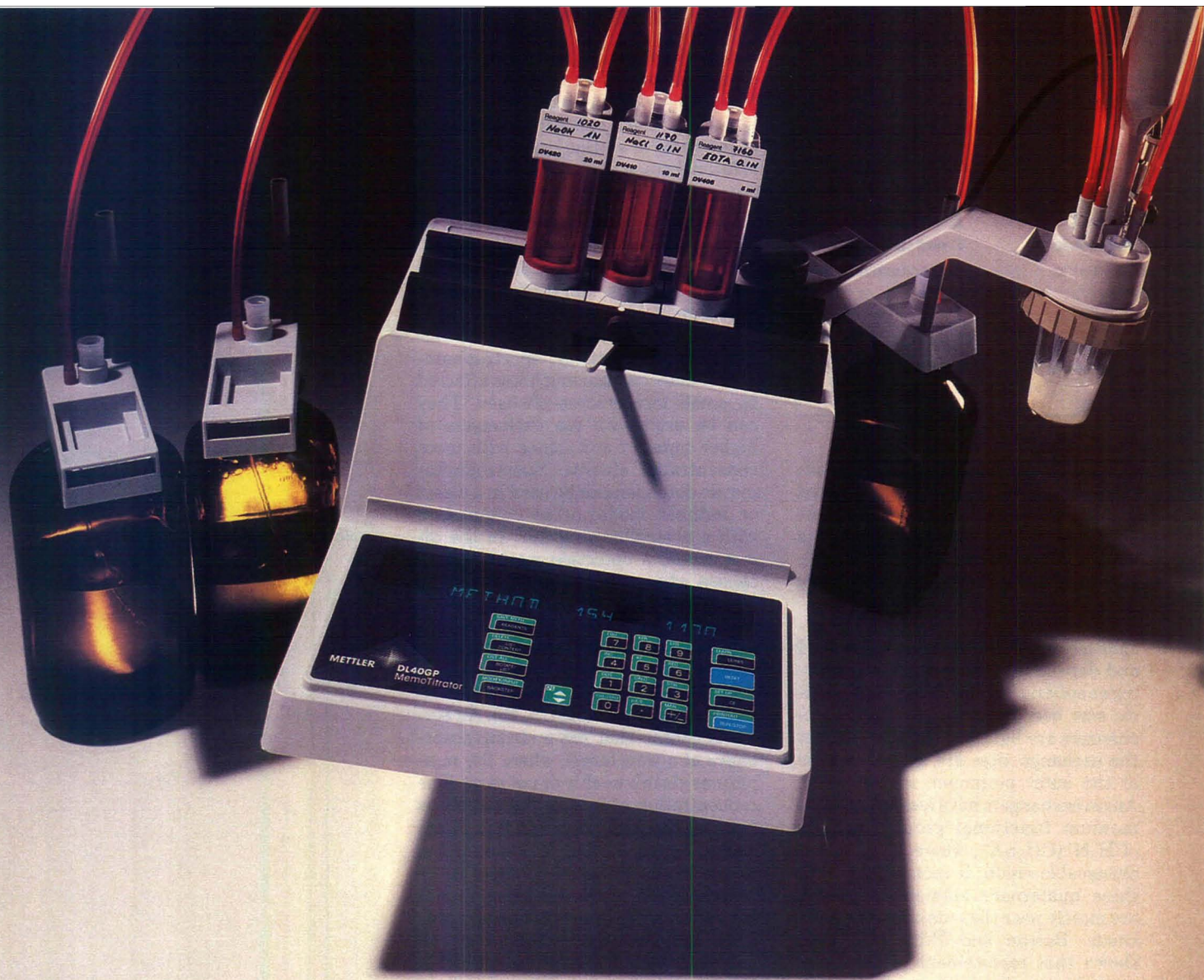
1 = Sulfuric acid, 2 = formic acid, 3 = acetic acid, 4 = propionic acid, 5 = butyric acid, 6 = valeric acid.

ing acid by the hydrogen ions in the ion exchange separation column. Weak molecular bases and their salts can be separated on an anion exchange column in the  $OH^-$  form.

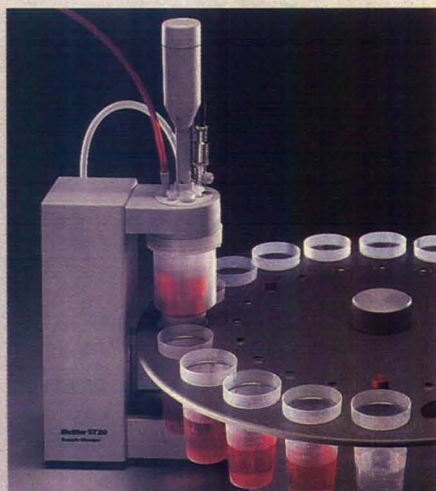
#### **Column packings used in ion chromatography**

The ion exchange materials used in ion chromatography fall into three general





## The new METTLER DL40GP MemoTitrator: Boosted by flexibility and diversity.



Mettler's new DL40GP MemoTitrator teams up with the ST20 Sample Changer to help you improve productivity.

Now you can completely master a diverse range of applications with the new METTLER DL40GP MemoTitrator. It gives you the flexibility to perform potentiometric, voltametric or colorimetric analyses virtually anywhere—in R&D and QA/QC labs, even in production areas.

Forty programmable methods, data storage and evaluation software are all standard features. Optional graphics dot matrix printers can record results, data tables, titration curves and their first derivative.

Using a convenient prompting routine, you can easily develop, store and execute new methods. With the touch of a button, the METTLER DL40GP titrates and calculates the result quickly and reliably. Increase your automation even more by connecting

the DL40GP to a computer, lab information system, robot or the METTLER ST20 Sample Changer.

As with all METTLER products, the new DL40GP MemoTitrator is backed by our respected team of application specialists and service technicians. They're ready to put years of titration experience to work for you nationwide.

For more information on the METTLER DL40GP and other innovative titrators, write Mettler Instrument Corporation, Box 71, Hightstown, NJ 08520. Or call 1-800-METTLER. (In New Jersey, 609-448-3000.)

# METTLER



**Table I. Detectors used in ion chromatography**

Detector	Detection mode
Conductivity, suppressed	Direct
Conductivity, SCIC	Direct or indirect
Spectrophotometric	Direct or indirect
Spectrophotometric	Postcolumn reactor
Fluorometric (17)	Indirect
Refractive index	Indirect
Electrochemical	Direct
Atomic absorption or emission	Direct

classes: polymeric ion exchangers, silica-based ion exchangers, and coated materials. The exchange capacity must be low so that a dilute eluent can be used. A low capacity is particularly necessary for SCIC with a conductivity detector.

Polystyrene-divinylbenzene ion exchangers are probably the most rugged and dependable. Efficiency is improving as spherical resins of uniform particle size become available. Cation exchangers are lightly sulfonated so that the exchange sites are in a thin zone at the outer perimeter of the beads. Anion exchangers have quaternary ammonium functional groups, usually  $-\text{CH}_2\text{N}^+(\text{CH}_3)_3\text{A}^-$ , where  $\text{A}^-$  is an exchangeable anion. It seems likely that these quaternary ammonium groups are mostly near the outside of the resin beads. Barron and Fritz (12) have shown that replacement of the three methyl groups with larger alkyl or hydroxyalkyl groups changes the affinity of the exchanger for certain anions.

Although silica-based ion exchangers can give excellent separations, they should not be used in conjunction with eluents that are very basic. Silica-based ion exchangers are less rugged than polymeric resins, and their exchange capacity tends to decrease gradually.

Column packings prepared by coating a resin with an ion exchange material also work quite well in ion chromatography. The anion exchangers originally used by Dionex Corporation were prepared by coating surface-sulfonated polymeric beads with a quaternized latex. Efficient ion exchangers for ion chromatography can also be prepared by coating porous polymeric beads with a suitable monomer such as cetylpyridinium chloride. The coating may be done in a static (5) or dynamic mode (13). These ion exchangers are stable and can be prepared in a range of exchange capacities by varying the coating conditions.

Pietrzyk and co-workers (14) used porous alumina as a column packing for ion chromatography. Alumina is an anion exchanger at acidic pH values

and a cation exchanger in contact with a basic eluent. The retention times of halide ions with alumina are  $\text{I}^- < \text{Br}^- < \text{Cl}^- < \text{F}^-$ , which is exactly the reverse of the order of elution using more conventional anion exchangers.

### Detectors

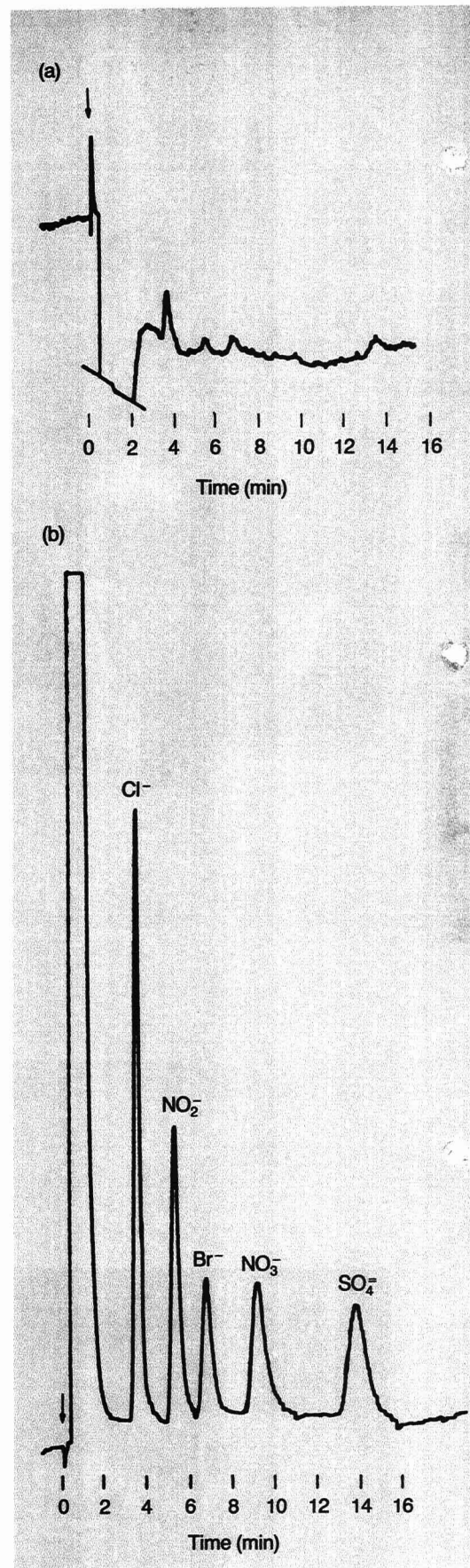
The major detectors used in ion chromatography are listed in Table I.

Conductivity detectors are generally the most versatile and useful; however, spectrophotometric detectors are receiving considerable attention. Compared to conductivity, spectrophotometric detectors are much less affected by small temperature changes. They can be used with ion exchangers of higher capacity and hence with more concentrated eluents. Spectrophotometric detection can be used in a direct or indirect mode, or in conjunction with a postcolumn reactor. In the direct mode, a detection wavelength is chosen where the sample ions absorb but the eluent does not. The use of this mode is somewhat limited because sample ions often lack the requisite absorbance.

Indirect spectrophotometric detection is usually possible (15, 16). An eluent is chosen that has a strong absorbance at a wavelength where the sample ions absorb weakly or not at all. The concentration of ions in the column is fixed by the ionic concentration of the eluent; hence, elution of a sample ion results in an equivalent decrease in the concentration of the absorbing eluent ion and in a negative chromatographic peak. Indirect spectrophotometry can be an exceptionally sensitive method of detection, as shown in Figure 5 (18). In this case, a resin of low capacity and a dilute eluent were used to make possible such excellent sensitivity.

A postcolumn reactor, coupled with spectrophotometric detection of the absorbing product, is capable of great versatility. To detect metal cations, the column effluent is simply mixed with a buffered color-forming reagent that is also pumped into the reactor. The detection can be general, or it can be selective for certain ions if the reagent and conditions for the postcolumn reaction are carefully chosen.

Note from Table I that fluorometry and refractive index detectors may also be used in an indirect detection mode. Haddad and Heckenberg (19) found that the detection limit obtainable for anions with indirect refractive-index detection was lower than with direct conductance, and it was frequently lower than with indirect UV detection. Electrochemical detectors (other than conductance) include polarographic, amperometric, and coulometric modes. Electrochemical detectors are capable of excellent selectivity for certain ions and low limits of detection. The pulsed amperometric detector (PAD) invent-

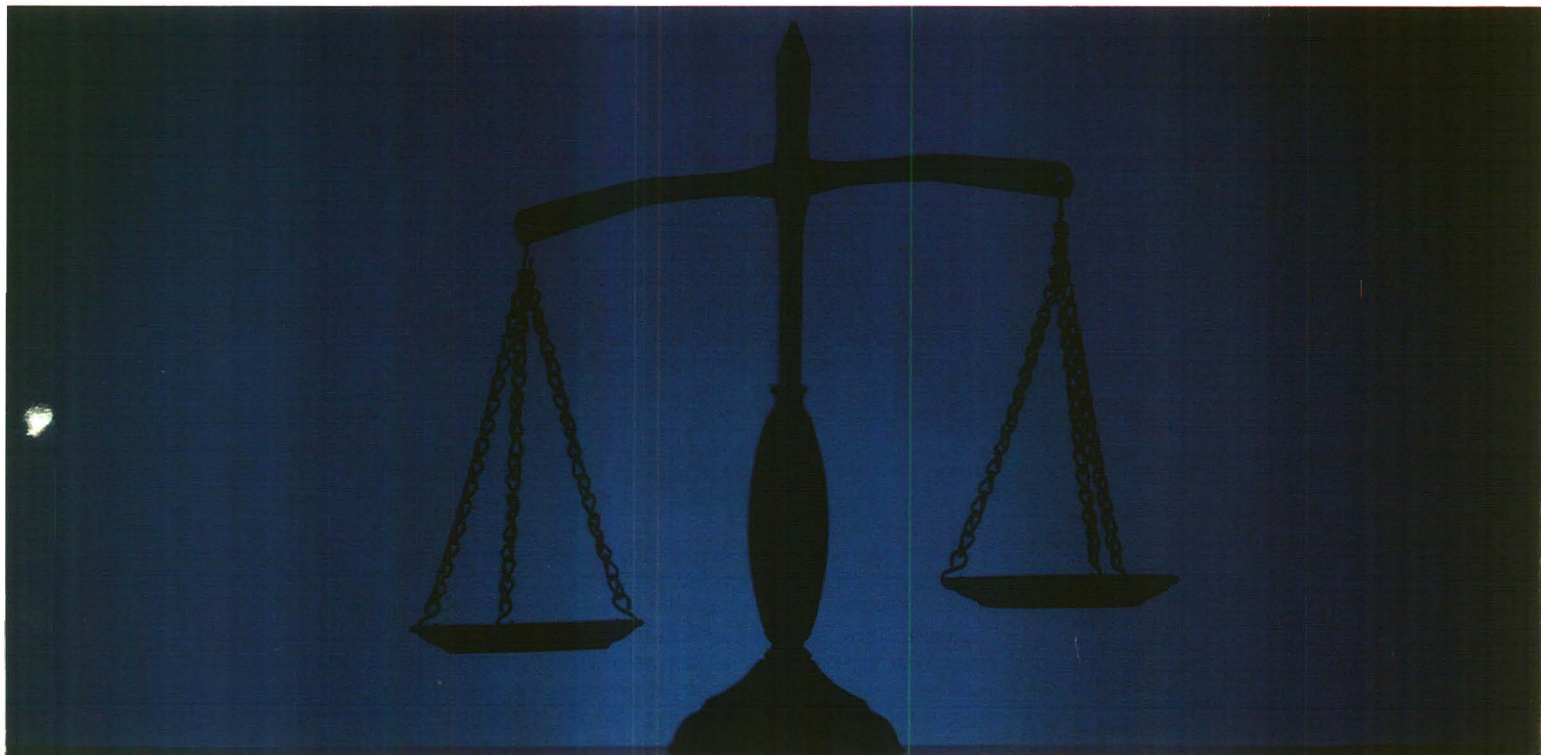


**Figure 5.** Separation of 1-ppm levels of common anions. TSK gel anion exchange column (1.0 meq/g),  $7 \times 10^{-4}$  M  $\text{MoO}_4^{2-}$  at 1.0 mL/min.

(a) Conductivity detection, 0.1  $\mu\text{S}$  full scale; (b) spectrophotometric detection, 250 nm, 0.003 absorbance units full scale.



# Perkin-Elmer LIMS 2000. Because all LIMS are not created equal.



## **Perkin-Elmer. One company for all your LIMS needs.**

No other company offers you everything you need. We'll provide you with the exact combination of software and hardware to fit your application and your lab. We'll interface our own and other vendors' instruments so your normal lab operations will continue as before—only now there's a central place where all data and results are stored. And, if you have special requirements, our LIMS Implementation Department will customize your system for a perfect fit.

## **Perkin-Elmer. 200 installed LIMS—more than any other company.**

There's a very good reason why

we have over 200 LIMS installed worldwide. We make it our job to understand your requirements for lab automation. We successfully implemented the first LIMS and we continue to introduce innovative, solution-oriented software for laboratories.

## **Perkin-Elmer. The most comprehensive LIMS support available.**

To ensure customer satisfaction, we offer professional training for all levels of expertise, comprehensive software and hardware maintenance contracts, and a central telephone hotline. Our Product Specialists and System Analysts will help you optimize and expand your system to fit your changing needs. We encourage customers to communicate

with us and with each other through national and regional LIMS 2000 Users Groups, an electronic bulletin board system, and an information-packed quarterly newsletter.

If you're ready for the best, call your Perkin-Elmer representative. Or, for literature in the U.S., call 1-800-762-4000.

Perkin-Elmer Corp., 761 Main Ave.  
Norwalk, CT 06859-0012 U.S.A.  
Tel: (203) 762-1000. Telex 965-954.

Bodenseewerk Perkin-Elmer & Co.,  
GmbH, Postfach 1120, 7770  
Ueberlingen, Federal Republic of  
Germany. Tel: (07551) 810.

Perkin-Elmer Ltd., Post Office Lane,  
Beaconsfield, Bucks HP9 1QA, England.  
Tel: Beaconsfield (049 46) 6161.

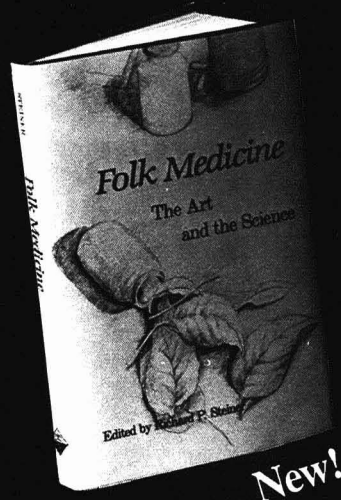


# PERKIN-ELMER



# Folk Medicine

## The Art and the Science



Richard P. Steiner, *Editor*

**Takes the mystery out of miracle cures. Explores the medical practices of nonwestern cultures to establish a scientific basis for the successes of folk remedies. Explains why western medical researchers are increasingly turning their attention to folk medicine for new drugs. Brings together work from many countries and a variety of cultures.**

### CONTENTS

Aztec Sources of Some Mexican Folk Medicine • Zuni Indian Medicine: Folklore or Pharmacology, Science or Sorcery? • Ayurveda: The Traditional Medicine of India • Fijian Medicinal Plants • Medicinal Plants of Papua New Guinea • Australian Medicinal Plants • Plants Used in African Traditional Medicine • Antithrombotic Agent of Garlic: A Lesson from 5000 Years of Folk Medicine • Scientific Basis of the Therapeutic Effects of Ginseng • Anticancer Chinese Drugs: Structure-Activity Relationships • Some Recent Biological Characterizations of Chinese Herbal Preparations • Bioactive Compounds from Three Chinese Medicinal Plants • Zingiberaceous Plants • Alkaloid Components of Zizyphus Plants

215 pages Clothbound (1985)  
LC 85-22904 ISBN 0-8412-0939-1  
US & Canada \$22.95 Export \$27.95

Order from:  
American Chemical Society  
Distribution Dept. 99  
1155 Sixteenth St., N.W.  
Washington, DC 20036  
or CALL TOLL FREE 800-424-6747  
and use your credit card!

ed by Johnson and his students at Iowa State University (20, 21) is particularly attractive for organic compounds and ions that are difficult to detect by other means. This detector makes constructive use of a long-standing enemy of electrochemists—the adsorption of organic compounds on a noble metal electrode. The PAD detects organic molecules and radicals using the faradaic signal resulting from their oxidative desorption. The separation of 13 carbohydrates on an anion exchange column with electrochemical detection is a good example of the usefulness of the PAD detector (22).

### Programming

The use of temperature programming in gas chromatography and solvent (eluent) programming in high-performance liquid chromatography (HPLC) is considered to be almost essential for resolving complex samples. The majority of ion chromatographic separations up to now, however, have been performed using isocratic elution. Maintaining a steady baseline with a conductivity detector while gradually increasing the eluent concentration has proved to be difficult.

Some success is now being achieved in suppressed anion chromatography with a basic eluent such as sodium hydroxide. The newer membrane suppressors can handle a higher concentration of sodium hydroxide (converting it to H<sub>2</sub>O) and still maintain a reasonable baseline. It is difficult, however, to prepare and maintain a solution of sodium hydroxide that is completely free of carbonate. As the programmed concentration of sodium hydroxide increases, the baseline conductance increases because of higher concentrations of carbonic acid from the eluent impurities.

Eluent programming is fairly easy in ion chromatography when the sample ions are detected by a direct method that is not affected by changes in the eluent composition. Detection of metal cations using a postcolumn reactor and spectrophotometric detector lends itself to eluent programming (9). Eluent programming has also been successful in the separation and potentiometric detection of halides and pseudohalides (23). The time required for separation of five anions was reduced from 8 min to just over 4 min by eluent programming.

### Sample pretreatment

Anions and cations can be separated and measured in extremely dilute samples, such as condensed high-purity steam and rainwater, provided a preconcentration step is included in the analytical procedure. Separation is usually accomplished by passing a relatively large aqueous sample through a

small ion exchange precolumn. Then a switching valve is turned so that the eluent sweeps the accumulated ions from the precolumn onto the separation column. Ion concentrations down to the very low parts-per-billion range can be determined by this method.

Concentration of dilute samples can also be achieved by injecting a larger than usual sample volume directly onto the separation column, but this may cause a broad dip or peak in the chromatogram as the sample plug flows through the separation column.

Organic matter in samples to be analyzed by ion chromatography may foul the column by being irreversibly adsorbed. This result can often be prevented by first passing the sample through a resin column (such as Rohm and Haas XAD-2) that adsorbs organic material and permits inorganic ions to pass through unchanged.

### Applications

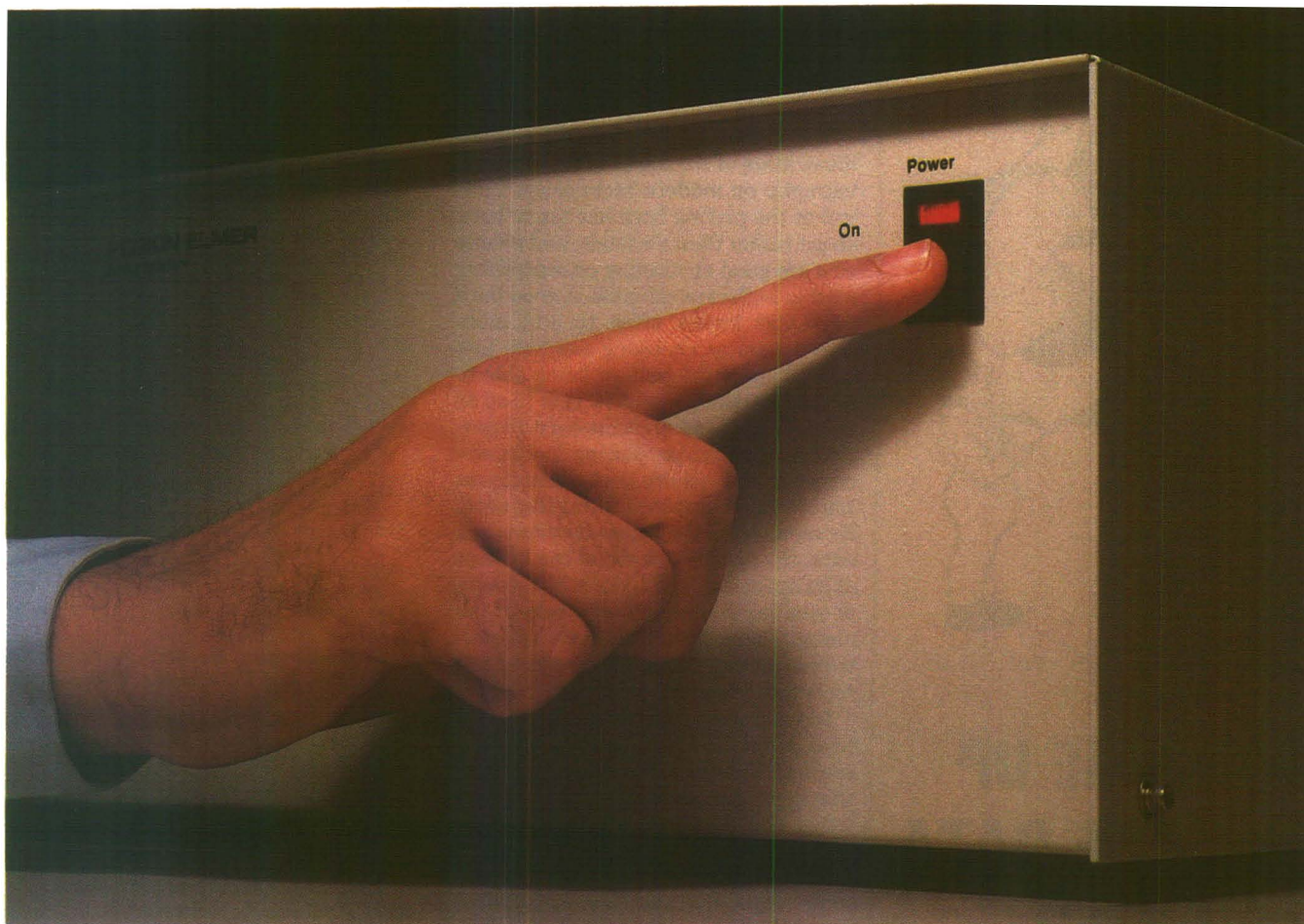
Ion chromatography is no stranger to the "real world" of chemical analysis. It is being used extensively for the determination of ions in drinking water, natural water, wastewater, air, aerosols, detergents, polymers, food and plant matter, soils, sediments, and rocks. Ion chromatography is also used in clinical analysis and in industries such as pharmaceuticals, pulp and paper, and metal plating, to name just a few.

One reason for such popularity is that the technique is rapid and easy to perform. Analysis takes only a few minutes, even for complex samples, and several ions can usually be determined in each chromatogram. Sample preparation is usually simple—just "dilute and shoot." Before ion chromatography, determination of ions sometimes took hours for each sample, and usually only one ion could be measured at a time.

Another point worth mentioning is that ion chromatography has brought ion analysis to the "masses"—to people who previously had no other methods for measuring ions. One example is its use in studies on acid rain. There are two problems here: Ion concentrations in the samples are often so low that a very sensitive analytical method must be used, and analysis of a large number of samples is usually necessary. With ion chromatography, samples can be concentrated in the field using small ion exchange cartridges. Later, a cartridge can be placed in the injection valve of an ion chromatograph, and a chromatogram of the sample can be generated.

In power plants it was impossible to measure chloride in water at low concentration levels before ion chromatography came into use. Because the levels of chloride in the boiler were not known, the harmfulness of corrosive





## Here's all you need to do to get our robotics system to work.

Because we will do the rest.

First, our robotics specialist analyzes your lab to determine how the MasterLab™ Robotics System can help you the most. We draw on our extensive background in analytical chemistry and our familiarity with your applications to custom design a system for your lab.

### **It works for us before it works for you.**

When your application has been determined, we can set up a system in our lab and program it to work just as if it were in your lab. Most of the programming and adjusting can be completed at this stage.

Once the system is running as planned, we ship it to your lab. There, our field engineer installs the system and makes any necessary minor adjustments. Our engineer will

even turn it on for you, if you wish.

### **Count on our continuing support.**

Following installation, a systems analyst specializing in robotics will continue working with you until you're totally comfortable and satisfied with all aspects of the system.

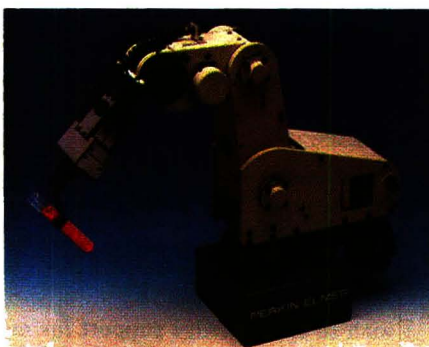
The MasterLab System can be easily programmed for a wide range of lab

applications. Today, MasterLab Systems are working around the clock — and around the world — with materials as diverse as cancer drugs and rocket fuels. And new applications for the MasterLab System are being developed all the time.

Our people will continue to work with you to develop new applications as you need them.

Get in touch with the MasterLab System today. Contact your local Perkin-Elmer representative. Or in the U.S., use our special robot hotline: 1-800-ROBOT-PE.

Perkin-Elmer Corp., 761 Main Ave., Norwalk, CT 06859-0012 U.S.A.  
Tel: (203) 762-1000. Telex 965-954.  
Bodenseewerk Perkin-Elmer & Co., GmbH, Postfach 1120, 7770 Ueberlingen, Federal Republic of Germany. Tel: (07551) 810.  
Perkin-Elmer Ltd., Post Office Lane, Beaconsfield, Bucks HP9 1QA, England. Tel: Beaconsfield (049 46) 6161.



# PERKIN-ELMER

CIRCLE 126 ON READER SERVICE CARD





## CONJURE UP ALL THE DATA YOU NEED

If you need information about laboratory instruments, equipment, apparatus, or supplies, you've come to the right one-stop genie: *Analytical Chemistry*.

Here, you'll find ads from just about everyone you need product data from. And most of the ads have a key number at the bottom.

Simply circle on one of our reader service reply cards those key numbers that pertain to the advertised products on which you need more information.

And, presto. Like magic, the data you need will be spirited to you at no charge or obligation.

**Analytical**  
CHEMISTRY

chloride was also not known for a while. A good quality-control program on boiler water now includes a chloride determination.

The metal plating industry is a good illustration of the effect of ion chromatography on modern technology. Control of the plating bath has really been an art rather than a science, and people who are good at running or controlling plating baths are valuable. A good bath controller knows when to add more brighteners or chelating reagents just by looking at the bath or being able to sense something about it. It is hard to transfer this kind of technology. In particular, electroless plating baths are complex and require periodic analysis. Ion chromatography is filling this need. By monitoring the key components of a bath, the plating of a metal can be kept at its optimum, and there is less chance of spoiling a product. The role of ion chromatography in the analysis of electroless plating baths was discussed in a recent article (24).

Ion chromatography is also saving time, effort, and money in the pharmaceutical industry. Although it is true that many pharmaceutical analyses involve the determination of organic chemicals by gas or liquid chromatography, a number of the more burdensome (expensive and time-consuming) determinations deal with ionic-inorganic components. Here are some examples:

- High-purity water is needed for pharmaceutical processing. Concentrations of common ionic impurities can be checked quickly by ion chromatography.
- Impurities in raw materials, such as iodide in sodium chloride USP and chloride in boric acid, can be determined.
- Dosage-form assay, such as hydrochloride salts of amine drugs and sodium or ethanolamine salts of acids, can be determined.
- Fluoride (used as a preservative for forensic specimens) in serum can be determined by ion-exclusion chromatography.
- Fluoride in mouthwash and monofluorophosphate in toothpaste is easily determined by SCIC.

### Literature

Several recent books (25, 26) and review articles (27, 28) on ion chromatography are available.

### Acknowledgment

I wish to acknowledge support for my research in ion chromatography by the U.S. Department of Energy under Contract No. W-7405-ENG-85. I also thank Doug Gjerde for his comments and information relating to applications of ion chromatography.

### References

- (1) Small, H.; Stevens, T. S.; Bauman, W. C. *Anal. Chem.* 1975, 47, 1801.
- (2) Stillian, J. *LC Magazine*, 1985, 3, 802.
- (3) Gjerde, D. T.; Fritz, J. S.; Schmuckler, G. *J. Chromatogr.* 1979, 186, 509.
- (4) Gjerde, D. T.; Schmuckler, G.; Fritz, J. S. *J. Chromatogr.* 1980, 186, 509.
- (5) Fritz, J. S.; Gjerde, D. T.; Becker, R. M. *Anal. Chem.* 1980, 52, 1519.
- (6) Fritz, J. S.; DuVal, D. L.; Barron, R. E. *Anal. Chem.* 1984, 56, 1177.
- (7) Sevenich, G. J.; Fritz, J. S. *Anal. Chem.* 1983, 55, 12.
- (8) Sevenich, G. J.; Fritz, J. S. *J. Chromatogr.* 1985, 347, 147.
- (9) Iskandarini, Z.; Pietrzyk, D. J. *Anal. Chem.* 1982, 54, 2427.
- (10) Knight, C. H.; Cassidy, R. M.; Recoskie, B. M.; Green, L. W. *Anal. Chem.* 1984, 56, 474.
- (11) Tanaka, K.; Fritz, J. S. *J. Chromatogr.* 1986, 361, 151.
- (12) Barron, R. E.; Fritz, J. S. *J. Chromatogr.* 1984, 24, 13.
- (13) Elchuk, S.; Cassidy, R. M. *Anal. Chem.* 1979, 51, 1434.
- (14) Schmitt, G. L.; Pietrzyk, D. J. *Anal. Chem.* 1985, 57, 2247.
- (15) Denkert, M.; Hackzell, L.; Schill, G.; Sjogren, E. *J. Chromatogr.* 1981, 218, 31.
- (16) Small, H.; Miller, T. E., Jr. *Anal. Chem.* 1982, 54, 462.
- (17) Mho, S.; Yeung, E. S. *Anal. Chem.* 1985, 57, 2253.
- (18) Warth, L.; Fritz, J. S.; unpublished work, 1986.
- (19) Haddad, P. R.; Heckenberg, A. L. *J. Chromatogr.* 1982, 252, 177.
- (20) Hughes, S.; Meschi, P. L.; Johnson, D. C. *Anal. Chim. Acta* 1981, 132, 1.
- (21) Hughes, S.; Johnson, D. C. *Anal. Chim. Acta* 1981, 132, 11.
- (22) Johnson, D. C. *Nature* 1986, 321, 481.
- (23) Lockridge, J. E.; Fortier, N. E.; Schmuckler, G.; Fritz, J. S., submitted for publication in *Anal. Chim. Acta*.
- (24) Barthel, P. J., Jr. *Metal Finishing* 1986 (March).
- (25) Smith, F. C., Jr.; Chang, R. C. *The Practice of Ion Chromatography*; Wiley-Interscience: New York, 1983.
- (26) Gjerde, D. T.; Fritz, J. S. *Ion Chromatography*, 2nd ed.; Huthig: Heidelberg, 1987.
- (27) Haddad, P. R.; Heckenberg, A. L. *J. Chromatogr.* 1984, 300, 357.
- (28) Fritz, J. S. *LC Magazine* 1984, 2, 446.



James Fritz is a professor of chemistry at Iowa State University and a senior chemist at Ames Laboratory (U.S. Department of Energy). He received his B.S. degree from James Millikin University and his Ph.D. from the University of Illinois. His research interests include various types of separations, especially chromatography.



# NESLAB REPLACES DRY ICE



Now you can do away with the hassle, storage and handling problems associated with dry ice and liquid nitrogen cooling. NESLAB Cryocool refrigeration systems provide constant temperatures over a range of  $-25^{\circ}\text{C}$  to  $-100^{\circ}\text{C}$  continuously, without monitoring. Ideal for specimen freezing, shell freezing, lyophilization, diffusion pump trapping, solvent trapping. NESLAB immersion coolers save you time and eliminate the cost of dry ice and liquid nitrogen. Average payback is one year. For application information, contact our technical staff. Toll Free Direct 1-800-258-0830.



Send for 72-page catalog, and the location of the NESLAB Sales and Service Center nearest you.

**HEADQUARTERS:** NESLAB Instruments, Inc. P.O. Box 1178 Portsmouth, NH 03801 Tel. 603-436-9444. Telex 940830

CIRCLE 107 ON READER SERVICE CARD

## Fifth International Symposium on Laboratory Robotics - 1987 October 18-21, 1987 Boston, MA

Chairpersons:  
Gerald L. Hawk, Ph.D.  
Janet R. Strimaitis

Zymark Corporation  
Zymark Center, Hopkinton, MA 01748  
(617) 435-9501

## CALL FOR PAPERS *Deadline: April 1, 1987*

If you would like to make a presentation, please send an abstract of 500 words or less by April 1st to the chairpersons. The program will include over 60 Technical presentations illustrated by slides and video tapes. A proceedings of the Symposium will be published.

Application of Laboratory Robotics include the following areas:

- BIOCHEMISTRY • RADIOCHEMISTRY • ELEMENTAL ANALYSIS • METHODS DEVELOPMENT**
- PHARMACEUTICAL ANALYSIS • ROBOTIC IMPLEMENTATION STRATEGIES • ANALYTICAL CHEMISTRY**
- MATERIALS TESTING • BIOTECHNOLOGY • MICROBIOLOGY**

Preliminary program request:



\_\_\_\_\_ Please send me a copy of the ISLR '87 preliminary program.

Attach business card or complete coupon.

AC

Name \_\_\_\_\_

Address \_\_\_\_\_

City \_\_\_\_\_ State \_\_\_\_\_ Zip \_\_\_\_\_

Telephone (\_\_\_\_) \_\_\_\_\_

Mail to: ISLR '87, Zymark Corporation, Zymark Center, Hopkinton, MA 01748

CIRCLE 181 ON READER SERVICE CARD



# Your key to MS-MS...VG 70-250SQ

We've designed the mass spectrometer to be a fully automated system that can operate with maximum reliability in either a research or routine environment.

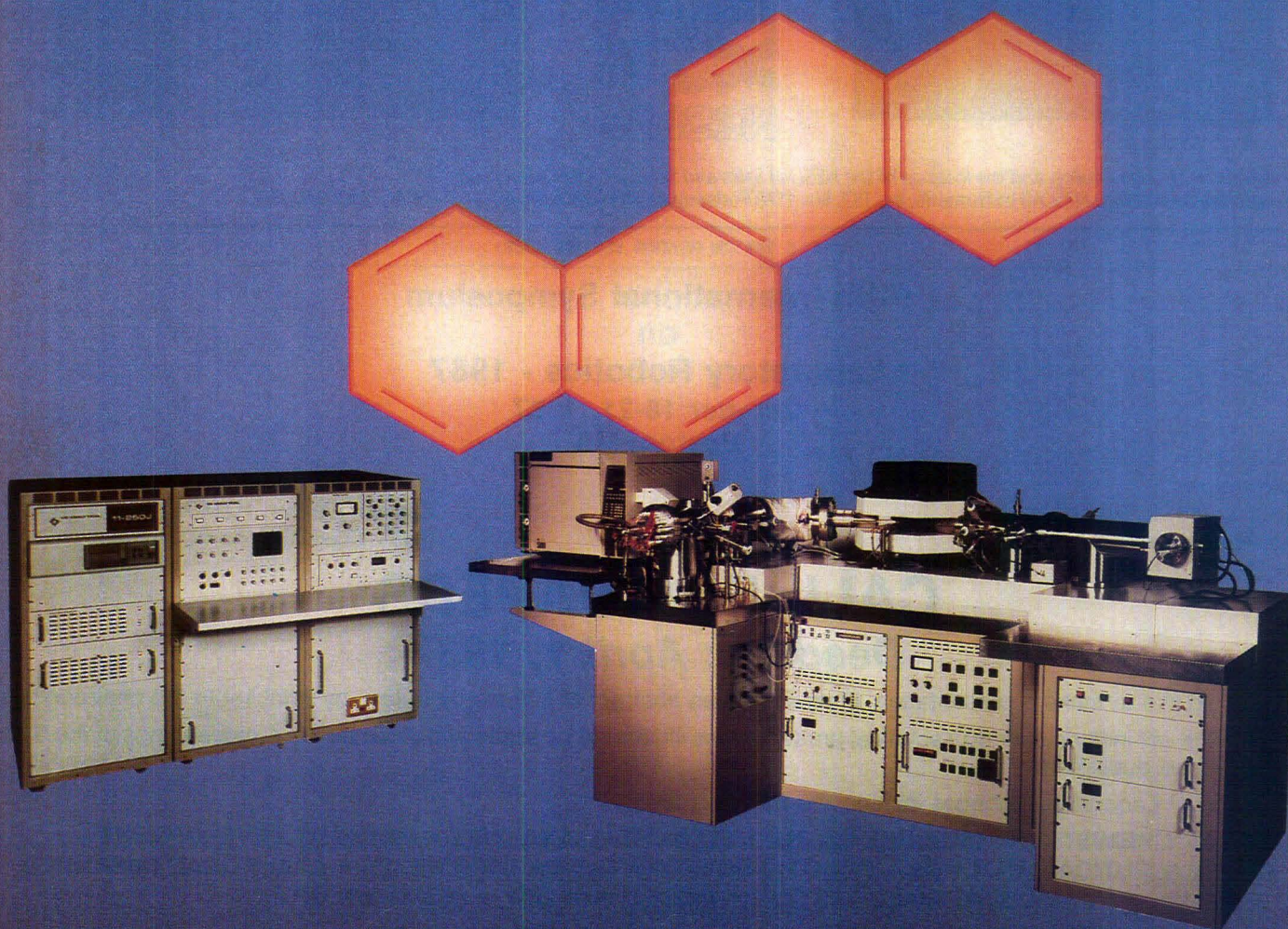
The VG 70-250SQ, with its high primary ion selectivity, good daughter ion efficiency and resolution gives the user a

powerful tool for mixture analysis and structural elucidation.

For trace level GC-MS-MS experiments the combination of selected reaction monitoring techniques with either high or low parent ion resolution enhances both selectivity and sensitivity.

Our extensive experience in MS-MS has enabled VG to use the latest digital electronic computer technology to put routine tune-up procedures, data acquisition and processing at your fingertips.

With the 70-250SQ you get MS-MS at the touch of a key.



**VG INSTRUMENTS**  
Organic mass spectrometry

A VG INSTRUMENTS GROUP COMPANY

USA: VG Instruments Inc., 300 Broad Street, Stamford, CT 06901. Tel. (203) 322-4546.  
VG Analytical Ltd., Flocks Road, Wythenshawe, Manchester M23 9LE. Tel. 061-945 4170.  
WEST GERMANY: VG Instruments GmbH, Gustav-Nachtigal-Strasse 4, 6200, Wiesbaden. Tel. (6121) 713030.  
FRANCE: VG Instruments, 3 Rue du Marechal de Lattre de Tassigny, 78150 Le Chesnay. Tel. (1) 3955 5120.  
ITALY: VG Instruments Limited, Viale Dell'Assunta 101, 20063 Cernusco Sul Naviglio, Milano. Tel. (2) 924 8808.  
THE NETHERLANDS: VG Instruments bv, PO Box 171, 1380 AD Weesp. Tel. (2940) 80484.  
CHINA: VG Instruments, Room 7059, Xi Yuan Hotel, Erilgou Xijiao, Beijing. Tel. 890721 Ext 759.  
HONG KONG: VG Instruments Asia Limited, GPO Box 217, Hong Kong. Tel. (5) 8613651.  
JAPAN: Jasco International Co. Ltd, 2-4-21, Sennin-cho, Hachioji City, Tokyo 193. Tel. (426) 661321.

Circle 170 for literature. Circle 171 to have sales representative contact you.  
See us at the Pittsburgh Conference Booth #844-851.



# Electroanalytical Chemistry

## Allen Bard discusses past successes and future promises

Electroanalytical chemistry has come a long way from the polarographic era, when most work involved aqueous solutions and mercury electrodes. During the 1960s and 1970s, new technology was introduced that included the incorporation of operational amplifiers and computers into electrochemical instrumentation, an expansion into non-aqueous solvents such as dimethylformamide and acetonitrile, and greater use of solid electrodes made of gold, platinum, and carbon. More recently, exotic solvents such as liquid ammonia have been brought into the fold, and development has proceeded apace on microelectrodes and on new types of semiconductor and chemically modified electrodes.

Nevertheless, many of the most significant electroanalytical advances may still lie ahead, according to Allen J. Bard of the University of Texas at Austin. Listening to Bard's presentation at the Eastern Analytical Symposium last November, one could not help but come away with the impression that electroanalytical chemistry may be entering the most exciting era in its history. It is an era in which we will see electrochemistry in the gas and solid phases, electrochemical resolution on the order of angstroms (scanning tunneling electrochemistry), and electrochemical expert systems.

The symposium honored George H. Morrison of Cornell University and Editor of *ANALYTICAL CHEMISTRY*, who received the first EAS Award for Outstanding Achievements in the Fields of Analytical Chemistry. Peter Keliher of Villanova University organized the symposium. Co-chairs were Tom Isenhour of Utah State University (Logan) and Andrew T. Kashuba of Teepac (Danville, Ill.).

### Ultramicroelectrodes

An area of electroanalytical chemistry that has already seen considerable development is ultramicroelectrode tech-

nology. Ultramicroelectrodes, which are constructed by sealing very small wirelike strands of gold, platinum, or carbon in glass or epoxy, are interesting for a number of reasons, according to Bard. For example, as an electrode is downsized, diffusion of species to the electrode surface becomes increasingly spherical—that is, material approaches the electrode from all sides, tending to increase the mass transfer rate tremendously (see Wightman, R. Mark, *Anal. Chem.* 1981, 53, 1125–34 A). The mass transfer rate to the surface of a 5- $\mu$ m diameter electrode is approximately equivalent to that associated with a rotating disk electrode at 10,000 revolutions per second, which represents a very highly stirred solution. High mass transfer rates such as these make it possible to do experiments involving shorter time scales and faster kinetics.

Ultramicroelectrode currents are sufficiently small—in the nA or sub-nA range—that it is possible to work in highly resistive solutions that would normally develop large  $iR$  drops, which distort the electrochemical response. Lower  $RC$  time constants at the ultramicroelectrode – solution interface permit high scan rates, up to 1000 V/s in highly resistive solutions (Howell, J. O. and Wightman, R. M., *J. Phys. Chem.* 1984, 88, 3915–18).

In addition, the advent of ultramicroelectrodes is making it possible to achieve improved time resolution. "As I shrink my electrode dimensions down, I shrink time down in the same way," said Bard. "A 1000 V/s scan rate really is putting us in the sub-microsecond region, and I think that is a direction in which electrochemistry has to go. There has only been a little bit of electrochemistry in the microsecond region, whereas spectroscopy is already being done in the femtosecond range."

### New solvents and phases

Considerable progress is also expected in the development of gas- and solid-

phase electrochemistry, an exciting new departure in view of the longtime restriction of electroanalytical chemistry to work in the liquid phase.

Solid-phase electrochemistry has already been demonstrated by Ulrich Stimming and Wolfgang Schmickler (*J. Electroanal. Chem.* 1983, 150, 125–31), who performed a ferric-ferrous reduction in 5M perchloric acid ice. In a paper by A. M. Bond, M. Fleischmann, and J. Robinson (*J. Electroanal. Chem.* 1984, 180, 257), electrochemistry was done at platinum microelectrodes in nonaqueous solvent glasses.

Recent work in the gas phase includes a paper from Stanley Pons's group (*Anal. Chem.* 1986, 58, 2278–82) in which ultramicroelectrodes were used for the detection of analytes in the gas-phase effluent of a gas chromatograph. Another example is a recent paper by Royce Murray's group (*J. Am. Chem. Soc.* 1985, 107, 2824–26) in which a polymeric layer in a sandwich electrode underwent oxidation and re-

“The future still lies in the minds of its practitioners”



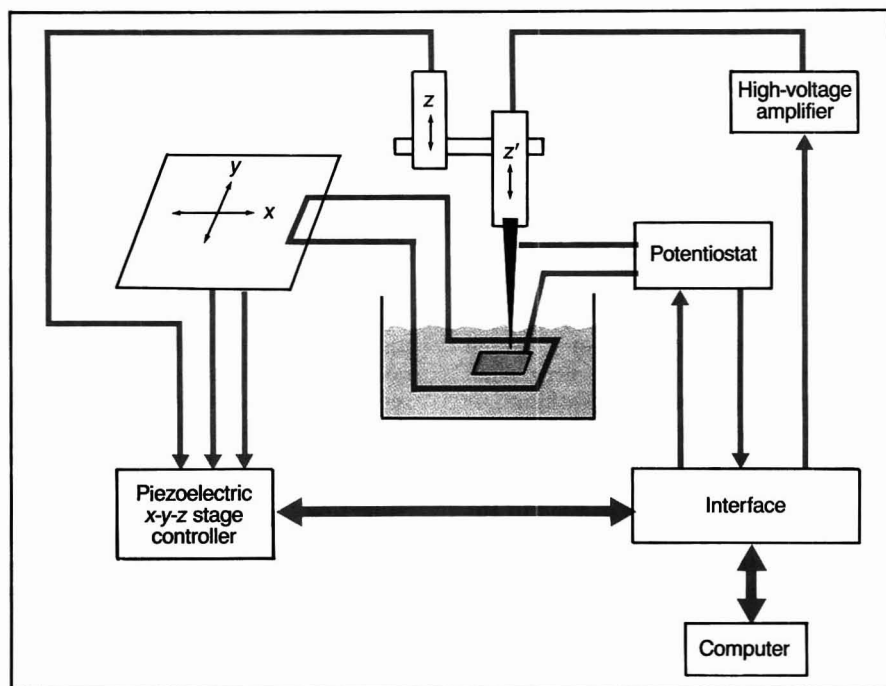
duction when an adjacent layer was exposed to acetonitrile vapor or dry nitrogen gas.

In addition to research on new phases, progress will continue in the extension of electrochemistry to new solvents. Recent promising investigations have centered around the use of freon, hexane, toluene, and various near-critical and supercritical fluids.

### Scanning tunneling electrochemistry

A new frontier for electrochemistry involves an electrochemical version of scanning tunneling microscopy (STM), the technology that recently won a Nobel prize for its developers. In STM, a





**Figure 1.** Design for a scanning electrochemical microscope (Liu, H.-Y.; Fan, F.-R.F.; Lin, Charles W.; Bard, A.J. *J. Am. Chem. Soc.* **1986**, *108*, 3838-39). The substrate is green in the figure.

needle tip sharpened to atomic dimensions is brought close to a conducting surface so that there is an overlap of

electron density distributions between the tip and the surface, permitting a current of electrons to tunnel across

the gap. As the tip is rastered over the surface, the current can be maintained at a constant level by moving the needle up and down to maintain a constant distance. The movement of this needle, which is controlled by a piezoelectric device, results in an atomic-resolution trace of the surface.

"This same technique should be applicable to the solid-solution interface," Bard explained. "We've built an apparatus to do this [Figure 1] in which the STM tip, immersed in solution, is used as one electrode, with the substrate serving as a second electrode." Movement of the STM tip in the  $z$  direction in response to perceived variations in the current serves to generate an electrochemical image of the substrate as it is moved in the  $xy$  plane by a piezoelectric controller.

The electrochemical STM technique is done at lower resolution than conventional STM. "For chemists there may be more interest in low resolution than high resolution," said Bard. "It's very nice to look at individual atoms tunneling 10 angstroms across the surface, but sometimes you want to find a micron-size spot and go back and look at it by scanning electrochemical spectroscopy. Now you can't tunnel any more because you have to move your tip further back. You are really doing electrochemistry at short distances.

"I think this is a coming technique," Bard continued. "We don't have any interesting chemical information yet, I'm afraid—it's fairly new. But I think this is a technique that will be useful in really looking at surfaces in situ."

## Sensors

Bard predicts that the development of new electrochemical sensor technologies based on microelectrode arrays, modified electrode surfaces, and solid-state devices will continue to progress over the next few years. Although research into sensors is proceeding in a number of interesting directions, Bard drew particular attention to the work of Mark Wrighton and his co-workers at the Massachusetts Institute of Technology. They are using microelectronics technology to deposit selective polymers of various types over small micron-size electrodes on silicon substrates (Figure 2). "The hardest part of this whole sensor game, as far as I'm concerned," said Bard, "is in the nature of the polymer layer. To get the selectivity and the sensitivity one needs, there's a lot of chemistry that's going to have to go into that layer.

"The basic idea is that one can put on a polymer, for example, that doesn't conduct in its reduced state," Bard continued. "When the polymer is in the

# New HPLC Autosampler



## Highest reliability and precision

- RS-232-C standard
- Requires no auxiliary gas
- Works with any HPLC system
- Interfaces with any valve

Micromeritics' new Model 728 Autosampler uses a patented positive displacement sampling technique to eliminate the need for an auxiliary gas supply. It provides the highest reliability and precision on the market at the lowest cost, using state-of-the-art microcomputer technology.

**micromeritics®**

One Micromeritics Drive, Norcross, GA 30093-1877, Telephone: (404) 662-3669

CIRCLE 98 ON READER SERVICE CARD





## Discover the new TSQ 70. Discover a new MS/MS.

It's a whole new generation in triple-stage quadrupole mass spectrometry, built upon experience gained from 60 successful installations. Much more powerful. Far easier to use. Unusually versatile. And surprisingly affordable.

Start with our mass range (2000 extendable to 4000), and marvel at the detection limit. Novel ion optics (patent applied for) minimizes neutral noise associated with soft ionization techniques such as thermospray and fast atom bombardment.

Discover our expert system approach to instrument control and user interaction. Dynamic adjustment of instrument parameters in real time gives you control over an inherently complex and sophisticated technique. A proprietary Instrument Control Language (ICL) makes it easy to create, optimize and duplicate your MS/MS experiments.

Discover the vacuum cradle. There isn't an inlet system it won't accept. It's that versatile.

The TSQ 70. For MS/MS at the price of MS, ask your Finnigan MAT representative.

Finnigan MAT did it.  
Again.

See us at Booth No. 2044,  
Pittsburgh Conference.

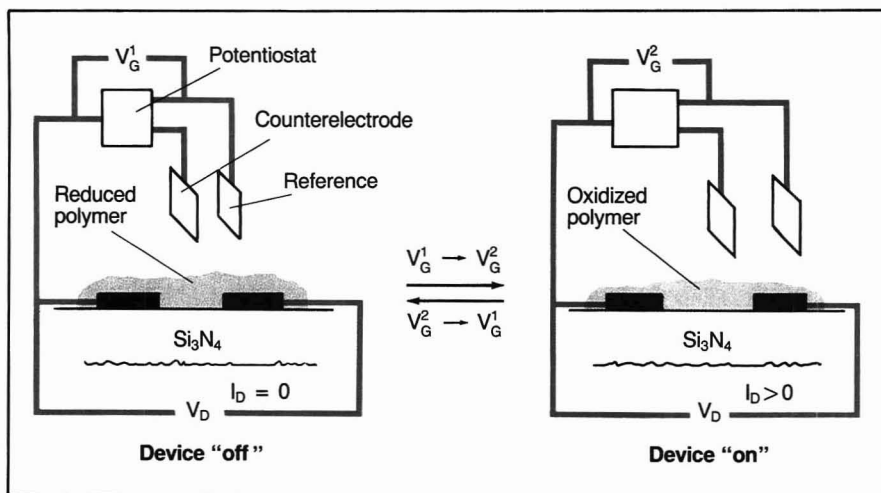


U.S.A., 355 River Oaks Parkway, San Jose, CA 95134. (408) 433-4800  
Germany, Postfach 14 40 62, D-2800 Bremen 14. (0421) 54 93-0  
U.K., Paradise, Hemel Hempstead, Herts HP2 4TG. (0442) 4 04 91  
France, 69 rue de Paris, F-91400, Orsay. (1) 69 28 52 53  
Benelux, Landjuweel 7, 3906 PE Veenendaal. 08385 27266  
Italy, Via Valadier, 37B, 00193 Rome. (06) 316000  
Japan, Shiozaki Bldg., 2-7-1 Hirakawa-cho, Chiyoda-ku, Tokyo 102. (03) 221-1001

Circle 50 for literature.

Circle 51 to have a representative contact you.





**Figure 2.** Selective polymer sensor developed by E. P. Lofton, J. W. Thackeray, and Mark S. Wrighton (*J. Phys. Chem.* **1986**, *90*, 6080-83).

In analogy to a field effect transistor,  $V_G$  = gate potential,  $V_D$  = drain potential, and  $I_D$  = drain current.

oxidized state it's either electronically or ionically conductive and a current will flow. The amount of charge it takes to switch this on and off is very small. Wrighton points out that it's an electrochemical analogue of a field effect transistor. You can think of one electrode as the source, one electrode as the drain, and the chemistry at the poly-

mer as the gate. By making very thin layers of this material one can get very sensitive sensors."

### Cybernetic electrochemistry

The state of the art of cybernetic electrochemistry is based on work done by Larry Faulkner and his co-workers, who developed a digital instrument

with built-in instructions to control the electrochemical repertoire and interpret the data (He, Peixin et al. *Anal. Chem.* **1982**, *54*, 1313-26 A). But Bard explained that "the loop hasn't really been closed yet, and I think it will be closed. Closing the loop means feeding the data to a computer that's attached to the instrument through a communications port and then having a resident expert system analyze the data. Then the expert system will close the loop by saying, 'The conclusion from the first experiment indicates that another experiment should be done.' System control will then return to the cell, the next experiment will be done, and the data will be reanalyzed. You let this cycle around until it's happy and it tells an observer what the answers are.

"But my own feeling is that the human being is still the most important part of the system," he continued. "If we look at the history of electroanalytical chemistry, I think the blessing has not been in the instrumentation. The instrumentation has helped a lot, but it's really the great ideas and the people who implement them that have made it such a productive field, and I think the future still lies in the minds of its practitioners." *Stu Borman*

## Mettler takes the hassle out of density measurement.



DMA45 with optional sample changer.

CIRCLE 97 ON READER SERVICE CARD

Mettler/Paar density meters provide reproducible, accurate density measurements without pycnometers or hydrometers—usually in less than three minutes. And Mettler/Paar density meters are so easy to use that no special training or skills are required.

### Results in units you prefer.

Obtain results that can be used immediately, such as g/cm<sup>3</sup>, °Brix, specific gravity, API number, % alcohol, % concentration, or dimensionless engineering units. Results can be transmitted directly to your computer for storage or analytical calculations.

### Flexible and versatile.

Check incoming and finished goods samples. Improve cost controls by ensuring that components are mixed in exactly the right ratio, and even standardize the quality control procedures for all lab and plant locations.

### Choose exactly what you need.

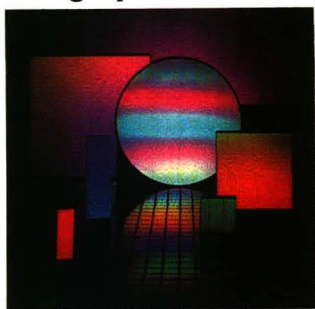
You can select from a complete line of Mettler/Paar density meters, including hand-held field units precise to 10<sup>-3</sup> g/cm<sup>3</sup>, laboratory models with precisions of 10<sup>-4</sup> to 10<sup>-6</sup> g/cm<sup>3</sup>, and in-line process control models with a precision of 10<sup>-5</sup> g/cm<sup>3</sup>.

Let Mettler take the hassle out of density measurement for you. Call 1-800-257-9535; in NJ, (609) 448-3000. Or write to Mettler Instrument Corporation, Box 71, Hightstown, NJ 08520 for complete technical details and pricing.

**Mettler**



## Diffraction Gratings Ruled and Holographic



The finest classically ruled and holographic gratings for research quality monochromators and spectrographs are available from Instruments SA. Plano gratings range in size from 12 x 12 to 120 x 140 mm with groove densities up to 3600 g/mm.

For OEM customers, blazed aberration corrected holographic gratings may greatly simplify and reduce the cost of traditional designs. Typical uses include blood analyzers, LC Detectors, lasers, and spectrophotometers. For further information contact Jobin Yvon/Instruments SA.

(201) 494-8660  
CIRCLE 73

## Versatile Monochromator/ Spectrograph System

This monochromator offers dual entrance and exit ports to allow the user to set up two or more experiments simultaneously.

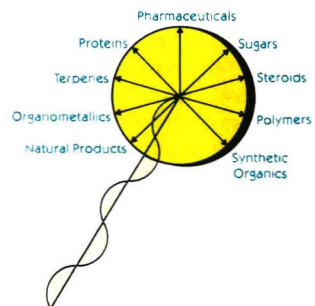


The instrument can be configured to present a 25mm flat field to a multichannel detector, with the capability to be used as a scanning monochromator as well. Instruments SA can provide gratings optimized for specific applications. For further information contact Jobin Yvon/Instruments SA.

(201) 494-8660  
CIRCLE 74

## Circular Dichroism R&D, Q.C., Q.A.

The Mark V CD Spectrometer shows outstanding performance in the U.V., down to 180nm. This is most important for those studying amino acids, proteins, hormones and DNA/RNA. The Mark V is fully computer controlled and includes an advanced, proven software package.

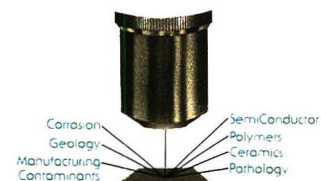


C.D., L.D., and or O.R.D. can solve your problems. Perform conformational, optical purity, and enantiomeric purity analyses under computer control. For further information contact Jobin Yvon/Instruments SA.

(201) 494-8660  
CIRCLE 75

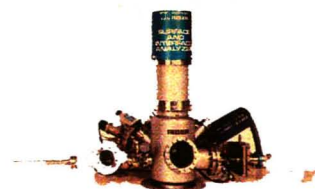
## MOLE® Molecular and Crystalline Characterization

The MOLE® Molecular Microprobe provides the capability for contaminant identification and device materials characterization by fingerprinting molecular composition and crystalline species.



Spatial resolution is 1µm and sample preparation requirements are identical to those for optical microscopy. Transparent substrates are not required. For further information contact Jobin Yvon/Instruments SA.

(201) 494-8660  
CIRCLE 77



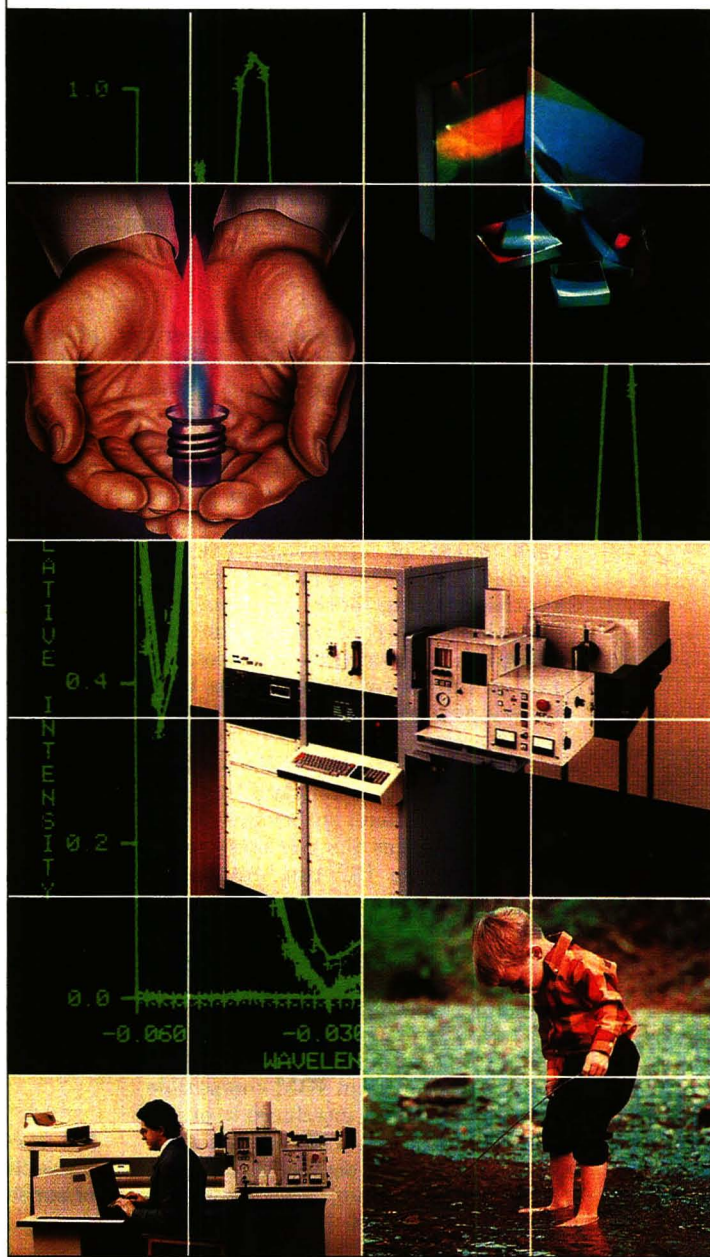
## SIA 200, Surface and Interface Analyzer

Winner of the 1985 IR-100 Award, the Riber SIA 200 combines ease of operation with the ability to perform high quality Auger, XPS, and ELS using a single analyzer optimized for these techniques. This powerful new analysis tool is the result of CAD and extensive prototype testing.

Features include: excellent energy resolution, insensitivity to sample positioning ( $\pm 5$ mm), rapid analysis (10 min. per sample), ease of selection between XPS, Auger and ELS spectrometries, ability to perform angle-resolved XPS, optional processing accessories, and excellent cost/benefit ratio. For further information contact Riber Division of Instruments SA.

(201) 494-8660  
CIRCLE 78

## ICP Emission Spectrometers



## The Finest ICP Systems Begin with The Finest Optics

That's why our instruments and diffraction gratings are used in everything from ozone monitoring satellites to laser isotope separation, synchrotron radiation... even the high resolution spectrograph of the Space Telescope. If you need *genuine* high performance at reasonable cost, Jobin Yvon/Instruments SA offers you a choice of emission spectrometers.

The JY 38 Plus Sequential ICP for the ultimate in flexibility. Our JY 32P for the Simultaneous ICP analysis of up to 40 elements — ideal for high sample throughput and low sample volume. And the JY-70 Combination for the very best of both worlds. Spark and Glow Discharge Spectroanalyzers for metal alloy and super alloy analysis with highest precision and linearity. Jobin Yvon/Instruments SA offers you a choice!

For further information contact Instruments SA, Inc., 173 Essex Ave., Metuchen, N.J. 08840 201/494-8660. Telex 844-516. In Europe, Jobin Yvon, Division d'Instruments SA, 16-18 Rue du Canal, 91160 Longjumeau, France, Tel. 909.34.93, Telex JOBYVON 692882.

(201) 494-8660  
CIRCLE 79

**JY**  
JOBIN  
YVON  
Instruments SA, Inc.  
J-Y Optical Systems Division  
EXCELLENCE IN OPTICS

See us at the Pittsburgh Conference, Booths #9044-10049.

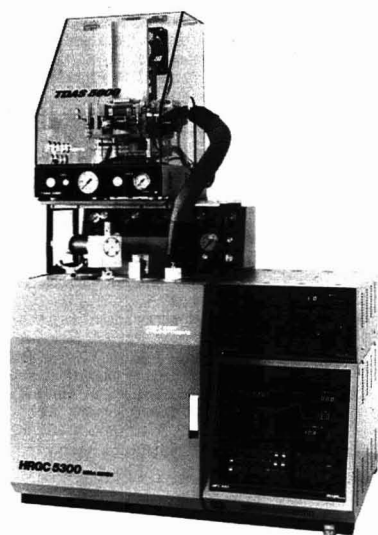


# NEW PRODUCTS

**GC detector.** HP 19256A flame photometric detector provides selective detection of sulfur and phosphorus compounds by burning them in a hydrogen flame and then measuring the emitted light with a photomultiplier tube. It is compatible with both packed and capillary columns and features a fused silica transfer line and a stainless steel burner. Hewlett-Packard 403

**TLC/FT-IR.** Chromalect sample transfer system allows separation of nonvolatile compounds followed by FT-IR identification. The complete system includes a computer-controlled stage, narrow band cadmium telluride detector, a development tank, TLC plates, transfer assembly, two strips, and ground glass. Analect Instruments 404

**Photomicroscope.** Axlophot, intended for use in materials testing and materials science applications, features Infinity Color Corrected optics that provide flat images over a wide field of view and a system-integrated design that permits integration of compo-



**TDAS 5000,** a thermal desorption accessory designed for determination of trace organics in environmental monitoring, forensic science, and the food industry, features rapid desorption, an inert low-volume interface, and an optional automatic cold trap sample concentrator. Haake Buchler Instruments 401



**LC/9570 programmable diode array detector** features single- or dual-wavelength monitoring, time-programmable wavelengths, and absorbance ratioing. Up to nine spectra can be collected per run, and an auto-store function detects emerging peaks and stores the spectrum when the peak maximum occurs. IBM Instruments 402

nents for illuminating and contrast-enhancing techniques, including bright-field and darkfield. Carl Zeiss 405

**DNA synthesis.** Cyclone bench-top automated DNA synthesizer has an easy-to-read CRT display that guides even the inexperienced user through each phase of operation. Preprogrammed memory cartridges permit synthesis using both  $\beta$ -cyanoethyl phosphoramidite chemistry and  $H$ -phosphonate synthesis protocols as well as future methodologies as they become available. Biosearch 406

**Ion trap detector.** Model 800 ion trap detector provides lower detection limits than other mass spectrometric detectors and scans the full mass range throughout the GC run. Automatic gain control software continuously adjusts the detector's operating parameters based on the amount of sample eluting from the GC column into the detector. Finnegan MAT 407

**Weighing system.** The Better Weigh, which consists of an IBM-compatible personal computer interfaced to one or more digital scales, is intended to automate the manual weighing of formulas, batches, and recipes. Scale capacities from 300 g to 5000 lbs are available,

along with optional bar-code reading equipment for ingredient identification. Eastern Scientific 408

**Gas chromatograph.** Model 3600 gas chromatograph, designed for research and methods development laboratories, features a large oven to accommodate extra columns, integrated data handling, a wide range of available injectors, and self-diagnostics. A variety of detectors, including FID, ECD, TCD, TSD, FPD, PID, and HECD, are available, and up to five detectors can be mounted on the gas chromatograph at a time. Varian 409

**Electrode.** Model S925CD combination pH electrode is designed to provide fast, accurate pH measurements for gel electrophoresis and isoelectric focusing. It has a 2.5-mm flat sensing surface and can be easily positioned at the location of interest. A sealed, double-junction reference electrode with a peripheral porous polyethylene junction is built into the system. Sensesorex 410

**For more information on listed items, circle the appropriate numbers on one of our Readers' Service Cards**



# Productivity

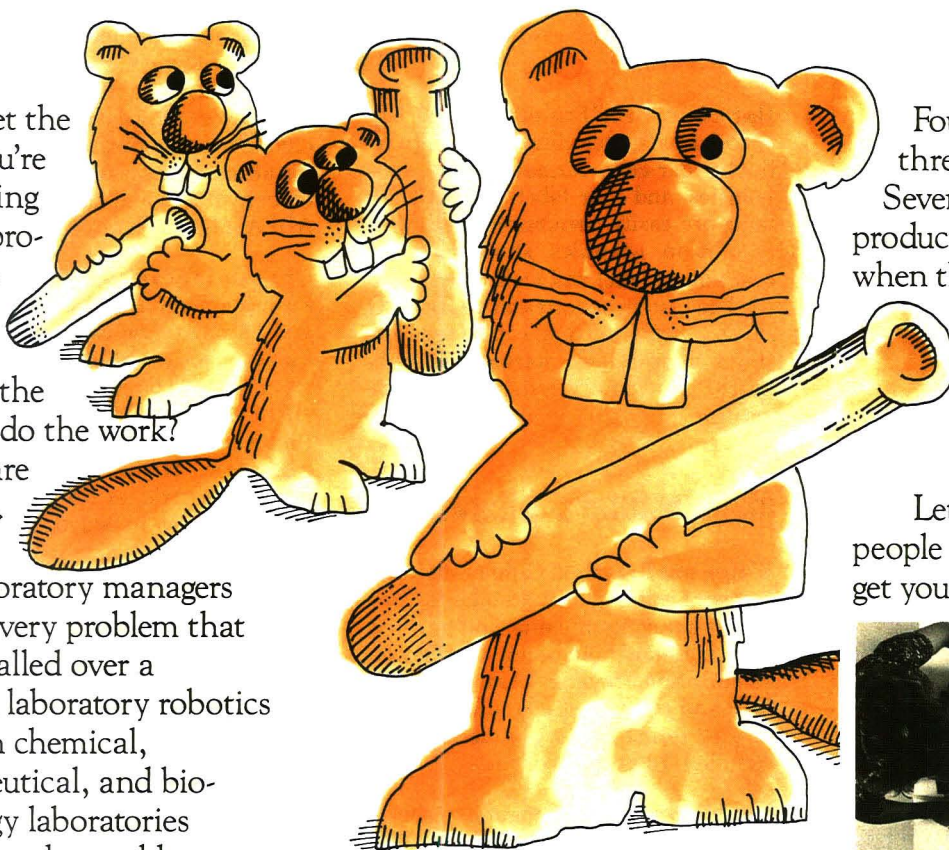
Increase it in seven days  
with Zymark Robotics.

Do you get the feeling you're always being asked to process more samples, never being given the people to do the work?

You are not alone. In fact so many laboratory managers have this very problem that we've installed over a thousand laboratory robotics systems in chemical, pharmaceutical, and biotechnology laboratories throughout the world.

## Robotics Without Tears

Now we've drastically shortened set-up time with a modular system called PyTechnology™. You simply plug in selected hardware



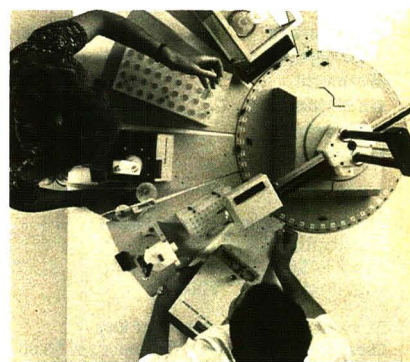
modules, insert a pre-programmed diskette, and begin automating your sample preparation immediately.

## Zymark Will Help

You'll need to know a few things first, of course, but we've made that part easier and faster, too. First comes hands-on training from the pioneers and world leaders in laboratory robotics, then installation assistance when your system is delivered.

Four days for training, three for installation: Seven days to increased productivity. From then on, when they ask you to increase sample throughput, you just leave the robot on when you turn off the lights at night.

Let the most experienced people in laboratory robotics get you started. Call us now



*PyTechnology: Simplified Robotics*

and ask for your free Robotics Starter Kit. (617) 435-9501. Zymark, Zymark Center, Hopkinton, MA 01748.

# Zymark

Visit us at Pittcon Booth 160

CIRCLE 180 ON READER SERVICE CARD



# Key Chemicals & Polymers All New 7th Edition

One-page reviews packed with data on the current economic status and short-term outlook for 46 large-volume chemical industry products.

The 46 products are:

Acetone	Nylon
Acrylics	Oxygen
Ammonia	Phenol
Benzene	Phenolics
Butadiene	Phosphoric acid
Carbon black	Phosphorus
Carbon dioxide	Polyester
Caustic soda	Polyesters
Chlorine	Polypropylene
Cyclohexane	Polystyrene
DMT/PTA	Polyvinyl chloride
Epoxies	Potash
Ethanol	Propylene
Ethylene	Soda ash
Ethylene oxide	Styrene
Formaldehyde	Sulfur
High-density polyethylene	Sulfuric acid
Hydrogen	Titanium dioxide
Lime	Toluene
Low-density polyethylene	diisocyanate (TDI)
Methanol	Urea
Methylene chloride	Vinyl acetate
Nitrogen	Vinyl chloride
	p-Xylene

**Chemical & Engineering News**  
Distribution Dept.  
1155 — 16th St., N.W.  
Washington, D.C. 20036

Please send \_\_\_\_\_ copies of **Key Chemicals & Polymers** (7th Edition) at \$5.00 per copy (\$4.00 per copy for orders of more than 10). On orders of \$20 or less please send payment with order.

☐ Payment enclosed ☐ Bill me  
Charge my ☐ MasterCard ☐ Diners Club  
☐ VISA ☐ American Express

Card # \_\_\_\_\_

Interbank # \_\_\_\_\_  
(MasterCard only)

Exp. date \_\_\_\_\_

Signature \_\_\_\_\_

Name \_\_\_\_\_

Address \_\_\_\_\_

City \_\_\_\_\_

State \_\_\_\_\_ ZIP \_\_\_\_\_

**Call Toll Free 800-424-6747**

## NEW PRODUCTS

### Software

**Data acquisition.** Unkelscope Junior acquires, displays, stores, and retrieves data using an IBM PC-XT, PT-AT, or compatible computer. Cursor scrolling allows the user to move two independent cursors through stored data showing numerical voltage and time values corresponding to each of the cursors on the screen, and data can also be ported to other programs or spreadsheets. A data acquisition board and an IBM or Hercules graphics card are required. Unkel Software 413

**Bar-code.** LabelPro provides 10 bar-code formats, including four health industry bar-code formats, seven symbologies, and four label sizes. All formats are easily customized, and high-resolution graphics show how the customized label will look when printed. The system operates on an IBM PC, PC-XT, or PC-AT and can be used as a stand-alone unit or interfaced with the StockPro inventory system. Fisher Scientific 414

### Manufacturers' Literature

**Water purification.** Guide provides a review of water quality standards, common water contaminants, and purification methods, including distillation, deionization, reverse osmosis, filtration, and ultraviolet oxidation. A glossary of terms and a bibliography are included. 12 pp. Labconco 417

**Newsletter.** The inaugural issue of *Chromatography* contains a variety of applications information and how-to tips on HPLC and SFC separations, including articles on determination of carbohydrates, organic acids, and catecholamines, and a guide to the selection of reversed-phase columns. 8 pp. Brownlee Labs 418

**ICP spectrometry.** Booklet describes how to select an ICP spectrometer that best fits the needs of a particular laboratory. Included is information on how to determine the lab's analytical needs and which features and specifications are important to good analytical performance. A glossary of ICP terminology is included. 8 pp. Leeman Labs 419

**Viscometry.** Brochure discusses the use of high-temperature viscometry for measuring the viscosity of glasses, tars, slags, molten salts, metals, ceramics, and dental materials. Several different viscometer models, each suitable for

particular applications, are described. 12 pp. Theta Industries 420

**Liquid handling.** Product bulletin includes basic descriptions and specifications of popular models of fixed- and tri-volume pipettes, dispensettes, macrodispensers, microcentrifuges and related accessories, bottle-top diluters, and digital burets. 12 pp. Brinkmann Instruments 421

**HPLC.** Brochure features a complete line of HPLC components, including absorbance and fluorescence detectors, solvent delivery systems, injectors, postcolumn reaction systems, and chromatography data systems. Also included are descriptions of turnkey applications systems for determination of carbohydrates and carbamates. 26 pp. ABI Analytical/Kratos 422

**Chromatography.** Brochure describes a complete line of membranes and chromatography products for reagent purification and sample management. Details on Millex filter units for HPLC sample filtration, the Milli-Q Plus water system for production of organic-free, HPLC-grade water, and Sep-Pak cartridges for sample preparation are also included. 16 pp. Millipore 423

### Catalogs

**Materials standards.** 1987 catalog contains more than 4000 items, including high-purity rare earth metals and compounds, inorganic compounds, metal single crystals, platinum labware, electronic chemicals, crystal growing materials, laboratory test equipment, and gas purifiers. All products are available in either bulk or catalog quantities. Aesar Group/Johnson Matthey 424

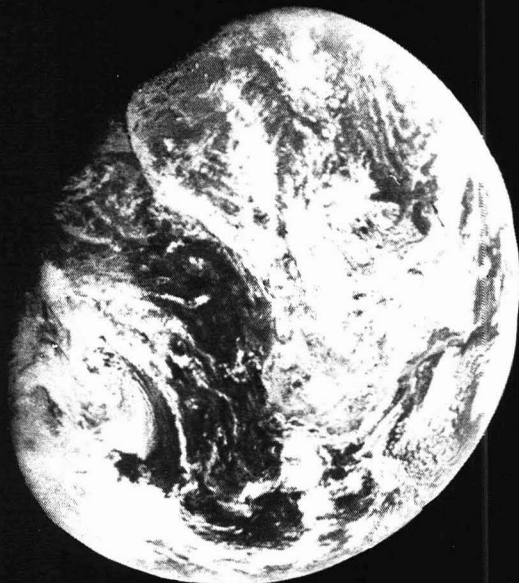
**Syringes.** Catalog includes information of the full line of Microliter and Gastight syringes, syringe packs, manual dispensers, and accessories. A guide assists users in choosing the appropriate syringe for their particular application. Hamilton 425

**Chromatography supplies.** Catalog features columns for both GC and HPLC, a wide range of chromatography accessories and chemical standards, and an extensive listing of column applications. New products include an indicating tube for detection of oxygen and moisture in GC carrier gas and a column for hydrophobic interaction chromatography. 260 pp. Supelco 426



ENVIRONMENTAL SCIENCE & TECHNOLOGY

ES&T



**The premiere  
research  
publication in the  
environmental  
field.**

Environmental science continues to be one of the fastest growing fields. And ES&T has grown right along with it!

ES&T continues to give you the practical, hard facts you need on this science . . . covering research, techniques, feasibility, products and services.

Essential reading for environmental scientists both in the business and academic world . . . ES&T has increased its emphasis on peer-reviewed research dealing with water, air, and waste chemistry in addition to adding critical reviews of important environmental science issues—all relevant to understanding the management of our natural environment.

Also included are discussions on environmental analyses, governmental regulations, current environmental lab activities, and much more!

**For rate information, and to subscribe, call toll free:**

**(800) 424-6747**

- ✓ single shot or up to 50 automatic multi-sequential runs
- ✓ improved static or dynamic combustion at selectable oxygen concentration
- ✓ sample amount up to 100 mg
- ✓ extreme compactness

no gaschromatographic column separation of the combustion products

*but*

thermal focusing and programmed temperature desorption PTD technique\*

\* patent pending

**THE NEW ELEMENTAL ANALYZER**

**DANI CHN 89.00**



**DANI S.p.A.** ■ I 20052 MONZA (MI) ■ VIA ROVANI 10 ■ ITALY  
■ TEL. (039) 323993 - 324448 ■ TELEX 332280 DANI I ■

CIRCLE 32 ON READER SERVICE CARD

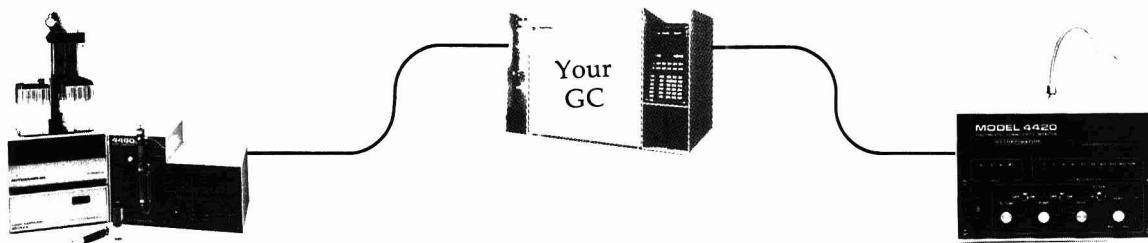


# PRIORITY POLLUTANT ANALYSIS

## Purge and Trap Concentrator and Selective Detector

EPA Methods: 601, 602, 603, 608, 611, 624, 502.1, 503.1, 524.1, 8010, 8020, 8030, 8240 . . .

The **Model 4460** Purge and Trap and the **Model 4420** Electrolytic Conductivity Detector teamed with your gas chromatograph is the right combination for performing priority pollutant analysis.



The **Model 4460** Purge and Trap with Autosampler is a microprocessor-based system that eliminates time-consuming manual operations of earlier purge and trap systems. Call today for details about advanced technology in purge and trap.

CIRCLE 120 ON  
READER SERVICE CARD

The **Model 4420** Detector provides selective detection of halogen compounds with the sensitivity and ease not found in other electrolytic conductivity detectors. Contact OIC for information on a selectively better detector.

CIRCLE 121 ON  
READER SERVICE CARD

## O.I. CORPORATION

Graham Rd. at Wellborn Rd. • P.O. Box 2980 • College Station, Texas 77841-2980  
Telephone (409) 690-1711 • Cable Address: O.I.COSN • TWX No.: 510-892-7944

Visit O.I. at PITCON booths 306, 308, 310.

## LABORATORY SERVICE CENTER

Acetylthiourea • L(+)-Arabinose • Cesium Chloride • Digitonin  
1,2-Dihydronaphthalene • Dihydroxyacetone • Dithiol • Esculin  
N-Ethyl Maleimide • Glutaric Acid & Anhydride • 1,6-Hexanediol  
8-Hydroxyquinoline-5-sulfonic Acid • INT •  $\alpha$ -Ketoglutaric Acid  
Levulinic Acid • Maltose • Methyl Acetamide • Nadic Anhydride  
Neutral Red • 3-Nitrophthalic Acid • Phenylthiourea • Phenylurea  
Potassium Hydrogen Phthalate • Sodium Diethyldithiocarbamate  
Sodium Pyruvate • Toluidine Blue • Triphenylphosphine • Xylitol

Write for our Products List of over 3000 chemicals

Tel: 516-273-0900 • TOLL FREE: 800-645-5566 • Telefax: 516-273-0858 • Telex: 497-4275

**EASTERN CHEMICAL**  
A Division of UNITED-GUARDIAN, INC.

P. O. Box 2500  
DEPT. AC  
SMITHTOWN, N. Y. 11787

**ORS** ONEIDA  
RESEARCH  
SERVICES, INC.

**SYNTHETIC  
COMPOUND  
ANALYSES**

### 2-DAY SERVICE FOR:

- Molecular Weights
- C, H, N Microanalyses
- Structural Mass Spectra
- X-ray Elemental Scans

See us at the **Pittsburgh Conference**  
**Booth 7061, 7059B**

One Halsey Rd., Whitesboro, NY 13492  
Telephone (315) 736-3050

**Laboratory Service Center** (Equipment, Materials, Services, Instruments for Leasing), Maximum space — 4 inches per advertisement. Column width, 2-3/16"; two column width, 4-9/16". Artwork accepted. No combination of directory rates with ROP advertising. Rates based on number of inches used within 12 months from first date of first insertion. Per inch: 1" — \$141; 12" — \$139; 24" — \$136; 36" — \$131; 48" — \$128.

CALL OR WRITE JANE GATENBY

**ANALYTICAL CHEMISTRY**  
500 Post Road East  
P.O. Box 231  
Westport, CT 06880  
203-226-7131

## FREE DATA, FAST

To quickly amass data on all of the products you need, consult the Lab Data Service section on our *Analytical Chemistry* reader reply card insert.



# INDEX TO ADVERTISERS IN THIS ISSUE

CIRCLE INQUIRY NO.	ADVERTISERS	PAGE NO.
17	Beckman Altex Cochrane, Chase & Livingston Company	304A-305A
18-19	Bioanalytical Systems Kissinger Advertising Associates	314A
25	CEM Corporation Union Agency	302A
27	Chrompack, Inc. Sardi & Blecker	332A
32	DANI S.p.A.	355A
40-42	ESA, Inc. James F. Balderson & Associates	327A, 329A, 331A
50-51	Finnigan MAT Corporation Lena Chow, Inc.	349A
49	Fluid Metering, Inc. Arnold H. Nachman Associates	326A
60	Great Lakes Environmental Services Alden Design Associates	330A
-	*Hewlett-Packard Company Pinné, Garvin, Herbers & Hock	OBC
73-79	*Instruments SA, Inc. Kathy Wyatt & Associates	351A
72	*Isco, Inc. Farneaux Associates	307A
81	*J&W Scientific, Inc.	326A
85	**Kontron, Ltd. Promotion Kontron AG	334I
91	*LDC/Milton Roy HRS Communications	324A
90	Lotus Development Corporation Leonard Monahan Saabye	322A-323A
100	Matheson Gas Products Kenyon Hoag Associates	309A
97	*Mettler Instrument Corporation Arnold, Brennan & Guariglia, Inc.	350A
94-95	*Mettler Instrument Corporation McKinney, Inc.	IFC, 339A
98	Micromeritics Fahlgren & Swink, Inc.	348A
99	Molytek, Inc. M.S.I., Inc.	299A
107	*Neslab Instruments, Inc. The Ramphastos Agency	345A
110-111	*Nicolet Corporation Nicolet Agency	311A, 313A
120-121	*O.I. Corporation	356A
125-126	*Perkin-Elmer Corporation AC&R Advertising, Inc.	341A, 343A
130-133	**Pye Unicam, Ltd. Spectrum/SSC&B: Lintas Worldwide	334B, 334D, 334F, 334H
141	Rheometrics Bliss, Barefoot & Associates	328A
151	*Scientific Glass Engineering Arden Advertising Associates	319A
152	Scott Specialty Gases The Matlin Company, Inc.	312A
150	Siemens AG Barbeau-Hutchings Advertising, Inc.	321A
1-3	Spex Industries, Inc. The Ad Lab, Inc.	316A
170-171	VG Instruments Barbeau-Hutchings Advertising, Inc.	346A

CIRCLE INQUIRY NO.	ADVERTISERS	PAGE NO.
173	*Wescan Instruments, Inc. Chromad	337A
174	Westinghouse Bio-Analytic Systems Company	301A
176	*Wheaton Instruments The Wheaton Agency	310A
180-181	Zymark Corporation Grover & Carroll, Inc.	345A, 353A

Directory section, see page 356A.

\* See ad in ACS Laboratory Guide.

\*\* Company so marked has advertisement in Foreign Regional edition only.

Advertising Management for the American Chemical Society Publications

## CENTCOM, LTD

President

Thomas N. J. Koerwer

Executive Vice President Senior Vice President

James A. Byrne Benjamin W. Jones

Alfred L. Gregory, Vice President

Clay S. Holden, Vice President

Robert L. Voepel, Vice President

Joseph P. Stenza, Production Director

500 Post Road East

P.O. Box 231

Westport, Connecticut 06880

(Area Code 203) 226-7131

Telex No. 643310

## ADVERTISING SALES MANAGER

James A. Byrne, VP

## ASSISTANT ADVERTISING SALES MANAGER

Bruce E. Poorman

## ADVERTISING PRODUCTION MANAGER

Jane F. Gatenby

## SALES REPRESENTATIVES

Philadelphia, PA ... Patricia O'Donnell, CENTCOM, LTD., GSB Building, Suite 725, 1 Belmont Avenue, Bala Cynwyd, Pa. 19004. Telephone: 215-667-9666

New York, NY ... Dean A. Baldwin, CENTCOM, LTD., 60 East 42nd St., New York, N.Y. 10165. Telephone: 212-972-9660

Westport, CT ... Edward M. Black, CENTCOM, LTD., 500 Post Road East, P.O. Box 231, Westport, Ct. 06880. Telephone: 203-226-7131, Telex 643310

Cleveland, OH ... Bruce E. Poorman, John C. Guyot, CENTCOM, LTD., 325 Front St., Suite 2, Berea, Ohio 44017. Telephone: 216-234-1333

Chicago, IL ... Michael J. Pak, CENTCOM, LTD., 540 Frontage Rd., Northfield, Ill. 60093. Telephone: 312-441-6383

Houston, TX ... Michael J. Pak, CENTCOM, LTD. Telephone: 312-441-6383

San Francisco, CA ... Paul M. Butts, CENTCOM, LTD., Suite 1070, 2672 Bayshore Frontage Road, Mountain View, CA 94043. Telephone: 415-969-4604

Los Angeles, CA ... Clay S. Holden, CENTCOM, LTD., Newton Pacific Center, 3142 Pacific Coast Highway, Suite 200, Torrance, CA 90505. Telephone: 213-325-1903

Boston, MA ... Edward M. Black, CENTCOM, LTD. Telephone: 203-226-7131

Atlanta, GA ... Edward M. Black, CENTCOM, LTD. Telephone: 203-226-7131

Denver, CO ... Paul M. Butts, CENTCOM, LTD. Telephone: 415-969-4604

## United Kingdom

Reading, England ... Malcolm Thiele, Technomedia Ltd., Wood Cottage, Shurlock Row, Reading RG10 0QE, Berkshire, England. Telephone: 073-434-3302, Telex #848800

Lancashire, England ... Technomedia Ltd., c/o Meconomics Ltd., Meconomics House, 31 Old Street, Ashton Under Lyne, Lancashire, England. Telephone: 061-308-3025

Continental Europe ... Andre Jamar, International Communications, Inc., Rue Mallar 1, 4800 Verviers, Belgium. Telephone: (087) 22-53-85, Telex #49263

Tokyo, Japan ... Shuji Tanaka, International Media Representatives Ltd., 2-29 Toranomon, 1-Chome Minato-ku Tokyo 105 Japan. Telephone: 502-0656, Telex #22633



**COMPLETE  
1987 SCHEDULE!**

# **ACS SHORT COURSES**

at

## **Virginia Tech, Blacksburg, VA**

**Get the Hands-On Experience You Need to Do Your Job Better!  
Register TODAY for These Popular Lecture-Lab Courses!**

### **Polymer Chemistry: Principles and Practice**

*Dr. James E. McGrath, Course Director*

Perform a variety of practical, industry-oriented experiments in polymer topics—from synthesis to manufacture.

Sunday–Friday, March 15–20, 1987

Sunday–Friday, August 9–14, 1987

Sunday–Friday, November 15–20, 1987

### **Gas Chromatography: Packed and Capillary Columns**

*Dr. Harold M. McNair, Course Director*

Gain valuable experience in the operation and maintenance of state-of-the-art GC systems.

Monday–Friday, March 16–20, 1987

Monday–Friday, September 28–October 2, 1987

### **Applied Rheology and Polymer Processing**

*Dr. Donald G. Baird, Course Director*

Learn how certain rheological measurements can be used to assess polymer processability when all other standard techniques are of no value.

Sunday–Friday, March 29–April 3, 1987

Sunday–Friday, September 13–18, 1987

### **The Computer-Integrated Laboratory: A Hands-On Experience in Lab Automation**

*Dr. Raymond E. Dessy, Course Director*

Gain a sound understanding of how to manage the computer-integrated laboratory—the key to successful implementation.

Sunday–Friday, June 7–12, 1987

Sunday–Friday, September 20–25, 1987

### **Polymer Characterization: Thermal, Mechanical, and Optical**

*Dr. James E. McGrath, Course Director*

Learn the principal approaches to understanding polymeric solids and their behavior.

Sunday–Friday, June 7–12, 1987

### **Liquid Chromatography: Theory and Practice**

*Dr. Harold M. McNair, Course Director*

Learn how to perform qualitative and quantitative analyses as well as how to maintain state-of-the-art HPLC systems.

Monday–Thursday, June 8–11, 1987

Monday–Thursday, December 14–17, 1987

### **Modern NMR Spectrometry: Principles and Practice**

*Dr. Harry C. Dorn, Course Director*

Be able to optimize, maintain, and troubleshoot an NMR spectrometer on a daily basis.

Monday–Friday, June 8–12, 1987

### **Polymer Synthesis: Fundamentals and Techniques**

*Dr. James E. McGrath, Course Director*

Learn the theory and practice of polymer production, including a broad spectrum of synthetic techniques.

Sunday–Friday, June 21–26, 1987

### **Send in this coupon for a free brochure!**

American Chemical Society  
Education Division  
1155 Sixteenth Street, NW  
Washington, DC 20036

*Please send me a free brochure giving details on the lecture-lab short courses to be offered at Virginia Tech in 1987.*

Name \_\_\_\_\_  
Title \_\_\_\_\_  
Organization \_\_\_\_\_  
Address \_\_\_\_\_  
City, State, ZIP \_\_\_\_\_

**CALL TODAY! To register by phone  
or to request a free brochure—CALL  
COLLECT (202) 872-4508.**



**EDITOR: GEORGE H. MORRISON**

**ASSOCIATE EDITORS:** Klaus Blemann,  
Georges Gulochon, Fred Lytle,  
Robert Osteryoung

**Editorial Headquarters**  
1155 Sixteenth St., N.W.  
Washington, D.C. 20036  
Phone: 202-872-4570  
Teletype: 710-8220 151

**Managing Editor:** Sharon G. Boots  
**Associate Editors:** Stuart A. Borman,  
Rani A. George, Louise Voress  
**Assistant Editor:** Mary D. Warner  
**Editorial Assistant:** Grace K. Lee  
**Production Manager:** Leroy L. Corcoran  
**Art Director:** Alan Kahan  
**Designer:** Sharon Harris Wolfgang  
**Production Editor:** Elizabeth E. Wood  
**Circulation:** Cynthia G. Smith  
**Editorial Assistant, LabGuide:** Joanne Mullican

**Journals Dept., Columbus, Ohio**  
**Associate Head:** Marianne Brogan  
**Associate Editor:** Rodney L. Temos

**Advisory Board:** Shier S. Berman, Brian S.  
Bidlingmeyer, Henry N. Blount, Gary D. Chris-  
tian, Harry V. Drushel, Larry R. Faulkner, Peter  
R. Griffiths, Gary M. Hieftje, Nobuhiko Ishiba-  
shi, Mary A. Kaiser, David L. Nelson, Erno Pun-  
gor, Dennis Schuetzle, Nicholas Winograd, Ed-  
ward S. Yeung, Andrew T. Zander

**Instrumentation Advisory Panel:** Howard G.  
Barth, Richard F. Browner, James B. Callis,  
Richard S. Danchik, Thomas C. Farrar, Joel M.  
Harris, John F. Holland, Ronald E. Majors, Linda  
B. McGown

**The Analytical Approach Advisory Panel:** Ed-  
ward C. Dunlop, Robert A. Hofstadter, Wilbur D.  
Shults

*Published by the*  
**AMERICAN CHEMICAL SOCIETY**  
1155 16th Street, N.W.  
Washington, D.C. 20036

## Books and Journals Division

**Director:** D. H. Michael Bowen

**Journals:** Charles R. Bertsch

**Research and Development:** Lorrin R. Garson

Manuscript requirements are published in the  
January 1, 1987 issue, page 219. Manuscripts  
for publication (4 copies) should be submitted  
to ANALYTICAL CHEMISTRY at the ACS Washing-  
ton address.

The American Chemical Society and its editors  
assume no responsibility for the statements  
and opinions advanced by contributors. Views  
expressed in the editorials are those of the  
editors and do not necessarily represent the  
official position of the American Chemical  
Society.

Albers, D., 593

Baranski, A. S., 662  
Barcelona, M. J., 582  
Beauchemin, D., 610  
Benson, D. M., 658  
Berman, S. S., 610  
Bier, M. E., 597  
Bright, F. V., 572  
Bryan, J., 658

Cantwell, F. F., 586  
Chang, T. T., 614  
Collin, P. J., 558  
Cooks, R. G., 597  
Cueto-Rejón, A. F., 645

Dasgupta, P. K., 629  
DesJarlais, S., 670

Engstrom, R. C., 670  
Ewing, A. G., 678

Frye, S. R., 640

George, G. K., 582  
Glerum, C., 687  
Greenberg, R. R., 688

Hieftje, G. M., 572  
Holm, T. R., 582

Isenhour, T. L., 649

Jang, G.-W., 684  
Jenke, D., 624  
Jeričević, Ž., 658  
Johns, R. B., 636  
Johnson, K. W., 670  
Johnston, M. V., 567  
  
Khan, A., 654  
Kim, Y. T., 687  
Kolling, O. W., 674  
Kratochvil, B., 586

Laude, D. A., Jr., 546, 576  
López-Cueto, G., 645  
Lucyk, D., 586  
Luque de Castro, M. D., 666

Malcolm, R. L., 558  
McLaren, J. W., 610  
McMinn, D. G., 640  
Mottola, H. A., 666  
Müller, M. D., 617

Nozoye, H., 681

Oades, J. M., 558  
Ogasawara, I., 681

Perdue, E. M., 551  
Phillips, D. A., 629  
Poirier, G. E., 572

Rajeshwar, K., 684  
Reuter, J. H., 551  
Rios, A., 666

Sacks, R., 593  
Segal, R., 684  
Siegel, M. M., 614  
Smith, L. C., 658  
Smith, R. D., 640  
Soroka, K., 629  
Stiller, S. W., 567  
Strachan, M. G., 636  
Sweileh, J. A., 586

Trainor, T. M., 601  
Tsou, H.-R., 614

Valcárcel, M., 666  
Vassallo, A. M., 551, 558  
Vithanage, R. S., 629  
Vouros, P., 601

Wakayama, N. I., 681  
Walker, B., 629  
Wallingford, R. A., 678  
Wang, C. P., 649  
Waters, A. G., 558  
Wenzel, T. J., 562  
Wilkins, C. L., 546, 576  
Wilson, M. A., 551, 558  
Wright, B. W., 640  
Wyatt, W. A., 572

Zaia, J., 562



# Reverse-Phase High-Performance Liquid Chromatography/Nuclear Magnetic Resonance Spectrometry in Protonated Solvents

David A. Laude, Jr., and C. L. Wilkins\*

Department of Chemistry, University of California, Riverside, California 92521

**On-line continuous flow high-performance liquid chromatography/nuclear magnetic resonance (HPLC/NMR) separations are performed in fully protonated reverse-phase solvent systems by using the 1-1 hard pulse NMR sequence for the dual suppression of solvent resonances. An analgesic mixture is separated in 50:50 H<sub>2</sub>O-acetonitrile and a phenol mixture is separated in 20:80 H<sub>2</sub>O-methanol. Outside the two suppression regions, the 1-1 hard pulse retains the spectral quality achieved in deuteriated solvents as spectral resolution remains data point limited and a 50- $\mu$ g injection of caffeine yields a signal to noise (S/N) ratio of 12:1 in continuous flow mode for a 28- $\mu$ L cell volume. The effects of solvent gradients on the NMR signal are examined for H<sub>2</sub>O-acetonitrile and H<sub>2</sub>O-methanol at pH 7 and 4.4. Conditions are then chosen to perform a gradient separation of vitamins by HPLC/NMR.**

A serious limitation to the general application of nuclear magnetic resonance (NMR) as an on-line detector for high-performance liquid chromatography (HPLC) is the difficulty of observing weak analyte signals in protonated solvents because of the dynamic range limitations of the analog-to-digital converter (ADC) associated with the spectrometer. Although nonprotonated solvent systems for normal-phase systems have been employed in HPLC/NMR separations (1-3), substitutes for reverse-phase systems (other than prohibitively expensive deuteriated analogues) do not exist. Of the many NMR pulse sequences developed for suppression of the water signal in aqueous biological systems, a few have been extended to HPLC/NMR in an attempt to find a general solution to the dynamic range problem (4-6). Characteristics of an ideal solvent suppression method for HPLC/NMR would include (1) elimination of solvent resonances without perturbation of the analyte signal, (2) simultaneous applicability to multiple solvent resonances, (3) a short preacquisition time to permit use of the maximum scan rate, and (4) invariance to the changes in chemical shifts associated with solvent gradients. Although several pulse sequences satisfy a few of these requirements, none exist which provide a universal solution to the problem.

In 1982 Bayer and co-workers performed the first extensive work with reverse-phase HPLC/NMR separations (7). In addition to employing a larger ADC (16-bit compared to the 12-bit ADC which was standard at that time), a gated homodecoupled presaturation pulse sequence was applied to the suppression of water and acetonitrile solvent resonances. Buddress and Herzog utilized a similar presaturation procedure for the suppression of [<sup>1</sup>H]chloroform in a normal-phase separation of steroids (8). The principal limitation of these suppression procedures is that because of the long presaturation time (0.5-2 s), the scan rate is significantly reduced, with a concomitant decrease in signal enhancement that is derived from ensemble averaging during dynamic flow NMR

measurements. However, because both researchers used relatively large observe cells (at the expense of chromatographic performance) the decreased scan rate was compensated by an increased observe time. In 1984 we reported the use of a selective excitation pulse sequence, the 1-1 hard pulse (1-1HP) developed by Clore and co-workers (4), which was amenable to the micro observe cell design employed for analytical scale HPLC/NMR (9). This pulse sequence, which permitted a rapid scan rate and the simultaneous suppression of H<sub>2</sub>O and acetonitrile resonances, was utilized for the isocratic reverse-phase separations of several mixtures of biomolecules. An obvious criticism of that work was the use of deuterium oxide (D<sub>2</sub>O) as a substitute for protonated water, as separations and columns were chosen such that a maximum of 3% acetonitrile in D<sub>2</sub>O was required for each separation.

The intent of this paper is to demonstrate the feasibility of on-line HPLC/NMR for any isocratic reverse-phase separation which utilizes the two principal solvent systems, protonated water-acetonitrile and protonated water-methanol. First, separations in both deuteriated and protonated solvents are performed to characterize the effects of the 1-1 hard pulse sequence, observe volume, and data acquisition parameters on analyte signals in the NMR spectrum. This information is then used for the separation of analgesics in 50:50 H<sub>2</sub>O-acetonitrile and phenols in 20:80 H<sub>2</sub>O-methanol. In addition, the effects of solvent gradients on chemical shift are defined for these two solvent systems at neutral pH and in an acetate buffer at pH 4.4.

## EXPERIMENTAL SECTION

HPLC/NMR instrumentation and system interface are described elsewhere (3). A postcolumn transfer volume of 2 to 3  $\mu$ L was obtained by inserting the stainless steel HPLC column directly in the bore of a 300-MHz superconducting solenoid magnet. Microcell observe volumes of 28 or 53  $\mu$ L, coupled with the small transfer volume, permitted analytical-scale separations for which band-broadening contributions due to chromatographic dead volume were small. All separations were performed at 0.5 mL/min flow rates by using a 10- $\mu$ m particle size 30 cm  $\times$  4.6 mm C<sub>8</sub> bonded phase column.

The three HPLC solvents used were deionized and distilled water, HPLC grade acetonitrile from Fischer Scientific, and anhydrous methanol from Mallinckrodt. The water was degassed for 30 min to remove dissolved CO<sub>2</sub>. In addition to the two unbuffered solvent systems, H<sub>2</sub>O-acetonitrile and H<sub>2</sub>O-methanol, a second set of solvent pairs, with 0.5 M potassium acetate added to H<sub>2</sub>O and adjusted to pH 4.4 with acetic acid, were used. The effect of solvent concentration on NMR chemical shift was determined for each of the four solvent systems, by varying the gradient from 100% H<sub>2</sub>O to 100% organic solvent, with spectra acquired in stopped-flow mode for every 10% change in solvent composition. An examination of the gradients in continuous-flow mode was also performed to observe concentration effects in the observe cell.

When collecting data during an HPLC/NMR analysis, four coadded spectra with a 512 ms acquisition time (4096 data points for a  $\pm 2000$  Hz spectral width) were stored in each data file. With a 0.3-s disk access time, a total chromatographic time resolution



Table I. Tabulation of Pertinent Mixture and Chromatographic Information for LC/NMR Measurements

separation	solvent system	compound	amt injected, μg	relevant figures
analgesics	50:50 H <sub>2</sub> O-ACN (buffered, pH 4.4)	acetaminophen	200	3
		caffeine	400	
		acetylsalicylic acid	500	
phenols	20:80 H <sub>2</sub> O-MeOH (buffered, pH 4.4)	phenol	200	4 and 5
		<i>p</i> -nitrophenol	200	
		<i>m</i> -cresol	200	
		2-methyl-3-methoxyphenol	300	
vitamins	10% to 20% ACN in D <sub>2</sub> O	ascorbic acid	200	8
		niacin	200	
		pyridoxine		
		hydrochloride	400	

Table II. Compilation of NMR Data Acquisition Parameters in Deuteriated Solvents for 28- and 53-μL Observe Volumes<sup>a</sup>

cell size, μL	sample	pulse sequence	flip angle, deg	recycle time, s	S/N <sup>b</sup>	
					long T <sub>1</sub>	short T <sub>1</sub>
53	acetaminophen	1 pulse	90	0.5	12.2	
			68	0.5	33.4	
	caffeine	1 pulse	90	0.5	7.3	51.7
			90	0.8	11.5	71.7
			68	0.5	14.9	70.6
	acetylsalicylic acid	1 pulse	90	0.5	12.3	
			90	0.8	14.0	
			68	0.5	19.1	
28	acetaminophen	1 pulse	90	0.5	10.2 (3.6)	
		1-1 hard pulse	68		20.3	
	caffeine	1 pulse	68		22.4	
		1 pulse	90		4.6 (5.4)	27.6 (2.0)
		1-1 hard pulse	68		11.5	40.8
		1 pulse	68		12.5	47.4
	acetylsalicylic acid	1 pulse	90		6.2 (4.7)	62.2 (3.8)
		1-1 hard pulse	68		9.6	34.4 <sup>c</sup>
		1 pulse	68		13.3	121.0

<sup>a</sup> All separations were in deuteriated H<sub>2</sub>O-ACN with 500 μg per component injected on column. <sup>b</sup> Relaxation time(s) are included in parentheses. <sup>c</sup> Methyl resonance is partially suppressed by 1-1 hard pulse because of chemical shift proximity to acetonitrile.

of 2.3 s per file was obtained. The 1-1 hard pulse sequence was applied to the dual solvent suppression of protonated H<sub>2</sub>O-methanol and H<sub>2</sub>O-acetonitrile resonances. Various pulse widths (a 90° excitation was 16 μs in length) and delay times were combined to compare spectral S/N as a function of analyte proton spin-lattice relaxation times (*T*<sub>1</sub>). Reconstructions of the chromatographic separations were generated by extracting the maximum absorbance from a selected portion of the NMR spectrum.

A three-component analgesic mixture, a four-component phenol mixture, and a three-component vitamin mixture were analyzed by reverse-phase HPLC/NMR. The analgesic and vitamin compounds were obtained from Sigma. The phenols were obtained from Aldrich Chemical. Table I details the significant chromatographic and spectral parameters for each separation.

## RESULTS AND DISCUSSION

**Optimized Data Acquisition Parameters.** For any given observe cell volume, flow rate, and spin-lattice relaxation time (*T*<sub>1</sub>), the NMR data acquisition parameters chosen will profoundly influence spectral signal-to-noise (S/N) ratio, spectral resolution, and chromatographic resolution. Equation 1 defines the scan rate (SR) for an HPLC/NMR experiment as the reciprocal of the NMR cycle time, *T*<sub>c</sub>, obtained from

$$SR = 1/T_c = 1/[(NDP \cdot SW) + T_d + T_s] \quad (1)$$

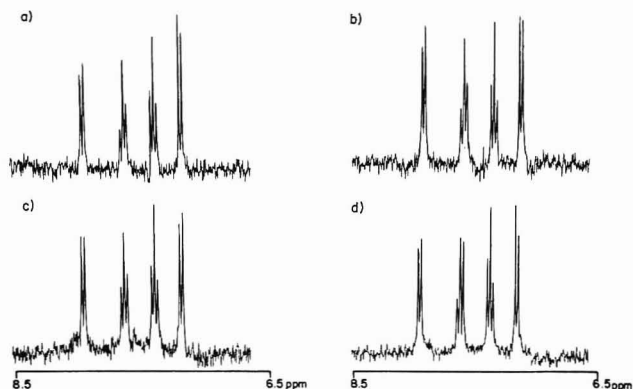
the summation of the acquisition time, *T*<sub>a</sub> (which is a function of spectral width, SW, and number of data points, NDP), delay time, *T*<sub>d</sub>, and disk storage time, *T*<sub>s</sub>. As with any discrete separation/characterization procedure, SR should be maximized, within the constraints of disk storage capability, to permit

adequate reconstruction of a representation of the separation. For analytical scale separations, elution volumes usually exceed 0.1 mL so that at common chromatographic flow rates (0.5–2.0 mL/min), a cycle time of a few seconds will adequately define chromatographic peak shapes.

A consideration of the limited sensitivity of NMR spectrometers suggests that scan rates be maximized to improve detector response. Unfortunately, because the proton NMR spin-lattice relaxation time may vary by as much as 2 orders of magnitude between sample nuclei, there is no ideal scan rate for HPLC/NMR separations. For a slowly relaxing nucleus, the use of large observe volumes and rapid scan rates would have a deleterious effect on NMR signal because of saturation effects in the cell. For any given average lifetime of a nucleus in the observe cell, *τ* (defined as the product of cell volume and flow rate), some compromise *T*<sub>c</sub> value, which reflects the *T*<sub>1</sub> values of compounds to be analyzed, should be selected.

Table II illustrates the effects of various data acquisition parameters on the S/N ratio for acetaminophen, caffeine, and acetylsalicylic acid analyzed individually by HPLC/NMR at 0.5 mL/min flow rates in 50:50 D<sub>2</sub>O-acetonitrile-*d*<sub>3</sub>. Spin-lattice relaxation times, which varied from a minimum of 2.0 s to a maximum of 5.4 s, significantly influenced the S/N ratio for a given *T*<sub>c</sub> and excitation angle, *θ*. For slowing relaxing aromatic protons of the three components, S/N decreased by 53% for the 53-μL cell and 56% for the 28-μL cell when *θ* was increased from 68° to 90° at a constant *T*<sub>c</sub> of 0.5 s. A smaller decrease, 27% and 42% for the two cells, was observed for



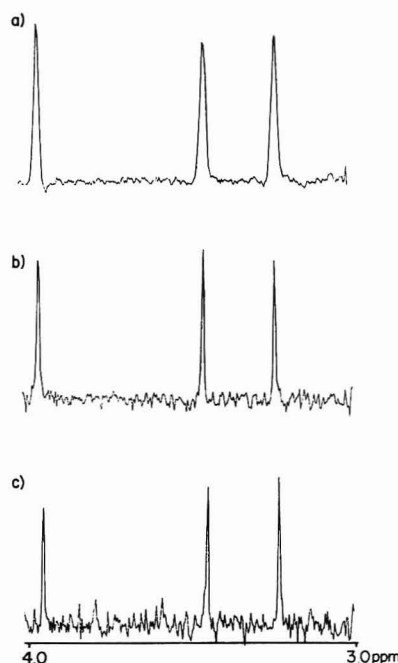


**Figure 1.** Comparison  $^1\text{H}$  NMR spectra of the aromatic region for 500  $\mu\text{g}$  of acetylsalicylic acid analyzed by HPLC/NMR: (a) buffered 50:50  $\text{H}_2\text{O}$ -acetonitrile in a 28- $\mu\text{L}$  cell with 1-1HP suppression; (b) buffered 50:50  $\text{H}_2\text{O}$ -acetonitrile in a 53- $\mu\text{L}$  cell with 1-1HP suppression, amplification was decreased by 30%; (c) buffered 50:50  $\text{D}_2\text{O}$ - $\text{CD}_3\text{CN}$  in 28- $\mu\text{L}$  cell with no suppression; (d) buffered 50:50  $\text{D}_2\text{O}$ - $\text{CD}_3\text{CN}$  in 53  $\mu\text{L}$  cell with no suppression.

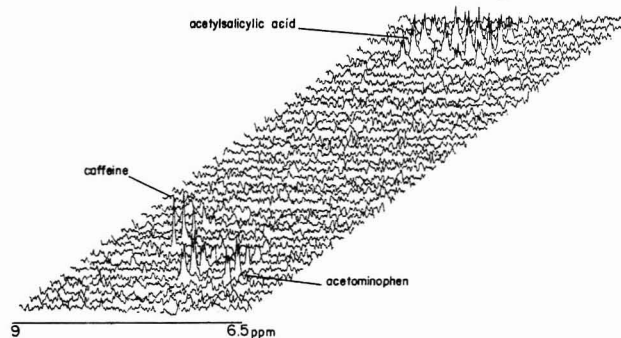
the more rapidly relaxing proton in caffeine. Also in Table II for the 53- $\mu\text{L}$  cell,  $T_c$  is increased to 0.8 s at a pulse angle of  $90^\circ$  and the expected improvement in S/N is observed as saturation effects are reduced. The actual selection of optimum  $T_c$  and  $\theta$  values for a given  $T_1$  cannot be derived from the Ernst angle expression which applies in static systems because  $\tau$  influences the determination of flow system parameters.

Although the S/N data in Table II were acquired in deuteriated solvents, they should be indicative of the data obtained from protonated solvent systems, independent of the suppression technique implemented. To test the effect of 1-1 hard pulse suppression on S/N, it was used in both deuteriated and undeuteriated solvents with the 28- $\mu\text{L}$  cell. The 1-1HP S/N for  $T_c$  and  $\theta$  values of 0.5 s and  $68^\circ$  in deuteriated solvents was within an average of 14% of the one-pulse measurement. The S/N ratios for spectra obtained in protonated solvents by using 1-1HP likewise exhibit little difference from the one-pulse deuteriated S/N data; the comparison spectra from the aromatic region of acetylsalicylic acid which are presented in Figure 1 for both the 28- and 53- $\mu\text{L}$  cells demonstrate this. It is also seen in Figure 1 that spectral resolution is unperturbed by either the pulse sequence or interface design. Rather, it is limited by the acquisition time to about 2 Hz, which is still sufficient to resolve common  $J_{\text{H-H}}$  coupling constants. In Figure 1, the S/N for the 28- $\mu\text{L}$  cell is equivalent in the protonated and nonprotonated solvents; however, the S/N for the 53- $\mu\text{L}$  cell does not exhibit the improvement expected for a larger  $\tau$ . This resulted because even with 1-1HP suppression, in order to maintain spectral integrity, the amplifier gain was reduced to avoid overloading the ADC for the 53- $\mu\text{L}$  cell, although maximum amplification was retained with the 28- $\mu\text{L}$  cell. The use of a 16-bit ADC or more efficient suppression method would permit extension to larger cell volumes.

Microgram detection limits have been reported previously for flow HPLC/NMR measurements with this system interface (3). These results are comparable to those achieved by others using much larger observe volumes with increased signal averaging, both of which degrade chromatographic performance. Figure 2 contains the spectra obtained from coaddition of two four-scan files for various quantities of caffeine analyzed by HPLC/NMR using protonated  $\text{H}_2\text{O}$ -acetonitrile. For 50  $\mu\text{g}$  of material injected on the HPLC column, a S/N ratio of 12 was obtained which, with the accompanying data, extrapolates to a detection limit of 10  $\mu\text{g}$  for the 28- $\mu\text{L}$  cell at a 0.5 mL/min flow rate. Although detection limits vary widely between samples as a function of  $T_1$ , number of equivalent



**Figure 2.**  $^1\text{H}$  NMR spectra of caffeine resonances acquired from increasingly dilute injections on column at a 0.5 mL/min flow rate: (a) 400  $\mu\text{g}$  injected,  $S/N = 48$ ; (b) 100  $\mu\text{g}$  injected,  $S/N = 20$ ; (c) 50  $\mu\text{g}$  injected,  $S/N = 12$ . Two files of four scans were coadded and a 0.5-Hz line-broadening smoothing was used.

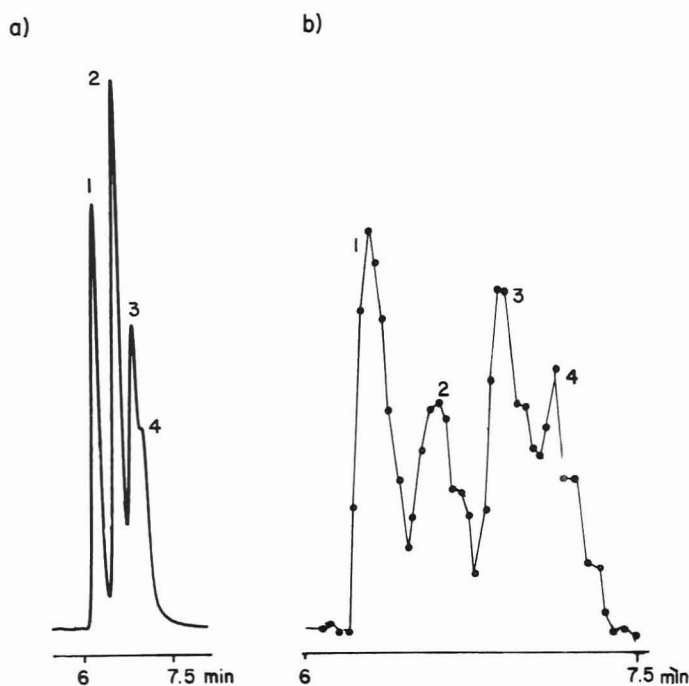


**Figure 3.** Stacked plot of aromatic region of proton spectrum from the HPLC/NMR separation of a three-component mixture of analgesics including 200  $\mu\text{g}$  of acetaminophen, 400  $\mu\text{g}$  of caffeine, and 500  $\mu\text{g}$  of acetylsalicylic acid. The 1-1 hard pulse procedure was used to suppress both resonances in a buffered 50:50  $\text{H}_2\text{O}$ -acetonitrile solvent system in a 28- $\mu\text{L}$  cell. Each spectrum is from a file of four coadded scans stored every 2.3 s. The 3-Hz line-broadening smoothing was used to improve the appearance of the stacked plot.

protons, and spin-spin splitting, these data indicate that HPLC/NMR in protonated solvents should be feasible with little degradation in system performance.

The selection of observe cell volume is usually dictated by the minimum chromatographic performance required for a particular separation, so that S/N ratio is maximized. However, in the choice between the 28- and 53- $\mu\text{L}$  cell for HPLC/NMR analysis in protonated solvents, the inability of the 1-1HP to achieve sufficient signal suppression at full amplification within the limits of the 12-bit ADC reduces the expected gains for the larger cell to just 50% (Table II). Hence the 28- $\mu\text{L}$  cell is employed for all separations in protonated solvents. With such a small observe volume, the flow rate must be decreased to increase  $\tau$ . The low microgram detection limits for the 28- $\mu\text{L}$  cell depicted in Figure 2 are obtained at a flow rate of 0.5 mL/min. At flow rates in excess of 1.0 mL/min the S/N ratio is markedly reduced.

**Analgesics Separation.** A three-component mixture consisting of 200  $\mu\text{g}$  of acetaminophen, 400  $\mu\text{g}$  of caffeine, and

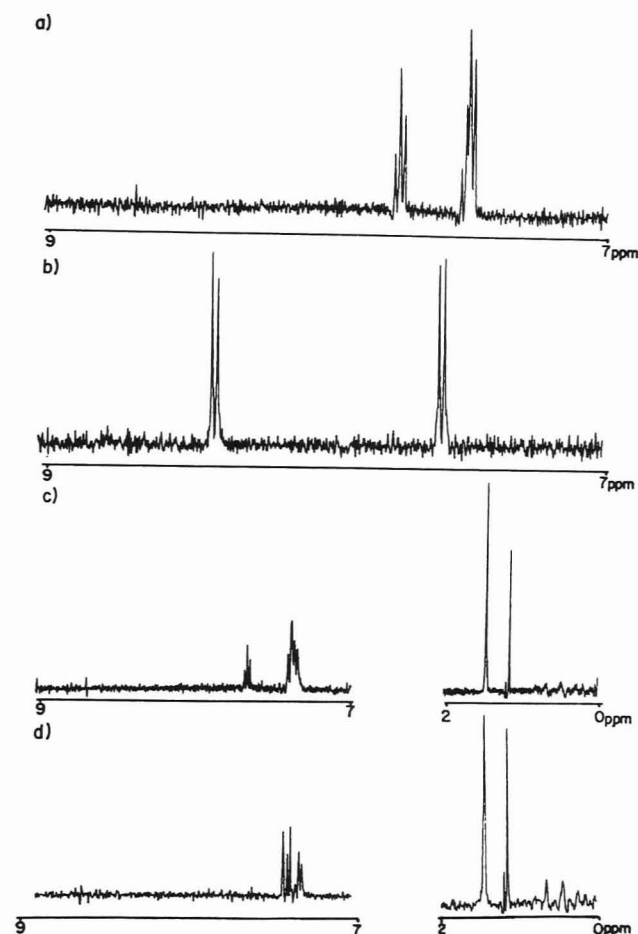


**Figure 4.** Comparison chromatograms from the separation of a four-component phenol mixture in buffered 20:80  $\text{H}_2\text{O}$ -methanol: (a) UV trace from injection of less than 200 ng of each component; (b) HPLC/NMR reconstruction generated from the maximum absorbance in the region 7–9 ppm. Each dot corresponds to an NMR file collected every 2.3 s. Peaks 1–4 correspond to NMR spectra a–d in Figure 5.

500  $\mu\text{g}$  of acetylsalicylic acid was separated in 50:50  $\text{H}_2\text{O}$ -acetonitrile (with  $\text{H}_2\text{O}$  buffered at pH 4.4), by using the 1–1 hard pulse technique for dual suppression of the solvent resonances. Figure 3 is a stacked plot of the aromatic region with a spectrum plotted from a file of four scans stored every 2.3 s. The three components were base-line-separated.

**Phenol Separation.** A four-component phenol mixture was separated by HPLC/NMR in an 80:20 methanol-water solvent system (with  $\text{H}_2\text{O}$  buffered at pH 4.4), again using 1–1 hard pulse method for dual solvent suppression. As will be described later, only two solvent resonances are observed because, at a pH of 4.4, the acidic  $\text{H}_2\text{O}$  and methanol protons coalesce under fast exchange conditions to form a single narrow resonance, in addition to the methyl resonance from methanol. Figure 4 presents a comparison of the UV trace and HPLC/NMR reconstruction for the separation. Four peaks may be distinguished from the UV trace although none are base-line-resolved. Similarly the HPLC/NMR reconstruction, with a time resolution of 2.3 s, also indicates the presence of four components. Thus chromatographic performance with NMR as a detector is similar to that with the conventional detector; this would be expected, assuming good postcolumn flow characteristics, because the total transfer and observe volume for both detectors is about 30  $\mu\text{L}$ .

Figure 5 contains the NMR spectra for each of the phenols. Each spectrum results from coaddition of all NMR files within  $\pm 1$  standard deviation of the maximum intensity spectrum, assuming a Gaussian peak shape. A 0.5-Hz line-broadening smoothing and one zero fill are performed. Suppression of the dual solvent resonances by the 1–1 hard pulse procedure seriously perturbs a several hundred hertz region around the peaks. For the 80:20 methanol- $\text{H}_2\text{O}$  system the regions 2–2.5 and 4–5 ppm are suppressed; however, all other regions are observable with little or no loss in spectral integrity, as is demonstrated with the various spectra of the phenols. A further value of NMR as a detector for HPLC, the ability to extract uncontaminated spectra from the non-base-line-resolved chromatographic peaks, permits verification of the



**Figure 5.** Coadded phenol spectra from HPLC/NMR analysis with the regions containing analyte resonances displayed: (a) 200  $\mu\text{g}$  of phenol, (b) 200  $\mu\text{g}$  of *p*-nitrophenol, (c) 200  $\mu\text{g}$  of *m*-cresol, (d) 300  $\mu\text{g}$  of 3-methyl-2-methoxyphenol. A 0.5-Hz line-broadening smoothing and one zero fill were applied to all spectra. In c and d a resonance at  $\sim 1.5$  ppm corresponds to the methyl group in acetate, a contaminant from the buffer.

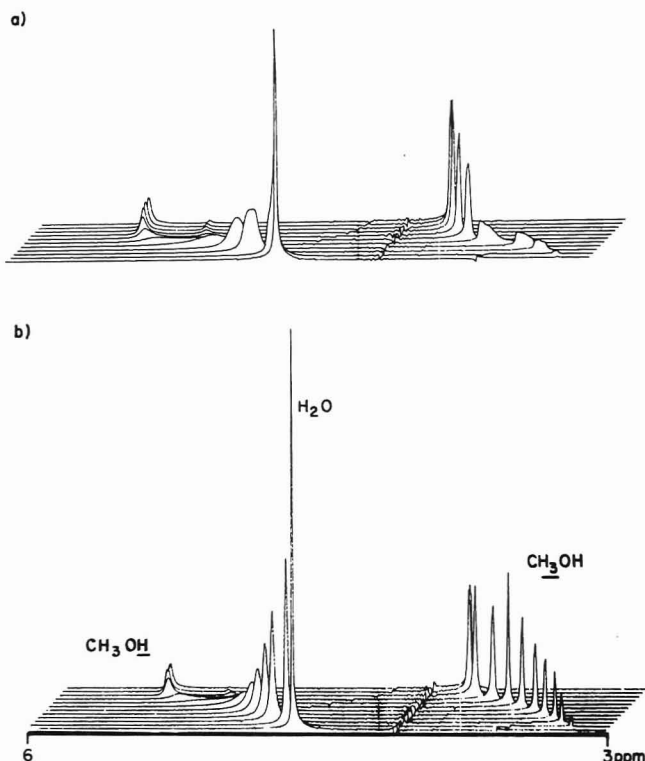
number of eluting components despite inadequate chromatographic resolution.

**Solvent Gradients.** Although use of solvent gradients enhances the versatility of HPLC separations, they have not been applied to HPLC/NMR analyses with protonated solvents. Figure 6 presents stacked plots of solvent spectra for two HPLC gradients (100%  $\text{H}_2\text{O}$  to 100% methanol) detected by NMR, which indicate a few of the technical difficulties associated with gradient elution analyses. Whereas isocratic HPLC/NMR separations permit the finely tuned application of specific pulse sequence spectral parameters to the suppression of solvent resonances, significant changes in solvent chemical shift values, line width, and line shape require the dynamic on-line reevaluation of NMR parameters to achieve effective suppression.

Figure 6 compares the NMR peak shapes obtained from a 100% change in solvent composition achieved in 2 min and 20 min. The significant distortion in peak shapes for the fast ramp, Figure 6a, is attributed to the concentration gradient in the cell which perturbs the homogeneity of the field. This effect is more pronounced for solvent systems with significant differences in dielectric constants. An obvious solution is the use of less abrupt gradients which, as seen in Figure 6b where the change in concentration is a factor of 10 less, yield spectral line shapes unperturbed by these effects.

Perturbation of NMR line shape is not limited to solvent-solvent interactions, but also is observed for solvent-analyte interactions. For example, the line widths of the caffeine resonances in Figure 2a for 400  $\mu\text{g}$  injected are sig-



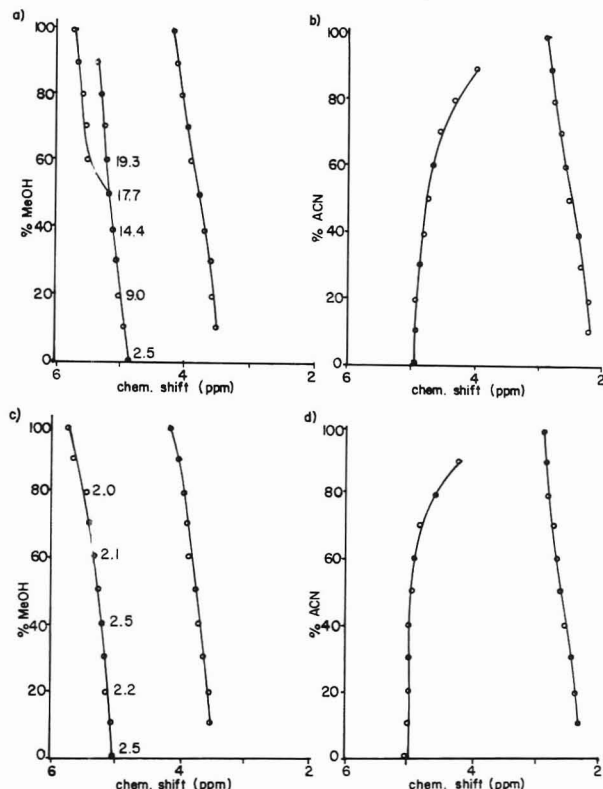


**Figure 6.** Stacked plots of the NMR spectra for the gradient 100:0  $\text{H}_2\text{O}$ -methanol to 0:100  $\text{H}_2\text{O}$ -methanol: (a) spectra acquired at 2 mL/min during a ramp of 2 min duration; (b) spectra acquired at 2 mL/min during a ramp of 20 min duration.

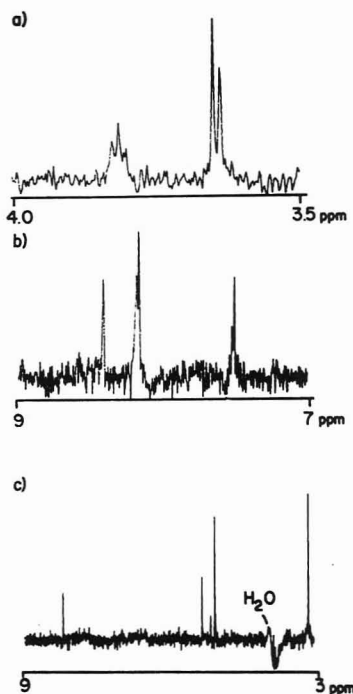
nificantly broader than those in Figure 2c for 50  $\mu\text{g}$  injected. In this example, even though an isocratic separation is used, the high concentration of caffeine in the water-methanol system degrades the spectral line shape.

Figure 6b suggests a second limitation of gradient systems which is not so readily overcome. Chemical shift values for both the methyl and acidic protons are observed to change by several hundred hertz during the gradient. Unless some means is employed to minimize the change in chemical shift for the solvent systems, then an interactive procedure would be required in which the NMR would track the solvent gradient, implementing changes in NMR pulse sequence parameters for the particular solvent concentration in the observe cell. For example, the 1-1 hard pulse parameters to be modified would be the spectrometer frequency which must be placed halfway between the solvent resonances, and the delay equal to  $1/2\Delta\nu$ , where  $\Delta\nu$  is the chemical shift difference between the two solvent peaks.

Figure 7 provides a comparison of changing chemical shift values for  $\text{H}_2\text{O}$ -methanol and  $\text{H}_2\text{O}$ -acetonitrile gradients in which both buffered and pure  $\text{H}_2\text{O}$  are used. A change of chemical shift in excess of 200 Hz is observed for all resonances during the course of the gradient elution. However, an interesting phenomenon is observed for the pure  $\text{H}_2\text{O}$ -methanol system (Figure 6b) in which, with increasing methanol, the acidic resonance around 5 ppm becomes increasingly broad (in excess of 20 Hz wide near 50:50  $\text{H}_2\text{O}$ -methanol), followed by separation of the acidic methanol and  $\text{H}_2\text{O}$  resonances. Peak broadening and the formation of three separate resonances would not permit the use of the 1-1HP method for suppression of dual resonances during an isocratic separation, effectively eliminating use of the  $\text{H}_2\text{O}$ -methanol system when greater than 40% methanol is required. Fortunately, this limitation can be remedied because, as seen in Figure 7c for the buffered  $\text{H}_2\text{O}$ -methanol system, the fast exchange conditions are retained at acidic (and, although not shown, also at basic pH) as peak widths remain below 3 Hz for all reso-



**Figure 7.** Graphs of proton chemical shift values as a function of relative concentration for (a) pure  $\text{H}_2\text{O}$  and methanol, (b) pure  $\text{H}_2\text{O}$  and acetonitrile, (c) buffered  $\text{H}_2\text{O}$  and methanol, and (d) buffered  $\text{H}_2\text{O}$  and acetonitrile. Numbers correspond to line width (fwhh, Hz) for selected resonances.



**Figure 8.**  $^1\text{H}$  NMR spectra from HPLC/NMR experiment with gradient from 90:10  $\text{D}_2\text{O}$ -acetonitrile to 80:20  $\text{D}_2\text{O}$ -acetonitrile: (a) 200  $\mu\text{g}$  of ascorbic acid, (b) 200  $\mu\text{g}$  of niacin, (c) 300  $\mu\text{g}$  of vitamin  $\text{B}_6$ .

nances. The phenol separation for which spectra are presented in Figure 5, was acquired in a buffered 20:80  $\text{H}_2\text{O}$ -methanol solvent system.

An examination of the buffered and unbuffered  $\text{H}_2\text{O}$ -acetonitrile systems in Figure 7b,d reveals little difference in chemical shift values during the gradient elution. One interesting observation, however, is the relative invariance in

chemical shift for the H<sub>2</sub>O resonance between 100% and 40% H<sub>2</sub>O for the buffered case (less than 20 Hz). Because the 1-1 hard pulse technique provides effective suppression over a range of 25 Hz around the peak centroid (6), it should be possible to implement a gradient separation in this region of relative stability without altering 1-1HP parameters. A gradient elution of 90:10 D<sub>2</sub>O-acetonitrile to 80:20 D<sub>2</sub>O-acetonitrile was used to separate a three-component mixture of vitamins. The chemical shift change of 10 Hz for the H<sub>2</sub>O and 18 Hz for the acetonitrile resonances permitted the selection of a single spectrometer frequency and delay for the 1-1HP pulse sequence. Figure 8 contains the coadded spectra from this separation.

In conclusion, the application of HPLC/NMR to reverse-phase separations in protonated solvents has been demonstrated. Either protonated H<sub>2</sub>O-acetonitrile or H<sub>2</sub>O-methanol may be employed in any relative concentration for isocratic analysis with 1-1 hard pulse NMR sequence permitting the effective suppression of dual solvent resonances while leaving unperturbed the majority of the <sup>1</sup>H NMR spectrum.

**Registry No.** Acetaminophen, 103-90-2; caffeine, 58-08-2; acetylsalicylic acid, 50-78-2; phenol, 108-95-2; *p*-nitrophenol,

100-02-7; *m*-cresol, 108-39-4; 2-methyl-3-methoxyphenol, 6971-52-4; ascorbic acid, 50-81-7; niacin, 59-67-6; vitamin B<sub>6</sub>, 8059-24-3.

## LITERATURE CITED

- (1) Dorn, H. C. *Anal. Chem.* **1984**, *56*, 747A-758A.
- (2) Bayer, E.; Albert, K.; Nieder, M.; Grom, E. *J. Chromatogr.* **1979**, *186*, 497-507.
- (3) Laude, D. A., Jr.; Wilkins, C. L. *Anal. Chem.* **1984**, *56*, 2471-2475.
- (4) Clore, G. M.; Kimbrev, B. J.; Gronenborn, A. M. *J. Magn. Reson.* **1983**, *54*, 170-173.
- (5) Turner, D. L. *J. Magn. Reson.* **1983**, *54*, 146-148.
- (6) Hore, P. J. *J. Magn. Reson.* **1983**, *55*, 283-300.
- (7) Bayer, E.; Albert, K.; Nieder, M.; Grom, E.; Woolf, G.; Rindlisbacher, M. *Anal. Chem.* **1982**, *54*, 1747-1750.
- (8) Buddruss, J.; Herzog, H. *Anal. Chem.* **1983**, *55*, 1611-1614.
- (9) Laude, D. A., Jr.; Lee, R. W.-K.; Wilkins, C. L. *Anal. Chem.* **1985**, *57*, 1464-1469.

RECEIVED for review July 7, 1986. Resubmitted October 16, 1986. Accepted October 30, 1986. Support from the National Science Foundation under Grant CHE-85-19087 and a Department Research Instrument Grant, CHE-82-03497, is gratefully acknowledged. Partial support of D.A.L. by the University of California, Riverside, Toxic Substances Research and Training Program is also acknowledged.

# Compositional and Solid-State Nuclear Magnetic Resonance Study of Humic and Fulvic Acid Fractions of Soil Organic Matter

Michael A. Wilson\* and Anthony M. Vassallo

CSIRO Division of Fossil Fuels, P.O. Box 136, North Ryde, New South Wales 2113, Australia

E. Michael Perdue\* and J. Helmut Reuter

School of Geophysical Sciences, Georgia Institute of Technology, Atlanta, Georgia 30332

Four soil organic matter samples (two humic acid fractions and two fulvic acid fractions) were obtained from two proximate soils in the flood plain of the Altamaha River in southeastern Georgia. Each sample was characterized by elemental and functional group analyses and by <sup>13</sup>C nuclear magnetic resonance spectrometry using cross polarization magic angle spinning (CP-MAS) with spin counting. The elemental and functional group analyses provided input for a series of analytical constraints calculations that yield an absolute upper limit for the amount of aromatic carbon and most probable estimates of both aromatic and non-carboxyl aliphatic carbon in each sample. Spin counting experiments demonstrate that less than 50% of the carbon in three of the fractions is observed in the NMR experiment, and even after correction for differential relaxation, the amounts of aromatic and non-carboxyl aliphatic carbon determined by <sup>13</sup>C CP-MAS NMR are dissimilar to those obtained by calculation. Unambiguous evidence is presented for the predominance of aliphatic carboxyl groups in one of the fulvic acid fractions.

Humic substances have been widely reported to contain amino acids, carbohydrates, and lignin-derived phenols that are of undeniably biochemical origin (1). The overall per-

centage of humic carbon that has been identified as these biochemical substances is small, as exemplified by the analytical chemical results of Perdue and co-workers for amino acids (about 1% (2)), carbohydrates (about 2% (3)) and lignin-derived phenols (about 5% (4)). The structure of the remaining organic matter in a typical humic substance is unknown and may be sufficiently altered by oxidation and hydrolysis that analysis detects insignificant amounts of identifiable compounds.

While the highly compound-specific methods that are used to quantify biochemical precursors in humic substances cannot detect even slightly modified compounds that result from oxidation and/or hydrolysis of biochemical precursors, functional-group-specific spectroscopic methods can detect unaltered functional groups even if some part of a compound has been chemically modified. Nuclear magnetic resonance spectrometry, in particular, has emerged as a very useful tool for characterizing the structural features of unfractionated humic substances, and, with some dissent (5, 6), it is now widely accepted that humic substances and their soluble solvent extracts contain a wide and variable array of structural carbon types (7-11).

Even though <sup>13</sup>C NMR spectrometry is becoming increasingly popular for the characterization of humic substances, questions remain concerning its use as a quantitative tool. In the related literature on the structural chemistry of coals, the



**Table I. Analytical Data for Samples Used in NMR Studies<sup>a</sup>**

parameter	HA3	FA3	HA5	FA5
C	54.1	45.9	50.9	42.5
H	3.5	4.5	4.5	4.7
N	1.8	1.3	2.9	1.1
O + S	40.6	48.3	41.7	51.7
ash	2.1	3.1	2.6	1.3
COOH	3.9	5.5	3.4	5.6
ArOH	4.3	3.7	4.2	3.5

<sup>a</sup> Elemental data in wt % on a dry, ash-free basis. S is small < 3%. COOH and ArOH in mmol/g. See ref 36 for details.

quantitative capabilities of <sup>13</sup>C NMR have been evaluated through model compound studies, direct <sup>1</sup>H and indirect <sup>13</sup>C spin-lattice relaxation time measurements in the rotating frame (12–14), Bloch decay experiments (15–19), comparative solution NMR experiments (15, 19–21), and spin counting (22–27). Only a few comparable detailed quantitative studies of <sup>13</sup>C NMR of humic substances, including a Bloch decay (28) and several studies of the contact time dependency of cross polarization (29–31), have been conducted. Spin counting, which has not previously been applied to NMR studies of humic substances, allows the fraction of “observed” carbon in a sample to be determined. Even with isotopic labeling (27), however, it is not possible to determine whether the “observed” carbon (when less than 100%) is actually representative of all the carbon in the sample.

Perdue (32) has demonstrated that basic data such as elemental and wet chemical functional group analyses can place unambiguous constraints on the level of aromatic carbon in a humic substance and can even be used to predict the most probable levels of aromatic and aliphatic carbon. The methods used by Perdue (32) allow the development of a series of analytically imposed constraints and probabilities against which other structural and/or compositional data can be evaluated. Like spectroscopic data, elemental and wet chemical functional group data are not compound-specific and may be only slightly affected by minor oxidation and/or hydrolysis of a humic substance.

We therefore wish to present the results of a compositional and spin counting study of four humic substances from a river floodplain in southeastern Georgia. Analytical constraints calculations of limiting and most probable carbon compositions were combined with <sup>13</sup>C NMR spectra to obtain more than one perspective on the compositions and structures of these samples and to check the internal consistency of the two approaches. These results demonstrate the high degree of structural and compositional variability that exists between samples extracted from the same general environment and shed some light on the ongoing controversy over the existence of aliphatic carboxyl groups in humic substances (33–35).

## EXPERIMENTAL SECTION

**Samples.** Elemental compositions and functional group data for the samples used in this study are given in Table I. Soil samples from the flood plain of the Altamaha River in southeastern Georgia were extracted under nitrogen with sodium hydroxide solution. The alkaline extracts were hydrogen-exchanged and freeze-dried. The solid products were then exhaustively extracted with water to obtain water-soluble samples (FA3, FA5) and water-insoluble samples (HA3, HA5). These samples are operationally similar to soil fulvic and humic acids, in that similar extraction procedures are used, but no special efforts were made to isolate the hydrophobic fractions that can be adsorbed from acidic solutions by macroporous XAD resins. Further details are given elsewhere (36).

**Analytical Constraints on Composition.** The methods described by Perdue (32) were used to place structural limits on the compositions of the samples used in this study and to estimate

the most probable distribution of aliphatic, aromatic, and “excess” carbon in these samples. Just as the number of moles of rings and  $\pi$  bonds in a pure substance (referred to collectively as *unsaturation*) can be computed from its elemental composition, the amount of unsaturation in a mixture is rigorously given by the equation

$$\phi_{\text{total}} = C_{\text{total}} + N_{\text{total}}/2 - H_{\text{total}}/2 + 1000/\bar{M}_n \quad (1)$$

where all terms are in units of mmol/g and  $\bar{M}_n$  is the number-average molecular weight of the mixture. It is easily shown that  $\phi_{\text{total}}$  is insensitive to  $\bar{M}_n$  for mixtures such as humic substances, for which  $\bar{M}_n$  values are approximately  $10^3$  or greater. Unsaturation exists in COOH and C=O groups, in aromatic and aliphatic rings, and in other “excess” functional groups that may exist in humic substances (alkenes, esters, amides). Thus

$$\phi_{\text{total}} = [\text{COOH}] + [\text{C=O}] + C_{\text{ar}}(\phi/C)_{\text{ar}} + C_{\text{al}}(\phi/C)_{\text{al}} + C_{\text{xs}}(\phi/C)_{\text{xs}} \quad (2)$$

where the “xs” subscript refers to “excess” functional groups. The maximum possible amount of aromatic carbon that could exist in a humic substance containing known concentrations of COOH and C=O groups corresponds to the unique case in which the sample has absolutely no aliphatic or excess unsaturation ( $C_{\text{al}}$  and/or  $(\phi/C)_{\text{al}}$  equal zero and  $C_{\text{xs}}$  and/or  $(\phi/C)_{\text{xs}}$  equal zero)

$$(C_{\text{ar}})_{\text{max}} = (\phi_{\text{total}} - [\text{COOH}] - [\text{C=O}]) / (\phi/C)_{\text{ar}} \quad (3)$$

It turns out that the smallest value for  $(\phi/C)_{\text{ar}}$ , corresponding to the largest value for  $C_{\text{ar}}$ , is that of simple benzene rings, which contain four rings and  $\pi$  bonds per six aromatic carbons. Thus, the maximum fraction of aromatic carbon in a humic substance is given by

$$(f_{\text{a}})_{\text{max}} = \frac{(C_{\text{ar}})_{\text{max}}}{C_{\text{total}}} = \frac{\phi_{\text{total}} - [\text{COOH}] - [\text{C=O}]}{C_{\text{total}}(4/6)} \quad (4)$$

Equation 4 can be evaluated simply from commonly available elemental and functional group analyses, using estimates of 1000 and 5000 g/mol for the  $\bar{M}_n$  values of fulvic and humic acids, respectively (recall that  $\phi_{\text{total}}$  is not very sensitive to  $\bar{M}_n$ ). Such basic data thus provide an unequivocal upper limit on the abundance of aromatic carbon in a humic substance.

Perdue (32) also described numerical methods for estimating the most probable abundances of  $C_{\text{al}}$ ,  $C_{\text{ar}}$ , and  $C_{\text{xs}}$  in a humic substance. Mass balance equations for  $C_{\text{total}}$  and  $H_{\text{total}}$  can be written in the form of eq 2 to obtain

$$C_{\text{total}} = [\text{COOH}] + [\text{C=O}] + C_{\text{ar}} + C_{\text{al}} + C_{\text{xs}} \quad (5)$$

$$H_{\text{total}} = [\text{COOH}] + C_{\text{ar}}(H/C)_{\text{ar}} + C_{\text{al}}(H/C)_{\text{al}} + C_{\text{xs}}(H/C)_{\text{xs}} \quad (6)$$

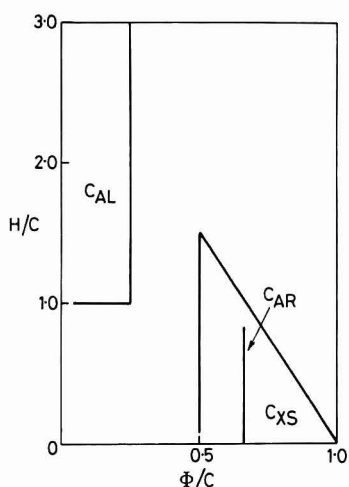
Estimates of  $C_{\text{al}}$ ,  $C_{\text{ar}}$ , and  $C_{\text{xs}}$  can be obtained, in principle, by simultaneous solution of eq 2, 5, and 6. These equations cannot be evaluated, unless the average  $(H/C)$  and  $(\phi/C)$  ratios of aliphatic, aromatic, and excess carbon are known, which is certainly not the case for humic substances. However, Perdue (32) was able to establish lower and upper limits on average  $(H/C)$  and  $(\phi/C)$  ratios based on the bonding characteristics and assumed composition of each carbon type and by randomly generating plausible solutions of calculated most probable values of  $C_{\text{al}}$ ,  $C_{\text{ar}}$ ,  $C_{\text{xs}}$ , and hence  $f_{\text{a}}$  and  $f_{\text{al}}$  (fraction of aliphatic carbon).

The allowed ranges of  $(H/C)$  and  $(\phi/C)$  for the three classes of carbon are given in Figure 1 (see ref 32 for derivation). It is anticipated that “most probable” estimates will be best for  $C_{\text{al}}$  and that  $C_{\text{ar}}$  will be somewhat underestimated because it is possible for  $C_{\text{xs}}$  to have the same  $(H/C)$  and  $(\phi/C)$  values as  $C_{\text{ar}}$ , and hence solutions may place some  $C_{\text{ar}}$  as  $C_{\text{xs}}$  (32). In light of the ongoing debate over the quantitative capabilities of <sup>13</sup>C NMR cross polarization magic angle spinning (CP-MAS) spectrometry, an independent method of calibrating the computational method was considered to be necessary. A series of entirely hypothetical “compounds” that contain a wide range of  $C_{\text{al}}$  values was constructed from some of the biochemical precursors that occur in humic substances. These “compounds” are shown in Figure 2 and the corresponding analytical data are given in Table II. The

**Table II. Compositional Parameters of Calibration "Compounds"**<sup>a</sup>

compd	% C	% H	% N	% O	COOH	C=O	$M_n$	$f_{al}$
1	54.3	3.8	0.0	41.9	3.57	0.00	840	0.16
2	55.0	4.4	1.5	39.2	4.26	0.00	939	0.28
3	53.5	5.2	4.3	36.9	4.62	0.00	650	0.41
4	60.2	6.4	4.3	29.2	4.56	0.00	658	0.42
5	41.8	4.3	0.0	53.9	6.74	0.00	890	0.61
6	52.5	6.4	3.3	37.8	4.73	1.18	846	0.65
7	47.9	5.8	0.0	46.3	6.89	0.00	726	0.72
8	41.8	5.6	0.0	52.6	2.90	0.00	1034	0.92

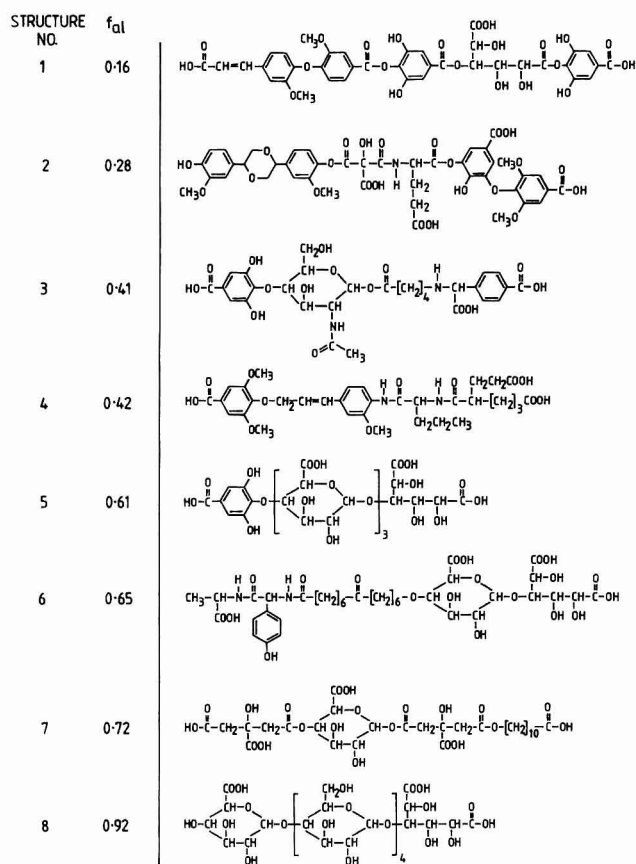
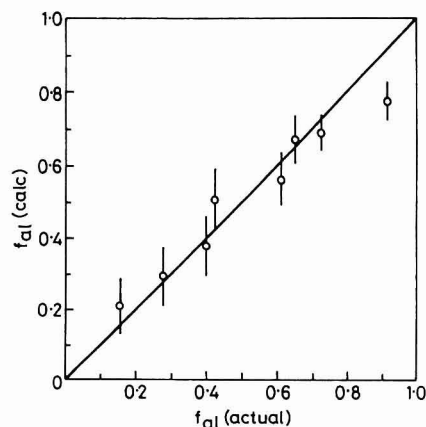
<sup>a</sup>Elemental data in wt % on a dry, ash-free basis. COOH and C=O in mmol/g.  $M_n$  = number-average molecular weight (g/mol).  $f_{al}$  = fraction aliphatic carbon.

**Figure 1.** Allowed ranges of (H/C) and ( $\phi$ /C) for aliphatic, aromatic, and excess carbon in humic substances.

computational method was "calibrated" by comparing the actual  $C_{al}$  values of these "compounds" with the predictions of the carbon distribution calculations.

**NMR Spectrometry.** Solid-state  $^{13}\text{C}$  NMR spectra were obtained by the cross polarization method at 22.5 MHz using magic angle spinning (CP-MAS). Full details of methods have been described elsewhere (29). Contact time was 0.5–12 ms with a recycle time of 1 s. Rotors were constructed from boron nitride with a Kel-F base and were used at rotor speeds of up to 3.5 kHz. Sidebands were insignificant. In some experiments, the dipolar dephasing technique (37) was used to distinguish protonated from nonprotonated carbon. Full details of the application of this method to humic substances are given by Wilson et al. (29). About 20 000 scans were needed for adequate signal and phasing but up to 100 000 scans were collected in spin counting experiments. To obtain reproducible results, compromise has to be made between adequate signal and deviation from the Hartmann–Hahn match when longer experimental times are used. Natural valleys in the spectra were used in integrating the broad resonances from different functional groups.

**Spin Counting.** Spin counting experiments involved recording the spectrum of mixtures of sample and glycine (accurately weighed and intimately mixed) at different contact times (1–12 ms) to determine the spin-lattice relaxation in the rotating frame ( $T_{1\rho}H$ ) behavior of both sample and glycine under identical conditions. Even though the glycine resonances overlap with those of the humic substances, it was possible to calculate the contribution of the glycine to the total signal. At long contact times only the resonances from the glycine were observed and the signal intensities of these resonances could be fitted to a simple single exponential function from which the  $T_{1\rho}H$  and the signal intensity in the absence of relaxation were determined. The contribution of signal from humic substance at each contact time was calculated from the region of the spectrum free from glycine resonances (55–165 ppm). These areas were then scaled up to account for the signal under the glycine resonances using the known ratio in the absence of glycine. Assuming 100% carbon detection from glycine, the normalized area per milligram of carbon in the sample can be calculated and compared with what is observed. The

**Figure 2.** Structures of hypothetical organic "compounds" used to evaluate the analytical constraints calculation method.**Figure 3.** Comparison of most probable estimates of aliphatic carbon with actual values for the "compounds" in Figure 2. Vertical bars represent one standard deviation unit.

percent carbon seen is thus the percent ratio of the area of the sample spectrum to the area expected from the carbon content. This method was checked by using hexamethylbenzene as a sample and showed that, as expected, 100% ( $\pm 5\%$ ) of the hex-



**Table III. Results of Analytical Constraints Calculations<sup>a</sup>**

parameter	HA3	FA3	HA5	FA5
[COOH]	9	14	8	16
$C_{al}$	16 ± 8	48 ± 8	36 ± 8	60 ± 7
$C_{ar}$	43 ± 20	19 ± 11	30 ± 16	12 ± 8
$C_{xs}$	32 ± 18	19 ± 13	26 ± 18	12 ± 9

<sup>a</sup> Units in mol %, COOH was calculated from Table I.

amethylbenzene carbon is detected. It should be noted that the  $T_{1\rho}H$  of glycine sometimes increased greatly on mixing with humic/fulvic material.

## RESULTS AND DISCUSSION

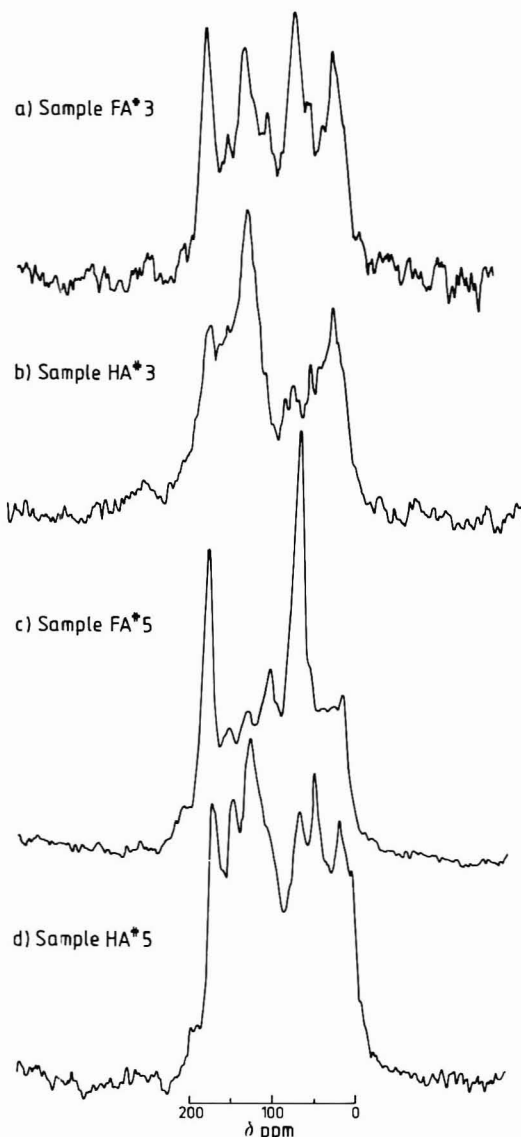
**Analytical Constraints Calculations.** The results of the computational exercise are given in Figure 3. Over most of the range of  $C_{al}$  values, the predicted value was within one standard deviation unit of the actual  $C_{al}$  value, the exception being the highest  $C_{al}$  value, which was underestimated by the probability calculations. In as much as the calculations procedure is equally applicable to pure substances and mixtures, the results of this limited calibration indicate that the probability calculations should provide reasonably accurate estimates of  $C_{al}$  in actual humic substances.

Calculated results for maximum percent  $C_{ar}$  and for most probable percent  $C_{al}$ ,  $C_{ar}$ , and  $C_{xs}$  for the four humic substances are given in Table III. As expected, predictions of  $C_{al}$  have less uncertainty than predictions of the other carbon types. These results clearly predict a considerable range of compositions for the four samples, even though the samples were isolated from very similar environments and were fractionated by simple water extraction. There is an obvious enrichment of  $C_{ar}$  in the humic acid samples. The most aliphatic sample is FA5 (60%  $C_{al}$ ) and the least aliphatic sample is HA3 (16%  $C_{al}$ ). Conversely, HA3 has the highest and FA5 has the lowest  $C_{ar}$  value.

Although not shown in Table III, most probable  $(H/C)_{ar}$  values for all four samples were predicted to lie in the 0.36–0.40 range, corresponding to an average of 2.2–2.4 unsubstituted carbons per aromatic ring. Interestingly, the principal phenolic building blocks in woody angiosperms and gymnosperms (syringyl and vanillyl phenols) contain two to three unsubstituted carbons per aromatic ring. These phenols accounted for about 5% of the carbon in two aquatic humic substances and were enriched in the humic acid fractions of those samples (4).

**NMR Peak Assignments.** Up to seven distinct broad resonances are observed in the CP-MAS spectra (Figure 4). These arise from the presence of ketone or aldehyde carbon (centered at 200 ppm), carboxylic acid, ester, and amide carbon (171–173 ppm), phenolic and aryl ether (147–151 ppm), aryl (129–132 ppm), acetal, ketal, or similar structures (104–106 ppm), alcoholic or dialkyl ether (73–76 ppm), alkoxy (55–57 ppm), and alkyl (19–32 ppm) carbons. Some olefinic carbon may resonate between 107 and 160 ppm. It is evident from Figure 4 that the proportions of these various types vary greatly between the fractions. For example, HA5 contains predominantly carboxyl and alcoholic or dialkyl ether carbon, while HA3 contains mainly aryl and alkyl carbon.

Some further indication of the various structural types present is given by the dipolar dephased spectra, which contain resonances only for nonprotonated and methyl carbons. In particular, substituted aryl carbons, methyl, and methoxyl groups are readily detected, while other protonated carbons give little signal. By comparison of the dipolar dephased spectra in Figure 5 with the normal spectra in Figure 4, methyl groups (~19 ppm), methoxyl groups (57 ppm), and substituted aryl carbons (129–151 ppm) are clearly present in all



**Figure 4.**  $^{13}\text{C}$  CP-MAS NMR spectra of the samples used in this study. Contact time was 1 ms; recycle time was 1 s.

samples. However, signal intensities are substantially reduced for alcoholic or dialkyl ether carbons (70–80 ppm), indicating that such carbons are protonated.

The resonance at ~70 ppm, which we have assigned to carbohydrate carbon, has plausibly been assigned to polyethers by Bayer et al. (38). Other evidence, however, supports our assignment. Wershaw et al. (39), using a soil fulvic acid, have shown by derivatization that this resonance arises mainly from carbohydrates. In our extracts, the presence of dioxygenated aliphatic carbons (which form acetal and ketal links in carbohydrates) also suggests the presence of carbohydrate carbon. In addition, the infrared (IR) spectra of these samples (36) exhibit strong absorption in the 1050- $\text{cm}^{-1}$  range that typifies carbohydrates. Moreover, the intensity of IR absorption in this region is proportional to the intensity of the  $^{13}\text{C}$  NMR peak in the 70–80 ppm region. The detection of furans (40) in the pyrolysis gas chromatograms of these samples is consistent with the presence of carbohydrates. The presence of polyethers (38) cannot be ruled out, however, simply because humic substances have great structural diversity.

**Variable Spin-Lattice Rotating Frame Relaxation Times ( $T_{1\rho}H$ ) and Quantitation.** Although the quantitative accuracy of  $^{13}\text{C}$  CP-MAS NMR measurements on geochemical samples has not been fully assessed, it is common to integrate spectra obtained at 1 ms contact time (e.g., Figure 4) to measure the proportions of various classes of carbon types in

**Table IV. Integrated Areas of  $^{13}\text{C}$  NMR Spectra, Corrected for Variable  $T_{1\rho}H$ 's<sup>a</sup>**

carbon type	HA3		FA3		HA5		FA5	
	N	D	N	D	N	D	N	D
total aliphatic	42	14	51	31	49	19	73	28
alkyl	23	9	16	↑	18	9	18	8
methoxyl	4	↑ 5		25	16	3	tr	tr
alcoholic	12	↓	27	↓	15	4	39	10
acetal + ketal	3		8	6		3	16	10
total aromatic	42	26	29	23	35	22	12	12
aryl-H,R	↑	↑	↑	↑	24	12	8	8
	42	26	29	23				
aryl-O	↓	↓	↓	↓	11	10	4	4
COOH	15	10	19	15	13	7	18	13
carbonyl	2	2			1	1		

<sup>a</sup> Units in mol %, and tr, N, and D are defined as follows: tr, trace amount detected; N, normal spectra, corrected for effects of  $T_{1\rho}H$ 's; D, dipolar dephased spectra (40  $\mu\text{s}$ ). Arrows imply integrated areas for regions which could not be accurately further subdivided.

a sample. Recycle times of  $\leq 5$  s must be used because of the necessity to collect large (20 000) numbers of scans for adequate signal to noise. One source of error in solid-state spectra is the potential variability of  $T_{1\rho}H$ 's for different carbon types in complex mixtures (only one  $T_{1\rho}H$  is normally observed in pure solids). In coals, all carbon types usually appear to have comparable  $T_{1\rho}H$  values (with some exceptions (14, 15)), but this is not necessarily true for humic substances. In this study, decay of signal intensity was found to be exponential over six data points from 2 to 7 ms (correlation coefficients  $\geq 0.98$ ) so that an average  $T_{1\rho}H$  for the sample could be measured (contact times up to 12 ms were used for spin counting experiments). However, in some samples,  $T_{1\rho}H$ 's for different functional groups were found to range from 1.4 to 5.8 ms (Table V). These observations may indicate that various structural groups with different  $T_{1\rho}H$ 's are not bonded to each other, although it is possible that differences in molecular motion or local effects of paramagnetic ions are responsible (30, 31).

It is noteworthy that the  $T_{1\rho}H$  of the carbohydrate components of some of the extracts is much shorter than that for other components of the same extract (Table V). This behavior is illustrated by the spectra obtained at 0.5 and 1 ms for sample FA5 and 0.8 and 5 ms for sample HA5 (Figure 6), which show diminished carbohydrate signals at longer contact times.

It is also true that the buildup of  $^{13}\text{C}$  magnetization takes a finite time, characterized by a constant termed  $T_{\text{CH}}$ , the cross polarization time constant. The exact value of  $T_{\text{CH}}$  depends on a number of factors such as molecular motion and the distance of carbons from protons. In general  $T_{\text{CH}}$  for  $\text{CH}_2$  and  $\text{CH}$  carbons is smaller than for  $\text{CH}_3$  carbons which in turn is shorter than nonprotonated carbons. A considerable amount of attention has gone into establishing  $T_{\text{CH}}$  values for model compounds which are relevant in geochemistry (12, 13, 23). It suffices to say that  $T_{\text{CH}}$ 's for most carbons are  $\leq 0.5$  ms and methine and methylene carbon  $\leq 0.2$  ms. Since buildup in magnetization is given by  $T_{\text{CH}}$ , and decrease in magnetization given by  $T_{1\rho}H$ , the actual magnetization at contact time,  $t$ , and thus signal intensity  $S_t$  is given as a combination of these by

$$S_t = S_0 \left( \frac{T_{1\rho}H}{T_{1\rho}H - T_{\text{CH}}} \right) (1 - \exp(-\alpha t / T_{\text{CH}})) (\exp(-t / T_{1\rho}H)) \quad (7)$$

where  $\alpha = (1 - T_{\text{CH}}/T_{1\rho}H)$  and  $S_0$  is the signal intensity in the absence of relaxation.

**Table V. Relaxation Data**

structural unit	$T_{1\rho}H$ , ms			
	HA3	FA3	HA5	FA5
sample averaged	2.5	2.5	3.5	2.0
methyl (17 ppm)			5.8	
methylene (29 ppm)			3.8	
methoxyl (57 ppm)			2.7	
alcoholic (76 ppm)			2.3	1.5
acetal + ketal (108 ppm)		1.4		1.8
aryl (132 ppm)			4.8	
aryl-O (152 ppm)			4.3	
COOH (173 ppm)			3.3	2.5

For the purposes of comparing signal intensities from each functional group it is necessary therefore to calculate  $S_0$  for each functional group in the substance. This requires a knowledge of  $T_{\text{CH}}$ . We have attempted to measure real  $T_{\text{CH}}$ 's, for humic substances from  $S_t$  vs  $t$  plots at short  $t$  values ( $< 1$  ms) but were unsuccessful due to an inability to delineate individual signal intensities within broad resonance bands. Instead, since the data appear to be exponential, we have calculated  $S_0$  from eq 8, which is derived from eq 7 if  $(\exp(-\alpha t / T_{\text{CH}})) \rightarrow 0$ .

$$S_0 = S_t(T_{1\rho}H - T_{\text{CH}})T_{1\rho}H^{-1}(e - t/T_{1\rho}H)^{-1} \quad (8)$$

In the case when  $T_{1\rho}H \gg t \gg T_{\text{CH}}$ , i.e., eq 7 reduces to eq 8,  $S_0$  is a measure of the number of  $^{13}\text{C}$  nuclei which yield the signal intensity (24). Assuming an upper limit of  $T_{\text{CH}}$  of 0.5 ms and a lower limit of  $T_{1\rho}H$  of 2.0 ms, calculation of  $S_0$  from eq 8 using our data should introduce  $< 10\%$  error in  $S_0$ . The values so obtained represent the relative proportions of functional groups in the sample and are listed in Table IV. It should be appreciated that material which might be in the humic substance but for which  $T_{1\rho}H/T_{\text{CH}}$  is small or for which  $T_{1\rho}H$  is long (e.g., 100 s) will not be observed. Hence functional group analyses employing eq 8 yield estimates which, although better approximations than values obtained by single contact experiments, may still be in error. An estimate of how much carbon is seen as  $S_0$ , however, can be made by spin counting experiments. The presence of undetected carbon in the humic and fulvic acid fractions is confirmed by the spin counting experiments. Estimates of the amount of carbon detected by this technique are shown in Table VI. It is clear from these data that less than 100% of the carbon is being detected in all cases.

Different effects may reduce  $T_{1\rho}H/T_{\text{CH}}$  or increase  $T_{1\rho}H$  for different functional groups to render some signal unobservable. Low frequency motion may reduce  $T_{1\rho}H$  for aromatic or aliphatic carbon. Organic paramagnetic species are intrinsically



Table VI. Results of Spin Counting Experiments on Humic and Fulvic Acid Fractions

expt no.	substrate	C <sup>a</sup> glycine, mg	C <sup>a</sup> substrate, mg	T <sub>1ρ</sub> H <sup>b</sup> glycine, ms	T <sub>1ρ</sub> H substrate, ms	% C <sup>c</sup> obsd
1	HA3	25.0	102.8	30.0	3.0	30
2	HA3	8.0	81.15	30.0	3.4	30
3	HA5	46.9	56.0	5.2	2.4	62
4	FA3	5.8	58.1	27.2	2.7	33
5	FA5	6.1	53.6	21.7	2.5	47

<sup>a</sup>Carbon in mixture of humic/fulvic-glycine mixture studied by NMR. <sup>b</sup>Spin-lattice relaxation time in the rotating frame measured through carbon. These values are considerably higher than those obtained for glycine alone (4.1 ms). <sup>c</sup>Carbon in humic or fulvic acid predicted from known carbon content of glycine. This is uncorrected for the term  $T_{1\rho}H/(T_{1\rho}H - T_{CH})$  and thus is an upper limit.

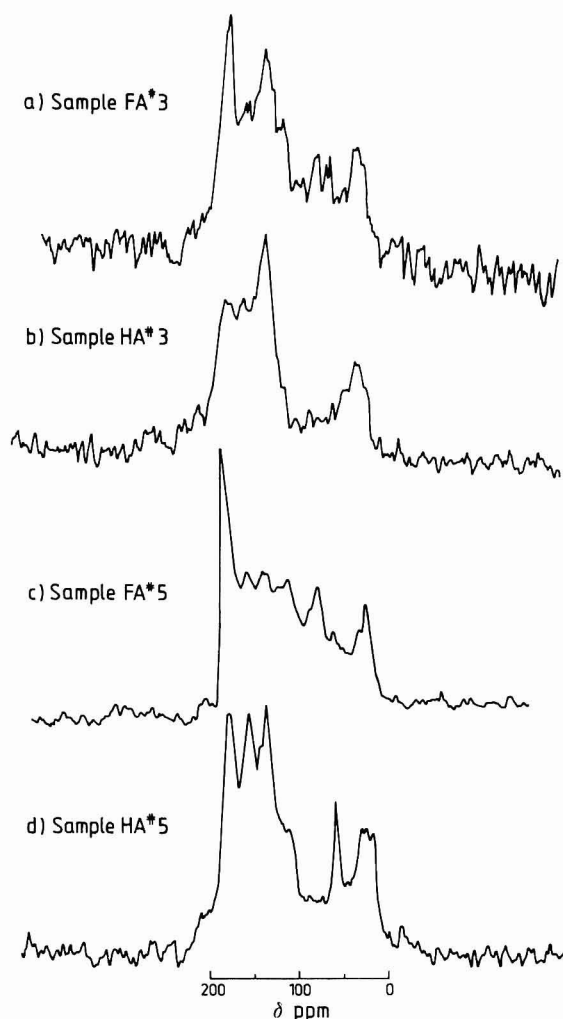


Figure 5. Dipolar dephased <sup>13</sup>C CP-MAS NMR spectra of the samples used in this study. Dipolar dephasing time was 40 μs.

aromatic, and they may reduce  $T_{1\rho}H$  for these species or broaden the resonance frequency so that insufficient power is available to produce a 90° pulse. Inorganic paramagnetics may selectively reduce  $T_{1\rho}H$ 's from polar bonding functional groups (30, 31) or the effect may be felt through all functional groups in the molecule (25).  $T_{1\rho}H$ 's are long for small rigid aromatic molecules (41). Some insight into which structural groups are not observed can be gleaned from the analytical constraint data.

**Structural Interpretations.** The analytical constraint calculations show that the maximum percent aromatic carbon is 63% or less for the humic acid fractions and 30% or less for the fulvic acid fractions. Moreover these calculations suggest that the aromatic carbon is largely nonprotonated, with an average of 2.2–2.4 unsubstituted carbons per aromatic ring. A very rough estimate of the  $(H/C)_{ar}$  value can be calculated from the spectral areas estimated by dipolar dephasing (Table VI). Since the area assigned as aromatic

carbon at 40 μs ( $A_{40}$ ) is almost all nonprotonated (29), then the fraction of aromatic carbon which is protonated is given by  $(A_0 - A_{40})/A_0$  where  $A_0$  is the area at 0 μs. This method ignores the fact that nonprotonated carbon also decays in intensity during dephasing albeit at a slower rate (29). For HA3, the ratio of protonated aromatic carbon to total aromatic carbon is  $(42 - 26)/42 = 0.38$  (Table IV). For HA5,  $(H/C)_{ar} = 0.37$ , i.e., 2.2 unsubstituted carbons per aromatic ring. Thus there is good agreement between the analytical constraint calculations and the NMR data for the humic acids. Less agreement is found for the fulvic acids, because the NMR suggests the aromatic structures are even more highly substituted. The NMR data show enrichment of both aromatic carbon and methoxyl carbon in the humic acid fractions compared with the fulvic acid fractions. This is consistent with the reported enrichment of lignin-derived phenols in humic acid fractions of aquatic humus (4) and with the analytical constraints calculations of aromatic carbon. The expected enrichment of carbohydrates in the water-soluble "fulvic acid" fractions is also confirmed by the NMR results, which indicate significantly greater levels of both alcoholic and acetal/ketal carbon in the FA samples. It should be noted, however, that FA3 contains nearly three times as much aromatic carbon as FA5. Likewise, the methoxyl content is variable and is particularly high in sample HA5.

Estimates of aliphatic carbon (Table IV) by NMR appear to be high. This conclusion is strongly supported by the analytical constraint calculations (Table III), which clearly show that the NMR data consistently overestimate the aliphatic contribution. Nevertheless, notwithstanding the reservations expressed above, the NMR estimates of  $C_{ar}$  (Table IV) are for the most part in reasonable agreement with most probable estimates in Table III. The NMR data can only be used with confidence for quantitative comparisons between humic/fulvic fractions if they are consistent with other analytical data.

All NMR estimates of carboxyl content in Table IV exceed the values in Table III that were calculated from the functional group analytical data in Table I. Since lack of cross polarization should produce an artificially low value for COOH, some other explanation must be sought. The wet chemical estimates of COOH are inherently operational (42, 43) and cannot detect weak carboxylic acids at all, so the COOH values in Table I may be too low. Alternatively, the NMR estimates may include esters, lactones, and amides (amides cannot be very important because of the low nitrogen content of these samples). Hatcher et al. (44) reported that NMR estimates of COOH were in better agreement with wet chemical measurements of total acidity than wet chemical measurements of COOH. In this study, however, if the total acidities in Table I are converted into equivalent concentrations of COOH groups, the resulting maximum possible COOH contents are too high. The total acidities of these samples must therefore include some weak acids other than COOH groups.

Sample FA5 has the best agreement between analytical constraint, titration, and NMR estimates of COOH and  $C_{ar}$ . The combination of a very low  $C_{ar}$  and a high COOH content

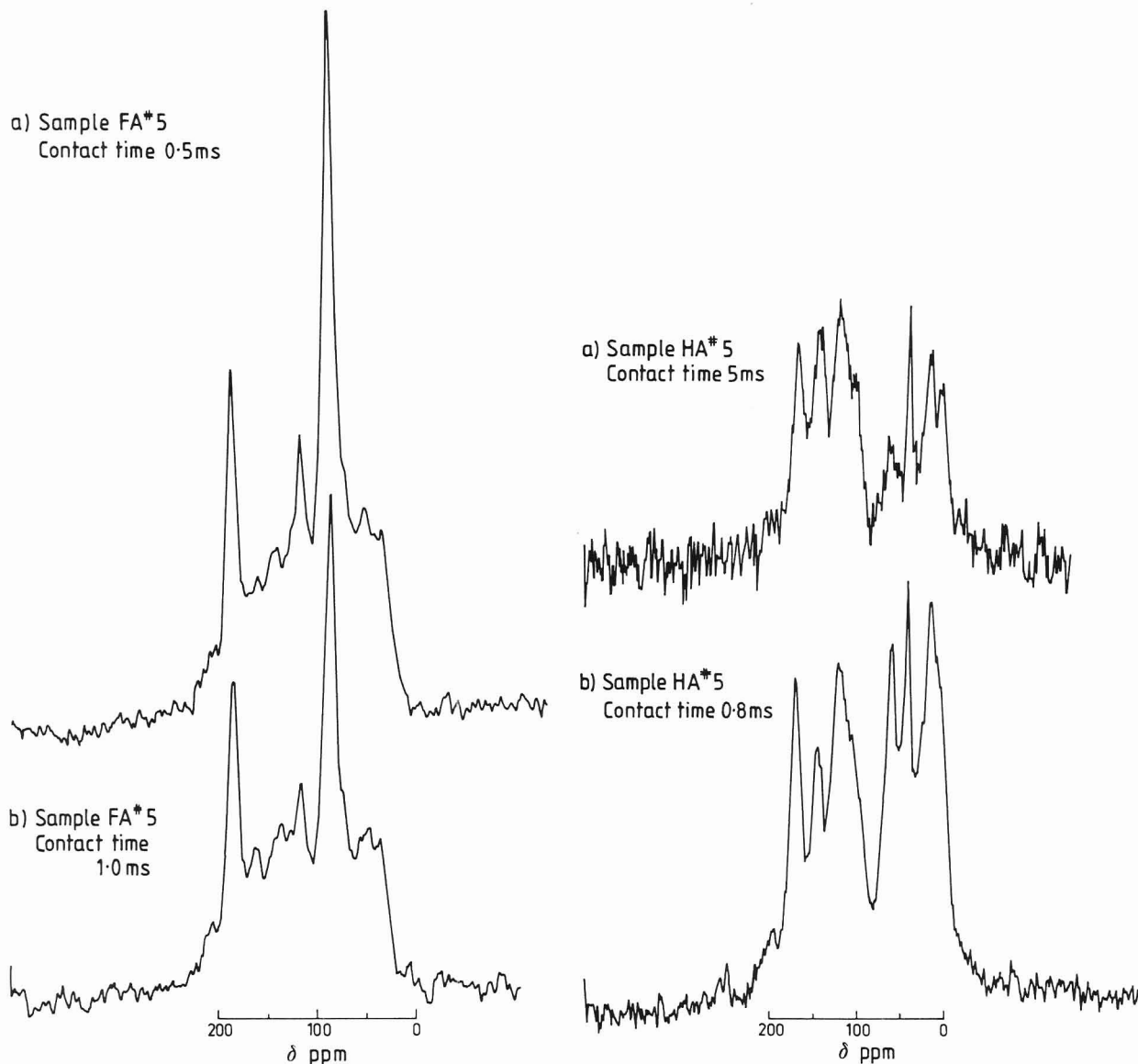


Figure 6. Effect of contact time on quantitation of relative carbon types.

indicates that this sample does not fit the commonly held perception of humic substances as phenolic benzenepoly-carboxylic acids. The 12% aromatic carbon in this sample represents 0.7 mmol of benzene rings per gram of sample. The NMR results show that one-third of the aromatic carbon is bonded to oxygen (two oxygens per benzene ring), so the phenolic content of this sample could not exceed 1.4 mmol/g. Likewise, even if all four remaining positions on an *average* benzene ring are all bonded to COOH groups, the aromatic carboxyl content could not exceed 2.8 mmol/g. Assuming that at least one carbon per aromatic ring forms bonds to bridging groups that link structural units in the humic substance, the actual combined phenolic and aromatic carboxyl group content is probably less than 3.5 mmol/g. This leaves at least 5.6 mmol/g (9.1–3.5) of the total acidity of FA5 associated with aliphatic components of the mixture. Given the very high levels of sugarlike carbon in this sample, the aliphatic acidity may well be partially attributed to the presence of complex mixtures of alduronic, aldonic, and aldaric acids that are produced by oxidation of C<sub>1</sub> and/or C<sub>6</sub> in carbohydrates. Indeed, the carboxylic carbon content of humic substances is decreased when carbohydrates are removed (45). Alternatively, the significant level of aliphatic carboxyl groups in this sample is also consistent with earlier suggestions that humic substances contain "polymaleic acid like" structures (34). In any case, the notion that carboxyl groups in humic

substances are always attached to aromatic rings is clearly inappropriate.

#### LITERATURE CITED

- (1) Aiken, G. R.; McKnight, D. M.; Wershaw, R. L.; MacCarthy, P. *Humic Substances in Soil, Sediment and Water*; Wiley-Interscience: New York, 1985; 692 pp.
- (2) Lytle, C. R.; Perdue, E. M. *Environ. Sci. Technol.* **1981**, *15*, 224–228.
- (3) Sweet, M. S.; Perdue, E. M. *Environ. Sci. Technol.* **1982**, *16*, 692–698.
- (4) Ertel, J. R.; Hedges, J. I.; Perdue, E. M. *Science* **1984**, *223*, 485–487.
- (5) Ruggiero, P.; Interesse, F. S.; Sciacovelli, O. *Geochim. Cosmochim. Acta* **1981**, *45*, 491–492.
- (6) Saiz-Jimenez, C.; de Leeuw, J. W. *Org. Geochem.* **1984**, *6*, 287–293.
- (7) Hatcher, P. G.; Maciel, G. E.; Dennis, L. W. *Org. Geochem.* **1981**, *2*, 43–48.
- (8) Wilson, M. A. *J. Soil Sci.* **1981**, *32*, 167–186.
- (9) Wilson, M. A.; Goh, K. M. *J. Soil Sci.* **1983**, *34*, 305–313.
- (10) Wershaw, R. L. In *Humic Substances in Soil, Sediment and Water*; Aiken, G. R.; McKnight, D. M.; Wershaw, R. L.; MacCarthy, P., Eds.; Wiley-Interscience: New York, 1985; pp 561–582.
- (11) Skjemstad, J. O.; Frost, R. L.; Barron, P. F. *Aust. J. Soil Res.* **1983**, *21*, 539–547.
- (12) Alemany, L. B.; Grant, D. M.; Pugmire, R. J.; Alger, T. D.; Zilm, K. W. *J. Am. Chem. Soc.* **1983**, *105*, 2133–2141.
- (13) Alemany, L. B.; Grant, D. M.; Pugmire, R. J.; Alger, T. D.; Zilm, K. W. *J. Am. Chem. Soc.* **1983**, *105*, 2142–2147.
- (14) Packer, K. J.; Harris, R. K.; Kenwright, A. M.; Snape, C. E. *Fuel* **1983**, *62*, 999–1002.
- (15) Dudley, R. L.; Fyfe, C. A. *Fuel* **1982**, *61*, 651–657.
- (16) Yoshida, T.; Nakata, Y.; Yoshida, R.; Ueda, S.; Kanda, N.; Mackawa, Y. *Fuel* **1982**, *61*, 824–830.
- (17) Sullivan, M. J.; Maciel, G. E. *Anal. Chem.* **1982**, *54*, 1615–1623.
- (18) Wilson, M. A.; Vassallo, A. M. *Org. Geochem.* **1985**, *8*, 299–312.



- (19) VanderHart, D. L.; Retkofsky, H. L. *Fuel* **1976**, *55*, 202-206.
- (20) Retkofsky, H. L. In *Coal Science*; Gorbarty, M. L., Larsen, J. M., Wender, I., Eds.; Academic: New York, 1982; Vol. 1, pp 43-80.
- (21) Wilson, M. A.; Collin, P. J.; Pugmire, R. J.; Grant, D. M. *Fuel* **1982**, *61*, 959-967.
- (22) Botto, R. E.; Wilson, R.; Hayatsu, R. J.; McBeth, R. L.; Scott, R. G.; Winans, R. E. *Prepr. Pap—Am. Chem. Soc., Div. Fuel Chem.* **1985**, *30*(4), 187-192.
- (23) Sullivan, M. J.; Maciel, G. E. *Anal. Chem.* **1982**, *54*, 1606-1614.
- (24) Kalman, J. R. In *Magnetic Resonance, Introduction, Advanced Topics and Applications to Fossil Energy*; Petrakis, L., Fraissard, J. P., Eds.; D. Reidel: Dordrecht, 1984; pp 557-567.
- (25) Vassallo, A. M.; Wilson, M. A.; Collin, P. J.; Oades, J. M.; Waters, A. G.; Malcolm, R. J. *Anal. Chem.* **1987**, *59*, 558-562.
- (26) Wemmer, D. E.; Pines, A.; Whitehurst, D. D. *Philos. Trans. R. Soc. London, A* **1981**, *300*, 15-41.
- (27) Hagaman, E. W.; Chambers, R. R., Jr.; Woody, M. C. *Anal. Chem.* **1986**, *58*, 387-394.
- (28) Hatcher, P. G.; Breger, I. A.; Dennis, L. W.; Maciel, G. E. In *Aquatic and Terrestrial Humic Material*; Christman, R. F., Gjessing, E. T., Eds.; Ann Arbor Science: Ann Arbor, MI, 1983; pp 37-82.
- (29) Wilson, M. A.; Pugmire, R. J.; Grant, D. M. *Org. Geochem.* **1983**, *5*, 121-129.
- (30) Pfeffer, P. E.; Gerasimowicz, W. V.; Piotrowski, E. G. *Anal. Chem.* **1984**, *56*, 734-741.
- (31) Preston, C. M.; Dudley, R. L.; Fyfe, C. A.; Mathur, S. P. *Geoderma* **1984**, *33*, 245-253.
- (32) Perdue, E. M. *Geochim. Cosmochim. Acta* **1984**, *48*, 1435-1442.
- (33) Wilson, M. A.; Philp, R. P.; Gillam, A. H.; Gilbert, T. D.; Tate, K. R. *Geochim. Cosmochim. Acta* **1983**, *47*, 497-502.
- (34) Anderson, H. A.; Russell, J. D. *Nature (London)* **1976**, *260*, 597.
- (35) Bracewell, J. M.; Robertson, G. W.; Welch, D. I. *J. Anal. Appl. Pyrolysis* **1980**, *2*, 239-248.
- (36) Reuter, J. H. Chemical and Spectroscopic Characterization of Humic Substances Derived from River Swamps in the Flood Plains of Southeastern Georgia; U.S. Coastal Streams Technical Report USOI/OWRT Project No. B-132-GA; Georgia Institute of Technology, Atlanta, GA, 1980.
- (37) Opella, S. J.; Frey, M. H. *J. Am. Chem. Soc.* **1979**, *101*, 5854-5856.
- (38) Bayer, E.; Albert, K.; Bergmann, K. J.; Eusener, W.; Peters, H. K. *Angew. Chem., Int. Ed. Engl.* **1984**, *23*, 147-149.
- (39) Wershaw, R. L.; Mikita, M. A.; Steelink, C. *Environ. Sci. Technol.* **1981**, *15*, 1461-1463.
- (40) Simmonds, P. G.; Schulman, G. P.; Stembridge, C. H. *J. Chromatogr. Sci.* **1969**, *29*, 36-41.
- (41) Wilson, M. A.; Vassallo, A. M.; Collin, P. J.; Rottendorf, H. *Anal. Chem.* **1984**, *56*, 433-436.
- (42) Perdue, E. M.; Reuter, J. H.; Ghosal, M. *Geochim. Cosmochim. Acta* **1980**, *44*, 1841-1851.
- (43) Perdue, E. M. In *Humic Substances in Soil, Sediment, and Water—Geochemistry, Isolation, and Characterization*; Aiken, G., McKnight, D., Wershaw, R., MacCarthy, P., Eds.; Wiley-Interscience: New York, 1985; pp 493-526.
- (44) Hatcher, P. G.; Schnitzer, M.; Dennis, L. W.; Maciel, G. E. *Soil Sci. Soc. Am. J.* **1981**, *45*, 1089-1094.
- (45) Wilson, M. A.; Heng, S.; Goh, K. M.; Pugmire, R. J.; Grant, D. M. *J. Soil Sci.* **1983**, *34*, 83-97.

RECEIVED for review June 30, 1986. Accepted October 20, 1986.

## Structural Analysis of Geochemical Samples by Solid-State Nuclear Magnetic Resonance Spectrometry. Role of Paramagnetic Material

Anthony M. Vassallo,\* Michael A. Wilson, and Philip J. Collin

CSIRO Division of Fossil Fuels, P.O. Box 136, North Ryde, New South Wales, Australia

J. Malcolm Oades and Angela G. Waters

Department of Soil Science, Waite Agricultural Research Institute, University of Adelaide, Glen Osmond, South Australia, Australia

Ronald L. Malcolm

U.S. Geological Survey, Denver Federal Center, Denver, Colorado 80225

An examination of coals, coal tars, a fulvic acid, and soil fractions by solid-state  $^{13}\text{C}$  NMR spectrometry has demonstrated widely differing behavior regarding quantitative representation in the spectrum. Spin counting experiments on coal tars and the fulvic acid show that almost all the sample carbon is observed in both solution and solid-state NMR spectra. Similar experiments on two coals (a lignite and a bituminous coal) show that most (70-97%) of the carbon is observed; however, when the lignite is ion exchanged with 3% (w/w)  $\text{Fe}^{3+}$ , the fraction of carbon observed drops to below 10%. In additional experiments signal intensity from soil samples is enhanced by a simple dithionite treatment. This is illustrated by  $^{13}\text{C}$ ,  $^{27}\text{Al}$ , and  $^{29}\text{Si}$  solid-state NMR experiments on soil fractions.

Over the last few years there has been extensive application of high-resolution solid-state, nuclear magnetic resonance (NMR) spectrometry in the study of fossil fuels, soils, and humic substances. This work has demonstrated the enormous

usefulness that solid-state NMR can have in such areas of structure elucidation, chemical reactivity, and biogenesis. One of the problems however in the interpretation of these data has been, and remains, the uncertainty of how much of the substance under investigation is represented in the final spectrum. For example, in  $^{13}\text{C}$  cross polarization with magic angle spinning (CP-MAS) it has been demonstrated that in some samples, proton spin-lattice relaxation times in the rotating frame ( $T_{1\rho}H$ ) are reduced by paramagnetic material (1, 2). Relative signal intensity may also be not quantitatively represented in a single spectrum because of inhomogeneous  $T_{1\rho}H$  and  $T_{1\rho}H$ 's (3-7). Some of these latter problems can be overcome by a judicious choice of contact time or recycle delay or by curve fitting the relaxation behavior to obtain the signal intensity in the absence of relaxation effects. However, although this approach may produce the correct representation of observable carbons, it does not indicate how much carbon is actually being observed.

There have been several reports concerning the estimation of how much carbon is represented in the spectra of problem materials, such as coal (5, 8-11). The approach has generally

**Table I. Elemental Analysis of Samples Used in CP-MAS NMR Studies**

sample	% C	% H	% ash	% Fe <sup>a</sup>	% Mn <sup>a</sup>
Morwell coal	69.0	4.8	2.3	0.07	
Morwell coal <sup>b</sup>	66.8	4.6	N.D.	3.25	
Millmerran coal	78.5	6.5	15.1	N.D.	
coal tar 1	87.4	7.0	<0.1	<0.1	
2	87.1	6.5	<0.1	<0.1	
3	88.1	6.6	<0.1	<0.1	
4	89.8	6.1	<0.1	<0.1	
5	88.2	6.7	<0.1	<0.1	
Soil PPO12	4.6	N.D. <sup>d</sup>	N.D.	14.8	0.35
Soil PPO12 <sup>c</sup>	3.94	N.D.	N.D.	6.4	0.03
Suwannee fulvic acid	51.3	4.32	<0.05	N.D.	N.D.

<sup>a</sup> Measured by X-ray fluorescence. <sup>b</sup> Fe<sup>3+</sup> exchanged coal. <sup>c</sup> Dithionite treated. <sup>d</sup> N.D., not determined.

been that of "spin counting" where a standard (assumed to be quantitatively represented) is added to the sample under investigation. While this approach has some problems, such as distinguishing between resonances from standard and sample, it is nevertheless capable of providing a reasonable estimate of how much carbon in a sample is actually being "seen". This approach has been used in this work to elucidate the role of organic and inorganic paramagnetics in CP-MAS experiments. We report results of spin counting on coal tars (which can also be examined by solution NMR spectrometry), coal, and a fulvic acid. In addition some preliminary results are presented on a simple method that can greatly enhance the signal from certain troublesome samples.

### EXPERIMENTAL SECTION

Solution <sup>13</sup>C NMR measurements were obtained on a Jeol FX90Q spectrometer operating at 22.5 MHz. Solid-state NMR measurements were carried out on either a Bruker CXP-100 (for carbon spectra at 22.5 MHz) or a Bruker CXP-300 (for silicon or aluminum spectra at 59.2 MHz or 75.6 MHz, respectively) using cross polarization for carbon or single pulse excitation for silicon and aluminum, and magic angle spinning techniques. A 5-μs 90° pulse was used for carbon with pulse delays of 1 s for coals, soils, and fulvic acid and a pulse delay of 5 s for coal tars. For silicon experiments a 6-μs (90°) pulse and 10-s pulse delay were used while for aluminum a 2-μs pulse and 1-s pulse delay were used. Samples were spun in rotors constructed of boron nitride or partially stabilized zirconia at speeds of approximately 3.5 kHz. Both rotors were equipped with Kel-F caps. Carbon-13 chemical shifts were determined by using external hexamethylbenzene and recalculated relative to Me<sub>4</sub>Si. Silicon chemical shifts were referenced to kaolin and reported relative to Me<sub>4</sub>Si. Aluminum chemical shifts are reported relative to Al(H<sub>2</sub>O)<sub>6</sub>Cl<sub>3</sub>. About 100 000

scans were required to obtain <sup>13</sup>C spectra of soils and fulvic acid, about 5000 scans were needed for tars and coals, and about 1000 and 3000 scans were needed to obtain <sup>27</sup>Al and <sup>29</sup>Si spectra of soils.

**Samples.** Element analyses of the samples used are shown in Table I. The coal tars were prepared from an Australian bituminous coal (Liddell) in a batch autoclave at temperatures of 400–450 °C using tetralin as a hydrogen-donating solvent. Full details are available elsewhere (12). The bituminous coal was from Millmerran, Queensland. The brown coal sample was a medium to light lithotype from Morwell, Latrobe Valley. Details of the brown coal and the preparation of its Fe<sup>3+</sup> exchanged salt are described elsewhere (13). Suwannee fulvic acid is the International Humic Substances Standard (14).

Soil samples were obtained from Urrbrae Red-brown earth in Adelaide, South Australia, and fractionated according to size and density using ZnBr<sub>2</sub> solutions for further study. These samples are part of a larger investigation of size fractionation of soil organic matter which will be reported elsewhere (15). The size fractions of this soil were treated with a 4% (w/v) sodium dithionite solution and 0.05 M hydrochloric acid and then washed with neutral sodium chloride solution and water. The solutions were then dialyzed overnight to remove salt and finally freeze-dried.

**Solution Spin Counting Experiments.** The procedures used to obtain solution <sup>13</sup>C NMR measurements on coal tars have been described elsewhere (12, 16) and shown to give quantitative results. The standard used for comparison of signal intensities with sample was *n*-octane. The tars and *n*-octane reference sample were prepared as 20% (w/v) solutions in CDCl<sub>3</sub>.

The area response curve for *n*-octane increased as expected with increasing pulse delays up to 20 s and then remained virtually constant at longer pulse delays. Therefore the area of the resonances obtained for *n*-octane at a pulse delay of >20 s was given a value of unity. Repeated estimations gave results within ±5%. The total area of the aromatic and aliphatic carbon resonances from the coal tars increased with increasing pulse delays up to 10 s and remained virtually constant up to 20 s. Spin counting was achieved by comparing the integrated area from the standard with that of the coal tar. Results obtained in the spin counting experiments are listed in Table II. They clearly show that 88% or more of the carbon is observed by solution <sup>13</sup>C NMR. In similar experiments using a relaxation reagent, namely, a 0.03 M solution of chromium(III) 2,4-pentanedionate in CDCl<sub>3</sub> instead of CDCl<sub>3</sub> solvent, the percent carbon observed was also found to be 88% or more.

**Spin Counting in Solids.** Spin counting experiments involved recording the spectrum of mixtures of sample and glycine (accurately weighed and intimately mixed) at different contact times (1–12 ms) to determine the *T*<sub>1ρ</sub>*H* behavior of both sample and glycine under identical conditions. In most cases, the carboxyl resonance of glycine was sufficiently removed from resonances of the sample that it could be used to determine the amount of signal derived from both the sample and glycine. In some cases however, interferences from sample carboxylic resonances ne-

**Table II. Parameters Required for Spin Counting Experiments, Aromaticities, and Percent Carbon Observed for Coals and Coal Tars<sup>a</sup>**

sample	<i>T</i> <sub>1ρ</sub> <i>H</i> , ms		mg of C		aromaticity <sup>f</sup>		% carbon seen <sup>f</sup>	
	glycine <sup>i</sup>	sample <sup>j</sup>	glycine	sample	soln	s.s.	soln	s.s.
coal tar 1	3.6	15.9	94.8	89.9	0.65	0.66	88	66
2	4.2	10.1	97.5	91.2	0.72	0.75	100	100
3	4.1	17.2	95.7	89.2	0.72	0.68	95	87
4	20.1	12.1	82.6	92.5	0.75	0.76	100	70
4	30.1	11.0	69.8	74.5	0.75	0.76	100	86
5	3.9	9.8	107.6	92.6	0.68	0.70	100	86
Morwell 1	38.2	7.5	120.6	144.2		0.45		74
2 <sup>c</sup>	29.0	4.4	105.0	94.7		<i>d</i>		70
3 <sup>c</sup>	22.3	5.7	64.0	64.6		<i>d</i>		63
Morwell <sup>e</sup>	38.5	<i>b</i>	98.2	107.6		0.46		<10
Millmerran	3.8	3.2	102.4	95.6		0.55		90
Suwannee fulvic	23.5	7.1	51.2	52.8	0.30 <sup>h</sup>	0.24		97

<sup>a</sup> 5-μs 90° pulse used unless otherwise stated. <sup>b</sup> Not measured. <sup>c</sup> 8-μs 90° pulse. <sup>d</sup> Not measured at this 90° pulse length. <sup>e</sup> Fe<sup>3+</sup> exchanged coal. <sup>f</sup> Key: soln, solution; s.s., solid state. <sup>g</sup> 6.5-μs 90° pulse. <sup>h</sup> Measured with 10-s pulse delay. <sup>i</sup> Measured in the presence of sample. <sup>j</sup> Measured in the presence of glycine.



cessitated an estimate of the contribution to the glycine resonance from sample carboxyl. This was obtained from the spectrum of the sample in the absence of glycine.

The development of signal intensity ( $S_t$ ) for a particular functional group in the cross polarization process can be described by

$$S_t = S_0 \left\{ \frac{T_{1\rho}H}{T_{1\rho}H - T_{CH}} \right\} \{1 - \exp(-\alpha t/T_{CH})\} \exp(-t/T_{1\rho}H) \quad (1)$$

where  $\alpha = 1 - [T_{CH}/T_{1\rho}H]$  and  $t$  is the contact time.

The calculation of  $S_0$ , the maximum intensity in the absence of signal losses, can be simplified to a simple exponential (eq 2) if  $T_{CH} \ll t \ll T_{1\rho}H$

$$S_t = S_0 \exp(-t/T_{1\rho}H) \quad (2)$$

In this work,  $S_0$  has been calculated from the intercept obtained by fitting eq 2 to the data at values of  $t > 2$  ms for both glycine and sample. In all experiments at least six data points were used and the correlation coefficient ( $r$ ) was always greater than 0.93. From these data, the normalized area of the spectrum due to sample and glycine is obtained and compared with the area expected from knowledge of the amount of carbon in each substance. Assuming 100% carbon detection from glycine, the normalized area per milligram of carbon in the sample can be calculated and compared with what is observed. The percent carbon seen is thus the percent ratio of the area of the sample spectrum to the area expected from the carbon content. It should be noted however that in samples in which  $T_{1\rho}H/T_{CH} < \sim 10$ , the value of the term  $T_{1\rho}H/[T_{1\rho}H - T_{CH}]$  in eq 1 becomes nonnegligible and introduces an error in the value of  $S_0$  obtained by using eq 2. This error results in the overestimation of observed carbon and thus calculated values of observed carbon should be interpreted as upper limits. The relevant data are shown in Table II.

## RESULTS AND DISCUSSION

**Coal Tars and Coals.** There can be many reasons for not observing carbon in cross polarization solid-state NMR experiments. Ollivier and Gerstein (17) showed that for some tar samples, aliphatic carbon signal intensity was lost under magic angle spinning conditions. They suggest that this may be due to a decoupling of the proton-carbon interaction by a combination of magic angle spinning and low-frequency motion. As the results in Table II show, this cannot be occurring here, since the aromaticity measured in the solid state is nearly identical with that obtained from solution measurements. Another reason for nonquantitative measurements can be the presence of paramagnetic inorganic materials. The coal tars examined here have no mineral matter content and thus the only paramagnetic material that could influence the magnetic resonance behavior must be organic in nature. Stable organic radicals have been identified in coal and coal tar previously (18–20) and may range in concentration from  $10^{16}$  to  $10^{20}$  spins/g. The concentration of organic radicals in coal tar can vary significantly and depends on the temperature at which the tar was prepared and the type and amount of donor solvent present during its preparation (19). Our observation that 88% or more of the carbon is detected in solution indicates that the effect of these radicals has been minimized or eliminated by molecular motion in solution. Moreover, the addition of paramagnetic relaxation reagents did not reduce the amount of observable carbon. In the solid state however, it is likely that the influence of organic radicals will be more significant, and it has been demonstrated that the interaction between protons and unpaired electrons results in the loss of approximately 5% of the total proton signal (21). This lost signal was, however, recoverable by swelling the coal. A loss of proton signal intensity, presumably through the inability to cover their now broadened resonance frequency with a 90° proton pulse of sufficient power, could easily influence the observation of carbon signal intensity in CP-MAS experiments. Within experimental error ( $\sim 10\%$ ) our results

demonstrate that all tar carbon is seen in solution. The differences between the amount of carbon seen in the solid state and solution are also not large (Table I). Thus it is clear that organic paramagnetic materials do not play significantly different roles in solution and in the solid state.

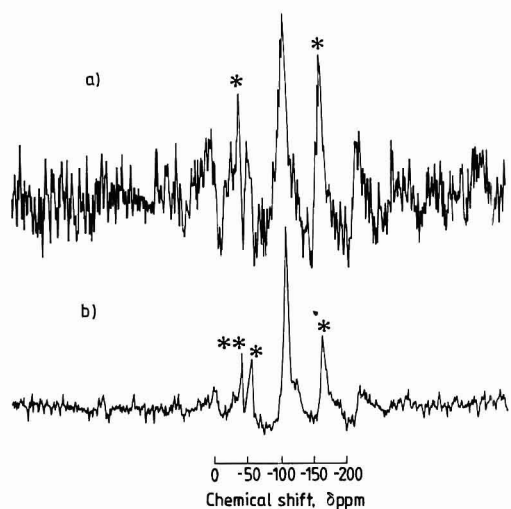
In view of the results from the coal tar experiments, two different coals were examined using the same spin-counting techniques in the solid state. The results obtained are shown in Table II. The observed value of 90% for Millmerran coal is surprising in view of recent reports (5, 8) claiming only 35–70% of the organic carbon is visible in some coals; however, it is likely that many factors, such as the type of coal, inorganic constituents, and thermal history will affect how much carbon is detected.

It should be noted that the measured  $T_{1\rho}H$  of glycine in the presence of Morwell coal was different to its value of 4.1 ms determined on its own or with other samples. The  $T_{1\rho}H$  increased in some cases to almost 10 times this value when mixed with the coal (Table II). Repeated determinations using materials from different samples produced the same, or nearly equivalent, values. In addition, the same effect was observed for natural and  $\text{Fe}^{3+}$  exchanged coal, the fulvic acid, and one tar. It appears that there is an interaction in the solid state between glycine and these samples, which may alter the components of molecular motion responsible for normal  $T_{1\rho}H$  relaxation (motion in the tens of kilohertz region). It is clear therefore, that it is quite inappropriate to use a  $T_{1\rho}H$  value of a standard measured in isolation. It is necessary to determine the  $T_{1\rho}H$  in situ with the material being measured.

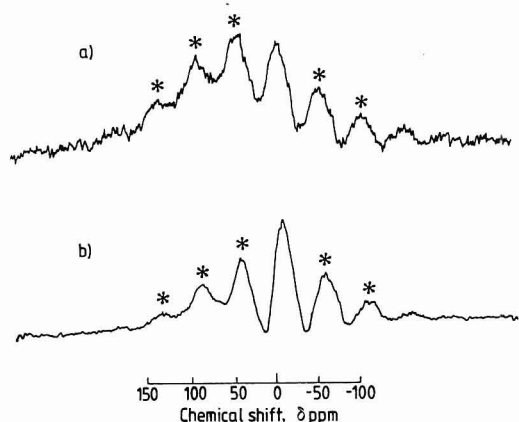
Some further comment should be made concerning the suitability of standards in these spin counting experiments. It is desirable that the standard (in this case, glycine) not interact with the sample. As noted above, this does occur. If the interaction produces spin diffusion between sample and standard, then the properties of the sample may be transferred to the standard and, hence, the same amount of the standard will be seen as the sample; i.e., the results will produce a false sense of quantitation since they will show that 100% of the carbon in the sample is observed. This effect is not operating here. Mixing glycine and sample increased the  $T_{1\rho}H$  of the glycine but had little or no effect on the sample. Clearly, in this case spin diffusion does not average the  $T_{1\rho}H$ 's of standard and sample. It is likely that the change in glycine  $T_{1\rho}H$  arises from altered molecular motion in the glycine due to ionic bonding between acidic groups in the coal (or tar) and the glycine amine group.

In order to determine the effect of inorganic paramagnetic materials on the NMR spectrum of coal, a lignite was examined, using spin-counting techniques with glycine, before and after exchange of  $\text{H}^+$  from  $\text{COOH}$  groups with  $\text{Fe}^{3+}$ . These results are also presented in Table II. Clearly, the effects of  $\text{Fe}^{3+}$  on the coal spectrum are such that almost all the carbon in the coal is rendered undetectable under our experimental conditions. Thus we see that  $\text{Fe}^{3+}$  levels of about 3% (w/w) all but destroy the coal signal when examined under CP-MAS conditions although the glycine signal appears to be unaffected. The most probable explanation for this phenomenon is that the  $\text{Fe}^{3+}$  shortens the  $T_{1\rho}H$  of protons in its immediate vicinity so that  $T_{CH} \gg T_{1\rho}H$  and  $S_t$  in eq 1 tends to zero. It is also likely that the resonance frequency of the protons is now so broad that they cannot be adequately irradiated with a 5- $\mu\text{s}$  pulse.

Although different amounts of carbon are seen in the  $\text{Fe}^{3+}$ -exchanged and natural coal, the aromaticity measurements are almost identical. This suggests that reasons other than paramagnetics must be sought to explain why some data on coals can be shown to be nonquantitative (3, 4). A probable explanation is found in the heterogeneity of coal. Minerals,



**Figure 1.** Solid-state  $^{29}\text{Si}$  dipolar decoupled MAS spectra of Urrbrae soil fraction  $<0.2\ \mu\text{m}$ : (a) untreated, (b) dithionite treated; \*, spinning sideband; \*\*, silicon rubber artifact. Equal numbers of scans (5760) were collected in both experiments.

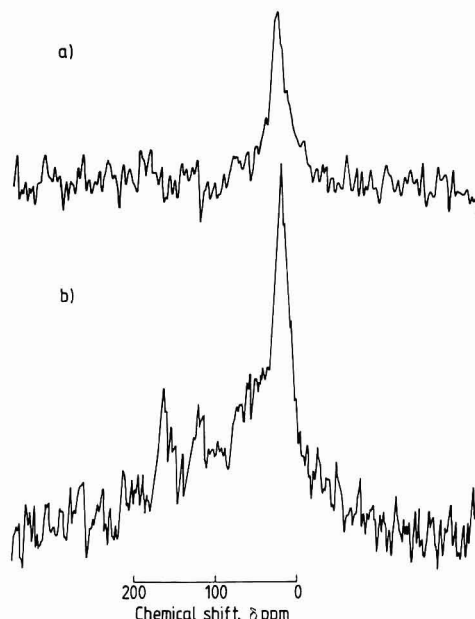


**Figure 2.** Solid-state  $^{27}\text{Al}$  dipolar decoupled MAS spectra of Urrbrae soil fraction  $<0.2\ \mu\text{m}$ : (a) untreated, (b) dithionite treated; \*, spinning sidebands. Equal numbers of scans ( $\sim 3000$ ) were collected for both experiments.

and hence inorganic paramagnetics, are known to concentrate in the inertinite macerals. Thus the amount of carbon observed will differ for different macerals (5) so that the average aromaticity of the coal will be biased toward that of the paramagnetic deficient macerals such as exinite and vitrinite. Since the aromaticities of inertinites are invariably higher than the vitrinite and exinite from the same coal (22–27), aromaticity measurements may be too low in the case of inertinite-rich coals.

**Silicon and Aluminum Spectra from Soils.** The degradation of NMR signal by paramagnetic materials is also a well-known problem in the measurement of spectra from silicon and aluminum nuclei. In a recent solid-state NMR study of the organic and inorganic structure of a soil under old pasture (15), it was evident that the signal-to-noise (S/N) ratio of certain samples was well below the expected levels. However after a simple sodium dithionite treatment, the same sample under identical conditions presented a much more intense spectrum. The comparison is shown in Figure 1. The effect of dithionite treatment on the structure appears minimal but the improvement in S/N ratio is large. Element analysis (Table I) before and after dithionite treatment show that the iron content has been reduced by almost 60% with an even greater reduction in the manganese content.

The S/N ratio in aluminum spectra from the same sample has also been improved by the dithionite treatment, although the improvements are less spectacular. These spectra are



**Figure 3.** Solid-state  $^{13}\text{C}$  CP-MAS spectra of Urrbrae soil fraction  $<0.2\ \mu\text{m}$ : (a) untreated, (b) dithionite treated. Equal numbers of scans (100 000) were collected for both experiments.

shown in Figure 2. The prominent sidebands still present in both  $^{29}\text{Si}$  and  $^{27}\text{Al}$  spectra of the treated sample may indicate that some paramagnetic impurities are incorporated within the aluminosilicate lattice and cannot be removed by this simple treatment. It is noteworthy that not all iron could be removed by dithionite treatment (Table I).

**Effect of Dithionite Treatment on Carbon Spectra from Soils.** The dithionite treatment mentioned above can also be used to improve the signal intensity arising from organic carbon in the same or similar samples. An example of the improvement attainable is shown in Figure 3. Both spectra represent the same amount of carbon (6.9 mg) in the rotor for an equal number of scans under identical conditions. From the integral intensities there is an approximately 5-fold improvement in the signal strength of the dithionite treated sample. This effect has been seen on a number of similar samples (not shown). Because of the improvement in S/N offered by the treatment, it is apparent that additional resonances have become visible (Figure 3b). These may be assigned to carboxyl (171 ppm) and aromatic carbon (127 ppm). Clearly sodium dithionite treatments may allow CP-MAS spectra to be obtained on samples containing high concentrations of paramagnetic iron.

**Fulvic Acid.** Although, like coal, Suwannee fulvic acid contains organic paramagnetic species, it is different from the coal and soil samples examined in that it has virtually no ash content. Hence signal intensity cannot be lost through interaction with inorganic paramagnetic material such as  $\text{Fe}^{3+}$ , and all carbon should be seen if organic radicals are inconsequential. This is confirmed by the spin counting experiments which show that 97% of carbon is observed.

**Registry No.** Fe, 7439-89-6.

#### LITERATURE CITED

- (1) Preston, C. M.; Dudley, R. L.; Fyfe, C. A.; Mathur, S. P. *Geoderma* **1984**, *33*, 245–253.
- (2) Pfeffer, P. E.; Gerasimowicz, W. V.; Piotrowski, E. G. *Anal. Chem.* **1984**, *56*, 834–741.
- (3) Dudley, R. L.; Fyfe, C. A. *Fuel* **1982**, *61*, 651–657.
- (4) Packer, K. F.; Harris, R. K.; Kenwright, A. M.; Snape, C. E. *Fuel* **1983**, *62*, 999–1992.
- (5) Botto, R. E.; Wilson, R.; Hayatsu, R.; McBeth, R. L.; Scott, R. G.; Winans, R. E. *Prepr. Pap.—Am. Chem. Soc., Div. Fuel Chem.* **1985**, *30*(4), 187–192.
- (6) Sullivan, M. J.; Maciel, G. E. *Anal. Chem.* **1982**, *54*, 1615–1623.
- (7) Wilson, M. A.; Vassallo, A. M.; Collin, P. J.; Rottendorf, H. *Anal. Chem.* **1984**, *56*, 433–436.



- (8) Hagaman, E. W.; Chambers, R. R., Jr.; Woody, M. C. *Anal. Chem.* **1986**, *58*, 387-394.
- (9) Kalman, J. R. In *Magnetic Resonance. Introduction, Advanced Topics and Applications to Fossil Energy*; Petrakis, L., Fraissard, J. P., Eds.; D. Reidel: 1984; pp 557-567.
- (10) VanderHart, D. L.; Retcofsky, H. L. *Fuel* **1976**, *55*, 202-204.
- (11) Wemmer, D. E.; Pines, A.; Whitehurst, D. D. *Philos. Trans. R. Soc. London, A* **1981**, *300*, 15-41.
- (12) Willson, M. A.; Rottendorf, H.; Collin, P. J.; Vassallo, A. M.; Barron, P. F. *Fuel* **1982**, *61*, 321-328.
- (13) Schafer, H. N. S. *Fuel* **1972**, *51*, 4-9.
- (14) Thurman, E. M.; Malcolm, R. L. In *Aquatic and Terrestrial Humic Materials*; Ann Arbor Science: Ann Arbor, MI, 1983; pp 1-24.
- (15) Oades, J. M.; Vassallo, A. M.; Waters, A. G.; Wilson, M. A. *Aust. J. Soil Res.*, in press.
- (16) Wilson, M. A.; Collin, P. J.; Pugmire, R. J.; Grant, D. M. *Fuel* **1982**, *61*, 959-967.
- (17) Ollivier, P.; Gerstein, B. C. *Carbon* **1984**, *22*, 409-412.
- (18) Retcofsky, H. L. In *Coal Science, Volume 1*; Gorbarty, M. L., Larsen, J. W., Wender, I., Eds.; Academic: New York, 1982; pp 43-80.
- (19) Petrakis, L.; Grandy, D. W. *Free Radicals in Coals and Synthetic Fuels*; Elsevier: Amsterdam, 1983.
- (20) Schlick, S.; Narayana, P. A.; Kevan, L. J. *Am. Chem. Soc.* **1978**, *100*, 3322-3326.
- (21) Barton, W. A.; Lynch, L. J.; Webster, D. S. *Fuel* **1984**, *63*, 1262-1268.
- (22) Pugmire, R. J.; Zilm, K. W.; Grant, D. M.; Larter, S. R.; Allen, J.; Sentfle, J. R.; Davis, A.; Spackman, W. *ACS Symp. Ser.* **1981**, No. 169, 23-42.
- (23) Pugmire, R. J.; Zilm, K. W.; Woolfenden, W. R.; Grant, D. M.; Dyrkacz, G. R.; Bloomquist, C. A. A.; Horwitz, E. P. *Org. Geochem.* **1982**, *4*, 79-84.
- (24) Pugmire, R. J.; Woolfenden, W. R.; Mayne, C. L.; Karas, J.; Grant, D. M. *ACS Symp. Ser.* **1984**, No. 252, 79-97.
- (25) Wilson, M. A.; Pugmire, R. J.; Karas, J.; Alemany, L. B.; Woolfenden, W. R.; Grant, D. M.; Given, P. H. *Anal. Chem.* **1984**, *56*, 933-943.
- (26) Zilm, K. W.; Pugmire, R. J.; Larter, S. R.; Allen, J.; Grant, D. M. *Fuel* **1981**, *60*, 717-722.
- (27) Karas, J.; Pugmire, R. J.; Woolfenden, W. R.; Grant, D. M.; Blair, S. *Int. J. Coal Geol.* **1985**, *5*, 315-338.

RECEIVED for review June 30, 1986. Accepted October 20, 1986.

## Organic-Soluble Lanthanide Nuclear Magnetic Resonance Shift Reagents for Sulfonium and Isothiuronium Salts

Thomas J. Wenzel\* and Joseph Zaia

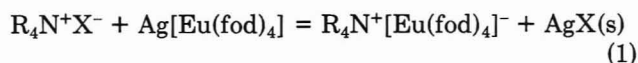
Department of Chemistry, Bates College, Lewiston, Maine 04240

**Lanthanide complexes of the formula  $[\text{Ln}(\text{fod})_4]^-$  (fod, 6,6,7,7,8,8,8-heptafluoro-2,2-dimethyl-3,5-octanedione) are effective organic-soluble nuclear magnetic resonance shift reagents for sulfonium and isothiuronium salts. The shift reagent is formed in solution from  $\text{Ln}(\text{fod})_3$  and  $\text{Ag}(\text{fod})$  or  $\text{K}(\text{fod})$ . The selection of  $\text{Ag}(\text{fod})$  or  $\text{K}(\text{fod})$  in forming the shift reagent is dependent on the anion of the organic salt.  $\text{Ag}(\text{fod})$  is more effective with halide salts, whereas  $\text{K}(\text{fod})$  is preferred with tetrafluoroborate salts. Resolution of diastereotopic hydrogen atoms was observed in the shifted spectra of certain substrates. Enantiomeric resolution was obtained in the spectrum of *sec*-butylisothiuronium chloride with a chiral shift reagent. The reagents can be employed in solvents such as chloroform and benzene.**

Lanthanide shift reagents are used to expand the utility of nuclear magnetic resonance (NMR) spectroscopy. In addition to their obvious application in stereochemical analysis, NMR shift reagents have often been employed in the analysis of mixtures. Lanthanide tris chelates have been used to analyze mixtures of straight chain alcohols (1), methylbenzyl alcohols (2), phenols (3-5), ketoterpenes (6), methyl esters (7, 8), fatty acid methyl esters (9), esters of tocopherols and retinols (10), cresol esters (10), methyl esters of toluic acids (2, 11), vitamin D<sub>2</sub> isomers (12), methylbenzylamines (2), toluamides (2), alkane- and alkenesulfonates (13), steroids (14), and triglycerides (15, 16). Binuclear lanthanide(III)-silver(I) shift reagents have been used to analyze mixtures of *cis* and *trans* olefins (17-19), xylenes (20, 21), and methylbenzenes in gasoline (21).

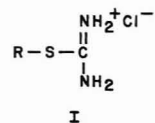
We have recently reported that the binuclear complex  $\text{Ag}[\text{Eu}(\text{fod})_4]$  formed in solution from  $\text{Eu}(\text{fod})_3$  and  $\text{Ag}(\text{fod})$  (fod = 6,6,7,7,8,8,8-heptafluoro-2,2-dimethyl-3,5-octanedione) is an effective organic-soluble NMR shift reagent for ammo-

nium salts (22). The interaction between an ammonium salt and  $\text{Ag}[\text{Eu}(\text{fod})_4]$  is believed to involve an ion pair between the ammonium cation and  $[\text{Eu}(\text{fod})_4]^-$ . The equilibrium representative of this process is shown in eq 1. Precipitation



of the silver salt favors formation of the ion pair between the organic cation and the lanthanide tetrakis chelate anion. The shifts in the spectrum of  $\text{R}_4\text{N}^+$  with  $[\text{Eu}(\text{fod})_4]^-$  were significantly larger than those with  $\text{Eu}(\text{fod})_3$  (22).

We have since determined that the species  $[\text{Ln}(\text{fod})_4]^-$  is an effective NMR shift reagent for sulfonium and isothiuronium salts (I) (isothiuronium salts are often prepared as



derivatives of alkyl halides) as well (23-25). The species  $[\text{Ln}(\text{fod})_4]^-$  would therefore appear to be a useful anionic organic-soluble NMR shift reagent applicable to a wide range of cations. Other workers have noted that the spectra of sulfonium salts are shifted in the presence of  $\text{Eu}(\text{fod})_3$  (26-28). We have found that the shifts in the spectra of sulfonium and isothiuronium salts with  $[\text{Eu}(\text{fod})_4]^-$  are significantly larger than those with  $\text{Eu}(\text{fod})_3$ . The shifts in the spectra of sulfonium salts with  $[\text{Ln}(\text{fod})_4]^-$  are also appreciably larger than those in the spectra of the corresponding sulfides with  $\text{Ln}(\text{fod})_3$ . The shifts in the spectra of isothiuronium salts with  $[\text{Ln}(\text{fod})_4]^-$  are larger than those for the corresponding alkyl halide with  $\text{Ln}(\text{fod})_3$  (29) or the binuclear reagent  $\text{Ag}[\text{Ln}(\text{fod})_4]$  (17, 30).

### EXPERIMENTAL SECTION

**Reagents.** The compounds 1-iodobutane, iodomethane, 1-bromopentane, 1-bromononane, 1-chlorobutane, benzyl chloride,

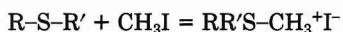
2-bromobutane, 2-chlorobutane, methyl sulfide, *n*-butyl sulfide, tetrahydrothiophene, benzothiophene, and diphenyl sulfide were purchased from commercial sources and used as received. Silver tetrafluoroborate was purchased from Aldrich Chemical Co. and stored in a desiccator over  $P_4O_{10}$ . Trimethyloxonium tetrafluoroborate was purchased from Alfa Products Co. and stored at 0 °C prior to use. Methylene chloride was distilled from  $P_4O_{10}$  under an atmosphere of dry nitrogen and stored over  $K_2CO_3$ . Nitromethane was stored over  $K_2CO_3$ . All other solvents were used as received.

Chloroform-*d* was purchased from Aldrich Chemical Co. and stored over molecular sieves. Deuterium oxide, benzene-*d*<sub>6</sub>, and 3-(trimethylsilyl)propanesulfonic acid sodium salt (DSS) was purchased from Wilmad Glass Co., Inc. Acetone-*d*<sub>6</sub> was purchased from Norell, Inc. Acetonitrile-*d*<sub>3</sub> was purchased from Stohler Isotope Chemicals. The  $Ln(fod)_3$  (31),  $Ag(fod)$  (32),  $Ag(ptb)$  (33) ( $ptb = 4,4,4$ -trifluoro-1-phenyl-1,3-butanedione), and  $K(fod)$  (34) chelates were synthesized by literature methods and stored in a desiccator over  $P_4O_{10}$ . The  $H(fod)$  ligand,  $Pr(facam)_3$ ,  $Pr(hfbc)_3$ ,  $Eu(facam)_3$ , and  $Eu(hfbc)_3$  ( $facam = 3$ -trifluoroacetyl-*d*-camphor,  $hfbc = 3$ -heptafluorobutyl-*d*-camphor) were purchased from Aldrich Chemical Co. All chiral shift reagents were stored in a desiccator over  $P_4O_{10}$  prior to use.

**Apparatus.** All NMR spectra were recorded on a Varian EM-360L 60-MHz instrument at ambient probe temperature.

**Synthetic Preparations.** The procedures employed in the preparation of sulfonium (35–44) and isothiuronium salts (23–25) were modifications of literature methods. Representative examples of each will be described.

**Conversion of Sulfides into Sulfonium Salts. Method 1.** Direct methylation with iodomethane

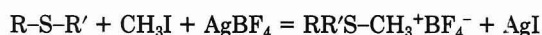


This procedure has been described in the literature for the preparation of trimethylsulfonium iodide (35–37). It is only suitable for the derivatization of highly nucleophilic sulfides. Trimethylsulfonium iodide, *S*-methyltetrahydrothiophenium iodide, and di-*n*-butylmethylsulfonium iodide were prepared by this method.

(A) *Preparation of S-Methyltetrahydrothiophenium Iodide.* Tetrahydrothiophene (2.20 g, 0.0211 mol) and iodomethane (3.00 g, 0.0211 mol) were added to a small Erlenmeyer flask that was stoppered and allowed to stand overnight. The solid that formed was removed and recrystallized from ethanol. After washing with cold ethanol the light yellow solid was washed with anhydrous ether. It was then dried in vacuo over  $P_4O_{10}$  for 18 h: mp 201–206 °C (sealed capillary) (sublime) [lit. (45) mp 185–190 °C (sublime)]; NMR ( $D_2O$ )  $\delta$  3.50 (m, 4), 2.85 (s, 3,  $CH_3$ ), 2.30 (m, 4).

(B) *Preparation of Di-n-butylmethylsulfonium Iodide.* After 24 h an orange oil that had settled to the bottom of the flask was removed and triturated three times with anhydrous ether. The oil remaining after trituration was dried for 24 hours in vacuo over  $P_4O_{10}$ . A waxy orange solid formed on drying: NMR ( $CDCl_3$ )  $\delta$  3.80 (m, 4  $CH_2$ ), 3.25 (s, 3,  $CH_3$ ), 1.1–2.0 (broad, 8), 0.95 (t, 6,  $CH_3$ ).

**Method 2.** Methylation with iodomethane in the presence of silver tetrafluoroborate (37–42)



In comparison to method 1, this procedure can be used for the derivatization of less nucleophilic sulfides. Ethyldiphenylsulfonium tetrafluoroborate and *S*-methyltetrahydrothiophenium tetrafluoroborate were prepared by this method.

(A) *Preparation of S-methyltetrahydrothiophenium Tetrafluoroborate.* To a flame-dried three-necked flask equipped with a nitrogen inlet, reflux condenser, and magnetic stirrer was added a solution of iodomethane (0.36 g, 0.00254 mol) and tetrahydrothiophene (0.45 g, 0.00511 mol) in 15 mL of dry nitromethane. Silver tetrafluoroborate (1.00 g, 0.00514 mol) was added to the solution as a solid over several minutes. The reaction was stirred at room temperature under an atmosphere of nitrogen for 6 h. An additional 15 mL of dry nitromethane was added and the solution was filtered by gravity. The nitromethane was removed by rotary evaporation and the resulting brown solid was washed with anhydrous ether and collected by suction filtration. It was

then dried in vacuo over  $P_4O_{10}$  for 24 h: mp 239–245 °C [lit. (46) mp 250–251 °C]; NMR ( $D_2O$ )  $\delta$  3.48 (m, 4), 2.81 (s, 3,  $CH_3$ ), 2.36 (m, 4).

(B) *Preparation of Ethyldiphenylsulfonium Tetrafluoroborate.* The reaction of phenyl sulfide and iodoethane with silver tetrafluoroborate in dry methylene chloride resulted in a brown oil that did not solidify on drying in vacuo: NMR ( $CDCl_3$ )  $\delta$  7.2–7.6 (broad, 10, aryl), 3.48 (q, 2,  $CH_2$ ), 1.18 (t, 3,  $CH_3$ ).

**Method 3.** Methylation with trimethyloxonium tetrafluoroborate (41, 43, 44)



This procedure is recommended for the least nucleophilic sulfides and was employed successfully with *n*-butyl sulfide and thianaphthene.

(A) *Preparation of Di-n-butylmethylsulfonium Tetrafluoroborate.* To a flame-dried three-necked flask equipped with a magnetic stirrer, rubber septum, nitrogen inlet, and reflux condenser was added trimethyloxonium tetrafluoroborate (1.00 g, 0.00676 mol) and 20 mL of dry methylene chloride. A solution of *n*-butyl sulfide (0.99 g, 0.0068 mol) in 5 mL of methylene chloride was added via syringe. The reaction was stirred at room temperature for 4 h and then filtered by gravity. The filtrate was triturated with 40 mL of anhydrous ether. An oil formed at the bottom of the flask and was removed and dried in vacuo over  $P_4O_{10}$  for 24 h. No visible changes occurred during this time: NMR ( $CDCl_3$ )  $\delta$  3.32 (t, 4,  $CH_2$ ), 2.85 (s, 3,  $CH_3$ ), 1.1–2.0 (broad, 8), 0.95 (t, 6,  $CH_3$ ).

(B) *Preparation of S-Methylbenzothiophenium Tetrafluoroborate.* The mixture of reactants was heated under reflux for 2 h and then stirred at room temperature for 60 h. Trituration with anhydrous ether resulted in the formation of a red oil. Drying the oil in vacuo over  $P_4O_{10}$  for 18 h resulted in a red-brown solid. The solid softened at 70 °C and melted from 110 to 112 °C [lit. (41) mp 72–73 °C]; NMR ( $CDCl_3$ )  $\delta$  7.6–7.9 (broad, 6), 3.50 (s, 3,  $CH_3$ ).

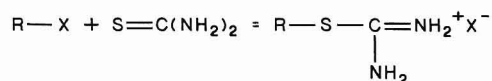
**Conversion of Alkyl Halides into Sulfonium Salts.** Sulfonium salts of alkyl halides such as iodomethane, 1-iodobutane, and benzyl chloride were prepared by modifying methods 1 and 2 (35–37). In these reactions the alkyl halide was derivatized with methyl sulfide.

(A) *Preparation of n-Butyldimethylsulfonium Iodide by Method 1.* A light brown solid formed from a mixture of 1-iodobutane and methyl sulfide that was allowed to stand over a period of 4 days. It was collected, washed with anhydrous ether, recrystallized from acetone, and dried in vacuo over  $P_4O_{10}$  for 18 h: mp 81–82 °C [lit. (47) mp 82 °C]; NMR ( $CDCl_3$ )  $\delta$  3.85 (t, 2,  $CH_2$ ), 3.42 (s, 6,  $CH_3$ ), 1.4–2.0 (broad, 4), 1.05 (t, 3,  $CH_3$ ).

(B) *Preparation of n-Butyldimethylsulfonium Tetrafluoroborate by Method 2.* The reactants (1-iodobutane, methyl sulfide, and silver tetrafluoroborate) were stirred in dry methylene chloride at room temperature for 18 h. The yellow solid obtained from the workup of the reaction was dried in vacuo over  $P_4O_{10}$ : mp 70–72 °C [lit. (48) mp 67.5–68 °C]; NMR ( $CDCl_3$ )  $\delta$  3.28 (t, 2,  $CH_2$ ), 2.84 (s, 6,  $CH_3$ ), 1.2–1.9 (broad, 4), 0.91 (t, 3,  $CH_3$ ).

(C) *Preparation of Benzyldimethylsulfonium Tetrafluoroborate by Method 2.* The reactants (benzyl chloride, methyl sulfide, and silver tetrafluoroborate) were stirred in nitromethane at room temperature for 60 h. After suitable workup, and recrystallization from 2-propanol, the white solid was dried in vacuo over  $P_4O_{10}$ : mp 96–100 °C [lit. (49) mp 99–101 °C]; NMR ( $CDCl_3$ )  $\delta$  7.3–7.6 (broad, 5, aryl), 4.61 (s, 2,  $CH_2$ ), 2.86 (s, 6,  $CH_3$ ).

**Conversion of Alkyl Halides into Isothiuronium Salts.**



The isothiuronium salts were prepared by a modification of literature methods (23–25). This procedure was used in the derivatization of 1-chlorobutane, 1-bromopentane, 1-bromononane, 1-iodobutane, benzyl chloride, 2-chlorobutane, and 2-bromobutane.

(A) *Preparation of n-Pentylisothiuronium Bromide.* A mixture of 1-bromopentane (5.00 g, 0.0331 mol), thiourea (2.52 g, 0.0331 mol), and 20 mL of 95% ethanol was heated under reflux, with stirring, for 24 h. The course of the reaction can be monitored



by the disappearance of the slightly soluble thiourea. The reflux condenser was removed and the volume of solution was reduced until the first sign of solid material. The mixture was then cooled in an ice bath. The resulting solid was collected by suction filtration and recrystallized from 95% ethanol. A waxy material was obtained that was dried in vacuo over  $P_4O_{10}$  for 18 h (33% yield, mp 78–84 °C): NMR ( $CDCl_3$ )  $\delta$  3.36 (t, 2,  $CH_2$ ), 1.1–2.0 (broad, 6), 0.94 (t, 3,  $CH_3$ ).

(B) *Preparation of n-Nonylthiuronium Bromide.* Thiourea and 1-bromononane were heated under reflux for 18 h. The desired product was obtained in 78% yield (mp 84–87 °C) as a white, waxy material: NMR ( $CDCl_3$ )  $\delta$  3.35 (t, 2,  $CH_2$ ), 1.1–2.0 (broad, 14), 0.90 (t, 3,  $CH_3$ ).

(C) *Preparation of Benzylthiuronium Chloride.* Benzyl chloride and thiourea were heated under reflux for 24 h. The product was obtained in 97% yield as a white, waxy material (mp 136–137 °C): NMR ( $D_2O$ )  $\delta$  7.51 (s, 5, aryl), 4.43 (s, 2,  $CH_2$ ).

(D) *Preparation of n-Butylthiuronium Iodide.* Thiourea and 1-iodobutane were heated under reflux for 1 h. After reduction of the volume and cooling, anhydrous ether was added and a white precipitate formed. Recrystallization from 95% ethanol afforded the product in 60% yield as a fine white powder (mp 95–101 °C): NMR ( $D_2O$ )  $\delta$  3.13 (t, 2,  $CH_2$ ), 1.1–2.0 (broad, 4), 0.92 (t, 3,  $CH_3$ ).

(E) *Preparation of n-Butylthiuronium Chloride.* Thiourea and 1-chlorobutane were heated under reflux for 24 h. After reduction of the volume and cooling, the product was obtained as a precipitate by the addition of anhydrous ether. The crude product was recrystallized from 95% ethanol and obtained in 73% yield as fine white crystals (mp 69–75 °C): NMR ( $D_2O$ )  $\delta$  3.16 (t, 2,  $CH_2$ ), 1.1–2.0 (broad, 4), 0.92 (t, 3,  $CH_3$ ).

(F) *Preparation of sec-Butylthiuronium Bromide.* Thiourea and 2-bromobutane were heated under reflux for 2.5 h. After the product was isolated by removal of the solvent, it was dissolved in ethanol and triturated with anhydrous ether. The sticky white material was collected and dried in vacuo over  $P_4O_{10}$  for 12 h. Its appearance did not change on drying: NMR ( $D_2O$ )  $\delta$  3.66 (m, 1, CH), 1.77 (m, 2,  $CH_2$ ), 1.43 (d, 3,  $CH_3$ ), 1.01 (t, 3,  $CH_3$ ).

(G) *Preparation of sec-Butylthiuronium Chloride.* Thiourea and 2-chlorobutane were heated under reflux for 144 h. The solution was cooled and unreacted thiourea was removed by gravity filtration. The filtrate was triturated with ether and reducing the volume resulted in a light brown solid. The solid was collected, recrystallized from 100% ethanol, and washed with anhydrous ether. The desired product was obtained as an off-white solid in 6.4% yield (mp 75–80 °C): NMR ( $D_2O$ )  $\delta$  3.66 (m, 1, CH), 1.76 (m, 2,  $CH_2$ ), 1.43 (d, 2,  $CH_3$ ), 1.02 (t, 3,  $CH_3$ ).

**Procedures.** To record the spectrum of a substrate in the presence of  $[Ln(fod)_4]^-$ , the appropriate amount of  $Ln(fod)_3$ ,  $M(fod)$  ( $M = Ag$  or  $K$ ), and substrate were weighed into a test tube. The correct amount of solvent was added and the test tube was stoppered and shaken vigorously for a period of 2 min. In instances when the substrate was sparingly soluble in  $CDCl_3$ , the mixture was periodically shaken over the course of an hour to ensure solubilization of the cation. Insoluble material, including the silver halide or potassium tetrafluoroborate salt, was removed by centrifugation and decantation of the supernatant. Prior to recording of the spectrum, the test tube and NMR tube were covered with foil to exclude light.

## RESULTS AND DISCUSSION

The reason for the superior effectiveness of  $[Ln(fod)_4]^-$  compared to  $Ln(fod)_3$  as a shift reagent for organic salts is not known with certainty. It has been postulated that the mechanism by which  $Ln(fod)_3$  complexes cause shifts in the spectra of organic salts involves the formation of the anionic species  $[Ln(fod)_3X]^-$  ( $X =$  original anion of the organic salt) (eq 2) (26–28, 50–56). The binding constants of the anions of organic salts with  $Ln(fod)_3$  to form  $[Ln(fod)_3X]^-$  are of intermediate values (26). The binding constant of  $Ag(fod)$  with  $Ln(fod)_3$  (eq 3) has a calculated value of  $500 M^{-1}$  (57). This reaction is in the slow exchange region below 20 °C and discrete resonances for the binuclear species  $Ag[Ln(fod)_4]$  are observed (57). The values reported in the literature for the association constants of  $X^-$  (chloride or bromide) with  $Ln(fod)_3$

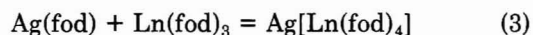
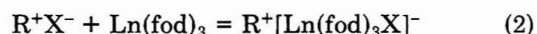
**Table I. Lanthanide Induced Shifts (ppm) in the Proton NMR Spectra of Butyl Sulfide (0.1 M), Di-n-butylmethylsulfonium Iodide (0.1 M), and Di-n-butylmethylsulfonium Tetrafluoroborate (0.1 M) in  $CDCl_3$  with Various Shift Reagents (0.05 M)**

$(CH_3CH_2CH_2CH_2)_2S$						
shift reagent	1	2	3	4		
Eu(fod) <sub>3</sub>	0.07	0.10	0.10	0		
$(CH_3CH_2CH_2CH_2)_2SCH_3^+I^-$						
shift reagent	$CH_3$	1 <sub>a</sub>	1 <sub>b</sub>	2	3	4
Eu(fod) <sub>3</sub>	0.15	0.09	0.09	– <sup>b</sup>	–	0
Eu(fod) <sub>3</sub> –K(fod)	0.17	0.34	0.34	0.30	0.30	0.09
Eu(fod) <sub>3</sub> –Ag(fod)	14.35	4.37	3.77	2.32	1.13	0.75
$(CH_3CH_2CH_2CH_2)_2SCH_3^+BF_4^-$						
shift reagent	$CH_3$	1 <sub>a</sub>	1 <sub>b</sub>	2	3	4
Eu(fod) <sub>3</sub>	0.88	0.44	0.44	0.30	0.10	0.05
Eu(fod) <sub>3</sub> –K(fod)	12.43	4.28	3.65	2.01	0.95	0.58
Eu(fod) <sub>3</sub> –Ag(fod)	0.25	0.09	0.09	0.10	0.10	0

<sup>a</sup> With certain shift reagents, the resonances of the diastereotopic hydrogen atoms at position 1 were resolved.

<sup>b</sup> Masked by the shift reagent resonance.

(eq 2) range from 27 to  $954 M^{-1}$  (26, 50). A further consideration with  $[Ln(fod)_4]^-$ , however, is that the anion of the organic salt precipitates with the  $Ag^+$  or  $K^+$  (eq 4). The



formation of such a precipitate was obvious from both the volume of insoluble material and unmistakable appearance of the silver halide. The formation of a precipitate was verified by adding a solution of *N*-methylnicotinium iodide in chloroform to a filtered solution of  $Ag[Eu(fod)_4]$  in chloroform. A gray-white solid formed on mixing the two solutions. This precipitation forces the association of the organic cation with the shift reagent and seems to be the most plausible reason for the enhanced shifts with  $[Ln(fod)_4]^-$  compared to  $Ln(fod)_3$ .

Other mechanisms cannot be ruled out, however, in explaining the relative effectiveness of  $[Ln(fod)_4]^-$  and  $Ln(fod)_3$  as shift reagents for organic cations. The shifts in the spectrum of an organic cation in the presence of an anionic shift reagent are probably predicted by the dipolar shift equation (58). It may be that the geometric term of the dipolar shift equation (distance and angle terms) with  $[Ln(fod)_4]^-$  results in larger shifts than for  $[Ln(fod)_3X]^-$ .

**Sulfonium Salts.** The NMR spectra of sulfonium salts with halide or tetrafluoroborate counterions exhibit large shifts in the presence of  $[Eu(fod)_4]^-$ . The shifts recorded in the spectra of di-n-butylmethylsulfonium iodide and tetrafluoroborate with several shift reagents are listed in Table I. The shifts in the NMR spectra of both salts with  $Eu(fod)_3$  are included in the table for comparison. The effectiveness of the species  $[Eu(fod)_4]^-$  relative to  $Eu(fod)_3$  as a shift reagent for sulfonium salts is apparent. One interesting observation is that the resonances of the diastereotopic hydrogen atoms of the methylene group  $\alpha$  to the sulfur atom are resolved in the spectra with  $[Eu(fod)_4]^-$ . No resolution of these diastereotopic protons was observed in the presence of  $Eu(fod)_3$ .

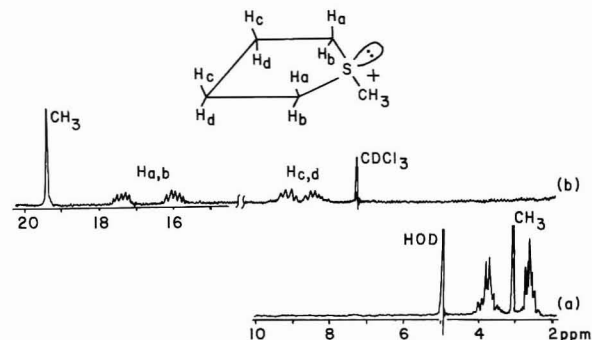
The selection of  $M(\text{fod})$  to use in the formation of  $[\text{Eu}(\text{fod})_4]^-$  depends on the identity of the counterion of the sulfonium salt. The data presented in Table I for di-*n*-butylmethylsulfonium iodide and di-*n*-butylmethylsulfonium tetrafluoroborate illustrate this conclusion. The species  $[\text{Eu}(\text{fod})_4]^-$  formed from  $\text{Eu}(\text{fod})_3\text{-Ag}(\text{fod})$  was more effective as a shift reagent for the sulfonium halide than  $[\text{Eu}(\text{fod})_4]^-$  formed from  $\text{Eu}(\text{fod})_3\text{-K}(\text{fod})$ . The opposite was found for the sulfonium tetrafluoroborate salt. A similar pattern was noted for the shifts in the spectra of the halide and tetrafluoroborate salts of the *S*-methyltetrahydrothiophenium and *n*-butyldimethylsulfonium cations with  $\text{Eu}(\text{fod})_3\text{-Ag}(\text{fod})$  and  $\text{Eu}(\text{fod})_3\text{-K}(\text{fod})$ .

The influence of  $M(\text{fod})$  on the magnitude of the shifts most likely reflects differences in the solubility of the  $\text{K}^+$  and  $\text{Ag}^+$  salts with the halide and tetrafluoroborate ions. This was shown by adding a solution of the chloroform-soluble salt benzyldimethylsulfonium tetrafluoroborate to solutions of  $\text{Ag}[\text{Eu}(\text{fod})_4]$  and  $\text{K}[\text{Eu}(\text{fod})_4]$ . With the silver reagent no precipitation was observed until high substrate concentrations were employed. With the potassium reagent a precipitate (presumably  $\text{KBF}_4$ ) was noted on the first addition of substrate. By an analogous study the reverse properties were shown using a solution of *N*-methylnicotinium iodide in chloroform. The first introduction of substrate to the silver reagent resulted in a precipitate, presumably  $\text{AgI}$ . With the potassium reagent, the solution only developed a slight cloudiness until high concentration of substrate were added. If the anion of the organic salt does not precipitate with the cation of the shift reagent, the association of the organic cation with the shift reagent will be reduced and smaller shifts will result. The use of  $\text{K}(\text{fod})$  is therefore recommended with tetrafluoroborate salts and  $\text{Ag}(\text{fod})$  is recommended for halide salts.

As can be seen from the data in Table I, the shifts in the spectrum of di-*n*-butylmethylsulfonium tetrafluoroborate with  $\text{Eu}(\text{fod})_3\text{-K}(\text{fod})$  are similar in magnitude to those of di-*n*-butylmethylsulfonium iodide with  $\text{Eu}(\text{fod})_3\text{-Ag}(\text{fod})$ . The same shifts would result if the anion of the salt precipitated with the cation of the shift reagent. Each sample would then contain an ion pair of the sulfonium cation with  $[\text{Eu}(\text{fod})_4]^-$ . Identical observations have been noted with the tetrafluoroborate and iodide salts of the *S*-methyltetrahydrothiophenium and *n*-butyldimethylsulfonium cations.

The shifts in the spectrum of butyl sulfide with  $\text{Eu}(\text{fod})_3$  are also presented in Table I. These shifts are small and agree with a previous conclusion that chelates of  $\text{fod}$  are relatively ineffective as NMR shift reagents for organosulfides (59). Chelates with 1,1,1,2,2,3,3,7,7,8,8,9,9,9-tetradecafluoro-4,6-nonanedione were reportedly more effective NMR shift reagents for organosulfides (59), but the magnitudes of the shifts do not compare with those in the spectra of sulfonium cations in the presence of  $[\text{Ln}(\text{fod})_4]^-$ .

The proton NMR spectra of the *S*-methyltetrahydrothiophenium cation with and without  $[\text{Eu}(\text{fod})_4]^-$  are shown in Figure 1. This compound has four different ring protons, the resonances of which were completely resolved in the shifted spectrum. No resolution of the geminal pairs ( $H_a$  from  $H_b$  and  $H_c$  from  $H_d$ ) was observed in the unshifted spectrum recorded at 60 MHz. Only small shifts were recorded in the spectrum of the *S*-methyltetrahydrothiophenium cation with  $\text{Eu}(\text{fod})_3$ . This confirms that  $[\text{Eu}(\text{fod})_4]^-$  forms an ion pair with the cation rather than associating with the cation at the lone pair of electrons of the sulfur atom. Assuming that the  $[\text{Eu}(\text{fod})_4]^-$  associates near the sulfur atom, the shifts of  $H_a$  and  $H_b$  would be larger than those of  $H_c$  and  $H_d$ . Resolution of the four different hydrogen atoms of the ring indicates that  $[\text{Eu}(\text{fod})_4]^-$  must be preferentially located toward one face of



**Figure 1.** Proton NMR spectrum of *S*-methyltetrahydrothiophenium iodide (0.1 M) in (a)  $\text{D}_2\text{O}$  and (b) in  $\text{CDCl}_3$  with  $[\text{Eu}(\text{fod})_4]^-$  (0.05 M).  $[\text{Eu}(\text{fod})_4]^-$  was formed in solution from  $\text{Eu}(\text{fod})_3$  and  $\text{Ag}(\text{fod})$ .

the ring. This would place the shift reagent closer to either the methyl group or the lone pair of electrons of the sulfur atom. The exact geometry of the shift reagent-substrate complex cannot be determined from the shift data and unequivocal assignment of the  $H_a, H_b$  and  $H_c, H_d$  pairs cannot be made at this time.

The spectra of sulfonium salts of aromatic sulfides such as phenyl sulfide and benzothiophene (II) are shifted in the

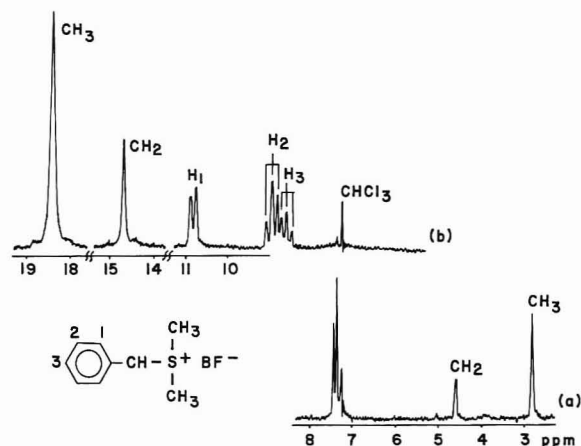


presence of  $[\text{Ln}(\text{fod})_4]^-$ . The shifts in the spectrum of ethyldiphenylsulfonium tetrafluoroborate with  $[\text{Eu}(\text{fod})_4]^-$  were too small to be of practical utility. In a solution containing  $[\text{Yb}(\text{fod})_4]^-$  (0.1 M) and this substrate (0.1 M) the resonances of the protons ortho to the sulfur atom were shifted by 1.60 ppm. The protons meta and para to the sulfur atom were unresolved and exhibited shifts of approximately 0.5 ppm. The shifts for the methylene resonance of the ethyl group were less than 0.5 ppm. The steric encumbrance of this substrate probably reduces the association constant with the shift reagent causing the small shifts. A similar conclusion was postulated to explain the small shifts in the spectrum of diphenylamine hydrochloride with  $[\text{Eu}(\text{fod})_4]^-$  (22).

In the spectra of benzothiophene and the *S*-methylbenzothiophenium ion at 60 MHz, none of the aromatic protons exhibit unique resonances. Essentially no shifts are observed in the spectrum of benzothiophene with  $\text{Eu}(\text{fod})_3$ . Shifts are observed in the spectrum of benzothiophene with binuclear shift reagents (18, 60). By use of  $\text{Pr}(\text{fod})_3\text{-ag}(\text{tfa})$  (0.15 M) first-order spectrum was obtained at 250 MHz for benzothiophene (0.1 M) (18). The largest shift with this reagent was  $-2.87$  ppm for the H-2 resonance. The spectrum of *S*-methylbenzothiophenium tetrafluoroborate (0.1 M) with  $[\text{Eu}(\text{fod})_4]^-$  (0.05 M) is shifted and three doublets and one complex multiplet are observed between 7 and 10 ppm. The three doublets are probably the resonances for the protons at the 2, 3, and 7 positions. Assuming the resonance furthest shifted is that of H-2, a shift of 2.57 ppm was obtained. Unfortunately the resonances were too close together in the shifted spectrum to permit decoupling experiments and assignment.

Large shifts were observed in the spectra of *n*-butyldimethylsulfonium iodide and -tetrafluoroborate and benzyldimethylsulfonium tetrafluoroborate with  $[\text{Eu}(\text{fod})_4]^-$ . The NMR spectra of benzyldimethylsulfonium tetrafluoroborate (0.1 M) with and without  $[\text{Eu}(\text{fod})_4]^-$  (0.1 M) are shown in Figure 2. In this example the shift reagent was formed from  $\text{Eu}(\text{fod})_3$  and  $\text{K}(\text{fod})$ . The spectrum with the shift reagent is first order. Both the *n*-butyldimethylsulfonium and benzyldimethylsulfonium salts were prepared by reacting the corresponding alkyl halide with methyl sulfide in the presence





**Figure 2.** Proton NMR spectrum of benzyldimethylsulfonium tetrafluoroborate (0.1 M) in  $\text{CDCl}_3$  with (a) no shift reagent and (b)  $[\text{Eu}(\text{fod})_4]^-$  (0.1 M).  $[\text{Eu}(\text{fod})_4]^-$  was formed in solution from  $\text{Eu}(\text{fod})_3$  and  $\text{K}(\text{fod})$ .

**Table II. Lanthanide Induced Shifts (ppm) in the NMR Spectra of 1-Iodobutane (0.2 M), *n*-Butyldimethylsulfonium Iodide (0.1 M), and *n*-Butylisothiuronium Iodide (0.1 M) in  $\text{CDCl}_3$**

shift reagent (concn)	1	2	3	4
	4 3 2 1			
	$\text{CH}_3\text{CH}_2\text{CH}_2\text{CH}_2\text{I}$			
$\text{Yb}(\text{fod})_3\text{-Ag}(\text{fod})$ (0.1 M)	1.57 <sup>a</sup>	1.00	0.64	0.47
	4 3 2 1			
	$\text{CH}_3\text{CH}_2\text{CH}_2\text{CH}_2\text{S}(\text{CH}_3)_2^+\text{I}^-$			
$\text{Eu}(\text{fod})_3\text{-Ag}(\text{fod})$ (0.05 M)	7.3	4.3	2.5	1.6
	4 3 2 1			
	$\text{CH}_3\text{CH}_2\text{CH}_2\text{CH}_2\text{S}-\text{C}(\text{NH}_2)=\text{NH}_2^+\text{I}^-$			
$\text{Eu}(\text{fod})_3\text{-Ag}(\text{fod})$ (0.05 M)	3.8	2.7	1.9	1.2
$\text{Yb}(\text{fod})_3\text{-Ag}(\text{fod})$ (0.05 M)	14.5	9.9	6.3	3.7

<sup>a</sup> From ref 9.

of  $\text{AgBF}_4$ . The spectra of alkyl chlorides, bromides, and iodides are not shifted in the presence of lanthanide tris chelates (29) and are shifted only slightly in the presence of binuclear lanthanide-silver reagents (17, 30). Conversion of alkyl halides to their corresponding sulfonium salts represents a useful method to obtain a shifted NMR spectrum of the alkyl group. Unfortunately, only reactive alkyl halides can be converted into sulfonium salts. A more general scheme for the conversion of primary and secondary alkyl halides into salts is to prepare isothiuronium derivatives (23-25).

**Isothiuronium Salts.** Table II presents shift data for the spectra of 1-iodobutane, *n*-butyldimethylsulfonium iodide, and *n*-butylisothiuronium iodide with several shift reagents. The  $\text{H}_2$  and  $\text{H}_3$  resonances partially overlap in the unshifted spectra of 1-iodobutane and the two salts. The shifts observed in the spectrum of 1-iodobutane with  $\text{Yb}(\text{fod})_3\text{-Ag}(\text{fod})$  were small (17), and the  $\text{H}_2$  and  $\text{H}_3$  resonances were not fully resolved at 60 or 90 MHz. Previous reports have concluded that the binuclear reagents are marginally effective shift reagents for primary alkyl halides (17, 30). The largest shifts are observed for iodo derivatives with the binuclear reagents (17).

As evidenced from the data in Table II, the shifts in the spectra of the sulfonium and isothiuronium salts with  $[\text{Ln}(\text{fod})_4]^-$  are significantly larger than those in the spectrum of the alkyl halide with  $\text{Ln}(\text{fod})_3$  (29) or  $\text{Ag}[\text{Ln}(\text{fod})_4]$  (17). Whereas the shifts in the spectra of sulfonium salts are adequate with  $[\text{Eu}(\text{fod})_4]^-$ , the shifts in the spectra of isothiuronium salts with  $[\text{Eu}(\text{fod})_4]^-$  are not of much practical utility. This observation probably reflects the longer distance between the lanthanide ion and alkyl portion of the molecule in the isothiuronium derivatives. Employing  $[\text{Yb}(\text{fod})_4]^-$ , a more

powerful downfield shift reagent than  $[\text{Eu}(\text{fod})_4]^-$ , results in larger and more useful shifts. The spectra of isothiuronium salts with  $[\text{Yb}(\text{fod})_4]^-$  exhibit more broadening than those observed with  $[\text{Eu}(\text{fod})_4]^-$ . The broadening is within acceptable levels, however, and the fine structure due to coupling was usually present in the spectrum. The species  $[\text{Yb}(\text{fod})_4]^-$  is therefore recommended over  $[\text{Eu}(\text{fod})_4]^-$  for the study of isothiuronium salts.

The spectra of the isothiuronium salts of primary halides including 1-bromopentane, 1-bromononane, 1-chlorobutane, and benzyl chloride exhibited large shifts in the presence of  $[\text{Yb}(\text{fod})_4]^-$ . The first five methylene resonances of *n*-nonylthiuronium bromide (0.1 M) were fully resolved in the presence of  $[\text{Yb}(\text{fod})_4]^-$  (0.1 M). The proton NMR spectrum of benzyliothiuronium chloride (0.1 M) was first order in the presence of  $[\text{Pr}(\text{fod})_4]^-$  (0.05 M) and  $[\text{Yb}(\text{fod})_4]^-$  (0.05 M) at 60 MHz. The shifts in the spectrum of *n*-butylisothiuronium chloride with  $[\text{Yb}(\text{fod})_4]^-$  were essentially the same as those in the spectrum of *n*-butylisothiuronium iodide with  $[\text{Yb}(\text{fod})_4]^-$  (see Table II). Such an observation is consistent with precipitation of the halide counterion from solution as a silver halide salt.

Similar shifts were also noted in the spectra of *sec*-butylisothiuronium chloride and bromide in the presence of  $[\text{Yb}(\text{fod})_4]^-$ . The hydrogen atoms of the methylene group of these substrates are diastereotopic and were fully resolved (shift difference of 1.2 ppm) in the presence of the shift reagent. The two secondary butylisothiuronium salts are chiral and attempts were made to resolve resonances of the dextro and levo enantiomers using chiral shift reagents. The chiral shift reagents formed from  $\text{Eu}(\text{facam})_3\text{-Ag}(\text{fod})$ ,  $\text{Eu}(\text{hfb})_3\text{-Ag}(\text{fod})$ ,  $\text{Pr}(\text{hfb})_3\text{-Ag}(\text{ptb})$ , and  $\text{Pr}(\text{facam})_3\text{-Ag}(\text{fod})$  were evaluated. These particular binuclear reagents were selected because of their demonstrated effectiveness at causing enantiomeric resolution in the spectra of olefins and aromatics (33, 61-64). Only with  $[\text{Eu}(\text{facam})_3(\text{fod})]^-$  was any enantiomeric resolution obtained in the spectrum of *sec*-butylisothiuronium bromide. In this case the methyl resonance  $\alpha$  to the asymmetric carbon was slightly resolved ( $\Delta\delta = 0.05$  ppm) when both the substrate and shift reagent were at 0.1 M.

**Solvents.** The effectiveness of  $[\text{Ln}(\text{fod})_4]^-$  as a shift reagent for organic salts was compared in chloroform- $d_3$ , acetonitrile- $d_3$ , acetone- $d_6$ , and benzene- $d_6$ . Essentially no shifts were observed in the spectra of benzyldimethylsulfonium tetrafluoroborate and *n*-butylisothiuronium iodide in the presence of  $[\text{Eu}(\text{fod})_4]^-$  in acetonitrile- $d_3$  and acetone- $d_6$ . One possibility is that these solvents bond to the europium and prevent adequate formation of  $[\text{Eu}(\text{fod})_4]^-$  and/or the ion pair. An alternative explanation is that the anion of the organic salt may not precipitate with the cation of the shift reagent. In the case of the iodide salt, precipitation of silver iodide was apparent in both acetone and acetonitrile, ruling out the second mechanism. With the tetrafluoroborate salt, no precipitate was observed with the potassium reagent and both mechanisms may be operative. The shifts for the same two substrates in benzene- $d_6$  and chloroform- $d$  were comparable in magnitude. Both solvents are suitable for use with the anionic shift reagents.

## LITERATURE CITED

- (1) Rabenstein, D. L. *Anal. Chem.* **1971**, *43*, 1599.
- (2) Rajeswari, K.; Dubey, R.; Ranganayakulu, K. *Indian J. Chem., Sect. B* **1979**, *17B*, 504.
- (3) Meshimo, K.; Hayashibe, T.; Wainai, T. *Bunseki Kagaku* **1977**, *26*, 672.
- (4) Werstler, D. D.; Suman, P. T. *Anal. Chem.* **1975**, *47*, 144.
- (5) Shoffner, J. P. *Anal. Chem.* **1975**, *47*, 341.
- (6) Enriquez, R.; Taboada, J.; Salazar, I.; Diaz, E.; *Org. Magn. Reson.* **1973**, *5*, 291.
- (7) Walters, D. B. *Anal. Chim. Acta* **1973**, *66*, 134.
- (8) Walters, D. B.; Horvat, R. J. *Anal. Chim. Acta* **1973**, *65*, 198.

- (9) Noda, M.; Takahashi, T. *Yukagaku* **1979**, *28*, 411.
- (10) Tsukida, K.; Ito, M.; Ikeda, F. *J. Vitaminol.* **1972**, *18*, 24.
- (11) Ranganayakulu, K.; Dubey, R.; Rajeswari, K. *Tetrahedron Lett.* **1981**, *22*, 4359.
- (12) Tsukida, K.; Akutsu, K.; Ito, M. *J. Nutr. Sci. Vitaminol.* **1976**, *22*, 7.
- (13) Hashimoto, S.; Nagai, T. *Bunseki Kagaku* **1977**, *26*, 10.
- (14) Lala, A.K.; Kulkarni, A.B. *Indian J. Chem.* **1974**, *12*, 926.
- (15) Pfeffer, P. E.; Rothbart, H. L. *Tetrahedron Lett.* **1972**, 2533.
- (16) Wedmid, Y.; Litchfield, C. *Lipids* **1975**, *10*, 145.
- (17) Wenzel, T. J.; Sievers, R. E. *Anal. Chem.* **1981**, *53*, 393.
- (18) Audit, M.; Demerseman, P.; Goasdoue, N.; Platzer, N. *Org. Magn. Reson.* **1983**, *21*, 698.
- (19) McKenna, M.; Wright, L. L.; Miller, D. J.; Tanner, L.; Hattiwanger, R. C.; DuBois, M. R. *J. Am. Chem. Soc.* **1983**, *105*, 5329.
- (20) Damska, A.; Janowski, A. *Org. Magn. Reson.* **1980**, *13*, 122.
- (21) Wenzel, T. J.; Sievers, R. E. *Anal. Chem.* **1982**, *54*, 1602.
- (22) Wenzel, T. J.; Zala, J. *J. Org. Chem.* **1985**, *50*, 1322.
- (23) Uguhart, G. G.; Gates, J. W., Jr.; Connor, R. *Organic Syntheses Collective Volume 3*; Wiley: New York, 1955; p 363.
- (24) Speziale, J. A. *Organic Syntheses Collective Volume 4*; Wiley: New York, 1963; p 401.
- (25) Pado, D. J.; Johnson, C. R. *Organic Structure Determination*; Prentice-Hall: Englewood Cliffs, NJ, 1964; p 350.
- (26) Lipkowitz, K. B.; Chevalier, T.; Mundy, B. P.; Theodore, J. J. *Tetrahedron Lett.* **1980**, *21*, 1297.
- (27) Caret, R. L.; Vennos, A. N. *J. Org. Chem.* **1980**, *45*, 361.
- (28) Caret, R. L.; Vennos, A.; Zapf, M.; Uebel, J. J. *Tetrahedron Lett.* **1981**, *22*, 2085.
- (29) San Filippo, J., Jr.; Nuzzo, R. G.; Romano, L. J. *J. Am. Chem. Soc.* **1975**, *97*, 2546.
- (30) Wenzel, T. J. *J. Org. Chem.* **1984**, *49*, 1834.
- (31) Springer, C. S., Jr.; Meek, D. W.; Sievers, R. E. *Inorg. Chem.* **1967**, *6*, 1105.
- (32) Wenzel, T. J.; Bettis, T. C.; Sadlowski, J. E.; Sievers, R. E. *J. Am. Chem. Soc.* **1980**, *102*, 5903.
- (33) Wenzel, T. J.; Ruggles, A. C.; Lalonde, D. R., Jr. *Magn. Reson. Chem.* **1985**, *23*, 778.
- (34) Hammond, G. S.; Nonhebel, D. C.; Wu, C. S. *Inorg. Chem.* **1963**, *2*, 73.
- (35) Corey, E. J.; Chaykovsky, M. *J. Am. Chem. Soc.* **1965**, *87*, 1353.
- (36) Bost, R. W.; Everett, J. E. *J. Am. Chem. Soc.* **1940**, *62*, 1752.
- (37) Trost, M.; Melvin, L. S., Jr. *Sulfur Ylides, Emerging Synthetic Intermediates*; Academic: New York, 1975; pp 6-11.
- (38) Trost, B. M.; Bogdanowicz, M. J. *J. Am. Chem. Soc.* **1973**, *95*, 5298.
- (39) LaRochelle, R. W.; Trost, B. M.; Krepski, L. *J. Org. Chem.* **1971**, *36*, 1126.
- (40) Tang, C. S. F.; Rapoport, H. *J. Org. Chem.* **1973**, *38*, 2806.
- (41) Acheson, R. M.; Harrison, D. R. *J. Chem. Soc. C* **1970**, 1764.
- (42) Acheson, R. M.; Harrison, D. R. *J. Chem. Soc., Chem. Commun.* **1969**, 724.
- (43) Brumlik, G. C.; Kosak, A. I.; Pitcher, R. *J. Am. Chem. Soc.* **1964**, *86*, 5360.
- (44) Andersen, K. K.; Caret, R. L.; Karup-Nielsen, I. *J. Am. Chem. Soc.* **1974**, *96*, 8026.
- (45) Braun, J. V.; Trumpler, A. *Ber. Dtsch. Chem. Ges.* **1910**, *43*, 549.
- (46) Umehara, M.; Kanai, K.; Kitano, H.; Fukui, K. *Nippon Kagaku Zasshi* **1962**, *83*, 1060.
- (47) Yano, Y.; Okonogi, T.; Tagaki, W. *J. Org. Chem.* **1973**, *38*, 3912.
- (48) Ohkubo, K.; Yamabe, T. *J. Org. Chem.* **1971**, *36*, 3149.
- (49) van Bergen, T. J.; Hedstrand, D. M.; Kruizinga, W. H.; Kellogg, R. M. *J. Org. Chem.* **1979**, *44*, 4953.
- (50) Rackham, D. M.; Chitty, C. J. *Spectrosc. Lett.* **1981**, *14*, 249.
- (51) Graves, R. E.; Rose, P. I. *J. Chem. Soc., Chem. Commun.* **1973**, 630.
- (52) Seeman, J. I.; Bassfield, R. L. *J. Org. Chem.* **1977**, *42*, 2337.
- (53) Montaudo, G.; Kruk, G.; Verhoeven, J. W. *Tetrahedron Lett.* **1974**, 1845.
- (54) Balaban, A. T. *Tetrahedron Lett.* **1978**, 5055.
- (55) Bassfield, R. L. *J. Am. Chem. Soc.* **1983**, *105*, 4168.
- (56) Lefevre, F.; Rabiller, C.; Mannschreck, A.; Martin, G. J. *J. Chem. Soc., Chem. Commun.* **1979**, 942.
- (57) Raber, D. J.; Hajek, M. *Magn. Reson. Chem.* **1986**, *24*, 297.
- (58) Bleaney, B. *J. Magn. Reson.* **1972**, *8*, 91.
- (59) Morrill, T. C.; Clark, R. A.; Bilobran, D.; Youngs, D. S. *Tetrahedron Lett.* **1975**, 397.
- (60) Rackham, D. M. *Spectrosc. Lett.* **1981**, *14*, 639.
- (61) Wenzel, T. J.; Sievers, R. E. *J. Am. Chem. Soc.* **1982**, *104*, 382.
- (62) Offermann, W.; Mannschreck, A. *Tetrahedron Lett.* **1981**, 3227.
- (63) Krasutsky, P. A.; Yurchenko, A. G.; Radionov, V. N.; Jones, M., Jr. *Tetrahedron Lett.* **1982**, 3719.
- (64) Wenzel, T. J.; Lalonde, D. R., Jr. *J. Org. Chem.* **1983**, *48*, 1951.

RECEIVED for review July 14, 1986. Accepted October 29, 1986.  
We thank Bates College and Roger C. Schmutz for their support through a College Research Grant.

## Supersonic Jet Spectroscopy with a Capillary Gas Chromatographic Inlet

Steven W. Stiller and Murray V. Johnston\*

Department of Chemistry and Biochemistry, and Cooperative Institute for Research in Environmental Sciences, Campus Box 215, University of Colorado, Boulder, Colorado 80309-0215

**Supersonic jet spectroscopy is a highly selective molecular detection method that has suffered from relatively poor sensitivity. Sensitivity problems arise in part from the sample dilution effect of a free jet expansion. We report a new type of jet nozzle based upon sheath flow gas dynamic focusing that enriches the central core of the jet with analyte to provide better overlap with the incident laser beam. For a constant flow of analyte, the fluorescence intensity along the center line of a focused jet expansion is 30 times greater than that of an unfocused jet expansion. This method allows a detection limit of 50 pg ( $S/N = 3$ ) to be achieved for naphthalene and provides a simple way to couple a capillary gas chromatograph to a supersonic jet expansion. The focusing and cooling properties of analyte enriched jets are presented, and spectral selectivity is illustrated for the detection of naphthalene in unleaded gasoline.**

The selectivity of supersonic jet spectroscopy as a potential analytical tool is now well established. In this method, the analyte is seeded into a free jet expansion of a rare gas (He,

Ar, Xe) from a high-pressure region into a vacuum. Isentropic cooling of the gas during the expansion reduces the thermal population of excited rotational and vibrational levels in the analyte. As a result, molecular absorption and/or excitation spectra are remarkably free of spectral congestion due to hot band transitions (1). The ability of supersonic jet spectroscopy to distinguish among similar compounds, thereby allowing a qualitative identification of an unknown sample, has been the subject of several recent publications (2-9). In contrast, only a few quantitative studies have been reported (8, 10). In each case, the sample was injected into a packed-column gas chromatograph. A small pinhole at the end of the column served as the supersonic jet orifice. The gas chromatograph served only as a quantitative injection device and was not designed for optimum separation efficiency. Detection limits were found to be in the 20-200 ng range.

The sensitivity of analytical jet spectroscopy is ultimately limited by the characteristics of the jet expansion itself. To achieve maximum cooling, the sample must be probed in the free-flow region of the jet, typically 50 nozzle diameters downstream from the jet orifice. At this position, the sample partial pressure is reduced by ca.  $10^4$  from its value prior to



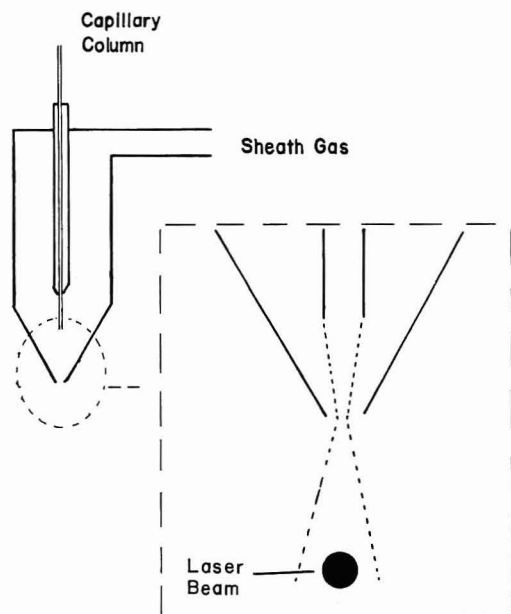


Figure 1. Schematic of the sheath flow nozzle.

expansion. Thus, the free jet expansion, which provides spectral selectivity through rotational and vibrational cooling, also contributes to decreased sensitivity since the sample concentration within the detection volume is significantly reduced.

In this paper, we report a new type of orifice that reduces the problem of sample "dilution" in the supersonic jet expansion. The central core of the jet is enriched with analyte through a gas focusing arrangement similar to that described by Keller and Nogar (11). The liquid-phase equivalent of this method, sheath flow hydrodynamic focusing, has been used routinely in flow cytometry for several years (12). The principle of sheath flow enrichment in supersonic jet spectroscopy is shown in Figure 1. The analyte gas flow is enveloped in a concentric sheath gas flow and then sent through a tapered jet orifice. The analyte is constrained to the central core of the jet, yielding better overlap between the sample and incident laser beam.

In addition to improved detection limits, this orifice can be used to couple a capillary gas chromatograph to the supersonic jet expansion. Interfacing these techniques with each other is not a trivial task since the gas flow rates needed are quite different. For example, a continuous supersonic jet expansion of argon at 250 torr through a 200- $\mu$ m orifice into a vacuum requires a gas flow rate of 370 mL/min. In contrast, optimum flow rates in capillary gas chromatography are on the order of 1 mL/min at atmospheric pressure. In the sheath flow nozzle, the end of the capillary column is inserted into the tapered orifice so that the column effluent becomes the analyte gas flow. The sheath gas provides the necessary gas flow for jet spectroscopy and focuses the analyte to achieve better sensitivity.

## EXPERIMENTAL SECTION

The sheath flow interface is shown schematically in Figure 1. The sheath gas flows down a 1/2-in.-o.d. stainless steel tube welded to a vacuum flange. This flange bolts into another flange containing the tapered jet orifice. The orifice consists of a 30° full angle cone that is machined in a stainless steel block. The open end of the cone matches the inner diameter of the sheath flow tube. The closed end of the cone has been milled back to give a 200- $\mu$ m-diameter orifice. The analyte flows through a 250- $\mu$ m-i.d. fused silica capillary that is fed through a 1/8-in. stainless steel tube. A series of spacers are used to center the capillary at the end of the inner 1/8-in. tube and to center the inner tube in the outer 1/2-in. tube. The capillary position in the tapered orifice

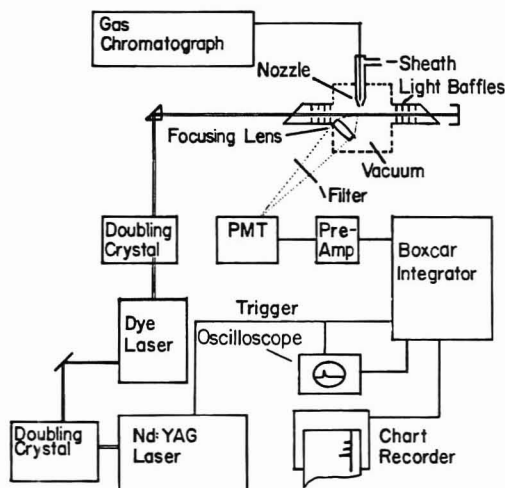


Figure 2. Block diagram of the experimental apparatus.

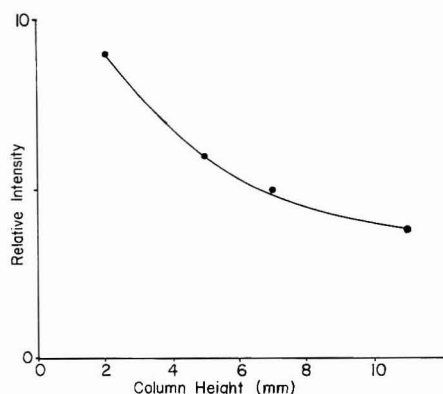
can be varied by raising or lowering the 1/8-in. tube relative to the outer tube. The entire interface is wrapped with heating tape and enclosed in a 1 1/2-in.-o.d. stainless steel tube that is mounted in a vacuum chamber with an xz translation stage.

A block diagram of the entire GC-fluorescence instrument is shown in Figure 2. The laser source is a Nd:YAG pumped frequency-doubled dye laser. Laser radiation enters and exits the vacuum chamber perpendicular to the supersonic beam through 12 in. arms that contain four baffles each. The baffles are similar in design to those described by Guyer (13). An xz translation stage is used to overlap the molecular and laser beams and to set the distance between the jet orifice and laser beam. Fluorescence is collected perpendicular to both the molecular and laser beams by a  $f/2$  lens assembly. Interference filters having peak transmissions of 30% and 10-nm band-passes centered at 321.5 and 326.0 nm are used to isolate the analyte emission from naphthalene and aniline, respectively. The vacuum chamber is pumped by a 6-in. cryotrapped diffusion pump. Under normal conditions, backing pressures of 250–400 torr are maintained behind the jet orifice, yielding chamber pressures of  $5 \times 10^{-4}$  to  $1 \times 10^{-3}$  torr. For a flow rate of 1 mL/min (STP) through the capillary column, the chromatographic effluent constitutes less than 1% of the total gas flow through the jet orifice.

For chromatographic applications, a 30-m by 0.25-mm-i.d. polydimethylsiloxane (Alltech catalog no. 13638) capillary column is used. The column resides in a chromatograph oven. A zero dead volume union connects the coated capillary column to an uncoated column of the same nominal inside diameter. This second column extends from the oven into the sheath flow nozzle. In this work, the transfer line and interface were maintained at 150 °C. The entire assembly can be heated to greater than 200 °C if necessary. Excitation spectra are obtained by using a constant mass flow of analyte. For this application, the coated column is replaced by an uncoated capillary of the same nominal inside diameter. The inlet of the column is connected to an effusive source held at a constant temperature in the chromatograph oven.

## RESULTS

**Sheath Flow Focusing.** The focusing properties of the sheath flow nozzle were first examined by varying the capillary column height within the tapered nozzle and measuring the relative fluorescence of a probe molecule, naphthalene. This process gave a qualitative measure of the analyte density along the center line of the jet expansion. When the column was placed closer than 2 mm from the jet orifice, the sheath gas became choked off and the gas flow became effusive. (Under effusive flow, the vacuum chamber pressure decreases and the naphthalene fluorescence excitation spectrum broadens significantly.) The column height dependence above 2 mm is shown in Figure 3. The fluorescence intensity is very high at short distances and falls off slowly as the column is raised. These data indicate that maximum sensitivity is achieved

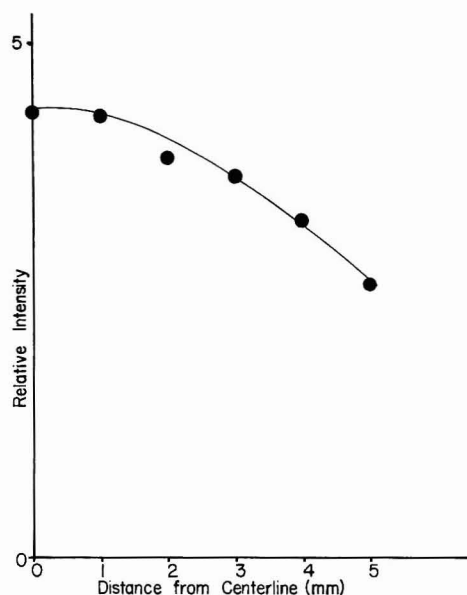


**Figure 3.** Naphthalene fluorescence intensity vs. capillary column height: argon sheath maintained at 250 torr; helium flow rate through capillary, 1 mL/min (STP); fluorescence probed 60 nozzle diameters downstream from the jet orifice.

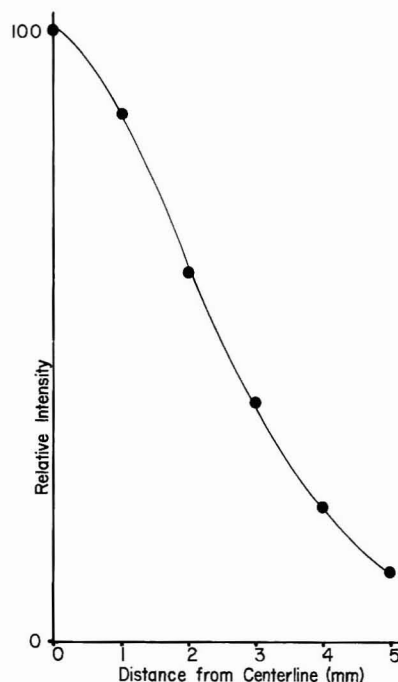
when the capillary is as close to the nozzle orifice as possible without choking off the sheath flow. The decrease in signal at longer distances from the nozzle is perhaps due to less efficient focusing through mixing of the analyte and sheath gas flows above the nozzle. These data were obtained by using a constant flow of naphthalene in helium as the "analyte" gas and argon at 250 torr as the sheath gas. Fluorescence was probed 12.5-mm (60 nozzle diameters) downstream from the orifice with a 1.0-mm-diameter laser beam. The laser was tuned to the  $8_0^1$  vibronic of the  $S_1 \leftarrow S_0$  transition of naphthalene at 308.12 nm.

The dependence shown in Figure 3 is observed only when extreme care is taken to maintain the concentric relationship between the inner and outer tubes. At short distances, a slight displacement of the inner column from the center-line axis of the outer tube can result in more than a 10-fold decrease in fluorescence intensity. The decrease in intensity may be explained as a deflection of the analyte stream off of the cone wall and subsequent mixing with the sheath. This observation is indicative of a substantial gas focusing effect within the sheath flow nozzle. At large distances, slight deviations from concentricity have a much smaller effect. This result is expected since the effective diameter of the sheath gas flow is much greater at large distances, and therefore, small changes in the lateral position of the inner capillary have only a minor effect upon the location of the (focused) analyte gas at the jet orifice.

The analyte profile across the jet expansion was examined by translating the center line of the jet expansion and measuring the relative fluorescence. Figure 4 shows the analyte profile of an unfocused jet expansion taken by mixing the analyte flow with the sheath gas prior to the bend in the sheath gas flow line (see Figure 1) so that focusing is destroyed. The density profile of this normal jet expansion has been described by a  $\cos^2 \theta$  dependence ( $\theta$  = angular displacement from the center line of the expansion) (14). Figure 5 is a profile of the focused jet when the capillary is positioned 2 mm above the jet orifice. The profile is significantly narrower than that in Figure 4. In addition, the absolute fluorescence intensity measured on the center line of the focused expansion is a factor of 30 greater than that of the nonfocused jet. Analyte profiles at 3 and 5 mm were found to be somewhat broader (as well as slightly less intense at the center line of the expansion) than the profile in Figure 5. These results indicate that the gas focusing that occurs upstream from the jet orifice leads to an enrichment of the analyte along the center line of the expansion downstream from the orifice. The profile obtained without any sheath gas flow is similar to the non-focused profile in Figure 4. In this case, the flow is effusive and no spectral cooling is observed.



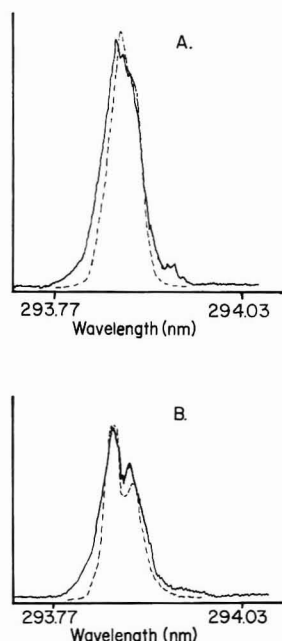
**Figure 4.** Naphthalene fluorescence intensity vs. linear displacement from the center line of the jet expansion: capillary column inlet into sheath gas stream prior to the nozzle interface; argon sheath maintained at 400 torr; helium flow rate through capillary, 1 mL/min (STP); fluorescence probed 60 nozzle diameters downstream, laser beam diameter 1.0 mm.



**Figure 5.** Naphthalene fluorescence intensity vs. linear displacement from the center line of the jet expansion: capillary column 2-mm upstream from the jet orifice; argon sheath maintained at 400 torr; helium flow rate through capillary, 1 mL/min (STP); fluorescence probed 60 nozzle diameters downstream, laser beam diameter 1.0 mm. Note that the vertical scale is related to that of Figure 4 but is a factor of 20 less sensitive.

Since fluorescence rather than concentration is being measured, it is important to show that the data in Figures 3, 4, and 5 do not simply reflect quenching processes or spectral differences due to changing rotational and vibrational temperatures. Quenching processes can be ruled out since the sample is probed in the free flow region where each molecule exists in a collision free regime on the fluorescence time scale. Spot checks of the excitation profile of the naphthalene  $8_0^1$  transition were made at several capillary heights and angular displacements. No significant changes in the spectrum were observed.

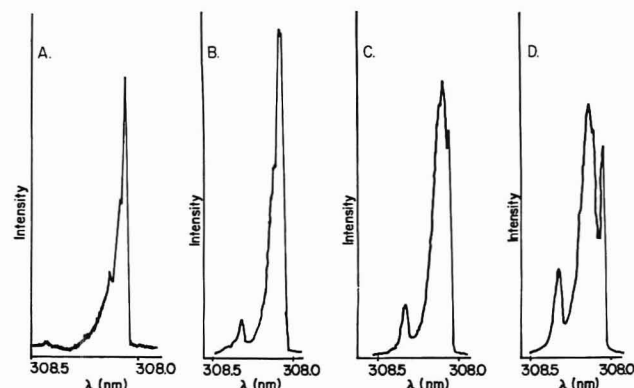




**Figure 6.** Excitation spectra of 0-0 transition of  $S_1 \leftarrow S_0$  of aniline. (A) Argon sheath pressure 400 torr. Dashed line indicates theoretical rotational contour for 10 K. (B) Argon sheath pressure 250 torr. Dashed line indicates theoretical rotational contour for 20 K.

Keller and Nogar (11) used a flow visualization apparatus to study the focusing properties of concentric gas flows. They found that the analyte gas could be constrained to an area as small as 0.1 mm in diameter *downstream* from the tapered orifice as long as the gas flow was subsonic. Their method was characterized by a low pressure differential across the orifice, a low gas velocity through the orifice, and nonturbulent flow downstream from the orifice. In contrast, the sheath flow nozzle in supersonic jet spectroscopy requires a high pressure differential across the orifice, a high gas velocity through the orifice, and turbulent flow downstream from the orifice. Thus, it would appear that tight focusing of the analyte flow and expansion cooling cannot be simultaneously produced downstream from the jet orifice. Nonetheless, significant enrichment of the central core of the supersonic beam can be achieved by this method, and as shown below, reasonable cooling is obtained.

**Supersonic Jet Spectroscopy.** The degree of rotational and vibrational cooling of a compound seeded into the jet expansion can be strongly influenced by the identity of the expansion gas and the geometry of the orifice (15, 16). Small molecules such as  $\text{NO}_2$  are commonly used as rotational thermometers in jets, but they are easier to cool than large molecules and therefore may overestimate the degree of cooling. Aniline is a more suitable choice since it is relatively "large" and rotational constants for both  $S_0$  and  $S_1$  are available (17). Parts A and B of Figure 6 show the comparison between experimental spectra obtained with the sheath flow nozzle and calculated rotational contours of aniline that are convoluted with the  $1.5 \text{ cm}^{-1}$  resolution of our dye laser. These spectra span the 0-0 transition of  $S_1 \leftarrow S_0$  of aniline at 293.87 nm and were obtained by using argon as the sheath gas at 400 torr in part A and 250 torr in part B of Figure 6. By comparison with the calculated rotational contours, it is estimated that rotational temperatures are approximately 10 K for the spectrum in part A and 20 K for the spectrum in part B of Figure 6. These spectra show that the degree of cooling is dependent upon sheath gas pressure. At sheath gas pressures below 250 torr, cooling becomes less efficient until the molecular beam becomes effusive and appreciable cooling is no longer observed. When helium is used as the sheath gas in the 250-400 torr range, cooling is much less efficient than with

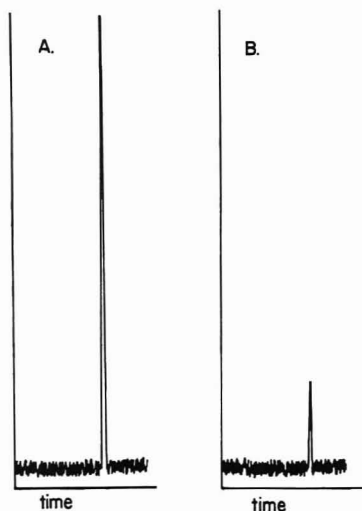


**Figure 7.** Excitation spectra of the  $8_0^1$  transition of naphthalene: fluorescence probed 60 nozzle diameters downstream from the orifice, capillary column height 2-mm upstream; argon sheath maintained at 250 torr; helium flow rate through capillary, 1 mL/min (STP). Naphthalene concentrations are as follows: (A) 5 ng/s, (B) 80 ng/s, (C) 500 ng/s, (D) 850 ng/s. Scale factors are  $\times 50$ ,  $\times 2.5$ ,  $\times 1$ , and  $\times 1$ , respectively.

argon. This observation is consistent with previous comparisons of the relative cooling efficiencies of helium and argon at relatively low backing pressures (15). Figure 7A is a wavelength scan across the  $8_0^1$  vibronic of  $S_1 \leftarrow S_0$  of naphthalene. This spectrum was taken under the same conditions as those in Figure 6B and therefore should reflect a rotational temperature of ca. 20 K.

Spectral resolution can be degraded if the sample partial pressure behind the jet orifice becomes too large. At partial pressures greater than 1 torr with conventional orifices, additional bands are observed in the optical spectra which arise from clustering of several molecules into large aggregates (18). Clustering may also affect quantitation since the analyte becomes distributed among several different chemical species. For these reasons, we explored the spectral changes that accompany large mass flows of naphthalene through the sheath flow nozzle. These changes are illustrated in Figure 7B,C,D. As the naphthalene flow increases above 50 ng/s, minor broadening of the  $8_0^1$  transition and a new band are observed. Major broadening and a change in band shape occur at flow rates on the order of 500 ng/s or greater. The scale calibration factors in Figure 7B,C,D show that a plot of fluorescence intensity vs. mass flow rate also becomes nonlinear in this region. Similar broadening would be expected in the case where a high-concentration impurity coelutes with a trace amount of naphthalene.

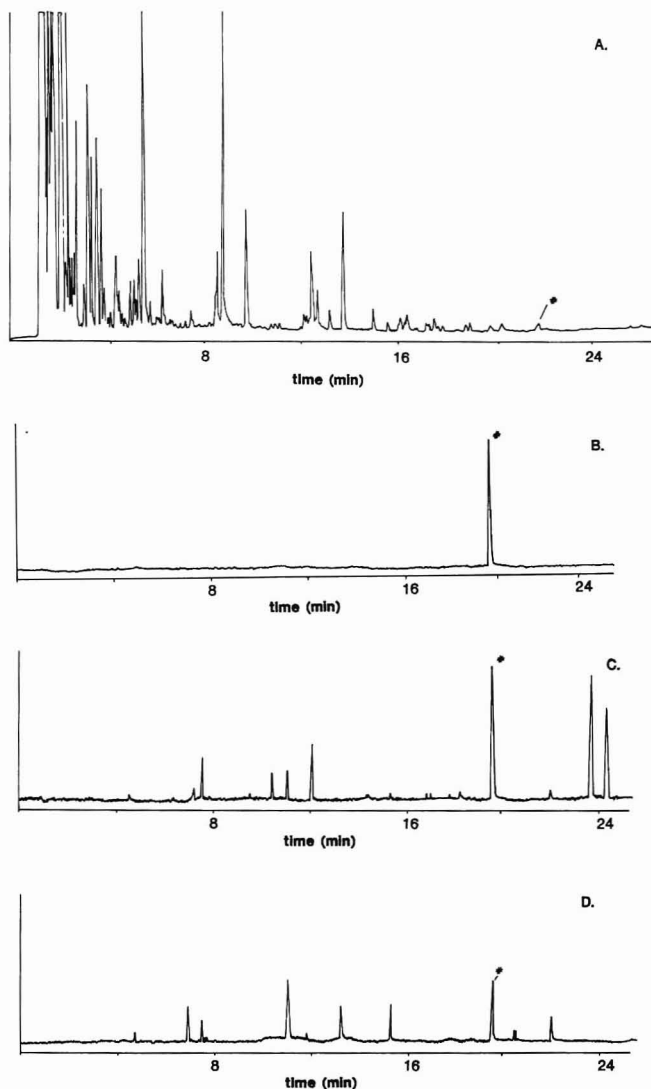
For chromatographic applications, the largest amount of analyte that can be eluted into the sheath flow nozzle without the loss of spectral resolution can be estimated from the above results. If one assumes a chromatographic peak width of 6 s at the base and that the mass flow rate near the peak maximum is roughly twice the average flow rate, then the mass flow rates in Figure 6 can be related to the absolute amount of sample eluted in a single chromatographic band that would produce a similar peak flow rate by the following: (ng eluted) = 3 (ng/s). Thus, major broadening that occurs at flow rates greater than 500 ng/s should become important when ca.  $1.5 \mu\text{g}$  or more elutes from the column in a single chromatographic band. However, one must consider the upper concentration limit imposed by the chromatography as well. The maximum sample size that can be injected without overloading a WCOT column is on the order of 0.5-1  $\mu\text{g}$ . Therefore, we conclude that only minor broadening will be induced within the range of sample sizes that can be handled with capillary columns as long as high-concentration impurities (solvent, etc.) are adequately separated from the analyte. The need to separate the solvent and analyte implies that at least a crude separation must be performed to retain maximum spectral selectivity.



**Figure 8.** (A) 500 pg of naphthalene injected into the gas chromatograph. (B) 100 pg of naphthalene injected. Oven and transfer line maintained at 150 °C. Laser: 1-mm beam diameter, 0.25 mJ/pulse, 60 nozzle diameters downstream. Capillary height was 2 mm.

**Gas Chromatography/Jet Spectroscopy.** When used in the chromatographic mode, the laser is fixed at a particular wavelength for the entire run. Figure 8 is an example of the sensitivity that can be achieved with the sheath flow nozzle. Figure 8A is a chromatogram of a 500-pg injection of naphthalene. Figure 8B is that of an injection of 100 pg. The estimated detection limit at  $S/N = 3$  is 50 pg. Although sensitivity is determined by several factors in addition to the nozzle performance, we note that this value is 3 orders of magnitude lower than that reported previously for naphthalene when using a conventional jet orifice (10). Of this amount, a factor of 30 can be attributed to sheath flow enrichment and the remainder from other factors such as improved chromatography, collection optics, baffling, etc. A calibration curve was constructed of naphthalene fluorescence (excitation at  $8_0^1$  transition) vs. amount injected. The plot was found to be linear from the detection limit to 500 ng injected.

The ability of jet spectroscopy to perform selective determinations in complex mixtures is illustrated in Figure 9. Figure 9A is a chromatogram of unleaded gasoline obtained by using a flame ionization detector. Figure 9B–D are chromatograms of the same sample obtained by using fluorescence detection at 321 nm under varying excitation conditions. When the laser is tuned to the  $8_0^1$  transition of naphthalene (Figure 9B), only naphthalene is detected. The difference in retention time between parts A and B of Figure 9 is due to a combination of differing pressures at the column outlet and the additional span of uncoated column in the sheath flow nozzle. In Figure 9C, the excitation wavelength is changed to 266 nm. At this wavelength, several chromatographic peaks are observed. Thus, the degree of selectivity is highly dependent upon the excitation and fluorescence wavelengths chosen. An explanation of this effect is found in the nature of electronic absorption spectra. At excitation energies close to the 0–0 transition of  $S_1 \leftarrow S_0$ , the density of states is small and excitation bands are well resolved. At energies well above the 0–0 transition, vibronic transitions in the  $S_1 \leftarrow S_0$  manifold become more closely spaced. In addition, transitions to higher energy electronic states may overlap. Therefore, the density of states becomes large enough that narrow-band excitation transitions are not observed even at low temperatures. When the excitation and fluorescence wavelengths are widely separated, it is possible to simultaneously excite several compounds in a common diffuse spectral region and still detect the strongly red-shifted fluorescence. Thus, the greatest selectivity will be achieved when both the excitation and



**Figure 9.** Unleaded gasoline chromatograms, temperature programmed 50 °C to 150 °C at 4 °C/min, (#) denotes naphthalene: (A) flame ionization detector; (B) jet cooled fluorescence detection, excitation at 308.12 nm, laser beam 60 nozzle diameters downstream; (C) same as (B) except excitation at 266 nm; (D) same as (B) except laser beam ca. 10 nozzle diameters downstream.

fluorescence wavelengths are set close to the 0–0 transition of the targeted compound. On the other hand, excitation of diffuse spectral regions may be useful for performing class determinations of compounds that can be well separated by chromatography.

The importance of cooling to spectral selectivity is illustrated in Figure 9D. This chromatogram was obtained with the laser beam intercepting the molecular beam approximately 10 nozzle diameters downstream from the jet orifice. At this point in the expansion, the gas has cooled only slightly. The excitation and fluorescence wavelengths are identical to those used in Figure 9B. As in Figure 9C, many chromatographic peaks are observed, though at a much lower absolute intensity. In this case, the high temperature yields broad excitation transitions for several compounds that overlap with the laser wavelength.

## DISCUSSION

Although the current nozzle design provides an order of magnitude of improvement in detection, further improvements may be possible. The 30° cone angle of the tapered jet orifice was chosen arbitrarily. Other angles may result in better enrichment and/or cooling. In this work, the sheath gas backing pressure and orifice diameter were limited by the pumping speed of our instrument. Larger pressures and/or



orifices may be obtained by inserting a pulsed valve in the sheath gas line. A wider range of orifice diameters and backing pressures would allow more flexibility in achieving the proper gas flow for expansion cooling. In the current apparatus, fluorescence detection is limited by the amount of light collected. Fluorescence collection could be increased by a factor of 40 by using an elliptical reflectance mirror in the vacuum chamber (19). Therefore, we conclude that low-picogram detection limits should be achievable with this method for compounds that absorb strongly and possess reasonable fluorescence quantum yields.

Absorption (20), resonant two photon ionization (21), and phosphorescence (22) detection have also been reported in supersonic jets. Each of these methods can be interfaced to a gas chromatograph through the sheath flow nozzle. Other forms of chromatography may be coupled as well. In a separate publication (23), we describe the application of this technique to supercritical fluids. Finally, we note that the selectivity of supersonic jet spectroscopy dramatically reduces the demand placed upon a chromatographic separation. In this regard, short open tubular columns (24) can be used to provide crude separations for rapid and sensitive analysis of samples.

#### ACKNOWLEDGMENT

The authors acknowledge many helpful discussions with N. S. Nogar and R. A. Keller and the assistance of B. A. Anderson in modeling the rotational contours of aniline.

#### LITERATURE CITED

- (1) Levy, D. H. *Science* **1981**, *214*, 263.
- (2) Warren, J. A.; Hayes, J. M.; Small, G. J. *Anal. Chem.* **1982**, *54*, 138.

- (3) Amirav, A.; Even, U.; Jortner, J. *Anal. Chem.* **1982**, *54*, 1666.
- (4) Lubman, D. M.; Kronick, M. N. *Anal. Chem.* **1982**, *54*, 660.
- (5) Tembreull, R.; Lubman, D. M. *Anal. Chem.* **1984**, *56*, 1962.
- (6) Tembreull, R.; Sin, C. H.; Li, P.; Pang, H. M.; Lubman, D. M. *Anal. Chem.* **1985**, *57*, 1186.
- (7) Tembreull, R.; Sin, C. H.; Pang, H. M.; Lubman, D. M. *Anal. Chem.* **1985**, *57*, 2911.
- (8) Imasaka, T.; Fukuoka, H.; Hayashi, T.; Ishibashi, N. *Anal. Chim. Acta* **1984**, *156*, 111.
- (9) Imasaka, T.; Hirata, K.; Ishibashi, N. *Anal. Chem.* **1985**, *57*, 59.
- (10) Hayes, J. M.; Small, G. J. *Anal. Chem.* **1982**, *54*, 1204.
- (11) Keller, R. A.; Nogar, N. S. *Appl. Opt.* **1984**, *23*, 2146.
- (12) Melamed, M. R.; Mullaney, P. F.; Mendelsohn, M. L. *Flow Cytometry and Cell Sorting*; Wiley: New York, 1979.
- (13) Guyer, D. R. Ph.D. Thesis, University of Colorado, Boulder, 1983; p 48.
- (14) Levy, D. H.; Wharton, L.; Smalley, R. E. In *Chemical and Biochemical Applications of Lasers*; Academic Press: New York, 1977; Vol. 2, Chapter 1.
- (15) Amirav, A.; Even, U.; Jortner, J. *Chem. Phys.* **1980**, *51*, 31.
- (16) McClelland, Saenger, K. L.; Valentini, J. J.; Herschbach, D. R. *J. Phys. Chem.* **1979**, *83*, 947.
- (17) Amirav, A.; Even, U.; Jortner, J.; Birss, F. W.; Ramsay, D. A. *Can. J. Phys.* **1983**, *61*, 278.
- (18) Oikawa, A.; Abe, H.; Mikami, N.; Ito, M. *J. Phys. Chem.* **1983**, *87*, 5083.
- (19) Spangler, L. H.; Pratt, D. W. *J. Chem. Phys.* **1986**, *84*, 4789.
- (20) Amirav, A.; Even, U.; Jortner, J. *Chem. Phys. Lett.* **1981**, *83*, 1.
- (21) Dietz, T. G.; Duncan, M. A.; Liverman, M. G.; Smalley, R. E. *J. Chem. Phys.* **1980**, *73*, 4816.
- (22) Abe, H.; Kamei, S.; Mikami, N.; Ito, M. *Chem. Phys. Lett.*, **1984**, *109*, 217.
- (23) Anderson, B. D.; Stiller, S. W.; Johnston, M. V., submitted for publication.
- (24) Tréhy, M. L.; Yost, R. A.; Dorsey, J. G. *Anal. Chem.* **1986**, *58*, 14.

RECEIVED for review February 28, 1986. Accepted November 3, 1986. This research was supported by the National Science Foundation under Grant No. CHE8308049. S.W.S. acknowledges support through a Graduate Student Foundation Award from the University of Colorado.

## Fluorescence Spectra and Lifetimes of Several Fluorophores Immobilized on Nonionic Resins for Use in Fiber-Optic Sensors

Wayde A. Wyatt, Greg E. Poirier, Frank V. Bright, and Gary M. Hieftje\*

Department of Chemistry, Indiana University, Bloomington, Indiana 47405

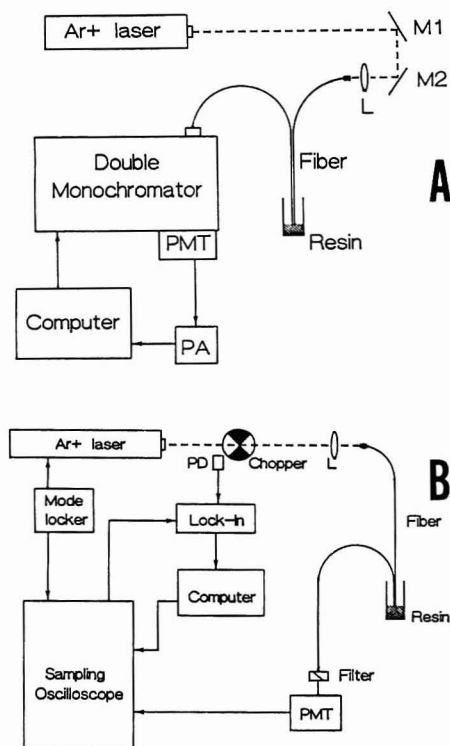
**Fluorescence emission spectra and lifetimes are reported for 0.01–1.0 mM samples of rhodamine B, rhodamine 6G, eosin Y, and fluorescein each adsorbed on XAD-2 and XAD-4 resins. Trends are discussed and comparisons made between bound fluorophore and fluorophore in solution. The systems appear to be useful in fiber-optic-based sensors.**

The development of fiber-optic sensors is one of the fastest growing new areas in analytical chemistry and is driven largely by the ability to use traditional spectroscopic techniques to make real-time, on-line measurements of a selected chemical species. Most of these sensors do not involve direct analyte determination, but instead measure the optical properties of a reagent attached to the fiber's distal end. This reagent is chosen so that one or many of its optical properties are changed upon interaction with the target substance. To date, fiber-optic sensors utilizing immobilized reagents have been developed based on reflectance (1–3), fluorescence complexation (4–7), and dynamic fluorescence quenching (8–10). As work continues in this area, fundamental knowledge of each

optrode component (optical design of probe, immobilization method, membrane choice, etc.) is becoming more important.

In sensors based on fluorescence or dynamic fluorescence quenching, both fluorescence lifetimes and excitation/emission spectra can be affected by immobilization in a way that depends upon the immobilization method (adsorption or covalent bonding), the type of solid support, and the amount of reagent present in or on the support medium. When a dynamic fluorescence quenching scheme is being used as a probe, it is desirable to choose the reagent concentration and solid support in a way that will minimize any decrease in the fluorescence lifetime. If the fluorescence lifetime is shortened greatly by immobilization, the probability of excited-state quenching by an analyte molecule is greatly reduced (11). Consequently, sensitivity is similarly reduced. Of course, the lifetime of a fluorophore can also increase upon immobilization. In such cases, the amount of analyte needed to achieve a particular quenching level will decrease and will result in improved dynamic range, sensitivity, and detection powers.

In the present study, two solid supports have been characterized (XAD-2 and XAD-4 nonionic polymeric resins); both have earlier been utilized in fiber-optic sensors reported in



**Figure 1.** (A) Schematic diagram of instrument for collecting fluorescence emission spectra utilizing optical fibers: M1, M2, mirrors; L, lens (7.0 cm focal length); PMT, photomultiplier tube; PA, picoammeter. (B) Schematic diagram of instrument for fluorescence-lifetime measurements utilizing optical fibers: L, lens (7.0 cm focal length); PMT, photomultiplier tube; PD, photodiode.

the literature (2, 3, 9). However, spectral or temporal changes in the immobilized reagent's fluorescence emission were not discussed. Here, fluorescence lifetimes and emission spectra were obtained for 0.01–1.0 mM concentrations of rhodamine B, rhodamine 6G, eosin Y, and fluorescein adsorbed on these resins. In general both parameters (lifetime and spectrum) were strongly dependent on the nature of the solid support and on the fluorophore concentration. At higher fluorophore concentrations, emission spectra became progressively more red-shifted. Lifetimes of some fluorophores were shortened by immobilization and to a degree that depended on concentration; other fluorophores exhibited longer lifetimes when immobilized. Possible reasons for this discrepancy in behavior are offered.

## EXPERIMENTAL SECTION

### Immobilization of Fluorophores on Nonpolar Resins.

Individual solutions of rhodamine B (Exciton Co.), rhodamine 6G (Exciton Co.), eosin Y (Aldrich Chemical Co.), and the disodium salt of fluorescein (Sigma Chemical Co.) are prepared at concentrations of 1.0, 0.1, 0.01, and 0.001 mM in reagent-grade ethanol. XAD-2 and XAD-4 polystyrene resin beads (Rohm and Haas Co.) are immersed for 24 h in each fluorophore solution at the ratio of 0.1 g of resin beads to 1.0 mL of fluorophore solution. The supernatant fluorophore solutions are then removed by vacuum filtration and the beads washed with distilled-deionized water and stored in disposable cuvettes (Fisher Scientific Co.) under distilled-deionized water.

**Determination of Emission Spectra Using Remote Fiber Spectrometry.** A schematic diagram of the instrument used for the measurement of emission spectra is shown in Figure 1A. The 488.0-nm line of an argon-ion laser (Spectra Physics, Inc., Model 171) operating at a plasma current of 30 A is focused onto one end of a 2-m optical fiber (Valtec 240- $\mu$ m core diameter). Radiant power measured at the fiber's distal end is 47 mW. The subsequent fluorescence is collected by a bundle of five 2-m fibers arranged concentrically about the input fiber and delivered to a double monochromator (Spex, Inc., Model 1680 Spectramate). The spectral band-pass used for obtaining all spectra is 9 nm. The

fluorescence is detected by a photomultiplier (RCA R928) operated at a biasing voltage of  $-900$  V dc. The output from the photomultiplier tube (PMT) is connected to a picoammeter (Keithley Instruments Model 414S) employed as a current-readout device. A computer (Digital Equipment Corp. MINC 11-23) drives the monochromator from 500 to 700 nm in 1-nm increments and collects the output from the picoammeter. The entire system is controlled by an interactive BASIC routine.

**Determination of Lifetimes Using a Sampling Oscilloscope.** A schematic diagram of the instrument used for the determination of fluorescence lifetimes is shown in Figure 1B. The 488.0-nm line of a mode-locked argon-ion laser (Spectra Physics, Inc., Model 171 laser, Model 342 mode locker, and Model 452 mode-locker drive) is mechanically chopped and focused into one end of the optical fiber described in the previous section. The mode-locker frequency is between 40.9900 and 40.9940 MHz, the laser plasma current is 35 A, and the radiant power measured at the distal end of the fiber is 9 mW. The optical fiber delivers excitation radiation to the sample holder and a bundle of five fibers collects the resulting fluorescence and sends it to a fast photomultiplier tube (RCA 31024) operated at a biasing voltage of  $-3500$  V dc. A long-pass filter which rejects light at wavelengths below 520 nm is located in a sliding mount and interposed between the return fiber bundle and the PMT. The filter is placed into or out of the path of the radiation depending on whether a fluorescence decay curve or instrument response curve is being collected, respectively. The output from the PMT is directed via a 50- $\Omega$  coaxial cable to a sampling oscilloscope (Tektronix, Inc.: Model 7844 mainframe, Model S4 sampling head, and Model 7S11 sampling unit) which is triggered by the synchronous output of the mode-locker driver. The output from the oscilloscope is connected to a lock-in amplifier (EG&G Princeton Applied Research, Model 5101, time constant set to 0.1 s), which is referenced to the mechanical chopper frequency. The lock-in amplifier reduces additive noise introduced after the chopper (12). The output from the lock-in amplifier is sampled by a computer (DEC, MINC 11-23) which collects 128 points across a 12-ns time window. A total of 128 points were chosen for convenience in the event that a fast-Fourier digital filter would need to be employed.

### Operation of the Time-Resolved Fluorescence Instrument.

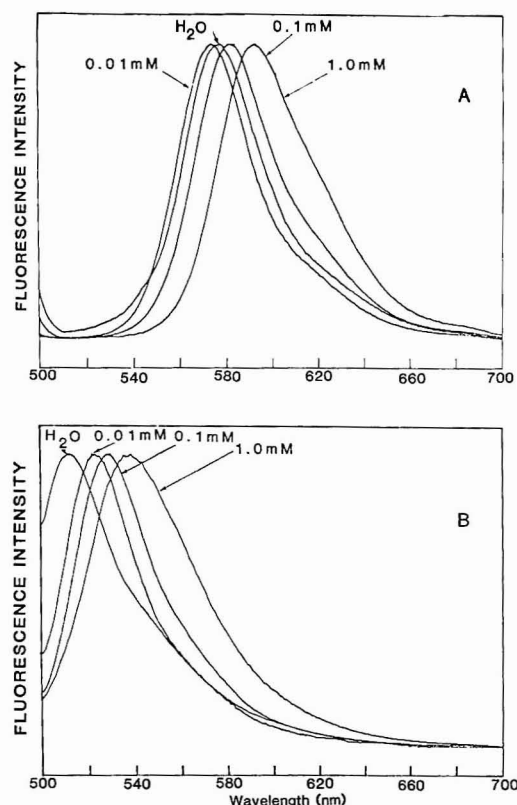
Depending on the required signal-to-noise ratio, between 200 and 500 data points are collected and averaged at each time increment of a fluorescence decay curve. An instrument response curve is measured before and after each fluorescence decay curve by collecting and averaging 200 data points of scattered radiation with the long-pass filter displaced from the light path. The lifetimes are extracted from fluorescence decay curves using a convolute-and-compare algorithm (13–15) on a VAX 11-780 computer.

## RESULTS AND DISCUSSION

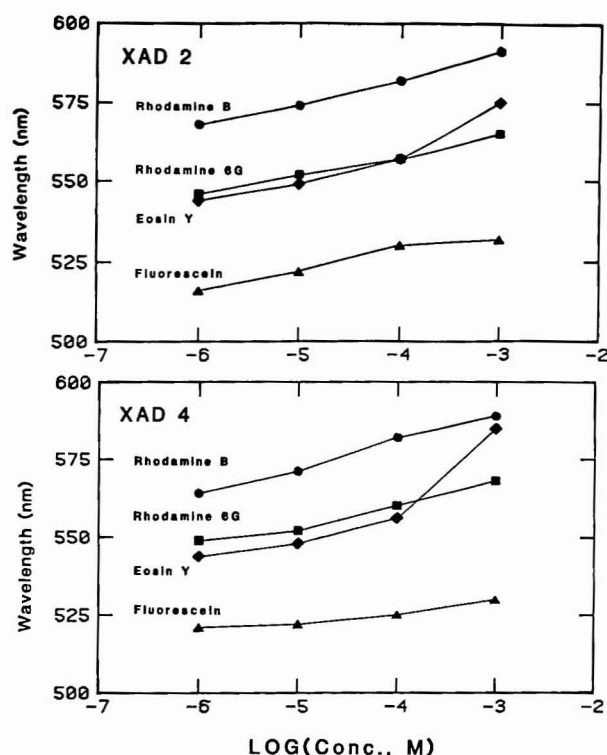
**Spectral Effects.** It was found that the fluorescence spectra of the immobilized fluorophores became progressively red-shifted with increasing fluorophore concentration. Typical fluorescence spectra for two of the immobilized fluorophores are shown in Figure 2. Figure 3 shows the shift in peak emission wavelength for each immobilized fluorophore as a function of its initial concentration in immobilizing solution. The shift toward longer wavelength upon immobilization indicates an average decrease in energy of the radiative decay from the excited electronic state ( $S_1$ ) to the ground electronic state ( $S_0$ ). Electronic spectral shifts related to chemical environment have been reported in the literature (16–18). In our case the spectral shifts can be broken down into three categories: solvent effects, adsorption effects, and spectral reabsorption.

Dissolving a fluorophore in increasingly polar solvents increases the degree of fluorescence red shift (19). Waggoner and Stryer (18) found that fluorophores entrapped in a non-polar lipid bilayer exhibited a blue shift in fluorescence peak relative to those in a methanol solution. They found also that the degree of blue shift was directly proportional to the depth the fluorophore was buried in the bilayer. Thus, a fluorophore close to the more polar surface of the bilayer was red-shifted





**Figure 2.** Typical fluorescence emission spectra of bound fluorophore. The concentrations listed on the figure refer to those of the solution which was used to immobilize the fluorophore on the XAD-2 resin. The H<sub>2</sub>O designation represents 0.01 mM fluorophore in aqueous solution: (A) XAD-2 immobilized rhodamine B; (B) XAD-2 immobilized fluorescein.



**Figure 3.** Fluorescence emission peak maxima for the fluorophores bound to (A) XAD-2 and (B) XAD-4 resins. (See Table II for peak maxima of the fluorophores in solution.)

from one nearer to the nonpolar center. In our case, if the fluorophores immobilized at low concentration preferentially occupy nonpolar sites deeper in the polystyrene resin's porous structure while those at higher concentrations must occupy sites closer to the polar aqueous environment, then the

**Table I.** Maximum Intensity and fwhm of Immobilized Fluorophore Fluorescence Spectra

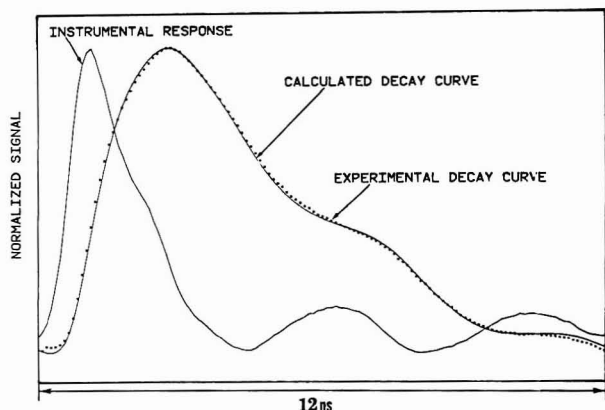
	intensity and fwhm at the following concns <sup>a</sup>			
	1.0 mM	0.1 mM	0.01 mM	0.001 mM
Maximum Intensity (Relative)				
rhodamine B				
XAD2	16.24	7.14	1.90	0.54
XAD4	8.46	10.65	1.84	0.39
rhodamine 6G				
XAD2	20.29	8.28	2.15	0.74
XAD4	5.30	2.43	2.55	0.52
fluorescein				
XAD2	8.99	5.92	2.89	0.69
XAD4	8.05	5.16	1.15	0.33
eosin Y				
XAD2	1.39	1.79	0.72	1.35
XAD4	0.70	1.32	1.04	0.39
Spectral fwhm <sup>b</sup> (nm)				
rhodamine B				
XAD2	49	40	36	40
XAD4	54	38	36	42
rhodamine 6G				
XAD2	52	47	39	41
XAD4	57	41	39	45
fluorescein				
XAD2	41	35	23	22
XAD4	40	33	24	27
eosin Y				
XAD2	77	66	35	35
XAD4	79	73	33	37

<sup>a</sup> Concentration of initial solution used in immobilization. <sup>b</sup> Full width at half maximum of emission spectrum.

fluorophores immobilized at higher concentrations would be red-shifted from those at lower concentrations. Peak broadening should also occur at the higher concentration as the total fluorescence emission is integrated over the range of environments. This behavior was observed (Table I).

Spectral shifts can arise also from changes in the equilibrium distance ( $\sigma_{RF}$ ) between the resin and the fluorophore in the excited state (17), from reabsorption of the short-wave portion of a fluorescence band, and from the aggregation of dye molecules. Franck-Condon considerations require that changes in  $\sigma_{RF}$  result in shifts in the absorption and emission lines. Similarly, short-wave absorption cannot be ruled out as a cause of the observed spectral shift, since no convenient method is available for measuring the absorption spectrum of the immobilized dye. The existence of simple first-order excited-state decay (see below) argues against this cause and against the aggregation of dye molecules, however.

**Temporal Effects.** The fluorescence decay curve for rhodamine 6G (immobilized on XAD-4 resin from 1.0 mM solution), the instrument-response function, and the same instrument response function convoluted with the calculated 4.98-ns lifetime (calculated decay curve) are shown in Figure 4. The ringing observed on the instrument response function was due to an impedance mismatch between the photomultiplier tube and the oscilloscope sampling head. The excellent fit between experimental and convoluted decay curves was found for the other immobilized fluorophores as well. The quality of this single-exponential fit is somewhat surprising in view of the apparent range of microenvironments in which the fluorophores are immobilized. However, a range of hydrophobicity does not always produce a commensurate shift in fluorescence lifetime (20); presumably, if such a shift occurs, it lies below the time resolution of our measurements. The fluorescence lifetimes obtained for each fluorophore in ethanol and water are shown in Table II and are in good agreement



**Figure 4.** Comparison of typical experimental (dotted line) with calculated (solid line) decay curves (4.98-ns lifetime) for rhodamine 6G immobilized on XAD-4 resin. Ringing is due to an impedance mismatch between the photomultiplier tube and oscilloscope sampling head.

**Table II. Lifetimes (ns) of Fluorophores in Solution**

fluorophore	exptl value		lit. value	
	deionized water	ethanol	deionized water	ethanol
rhodamine B	1.59 ± 0.05 <sup>a</sup>	3.00 ± 0.03	2.0 <sup>b</sup>	3.2 <sup>c</sup>
rhodamine 6G	4.23 ± 0.05	4.44 ± 0.04	4.1 <sup>d</sup>	3.7 <sup>e</sup>
fluorescein	3.64 ± 0.02	4.03 ± 0.03	4.0 <sup>f</sup>	5.0 <sup>b</sup>
eosin Y	1.18 ± 0.05	3.01 ± 0.07	1.9 <sup>b</sup>	2.78 <sup>g</sup>

<sup>a</sup>Standard deviation of three replicant samples. <sup>b</sup>From ref 24.

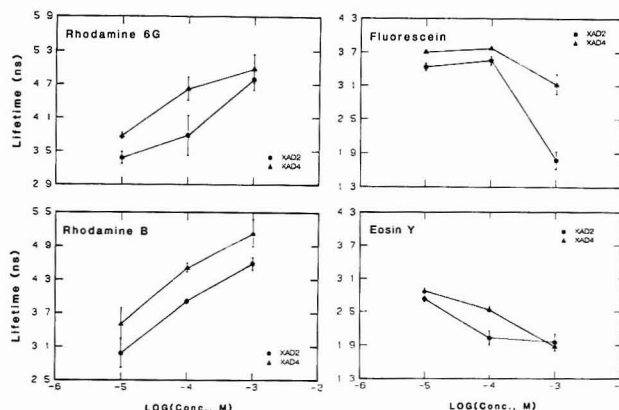
<sup>c</sup>From ref 21. <sup>d</sup>From ref 26. <sup>e</sup>From ref 22. <sup>f</sup>From ref 23. <sup>g</sup>From ref 25.

with literature values (21–26). Plots of fluorescence lifetime as a function of initial concentration of immobilizing solution are shown in Figure 5. It is clear that, for the same initial solution concentration, fluorophores immobilized on XAD-4 resin have longer lifetimes than those immobilized on XAD-2. Interestingly, lifetimes of rhodamine B and rhodamine 6G became longer with increasing fluorophore concentration whereas lifetimes of fluorescein and eosin Y became shorter.

Time-resolved emission spectroscopy studies by Badea et al. (27) of 2-anilinonaphthalene (2-AN) in a dimyristoyllecithin single-bilayer liposome showed that the deconvolved decay curves at the red end of the emission spectrum had a longer initial rise. This behavior indicates that some of these lower-energy emissions were from species generated during the lifetime of the excited state. That is, 2-AN self-absorption was occurring. Self-absorption will increase the radiative lifetime because emitted radiation can be reabsorbed and reemitted many times before finally reaching the detector (28). Self-absorption is a concentration-dependent process. In our case, because the adsorbed fluorophores undergo self-absorption, the radiative lifetime increases with concentration. Because XAD-4 has a smaller pore diameter and larger surface area than XAD-2, it should be more prone to self-absorption of radiation from the immobilized fluorophore and should exhibit longer lifetimes as was observed. The decrease in lifetime with increasing concentration of fluorophore, which was observed for eosin Y and fluorescein, could be attributable to concentration quenching of luminescence (CQL) (29, 30). This CQL occurs at high concentration when the dye molecules form nonluminescent aggregates which absorb energy from the luminescent monomers. In CQL the luminescence intensity will decrease with the excited-state lifetime. This behavior was observed for eosin Y but not for fluorescein.

## CONCLUSIONS

Each fluorophore was observed qualitatively to bleed from the resins. Since adsorption is an exothermic process, heating



**Figure 5.** Fluorescence lifetimes of XAD-2 and XAD-4-immobilized fluorophores vs. concentration of initial solution used for immobilization.

of the sample by laser irradiation would further cause the fluorophores to be desorbed. There was a direct correlation between the hydrophilicity of the fluorophore and the degree to which it bled from the resin.

The fundamental differences between the two resins studied are their surface areas and pore diameters. The surface areas of XAD-2 and XAD-4 are 300 and 725 m<sup>2</sup>/g, respectively, with corresponding average pore diameters of 900 and 400 nm. Among the fluorophores studied, a greater fluorescence intensity is observed from those immobilized on XAD-2 than on XAD-4 resin (see Table I). This finding would indicate that pore size is more important than surface area in determining the magnitude of fluorescence emission from resin-bound fluorophores.

From this work it is clear that the optical properties of the fluorophores that were examined are significantly altered upon adsorption to the resins studied. It appears that these systems might be useful for remote-fiber-optic chemical sensors which utilize an immobilized reagent. However, the pore size of the solid support and the concentration of the reagent should be coordinated in order to optimize sensitivity.

## LITERATURE CITED

- Peterson, J. I.; Goldstein, S. R.; Fitzgerald, R. V.; Buckhold, D. K. *Anal. Chem.* **1980**, *52*, 864–869.
- Kirkbright, G. F.; Narayanaswamy, R.; Welti, N. A. *Analyst (London)* **1984**, *105*, 15–17.
- Edmonds, T. E.; Ross, I. D. *Anal. Proc. (London)* **1985**, *22*, 206–207.
- Freeman, T. M.; Seitz, W. R. *Anal. Chem.* **1978**, *50*, 1242–1246.
- Saari, L. A.; Seitz, W. R. *Anal. Chem.* **1983**, *55*, 667–670.
- Saari, L. A.; Seitz, W. R. *Analyst (London)* **1984**, *109*, 655–657.
- Zhu, J.; Seitz, W. R. *Anal. Chim. Acta* **1985**, *171*, 251–258.
- Saari, L. A.; Seitz, W. R. *Anal. Chem.* **1982**, *54*, 823–824.
- Peterson, J. I.; Fitzgerald, R. V.; Buckhold, D. K. *Anal. Chem.* **1984**, *56*, 62–67.
- Urbano, E.; Offenbacher, H.; Wolfbeis, O. S. *Anal. Chem.* **1984**, *56*, 427–429.
- Hieftje, G. M.; Haugen, G. R. *Anal. Chim. Acta* **1981**, *123*, 255–256.
- Vickers, G. H.; Miller, R. M.; Hieftje, G. M., submitted for publication in *Anal. Chim. Acta*.
- Ware, W. R. *Transient Luminescence Measurements*; Marcel Dekker: New York, 1971; Vol. 1A, Chapter 5.
- Ramsey, J. M. Ph.D. Dissertation, Indiana University 1979.
- Demas, J. N. *Excited State Lifetime Measurements*; Academic: New York, 1983; pp 128–129.
- Longuet-Higgins, H. C.; Pople, J. A. *J. Chem. Phys.* **1957**, *27*, 192.
- McCarty, M.; Robinson, G. W. *Mol. Phys.* **1959**, *2*, 415.
- Waggoner, A. S.; Stryer, L. *Proc. Natl. Acad. Sci. U.S.A.* **1970**, *67*, 579–589.
- Lakowicz, J. R. *Principles of Fluorescence Spectroscopy*; Plenum: New York, 1983; pp 189–225.
- Bright, F. V.; McGown, L. B. *Talanta* **1985**, *32*, 15.
- Berlman, I. B. *Handbook of Fluorescence Spectra of Aromatic Molecules*; Academic: New York, 1965.
- Kubin, R. F.; Fletcher, A. N. *J. Lumin.* **1982**, *27*, 455.
- Bright, F. V. Ph.D. Dissertation, Oklahoma State University, 1985.
- Gaviola, E. Z. *Phys.* **1927**, *42*, 853.
- Gati, L.; Szalma, I. *Acta Phys. Chim.* **1968**, *14*, 3.
- Harris, J. M.; Lytle, F. E. *Rev. Sci. Instrum.* **1977**, *48*, 1469.
- Badea, M. G.; DeToma, R. P.; Brand, L. *Biophys. J.* **1978**, *24*, 197–212.
- Chandler, D. W.; Ewing, G. E. *Chem. Phys.* **1981**, *54*, 241–248.



- (29) Levshin, L. V.; Yuzhakov, V. I. *Opt. Spektrosk.*, **1974**, *34*, 503-508.  
(30) Zemshii, V. I.; Meshkovskii, I. K.; Sokolov, I. A. *Opt. Spectrosc. (Engl. Transl.)* **1985**, *59*(2), 197-199.

RECEIVED for review August 18, 1986. Accepted October 27,

1986. Supported in part by the Office of Naval Research, The Upjohn Co. and the National Science Foundation through Grant CHE 83-20053. We also thank the National Science Foundation for its support of the VAX 11-780 used in this work (Grants CHE 83-09446 and CHE 84-05851).

## Identification of Mixture Components in Organic Waste Materials by Carbon-13 Nuclear Magnetic Resonance

David A. Laude, Jr., and Charles L. Wilkins\*

Department of Chemistry, University of California, Riverside, Riverside, California 92521

**Carbon-13 nuclear magnetic resonance ( $^{13}\text{C}$  NMR) is used to determine mixture component identities and relative concentrations in organic waste materials without prior separation. A quantitative  $^{13}\text{C}$  NMR spectrum provides the data used in an algorithm to extract subspectrum resonances specific to each mixture component. The subspectra are then subjected to reverse searches of either a  $^{13}\text{C}$  NMR simulated spectrum library or a  $^{13}\text{C}$  NMR chemical shift library. The quantitative  $^{13}\text{C}$  NMR mixture analysis algorithm is applied to seven waste solvent mixtures procured from analytical and organic laboratories. The 34 subspectra comprised of NMR resonances above the 0.5% level in the mixtures yield 31 unambiguous identifications for the simulated library search and 27 unambiguous identifications from a search of the chemical shift library.**

Characterization of bulk components in organic mixtures is essential to the management of hazardous waste materials. Ideally, any method developed for mixture analysis should permit the rapid identification and quantitative measurement of all components in the mixture, with minimal sample preparation. Although gas chromatography/mass spectrometry (GC/MS) is presently the separation/characterization method of choice for unknown mixtures, the uncertainty associated with chromatographic separation of all sample components, the nonuniform detector response of the mass spectrometer, and the need for sample volatility all impose constraints on the general application of the technique.

In two recent publications (1, 2), we advocated the use of interpretation schemes for mixture analysis which incorporated  $^{13}\text{C}$  nuclear magnetic resonance (NMR) data. NMR is unique among the major molecular spectrometry techniques in that quantitative conditions can be achieved so that signal response is equivalent for all nuclei; coupled with a large spectral bandwidth relative to line width for  $^{13}\text{C}$  NMR, it becomes possible to extract the resonances specific to each compound in a mixture without prior separation. The peak intensity data from this quantitative data may be used to determine directly the relative concentrations of each compound. In addition, the well-defined relationship between a  $^{13}\text{C}$  NMR spectrum and chemical structure permits the implementation of elaborate computer-aided identification methods for unknowns. These properties of  $^{13}\text{C}$  NMR previously were exploited in procedures which utilized quantitative and multiplicity  $^{13}\text{C}$  NMR data to characterize petroleum distillate fractions (1) and to improve the reliability of GC/MS search results (2).

In the present work quantitative  $^{13}\text{C}$  NMR data facilitates the isolation of pure-component subspectra from the mixture spectrum in an algorithm denoted as Q $^{13}\text{C}$ NMR; subsequent identification procedures include two independent reverse search algorithms: (1) comparison of subspectrum chemical shift data with a library of  $^{13}\text{C}$  NMR chemical shift values (3); and (2) comparison with a library of simulated  $^{13}\text{C}$  NMR spectra created from quantitative, multiplicity, and functional group chemical shift ranges. Selection of any identification procedure is ultimately dependent upon the compounds to be analyzed and the availability of appropriate spectral libraries and computer software. Although the preponderance of mixtures would be conveniently analyzed with algorithms employing large chemical shift library data bases, the reliability of the library search applied to unknown mixtures is suspect because of potential solvent and pH effects on chemical shift data. It is therefore of interest to contrast the search results from a chemical shift  $^{13}\text{C}$  NMR library with a simulated library created specifically for the mixtures to be analyzed.


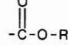


### EXPERIMENTAL SECTION

A Nicolet NMC 300 NMR spectrometer operating at 75.497 MHz for  $^{13}\text{C}$  nuclei was used for all measurements. Two commercial Nicolet probes, a 5-mm fixed-frequency  $^{13}\text{C}$  probe and a 12-mm wide-band ( $^1\text{H}$  to  $^{31}\text{P}$ ) probe, were used without modification. Processing of spectral data was performed on a Nicolet 1280 computer with Nicolet-developed software. Quantitative, multiplicity, and chemical shift data extracted from the spectra were used in Fortran programs written for the Q $^{13}\text{C}$ NMR analysis and executed on a Digital Equipment Corp. MicroVAX II.

Implementation of the mixture analysis algorithm requires the acquisition of quantitative  $^{13}\text{C}$  NMR data for the tabulation of relative peak areas. The quantitative NMR measurement is achieved when the recycle time between scans exceeds five times the longest spin-lattice relaxation time ( $T_{1\text{max}}$ ) in the sample and the nuclear Overhauser effect (NOE) is quenched (4). In order to satisfy these conditions in an efficient manner, chromium triacetylacetonate ( $\text{Cr}(\text{acac})_3$ ) was added to each mixture to achieve a 0.05 M concentration. A delay of between 5 and 15 s, depending upon the sample, was imposed between scans to ensure a leveling of  $T_1$  and NOE for each nucleus.

Reliable determination of relative peak areas from quantitative spectra is essential to the success of the algorithm. To ensure that measurement errors are minimized (less than 2%), adequate peak definition is required. These requirements were satisfied by choosing data acquisition parameters such that at least 8 to 10 points defined each peak with signal to noise (S/N) in excess of 20 to 1. Transients (32K and 64K) were acquired for spectra in which resonances encompassed a 200 ppm ( $\pm 7500$  Hz) region. The application of a line-broadening function (0.5-3.0 Hz) also increased the number of data points defining each peak for situations when maximum spectral resolution was not essential.

Table I. Simulated Library Subset of the Identified Spectra for Mixtures 1 and 6 in Table V

compd name	no. of carbons	no. of resonances	multiplicity <sup>a</sup>			
			CH <sub>3</sub>	CH <sub>2</sub>	CH	Q
<i>tert</i> -butyl alcohol	4	2	3 <sup>3</sup>			1 <sup>48</sup>
<i>sec</i> -butylamine	4	4	1 <sup>3</sup> , 1 <sup>3</sup>	1 <sup>4</sup>	1 <sup>28</sup>	
tartaric acid	4	2			2 <sup>47</sup>	2 <sup>62</sup>
1-chlorobutane	4	4	1 <sup>3</sup>	1 <sup>4</sup> , 1 <sup>4</sup> , 1 <sup>82</sup>		
methylcyclopropane	6	4	1 <sup>3</sup>	2 <sup>4</sup> , 2 <sup>4</sup>	1 <sup>5</sup>	
bromobenzene	6	4			2 <sup>12</sup> , 2 <sup>12</sup> , 1 <sup>12</sup>	1 <sup>92</sup>
acetophenone	8	6	1 <sup>41</sup>		2 <sup>12</sup> , 2 <sup>12</sup> , 1 <sup>12</sup>	1 <sup>13</sup> , 1 <sup>65</sup>
superscript no.	environment	chem shift range, ppm	superscript no.	environment	chem shift range, ppm	
3	CH <sub>3</sub> -	0-32	41	>CH-O-	20-30	
4	-CH <sub>2</sub> -	16-54	47	>C-O-	52-82	
5	-CH-	24-54	48	>C< <sup>0</sup>	68-86	
12		112-136	62		174-186	
13		130-150	82	>C=O	186-208	
			92	>CHCl	36-54	
28	>CHN<	48-66			104-126	

<sup>a</sup>Each number represents the equivalent nuclei of each carbon type within the molecule. Superscript refers to the particular molecular environment denoted above with appropriate chemical shift data.

However, for several of the more complex mixtures, for which smoothing could not be used, 64K data were insufficient to adequately define peaks for accurate quantitative measurements. Especially for resonances with low S/N, errors in peak areas were significant, limiting the reliability of the analysis for minor components below the 1% level.

A variety of identification procedures may be applied to the mixture subspectra. The simplest involves a comparison of library chemical shift values with the chemical shift data extracted from the quantitative <sup>13</sup>C NMR spectrum. Implementation of the more elaborate identification algorithm which employed simulated library spectra required multiplicity data to complement the quantitative and chemical shift information. Distortionless enhanced polarization transfer experiments (DEPT) (5) conveniently provide this information in two edited spectra from which the number of methyl (CH<sub>3</sub>), methylene (CH<sub>2</sub>), methine (CH), and nonprotonated (Q) carbons in a mixture are determined. Assuming an average coupling constant of 135 Hz (a 3.3-ms delay) and with an editing angle,  $\theta$ , equal to  $(3/4)\pi$ , a spectrum with CH<sub>3</sub> and CH upright, CH<sub>2</sub> inverted, and Q suppressed is obtained for most organic compounds. With  $\theta$  equal to  $\pi/2$ , only CH resonances are observed while CH<sub>3</sub>, CH<sub>2</sub>, and Q are suppressed. CH<sub>2</sub> and CH are determined directly from the edited spectra, CH<sub>3</sub> is inferred by its presence at  $\theta = 3\pi/4$  and absence at  $\theta = \pi/2$ , and Q is inferred by a presence in the quantitative spectrum and absence from the DEPT spectra. Because  $J_{C-H}$  coupling constants vary substantially above and below 135 Hz, some cross-talk contamination in the DEPT spectra will occur, especially at  $\theta = \pi/2$  when only CH should be observed. Despite this there was no difficulty in defining each multiplicity with certainty through a comparison of the relative intensity information in each DEPT spectrum.

Each of two 403-compound libraries were created to include all chemicals used as HPLC and organic solvents in selected analytical laboratories and as reagents in an organic laboratory course. One library contained only <sup>13</sup>C NMR chemical shift data extracted from a large <sup>13</sup>C NMR data base. The second, a simulated spectrum <sup>13</sup>C NMR library, contained quantitative, multiplicity, and functional group chemical shift range information; Table I presents sample spectra from this library. Each library was utilized in reverse search algorithms applied to identify identical mixture subspectra created from the quantitative <sup>13</sup>C NMR data.

Of seven samples subjected to Q<sup>13</sup>CNMR analysis, two were synthetic mixtures containing five and ten reagent-grade compounds. The remaining five mixtures were obtained from solvent waste containers located in departmental laboratories. Three

mixtures were waste from undergraduate organic laboratory experiments and two were from HPLC solvent waste in analytical and organic laboratories; no other information concerning the origin and identity of the mixtures was utilized.

Sample preparation prior to NMR measurement consisted of a filtration procedure to remove any observable particulate matter which might diminish spectral quality; otherwise the samples were analyzed directly without other cleanup procedures. A non-quantitative proton-decoupled <sup>13</sup>C NMR spectrum of each mixture yielded line widths of ~1 Hz which indicated no paramagnetic species were present that might degrade NMR performance.

## RESULTS AND DISCUSSION

**Q<sup>13</sup>CNMR Algorithm.** The Q<sup>13</sup>CNMR algorithm permits the evaluation of quantitative, multiplicity, and chemical shift information from <sup>13</sup>C NMR spectra in an integrated procedure which extracts and identifies each of the major components in a mixture. The premise for assigning the individual resonances to a specific compound without prior separation of the mixture is that within the quantitative NMR spectrum the integrated peak intensities of a particular compound will be simple integer multiples of each other. A compound's integrated peak areas are usually equivalent unless there are equivalent nuclei in the molecule that result from sites of topological symmetry. The possibility that different components in the mixture will yield equivalent peak areas within a particular tolerance is likely in more complex mixtures. However, in a procedure that is analogous to the application of reverse library search methods to unresolved chromatographic peaks during GC/MS analysis (6), Q<sup>13</sup>CNMR relies upon an algorithm for unknown identification which will consider any combination of library spectra that match subsets of NMR data extracted from the mixture spectrum.

Figure 1 contains a flow chart of the Q<sup>13</sup>CNMR algorithm which combines the creation of subspectra from quantitative data with the identification procedure based upon the search of a 403-compound library containing simulated <sup>13</sup>C NMR spectra. Following acquisition of the three-mixture spectra (one quantitative and two DEPT experiments), integrated peak area, multiplicity, and chemical shift data are tabulated, with the information for each resonance ranked by intensity. A first subset is created by setting a minimum window tolerance of 1% in peak area and extracting those resonances with simple integer (1 to 1, 1 to 2, or 1 to 3) ratios within that



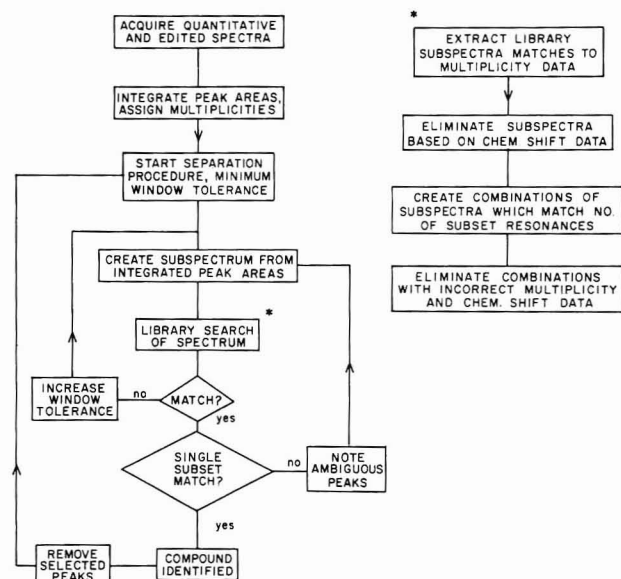


Figure 1. Flow chart of the Q<sup>13</sup>CNMR algorithm with simulated library reverse search procedure as applied to analysis of organic waste.

tolerance. This subset is then subjected to a reverse search identification procedure.

Should a unique match of subset and library spectrum occur, those resonances included in the identification are removed from the data table and a new subset is created with the 1% window. If there is no match, the window tolerance is increased by 1% up to a maximum of 5% so that a larger subset can be created by Q<sup>13</sup>CNMR before repeating the library search. If no match occurs within the 5% tolerance, it is assumed that the compound is not in the library and the initial resonance, around which the subset was created, is discarded and the next more intense resonance is selected to begin the analysis. Multiple matches with the library spectra which result because of the similarity between <sup>13</sup>C NMR library spectra cannot be corrected without increasing the chemical information available to the search. However, often multiple matches may be resolved because a particular resonance, initially placed incorrectly in the subset, is actually associated with resonances to be assigned later in the analysis. Therefore, if multiple matches occur for a subset, the individual resonances are still considered in the creation of new subsets, until the ambiguity is resolved.

**Simulated <sup>13</sup>C NMR Library.** The identification procedure which is applied to subsets generated from the quantitative spectrum may include any collection of <sup>13</sup>C NMR data in simple to very elaborate analysis schemes, depending upon the number and type of unknowns to be evaluated. For example, because a previous analysis of low-boiling petroleum distillate fractions encompassed only saturated and unsaturated C<sub>5</sub>–C<sub>7</sub> hydrocarbons, it was possible to create a library of 207 simulated hydrocarbon spectra which included only quantitative, multiplicity, and carbon hybridization information; over 80% of the compounds were unambiguously assigned (1). However, extension of the Q<sup>13</sup>CNMR procedure to the analysis of organic waste materials requires the incorporation of chemical shift data to distinguish between functional groups for compounds with identical carbon backbones. As an alternative to the utilization of a library of actual <sup>13</sup>C NMR spectra, a collection of 104 common chemical environments was assigned appropriate chemical shift ranges (Table I). This information, in addition to multiplicity and quantitative data obtained by inspection, was utilized to predict spectra.

The waste materials to be analyzed were collected from undergraduate organic laboratory experiments and HPLC

waste in organic and analytical laboratories. Hence, the collection of 403 compounds in the libraries included 109 chemicals described in the organic laboratory textbook (including solvents, reagents, and major products), 87 compounds used as common solvents and reagents in the research laboratories, and the 207-compound hydrocarbon library prepared for the petroleum fraction analysis. Table I lists, as examples, seven compounds present in the simulated library with their corresponding <sup>13</sup>C NMR information. The seven compounds are actually the matches from the analyses of a five-component synthetic mixture and a two-component unknown from an organic laboratory experiment. (A notation used to efficiently describe the simulated spectrum separates CH<sub>3</sub>, CH<sub>2</sub>, CH, and Q carbon types with slashes and includes the chemical shift environment index for each resonance as the superscript number. For example, *sec*-butylamine in Table I is described by 1<sup>3</sup>, 1<sup>3</sup>/1<sup>4</sup>/1<sup>28</sup>/0.)

As the flow chart logic in Figure 1 illustrates, the simulated library analysis requires first that all library spectra with multiplicity data that are a subset of the extracted NMR multiplicity data be noted, with those which do not conform to the accompanying chemical shift data for the mixture subset subsequently eliminated. Possible combinations of the remaining library subspectra are then selected as the identity of the subspectrum only if three match criteria are met: an equivalent number of total resonances, a combined multiplicity data match, and a combined chemical shift data match.

**Chemical Shift Library Search.** As an alternate procedure for analysis of each subspectrum, the 403-compound library of <sup>13</sup>C NMR chemical shift data was extracted from a larger library. A reverse binary search of the library was performed for each subspectrum generated by Q<sup>13</sup>CNMR with any coincidence between library and subspectrum resonance within a selected window tolerance (1 to 2 ppm) contributing to a match. Permutation of reverse search library spectra for which all resonances were a subset of the subspectrum was then performed to identify those combinations which yielded identical matches with the subspectrum.

**Q<sup>13</sup>CNMR Applications.** A detailed examination of Q<sup>13</sup>CNMR is presented for a five-component synthetic mixture to clarify the procedure. Figure 2 presents the three <sup>13</sup>C NMR spectra for the mixture. In Table II are tabulated <sup>13</sup>C NMR data (extracted from the three spectra in Figure 2), the subsets created for a particular window tolerance that provided a subset match with the library, and the identity and relative concentration of each component from the five-component mixture. For this relatively simple example in which a total of 20 resonances, including four CH<sub>3</sub>, six CH<sub>2</sub>, seven CH, and three Q were observed, five subsets of the data were defined and unambiguously matched to the correct <sup>13</sup>C NMR library spectra by both the simulated and chemical shift library reverse search procedures.

In Table III, a detailed flow chart of the simulated library identification procedure for the analysis of subset 3 in Table II is presented. A tolerance window of 2% permitted the extraction of a six resonance subset, with the multiplicity data (1/0/2,2,1/1,1), found to provide reverse search matches to 31 subspectra in the library. Of these, 24 were eliminated by use of chemical shift data, leaving the seven listed in the Table III. Assuming that the library includes all compounds that are in the unknown mixture, then some combination of the seven individual subspectra must exactly match all the <sup>13</sup>C NMR data for the subset. Three filters were sequentially employed to eliminate incorrect compounds. The first was a summation of the number of resonances in any combination to equal the six peaks for the unknown; three combinations met this requirement. The second criterion, a match of combined multiplicity data, eliminated all but one combina-

Table II.  $Q^{13}CNMR$  Analysis of Synthetic Five-Component Mixture Including Tabulated NMR Data and Results

peak no.	chem shift, ppm	multiplicity	rel area	subset no.	% window tolerance	intensity ratios			subset	identity	% rel concn
						1:1	1:2	1:3			
1	30.3	CH <sub>3</sub>	569	1	1	1			8	<i>tert</i> -butyl alcohol	25.2
2	129.2	CH	547	2	1	2, 3	4, 5		0/0/2,2,1/1		36.2
3	130.6	CH	546								
4	121.6	Q	274								
5	126.0	CH	273								
6	127.4	CH	201	3	2	6, 7	15, 16, 17, 18		1/0/2,2,1/1,1	acetophenone	13.1
7	127.6	CH	197								
8	67.6	CH <sub>2</sub>	191								
9	43.6	CH <sub>2</sub>	142	4	3	9, 10, 11, 12			1/1,1,1/0/0	1-chlorobutane	18.3
10	19.2	CH <sub>2</sub>	138								
11	12.4	CH <sub>3</sub>	137								
12	33.8	CH <sub>2</sub>	135								
13	24.4	CH <sub>2</sub>	110	5	4	13, 14	19, 20		1/2,2/1/0	methylcyclopentane	7.2
14	33.8	CH <sub>2</sub>	108								
15	196.4	Q	100								
16	136.2	Q	100								
17	132.0	CH	97								
18	25.4	CH <sub>3</sub>	97								
19	19.8	CH <sub>3</sub>	55								
20	33.7	CH	51								

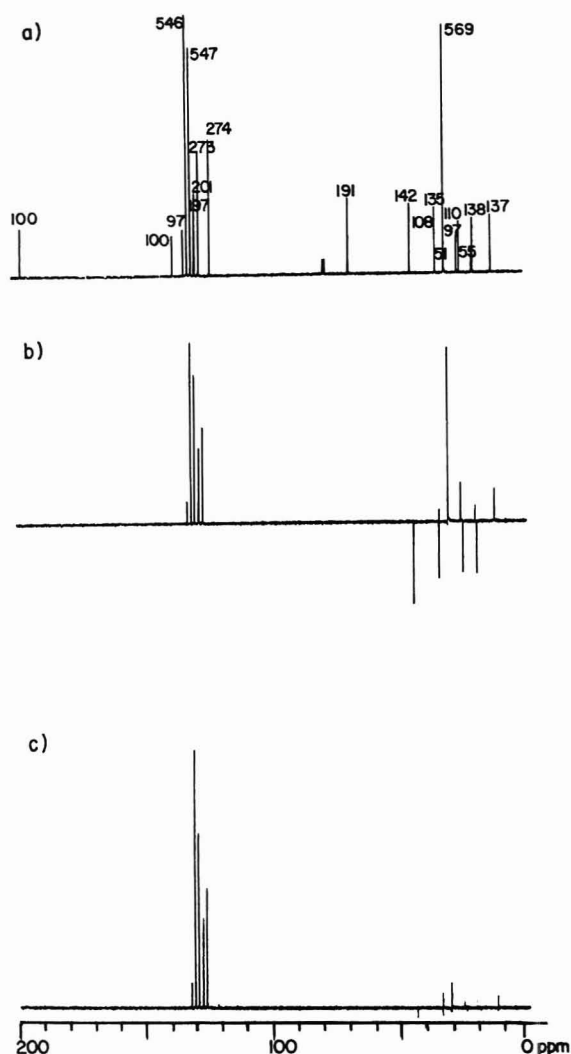


Figure 2. Three  $^{13}C$  NMR spectra for which tabulated  $Q^{13}CNMR$  data of a synthetic five-component mixture are found in Table II. (a) Quantitative spectrum with relative peak areas included. (b) DEPT spectrum with  $\theta = (3/4)\pi$  to suppress Q and invert  $CH_2$ ;  $CH_3$  and CH are upright. (c) DEPT spectrum with  $\theta = \pi/2$ ; CH is upright, all other resonances are suppressed.

tion, the single compound acetophenone, which is the correct result. A third criterion, the match of combined chemical shift data, confirmed the selection of acetophenone.

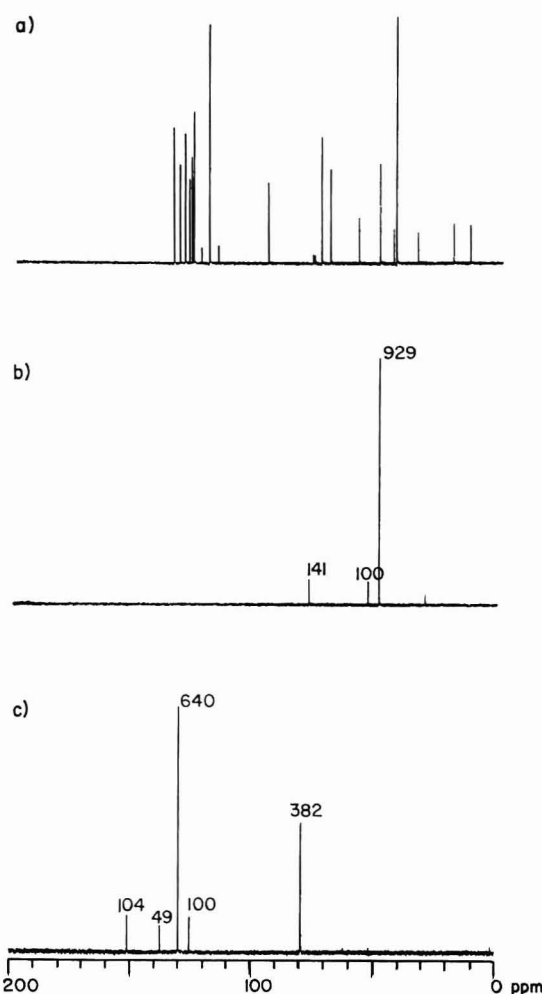


Figure 3. Quantitative  $^{13}C$  NMR spectra of mixtures 2-4 in Table V: (a) synthetic 10-component chlorinated solvent mixture with 20 resonances (mixture 2), (b) HPLC waste solvent (mixture 3), integrated areas included, (c) HPLC waste solvent (mixture 4), integrated areas included.

A second example of the  $Q^{13}CNMR$  analysis with simulated library analysis is presented in Table IV. Applied to a subset from an unknown organic laboratory waste solvent (mixture 7 in Table V), this example demonstrates the limitations of the particular identification procedure utilized. For the multiplicity subset 2,1/1/1/0, seven subspectrum matches (excluding single resonance matches) were found from which



**Table III. Flow Chart of Search Algorithm Applied to NMR Data of Subset 3 from Table II**

subset data:				
multiplicity	rel area	chem shift, ppm		
CH <sub>3</sub>	1	25		
CH	2	127		
CH	2	128		
CH	1	132		
Q	1	136		
Q	1	196		
match multiplicity data to 403-compound library				
subset = 1/0/2,2,1/1,1				
result	↓			
31 cmpds remain	31 reverse search subspectrum matches			
↓ match chemical shift data				
	compd no.	name	multiplicity	no. of resonances
7 compds remain	1	benzene	0/0/1/0	1
	2	benzenesulfonyl chloride	0/0/2,2,1/1	4
	3	toluene	1/0/2,2,1/1	5
	4	acetophenone	1/0/2,2,1/1,1	6
	5	2,4-hexadiene	1/0/1,1/0	3
	6	<i>p</i> -xylene	1/0/2/1	3
	7	biphenyl	0/0/2,2,1/1	4
↓ match no. of resonances to 6				
	comb no.	compd no.	combined multiplicity	
3 combinations remain	1	1, 3	1/0/2,2,1/1	
	2	5, 6	1,1/2/2,1,1/1	
	3	4	1/0/2,2,1/1,1	
↓ match combined multiplicity to 1/0/2,2,1/1,1				
	compd no.	name	multiplicity	no. of resonances
1 compd remains	4	acetophenone	1/0/2,2,1/1,1	6

ultimately two combinations, 2-propanone and ethanol and 2-propanone and ethyl ether, satisfied all match criteria. The identification of two compounds within the subspectrum resulted from the overlap of intensity information within a 2% tolerance window (a 1% tolerance window with a 2,1/0/0/0 subset produced no matches). However in a manner analogous to the identification of overlapping chromatographic peaks, the reverse search algorithm correctly identified two compounds despite the "unresolved" data.

Although 2-propanone is unambiguously identified by its inclusion in both matched combinations in Table IV, ethanol and ethyl ether cannot be distinguished based upon the quantitative, multiplicity, and chemical shift data used because the two compounds yield identical predicted spectra. Upon examination of the mixture results, ethanol would immediately be selected as the correct compound because ethyl ether is immiscible with 2-propanol and acetic acid. However, use of the actual <sup>13</sup>C NMR spectral library would permit the immediate identification of ethanol because of the greater discrimination afforded by precise chemical shift data.

The application of chemical shift data in identification procedures should be superior to the simulated library search because of the significant increase in information content

**Table IV. Flow Chart of Search Algorithm Applied to NMR Data for Subset in Mixture 7**

subset data:			
multiplicity	rel area	chem shift, ppm	
CH <sub>3</sub>	960	24	
CH <sub>3</sub>	480	17	
CH <sub>2</sub>	476	57	
CH	489	63	
match multiplicity data to 403-compound library			
subset = 2,1/1/1/0			
result	↓		
7 compds remain	ethanol (1/1/0/0), 2-propanone (2/0/1/0), ethyl ether (1/1/0/0), dimethoxyethane (1/1/0/0), chloroethane (1/1/0/0), 1,2-dichloropropane (1/1/1/0), 2-methylbutane (2,1/1/1/0)		
↓ match chemical shift data			
	compd no.	name	no. of reso- nances
4 compds remain	1	ethanol	2
	2	ethyl ether	2
	3	2-propanone	2
	4	1,2-dichloropropane	3
↓ match no. of resonances to 4			
	comb no.	compd nos.	combined multiplicity
3 combinations remain <sup>a</sup>	1	1, 2	1,1/1,1/0/0
	2	1, 3	2,1/1/1/0
	3	2, 3	2,1/1/1/0
↓ match combined multiplicity to 2,1/1/1/0			
	comb no.	name	
2 combinations remain <sup>a</sup>	2	2-propanone, ethanol	
	3	2-propanone, ethyl ether	
<sup>a</sup> No further distinction is possible with present identification procedure.			

<sup>a</sup>No further distinction is possible with present identification procedure.

afforded by precise measurement of chemical shift data. For example chemical shift data do resolve the ambiguity in simulated library search results presented in Table IV as ethanol is correctly identified. Unfortunately, chemical shift library spectra are often unreliable because of the strong dependence of shift values on solvent, pH, and analyte concentration. Although such affects may be controlled for pure compounds to conform to spectral and sample conditions for the library spectra, the analysis of unknown mixtures does not afford this opportunity and search results are often suspect. Especially for the case of a small controlled set of unknowns, as with the hydrocarbon analysis or the 403-compound library created for this work, the simulated library results actually compare favorably with a chemical shift library search. Of course reliability of the chemical shift library search algorithm would improve by using much larger tolerance windows for the small set of library compounds considered in these analyses.

Figures 3 and 4 contain the quantitative NMR spectra for six additional mixtures analyzed by Q<sup>13</sup>CNMR. For the less complicated spectra, integrated peak areas are included. The results of the analyses are summarized in Table V for both identification procedures. Table VI presents selected search results and relative concentrations for mixtures 1, 6, and 7. A total of 34 compounds were found in the seven mixtures above the 0.5% level, with all but three and seven unambig-

Table V. Comparison of Reverse Search Identification Procedures Used with Seven Mixtures Analyzed by  $Q^{13}CNMR$ 

mixture no.	source	no. $^{13}C$ resonances	$Q^{13}CNMR$ subsets	simulated search			chem shift search		
				iden- tified	ambig- uous	un- known	iden- tified	ambig- uous	un- known
1 <sup>a</sup>	synthetic	20	5	5			4	1	
2	synthetic (chlorinated hydrocarbons)	20	10	9	1		7	3	
3	waste solvent (LC)	4	3	3			3		
4	waste solvent (LC)	5	4	3			3		1
5	waste solvent (organic lab)	20	7	7			7		
6 <sup>a</sup>	waste solvent (organic lab)	6	2	2			1		1
7 <sup>a</sup>	waste solvent (organic lab)	10	3	2	1		2		1
totals			34	31	2	1	27	4	3

<sup>a</sup>Complete analysis in Table VI. <sup>b</sup>Minor component consisting of four peaks at 1% level was not identified in either 403-compound library.

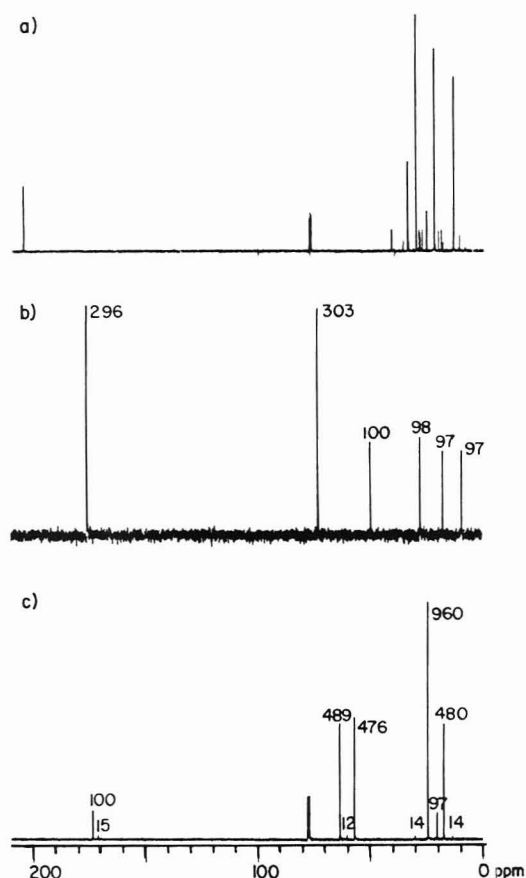


Figure 4. Quantitative  $^{13}C$  NMR spectra of mixtures 5–7 in Table V: (a) waste solvents from organic laboratory containing petroleum ether (mixture 5); (b) waste solvent from organic laboratory (mixture 6), integrated peak areas included; (c) waste solvent from organic laboratory (mixture 7), integrated peak areas included.

uously assigned by the simulated and chemical shift libraries, respectively. For the two synthetic mixtures containing five and ten components, 14 of 15 were correctly identified by the simulated search results, attesting to the validity of the procedure. Although the reliability of identifications for the other five mixtures cannot be determined without independent confirmation, some certainty in the analysis can be assumed from the percentage of consistent, unambiguous assignments made by both identification procedures.

$Q^{13}CNMR$  offers a novel complementary approach to the analysis of simple mixtures with the distinct advantage that

Table VI. Representative Mixture Analysis Results Comparing Simulated and Chemical Shift Reverse Search Algorithms

mixture	subset no.	% comp	identification	
			simulated	chem shift
1	1	36.2	bromobenzene	bromo- benzene
	2	25.2	tert-butyl alcohol	tert-butyl alcohol
	3	18.3	1-chlorobutane	1-chloro- butane
	4	13.1	acetophenone	aceto- phenone
	5	7.2	methylcyclopentane	methylcyclo- pentane
6	1	60.4	tartaric acid	tartaric acid
	2	39.6	sec-butylamine	— <sup>a</sup>
7	1	45	2-propanol	2-propanol
	2	45	ethyl alcohol or ethyl ether	ethyl alcohol
	3	9	acetic acid	— <sup>a</sup>

<sup>a</sup>Chemical shift data for all library spectra fell outside a 2 ppm tolerance window.

a nonchromatographic separation procedure is utilized. Although sensitivity limitations restrict the analysis to compounds at greater than 0.1% concentration in the mixture, direct quantitative measurement, reliable identification procedures, and minimal sample preparation recommend the method for the characterization of organic waste materials.

### LITERATURE CITED

- (1) Laude, D. A., Jr.; Wilkins, C. L. *Anal. Chem.* **1986**, *58*, 2820–2824.
- (2) Laude, D. A., Jr.; Cooper, J. R.; Wilkins, C. L. *Anal. Chem.* **1986**, *58*, 1213–1217.
- (3) Dalrymple, D. L.; Wilkins, C. L.; Milne, G. W. A.; Heller, S. R. *Org. Magn. Reson.* **1978**, *11*, 535–540.
- (4) Shoolery, J. N. *Prog. NMR Spectrosc.* **1977**, *11*, 79–93.
- (5) Bendall, M. R.; Pegg, D. T. *J. Magn. Reson.* **1983**, *53*, 272–296.
- (6) Martinsen, D. P.; Song, B. N. *Mass Spectrom. Rev.* **1985**, *4*, 461–490.

RECEIVED for review July 7, 1986. Accepted October 27, 1986. Support from the National Science Foundation under Grant CHE-85-19087 and a Department Research Instrument Grant CHE-82-03497 is gratefully acknowledged. Partial support of D.A.L. by the University of California, Riverside, Toxic Substances Research and Training Program is also acknowledged.



# Fluorometric Determination of Hydrogen Peroxide in Groundwater

Thomas R. Holm,\* Gregory K. George, and Michael J. Barcelona

State Water Survey Division, Illinois Department of Energy and Natural Resources,  
2204 Griffith Drive, Champaign, Illinois 61820

**The fluorometric scopoletin-horseradish peroxidase method has been modified for field determinations of hydrogen peroxide concentrations in groundwaters. Standard additions calibration compensates for background fluorescence and inconsistent stoichiometry of the fluorescence quenching reaction due to interferences by the matrix. The detection limit, defined as the blank plus three standard deviations, ranged from 3.6 to 44.6 nM. However, this limit was more an indication of the difficulty of preparing peroxide-free water than the actual limit imposed by the sensitivity of the method for the peroxide contamination introduced with the reagents. For 111 field determinations the weighted average (uncorrected) hydrogen peroxide concentration was 20.2 nM and the pooled standard deviation was 7.7 nM. The average of 45 field blanks was 7.8 nM with a pooled standard deviation of 5.2 nM. At nanomolar concentration levels, it is essential that samples are analyzed for  $H_2O_2$  in the field. Storage periods exceeding 1 h caused serious errors and irreproducible results.**

Oxidation and reduction processes play important roles in the solution chemistry and geochemistry of natural waters. Dominant redox couples, such as  $O_2/H_2O$  or  $Fe(II)/Fe(III)$ , influence the speciation of other chemical constituents by establishing a redox condition (1). The redox condition of a surface water/sediment or groundwater/aquifer system can control equilibria between dissolved and solid phases, influencing the solubility, mobility, and reactivity of metal ions or nutrient species as well as potential chemical pollutants (2, 3). Similarly, oxidizing conditions favor the oxidation or aerobic biotransformation of organic compounds, while reducing conditions may result in the preservation of organic matter (4). It is therefore important to identify redox-active species and controlling redox reactions because of their direct influence on the stability and transport of chemical substances which may impact the quality of our water resources.

The redox condition of groundwater systems is of great concern to environmental scientists involved in investigations of the fate of dissolved chemical contaminants as well as efforts to clean up contaminated aquifers. In the past, geochemists have considered groundwater to be in a reducing condition due to the depletion of dissolved oxygen in recharge waters during the oxidation of organic matter (5). A number of investigators have demonstrated that the predicted thermodynamic sequence of electron acceptors (i.e.,  $O_2$ ,  $NO_3^-$ ,  $Mn(IV)$ ,  $Fe(III)$ , and  $SO_4^{2-}$ ) may be evidenced by redox zonation within groundwater flow systems (6-8). However, the interpretive power of either redox potential measurements or calculated equilibrium potentials alone is only qualitative in many situations (9-12).

In order to effectively manipulate subsurface conditions to chemically oxidize chemical contaminants or stimulate microbial transformation of organic compounds, it is necessary to have more reliable indicators of redox condition than calculated or measured oxidation-reduction potentials. Be-

cause oxic (oxygen-containing) waters have been postulated to have an effective redox potential of the couple  $O_2/H_2O_2$  (13), it was felt that  $H_2O_2$  is an important intermediate in  $O_2$  reduction and may be found in oxic groundwaters. The reliable determination of  $H_2O_2$  in groundwater was the primary goal of this study.

The fluorometric horseradish peroxidase-scopoletin method was chosen for  $H_2O_2$  determinations because it is sufficiently sensitive to determine nanomolar concentrations and the procedure can be performed in the field (14). The basis of the method is fluorescence quenching of scopoletin in the reaction with  $H_2O_2$  catalyzed by horseradish peroxidase. The method has been shown to be applicable to  $H_2O_2$  determinations at micromolar to nanomolar concentrations in natural waters (15, 16).

## EXPERIMENTAL SECTION

**Site Description.** The groundwater samples which were collected for chemical analysis were taken from PTFE cells (5 cm o.d., Fluorocarbon Co., Anaheim, CA) finished at depths of 11, 15, 21, and 32 m between November 1984 and January 1986. The wells were constructed by hollow-stem auger techniques without the use of drilling aids or foreign additives. The study area is located in the Sand Ridge State Forest near Manito, IL. The geology and hydrology of the site have been described previously (17-19). Sampling was done with positive-displacement bladder pumps (Well Wizard, Q.E.D. Environmental Systems, Ann Arbor, MI) constructed of PTFE with PTFE gas and water transfer lines which were dedicated to each well.

**Water Sampling.** Sampling was conducted according to a published procedure (20) to assure that each well was purged of stagnant water prior to sample collection. Field measurements of pH, Eh (platinum electrode potential), temperature, and specific conductance were made at the surface with an in-line flow-cell device that was designed in our laboratories (21). Separate aliquots of each sample were taken for the determination of major cations, anions, trace metals, organic carbon, dissolved oxygen, and hydrogen peroxide. The  $H_2O_2$  samples were collected in a glass stoppered, aluminum foil covered, glass bottles. The sampling tubing from the wellhead was covered with commercial pipe insulation to minimize temperature changes and exposure to light.

**Apparatus.** A Turner Model 111 filter fluorometer, powered by a portable generator, was used for fluorescence measurements. Filters for the analysis were selected by choosing the combination which gave the highest sensitivity to scopoletin in distilled  $H_2O$ . The excitation filter was a Corning 7-60 (365-nm primary wavelength); the emission filter was a Wratten 65 (495-nm primary wavelength, transmittance falling to less than 1% below 430 and above 570 nm) coupled with a Wratten 2A (sharp cut off below 415 nm). The light source was a general purpose mercury ultraviolet lamp with its highest efficiency at 360 nm (range 310-390 nm).

Pyrex serum vials (7 cm  $\times$  0.75 cm i.d.) were used as cuvettes in the instrument. Vials were selected after measurement of the fluorescence of distilled water in the most sensitive range of the instrument. Vials which differed significantly from the mean reading were rejected.

**Reagents.** Water used for reagents and blanks was deionized and doubly distilled, with the final distillation within 24 h of use. Reagent water was stored in precombusted, dark glass bottles capped with Teflon-linked caps. All glassware used for fluores-

cence measurements was cleaned with laboratory detergent free of fluorescent dyes, soaked in 2 M HCl, and thoroughly rinsed with reagent water. A hydrogen peroxide standard was prepared fresh in the field, and renewed on evidence of deterioration, by dilution of a 30% w/w stock solution (Superoxol, Baker  $\text{Na}_2\text{SnO}_3 \cdot 3\text{H}_2\text{O}$  preservative). The concentration of the stock solution was determined periodically in the laboratory by titration with standard  $\text{KMnO}_4$  (22, 23). Scopoletin (7-hydroxy-6-methoxy-2H-1-benzopyran-2-one) stock solution ( $1 \times 10^{-5}$  M) was prepared fresh within 24 h of use by dissolving a weighed quantity of scopoletin crystals (Sigma) in double-distilled water. The stock solution was diluted 1:10 immediately before use in the field. The diluted reagent was stable in the dark for 24 h without refrigeration. A 0.05 M phosphate buffer (pH 6.86) was prepared from distilled water and commercial buffer salts (Beckman). Horseradish peroxidase (HRP) (Sigma P8125, type II, 150–200 purpogallin units/p mg of solid) reagent was prepared within 6 h of use. Twenty milligrams of solid HRP and 3 mg of  $\text{NaN}_3$  were dissolved in 5 mL of pH 6.86 buffer. Phenol (24, 25) is less effective than  $\text{NaN}_3$  at limiting the development of microbes, as evidenced by a strong odor and increasing fluorescence which developed in refrigerated, sealed, phenol-preserved enzyme preparations. When  $\text{NaN}_3$  was used, the enzyme was found to be useful for up to 8 h without refrigeration. Storage on ice prolonged its useful life. The crystalline enzyme develops increasing fluorescence after a period of months at  $-10^\circ\text{C}$ , and must be periodically replaced.

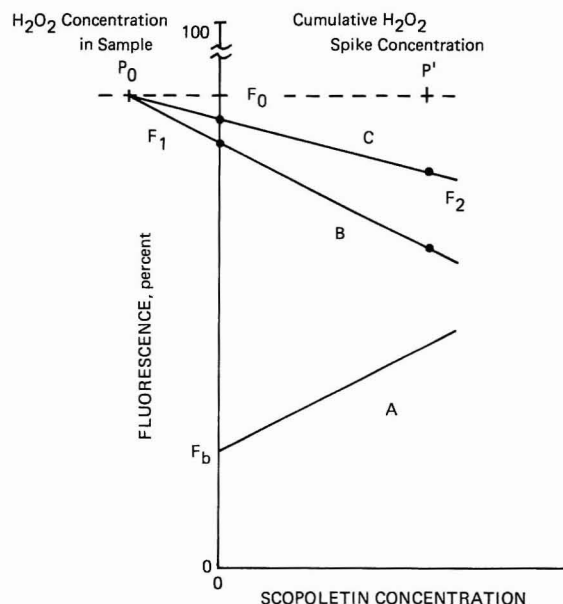
**Procedure.** All groundwater samples were analyzed within 10 min of collection. The fluorometer was zeroed by using an opaque rod in place of a cuvette. Five milliliters of groundwater was pipetted into a serum vial, and the background fluorescence was measured and recorded. Next, scopoletin reagent was added by using an adjustable micropipet, the sample was mixed for 5 s with a vortex mixer, and the fluorescence was measured and recorded. Next, 10  $\mu\text{L}$  of HRP reagent was added, the sample was mixed, and the fluorescence was measured and recorded. A decrease in fluorescence after HRP addition indicated the presence of  $\text{H}_2\text{O}_2$  in the sample. Three spikes of  $\text{H}_2\text{O}_2$  were added with mixing followed by measurement of the fluorescence after each addition. The  $\text{H}_2\text{O}_2$  concentration was calculated by the method of standard additions (26). Blanks were treated identically to samples except that 50  $\mu\text{L}$  of phosphate buffer was added before the scopoletin.

Preliminary  $\text{H}_2\text{O}_2$  determinations were necessary to optimize the amount of scopoletin added, the volume of the  $\text{H}_2\text{O}_2$  spikes, and the fluorometer sensitivity. The amount of scopoletin reagent was calculated to provide up to an 80% excess over the amount quenched by the natural  $\text{H}_2\text{O}_2$  with the constraint that fluorescence readings, i.e., background plus scopoletin, must remain on-scale. The optimum volume of the  $\text{H}_2\text{O}_2$  spikes was calculated to quench approximately half of the scopoletin fluorescence. One or two preliminary determinations on each sample were usually sufficient to optimize reagent volumes and instrument settings.

For a subset of groundwater samples, the stoichiometry of the fluorescence quenching reaction was determined. This was done by adding spikes of scopoletin to a fresh aliquot of groundwater and measuring the fluorescence. Scopoletin concentrations were adjusted to bracket the concentration range covered by the  $\text{H}_2\text{O}_2$  standard additions. The reaction stoichiometry, in moles of scopoletin per mole of  $\text{H}_2\text{O}_2$ , was calculated as the ratio of the slopes of the standard additions curve and the scopoletin calibration curve.

## RESULTS AND DISCUSSION

**Buffering.** Buffering of the pH of water samples for  $\text{H}_2\text{O}_2$  determinations is recommended (24, 25, 27). However, groundwaters commonly exhibit pH values close to the specified values and alkalinities in the range of 2–5 mequiv  $\text{L}^{-1}$  (28), which is much greater than the specified buffer concentrations. Added buffer would contribute very little to the pH buffering of the groundwater/reagent mixtures. The buffer was therefore only used for blank determinations. Buffering would be necessary for  $\text{H}_2\text{O}_2$  determinations in acidic or basic groundwaters having pH values far removed from the optimum for HRP or in the range in which scopoletin



**Figure 1.** Fluorescence quenching and standard additions: (A) scopoletin in groundwater ( $F_b$  is background fluorescence); (B) standard additions curve with ideal stoichiometry, i.e., 1 mol of  $\text{H}_2\text{O}_2$ /mol of scopoletin; (C) standard additions curve with nonideal stoichiometry. Concentration scales for scopoletin and  $\text{H}_2\text{O}_2$  are arbitrary but identical.

fluorescence is weak.

**Calibration Problems and Nonstoichiometry.** The stoichiometry of the fluorescence quenching reaction in distilled water has been shown to be 1 mol of scopoletin/mol of  $\text{H}_2\text{O}_2$  in distilled water (27). However, in the present study, the reaction stoichiometry in groundwater analyses, calculated as the ratio of the slope of the standard additions curve to the slope of the distilled water calibration curve, was observed to be as low as 0.1. For a groundwater sample in which 0.1 mol of scopoletin is oxidized for every mole of  $\text{H}_2\text{O}_2$ , comparison with a distilled water calibration curve (15, 16) would underestimate  $\text{H}_2\text{O}_2$  by a factor of 10. This potentially serious source of error has not been previously recognized in the literature.

There are many reactions that can compete with the fluorescence quenching reaction. Reducing substances such as ascorbic acid, glutathione, and manganous ion have been shown to interfere with the HRP catalyzed oxidation of scopoletin by  $\text{H}_2\text{O}_2$ . Nitrite and ethanol can be oxidized (14). Certain amino acids, phenols, thiols, diamines, and iodide also react (29). Maloney et al. (30) have shown that HRP can catalyze the oxidation of chlorinated phenols by  $\text{H}_2\text{O}_2$ . Perdue (31) has shown that phenolic functional groups account for a significant fraction of ionizable protons in aquatic humic substances. Thus, the reduced stoichiometry of the scopoletin- $\text{H}_2\text{O}_2$  reaction in groundwaters may have been caused by oxidative coupling of natural organic matter in the presence of HRP and  $\text{H}_2\text{O}_2$ .

The method of standard additions can be shown to correct for nonideal stoichiometry. The derivation of this follows the schematic diagram provided in Figure 1. The fluorescence of a solution containing scopoletin may be given by  $F = aS + F_b$ , where  $F$  is fluorescence,  $a$  is the slope of the calibration curve,  $S$  is scopoletin concentration, and  $F_b$  is background fluorescence. This scopoletin calibration curve is shown as line A in Figure 1. We define the stoichiometry of the fluorescence quenching reaction in a groundwater sample as  $f$  mol of scopoletin for every mole of  $\text{H}_2\text{O}_2$  ( $0 < f \leq 1$ ). The apparent concentration of  $\text{H}_2\text{O}_2$  by external calibration is then given by  $C = (F_0 - F_1)/a$ , where  $C$  is the calculated  $\text{H}_2\text{O}_2$  concentration and  $F_0$  and  $F_1$  are the fluorescence levels measured before and after addition of HRP, respectively. If



Table I. Field and Laboratory Performance of the Method

Blanks							
date	location <sup>a</sup>	n <sup>b</sup>	H <sub>2</sub> O <sub>2</sub> concn, nM	detection limit, nM <sup>c</sup>	precision (% RSD) <sup>d</sup>		
7/23/85	f	5	8.0	15.4	31		
11/18/85	f	2	4.0	13.9	105		
6/2/86	f	3	13.1	30.3	44		
5/16/86	l	7	2.3	4.6	33		
Spike Recoveries							
date	depth	N	initial H <sub>2</sub> O <sub>2</sub> concn, nM	H <sub>2</sub> O <sub>2</sub> added, nM	H <sub>2</sub> O <sub>2</sub> found, nM	recovery, <sup>g</sup> %	precision (% RSD)
7/23/85	11	2	0.0 <sup>f</sup>	20.0	21.5	108	12
11/18/85	21	1	2.0	40.0	39.5	94	
6/2/86	21	3	0.0 <sup>f</sup>	40.0	37.1	93	23
5/16/86	L <sup>e</sup>	6	2.3	20.0	13.0	53	47

<sup>a</sup>f, field; l, laboratory. <sup>b</sup>Number of replicates. <sup>c</sup>Mean blank + three standard deviations. Standard deviation for 11/18/85 estimated from range (37). <sup>d</sup>RSD is relative standard deviation. Standard deviation could not be calculated for the 11/18/85 21-m sample. <sup>e</sup>Distilled water spiked in the laboratory. <sup>f</sup>No quenching on HRP addition. <sup>g</sup>All initial concentrations were below detection limit, but recoveries were calculated by using these initial concentrations.

$P_0$  is the actual concentration of H<sub>2</sub>O<sub>2</sub> in the sample, then the calculated cumulative concentration is  $fP_0$ . If the stoichiometry is 1:1, then  $f = 1$  and the calibration method yields the correct result. Otherwise, the H<sub>2</sub>O<sub>2</sub> concentration may be seriously underestimated. The formula for calculating the H<sub>2</sub>O<sub>2</sub> concentration from a single standard addition is  $C = (F_0 - F_1)P'/(F_1 - F_2)$ , where  $P'$  is the concentration of the H<sub>2</sub>O<sub>2</sub> spike and  $F_2$  is the fluorescence after addition of the spike. In Figure 1, line B is the standard additions curve for ideal stoichiometry. Its slope is equal in magnitude and opposite in sign to the slope of the scopoletin calibration curve, line A. Line C is the standard additions curve for nonideal stoichiometry. For multiple standard additions ( $P', F_2$ ) is a point on the regression line. By straightforward algebra, this formula yields the correct H<sub>2</sub>O<sub>2</sub> concentration regardless of reaction stoichiometry.

**H<sub>2</sub>O<sub>2</sub> Background and Blank Determinations.** The detection limits (DL), calculated as the blank plus three standard deviations (32), were greater than calculated H<sub>2</sub>O<sub>2</sub> concentrations at all depths in three of the nine times when DL was estimated and at least at one depth in eight of the nine times, even though there was measurable quenching. We suspected that the distilled water used for blank determinations contained H<sub>2</sub>O<sub>2</sub> and tested this hypothesis by varying the concentrations of scopoletin and peroxidase and by adding the peroxidase before the scopoletin in groundwater samples. Varying the reagent concentrations had no effect on the blanks. The contribution of H<sub>2</sub>O<sub>2</sub> to the blank fluorescence was eliminated by addition of the enzyme prior to the scopoletin. Therefore, the measured quenching in the reagent blanks was probably due to H<sub>2</sub>O<sub>2</sub> present at the 5–25 nM range in the distilled water.

We further investigated the origin of the H<sub>2</sub>O<sub>2</sub> contamination in the distilled water. Storage did not produce increases in the levels of H<sub>2</sub>O<sub>2</sub> in the water over those in freshly distilled water. Also, sparging the distilled water with oxygen-free nitrogen for several hours did not reduce the levels of H<sub>2</sub>O<sub>2</sub>. Distillation and collection under nitrogen reduced the level of apparent H<sub>2</sub>O<sub>2</sub> in the distilled water by approximately 50%. The most likely sources of the H<sub>2</sub>O<sub>2</sub> contaminant are production in the distillation process or carry-over from the original amount in the deionized water.

Blanks for this method have not been addressed in detail in the literature. A number of authors have suggested that

H<sub>2</sub>O<sub>2</sub> can be produced in deionized distilled water by microbial activity (33), by photochemical reactions (34), by sparging with air (16), or even by free-radical reactions during storage under He (29). However, few of the previous workers reported any problems with background H<sub>2</sub>O<sub>2</sub> concentrations at the levels of interest in their experiments. Zika and Saltzman (25) distilled reagent water from a KMnO<sub>4</sub> solution. Perschke and Broda (27) suggested successive distillation of blank and reagent water from KMnO<sub>4</sub>, from AgNO<sub>3</sub>, and finally from a quartz still to achieve sufficient water purity. Perschke and Broda intended to establish the stoichiometry of the reaction. They did not report the background contribution of H<sub>2</sub>O<sub>2</sub> in the distilled water. Kok et al. (35) used catalase to prepare H<sub>2</sub>O<sub>2</sub>-free water. However, this may reduce the stoichiometry of the fluorescence quenching reaction through competition with the HRP. Also, the fluorescence of their blank was 8–12% of the fluorescence of a 1.2 μM H<sub>2</sub>O<sub>2</sub> solution. Thus, the blank reduction may not be adequate for H<sub>2</sub>O<sub>2</sub> determinations in the nanomolar concentration range. (While this manuscript was in review, a method was published (36) for reducing H<sub>2</sub>O<sub>2</sub> blanks in distilled water. The method involves pumping the distilled water through a MnO<sub>2</sub> column. Subsequent measurements in our laboratories confirm that the method effectively reduces blank levels of H<sub>2</sub>O<sub>2</sub> such that there is no detectable fluorescence quenching on addition of HRP. The method is recommended for field applications of the modified HRP-scopoletin method.)

It is likely that hydrogen peroxide is a normal trace component of distilled water, produced from the water itself and varying with inputs of radiation and dissolved oxygen. Because the fluorescence quenching method is so sensitive and because the H<sub>2</sub>O<sub>2</sub> concentrations in groundwaters are so low, distilled water blanks tested the ability to prepare H<sub>2</sub>O<sub>2</sub>-free water more than the validity of apparent H<sub>2</sub>O<sub>2</sub> signals in the analytical method.

**Laboratory Analytical Performance.** Table I contains averaged analytical performance measures for the modified HRP-scopoletin method determined on several occasions over a 12-month period. These data were collected on aliquots of H<sub>2</sub>O<sub>2</sub>-spiked groundwater or double-distilled water. The data show that the method is quite sensitive and precise over the concentration range of interest. In most cases recovery of the H<sub>2</sub>O<sub>2</sub> spike from groundwater exceeded 95%. The recoveries from spiked distilled water were erratic and averaged ap-

Table II. Field Determinations of Hydrogen Peroxide in Groundwaters<sup>d</sup>

date	blank			MDL <sup>e</sup>	11 m			15 m			20 m		
	av <sup>a</sup>	n <sup>b</sup>	SD <sup>c</sup>		av <sup>a</sup>	n <sup>b</sup>	SD <sup>c</sup>	av <sup>a</sup>	n <sup>b</sup>	SD <sup>c</sup>	av <sup>a</sup>	n <sup>b</sup>	SD <sup>c</sup>
12/13/84	8.16	6	0.64	10.1	60.6	6	13.2	27.4	2	12.8	66.3	2	2.69
1/17/85	20.4	7	8.07	44.6	61.2	3	6.2	—	—	—	39.6	2	2.38*
2/19/85	7.58	1	(6.07)	(25.8)	32.4	5	11.7	2.94	2	0.36*	7.59	2	1.58*
3/19/85	2.36	6	1.74	7.58	1.20	1	—*	7.89	1	—	8.97	5	0.37
4/23/85	6.37	6	2.20	13.0	11.2	3	0.78	9.59	3	2.22*	17.7	4	9.25
5/15/85	7.38	7	7.02	28.4	9.72	2	5.23*	22.5	2	10.3*	19.3	3	2.91*
7/23/85	8.0	5	2.4	15.4	-1.75	3	—*	11.0	2	13.1*	0.72	2	0.82*
9/19/85	1.07	3	0.85	3.61	14.3	3	17.7	-4.70	2	—*	-1.21	1	—*
10/17/85	0.65	1	(6.07)	(18.9)	20.8	6	10.4	—	—	—	25.2	2	4.54
11/18/85	4.0	2	3.32	13.9	7.63	3	6.41*	—	—	—	2.54	3	2.98*
12/9/85	16.7	2	1.42	20.9	2.21	3	2.02*	—	—	—	3.73	3	2.30*
1/28/86	(4.67)	—	(6.07)	(22.9)	18.1	5	2.48*	—	—	—	65.0	6	7.23
2/17/86	3.54	2	4.20	16.1	1.06	3	1.67*	—	—	—	8.20	4	4.95*
3/10/86	0.50	2	9.10	27.8	7.41	3	7.84*	—	—	—	15.0	5	10.6*
4/6/86	-1.43	1	(6.07)	(16.8)	2.19	4	1.77*	—	—	—	9.55	3	2.23*

<sup>a</sup> av, average (mean) concentration (nM). <sup>b</sup> n, number of replicates. <sup>c</sup> SD, standard deviation (nM). <sup>d</sup> —, quantity could not be calculated. (x), estimated quantity. \*, result was below detection limit established by lab blank. Blank space, analysis not performed. <sup>e</sup> MDL, method detection limit (MDL = blank + 3 SD) (nM).

proximately 50%. Also, one should recognize that the H<sub>2</sub>O<sub>2</sub> blank problem practically limits the precision and usefulness of an external calibration method. It should be noted that the potential errors involved in external calibration methods due to nonstoichiometric oxidative coupling reactions are far more serious at the nanomolar level than those which may arise from blanking problems. Thus, the minor methodological modifications and use of the standard additions methods permitted the routine quantitation of H<sub>2</sub>O<sub>2</sub> in the nanomolar concentration range in groundwater samples.

**Field Results.** In well-mixed natural surface waters it is generally accepted that dissolved oxygen controls the system redox potential (1). Similarly, the redox conditions of the shallow, unconfined sand and gravel aquifer were dominated apparently by the distribution of dissolved oxygen. The samples from the shallow well at 11 m consistently showed dissolved oxygen levels greater than 80% saturated at the in situ temperatures. The concentration gradient with depth from the 11-m well was approximately -0.3 mg·L<sup>-1</sup>·m<sup>-1</sup> O<sub>2</sub> to a depth of 32 m where the groundwater exhibited oxygen levels at or near the detection limit for both the azide-modified Winkler titration and Clark polarographic electrode methods. There was a correspondence between dissolved oxygen levels and measurements of platinum electrode potential. The gradient in O<sub>2</sub> noted above closely matched the corresponding gradient in Eh which was approximately -20 mV·m<sup>-1</sup> with depth in the aquifer. Oxygen was the most concentrated oxidant measured in the system, far exceeding the dissolved levels of other potential electron acceptors, such as Fe(III), NO<sub>3</sub><sup>-</sup>, or SO<sub>4</sub><sup>2-</sup> ions. Therefore, in this shallow sand and gravel aquifer we have observed strong vertical gradients in redox conditions which are bounded by the dissolved oxygen saturation near the water table and levels below the detection limit of practical field methods at a depth of 32 m below land surface. Reports of relatively high levels of dissolved oxygen in unconfined aquifers at depths exceeding 200 m suggest that subsurface oxygen removal processes may be quite slow in certain hydrogeologic settings (37). While we have not explored the kinetics of oxygen uptake in our study situation, there is evidence that the activity of the O<sub>2</sub>/H<sub>2</sub>O electrochemical couple is mediated by the persistence of H<sub>2</sub>O<sub>2</sub> in shallow groundwater. This would have the effect of substantially reducing the equilibrium oxidizing intensity of the O<sub>2</sub>/H<sub>2</sub>O redox couple (1).

The results of the H<sub>2</sub>O<sub>2</sub> field analyses are presented in Table II. When five or more replicates of a sample were run, the extreme high and low values were ignored in calculating av-

erages and standard deviations. When two replicates were run, the standard deviation was estimated from the range of concentrations (38). One replicate blank was run on 2/19/85, 10/17/85, and 4/6/85, and no blank was run on 1/28/86. The square root of the sum of squares of the blank variances of the other dates was used to estimate the standard deviation for these dates. The weighted average of the blanks was used to estimate the standard deviation for these dates. For 1/28/86, the weighted average of the blanks from the other dates was used to estimate the blank. Because of the difficulty of preparing H<sub>2</sub>O<sub>2</sub>-free water mentioned above, measured H<sub>2</sub>O<sub>2</sub> concentrations were frequently below the method detection limit (MDL). However, on 8 of the 15 sampling runs, observed H<sub>2</sub>O<sub>2</sub> concentrations for at least one depth were greater than the MDL or estimated MDL.

There was some indication that peroxide maxima were related to maxima in dissolved oxygen, particularly at a depth of 11 m. Although this shallow well consistently showed near-saturation oxygen levels and most frequent detectable peroxide concentrations, the actual concentrations were not correlated over time. Also, the increased reducing gradient with depth noted above for O<sub>2</sub> and Eh was not observable in the H<sub>2</sub>O<sub>2</sub> data.

If H<sub>2</sub>O<sub>2</sub> is to be applied to aquifer rehabilitation efforts, we must better understand the reactions that control oxidant or reductant stabilities. The scopoletin-horseradish peroxidase method with the modifications described in this paper permits reliable H<sub>2</sub>O<sub>2</sub> determinations in groundwaters and may be useful for the study of H<sub>2</sub>O<sub>2</sub> geochemistry.

#### ACKNOWLEDGMENT

The authors thank Pamela Beavers, Mark Sievers, and Ed Garske of the State Water Survey for their help in the field and laboratory aspects of this work.

#### LITERATURE CITED

- (1) Stumm, W.; Morgan, J. J. *Aquatic Chemistry*, 2nd ed.; Wiley: New York, 1981; Chapter 7.
- (2) Hem, J. D. U.S. Geological Survey, Water Supply Paper 1459-B, 1960.
- (3) Brezonik, P. L. *Nutrients in Natural Waters*; Allen, H. E., Kramer, J. R., Eds.; Wiley: New York, 1972; Chapter 1, pp 1-51.
- (4) Eglinton, G.; Barnes, P. J. *Environmental Biogeochemistry and Geomicrobiology*; Krumbein, W. E., Ed.; Ann Arbor Science: Ann Arbor, MI, 1978; Vol. 1, pp 25-46.
- (5) Garrels, R. M.; Christ, C. L. *Solutions, Minerals, and Equilibria*; Freeman, Cooper and Co.: San Francisco, CA, 1965; p 383.
- (6) Back, W.; Barnes, I. U.S. Geological Survey Professional Paper 498-C, 1965.
- (7) Champ, D. R.; Gulens, J.; Jackson, R. E. *Can. J. Earth Sci.* **1979**, *16*, 12-23.
- (8) Baedeker, M. J.; Back, W. J. *Hydrology* **1979**, *43*, 393-414.



- (9) Jackson, R. E.; Patterson, R. J. *Water Resour. Res.* **1982**, *18*, 4, 1255-1268.
- (10) Lindberg, R. D.; Runnels, Donald D. *Science (Washington, D.C.)* **1984**, *225*, 925-927.
- (11) Barcelona, M. J.; Garske, E. E. *Anal. Chem.* **1983**, *55*, 965-967.
- (12) Schwarzenbach, R. P.; Giger, W.; Schaffner, C.; Wanner, O. *Environ. Sci. Technol.* **1985**, *19*, 322-327.
- (13) Sato, M. *Econ. Geol.* **1960**, *55*, 928.
- (14) Andreae, W. A. *Nature (London)* **1955**, *175*, 859-860.
- (15) Cooper, W.; Zika, R. *Science (Washington, D.C.)* **1983**, *221*, 711-712.
- (16) Zika, R. E.; Saltzman, E.; Chameides, W. L.; Davis, D. D. *J. Geophys. Res.*, *B* **1982**, *87*, 5015-5017.
- (17) Walker, W. H.; Bergstrom, R. E.; Walton, W. C. *Preliminary Report on the Ground-Water Resources of the Havana Region in West-Central Illinois*; Illinois State Water Survey/Illinois State Geological Survey Coop. Report 3, 1985.
- (18) Naymik, T. G.; Sievers, M. E. *Ground Water Tracer Experiment (I) at Sand Ridge State Forest, IL*; State Water Survey Contract Report No. 317, 1983.
- (19) Naymik, T. G.; Sievers, M. E. *Ground Water* **1985**, *23*, 746-752.
- (20) Barcelona, M. J.; Gibb, J. P.; Helfrich, J. A.; Garske, E. E. *A Practical Guide for Ground Water Sampling*; prepared for USEPA, RSKERL, Ada, OK, and EMSL, Las Vegas, NV, State Water Survey Contract Report No. 374, Nov. 1985.
- (21) Schock, M. R.; Garske, E. E. *Ground Water Monit. Rev.* **1986**, *6*, 79-84.
- (22) Kok, G. L. *Atmos. Environ.* **1980**, *14*, 653-656.
- (23) Skoog, D. A.; West, D. M. In *Fundamentals of Analytical Chemistry*, 4th ed.; Saunders College Publishing: New York, NY, 1982; pp 755-761.
- (24) Van Baalen, C.; Marler, J. E. *Nature (London)* **1966**, 951.
- (25) Zika, R. G.; Saltzman, E. S. *Geophys. Res. Lett.* **1982**, *9*, 231-234.
- (26) Larsen, I. L.; Hartmann, N. A.; Wagner, J. J. *Anal. Chem.* **1973**, *45*, 1511-1513.
- (27) Perschke, H.; Broda, E. *Nature (London)* **1961**, *190*, 257-258.
- (28) Hem, J. D. U.S. Geological Survey Water Supply Paper No. 1473, 2nd ed., 1970.
- (29) Schumb, N. C. *ACS Monogr. Ser.* **1955**, No. 128, 421.
- (30) Maloney, S. M.; Manem, J.; Mallevialle, J.; Frissinger, F. *Environ. Sci. Technol.* **1986**, *20*, 249-253.
- (31) Perdue, E. M. *ACS Symp. Ser.* **1979**, No. 93, 99-114.
- (32) ACS Committee on Environmental Improvement. *Anal. Chem.* **1980**, *52*, 2242.
- (33) Lazrus, A. L.; Kok, G. L.; Gittlin, S. N.; Lind, J. A.; McLaren, S. E. *Anal. Chem.* **1985**, *57*, 917-922.
- (34) Zika, R. G. *Short-Lived Oxidants in Natural Waters, Extended Abstract 52*; Conference on Gas-Liquid Chemistry in Natural Waters, Brookhaven National Laboratory, April 1984.
- (35) Kok, G. L.; Thompson, K.; Lazrus, A. L.; McLaren, S. E. *Anal. Chem.* **1986**, *58*, 1192-1194.
- (36) Hwang, H.; Dasgupta, P. K. *Anal. Chem.* **1986**, *58*, 1521-1524.
- (37) Winograd, I. J.; Robertson, F. N. *Science (Washington, D.C.)* **1982**, *216*, 1227-1230.
- (38) Dean, R. B.; Dixon, W. J. *Anal. Chem.* **1951**, *23*, 636-638.

RECEIVED for review June 16, 1986. Resubmitted September 18, 1986. Accepted October 15, 1986. The support of the USEPA—R. S. Kerr Environmental Research Laboratory and the Campus Research Board of the University of Illinois, Urbana-Champaign, is gratefully acknowledged. The work was supported in part by donations of material and equipment by Q.E.D., Inc., Ann Arbor, MI; Fluorocarbon, Anaheim, CA; and Du Pont, Wilmington, DE. Although the research described in this article was funded wholly or in part by the United States Environmental Protection Agency, through its cooperative agreement program, it has not been subjected to the Agency's peer and policy review and, therefore, does not necessarily reflect the views of the Agency, and no official endorsement should be inferred.

## Specificity of the Ion Exchange/Atomic Absorption Method for Free Copper(II) Species Determination in Natural Waters

Jamal A. Sweileh, Dale Lucyk, Byron Kratochvil,\* and Frederick F. Cantwell\*

Department of Chemistry, University of Alberta, Edmonton, Alberta, Canada T6G 2G2

Concentrations of the free copper(II) species ( $\text{Cu}^{2+}$ ) measured by the ion exchange/atomic absorption (IEX) method in the presence of various concentrations of the ligands citrate, glycinate, phthalate, salicylate, chloride, and fulvate are compared to concentrations measured with a cupric ion selective electrode (ISE) and/or to concentrations calculated from known metal-ligand formation constants. The IEX method is considerably more sensitive for  $\text{Cu}^{2+}$  than the ISE method but is subject to interference from cationic and neutral copper complexes as well as from filterable colloid copper-hydroxo species at higher pH values. Accurate values of  $\text{Cu}^{2+}$  concentration are obtained by both methods in the presence of anionic copper-ligand complexes. Since fulvate, which is the principal ligand present in natural freshwaters, forms anionic copper complexes, the IEX method possesses adequate selectivity for measuring  $\text{Cu}^{2+}$  at trace levels in such waters. The complexing capacity of an acidic lake water with a very low dissolved organic carbon content was measured as  $3.0 \times 10^{-8} \text{ M}$  by monitoring  $\text{Cu}^{2+}$  concentration by the IEX method during titration with copper nitrate.

The determination of concentrations of individual metal-containing species as opposed to determining the total con-

centration of a metal is important, especially in the environmental, toxicological, and clinical fields. In previous studies it has been shown that a column-equilibration technique, employing a strong-acid-type cation exchange resin, can be coupled to an atomic absorption spectrophotometer to provide an "ion selective probe" for measuring the concentration of free (hydrated) metal ion species in the presence of kinetically labile complexes of the metal ion (1-3). In this technique the sample solution is passed through a small cation exchange resin column until complete breakthrough of the free metal ion has occurred and equilibrium has been achieved between the resin and sample solution. After a water wash, the sorbed metal ion is eluted from the resin and measured by atomic absorption spectroscopy.

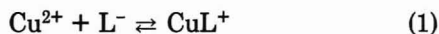
As is true for any species-selective method, including ion selective electrode (ISE) potentiometry, the term "selective" is relative, for there are always some conditions under which a method experiences interference. This study investigates interferences in the ion exchange (IEX) technique, which involves ion exchange column equilibration followed by atomic absorption, to determine free, hydrated  $\text{Cu}(\text{II})$  (hereinafter referred to as  $\text{Cu}^{2+}$ ) in natural waters. In the study,  $\text{Cu}^{2+}$  concentrations are measured by the technique in solutions containing known concentrations of ligands that are commonly found in natural waters or that contain functional groups similar to those present in ligands found in natural waters.

The measured  $\text{Cu}^{2+}$  concentrations are compared to concentrations obtained by ISE potentiometry and to concentrations calculated from known metal-ligand complex formation constants.

$\text{Cu}^{2+}$  is important in natural waters because it is the most toxic species of dissolved copper to fish, plants, and other aquatic organisms (4-8) and because copper sulfate is widely used for the control of algal growth in freshwater lakes and reservoirs (9, 10).

### THEORY

This subject is treated in greater detail in ref 11. When a ligand which is present in the test solution but not in the standard solution forms a copper complex that sorbs on the resin, then the IEX method yields an erroneously high value for  $\text{Cu}^{2+}$ . Consider a ligand  $\text{L}^-$  that forms a complex  $\text{CuL}^+$



If  $\text{CuL}^+$  is sorbed along with  $\text{Cu}^{2+}$ , then the sorption equilibria are



and



The distribution coefficients,  $\lambda$ , for the species  $\text{Cu}^{2+}$  and  $\text{CuL}^+$  are defined as

$$\lambda_{\text{Cu}^{2+}} = [\text{R}_2\text{Cu}]/[\text{Cu}^{2+}] \quad (4)$$

and

$$\lambda_{\text{CuL}^+} = [\text{RCuL}]/[\text{CuL}^+] \quad (5)$$

The distribution ratio for copper in the standard solution is given by

$$D_{\text{Cu},L=0} = \lambda_{\text{Cu}^{2+}}\alpha_{\text{Cu}^{2+},L=0} \quad (6)$$

where  $D_{\text{Cu},L=0}$  is the ratio of the total copper concentration in the resin to the total copper concentration in the solution and is measured experimentally by running a standard solution (containing no  $\text{L}^-$ ) through the IEX procedure. The quantity  $\alpha_{\text{Cu}^{2+},L=0}$  is the fraction of copper in the standard solution that is present as the  $\text{Cu}^{2+}$  species (12) and has a value less than 1 if species such as  $\text{CuOH}^+$  or  $\text{CuNO}_3^+$  are present.

In the test solution which contains  $\text{L}^-$  the distribution ratio for copper is given by

$$D_{\text{Cu},L\neq 0} = \lambda_{\text{Cu}^{2+}}\alpha_{\text{Cu}^{2+},L\neq 0} + \lambda_{\text{CuL}^+}\alpha_{\text{CuL}^+,L\neq 0} \quad (7)$$

where  $\alpha_{\text{Cu}^{2+},L\neq 0}$  and  $\alpha_{\text{CuL}^+,L\neq 0}$  are the fractions of copper in the test solution present as the  $\text{Cu}^{2+}$  and  $\text{CuL}^+$  species.

Dividing eq 7 by eq 6 gives

$$\frac{D_{\text{Cu},L\neq 0}}{D_{\text{Cu},L=0}} = \frac{\lambda_{\text{Cu}^{2+}}\alpha_{\text{Cu}^{2+},L\neq 0} + \lambda_{\text{CuL}^+}\alpha_{\text{CuL}^+,L\neq 0}}{\lambda_{\text{Cu}^{2+}}\alpha_{\text{Cu}^{2+},L=0}} \quad (8)$$

In the IEX method the peak area, PA (absorbance seconds), is measured for the eluted copper peak. PA is proportional to the concentration of copper in the resin,  $C_{\text{Cu},R}$  (moles/gram); according to

$$\text{PA} = (GS/F)C_{\text{Cu},R} \quad (9)$$

where the proportionality constant includes the sensitivity of the atomic absorption spectrophotometer,  $S$  ((absorbance/mol)/mL), the weight of resin in the column,  $G$  (grams), and the flow rate of eluate into the nebulizer,  $F$  (mL/s). Since peak area is directly proportional to the distribution ratio of copper, it has been shown (11) that

$$\text{PA}_{L\neq 0}/\text{PA}_{L=0} = D_{\text{Cu},L\neq 0}/D_{\text{Cu},L=0} \quad (10)$$

If the only copper-containing species sorbed by the resin is  $\text{Cu}^{2+}$  (and perhaps  $\text{CuOH}^+$  as discussed below), then  $\lambda_{\text{CuL}^+} =$

0 and the resin is selective (specific) for  $\text{Cu}^{2+}$ . Combining eq 8 and 10 gives

$$\text{PA}_{L\neq 0}/\text{PA}_{L=0} = \alpha_{\text{Cu}^{2+},L\neq 0}/\alpha_{\text{Cu}^{2+},L=0} \quad (11)$$

In this equation the ratio  $\alpha_{\text{Cu}^{2+},L\neq 0}/\alpha_{\text{Cu}^{2+},L=0}$  is identical with the relative fraction of  $\text{Cu}^{2+}$  in the test solution compared to the fraction (taken as 1) of  $\text{Cu}^{2+}$  in the standard solution. When this ratio of peak areas for test solution and standard solution,  $\text{PA}_{L\neq 0}/\text{PA}_{L=0}$ , is multiplied by the  $\text{Cu}^{2+}$  concentration of the standard solution, the  $\text{Cu}^{2+}$  concentration of the test solution is obtained.

If, on the other hand,  $\text{CuL}^+$  is sorbed, the resin is not selective for  $\text{Cu}^{2+}$ . From eq 8 and 10

$$\frac{\text{PA}_{L\neq 0}}{\text{PA}_{L=0}} = \frac{\alpha_{\text{Cu}^{2+},L\neq 0}}{\alpha_{\text{Cu}^{2+},L=0}} + \frac{\lambda_{\text{CuL}^+}\alpha_{\text{CuL}^+,L\neq 0}}{\lambda_{\text{Cu}^{2+}}\alpha_{\text{Cu}^{2+},L=0}} \quad (12)$$

and multiplying  $\text{PA}_{L\neq 0}/\text{PA}_{L=0}$  by the  $\text{Cu}^{2+}$  concentration of the standard solution will yield an erroneously high concentration of  $\text{Cu}^{2+}$  for the test solution.

The above concepts can be generalized for the simultaneous sorption of other Cu-L complexes and of copper complexes with other ligands.

In the experiments discussed below the ligands  $\text{L}^-$  present in the test solution are known so that  $\alpha_{\text{Cu}^{2+},L\neq 0}$  and  $\alpha_{\text{Cu}^{2+},L=0}$  can be predicted for any ligand concentration and pH from available equilibrium constants. The experimentally measured value of  $\text{PA}_{L\neq 0}/\text{PA}_{L=0}$  can then be compared with the value predicted from eq 11 to determine the specificity of the method for  $\text{Cu}^{2+}$ .

### EXPERIMENTAL SECTION

**Apparatus and Glassware.** The instrument used for the ion exchange column equilibration experiments was similar to the one described previously (1), with a few modifications. A third pump tube and an additional Cheminert four-way valve were used with the peristaltic pump to maintain a flow of water to the nebulizer of the atomic absorption spectrometer during the column loading step. An additional sample injection valve (Model 202-00, Altex Inc., Berkeley, CA) with a 135- $\mu\text{L}$  injection loop was placed between valve  $V_3$  and the resin column. This valve permitted injection of a standard copper solution to check for flow rate changes or instrument drift. The sample solution reservoir and the small ion exchange column (containing either 2 or 10 mg of Dowex 50W-X8) were thermostated at  $25 \pm 0.5^\circ\text{C}$  with a circulating water bath. The copper in the column eluate was monitored with a Model 4000 atomic absorption spectrometer (Perkin-Elmer).

Measurement of solution pH was made with an Accumet 320 meter (Fisher) using a 13-639-90 combination electrode (Fisher). Potentiometric measurement of  $\text{Cu}^{2+}$  concentration was made at  $25.0 \pm 0.1^\circ\text{C}$  with an Orion 94-29 cupric selective electrode, an Orion 90-02 double junction Ag/AgCl reference electrode with 0.1 M  $\text{NaNO}_3$  as the salt bridge, and an 825 MP Accumet meter (Fisher).

Ultraviolet-visible absorption spectra of molecular species in solution were made with an HP 8451A spectrophotometer (Hewlett-Packard), and flameless atomic absorption measurements were made with a PE 5000 atomic absorption spectrometer, PE HGA 2200 graphite furnace, and PE AS-1 autosampler (Perkin-Elmer).

All labware used for handling solutions was cleaned with detergent solution, rinsed with tap water, soaked overnight in either 30% (v/v) nitric acid or in 3:1 (v/v)  $\text{H}_2\text{SO}_4/\text{HNO}_3$ , and rinsed with distilled deionized water.

**Reagents and Chemicals.** A stock copper(II) solution was prepared by dissolved ACS reagent grade copper foil (Matheson, Coleman and Bell) in 1% (v/v) nitric acid and diluting with water. The buffer component 2,6-dimethylpyridine (2,6-lutidine, Terochem, Edmonton, AB) was distilled at atmospheric pressure and the middle fraction (132-136  $^\circ\text{C}$ ) was collected. A sample of fulvic acid which had been extracted from the Bh horizon of a podzol from Armadale, Prince Edward Island, Canada, was supplied by



C. H. Langford, Concordia University, Montreal, and was used without further treatment.

Analytical grade 100–200 mesh Dowex 50W-X8 strong-acid-type cation exchange resin (J. T. Baker) was treated as described in the literature (13). Its ion exchange capacity was 5.1 mequiv/g on a dry basis.

Water was distilled and passed through a mixed-bed ion exchange resin column (Amberlite MB-1, Rohm and Haas). All other chemicals were analytical or reagent grade and were used as received. Swamping electrolyte was prepared from a stock solution of 0.500 M sodium nitrate that had been passed through a bed of Chelex 100 resin (analytical grade, 100–200 mesh, sodium form) (Bio-Rad) to remove trace copper.

**Test Solutions and Blanks.** A series of test solutions, each  $1.00 \times 10^{-7}$  M in total dissolved copper, was prepared to contain variable ligand concentrations but constant total sodium concentration (0.100 M) and constant lutidine buffer concentration ( $10^{-3}$  M) as follows: A volume of 0.500 M  $\text{NaNO}_3$  solution that would yield a final total  $\text{Na}^+$  concentration, including the  $\text{Na}^+$  from the ligand solution, of 0.100 M was transferred into a 400-mL beaker. The calculated volume of ligand solution was added, followed by 5.00 mL of 0.05 M lutidine and enough water to adjust the volume to about 200 mL. The pH was adjusted to 6.0 with dilute  $\text{HNO}_3$ . This was followed by dropwise addition to the stirred solution of 10.00 mL of daily prepared  $2.50 \times 10^{-6}$  M copper standard solution. In some cases the pH had to be readjusted to 6.0 after adding the copper solution. The contents of the beaker were quantitatively transferred to a 250-mL volumetric flask and diluted to volume. These test solutions were used for the  $\text{Cu}^{2+}$  determination by the IEX method. For each test solution a corresponding blank solution was prepared in an identical manner, with the copper omitted.

For many of the ligand systems the  $\text{Cu}^{2+}$  concentration was also determined by ISE potentiometry. For this purpose five test solutions were prepared, each containing 0.100 M  $\text{NaNO}_3$ ,  $10^{-3}$  M lutidine buffer, and  $1.00 \times 10^{-6}$  M total dissolved copper. Four of these solutions contained varying concentrations of the ligand. The fifth, containing no added ligand, was used as a standard to calibrate the electrode-meter system. These solutions were prepared in a manner similar to that described above. The total dissolved copper concentration in these solutions was 10 times that used in the IEX measurements.

**Lake Water Sample.** The Bonneville Lake water sample was supplied by M. Papineau of Environment Canada, Inland Waters Directorate, Quebec Region. It was an integrated sample (0–4 m depth) collected by helicopter on October 3, 1985, divided into four 1-L subsamples, and shipped in ice. In our laboratory the subsamples were allowed to stand at room temperature for several hours before the pH was measured (pH 5.2). The subsamples were then filtered (0.45  $\mu\text{m}$ ) through acid-washed 47-mm-diameter Nylon 66 filters (Rainin Instruments Co., Woburn, MA). For each 1-L subsample a new filter was used. The first 200 mL of filtrate was used to rinse the receiving flask and discarded.

The lake water sample solutions were prepared for free copper determination as follows: To 20 mL of 0.500 M  $\text{NaNO}_3$  solution was added 2.00 mL of lutidine buffer (0.05 M); the pH was adjusted to 5.2 by dropwise addition of dilute nitric acid; into this solution was delivered 78.00 mL of the filtered lake water sample. The final pH was  $5.25 \pm 0.05$ . A blank test solution was prepared by the same procedure, except that the lake water sample was replaced with an equivalent volume of filtered distilled water. A standard copper solution ( $1.00 \times 10^{-7}$  M) was also prepared for calibration as described above except for pH adjustment to 5.2.

In another experiment the complexing capacity of the lake water was measured. Lake water solutions were prepared for this experiment as follows: Eighty milliliters of the filtered lake water was dispensed into each of eight 100-mL polyethylene bottles and spiked with 0, 10, 25, 50, 100, 200, 300, and 400  $\mu\text{L}$  of a standard copper solution ( $5 \times 10^{-5}$  M). The final pH did not drop by more than 0.06 unit from the initial value of 5.2. The next day 20.00 mL of a solution composed of 0.500 M  $\text{NaNO}_3$  and 0.005 M lutidine adjusted to pH 5.2 was added to each bottle. After the sample was shaken, the  $\text{Cu}^{2+}$  concentration was measured in these solutions by the IEX method.

**$\text{Cu}^{2+}$  by IEX.** Flow rates were 5 to 6 mL/min for all solutions. Test or blank solutions were pumped through a 10-mg ion ex-

change resin column for 15 min, a period of time found sufficient to achieve equilibrium at pH 6. During this resin loading step the column effluent was directed to waste to prevent plugging of the atomic absorption (AA) nebulizer by the high salt concentration. The resin was next backwashed for 4 min to remove interstitial solution, during which time the column effluent was directed to the nebulizer. Then eluent (2 M  $\text{HNO}_3$ ) was pumped through the resin column. A 50-s integration of the eluted copper peak area was triggered 15 s after switching from water to eluent flow. Before the next test or blank solution was pumped, the resin column was washed briefly with water.

$\text{Cu}^{2+}$  in a test sample is calculated from the ratio of peak areas of the test solution to the standard solution, each corrected for the appropriate blank area (eq 11).

**$\text{Cu}^{2+}$  by ISE.** Measurement and electrode cleaning procedures were similar to those of Blaedel and Dinwiddie (14). At the start of each series of measurements the ISE was polished and then placed in a stirred solution containing 10  $\mu\text{g/mL}$   $\text{Cu}(\text{NO}_3)_2$ , 0.100 M  $\text{NaNO}_3$ , and  $10^{-3}$  M lutidine (pH 6) for several hours. Before each measurement in a series, the electrode was placed in the above solution until it reached a stable potential (14), rinsed with water, placed in 0.025 M  $\text{H}_2\text{SO}_4$  until it reached a constant potential, rinsed with water, and blotted dry. The electrode was calibrated by placing it in a blank solution and adding successive small increments of copper nitrate solution. A constant potential was reached 2–7 min after each addition. Five calibration points were used between  $[\text{Cu}^{2+}]$  values of  $1 \times 10^{-6}$  and  $1 \times 10^{-7}$  M. Electrode responses were nonlinear, and precision was unsatisfactory, at  $\text{Cu}^{2+}$  concentrations below  $1 \times 10^{-7}$  M.

Measurements of  $\text{Cu}^{2+}$  in ligand-copper solutions were performed in duplicate with frequent electrode recalibration. For each solution the ratio of the fraction of  $\text{Cu}^{2+}$  in test solution ( $L \neq 0$ ) to that in standard solution ( $L = 0$ ) was calculated as

$$\frac{\alpha_{\text{Cu}^{2+}, L \neq 0}}{\alpha_{\text{Cu}^{2+}, L = 0}} = 10^{(E_{L=0} - E_{L \neq 0})/S} \quad (13)$$

where  $E$  is the measured potential and  $S$  is the slope of the best-fit line to the pooled values of the two calibration points bracketing the point in question.

## RESULTS AND DISCUSSION

**Copper(II)-Hydroxo and -Nitrate Species.** A condition of the IEX method is that all solutions are buffered at the same pH and that their electrolyte composition is swamped by the addition of the same large excess of an inert electrolyte such as  $\text{NaNO}_3$ . All solutions (test, standard, and blank) will therefore necessarily contain the same concentrations of  $\text{OH}^-$  and  $\text{NO}_3^-$ .

In the IEX method the area of the eluted copper peak is proportional to the moles of copper sorbed on the resin. A fundamental assumption of the method is that the moles of sorbed copper are proportional to the concentration of  $\text{Cu}^{2+}$  in the solution with which the resin was equilibrated. In solutions buffered at pH  $\leq 5$  there will be appreciable amounts of mononuclear copper-hydroxo complexes, such as  $\text{CuOH}^+$  ( $\beta = 10^{6.4 \pm 0.35}$ ) and  $\text{Cu}(\text{OH})_2$  ( $\beta = 10^{12 \pm 1}$ ) (15, 16), which might be expected to sorb on the cation exchange resin. It can be shown (11) that as long as the test solution and the standard solution have the same pH and swamping  $\text{NaNO}_3$  concentration, and as long as the  $\text{Cu}^{2+}$  concentration in the test solution is calculated via eq 11, then whether or not species such as  $\text{CuOH}^+$  are sorbed on the resin, the correct  $\text{Cu}^{2+}$  concentration will be obtained for the test solution even though the existence of copper-hydroxo species is ignored. In contrast, the presence of polynuclear copper-hydroxo species, especially colloidal species, can cause problems in the method (see Effect of pH, below).

Sodium nitrate was selected as swamping electrolyte for providing a constant concentration of  $\text{Na}^+$  because the  $\text{NO}_3^-$  ion is a poor ligand for  $\text{Cu}(\text{II})$  (17). IEX studies performed in this laboratory (11) show that there is no detectable difference between the complexing ability of  $\text{NO}_3^-$  and  $\text{ClO}_4^-$  for

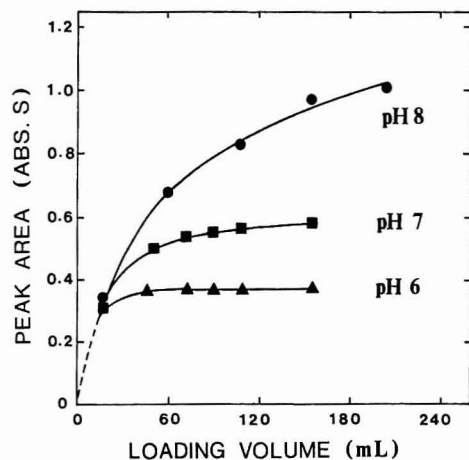


Figure 1. Effect of pH on loading curves of  $1 \times 10^{-6}$  M copper(II) solution for a 2-mg column of Dowex 50 W-X8.

Cu(II). Perchlorate is generally considered to be noncomplexing (17).

**Buffer and Eluent.** Several concentrations of nitric acid were investigated as eluents for removing copper from the ion exchange resin. The eluted copper peak became sharper as  $\text{HNO}_3$  concentration was increased up to about 2 M  $\text{HNO}_3$ . This concentration was chosen for subsequent work.

Lutidine (for lutidinium ion  $pK_a = 7.0$ ) (18) was chosen as buffer component because it is a poor ligand for Cu(II). Although the formation constant for the copper(II)-lutidine complex has not been reported, the formation constants of complexes between copper(II) and derivatives of lutidine are only about 1.3–1.6 (18) and the formation constant for the nickel(II)-lutidine complex is only 1.6 (18). Copper solutions containing 20 times the concentration of lutidine than that used in the IEX method for  $\text{Cu}^{2+}$  showed no shift in the visible absorption band of copper. Since, by analogy with the copper-pyridine complex (19), a copper-lutidine complex would be expected to produce a blue-shift and an increase in molar absorptivity compared to the hydrated  $\text{Cu}^{2+}$  band, it was concluded that the formation of a copper-lutidine complex could be neglected under the conditions of the ion exchange studies.

**Effect of pH.** In Figure 1 are shown plots of eluted peak area vs. volume of load solution that were obtained for  $1 \times 10^{-6}$  M copper standards buffered at pH 6, 7, and 8. These loading curves were obtained by pumping a solution through the resin for the specified load times, washing with water for 4 min, eluting with 2 M  $\text{HNO}_3$ , and measuring the area of the eluted peak. Column equilibration (complete breakthrough) is achieved when the plot becomes horizontal. For the solution at pH 6.0 equilibrium was achieved in less than 15 min (83 mL) but for the solutions at pH 7.0 and 8.0 equilibrium was not achieved even after 30 min (156 mL). Furthermore, a comparison of the peak areas for the three curves at any given time after about 5 min shows that peak area is greater at higher pH. This latter trend is opposite to that expected because at higher pH the fraction of copper present as  $\text{CuOH}^+$  increases at the expense of  $\text{Cu}^{2+}$  (i.e.,  $\alpha_{\text{Cu}^{2+},L=0}$  decreases in eq 7). The observed behavior of the pH 7.0 and 8.0 solutions suggests the presence of polynuclear copper-hydroxo complex species in addition to the  $\text{Cu}^{2+}$  and  $\text{CuOH}^+$  species. The continually increasing peak area at pH 8.0, in particular, suggests the presence of filterable, perhaps near-colloidal, copper-hydroxo species.

To test this, two 1-L volumes of identical standard solutions containing  $2 \times 10^{-6}$  M copper were prepared at pH 7.8. One was filtered through a 0.45- $\mu\text{m}$  pore size Nylon 66 membrane filter, discarding the first 250 mL of solution, while the second 1-L solution was not filtered. The loading curves obtained

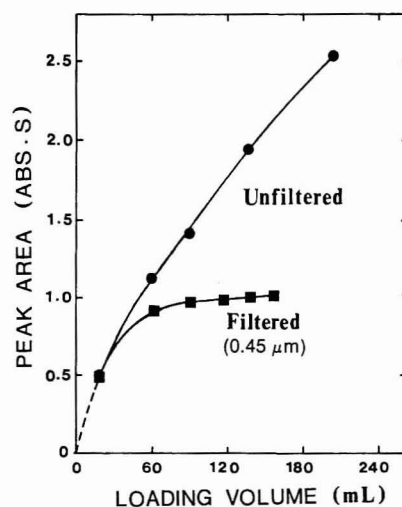


Figure 2. Effect of filtration of  $2 \times 10^{-6}$  M copper(II) solution on the shape of loading curve (pH 7.8). Resin column same as in Figure 1.

as above for both the filtered and unfiltered solutions are shown in Figure 2. The filtered solution is seen to more closely approach a plateau (equilibrium) than the unfiltered solution. This clearly demonstrates the presence in  $2 \times 10^{-6}$  M copper solution at pH 7.8 of filterable particulate copper-containing species, which are undoubtedly copper-hydroxo species. Washing of the Nylon 66 membrane filter with dilute nitric acid showed that about 10% of the total copper initially present in 1 L of solution had been retained by it. The presence of colloidal copper-hydroxo species has previously been reported in  $1 \times 10^{-6}$  M copper solutions at pH values as low as 8.5 (15).

It is expected that in more dilute copper solutions less readily filterable copper species would be formed. Indeed, at pH 8.0 loading curves for solutions with total copper concentrations  $\leq 2 \times 10^{-7}$  M achieved a plateau in about 20 min (figure not shown). The peak area plateau at pH 8.0 was higher, however, than that obtained for the same total copper concentration at pH 6.0. This is due, probably, to the presence of multiply charged cationic soluble polynuclear copper-hydroxo species at the higher pH. Under these conditions  $\text{Cu}^{2+}$  will vary with respect to the total copper, and the system can be used for  $\text{Cu}^{2+}$  measurements only if standards are prepared to contain an equilibrium concentration of  $\text{Cu}^{2+}$  close to that of the solution under study and if filterable copper-containing colloids are absent. In the present work it was decided to perform the selectivity studies at pH 6.0, where only mononuclear copper species are present.

**Effect of Added Ligands.** Five ligands were selected for study. The acid-base dissociation and copper(II) complex stability constants for the major species are listed in Table I. The principal copper-ligand complex species present under the conditions investigated are also given. The percent species distribution of soluble mononuclear copper(II) complexes at 0.1 M ionic strength and pH 6 was calculated for copper in the presence of various concentrations of each of the five ligands. For the calculations a slightly modified version of the speciation program COMICS (20) was used. Calculations were performed for total copper concentrations of both  $1 \times 10^{-7}$  M and  $1 \times 10^{-6}$  M. Equilibrium constants were taken from data compilations or from specific literature references, as indicated (16, 17, 21–24). If necessary, correction for ionic strength was made by using individual ionic activity coefficients based on values reported by Kielland (25) or calculated by the Davies equation (26).

In Figure 3a is shown, as an example, the copper-containing species diagram predicted for a total copper concentration of  $1 \times 10^{-7}$  at pH 6.0 in the presence of various total citrate



Table I. Summary of Equilibria for Copper-Ligand Studies

ligand	$K_a$ values	$\beta$ values	principal Cu complexes	ref
citrate	$K_{a1} = 10^{-2.87 \pm 0.08}$	$\text{CuCit}^-, 10^{5.9 \pm 0.1}$	$\text{CuCit}^-$	23, 24
	$K_{a2} = 10^{-4.35 \pm 0.05}$	$\text{CuHCit}, 10^{3.42}$		
	$K_{a3} = 10^{-5.69 \pm 0.05}$	$\text{CuH}_2\text{Cit}^+, 10^{2.26}$		
glycine	$K_{a1} = 10^{-2.36 \pm 0.03}$	$\text{CuGly}^+, 10^{8.15 \pm 0.09}$	$\text{CuGly}^+$	14, 25
	$K_{a2} = 10^{-9.56 \pm 0.04}$	$\text{Cu}(\text{Gly})_2, 10^{15.03 \pm 0.1}$		
phthalate	$K_{a1} = 10^{-2.75 \pm 0.02}$	$\text{CuPth}, 10^{3.22 \pm 0.05}$	$\text{CuPth}$ $\text{Cu}(\text{Pth})_2^{2-}$	14, 23, 24
	$K_{a2} = 10^{-4.92 \pm 0.05}$	$\text{CuHPth}^+, 10^{1.33}$		
		$\text{Cu}(\text{Pth})_2^{2-}, 10^{5.46}$		
salicylate	$K_{a1} = 10^{-2.81 \pm 0.01}$	$\text{CuSal}, 10^{10.6 \pm 0.1}$	$\text{CuSal}$	23, 24
chloride	$K_{a2} = 10^{-13.4 \pm 0.1}$	$\text{Cu}(\text{Sal})_2^{2-}, 10^{18.4}$	$\text{CuCl}^+$	15, 26
		$\text{CuCl}^+, 10^{0.12 \pm 0.15^a}$		

<sup>a</sup> Corrected to an ionic strength of 0.1.

concentrations up to  $1 \times 10^{-5}$  M. In Figure 3a the vertical axis value is calculated as  $100\alpha_{\text{Cu}^{2+}, L \neq 0}$ . The ligand species of citric acid is citrate anion,  $\text{Cit}^{3-}$ . As the total citric acid concentration increases along the horizontal axis, the percents of  $\text{Cu}^{2+}$  and  $\text{CuOH}^+$  in solution decrease and the percentage of copper(II)-citrate complex increases. The data for the  $\text{Cu}^{2+}$  species in the presence of citric acid from Figure 3a are used to calculate the solid line representing "Relative Free Copper", shown in Figure 3b, by dividing  $\alpha_{\text{Cu}^{2+}, L \neq 0}$  at a given citric acid concentration ( $L \neq 0$ ) by  $\alpha_{\text{Cu}^{2+}, L=0}$  at zero concentration of citric acid ( $L = 0$ ) and multiplying by 100. Comparisons of the predicted values ( $100\alpha_{\text{Cu}^{2+}, L \neq 0} / \alpha_{\text{Cu}^{2+}, L=0}$ ) with the experimentally measured values ( $100\text{PA}_{L \neq 0} / \text{PA}_{L=0}$ ) are based on eq 11. The uncertainties in the calculated solid line, estimated from the uncertainties in the equilibrium constants used, are indicated on the line by vertical error bars. The solid circles in Figure 3b denote experimental values obtained by the IEX method on solutions containing a total copper concentration of  $1 \times 10^{-7}$  M, and the solid triangles denote experimental values obtained by measurements with the copper ISE on solutions containing a total copper concentration of  $1 \times 10^{-6}$  M. A higher total copper concentration was used for the electrode measurements because of nonlinear response and unsatisfactory precision at  $\text{Cu}^{2+}$  concentrations below  $1 \times 10^{-7}$  M.

For citrate the use of the higher total copper concentration required for the ISE measurements resulted in citrate concentrations no longer being present in swamping excess over the copper. Under these conditions, the species distribution depended on both total citrate and total copper concentration. The dashed line in Figure 3b shows results calculated by the COMICS program for  $1 \times 10^{-6}$  M total copper. The triangular experimental points should be compared with this line.

The agreement between  $\text{Cu}^{2+}$  predicted (solid line) and  $\text{Cu}^{2+}$  measured by the IEX method (solid circles) (Figure 3b) is within experimental error, suggesting that the IEX method is specific for  $\text{Cu}^{2+}$  in the presence of  $\text{CuCit}^-$ . This is as expected since the negatively charged co-ion  $\text{CuCit}^-$  would be excluded from the resin (13). Agreement between the ISE measurements and the dashed line, though not as good, is still within experimental error.

For all ligands studied other than citrate the conditional stability constants of the copper-ligand complexes were small enough that the ligand concentration could be maintained in swamping excess over the copper for total copper concentrations from  $1 \times 10^{-6}$  to  $1 \times 10^{-7}$  M. Therefore the calculated species distributions as a function of ligand concentration for the copper-ligand complexes were independent of the total copper present over this range of copper concentrations. Figure 4 shows plots of relative  $\text{Cu}^{2+}$  vs. total ligand concentrations for the four other ligands studied.

For glycine, the IEX (circles) and ISE (triangles) values can be compared with those calculated for free copper (solid

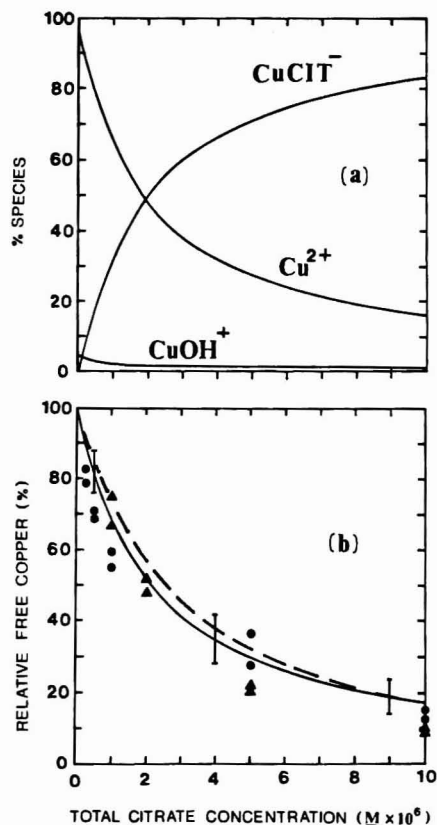
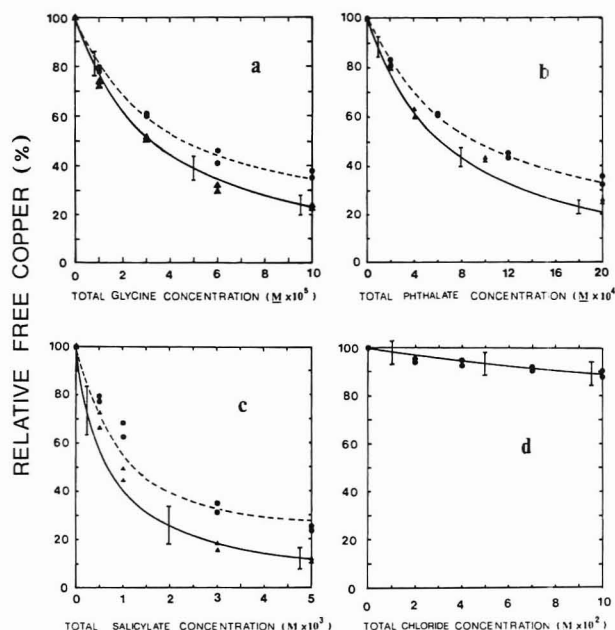


Figure 3. (a) Copper species distribution vs. total citrate concentration for  $1 \times 10^{-7}$  M total copper, at pH 6.0. (b) Dependence of relative free copper on total citrate concentration as obtained by the ion exchange method (●) and by the ion selective electrode method (▲). The solid line in (b) is calculated from the  $\text{Cu}^{2+}$  species distribution in (a). The dashed line in (b) is calculated from the  $\text{Cu}^{2+}$  species distribution curve (not shown) for  $1 \times 10^{-6}$  M total copper. The vertical error bars represent the uncertainty in the solid line.

line) in Figure 4a. The ISE values for free copper agree well with the predicted values, while the ion exchange results appear systematically to be higher. Evidently the cation exchange resin sorbs not only the free  $\text{Cu}^{2+}$  species but also the cationic complex species  $\text{CuGly}^+$ . From measurements on a standard copper solution, a value for  $\lambda_{\text{Cu}^{2+}}$  of 41 L/g is obtained. The dashed line in Figure 4a was calculated by using eq 12 with this value substituted for  $\lambda_{\text{Cu}^{2+}}$  and a value of 9 L/g assumed for  $\lambda_{\text{CuGly}^+}$ . This line fits well the experimental points measured by the IEX method. The selectivity coefficient,  $\lambda_{\text{Cu}^{2+}} / \lambda_{\text{CuGly}^+}$ , of the IEX method for  $\text{Cu}^{2+}$  over  $\text{CuGly}^+$  is thus only about 4.6, suggesting that the method is not highly selective for  $\text{Cu}^{2+}$  in the presence of univalent cationic copper complexes.

For phthalate the ISE values for free copper are within experimental error of the predicted values while the IEX



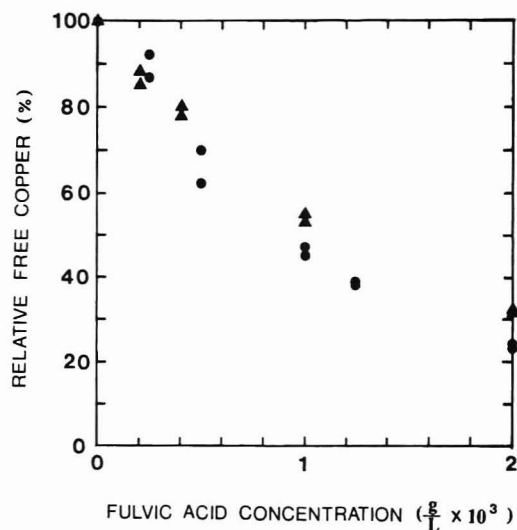
**Figure 4.** Dependence of relative free copper on ligand concentration as obtained by IEX (●) and by ISE (▲). The solid lines are those predicted from the copper species distributions for a total copper concentration of  $1 \times 10^{-7}$  M. The vertical error bars represent the uncertainty in the predicted solid lines. The dashed lines are calculated via eq 12, taking into account sorption of other species (see text for details).

values are somewhat high (Figure 4b). The two principal copper-phthalate complex species in solution are  $\text{CuPth}$  and  $\text{Cu(Pth)}_2^{2-}$ , with the former predominating. Since the anion  $\text{Cu(Pth)}_2^{2-}$  will be excluded from the resin, it is likely that it is sorption of the neutral species  $\text{CuPth}$  that interferes with the determination of  $\text{Cu}^{2+}$ . Evidently, water wash of the resin following the load step does not remove the interference, perhaps because during the water wash the species  $\text{CuPth}$  dissociates to  $\text{Cu}^{2+}$  and phthalate species and the  $\text{Cu}^{2+}$  is sorbed by cation exchange. This interference by neutral copper-containing species was unanticipated (2). The dashed line in Figure 4b, calculated via eq 12 using  $\lambda_{\text{Cu}^{2+}} = 41$  L/g, agrees well with the IEX values when  $\lambda_{\text{CuPth}}$  is taken as 8 L/g.

For *salicylate*, values of  $\text{Cu}^{2+}$  obtained with the ISE agree well with predicted values (Figure 4c). Values measured by the IEX method appear to be high, presumably due to sorption of the neutral complex  $\text{CuSal}$ . The dashed line in Figure 4c is obtained via eq 12 with  $\lambda_{\text{Cu}^{2+}} = 41$  L/g and  $\lambda_{\text{CuSal}} = 8$  L/g.

For *chloride*, the predicted  $\text{Cu}^{2+}$  concentrations were measured at total chloride concentrations up to 0.10 M (Figure 4d). To achieve this high sodium chloride concentration while maintaining a constant  $[\text{Na}^+]$ , the sodium nitrate concentration was correspondingly decreased. Values of  $\text{Cu}^{2+}$  were measured experimentally only by the IEX method since it is well-known that the ISE behaves anomalously in chloride media (27–29). The good agreement between the predicted solid line and the measured points must be considered somewhat fortuitous in light of the large standard deviation for the line ( $\pm 5\%$   $\text{Cu}^{2+}$ ). One cannot conclude, for example, that  $\text{CuCl}^+$  is not sorbed by the resin. Nevertheless the data in Figure 4d do show that the presence of substantial concentrations of  $\text{Cl}^-$  produces negligible errors when  $\text{Cu}^{2+}$  concentrations are to be measured, largely because very little copper-chloride complexation occurs.

**Fulvate Ligand.** Fulvic acid is the soluble fraction of humic substances in soil and water. It is a polydisperse polymer with a molecular weight of a few hundred to a few thousand, and it possesses both phthalic and salicylic acid type functional groups (30, 31). Armadale fulvic acid has been shown to have a total of 6.5 mequiv of acidic functional groups



**Figure 5.** Dependence of relative free copper on fulvic acid concentration as obtained by IEX (●) and by ISE (▲).

per gram and to be nearly completely ionized at  $\text{pH} > 5$  in 0.1 M KCl (32).

Because of the ill-characterized nature of fulvic acid and its complicated behavior as a ligand (31, 33), no attempt was made to utilize copper-fulvate formation constants reported in the literature to predict the variation of  $\text{Cu}^{2+}$  concentration with fulvic acid concentration. Instead, the experimental  $\text{Cu}^{2+}$  values obtained by the IEX method (at  $1 \times 10^{-7}$  M total copper) are compared in Figure 5 to those obtained by the ISE method (at  $1 \times 10^{-6}$  M total copper). It can be seen that the IEX values are similar to the electrode values. From this agreement we conclude that the IEX method is as selective as the ISE for  $\text{Cu}^{2+}$  in the presence of copper-fulvate complexes. This selectivity is probably due to the fact that copper-fulvate complexes are anionic and are therefore excluded from the cation exchange resin.

**Effect of Ionic Strength.** The method requires the addition of a relatively high concentration of an inert electrolyte to all samples and standards. The resulting increase in ionic strength will affect activity coefficients of ionic species and thereby alter equilibria involving free copper. The magnitude of the change produced in  $[\text{Cu}^{2+}]$  as a result of a change in ionic strength can be estimated from the Debye-Hückel equation if a few assumptions are made about the nature of the complexes expected to be present. For a change in ionic strength from 0 to 0.1, the change in  $[\text{Cu}^{2+}]$  in a natural water sample due to activity coefficient effects is estimated to be less than a factor of 2.

**Study of an Acidic Lake Water.** Bonneville Lake is an acidic freshwater lake ( $\text{pH}$  5.2–6.1) on the Canadian Precambrian shield. The  $\text{Cu}^{2+}$  content of this lake, measured at the original  $\text{pH}$  of 5.2 by the IEX method, was below the detection limit of the method ( $2 \times 10^{-8}$  M  $\text{Cu}^{2+}$ ).

Ligands present in natural waters serve to complex added metal ions, and the so-called complexing capacity of a natural water is an important measure of its ability to detoxify added metals. The complexing capacity of Bonneville Lake water was determined by titration with copper. A plot of  $\text{Cu}^{2+}$  vs. total copper in the sample is a typical two-segment plot (2). The concentration of  $\text{Cu}^{2+}$  (vertical axis) was measured by the IEX method at  $\text{pH}$  5.2. The total copper concentration (horizontal axis) was calculated as the copper added as titrant to the sample plus the copper present as an impurity in the reagents (swamping electrolyte and buffer) added to the sample. The copper concentration in the reagents was measured by graphite furnace atomic absorption spectroscopy as  $(1.8 \pm 0.3) \times 10^{-8}$  M (34). The intersection point of the two



linear segments of the complexing capacity curve at  $3.0 \times 10^{-8}$  M total copper gives the complexing capacity of the lake water sample.

This value is low compared to that of many lakes around the world, which range from  $1 \times 10^{-7}$  M to  $1 \times 10^{-4}$  M (35). This low complexing capacity for Bonneville Lake is not surprising, however, since the water has a very low total dissolved organic carbon content (3.9 mg/L) (36). A consequence of a low complexing capacity is that such a lake would be more vulnerable to metal ion pollution than other lakes.

### CONCLUSION

Comparison of the experimental and measured values in Figures 3 and 4 suggests that the ISE is generally selective for  $\text{Cu}^{2+}$  for the ligands studied. However, it is not applicable to  $\text{Cu}^{2+}$  concentrations below about  $1 \times 10^{-7}$  M. A similar comparison for the IEX method shows that it is subject to interference from cationic and neutral copper complexes as well as from filterable colloidal copper-hydroxo species at higher pH values. The IEX method has the advantages that it is more sensitive than the ISE method and can be adapted to metals such as  $\text{Ni}^{2+}$ , for which ISE's are not available (2). The IEX method may be particularly useful for the measurement of  $\text{Cu}^{2+}$  in natural waters where the copper is often present in low concentrations, where cationic and neutral copper complexes are likely to be absent, and where humates and fulvates are the principal complexing ligands (37).

### ACKNOWLEDGMENT

The authors thank N. Motkosky for performing the graphite furnace AAS measurements and M. Papineau, Environment Canada, Inland Waters Directorate—Quebec Region, for supplying the lake water sample.

**Registry No.** Cu, 7440-50-8;  $\text{H}_2\text{O}$ , 7732-18-5; citrate, 126-44-3; glycine, 23297-34-9; phthalate, 88-99-3; salicylate, 63-36-5.

### LITERATURE CITED

- (1) Treit, J.; Nielsen, J. S.; Kratochvil, B.; Cantwell, F. F. *Anal. Chem.* **1983**, *55*, 1650.
- (2) Cantwell, F. F.; Nielsen, J. S.; Hruddy, S. E. *Anal. Chem.* **1982**, *54*, 1498.
- (3) Nielsen, J. S. Ph.D. Thesis, Department of Civil Engineering, University of Alberta, Edmonton, Alberta, Canada, 1982.
- (4) Sunda, W. G.; Guillard, J. J. *Mar. Res.* **1976**, *34*, 511.
- (5) Anderson, D. M.; Morel, F. M. M., *Limnol. Oceanogr.* **1978**, *23*, 283.

- (6) Surda, W. G.; Gillespie, P. A. *J. Mar. Res.* **1979**, *37*, 761.
- (7) Jackson, G. A.; Morgan, J. J., *Limnol. Oceanogr.* **1978**, *23*, 268.
- (8) Gavis, J.; Guillard, R. R. L.; Woodward, B. L. *J. Mar. Res.* **1981**, *39*, 315.
- (9) Wagemann, R.; Barica, J. *Water Res.* **1979**, *13*, 515.
- (10) Hanson, J. M.; Stefan, G. H. *Water Resour. Bull.* **1984**, *20*, 889.
- (11) Swaileh, J. A. Ph.D. Thesis, Department of Chemistry, University of Alberta, Edmonton, Alberta, Canada, 1986.
- (12) Laitinen, H. A.; Harris, W. E. *Chemical Analysis*, 2nd ed.; McGraw-Hill: New York, 1975; Chapter 11.
- (13) Helfferich, F. *Ion Exchange*; McGraw-Hill: New York, 1962; Chapter 5.
- (14) Blaedel, W. J.; Dinwiddie, D. E. *Anal. Chem.* **1974**, *46*, 873.
- (15) Gulens, J.; Leeson, P. K.; Seguin, L. *Anal. Chim. Acta* **1984**, *156*, 19.
- (16) Martell, A. E.; Smith, R. M. *Critical Stability Constants*, Vol. 5: *First Suppl.*; Plenum: New York, 1985.
- (17) Martell, A. E.; Smith, R. M. *Critical Stability Constants*, Vol. 4: *Inorganic Complexes*; Plenum: New York, 1976.
- (18) Bips, U.; Ilias, H.; Hauröder, M.; Kleinhans, G.; Pfeifer, S.; Wannowius, K. J. *Inorg. Chem.* **1983**, *22*, 3862.
- (19) Bjerrum, J. *Acta Chem. Scand.* **1964**, *18*, 843.
- (20) Perrin, D. D.; Sayce, I. G. *Talanta* **1967**, *14*, 833.
- (21) Martell, A. E.; Smith, R. M. *Critical Stability Constants*, Vol. 3: *Other Organic Ligands*; Plenum: New York, 1977.
- (22) Perrin, D. D. *Stability of Metal-Ion Complexes, Part B, Suppl. 2: Organic Ligands*; IUPAC Chemical Data Series No. 22; Pergamon: Oxford, 1979.
- (23) Martell, A. E.; Smith, R. M. *Critical Stability Constants*, Vol. 1: *Amino Acids*; Plenum: New York, 1974.
- (24) Högfeldt, E. *Stability Constants of Metal-Ion Complexes, Part A: Inorganic Ligands*; IUPAC Chemical Data Series No. 21; Pergamon: Oxford, 1982.
- (25) Kelland, J. J. *Am. Chem. Soc.* **1937**, *59*, 1675.
- (26) Davies, C. W. *J. Chem. Soc.* **1938**, 2093.
- (27) Lewenstam, A.; Sokalski, T.; Hulanicki, A. *Talanta* **1985**, *32*, 531.
- (28) Westal, J. C.; Morel, F. M. M.; Hume, D. N. *Anal. Chem.* **1979**, *51*, 1792.
- (29) Lanza, P. *Anal. Chim. Acta* **1979**, *105*, 53.
- (30) Saar, R. A.; Weber, J. H. *Environ. Sci. Technol.* **1982**, *16*, 510A.
- (31) Gamble, D. S.; Marinsky, J. A.; Langford, C. H. In *Ion Exchange and Solvent Extraction*; Marinsky, J. A., Marcus, Y., Eds.; Marcel Dekker: New York, 1985; Vol. 9 Chapter 7.
- (32) Gamble, D. S. *Can. J. Chem.* **1972**, *50*, 2680.
- (33) Buffle, J. *Anal. Chim. Acta* **1980**, *118*, 29.
- (34) Motkosky, N., Department of Chemistry, University of Alberta, private communication, 1985.
- (35) Neubecker, T. A.; Allen, H. E. *Water Res.* **1983**, *17*, 1.
- (36) Papineau, M.; Inland Waters Directorate—Quebec Region, Environment Canada, private communication, 1985.
- (37) Murdoch, A.; Arafat, N.; Davies, S. *Environ. Technol. Lett.* **1984**, *5*, 237.

RECEIVED for review August 21, 1986. Accepted October 16, 1986. This work was supported by the Natural Sciences and Engineering Research Council of Canada and by the University of Alberta.

# Direct Atomic Emission Determination of Some Trace Metals in Solid Powder Samples with a Magnetically Tailored Capacitive Discharge Plasma

David Albers<sup>1</sup> and Richard Sacks\*

Department of Chemistry, University of Michigan, Ann Arbor, Michigan 48109

**A magnetic field is used to alter the structure of the plasma produced by the electrical vaporization of a 40 nm thick, 350  $\mu\text{g}$  silver film. The films are vacuum deposited on plastic substrates. The sample, as a particle suspension in isopropyl alcohol, is applied to the film surface and vaporized along with the film by interaction with the hot plasma gases. A magnetic field of a few kilogauss results in a significant drift motion of the plasma. This reduces the rate of plasma expansion, improves positional stability, and dramatically increases the rate of sample atomization. In addition, continuum background radiation is more localized near the substrate surface, and increased line-to-background ratios are obtained if this region is masked. General analytical features of the plasma are discussed and analytical data presented for several NBS solid powder reference materials. Relative errors typically are in the 5-10% range.**

Sample preparation for nonmetallic solids prior to elemental analysis by atomic spectroscopy may be lengthy, complex, and prone to sample loss and contamination. Direct methods, which eliminate matrix exchange and solution operations, may be much more rapid and less prone to contamination and loss. However, concomitant effects and particle size biasing of analytical data have frustrated development of these methods (1-4).

Goldberg and Sacks (5) used a novel plasma generation technique for the direct determination of some trace metals in solid, powder samples. Their method uses a capacitive discharge with total energy of about 1 kJ to vaporize a thin Ag film and generate a high-temperature plasma in the Ag vapor. A 1.0-mg powder sample deposited on the thin film surface is atomized by interaction with the hot plasma gases. Metallic elements in the sample are determined by measuring atomic emission intensities in the luminous, transient plasma. When circuit inductance is increased to about 1200  $\mu\text{H}$ , sample particles as large as 30  $\mu\text{m}$  are atomized completely. However, nearly 2 ms may be required to atomize these larger sample particles. To prevent particle size biasing, intensity integration must be delayed until the entire sample is atomized. During this measurement delay, rapid plasma expansion results in significant loss of sample vapor and increased plasma instability (6).

Recently, Albers and Sacks used a magnetic field to confine and stabilize the electrically vaporized thin film plasma (7) and increase analysis-line-to-background ratios (8). The magnetic field is generated by the plasma current in a large inductor. The magnetic field is oriented normal to the plasma electric field and produces an  $E \times B$  drift motion of the plasma ions and electrons. The drift motion moves the plasma toward the plastic substrate which originally supported the Ag film and the powder sample. This increases the plasma-sample

interaction and reduces sample atomization time typically by a factor of 5-10. Since the region of intense continuum background radiation also is more localized near the substrate surface, greater analysis-line-to-background ratios are obtained for neutral-atom emission lines if this region is optically masked.

In the study reported here, this magnetically altered plasma is used as a sample cell and excitation source for the direct determination of some trace metallic elements in National Bureau of Standards reference materials including opal glass (SRM-91), portland cement (SRM-635), urban particulates (SRM-1648), river sediments (SRM-1645), bauxite (SRM-696), and spinach leaves (SRM-1570). These materials were chosen because they represent cases where extensive sample preparation usually is required to obtain a representative solution for the determination of metallic elements by conventional atomic emission or atomic absorption techniques.

## EXPERIMENTAL SECTION

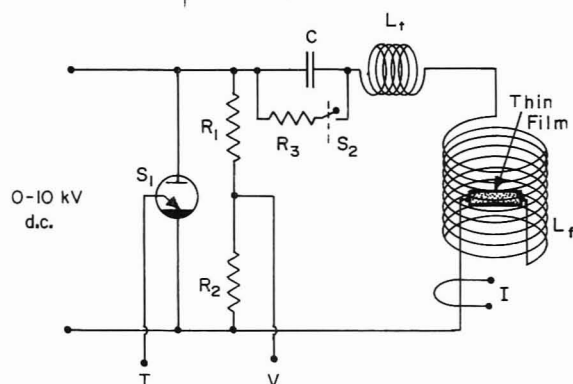
**Experiment Design.** Efficient interaction of the plasma with the sample requires that the drift motion of the plasma be directed toward the substrate which originally supported the thin film and the sample. The drift motion is normal to the plane defined by the magnetic field  $B$  and the electric field  $E$  in the plasma (vector cross product). This is called an  $E \times B$  drift (9, 10). Since the plasma is generated by capacitive discharge through an underdamped RCL tank circuit, the discharge current oscillates, and the electric field in the plasma changes direction by 180° for each half-cycle of the discharge current. By use of the plasma current to generate the magnetic field in a coil surrounding the plasma, the magnetic field direction also will change by 180° for each half-cycle, and the drift motion will be in the same direction for the entire duration of the discharge. In the present study, the coil axis was oriented normal to the electric field in the plasma, and the drift motion was directed toward the sample on the substrate surface. Radiation is viewed parallel to the coil axis.

**Apparatus.** Figure 1 shows important features of the high-voltage RCL tank circuit used to vaporize the thin Ag film and generate the high-current plasma in the Ag vapor. The 30- $\mu\text{F}$  capacitor,  $C$ , is charged to 5-10 kV by a high-voltage power supply. In addition to the capacitor, the discharge loop contains tuning inductor  $L_t$ , field-producing inductor  $L_f$ , the thin Ag film, and high-current ignitron switch  $S_1$ . A trigger pulse at point T drives the ignitron into conduction and thus initiates the discharge. Characteristics of the ignitron and its trigger circuit are provided elsewhere (11). Discharge current is monitored with a Pearson Model 1025 wide-band current probe (I), and the capacitor charging voltage is monitored at point V with the  $R_1$ - $R_2$  voltage divider and a DVM. High-current relay-type switch  $S_2$  together with resistor  $R_3$  is used to discharge the capacitor without vaporizing the thin film.

Inductor  $L_f$  was constructed from 25 turns of AWG-14 gauge solid copper wire which was cast in a rigid epoxy cylinder. The coil is 12.5 cm long and 19 cm in diameter. This inductor was designed to slip easily on or off the cylindrical nylon discharge chamber so that plasma properties with and without the magnetic field could be compared directly. However, the coil was always in the discharge circuit in order to maintain a constant inductance. The total circuit inductance is adjusted by air-core inductor  $L_t$ . For the studies reported here, a high-inductance discharge with

<sup>1</sup> Present address: Dow Chemical Co., Midland, MI.





**Figure 1.** High-current capacitive discharge circuit containing field-producing inductor,  $L_f$ , and tuning inductor,  $L_t$ . Other components are discussed in the text.

**Table I. Circuit Parameters and Discharge Conditions**

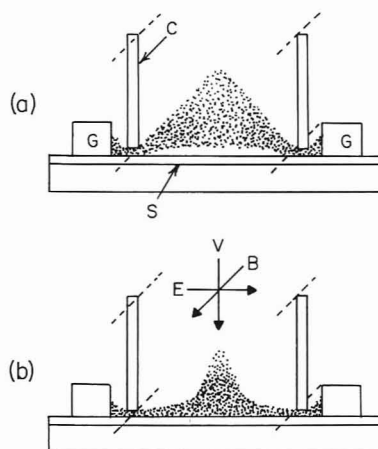
	low inductance	high inductance
charging voltage, kV	6.0	8.0
capacitance, $\mu\text{F}$	30	30
energy, J	540	960
circuit inductance, $\mu\text{H}$	105	940
peak current, kA	2.8	1.2
ringing frequency, kHz	2.8	0.95
peak magnetic field, kG	3.7	1.7
plasma support gas pressure	Ar (60%)/O <sub>2</sub> (40%) atmospheric	

$L_t = 835 \mu\text{H}$  and a low-inductance discharge with  $L_t = 0$  were evaluated. Table I summarizes the circuit parameters and discharge conditions for the two values of circuit inductance. Note that the peak current of the low-inductance discharge is more than twice as large as that of the high-inductance discharge despite the higher charging voltage of the latter.

The cylindrical nylon discharge chamber is similar to previous designs (12) except the cylinder axis is oriented parallel to the optical axis and normal to the current channel through the thin film and the plasma. Radiation was viewed through quartz windows in the chamber end plates. The plastic cassette used to support the thin film and substrate and provide electrical contact by graphite electrodes also was similar to previous designs (13).

Photographic spectra and photoelectric intensity measurements were obtained with a 1.0-m Czerny-Turner spectrometer used in the first order with a 1200 line/mm grating and equipped with a 1P28 photomultiplier tube. The tube usually was biased at about 600 V and used a 1.0-k $\Omega$  load in a current follower circuit. The output from the current follower could be displayed on a Nicolet 2090-III digital storage oscilloscope or integrated over any specified time gate using a gated integrator circuit (14). The output from the Pearson current transducer was displayed on the oscilloscope simultaneously with the photomultiplier signal. Photographic spectra for analysis line selection were obtained with Kodak SA#1 plates which were processed as per manufacturer recommendations. Spatially resolved spectra were obtained by use of an astigmatism-corrected optical system (13).

**Procedures.** Thin Ag films were prepared on polyethylene substrates as described previously (15). All films were 7.3 cm × 1.6 cm × 40 nm thick and weighed about 350 μg. All standard reference material (SRM) samples were examined with an electron microscope, and when necessary, materials were ground in a small mill to reduce particle size to under about 30 μm in diameter. Grinding times of 10–20 min were typical. Analytical standards were deposited on the thin films as aqueous solutions or as solid powders suspended in isopropyl alcohol. All SRM samples also were deposited as powder suspensions in isopropyl alcohol. Typically, a 0.5-mg sample of SRM was used for each determination. A disposable tip micropipet was used to transfer a 10–50-μL aliquot of solution or suspension. To obtain adequate uniformity, a suspension was rapidly stirred with a vortex stirrer while an aliquot was drawn. All experiments were conducted at



**Figure 2.** Drawings of the confinement cell and the plasma without (a) and with (b) an external magnetic field in an  $E \times B$  configuration. The vector diagram shows the orientation of the external magnetic field  $B$ , the plasma electric field  $E$ , and the drift motion  $V$ . Also shown are the following: G, graphite electrodes; S, plastic substrate supporting thin film and sample; C, walls of the plastic confinement cell.

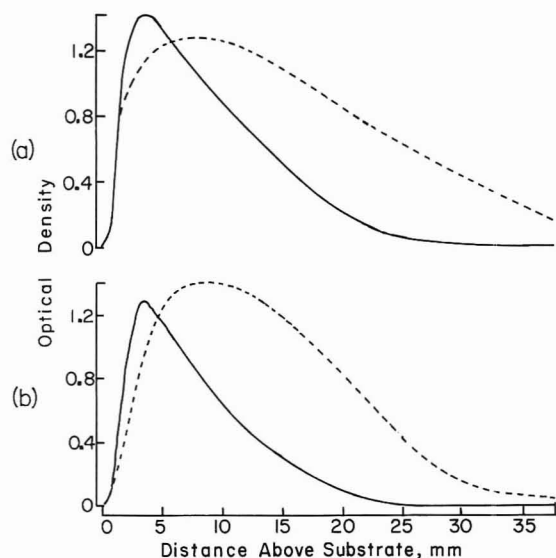
atmospheric pressure in a 60% Ar/40% O<sub>2</sub> gas mixture flowing through the chamber at 5 L/min. For all analytical studies, intensity values were averaged from four replicate determinations. For background correction, the average intensity from four blank determinations (bare Ag film) at the analysis wavelength was subtracted from the total average intensity.

## RESULTS AND DISCUSSION

**General Plasma Properties.** Time-integrated photographs of the plasma with and without the magnetic field (13) show that the plasma is significantly more localized near the substrate surface when the magnetic field is present. A nearly scaled drawing of the plasma and its physical environment is presented in Figure 2. The plasma is partially confined by a polycarbonate plastic cell. The plasma makes contact with the electrodes by passing through a pair of slots in the cell. Without the magnetic field (part a), the plasma expands freely in the vertical direction and forms a rather angular structure with a peak typically 2 cm from the substrate surface. The base of the plasma may not be in close contact with the substrate surface. With the field present (part b), the plasma is much more localized near the substrate surface, and it appears to be in direct contact with the substrate. It is not known if the plume near the center of the plasma is a real feature or a reflection artifact.

Continuum background radiation intensity integrated over the entire duration of the discharge and over the plasma volume is about a factor of 2 lower with the field present. Figure 3 shows microdensitometer traces from spatially resolved photographic spectra both with (solid lines) and without (broken lines) the magnetic field. Densitometer scans were made normal to the wavelength axis in a line-free region and thus reflect variations in continuum background intensity with respect to distance from the substrate surface. The top traces (part a) were obtained with the low inductance circuit, and the bottom traces (part b) were obtained with the high inductance circuit (see Table I).

Note that the low inductance discharge has a peak current in the first half cycle of about 2.8 kA and lasts about 1.3 ms; while the high inductance discharge has a peak current of 1.2 kA and lasts about 3 ms. In both cases, the presence of the magnetic field results in significantly greater localization of the most intense continuum background. This effect is somewhat more pronounced with the high-inductance discharges. Emission lines from ionized species of the Ag thin film material and the powder sample respond to the magnetic field in a similar fashion. That is, peak ion line intensities



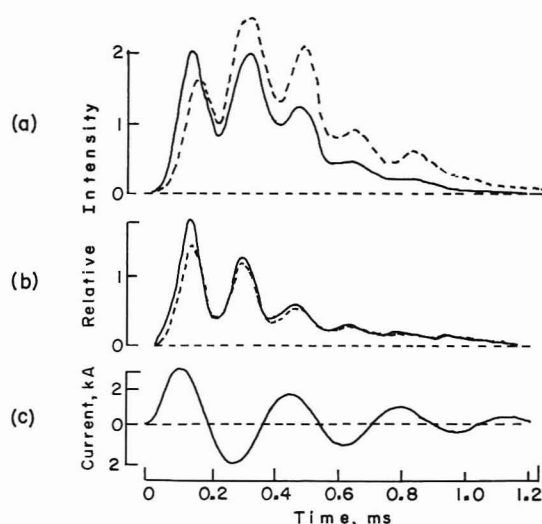
**Figure 3.** Continuum background microdensitometer traces from spatially resolved, time-integrated photographic spectra with (solid lines) and without (broken lines) the external magnetic field: (a) low-inductance discharges; (b) high-inductance discharges.

occur nearer to the substrate surface in the presence of the magnetic field. Emission line intensities from neutral-atom species, however, are less affected by the magnetic field and are more uniform over the 38 mm high observation window. These data suggest that optically masking the region of the plasma near the substrate surface may be useful in increasing analysis-line-to-background intensity ratios for neutral-atom lines.

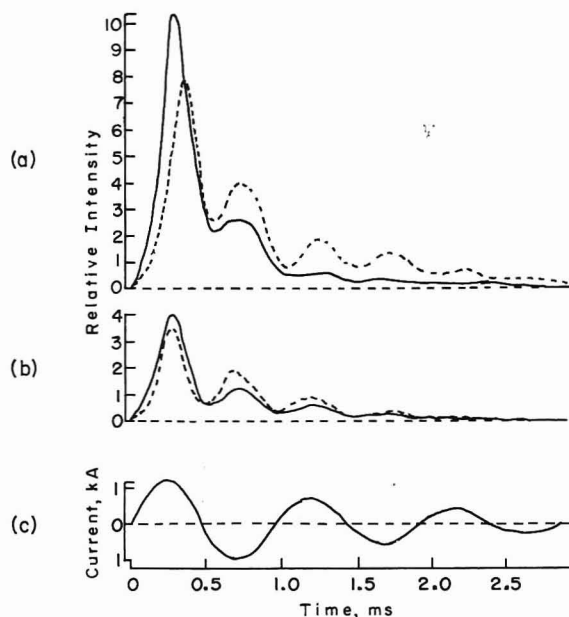
**General Analytical Features.** General analytical features of electrically vaporized thin films as atom cells and excitation sources for analytical atomic spectroscopy have been discussed in detail (5, 15, 16). Goldberg and Sacks (5) were able to minimize particle size and sample loading effects to the point where almost any sample particle less than about 30  $\mu\text{m}$  in diameter could be completely atomized in about three current half cycles of their 1200- $\mu\text{H}$  discharge. This corresponds to about 1.8 ms. More severe particle size effects were observed at lower circuit inductance despite a nearly 5-fold increase in peak discharge current.

Concomitant effects with electrically vaporized thin film atomic emission analysis generally have been sufficiently modest that matching the standard matrix to the sample matrix has been unnecessary (5, 15). Figure 4 shows radiation intensity vs. time profiles for the Mn 259.4 nm ion line from aqueous solution residues of  $\text{MnSO}_4 \cdot 7\text{H}_2\text{O}$  (solid lines) and powder suspension samples of SRM-1570 (broken lines). No spatial resolution was used, and the spectrometer viewed the entire plasma volume. The upper pair of profiles was obtained without the magnetic field and the lower pair with the magnetic field. All profiles were obtained from low-inductance discharges. Each profile is corrected for continuum background and is an average for four separate experiments. In all cases, the sample contained 83 ng of Mn.

The presence of the magnetic field results in a significant decrease in intensity for both the SRM and the aqueous residue sample. However, since continuum background intensity also is reduced in the magnetically confined plasma (7, 13), line-to-background intensity ratios may be larger in some cases. Without the field present, peak intensity from the SRM sample does not occur until the second half-cycle of the discharge current. With the field, the peak intensity occurs during the first half-cycle. This suggests that sample atomization is more rapid in the magnetically confined plasma. With the field present, the profiles for the SRM and the aqueous standard nearly coalesce after the first current half



**Figure 4.** Radiation intensity-time profiles for low-inductance discharges without (a) and with (b) the external magnetic field. The Mn II 259.4-nm line was monitored from 0.50-mg samples of SRM-1570 (broken lines) and from aqueous residues of  $\text{MnSO}_4$  containing the same amount of Mn (solid lines). The discharge current waveform (c) is shown to provide a time reference.



**Figure 5.** Radiation intensity-time profiles for high-inductance discharges without (a) and with (b) the external magnetic field. The Mn II 259.4-nm line was monitored from 0.50-mg samples of SRM-1570 (broken lines) and from aqueous residues of  $\text{MnSO}_4$  containing the same amount of Mn (solid lines). The discharge current waveform (c) is shown to provide a time reference.

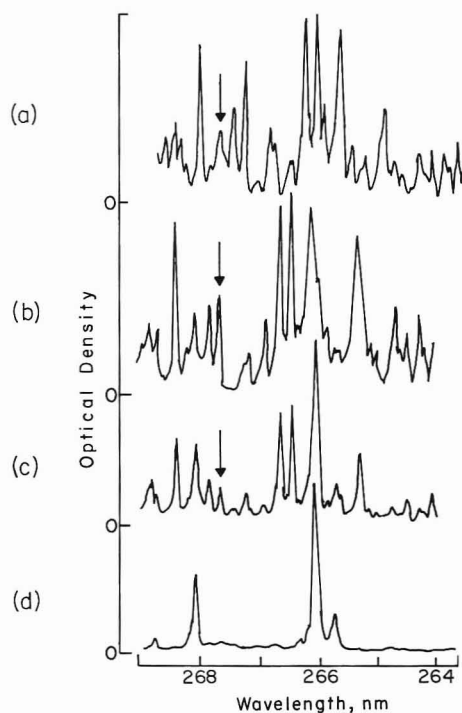
cycle or about 0.17 ms after the start of the discharge. Thus, if intensity integration is delayed until after the end of the first half-cycle, the aqueous standard should be quite satisfactory. Without the magnetic field, intensity from the aqueous residue sample is significantly lower than that from the SRM during most of the discharge duration, and thus there is no satisfactory measurement time interval for which aqueous standards would be satisfactory. Particle size studies with single-component powder samples (7) suggest that intensity integration should be delayed about two current half-cycles to adequately reduce particle size biasing for more refractory materials.

Figure 5 shows similar intensity-time profiles for high-inductance discharges. Again, the presence of the magnetic field results in a significant decrease in radiation intensity. While the profiles for the SRM sample and the solution standard are more nearly similar with the magnetic field, they are not



**Table II. Standard Materials, Analysis Lines, and Detection Limits**

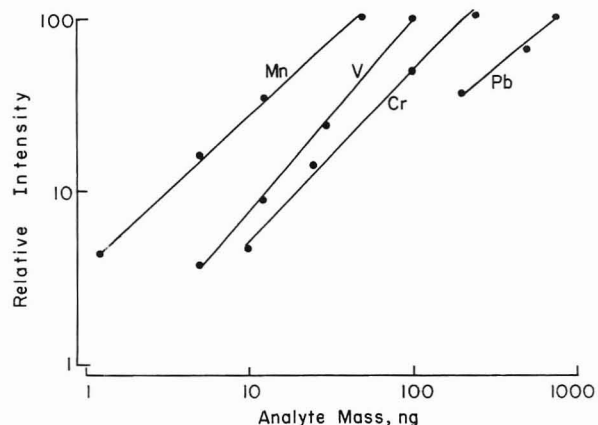
element	compound	analysis line, nm	log-log slope	corr coeff	detection limit, ng
Cr	K <sub>2</sub> Cr <sub>2</sub> O <sub>7</sub>	II 267.7	0.94	0.996	2.4
Mn	MnSO <sub>4</sub> ·7H <sub>2</sub> O	II 259.4	0.85	0.997	2.2
Mn	Mn	II 259.4	<i>a</i>	<i>a</i>	<i>a</i>
V	NH <sub>4</sub> VO <sub>3</sub>	II 310.2	1.09	0.998	1.6
Pb	Pb(NO <sub>3</sub> ) <sub>2</sub>	II 220.4	0.74	0.987	42

<sup>a</sup> Analytical curve was nonlinear.**Figure 6.** Microdensitometer traces from photographic spectra of some NBS reference materials: (a) urban particulates (SRM-1648); (b) bauxite (SRM-696); (c) portland cement (SRM-635); (d) bare silver film. The Cr II 267.7-nm analysis line is indicated by arrows.

as similar as for the low-inductance discharges with the magnetic field. Thus, when the magnetic field is used to slow plasma expansion and increase sample-plasma interaction, lower circuit inductance and its attendant increased plasma current and magnetic field strength (see Table I) may be more useful for the direct analysis of solid powder samples using aqueous solution standards. This is in contrast with earlier work without magnetic field confinement (5) where high circuit inductance was preferred for this applications.

**Analysis of NBS Materials.** Selected elements were determined in the SRM samples using the magnetically confined plasmas from low-inductance discharges. A 5 mm wide region starting at the substrate surface was masked, and radiation intensity integration was delayed until the start of the third discharge current half-cycle or about 0.34 ms after the start of the discharge. Analytical curves were constructed for Mn, Cr, V, and Pb using the materials listed in Table II. These materials were chosen based only on availability. Aqueous solutions were used in all cases except for the Mn metal powder which was used as a suspension in isopropyl alcohol of particles which passed through a 5-μm pore diameter sieve.

Analysis lines also are listed in Table II. These lines were chosen after detailed study of photographic spectra of all NBS materials. Microdensitometer traces of portions of these spectra for urban particulate material (a), bauxite (b), portland

**Figure 7.** Analytical curves used for the determination of selected metallic elements in NBS standard reference materials. Compounds and analysis lines are listed in Table II.**Table III. Analysis Results for NBS Materials**

NBS standard	element	amt found, <sup>b</sup> ppm	NBS value, <sup>c</sup> ppm	% rel error
bauxite (SRM 696)	Mn	28.1 ± 3.5	31 ± 8	-9.4
	Cr	351 ± 72	320 ± 22	+9.9
	V	390 ± 53	400 ± 12	-2.5
river sediments (SRM 1645)	Mn	837 ± 28 <sup>a</sup>	785 ± 97	+6.6
	V	25.3 ± 3.8	23.5 ± 6.9	+7.7
opal glass (SRM 91)	Pb	796 ± 173	714 ± 28	+11.5
	Pb	867 ± 123	930	-6.8
portland cement (SRM 635)	Mn	662 ± 116 <sup>a</sup>	630 ± 70	+5.1
	Cr	74.4 ± 12.8	68	+9.4
urban particulates (SRM 1648)	Cr	420 ± 117	403 ± 12	+4.3
	Pb	6070 ± 290	6550 ± 80	-7.3
spinach (SRM 1570)	Mn	171 ± 31	165 ± 6	+3.6

<sup>a</sup> Powder standards used. <sup>b</sup> Average ± standard deviation for four determinations. <sup>c</sup> ± values are intermethod ranges reported by NBS.

cement (c) and a bare Ag film (d) are shown in Figure 6. The arrows in the SRM spectra indicate the Cr ion line at 267.7 nm. For the complex solid matrices of these materials, the spectra are very line-rich, and the qualitative aspects of analysis line selection are nontrivial. In many cases, the most intense lines were unusable because of significant line interference problems. Greater wavelength dispersion certainly would be useful here.

Figure 7 shows the analytical curves used for the SRM analyses. Table II lists the log-log slopes and correlation coefficients for the analytical curves as well as the detection limits (signal-to-noise ratio = 3.0). These detection limits are single channel values where the shot-to-shot variation in continuum background intensity for bare Ag films is the principal noise source.

Table III presents the SRM analysis data for 0.50-mg samples. Relative errors generally are in the 5–10% range. Aqueous standards were used in all cases except for the Mn determinations in SRM-1645 and SRM-635. For these cases, the amounts of Mn found with the aqueous standards were about 25% higher than the NBS values. The reason for this is unclear, but the use of the small-particle powder suspension standards reduced the relative errors to +6.6% and +5.1%, respectively. With these Mn values, the average error magnitude for the 12 determinations is 7.0%. This is quite satisfactory for a rapid, direct, single-channel method requiring little if any attention to matching the composition of the

samples and the analytical standards.

The data in Table III suggest that the very simple techniques used for sample introduction can provide reasonably accurate results even for samples as small as 0.5 mg. It should be noted that NBS typically recommends a 1-g sample. The shot-to-shot reproducibility of analyte line intensities from the SRM samples is not significantly poorer than from the aqueous or the powder standards. This indicates that inhomogeneity of the NBS powder materials is not the principal source of measurement variance. Plasma instability and refractive index gradients (thermal lens) probably are the principal variance sources.

The use of an external magnetic field with the electrically vaporized thin film plasma technique significantly increases the rate of solid sample atomization, reduces particle size biasing, and improves analytical accuracy. While analysis-line-to-background intensity ratios and powers of detection typically are a factor of 2-10 greater with the magnetic field for the discharge conditions used in this study, powers of detection are not significantly greater than for previous work using much larger circuit inductance (5).

While delayed intensity integration has relatively little effect on line-to-background ratios, continuum background reproducibility is poorer with delayed integration. The result is poorer powers of detection. Detection limits can be reduced by a factor of 10 in some cases if intensity integration begins at the start of the discharge (7). However, this will result in increased particle size biasing. Thus, to preserve accuracy, either more elaborate standardization techniques or reduced sample particle size will be required.

The data presented here clearly show that a relatively modest magnetic field can significantly alter the analytical characteristics of these high-current plasmas. While significantly greater sample-plasma interaction occurs in the  $E \times B$  plasma-magnetic field configuration, confinement of the plasma by the magnetic field is very inefficient. There are

two reasons for this. First, as the  $E \times B$  drift motion compresses the plasma in the vertical direction, the plasma responds by expanding in the direction normal to the drift motion (see Figure 2). Since there is no mechanical confinement in the direction parallel to the optical axis, the plasma expands significantly in this direction. This can result in earlier loss of sample vapor (8) and increased self-absorption (7). Second, the magnetic field strength is proportional to plasma current. Thus, at the end of each current half-cycle the field vanishes, and for a short time, free expansion of the plasma occurs. More efficient plasma confinement may further reduce particle size biasing and obviate the need for delayed radiation measurements.

**Registry No.** Cr, 7440-47-3; Mn, 7439-96-5; V, 7440-62-2; Pb, 7439-92-1; bauxite, 1318-16-7.

## LITERATURE CITED

- (1) Dagnall, R. M.; Smith, D. J.; West, T. S. *Anal. Chim. Acta* **1976**, *54*, 397.
- (2) Ng, K. C.; Caruso, J. A. *Anal. Chem.* **1984**, *56*, 417.
- (3) Page, A. G.; Godbole, S. V.; Madraswala, K. H.; Kulkarni, M. J.; Mallapurkar, V. S.; Joshi, B. D. *Spectrochim. Acta, Part B* **1984**, *39B*, 551.
- (4) Lorber, A.; Goldbart, A. *Analyst (London)* **1985**, *110*, 155.
- (5) Goldberg, J.; Sacks, R. *Anal. Chem.* **1982**, *54*, 2179.
- (6) Collins, R.; Sacks, R. *Anal. Chem.* **1983**, *55*, 2179.
- (7) Albers, D.; Sacks, R., submitted for publication in *Appl. Spectrosc.*
- (8) Albers, D.; Sacks, R. *Spectrochim. Acta*, in press.
- (9) Chen, F. F. *Introduction to Plasma Physics*; Plenum: New York, 1974.
- (10) Boyd, T. J. M.; Sanderson, J. J. *Plasma Dynamics*; Barnes and Noble: New York, 1969.
- (11) Suh, S. Y.; Collins, R. J.; Sacks, R. D. *Appl. Spectrosc.* **1981**, *35*, 42.
- (12) Duchane, D. V.; Sacks, R. D. *Anal. Chem.* **1978**, *50*, 1752.
- (13) Albers, D.; Johnson, E.; Tisack, M.; Sacks, R. *Appl. Spectrosc.* **1986**, *40*, 60.
- (14) Swan, J.; Sacks, R. *Appl. Spectrosc.* **1985**, *39*, 704.
- (15) Clark, E. M.; Sacks, R. D. *Spectrochim. Acta, Part B* **1980**, *35B*, 471.

RECEIVED for review May 16, 1986. Accepted October 16, 1986. This work was supported by the National Science Foundation through Grant No. CHE 8411290.

# Membrane Interface for Selective Introduction of Volatile Compounds Directly into the Ionization Chamber of a Mass Spectrometer

M. E. Bier and R. G. Cooks\*

Department of Chemistry, Purdue University, West Lafayette, Indiana 47907

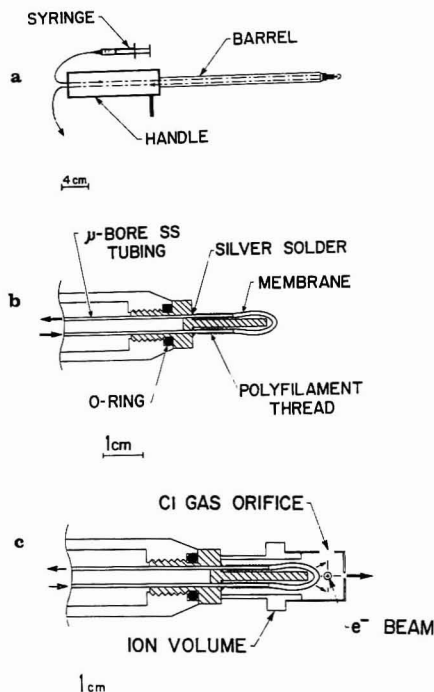
**A direct insertion membrane probe has been designed for the selective introduction of organic molecules from aqueous solutions, into a mass spectrometer. The probe transfers analyte directly into the ionization chamber from a fluid flowing within a capillary membrane. High sensitivity is obtained by placing the membrane in close proximity to the ionization region where the elevated source temperature enhances analyte permeation, improving response time and decreasing memory effects. Mass spectra and daughter spectra of a simple aqueous mixture of small alcohols and ketones, and of small oxygenated molecules in fermentation broth samples, are reported by using the interface with a tandem mass spectrometer.**

The selective introduction of components of a fluid into a mass spectrometer is a long-standing problem. Successful

devices include various types of membrane separators that have attractive features for monitoring organic compounds in aqueous media. These devices have allowed trace solution analysis (1-6), gas analysis (7, 8), and in vivo studies (1, 9, 10) particularly for low molecular weight molecules. They have also been applied to reaction monitoring, including indirect analysis of particular components through secondary product detection (5, 11, 12). Westover and co-workers used a hollow fiber device (1) and several others (2-6, 11, 13) have used membranes configured into films as is done in the gas chromatograph/mass spectrometer (GC/MS) interface of Littlejohn and Llewellyn (14).

All of these designs position the membrane exterior to the mass spectrometer ion source. In fact, recently, film membrane probes have been located inside fermentors (13, 15-19). Condensation along transfer lines can cause poor response times (15), memory effects, and analyte dilution for these otherwise useful configurations. In addition to the problems





**Figure 1.** (a) Direct insertion membrane probe (DIMP) showing sample introduction and the fluid flow in the system. (b) Cross section of the tip of the DIMP, showing coupling of capillary tubing to stainless steel inlet and outlet lines. (c) Cross section of the tip inserted into an EI or CI ion volume.

caused by the distance the analyte must travel to reach the source, room-temperature interfaces often give poor response times (1–5 min) (18) and suffer from memory effects due to low permeation rates. We describe here a new type of probe that allows the analyte solution, contained in a capillary membrane, to be transported directly into and through the heated ion source. This method of transporting the solution appears to have distinct advantages (18, 19) over vapor-phase analyte transport from a distant membrane. By use of this approach with tandem mass spectrometry, direct and continuous mixture analysis is facilitated.

## EXPERIMENTAL SECTION

**Description of the Device.** The direct insertion membrane probe (DIMP) is shown in Figure 1a. The handle and probe barrel of the DIMP were adapted from a Finnigan MAT ion-volume insertion/removal tool. The machined probe tip was designed to insert into a modified ionization volume as shown in Figure 1b,c. The membrane loop may be located within 1 mm of the electron beam. The interchangeable tip screws onto the probe barrel and is sealed with a viton O-ring. Two 50-cm lengths of stainless steel microbore tubing (0.51-mm o.d. × 0.13-mm i.d.) were silver-soldered into the barrel of the probe tip leaving 1 cm of inlet and exit line extending from its base. The membrane itself is a capillary tube (0.94-mm o.d., 0.51-mm i.d.) made of a dimethyl vinyl silicone polymer (ASTM: VMQ; Dow Corning). It is pushed over the stainless steel tubes at both ends forming a loop some 15 mm long. A polyfilament thread, coiled around each end of the membrane, secures the capillary membrane to the probe tip. Additional thread is coiled around the post and the 1-cm inlet and exit lines to increase the positional stability of the microbore tube. The post on the probe tip can also serve as a mount to attach the membrane when greater lengths are employed in order to increase surface area. The configuration shown in Figure 1 has an exposed internal membrane surface area of 24 mm<sup>2</sup> and a membrane internal volume of 3 μL.

The fluid flow in the system can be continuous, for steady-state determination, or segmented with solvent (e.g., water) as in flow injection analysis (FIA). Solution enters the probe through the inlet line and flows through the membrane located in the ionization chamber. Components of the analyte permeate the membrane and are ionized, while the remaining solution passes

out through the exit stainless steel line. Flow rates up to 0.7 mL/min have been achieved. The total internal volume of the whole device is less than 50 μL and the dead volume is negligible.

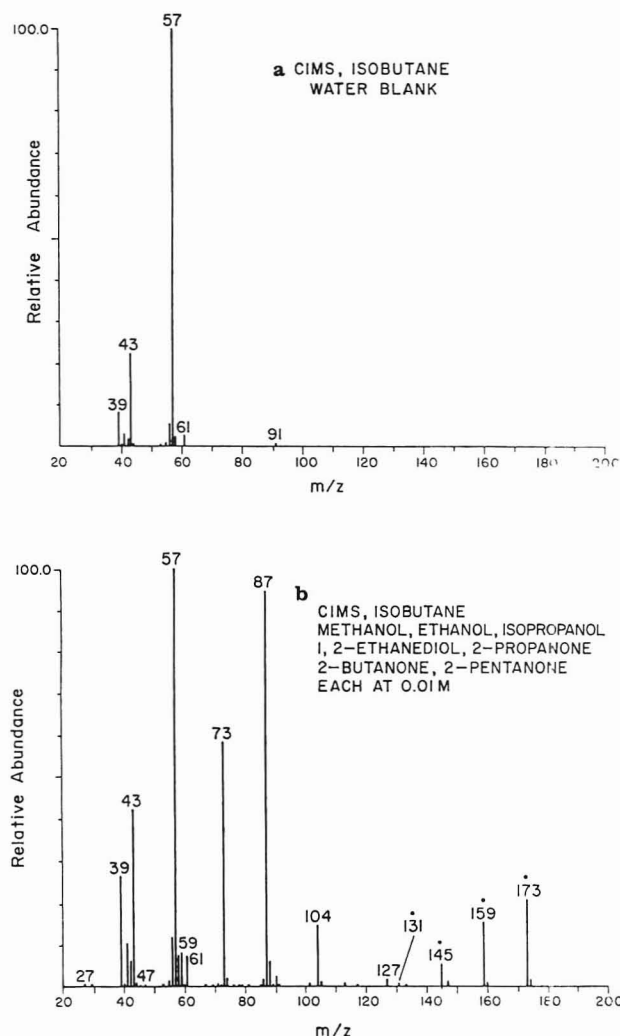
The DIMP may be heated to a constant temperature to enhance permeation rates, eliminate condensation, and decrease memory effects. The temperature of the DIMP tip after insertion into the source is not measured directly, but, at a constant liquid flow rate, it should be constant and below the source block temperature. The DIMP temperature is maintained by conduction of heat from source to probe tip and by radiant heat from the ion volume that is in intimate contact with the source block.

**Tests of the Probe.** Two types of samples were examined: one, a simple aqueous mixture of alcohols and ketones, and the second, various fermentation broths. The simple aqueous mixture contained methanol, ethanol, 2-propanol, 1,2-ethanediol, 2-propanone, 2-butanone, and 2-pentanone, each at a concentration of 0.01 M. The sample was continuously injected during the course of analysis to maintain steady-state conditions. Following and preceding each analyte run, a water plug was injected and analyzed. The water plug allows time for the signal to return to base line as residual molecules diffuse from the membrane. The broth on which most work was done was *Klebsiella oxytoca* cultured in PA medium with 200 g/L of xylose. A sample of the broth was centrifuged, filtered through a 0.2 μM filter, and then continuously injected into the DIMP for a steady-state analysis. Mass spectra and daughter spectra were recorded by using a triple quadrupole mass spectrometer (Finnigan MAT TSQ 4500) (20) operated via an INCOS data system. All samples were ionized by chemical ionization (CI) at a pressure of 0.4 torr. Isobutane was used as the reagent gas for the ketone alcohol mixture while methane was used in the fermentation broth experiments. The collision gas used to record the daughter spectra was argon at a pressure of 2 mtorr that corresponds to multiple-collision conditions. The collision energy was set at 20 eV.

## RESULTS AND DISCUSSION

The chemical ionization mass spectra (CIMS) of a water blank and of a seven-compound mixture (0.01 M each) of simple alcohols and ketones are shown in Figure 2. The blank spectrum shows only ions due to the reagent isobutane. Note the absence of peaks due to water that does not permeate the membrane. The mixture, introduced via the membrane probe, displays ions due to the individual components that are best seen by using CI. For example,  $m/z$  87 and 73 are assigned to protonated 2-pentanone and butanone, respectively. Note that cluster ions are also observed, e.g.,  $m/z$  173 is due to the proton-bound dimer of 2-pentanone and that some of the compounds do not give abundant ions in the mass spectrum. Even in these cases, the compounds in question can be characterized by recording daughter spectra. For example, even though the protonated 1,2-ethanediol molecule,  $m/z$  63, is barely observable in the mass spectrum (<1% relative abundance), it gives an excellent daughter spectrum when it is mass-selected and independently fragmented (Figure 3). The improvement (21) in signal-to-noise ratio observed in the tandem experiment results in a spectrum from the mixture that compares well with the daughter spectrum of the standard. While detection limits have not been measured for the membrane probe, they can be estimated to vary from ca. 10<sup>-3</sup> M for 1,2-ethanediol through 10<sup>-6</sup> M for 2-pentanone to below 10<sup>-6</sup> M for some hydrocarbons (21).

A sample of the *Klebsiella cerevisiae* broth was filtered and injected directly into the probe to yield the CIMS spectrum shown in Figure 4. Many of the ions are readily assigned; for example,  $m/z$  47 corresponds to protonated ethanol,  $m/z$  61 to protonated acetic acid, and  $m/z$  87 to protonated 2,3-butanediol. These assignments can be checked by obtaining daughter spectra on the individual ions. For example, the daughter spectra of  $m/z$  91 and 89 serve to identify the expected fermentation products, 2,3-butanediol and 2-hydroxy-2-butanone (acetoin), in the fermentation broth, Figure 5. This type of analysis suggests the possibility of

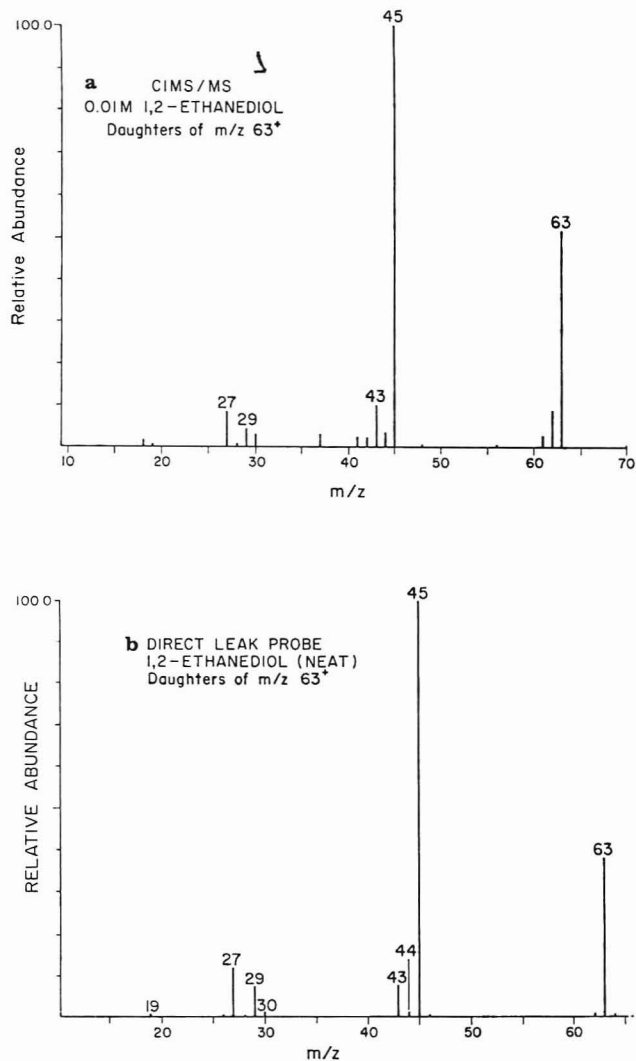


**Figure 2.** (a) Mass spectrum (CI, isobutane) of a water blank flowing through the capillary. (b) Mass spectrum of the mixture of 0.01 M each of methanol, ethanol, 2-propanol, 1,2-ethanediol, 2-propanone, 2-butanone, and 2-pentanone with  $(M + H)^+$   $m/z$  33, 47, 61, 63, 59, 73, and 87, respectively. Note the proton bound dimers (indicated with dots above the number).

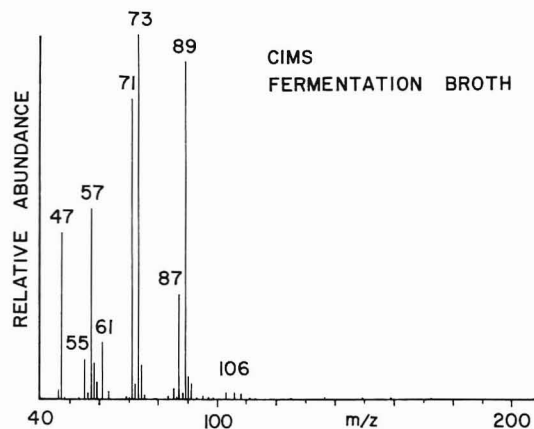
on-line monitoring of fermentation processes using the membrane probe and tandem mass spectrometer.

Some preliminary experiments have been done comparing the relative amounts of the small oxygenated compounds in different fermentation broths. Substantial difference are observed with the reactor conditions and microorganism type. For example, Figure 6, shows the results of screening for ethanol, monitoring dehydration of the protonated molecule ( $m/z$  47  $\rightarrow$   $m/z$  29), as a series of broths produced by five different organisms are successively introduced into the membrane probe. The expected large differences in ethanol levels are observed although precise quantitation will require the use of isotopically labeled standards as is commonly done in mass spectrometry.

The limitations of the device in its present state of development lie chiefly with the nonideal properties of the membrane. These limitations are (a) differential permeability, (b) zero permeability above a certain molecular size, and (c) finite response times associated with membrane transport. The first two limitations are essentially fixed by the choice of a particular membrane. The membrane selects only for small, nonpolar molecules and has a maximum transport size. Response time, however, may be decreased by avoiding transfer lines, by using a thinner walled capillary, or by heating the membrane. To characterize the dimethyl vinyl silicone capillary membrane, response times, rise times, and fall times



**Figure 3.** (a) Daughter spectrum of glycol  $(M + H)^+$ ,  $m/z$  63, from the 0.01 M mixture using the DIMP. (b) Daughter spectrum of glycol standard  $(M + H)^+$ ,  $m/z$  63, from direct probe. Note in comparison, the low relative intensity of  $m/z$  63 of glycol in Figure 2b.



**Figure 4.** Mass spectrum (CI, methane) of a *Klebsiella cerevisiae* fermentation broth sample examined via membrane introduction showing, inter alia, ions due to protonated ethanol, 3-hydroxy-2-butanone, and 2,3-butanediol at  $m/z$  47, 89, and 91, respectively.

of various constituents were examined.

We define response time as the time it takes for the signal to reach 50% of its maximum intensity. The time is measured from when the analyte first enters the capillary membrane. Rise time is the time it takes the signal to go from 10% to 90% of the maximum normalized signal. Fall time is due to membrane memory effects and is the time it takes the signal to fall from 90% to 10% of the maximum. To measure these



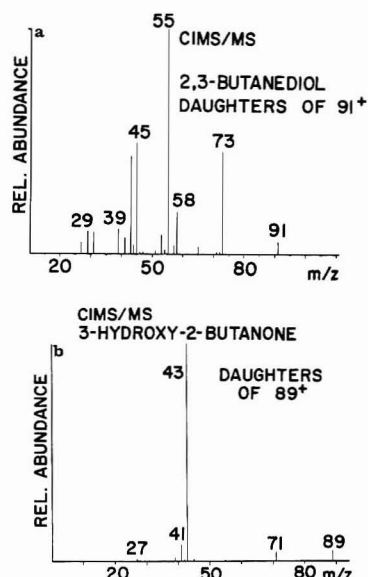


Figure 5. Daughter spectrum (CI, methane) of the fermentation products (a) 2,3-butanediol and (b) 3-hydroxy-2-butanone.

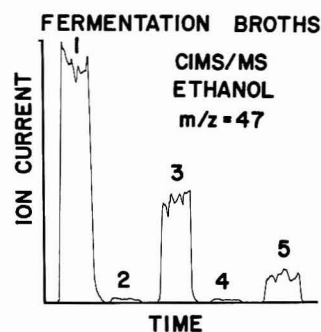


Figure 6. Comparison of ethanol levels in five fermentation broth samples using reaction monitoring ( $47^+ \rightarrow 29^+$ ). The microorganisms represented are *Saccharomyces cerevisiae* (1 and 3), *Klebsiella oxytoca* (2), *Candida utilis* (4), and *Bacillus polymyxa* (5).

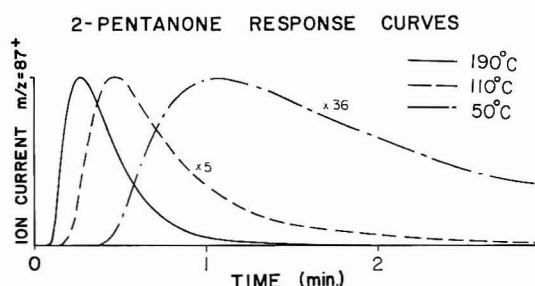


Figure 7. Normalized ion current curves for 2-pentanone,  $m/z$  87, showing the response time, rise time, and fall time at source temperatures of 190, 110, and 50 °C, respectively.

times, CI multiple ion monitoring scans were obtained for several 14- $\mu$ L injections of the 0.01 M mixture of alcohols and ketones. The injections were made with an eight-port valve (Altex) into an otherwise continuously pumped (0.5 mL/min) water stream. These injections were made at three source temperatures: 190, 110, and 50 °C. Figure 7 shows the typical response curves for 2-pentanone. As shown by comparing these curves, each characteristic time defined above is temperature dependent. In this case, the 190 °C response time was fivefold shorter than the 50 °C response time and considerably smaller than 1–5 min found with a prior device (18). Note that the curves shown in Figure 6 have been individually normalized for ease of comparison. Comparison of the areas under the peaks reveals that in this case the total response increased with temperature although there may be

Table I. Typical Response Times, Rise Times, and Fall Times (s) for the Membrane Probe

constituent <sup>a</sup>	response time	rise time	fall time
methanol	1.9	2.9	12.3
ethanol	3.5	4.2	18.4
2-propanone	3.9	4.5	20.2
2-butanone	4.4	4.6	23.2
2-pentanone	5.4	5.9	31.7

<sup>a</sup> Constituents introduced as 14- $\mu$ L injections of a 0.01 M mixture. The source temperature was at 190 °C, and the flow rate equaled 0.5 mL/min.

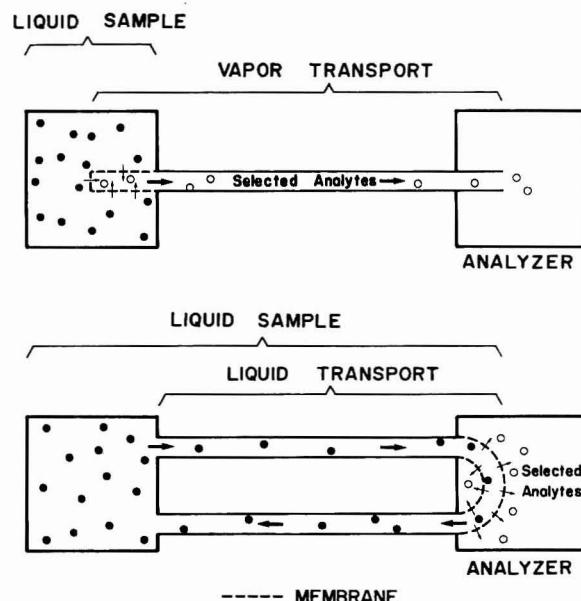


Figure 8. Comparison between placement of the membrane in the sample solution vs. having the solution flow through a capillary membrane.

a minor contribution due to the relationship between improved ionization efficiency at higher temperatures.

The ratio of the rise time and fall time measurements describe the symmetry of the response. Similarity of these two times implies high symmetry. A short rise time and fall time are necessary to resolve consecutive injections. Short fall times are also considerably more important when working at low concentrations where the residual effects are strongest. The 190 °C source temperature reduces the fall time for 2-pentanone by a factor of 8 compared to the 50 °C curve. As shown in Table I, the temporal data also provide an indication of the relative permeation rates for these molecules. Addition of a methyl group in place of a hydrogen results in a decrease in permeation rate, suggesting reduced mobility due to an increase in molecular size.

The direct insertion membrane probe combines several attractive features for selective introduction of organic molecules in aqueous solution into a mass spectrometer: the whole apparatus is inexpensive and is easily adapted to most mass spectrometers. Water does not permeate the membrane ( $m/z$  19 is always <1% relative abundance) that selectively transmits analyte over solvent. The ability to control the membrane temperature is advantageous as is the high sensitivity resulting from direct access to the ion volume and the access to the membrane once the probe is withdrawn. These features make the device attractive for on-line reaction monitoring. In addition, the DIMP has characteristics that suggest its use in specialized HPLC/MS applications. These factors include an extremely small internal volume (<50  $\mu$ L) with essentially zero dead volume, and the internal membrane sample volume is only 3  $\mu$ L. Naturally, initial applications

of membranes with HPLC will be limited to problems where due consideration is given their current limitations in terms of the molecular weight and polarity of analyte.

The results obtained in this paper depend on the operation of the hollow fiber membranes in the mode (18) in which the fluid sample stream flows *through* the capillary tube. This approach can be contrasted with that in which the permselective analyte itself moves through the capillary which is surrounded by fluid analyte (Figure 8). The permeation step is identical, but the method used herein has substantial analytical advantages. These include the efficiency of analyte transport by the fluid into the heart of the analyzer, applicability of flow injection analysis as a means of introducing standard samples and of controlling contact times, and the fact that the molecules emerge from the membrane directly into a low-pressure environment where they are effectively transported through the ionization region.

#### ACKNOWLEDGMENT

We express our appreciation to Weldon Vaughn for his precision machining and George Tsao and Norm Jensen for the fermentation samples.

#### LITERATURE CITED

- (1) Westover, L. B.; Tou, J. C.; Mark, J. H. *Anal. Chem.* **1974**, *46*, 568.
- (2) Weaver, J. C.; Abrams, J. H. *Rev. Sci. Instrum.* **1979**, *50*, 478.

- (3) Jones, P. R.; Yang, S. K. *Anal. Chem.* **1975**, *47*, 1000.
- (4) Kallos, G. J.; Mahle, N. H. *Anal. Chem.* **1983**, *55*, 813.
- (5) Calvo, K. C.; Weisenberger, C. R.; Anderson, L. B.; Klapper, M. H. *Anal. Chem.* **1981**, *53*, 981.
- (6) Eustache, H.; Histi, G. J. *Membr. Sci.* **1981**, *8*, 105.
- (7) Tou, J. C.; Kallos, G. T. *Anal. Chem.* **1974**, *46*, 1866.
- (8) Evans, J. E.; Arnold, J. T. *Environ. Sci. Technol.* **1975**, *9*, 1134.
- (9) Woldring, S.; Owens, G.; Woolford, D. C. *Science (Washington, D.C.)* **1966**, *153*, 885.
- (10) Roberts, M.; Cotton, E. T.; Owens, G.; Watkins, G. M. *Med. Biol. Eng.* **1975**, *13*, 535.
- (11) Weaver, J. C.; Mason, M. K.; Jarrell, J. A.; Peterson, J. W. *Biochim. Biophys. Acta* **1976**, *438*, 296.
- (12) Calvo, K. C.; Weisenberger, C. R.; Anderson, L. B.; Klapper, M. H. *J. Am. Chem. Soc.* **1983**, *105*, 6935.
- (13) Pungor, E.; Pecs, M.; Szigeti, L.; Nyeste, L. *Anal. Chim. Acta* **1984**, *163*, 185.
- (14) Llewellyn, P. M.; Littlejohn, D. P. U.S. Patent 3 429 105, Feb 1969.
- (15) Schmidt, W. J.; Meyer, H. D.; Schugert, K. *Anal. Chim. Acta* **1984**, *163*, 101.
- (16) Heinze, E.; Moes, J.; Griot, M.; Kramer, H.; Dunn, I. J.; Bourne, J. R. *Anal. Chim. Acta* **1984**, *163*, 219.
- (17) Reuss, M.; Piehl, H.; Wagner, F. *Eur. J. Appl. Microbiol.* **1975**, *1*, 323.
- (18) Brodbelt, J. S.; Cooks, R. G. *Anal. Chem.* **1985**, *57*, 153.
- (19) Bier, M. E.; Cooks, R. G.; Brodbelt, J. S.; Tou, J. C.; Westover, L. G. U.S. Patent pending.
- (20) Yost, R. A.; Fetterolf, D. D. *Mass Spectrom. Rev.* **1983**, *2*, 1.
- (21) Cooks, R. G.; Busch, K. L. *J. Chem. Educ.* **1982**, *13*, 535.

RECEIVED for review July 29, 1986. Accepted November 3, 1986. This work was funded by the National Science Foundation (CHE 84-08258).

## Electron Capture Negative Ion Chemical Ionization Mass Spectrometry of Derivatized Chlorophenols and Chloroanilines

Thomas M. Trainor\* and Paul Vouros

Barnett Institute of Chemical Analysis and Department of Chemistry, Northeastern University, Boston, Massachusetts 02115

The electron capture negative ion chemical ionization mass spectra of electrophilic derivatives (perfluoroacyl, pentafluorobenzyl, pentafluorobenzoyl, 3,5-bis(trifluoromethyl)-benzoyl, and (pentafluorophenyl)methanimine) of chloro-substituted phenols and anilines have been investigated. The formation of analyte-specific anions in the spectra of the derivatives is strongly influenced by the nature of the electrophilic group and the summed electron-donating or -withdrawing properties of the aromatic ring substituents. Hammett linear free energy relationships can be used to predict the stability of molecular anions, the direction of fragmentation pathways, and the usefulness of a given derivative for analytical purposes by using selective-ion monitoring. The influence of ion source temperature on the ionically induced dissociation of the derivatives was examined. The relative molar responses of different derivatives under conditions of GC-negative ion chemical ionization mass spectrometry and GC-electron capture detection were comparable.

At least three of the most sensitive techniques for the detection of organic compounds at the trace level are based on the process of gas-phase electron capture. These are the electron capture detector utilized in gas chromatography (GC-ECD), the conventional mass spectrometer operated in

the electron capture negative ion chemical ionization mode (EC-NCIMS), and the atmospheric pressure ionization mass spectrometer (API-MS). In each case, extremely low detection limits, approaching the low femtogram ( $10^{-15}$  g) range, have been demonstrated for compounds amenable to electron capture (1-3). In general, this ionization process is based on the production of near thermal energy electrons (ca. 0 eV) followed by electron-molecule reactions creating organic anions in the gas phase. The ionization efficiency of molecules by this process is highly structure dependent. This feature allows for selective techniques, with high sensitivity for favorable cases. The presence of structural elements possessing low level unoccupied molecular orbitals is found to facilitate this ionization. This translates to compounds containing halogens, nitro groups, and highly conjugated systems.

Unfortunately, many compounds of interest are not inherently electrophilic and must be converted to a suitable volatile derivative for analysis by any of the aforementioned EC techniques. A vast literature base has developed over the last 20 years concerning the synthesis of EC derivatives for the GC-ECD (4-6). Hunt (2, 7) has pioneered the use of popular GC-ECD derivative methodology for the analysis of nonelectrophilic compounds by negative ion mass spectrometric techniques. To be of use in EC-NCIMS, the derivatized molecule must not only favor the capture of electrons but, just as important, stabilize the negative charge in a manner in which anions characteristic of the derivative or original analyte



**Table I. Structures of Phenol and Aniline Derivatives ( $\phi = \text{C}_6\text{H}_5$ )**

1 ~ 	9 ~ 
2 ~ 	10 ~ 
3 ~ 	11 ~ 
4 ~ 	12 ~ 
5 ~ 	13 ~ 
6 ~ 	14 ~ 
7 ~ 	15 ~ 
8 ~ 	16 ~ 
-	17 ~ 

predominate in the mass spectrum. In many instances, the observed fragmentation of derivatives contains a preponderance of ions stemming from the introduced electrophore. For instance, acidic and alcoholic catecholamine metabolites converted to the corresponding pentafluoropropionyl derivatives have been shown to fragment under EC-NCIMS conditions to primarily a series of ions at  $m/z$  128, 147, and 163 corresponding to the fragments  $\text{C}_2\text{F}_4\text{CO}^-$ ,  $\text{C}_2\text{F}_5\text{CO}^-$ , and  $\text{C}_2\text{F}_5\text{CO}_2^-$ , respectively (8). This presents a limitation to the application of selected ion monitoring techniques, GC-SIM-MS, since the presence of ions specific to the original analyte is necessary for unequivocal characterization. Therefore, when a derivative is selected for the quantitative analysis of a compound by EC-NCIMS, major considerations in terms of derivative selection include (1) good chromatographic performance, (2) high synthetic yields, (3) high ionization efficiency, and (4) high relative abundance of analyte-specific ions.

Many of the perfluorinated acylation and alkylation reagents that have been described in the GC-ECD literature (4) will produce stable derivatives of a variety of functionalities that satisfy criteria 1 and 2. However, as noted in a review of the EC-NCIMS technique (8), systematic studies on the suitability of different electrophoric derivatives for the analysis of specific compounds by EC-NCIMS have not yet appeared. We report here on an examination by EC-NCIMS of five of the most popular EC derivatives (trifluoroacetyl, pentafluoropropionyl, heptafluorobutyryl, pentafluorobenzoic, and pentafluorobenzoyl), as well as several novel EC derivatives, of a series of test analytes. These derivatives were compared in terms of their fulfillment of criteria 3 and 4 above. Selected as test analytes were a number of chlorinated phenols and anilines. This selection was based, in part, on the substantial environmental concerns surrounding these compounds. Moreover, the aromatic hydroxy and amino functionalities are pervasive in the realm of industrially and biologically important chemicals, and their associated intermediates, degradation products, and metabolites.

The structures of the derivatives studied are presented in Table I. Hunt has previously reported the EC-NCIMS spectra of 5, 13, and 17 (2, 7). Shang-Zhi and Duffield reported the spectra of a number of derivatives of pentachlorophenol, 2,3,4,6-tetrachlorophenol, and 2,4,6-trichlorophenol (9). Unfortunately, these studies obtained spectra in a range above

$m/z$  60, thus failing to observe the ion  $\text{Cl}^-$  ( $m/z$  35 and 37), a prominent signal in the EC-NCIMS of many chlorinated species (10-12). In this work, we focused on the influence of both the analyte and final derivative structure on the resulting fragmentation pattern under methane EC-NCIMS conditions. A useful parameter to evaluate changes in the observed spectra was found to be the Hammett free energy relationship (13). Indeed, for several of the series of chlorinated derivatives, a correlation exists between the log ratio of analytically important ions and the Hammett  $\sigma$  substituent constants.

## EXPERIMENTAL SECTION

**Reagents.** Solvents used included methanol, cyclohexane, methylene chloride, and ethyl acetate and were residue grade (J. T. Baker). All derivatization reagents, phenols, and anilines were purchased from Aldrich and used as received. Stock solutions of the individual phenols and anilines were prepared by diluting each compound to a concentration of approximately  $1 \mu\text{g}/\mu\text{L}$  in methanol. All glassware and syringes were treated with hexamethyldisilazane (14) to minimize losses due to surface adsorption.

**Instrumentation.** All GC-MS analyses were carried out on a Finnigan 4021 GC-MS equipped with a 15-m DB-5 capillary column (J&W, 0.25- $\mu\text{m}$  film) directly inserted into the ion source. Helium (Matheson, UHP) was used as carrier gas, while methane (Matheson, UHP) served as the CI reagent gas. The ion source tuning was carried out in the negative ion mode by using perfluorotributylamine. Typical MS operating parameters included: 70-eV ionizing potential, 0.40-mA filament current, 0.30-torr source pressure, and 1000-V electron multiplier setting. The Finnigan-Incos data system was programmed to scan the range from  $m/z$  18 to 500 in 0.50 s for the full scan runs. In the case of the SIM experiments, the mass spectrometer was scanned over one amu in 0.25 s. The GC oven was initially set at  $110^\circ\text{C}$  and ramped linearly at  $15^\circ\text{C}/\text{min}$  to  $300^\circ\text{C}$ . Injections were made by using the on-column technique (15) utilizing an injector and fused silica needle syringe supplied by J&W. For the chlorinated compounds, only the most intense peak in each isotope cluster is reported here. The expected isotope pattern was observed in all instances. In the instances where no molecular anion  $\text{M}^-$  could be observed, derivative structures were confirmed by using both methane positive chemical ionization and electron-impact MS.

For the GC-ECD study, a Varian Model 3700 gas chromatograph equipped with a Varian constant-current variable-frequency  $^{63}\text{Ni}$  electron-capture detector and a Varian Model 11095 temperature programmable on-column injector was used. The GC-ECD chromatograms were recorded with a Spectra-Physics Model 4270 digital integrator. The identical 15-m DB-5 column utilized in the GC-MS experiments was installed in the GC-ECD. The carrier and ECD makeup gases were helium (UHP, Matheson) and nitrogen (UHP, Matheson), respectively. Flow rates, measured at  $20^\circ\text{C}$ , were  $5 \text{ cm}^3/\text{min}$  for helium and  $25 \text{ cm}^3/\text{min}$  for nitrogen. Injections were made by using a  $5\text{-}\mu\text{L}$  syringe equipped with a stainless-steel needle (Varian). The on-column injector was initially set at  $100^\circ\text{C}$  and heated to a temperature of  $290^\circ\text{C}$  at a rate of  $180^\circ\text{C}/\text{minute}$  upon sample injection. The GC oven was kept at  $120^\circ\text{C}$  for 1.0 min after injection and ramped linearly at  $20^\circ\text{C}/\text{min}$  to  $220^\circ\text{C}$ . The detector temperature was maintained at  $300^\circ\text{C}$ .

**Preparation of Derivatives. A. Phenols.** Appropriate volumes of the methanol solutions containing the five chlorophenols (3-Cl, 4-Cl, 3,4- $\text{Cl}_2$ , 3,5- $\text{Cl}_2$ , and 3,4,5- $\text{Cl}_3$ ) and phenol itself were transferred to a 1-mL reacti-vial (Pierce) to give  $10 \mu\text{g}$  of each compound. The methanol was removed under a gentle nitrogen stream, and the appropriate solvent and reagents were added immediately.

**1. Trifluoroacetates (1) and Pentafluoropropionates (2).** Ethyl acetate ( $200 \mu\text{L}$ ), triethylamine ( $1 \mu\text{L}$ ), and the perfluoroanhydride ( $10 \mu\text{L}$ ) were added to the analyte, and the solution was allowed to react for 30 min at  $75^\circ\text{C}$ . The mixture was then cooled, brought to dryness via nitrogen, and transferred to another vessel by using  $0.5\text{-mL}$  aliquots of cyclohexane. The solution was further diluted to give a concentration of  $1.0 \text{ ng}/\mu\text{L}$  for each derivative.

**2. Heptafluorobutyrylates (3), Pentafluorobenzoates (5), 3,5-Bis(trifluoromethyl)benzoates (6), 3-(Trifluoro-**

Table II. EC-NCI Mass Spectra of Phenol Derivatives

derivative	rel abundance		
	M <sup>-</sup>	ArO <sup>-</sup>	other
1	0	0.2	CF <sub>3</sub> CO <sub>2</sub> <sup>-</sup> (100)
2	0	0	C <sub>2</sub> F <sub>5</sub> CO <sup>-</sup> (100), C <sub>2</sub> F <sub>4</sub> CO <sup>-</sup> (23)
3	0	0	C <sub>3</sub> F <sub>7</sub> CO <sup>-</sup> (100), C <sub>3</sub> F <sub>6</sub> CO <sup>-</sup> (6)
4	0	100	
5	100	5	C <sub>6</sub> F <sub>5</sub> <sup>-</sup> (8)
6	100	2	
7	100	1	CF <sub>3</sub> C <sub>6</sub> H <sub>4</sub> CO <sub>2</sub> <sup>-</sup> (80)
8	100	1	CF <sub>3</sub> C <sub>6</sub> H <sub>4</sub> CO <sub>2</sub> <sup>-</sup> (19)

Table III. EC-NCI Mass Spectra of Aniline Derivatives

derivative	rel abundance		
	M <sup>-</sup>	(M - HF) <sup>-</sup>	other
9	0	0	(M - H) <sup>-</sup> (100)
10	0	100	(M - H <sub>2</sub> F) <sup>-</sup> (2)
11	0	100	
12	0	100	(M - H <sub>2</sub> F) <sup>-</sup> (30)
13	0	35	(M - H <sub>2</sub> F) <sup>-</sup> (100)
14	100		(M - H) <sup>-</sup> (57)
15	80		(M - H) <sup>-</sup> (100)
16	100		(M - H) <sup>-</sup> (30)
17	100	1	

methyl)benzoates (7), and 4-(Trifluoromethyl)benzoates (8). The above procedure (A.1) was followed with two exceptions. The quantity of derivatization reagent (heptafluorobutyric anhydride or the appropriate benzoyl chloride) was decreased to 5  $\mu$ L, and the cyclohexane solution was subjected to a wash with distilled water (3  $\times$  0.5 mL). These changes facilitated the removal of these less volatile derivatization reagents prior to the nitrogen drying step.

**3. Pentafluorobenzyl Ethers (4).** The extractive alkylation procedure of Ehrsson (16) was adapted. To the reaction vial containing 10  $\mu$ g of each phenol was added methylene chloride (0.5 mL), an aqueous solution of 0.2 M tetrabutylammonium sulfate in 0.1 M NaOH (0.5 mL), and pentafluorobenzyl bromide (1  $\mu$ L). After the reaction was allowed to proceed for 15 min with constant shaking at room temperature, the aqueous layer was discarded and the organic layer washed with distilled water (2  $\times$  0.5 mL). Next, the methylene chloride was removed via a nitrogen stream, and the contents were transferred to a clean vessel with cyclohexane and diluted to a concentration of 1 ng/ $\mu$ L.

**B. Anilines. 1. Trifluoroacetamides (9), Pentafluoropropionamides (10), Heptafluorobutyramides (11), (Pentafluorobenzyl)amines (12), Pentafluorobenzamides (13), 3,5-Bis(trifluoromethyl)benzamides (14), 3-(Trifluoromethyl)benzamides (15), and 4-(Trifluoromethyl)benzamides (16).** The reactions were conducted as described in procedure A.2, above, by using 10  $\mu$ g each of aniline and the five chloroanilines (3-Cl, 4-Cl, 3,4-Cl<sub>2</sub>, 3,5-Cl<sub>2</sub>, and 3,4,5-Cl<sub>3</sub>).

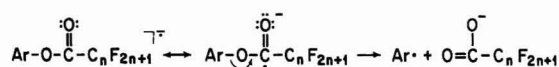
**2. (Pentafluorophenyl)methanimines (17).** To the reaction vial containing the anilines was added ethyl acetate (200  $\mu$ L) and pentafluorobenzaldehyde (1.0 mg). The mixture was heated at 75  $^{\circ}$ C for 1 h, cooled, and isolated as in A.2, above.

In addition to the microgram scale derivatizations, three derivatives of phenol (4–6) were prepared on a 0.5-g scale by using similar conditions and adding the derivatization reagents in a 1:1 molar ratio with phenol. The products were recrystallized from 95% ethanol to give white needles with sharp melting points (4, mp 74  $^{\circ}$ C; 5, mp 68  $^{\circ}$ C; 6, mp 34  $^{\circ}$ C). Silica gel TLC revealed in each case only one UV absorbing spot (ethyl acetate/hexane, 1:9).

## RESULTS AND DISCUSSION

Initially, eight derivatives of phenol and nine derivatives of aniline were prepared and EC-NCIMS spectra recorded by using methane as a moderator gas and an ion source temperature of 200  $^{\circ}$ C. The spectra are summarized in Tables II (phenols) and III (anilines). In general, all of the aniline

Scheme I



Scheme II

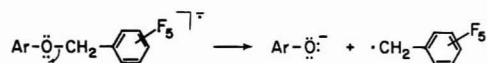


Table IV. EC-NCI Mass Spectra of Pentafluorobenzyl Ethers

Cl <sub>x</sub> PhOCH <sub>2</sub> C <sub>6</sub> F <sub>5</sub>	rel abundance	
	Cl <sub>x</sub> PhO <sup>-</sup>	Cl <sup>-</sup>
H	100	
4-Cl	100	0.9
3-Cl	100	1.9
3,4-Cl <sub>2</sub>	100	4.8
3,5-Cl <sub>2</sub>	100	7.5
3,4,5-Cl <sub>3</sub>	100	20

derivatives 9–17 exhibit ions suitable for GC-SIM-MS analysis; either the molecular anion M<sup>-</sup> or fragment ions characteristic of aniline are produced in high abundance. However, for phenol only the aryl derivatives 4–8 provide analyte specific ions. The nature of the spectra of the derivatives 4–17 was found to change with chlorine substitution on the phenol or aniline ring, and, furthermore the spectral patterns also exhibited a strong dependence on ion source temperature. The following discussion covers these results in more detail.

**A. Phenol Derivatives. I. Alkyl Perfluoroacyl Derivatives.** The alkyl perfluoroacyl derivatives 1–3, popular in the GC-ECD determination of phenols (17, 18), are not suitable for GC-SIM-MS analysis under EC-NCIMS conditions. For these compounds, retention of the negative charge with the fluoroacyl moiety leads to formation of anions derived from the derivatization reagent and not the original phenol analyte (Scheme I). Since these derivatives were found to be of little potential use in the case of phenols, additional substituted phenols were not examined.

**II. Pentafluorobenzyl Ether Derivatives.** The alkylation of phenols with pentafluorobenzyl bromide and subsequent analysis by GC-ECD is a well-known analytical approach (16, 19–21). Under EC-NCIMS conditions, 4 undergoes a dissociative electron capture process to produce the phenoxide anion (ArO<sup>-</sup>) as the sole peak in the mass spectrum (Scheme II). The ion ArO<sup>-</sup> is of course characteristic of the original phenol and should be useful for quantitation by GC-SIM-MS. The absence of an ion at *m/z* 181, corresponding to the pentafluorobenzyl anion, is noteworthy since none of the ion current is carried by nonspecific ions. Murphy (22) has previously reported the absence of the *m/z* 181 ion in the EC-NCIMS spectra of pentafluorobenzyl esters of prostaglandins and has attributed this to the lower relative stability of the pentafluorobenzyl anion vs. the corresponding radical species. Hence, in contrast to the alkyl perfluoroacyl derivatives, negative charge is preferentially retained by the phenoxide moiety.

Table IV contains the EC-NCIMS spectra of the five chlorinated phenols studied. Other than the substituted phenoxide species, the only additional ion noted in the spectra of these compounds is the chloride anion, Cl<sup>-</sup>, which is found to increase in relative abundance with the extent of chlorination.

**III. Pentafluorobenzoate Esters.** Lester has detected chlorinated phenols at the ppb level by GC-ECD of derivative 5 formed by treatment with pentafluorobenzoyl chloride (23). Under EC-NCIMS conditions, the molecular anion M<sup>-</sup> is



Table V. EC-NCI Mass Spectra of Pentafluorobenzoate Esters

$\text{Cl}_x\text{PhOC(O)C}_6\text{F}_5$	rel abundance						
	$\text{M}^-$	$(\text{M} - 20)^-$	$(\text{M} - 64)^-$	$\text{Cl}_x\text{PhO}^-$	$m/z$ 196 <sup>a</sup>	$m/z$ 167 <sup>b</sup>	$m/z$ 148 <sup>c</sup>
H	100	2.5	1.2	5	3.2	6	3.7
4-Cl	100	14	8	6.3	6	21	1.4
3-Cl	100	8	8	25	5.5	38	3.5
3,4-Cl <sub>2</sub>	78	19	16	44	14	58	3
3,5-Cl <sub>2</sub>	53	10	13	90	20	100	8
3,4,5-Cl <sub>3</sub>	8.5	4.5	4	73	31	100	6

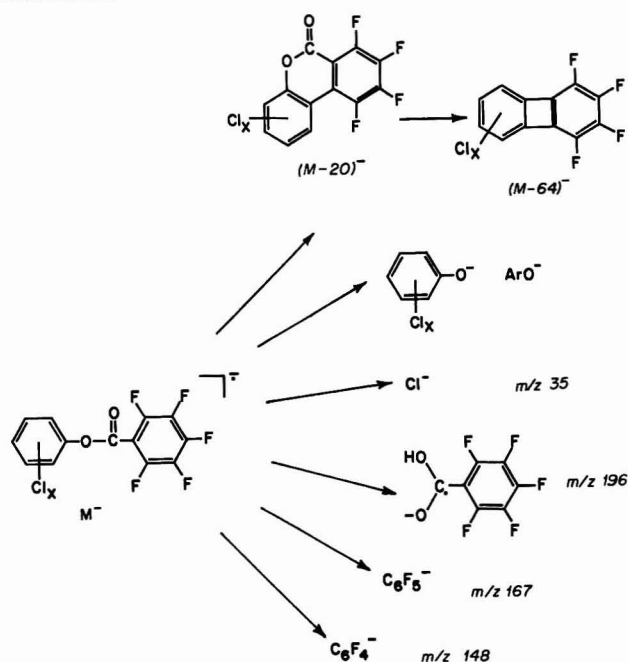
<sup>a</sup>  $\text{C}_6\text{F}_5\text{COH}^-$ . <sup>b</sup>  $\text{C}_6\text{F}_5^-$ . <sup>c</sup>  $\text{C}_6\text{F}_4^-$ .

Table VI. EC-NCI Mass Spectra of 3,5-Bis(trifluoromethyl)benzoate Esters

$\text{Cl}_x\text{PhOC(O)Ph(CF}_3)_2$	rel abundance				
	$\text{M}^-$	$\text{Cl}_x\text{PhO}^-$	$m/z$ 257 <sup>a</sup>	$m/z$ 213 <sup>b</sup>	$\text{Cl}^-$
H	100	2	0	1	
4-Cl	100	4.9	33	2	1
3-Cl	100	6.7	46	2	5
3,4-Cl <sub>2</sub>	78	11	100	3	11
3,5-Cl <sub>2</sub>	85	17	100	3	12
3,4,5-Cl <sub>3</sub>	41	21	100	4	47

<sup>a</sup>  $(\text{CF}_3)_2\text{C}_6\text{H}_3\text{CO}_2^-$ . <sup>b</sup>  $\text{C}_6\text{H}_3(\text{CF}_3)_2^-$ .

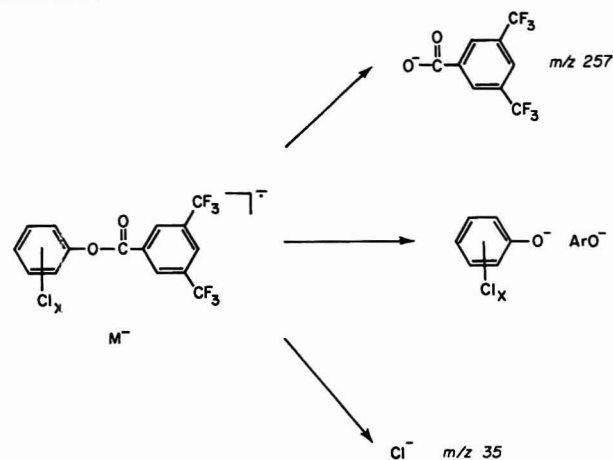
Scheme III



quite stable and represents the base peak in the spectrum. Apparently the conjugated carbonyl-aromatic system is capable of stabilizing the additional electron, and fragmentation is minimal. Upon chlorination, however, an increase in intensity of many of the fragment ions is observed as indicated in the spectra summarized in Table V. The fragmentation pathways of the pentafluorobenzoate esters of the chlorinated phenols are outlined in Scheme III.

**IV. 3,5-Bis(trifluoromethyl)benzoate Esters.** The use of the reagent 3,5-bis(trifluoromethyl)benzoyl chloride for the synthesis of electrophoric derivatives for EC-NCIMS has been reported by Murray (24) for the analysis of the drug clonidine, a secondary amine. The ester prepared from treatment of phenol with this reagent produces a derivative that exhibits a base peak corresponding to the molecular ion  $\text{M}^-$ . Table VI summarizes the EC-NCIMS spectra for the chlorinated phenol derivatives, and Scheme IV outlines their fragmentation. Even though derivatives of type 5 and 6 share the benzoate functionality, the different substitution on the

Scheme IV



aromatic ring of the electrophore, pentafluoro vs. 3,5-bis(trifluoromethyl), changes dramatically the fragmentation pattern. When the two sets of derivatives (Tables V and VI) are compared, two features can be noted. First, the number and intensity of nonspecific fragment ions is greater in the case of the pentafluorobenzoate esters. Second, the relative intensity of the molecular ion,  $\text{M}^-$ , is always enhanced in the 3,5-bis(trifluoromethyl)benzoate ester. Thus the stabilization of negative charge is highly dependent on the structure of the benzoyl ester.

**V. Substituent Effects.** A common feature of the three sets of chlorophenol derivatives discussed above is the increased fragmentation noted as the number of chlorines on the phenol ring is increased. Significantly, the application of the Hammett linear energy relationships can be shown to provide an insight into these observations. The correlation of ion abundances in the mass spectra of substituted aromatic compounds with the substituent Hammett  $\sigma$  values has found use in mass spectrometry (25-27). Typically, the log ratios of molecular ion intensities to selected fragment ions or ratios ( $R$ ) of two fragment ions are calculated and plotted vs. the appropriate  $\sigma$  value. A plot fit to the equation  $\log R = \rho\sigma + b$  with a reasonable correlation coefficient ( $r^2$ ) is significant, as the change in ion abundances in a mass spectrum can then be predicted for further substituent changes. For multiply substituted aromatics, the sum of the individual  $\sigma$  values,  $\sum\sigma$ ,

**Table VII. Values of  $\sum\sigma$  for Chlorinated Derivatives<sup>a</sup>**

Cl <sub>x</sub> Ph <sup>-</sup>	$\sum\sigma$	Cl <sub>x</sub> Ph <sup>-</sup>	$\sum\sigma$
H	0.00	3,4-Cl <sub>2</sub>	0.60
4-Cl	0.23	3,5-Cl <sub>2</sub>	0.74
3-Cl	0.37	3,4,5-Cl <sub>3</sub>	0.97

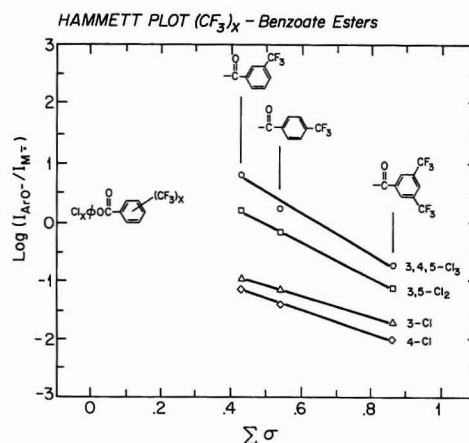
<sup>a</sup> Reference 28.

is calculated (27). Table VII lists the  $\sum\sigma$  values calculated for the chlorinated compounds in this report (28).

For the purposes of this study, we have been interested in isolating the factors responsible for the production of ions characteristic of the phenol and aniline derivatives so as to permit the selection of electrophoric derivatives on a predictive basis and thus facilitate the development of selective quantitative methods. Plotting the log ratios of the intensities of analytically important ions for the three sets of phenol derivatives has resulted in linear Hammett plots with excellent correlation coefficients. Presented in Table VIII are the values of  $\rho$ ,  $b$ , and  $r^2$  obtained from linear regression analysis of the plots  $\log I_{\text{Cl}^-}/I_{\text{Aro}^-}$  vs.  $\sum\sigma$  for the pentafluorobenzyl ethers and  $\log I_{\text{Aro}^-}/I_{\text{M}^-}$  vs.  $\sum\sigma$  for the two sets of benzoate esters. The results from experiments conducted at five different ion source temperatures are included.

The absolute value of  $\rho$ , the slope of the Hammett plot, is a measure of the degree of influence the substituents exert in directing the fragmentation. Chlorine is assigned positive  $\sigma$  values, reflecting electron-withdrawing properties at both the meta ( $\sigma = 0.37$ ) and para ( $\sigma = 0.23$ ) positions. There is a wide range in the absolute magnitude in  $\rho$  values for these derivatives, demonstrating the degree to which each type of derivative is affected by substitution. For the benzoate esters, as the value  $\sum\sigma$  becomes more positive, the abundance of the molecular ion  $\text{M}^-$  diminishes, while the abundances of the fragment ions increases. The ratio of the two ions potentially useful for quantitation,  $I_{\text{Aro}^-}/I_{\text{M}^-}$ , increases sharply as the value of  $\sum\sigma$  increases ( $\rho > 0$ ). This may be attributed in part to the increasing ability of the phenoxide anion to stabilize the resulting charge as chlorine substitution increases. In the case of the benzyl ethers, only two ions, both fragments, are observed in the mass spectra. The increase in the abundance of  $\text{Cl}^-$  with the increase in chlorine substitution in the molecule is not surprising. However, the linear Hammett plots indicate that the actual site of substitution is a major factor in the observed ratio  $I_{\text{Aro}^-}/I_{\text{Cl}^-}$ .

Since the changes in substitution on the phenol portion of the derivatives were found to lead to significant mass spectral changes, we next considered the effect of changes in fragmentation brought about by changing the substituent  $\sum\sigma$  value for the benzoate ring. A convenient set of derivatives for this purpose is those bearing the electrophores shown in compounds 6, 7, and 8. In these examples, the number and position of electrophoric trifluoromethyl groups are varied. A series of chlorophenols was derivatized with the appropriate substituted benzoyl chloride reagents, and the EC-NCIMS

**Figure 1.** Hammett plot for 3,5-bis(trifluoromethyl)benzoate esters.

spectra were recorded at an ion source temperature of 200 °C. Figure 1 shows the Hammett plots observed for these derivatives. In this instance, the log ratio  $I_{\text{Aro}^-}/I_{\text{M}^-}$  is plotted vs. the  $\sum\sigma$  value for the benzoate ring ( $\sigma_m = 0.43$  and  $\sigma_p = 0.54$  for  $\text{CF}_3$ ). In contrast to the change in the ratio  $I_{\text{Aro}^-}/I_{\text{M}^-}$  observed by varying  $\sum\sigma$  on the phenol ring ( $\rho > 0$ ), the increase in  $\sum\sigma$  on the benzoate ring leads to a decrease in  $I_{\text{Aro}^-}/I_{\text{M}^-}$  ( $\rho < 0$ ). Presumably, a higher value of  $\sum\sigma$  on the benzoate ring leads to stabilization of the molecular anion  $\text{M}^-$  formed by initial electron capture, suggesting that the site of electron capture is most likely the carbonyl group of the benzoate ring.

As noted earlier, an EC-NCIMS study conducted on derivatives of the chlorophenols 2,4,6-trichlorophenol, 2,3,4,6-tetrachlorophenol, and pentachlorophenol has been published (9). The authors reported that the spectra were dominated by the phenoxide anions. It is important to note, however, that all their spectra were not scanned below  $m/z$  60. Our results illustrate that for valid linear free energy relationship calculations inclusion of the chloride anion abundances is necessary, at least for the simple pentafluorobenzyl derivatives of chlorophenols.

**VI. Temperature Effects.** An increase in fragment ion abundances with increasing source temperature has been a general behavior reported for EC-NCIMS (29). We have obtained EC-NCIMS spectra of the phenol derivatives 4, 5, and 6 over the range of ion source temperatures between 100 and 300 °C and have noted some significant trends. In reviewing the change in relative ion abundances for the chlorinated series of derivatives 4 (Figure 2), 5 (Figure 3), and 6 (Figure 4) two points can be made. First, the changes in ion abundances are most pronounced for the higher chlorinated compounds, with the derivatives of phenol itself showing little change. Second, the temperature effects are minimal for compounds undergoing dissociative electron capture (i.e., 6) and most significant for compounds capable of nondissociative ionization.

**B. Aniline Derivatives. I. Alkyl Perfluoroacyl Derivatives.** Three alkyl perfluoroacyl derivatives have been

**Table VIII. Hammett  $\rho$  Constants for Phenol Derivatives<sup>a</sup>**

source temp, °C	derivative (ion ratio, $R$ )								
	ROCH <sub>2</sub> C <sub>6</sub> F <sub>5</sub> (Aro <sup>-</sup> /Cl)			ROC(O)C <sub>6</sub> F <sub>5</sub> (Aro <sup>-</sup> /M <sup>-</sup> )			ROC(O)C <sub>6</sub> H <sub>3</sub> (CF <sub>3</sub> ) <sub>2</sub> (Aro <sup>-</sup> /M <sup>-</sup> )		
	$\rho$	$r^2$	$b$	$\rho$	$r^2$	$b$	$\rho$	$r^2$	$b$
100	-1.49	0.991	2.16	1.49	0.978	-1.45	0.847	0.889	-1.56
150	-1.59	0.993	2.15	1.80	0.978	-1.44	1.18	0.985	-1.52
200	-1.77	0.996	2.41	2.37	0.960	-1.52	1.42	0.990	-1.71
250	-1.80	0.995	2.36	3.05	0.968	-1.63	1.95	0.990	-1.91
300	-1.83	0.995	2.31	4.24	0.976	-1.61	2.26	0.975	-1.96

<sup>a</sup>  $\log R = \rho \sum\sigma + b$ ;  $r^2$  = correlation coefficient.



Table IX. EC-NCI Mass Spectra of Trifluoroacetamides

Cl <sub>x</sub> PhNHC(O)CF <sub>3</sub>	rel abundance					
	M <sup>+</sup>	(M - H) <sup>+</sup>	(M - HF) <sup>+</sup>	(M - HCl) <sup>+</sup>	(M - H <sub>2</sub> Cl <sub>2</sub> ) <sup>+</sup>	CF <sub>3</sub> <sup>+</sup>
H	0	100	0			0
4-Cl	100	1	3	75	0	5
3-Cl	34	1	4	100	0	4
3,4-Cl <sub>2</sub>	8	0	0	100	2	9
3,5-Cl <sub>2</sub>	4	0	0	100	5	8
3,4,5-Cl <sub>3</sub>	0	0	0	100	11	3

Table X. EC-NCI Mass Spectra of Pentafluoropropionamides

Cl <sub>x</sub> PhNHC(O)CF <sub>2</sub> CF <sub>3</sub>	rel abundance				
	M <sup>+</sup>	(M - HF) <sup>+</sup>	(M - H <sub>2</sub> F) <sup>+</sup>	(M - HCl) <sup>+</sup>	Cl <sup>+</sup>
H	0	100	2		3
4-Cl	0	100	2	1	1
3-Cl	0	100	2	2	1
3,4-Cl <sub>2</sub>	0	100	1	5	4
3,5-Cl <sub>2</sub>	0	100	2	4	4
3,4,5-Cl <sub>3</sub>	0	100	1	12	9

Table XI. EC-NCI Mass Spectra of Heptafluorobutyramides

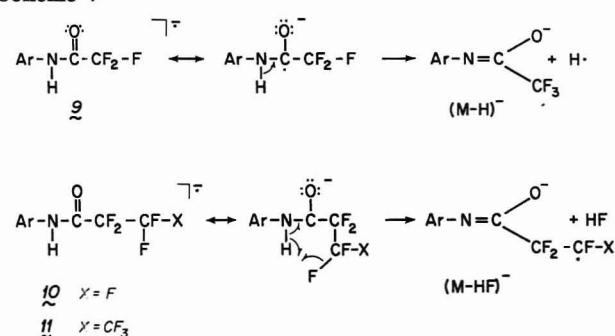
Cl <sub>x</sub> PhNHC(O)CF <sub>2</sub> CF <sub>2</sub> CF <sub>3</sub>	rel abundance				
	M <sup>+</sup>	(M - HF) <sup>+</sup>	(M - H <sub>2</sub> F) <sup>+</sup>	(M - HCl) <sup>+</sup>	Cl <sup>+</sup>
H	0	100	0		2
4-Cl	0	100	0	0	1
3-Cl	0	100	0	1	1
3,4-Cl <sub>2</sub>	0	100	0	3	1
3,5-Cl <sub>2</sub>	0	100	0	3	4
3,4,5-Cl <sub>3</sub>	0	100	1	4	9

Table XII. EC-NCI Mass Spectra of (Pentafluorobenzyl)amines

Cl <sub>x</sub> PhNHCH <sub>2</sub> C <sub>6</sub> F <sub>5</sub>	rel abundance				
	M <sup>+</sup>	(M - HF) <sup>+</sup>	(M - H <sub>2</sub> F) <sup>+</sup>	(M - H <sub>3</sub> F) <sup>+</sup>	Cl <sup>+</sup>
H	0	100	30	15	
4-Cl	0	100	46	15	7
3-Cl	0	100	37	11	53
3,4-Cl <sub>2</sub>	0	100	23	7	56
3,5-Cl <sub>2</sub>	0	24	0	0	66
3,4,5-Cl <sub>3</sub>	0	2	0	0	29

examined for the determination of anilines by EC-NCIMS: trifluoroacetamides (9), pentafluoropropionamides (10), and heptafluorobutyramides (11). Under methane EC-NCIMS conditions, these derivatives were observed to produce characteristic fragment ions unlike the situation noted earlier for phenols in Table II. The spectra for the series of the chlorinated aniline derivatives 9-11 are summarized in Tables IX-XI. The spectra of both the pentafluoropropionamides (10) and the heptafluorobutyramides (11) are dominated by the (M - HF)<sup>+</sup> ion, with no molecular anion M<sup>+</sup> and few additional fragment ions. Similar trends were also observed with the derivatized chloroanilines. In contrast, the EC-NCIMS spectra of the trifluoroacetamides (9) exhibited more dramatic changes as a function of chlorine substitution. Derivative 9 produced essentially the (M - H)<sup>+</sup> ion. However, with the addition of chlorine atoms to the aniline ring, significant abundances of molecular anion M<sup>+</sup> and fragments (M - HCl)<sup>+</sup> and Cl<sup>+</sup> were observed. Experiments carried out by using ring labeled [<sup>2</sup>H<sub>5</sub>]aniline confirm that the hydrogen bonded to the nitrogen atom is eliminated to form both the (M - H)<sup>+</sup> ion in 9 and the (M - HF)<sup>+</sup> ion in 10 and 11. The differences in fragmentation between the trifluoroacetyl derivatives 9 and those of the larger fluoroacetyl homologues (10 and 11) may be the result of the steric demands of the elim-

Scheme V



ination process that involves a six-member ring intermediate leading to the formation of the (M - HF)<sup>+</sup> ion. Conceivably a minimum length of the perfluorocarbon chain is critical to sustain the fragmentation process (30) (Scheme V).

II. (Pentafluorobenzyl)amines. Under EC-NCIMS conditions, the pentafluorobenzyl derivatives of anilines, 12, were found to undergo considerable fragmentation (Table XII). Major ions include (M - HF)<sup>+</sup>, (M - H<sub>2</sub>F)<sup>+</sup>, (M - HF - HCl)<sup>+</sup>, and Cl<sup>+</sup>, whose relative abundances were strongly affected by the chlorine ring substitution. Unlike the corre-

Table XIII. EC-NCI Mass Spectra of Pentafluorobenzanilides

$\text{Cl}_x\text{PhNHC(O)C}_6\text{F}_5$	rel abundance					
	$\text{M}^+$	$(\text{M} - \text{HF})^+$	$(\text{M} - \text{H}_2\text{F})^+$	$(\text{M} - \text{H}_2\text{F}_2)^+$	$(\text{M} - \text{HF} - \text{HCl})^+$	$\text{Cl}^+$
H	1	35	100	6		
4-Cl	0	52	100	3	2	4
3-Cl	0	81	100	3	7	4
3,4- $\text{Cl}_2$	0	100	80	2	9	14
3,5- $\text{Cl}_2$	0	100	17	0	11	12
3,4,5- $\text{Cl}_3$	0	100	10	0	9	33

Table XIV. EC-NCI Mass Spectra of 3,5-Bis(trifluoromethyl)benzanilides

$\text{Cl}_x\text{PhNHC(O)C}_6\text{H}_3(\text{CF}_3)_2$	rel abundance				
	$\text{M}^+$	$(\text{M} - \text{H})^+$	$(\text{M} - \text{HCl})^+$	$m/z$ 242 <sup>a</sup>	$\text{Cl}^+$
H	100	57		2	
4-Cl	100	50	1	9	0.1
3-Cl	100	51	2	4	0.5
3,4- $\text{Cl}_2$	100	48	17	10	7
3,5- $\text{Cl}_2$	100	46	19	7	7
3,4,5- $\text{Cl}_3$	100	47	99	16	31

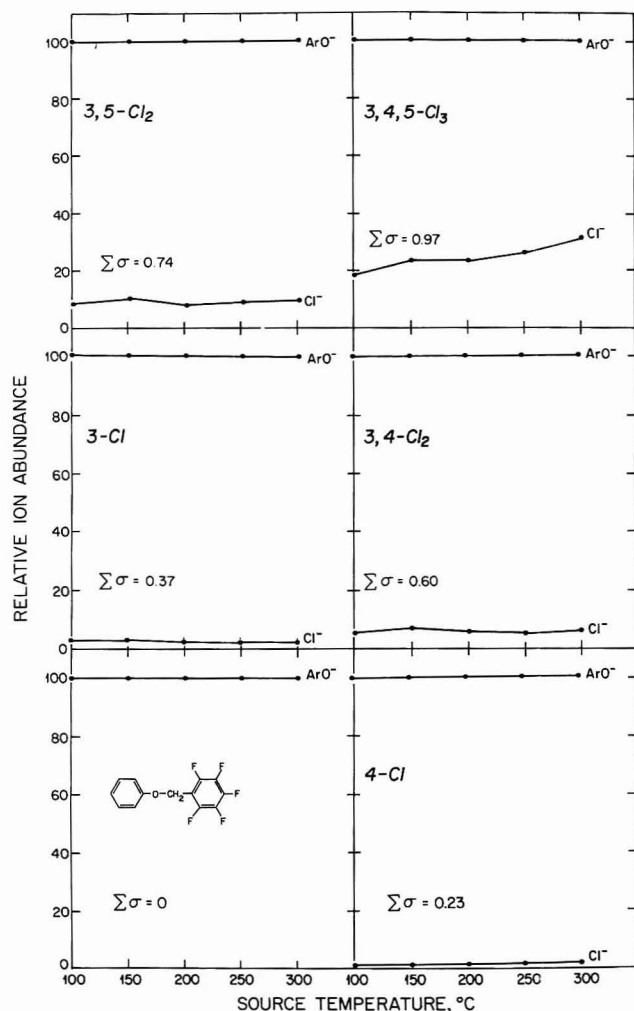
<sup>a</sup>  $\text{HCOCC}_6\text{H}_3(\text{CF}_3)_2^-$ .

Figure 2. Relative ion abundances vs. ion source temperature for pentafluorobenzyl ethers.

sponding phenol derivatives (4), no  $(\text{M} - 181)^+$  ion corresponding to the fragment  $\text{ArNH}^+$  was observed.

**III. Pentafluorobenzanilides.** In contrast to the case of phenol, the spectra of the derivatives obtained from treatment of the chlorinated anilines with pentafluorobenzoyl chloride did not exhibit a molecular anion,  $\text{M}^+$ , under EC-NCIMS conditions. For these derivatives, the spectra were

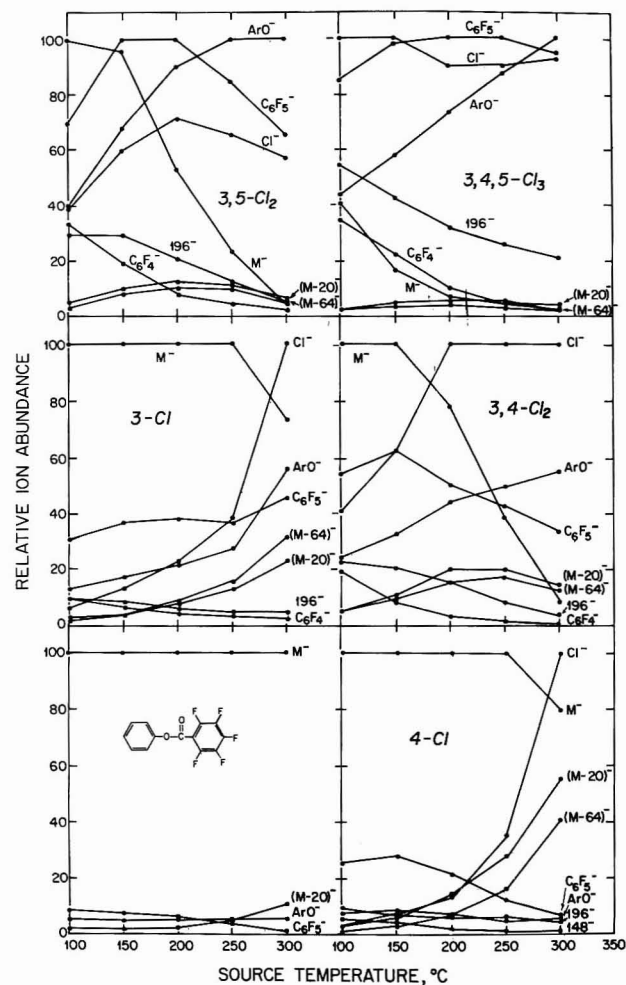


Figure 3. Relative ion abundances vs. ion source temperature for pentafluorobenzoate esters.

dominated by the fragments  $(\text{M} - \text{HF})^+$  and  $(\text{M} - \text{H}_2\text{F})^+$  (Table XIII and Scheme VI). For the case of aniline itself, the ion  $(\text{M} - \text{H}_2\text{F})^+$  was the base peak. With chlorine substitution on the ring the relative abundances of the  $(\text{M} - \text{HF})^+$  ion and chloride ion  $\text{Cl}^+$  increased, while that of the  $(\text{M} - \text{H}_2\text{F})^+$  ion decreased.

**IV. 3,5-Bis(trifluoromethyl)benzanilides.** The molecular anion  $\text{M}^+$  was the base peak in the EC-NCIMS spectra



Table XV. EC-NCI Mass Spectra of (Pentafluorophenyl)methanimines

Cl <sub>x</sub> PhN=CHC <sub>6</sub> F <sub>5</sub>	rel abundance					
	M <sup>+</sup>	(M - HF) <sup>+</sup>	(M - HCl) <sup>+</sup>	(M - F - Cl) <sup>+</sup>	C <sub>6</sub> F <sub>5</sub> <sup>+</sup>	Cl <sup>+</sup>
H	100	1			2	
4-Cl	100	1	0	1	3	1
3-Cl	100	2	0	0.5	3	0.5
3,4-Cl <sub>2</sub>	100	0.3	1	2	3	2
3,5-Cl <sub>2</sub>	100	2	0.3	1	3	2
3,4,5-Cl <sub>3</sub>	100	0.1	2	3	3	4

Table XVI. Hammett  $\rho$  Constants for Aniline Derivatives<sup>a,b</sup>

	derivative			
	RNHC(O)CF <sub>3</sub> (9) (M - HCl) <sup>+</sup> /M <sup>+</sup>	RNHCH <sub>2</sub> C <sub>6</sub> F <sub>5</sub> (12) (M - HF - HCl) <sup>+</sup> /(M - HF) <sup>+</sup>	RNH(O)CC <sub>6</sub> F <sub>5</sub> (13) (M - H <sub>2</sub> F) <sup>+</sup> /(M - HF) <sup>+</sup>	RNHC(O)C <sub>6</sub> H <sub>3</sub> (CF <sub>3</sub> ) <sub>2</sub> (14) (M - HCl) <sup>+</sup> /M <sup>+</sup>
$\rho$	3.05	3.24	-1.64	2.71
$r^2$	0.987	0.909	0.925	0.974
$b$	-0.75	-1.66	0.61	-2.62

<sup>a</sup>  $\log R = \rho \sum \sigma + b$ ;  $r^2$  = correlation coefficient. <sup>b</sup> Ion source temperature, 200 °C.

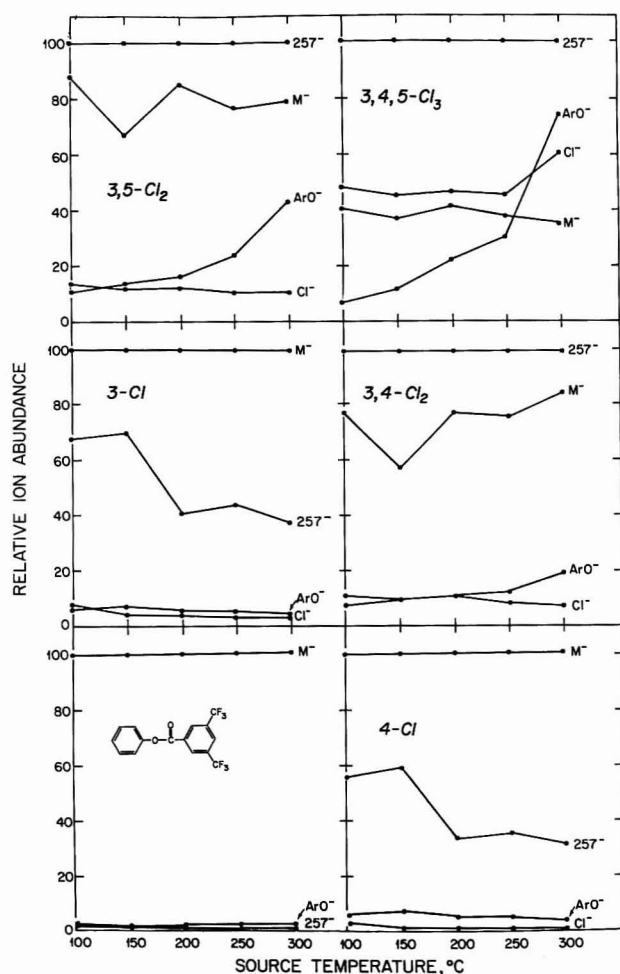
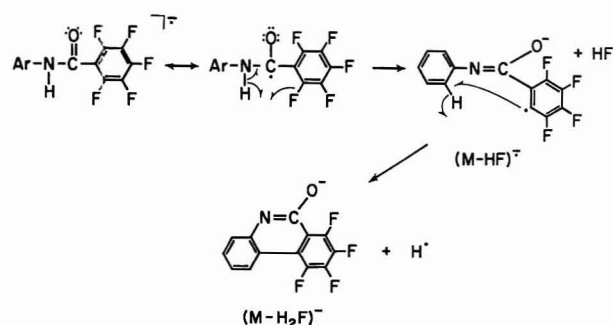


Figure 4. Relative ion abundances vs. ion source temperature for 3,5-bis(trifluoromethyl)benzoate esters.

of the anilines derivatized with 3,5-bis(trifluoromethyl)benzoyl chloride (Table XIV). Similar to the situation noted with the phenols, the change from a pentafluoro to a 3,5-bis(trifluoromethyl) electrophore had a major effect on the fragmentation pattern. No (M - HF)<sup>+</sup> ion was produced, and the major fragments include (M - H)<sup>+</sup>, (M - HCl)<sup>+</sup>, and Cl<sup>+</sup>. An ion derived from the derivative moiety, at  $m/z$  242, was also present.

**V. (Pentafluorophenyl)methanimines.** The formation of a Schiff's base derivative by treatment of primary amines

Scheme VI



with pentafluorobenzaldehyde has been utilized in both GC-ECD (31) and EC-NCIMS (7). Among the aniline derivatives studied here, the (pentafluorophenyl)methanimines of type 17 produced EC-NCIMS spectra with the least fragmentation (Table XV). Indeed, even for the chlorinated compounds, the molecular anion remained the base peak, accounting for over 80% of the total ion current. This reflects the stability of the highly conjugated anion formed upon initial electron capture.

**VI. Substituent Effects.** In a manner analogous to the phenols discussed above, the aniline derivatives examined in this study also exhibited fragmentation patterns under EC-NCIMS conditions that were consistent with the Hammett linear free energy relationships. Three types of derivatives (10, 11, and 17) showed very little variation in their mass spectral patterns as the number and position of chlorine substituents on the ring were varied. For the case of the Schiff's base, series 17, this is not surprising given the inherent high stability of the molecular anion. The derivatives in the series 10 and 11 exhibited only minor changes in ion abundances with increased chlorination, probably due to the very facile loss of HF (Scheme VI). However, derivatives of the type 9, 12, 13, and 14 produced EC-NCIMS spectra that showed considerable ion abundance variation with changes in chlorine substitution in agreement with the Hammett equation. This is illustrated in Table XVI that shows the Hammett equation constants obtained from linear regression analysis of the analytically most important ion abundance ratios.

When the conformity of the aniline and the phenol derivatives with the Hammett equation is compared, generally higher correlation coefficients may be noted for the phenols. For the anilines, the worst cases are for derivatives of type 12 and 13 where the ion ratios compared are formed via

Table XVII. GC-SIM-MS Relative Molar Response

compd	ion monitored	rel molar response (RMR) <sup>a</sup>		
		150 °C <sup>b</sup>	200 °C <sup>b</sup>	250 °C <sup>b</sup>
PhOCH <sub>2</sub> C <sub>6</sub> F <sub>5</sub> , 4	<i>m/z</i> 93 (C <sub>6</sub> H <sub>5</sub> O <sup>-</sup> )	1.8	2.1	2.5
PhOC(O)C <sub>6</sub> F <sub>5</sub> , 5	<i>m/z</i> 288 (M <sup>+</sup> )	0.73	1.1	1.0
PhOC(O)C <sub>6</sub> H <sub>3</sub> (CF <sub>3</sub> ) <sub>2</sub> , 6	<i>m/z</i> 234 (M <sup>+</sup> )	0.15	0.18	0.15

<sup>a</sup> RMR expressed in terms of area counts per picomole × 10<sup>6</sup>. <sup>b</sup> Source temperature.

Table XVIII. GC-ECD Relative Molar Response

compd	rel molar response, RMR <sup>a</sup>	RMR referenced to compd 5 <sup>b</sup>
PhOCH <sub>2</sub> C <sub>6</sub> F <sub>5</sub> , 4	3.9	1.3
PhOC(O)C <sub>6</sub> F <sub>5</sub> , 5	3.0	1.0
PhOC(O)C <sub>6</sub> H <sub>3</sub> (CF <sub>3</sub> ) <sub>2</sub> , 6	0.59	0.20

<sup>a</sup> RMR expressed in terms of area counts per picomole × 10<sup>6</sup>.<sup>b</sup> Calculated by dividing the RMR values for each compound by the RMR value of compound 5.

multistep processes. Thus it would appear that other factors, in addition to the simplified Hammett treatment, influence the mode of fragmentation of the molecular anion and other secondary fragments. Nevertheless, the selection of a derivative that yields abundant analyte-related ions for SIM can still be aided by applying the Hammett principles.

**C. Relative Sensitivity.** Any one type of the derivatives that produce abundant analyte-specific ions are, in principle, good candidates for trace level analysis by GC-SIM-MS using EC-NCIMS. For the examples considered in this study this criterion is met by most of the substituted anilines as long as the facile elimination of HF, HCl, or other related processes that yield analyte-related ions is a priori known. In the case of the phenols, derivatives of the type 4, 5, or 6 appear best suited for analytical purposes by GC-SIM-MS in the EC-NCIMS mode.

In previous work utilizing GC-ECD (4-6), it has been reported that significant differences in sensitivity exist among electrophoric derivatives of a specific analyte. The phenolic derivatives 4, 5, and 6 were used as models to assess the extent to which such differences in sensitivity may also exist under EC-NCIMS conditions. The experiment was carried out under selected ion monitoring conditions (500 pg injected) over a range of source temperatures. As shown in Table XVII, at all ion source temperatures studied, the relative molar responses remained in the order 4 > 5 > 6. It was further reasoned that, since all three of these compounds produce spectra composed of essentially a single ion, the differences in the MS response may also reflect the electron capturing ability of the compounds under methane EC-NCIMS conditions. Accordingly, we compared these molar response ratios to those exhibited for the same derivatives by the similar technique of GC-ECD. The data obtained, Table XVIII, indicate that the derivatives produce signals in the identical order as for the EC-NCIMS experiments, with some change in the ratio of responses between the three derivatives. This correlation does not imply that identical processes are taking place in the two detectors. However, unlike the information obtained with the mass spectrometer, the data from the ECD detector reveal little about the actual electron capture mechanism (i.e., dissociative vs. nondissociative) taking place in the ECD. A number of studies have been conducted on ECD detectors in combination with atmospheric ionization mass spectrometers (32-34) in order to study the actual ECD ionization products. None of these studies utilized any of the common electrophoric derivatives of the type discussed here. Consequently the identity of the anionic products formed in

the ECD remains unknown.

In conclusion, the data presented here show that selection of the appropriate electrophoric derivative is an important consideration in order to carry out trace level analysis by GC-EC-NCIMS. It is also shown that linear free energy relationships can be employed to predict stability of molecular anions, the direction of fragmentation pathways, and thus the extent to which a derivative will be useful under selective ion monitoring conditions. To that effect, the ion source temperature is an additional parameter that may play an important role in the efficient use of the EC-NCIMS selective ion detection process. Finally, the comparison of the molar responses of derivatives of the type 4, 5, and 6 when used in the GC-ECD vs. the GC-EC-NCIMS mode provides some interesting new insights regarding the operation of the two detectors. It appears, from the present data, that the EC-NCIMS and ECD are very similar in their mode of operation although, clearly, more information will be necessary before any definitive conclusions can be made. Work along these lines is currently in progress.

## LITERATURE CITED

- (1) Corkill, A.; Joppich, M.; Kuttub, H.; Giese, R. W. *Anal. Chem.* **1982**, *54*, 481-485.
- (2) Hunt, D. F.; Stafford, G. C., Jr.; Crow, F. W.; Russell, J. W. *Anal. Chem.* **1976**, *48*, 2098-2105.
- (3) Siegel, M. W.; McKeown, M. C. *J. Chromatogr.* **1976**, *122*, 397-413.
- (4) Zlatkis, A.; Poole, C. F. *Electron Capture. Theory and Practice in Chromatography*; Elsevier: New York, 1981; Chapter 8.
- (5) Poole, C. F.; Zlatkis, A. *Anal. Chem.* **1980**, *52*, 1002A-1016A.
- (6) Knapp, D. R. *Handbook of Analytical Derivatization Reactions*; Wiley: New York, 1979.
- (7) Hunt, D. F.; Crow, F. W. *Anal. Chem.* **1978**, *50*, 1781-1784.
- (8) Faull, K. F.; Barchas, J. D. In *Methods of Biochemical Analysis*; Glick, D., Ed.; Wiley: New York, 1983; Vol. 29, pp 325-383.
- (9) Shang-Zhi, S.; Duffield, A. M. *J. Chromatogr.* **1984**, *284*, 157-165.
- (10) Dougherty, R. C. *Biomed. Mass Spectrom.* **1981**, *8*, 283-292.
- (11) Crow, F. W.; Bjorseth, A. F.; Knapp, K. T.; Bennett, R. *Anal. Chem.* **1981**, *53*, 619-625.
- (12) Betowski, L. D.; Webb, H. M.; Sauter, A. D. *Biomed. Mass Spectrom.* **1983**, *10*, 369-376.
- (13) Grunwald, E. *CHEMTECH* **1984**, *14*, 698-705.
- (14) Fenimore, D. C.; Davis, M.; Whitford, J. H.; Harrington, C. A. *Anal. Chem.* **1976**, *48*, 2289-2290.
- (15) Grob, K.; Grob, K., Jr. *J. Chromatogr.* **1978**, *151*, 311-320.
- (16) Ehrsson, H.; Brothell, H.; Glyllenhaal, O. *J. Chromatogr.* **1973**, *78*, 293-301.
- (17) Ehrsson, H.; Walle, T.; Brothell, H. *Acta Pharm. Suec.* **1971**, *8*, 319-328.
- (18) Lamparski, L. L.; Nestrick, T. J. *J. Chromatogr.* **1978**, *156*, 143-150.
- (19) Lee, H.-B.; Weng, L.-D.; Chau, A. S. Y. *J. Assoc. Off. Anal. Chem.* **1984**, *67*, 1086-1091.
- (20) Davis, B. *Anal. Chem.* **1977**, *49*, 832-834.
- (21) Kawahara, F. H. *Anal. Chem.* **1968**, *40*, 1009-1010.
- (22) Strife, R. J.; Murphy, R. C. *J. Chromatogr.* **1984**, *305*, 3-12.
- (23) Buisson, R. S. K.; Kirk, P. W. W.; Lester, J. N. *J. Chromatogr. Sci.* **1984**, *22*, 339-342.
- (24) Murray, S.; Davies, D. S. *Biomed. Mass Spectrom.* **1984**, *11*, 435-440.
- (25) Bursey, M. M. In *Advances in Linear Free Energy Relationships*; Chapman, N. B., Shorter, J., Eds.; Plenum: New York, 1972; pp 445-461.
- (26) Bentley, T. W.; Johnstone, R. A. W. In *Advances in Physical Organic Chemistry*; Gold, V., Ed.; Academic: New York, 1970; Vol. 8, pp 151-269.
- (27) Exner, O. In *Advances in Linear Free Energy Relationships*; Chapman, N. B., Shorter, J., Eds.; Plenum: New York, 1972; pp 2-69.
- (28) Lowry, T. H.; Richardson, K. S. *Mechanism and Theory in Organic Chemistry*; Harper and Row: New York, 1976; p 62.
- (29) Miwa, B. J.; Garland, W. A.; Blumenthal, P. *Anal. Chem.* **1981**, *53*, 793-797.
- (30) Low, G. K. C.; Duffield, A. M. *Biomed. Mass Spectrom.* **1984**, *11*, 177-181.



- (31) Moffat, A. C.; Horning, E. C.; Matin, S. B.; Rowland, M. J. *Chromatogr.* **1971**, *66*, 255-260.  
 (32) Grimsrud, E. P.; Kim, S. H.; Gobby, P. L. *Anal. Chem.* **1979**, *51*, 223-229.  
 (33) Horning, E. C.; Carroll, D. I.; Dzidic, I.; Lin, S. N.; Stilwell, R. N.; The-  
 not, J. P. *J. Chromatogr.* **1977**, *142*, 481-495.  
 (34) Siegel, M. W.; McKeown, M. C. *J. Chromatogr.* **1976**, *122*, 397-413.

RECEIVED for review May 5, 1986. Accepted October 10, 1986.

This work was supported by funds provided from the National Institutes of Health (Grants RR07143, NS 15439, NCICA35843), Grant CR 812740 from the Reproductive Effects Assessment Group of the U.S. Environmental Protection Agency, and an ACS Analytical Division Graduate Fellowship sponsored by the Analytical Chemists of Pittsburgh (T.M.T.). Contribution no. 294 from the Barnett Institute of Chemical Analysis.

## Application of Isotope Dilution Inductively Coupled Plasma Mass Spectrometry to the Analysis of Marine Sediments

J. W. McLaren,\* Diane Beauchemin, and S. S. Berman

Analytical Chemistry Section, Division of Chemistry, National Research Council of Canada, Ottawa, Ontario, Canada K1A 0R9

Isotope dilution inductively coupled plasma mass spectrometry (ICP-MS) has been applied to the determination of 11 trace elements (Cr, Ni, Zn, Sr, Mo, Cd, Sn, Sb, Ti, Pb, and U) in the marine sediment reference materials MESS-1 and BCSS-1. Accuracy and, especially, precision are better than those that can be easily achieved by other ICP-MS calibration strategies, as long as isotopic equilibration is achieved and the isotopes used for the ratio measurement are free of isobaric interferences by molecular species. The measurement of the isotope ratios on unspiked samples provides a sensitive diagnostic of such interferences.

The detection power of inductively coupled plasma mass spectrometry (ICP-MS) makes possible the determination in geological reference materials of many trace elements for which relatively few reliable values have been previously established (1-4). This lack of data in many cases prevents a full assessment of the accuracy of ICP-MS results. A partial solution to this problem is the use of stable isotope dilution techniques (5) which are immune to many of the sources of error which can adversely affect ICP-MS results obtained by other calibration strategies. This approach would, for example, be an effective means to compensate for the suppression of ion sensitivities by concomitant elements (6) observed in many of the early applications of ICP-MS (4, 7-9). Also, more calibration drift can be tolerated in an isotope dilution analysis because an isotope ratio, rather than an absolute intensity measurement, is used in the calculation of the analyte concentration. This suggests that it may be easier to obtain accurate and precise ICP-MS results for solutions with appreciable dissolved solids concentrations if isotope dilution techniques are used.

Relatively little use has been made of isotope dilution techniques in ICP-MS. Its application to the determination of six trace metals in a coastal seawater sample after a separation by adsorption on silica-immobilized 8-hydroxyquinoline was recently reported (10). Ting and Janghorbani used a  $^{57}\text{Fe}$  spike for the accurate determination of  $^{54}\text{Fe}$  and  $^{58}\text{Fe}$  in human fecal matter after a chemical separation (11). Taylor and Garbarino (12) have applied isotope dilution ICP-MS to the determination of trace elements in natural

Table I. Operating Conditions for Isotopic Analysis by ICP-MS

ICP	
plasma Ar	14 L min <sup>-1</sup>
auxiliary Ar	2.0 L min <sup>-1</sup>
nebulizer Ar	0.9 L min <sup>-1</sup>
rf power	1.2 kW
Mass Spectrometer	
sampler	nickel, 1.2-mm orifice
skimmer	nickel, 0.9-mm orifice
Operating Pressures	
interface region	~1 torr
mass spectrometer chamber	~4 × 10 <sup>-5</sup> torr
Lens Voltages	
photon stop (S2)	-7.0 V
Bessel box barrel (B)	+2.95 V
einzel lenses 1 and 3 (E1)	-12.0 V
Bessel box end lenses (P)	-11.3 V
einzel lens 2	-130 V
entrance a.c. rods	0 V
exit a.c. rods	-5 V

waters. Longerich et al. (4) briefly described the determination of samarium using a  $^{147}\text{Sm}$  isotopic spike in three geological reference materials.

The purpose of the present work was to examine in detail the application of isotope dilution ICP-MS to the determination of trace elements in solutions of the marine sediment reference materials MESS-1 and BCSS-1. These materials were chosen with two objectives in mind: verification of the methodology by comparison of the results with published reliable values, and assessment of the potential of isotope dilution ICP-MS to contribute accurate data toward establishment of reliable values for additional elements.

### EXPERIMENTAL SECTION

**Instrumentation.** The inductively coupled plasma mass spectrometer used for this work was an ELAN 250 from SCIEX Division of MDS Health Group Ltd. (Thornhill, Ontario, Canada) that had recently undergone a modification of the original ion optics by the manufacturer to improve stability and reduce suppression of analyte ion sensitivity by concomitant elements. This involved replacement of a set of ac rods between the skimmer and Bessel box lenses with a three-cylinder einzel lens and re-

placement of a screen (termed the "ring" electrode), positioned immediately behind the skimmer and held at -10 to -50 V, with a 5-mm-diameter grounded stop. The lens voltage settings used for this work are listed in Table I.

As described in ref 10 a mass flow controller was used on the aerosol carrier gas line and solution uptake was controlled by a peristaltic pump. As described in ref 9 the extended torch provided with the instrument was replaced with a conventional ICP-AES torch and the torch box was positioned as close as possible to the sampler. Other details of the operating conditions are given in Table I.

**Reagents.** All acids were purified by subboiling distillation of reagent grade feedstocks in quartz or polypropylene stills prior to use. Enriched isotopes purchased from the Oak Ridge National Laboratory included  $^{53}\text{Cr}$ ,  $^{61}\text{Ni}$ ,  $^{67}\text{Zn}$ ,  $^{86}\text{Sr}$ ,  $^{100}\text{Mo}$ ,  $^{111}\text{Cd}$ ,  $^{117}\text{Sn}$ ,  $^{123}\text{Sb}$ ,  $^{203}\text{Tl}$ , and  $^{207}\text{Pb}$ . These stable isotopes were received as metals or oxides (lead as the nitrate) with an isotopic enrichment greater than 95%. Stock solutions of approximately 100 mg L<sup>-1</sup> of each were prepared by dissolution of an accurately weighed quantity of the material in nitric acid and dilution to volume.  $\text{Cr}_2\text{O}_3$  was dissolved by prolonged digestion with several milliliters of perchloric acid.  $\text{SnO}_2$  was dissolved by a lithium tetraborate fusion. The source of  $^{235}\text{U}$  was the U.S. National Bureau of Standards SRM U-930. The concentrations of the spike solutions were verified by reverse spike isotope dilution ICP-MS.

**Dissolution of Marine Sediments.** A series of solutions of the marine sediment reference materials MESS-1 and BCSS-1 was prepared by a mixed acid digestion procedure which results in a total dissolution of a 0.5-g sample in 50 mL of 0.5 M nitric acid. The initial digestion was performed by heating each sample with a mixture of 3 mL of hydrofluoric acid, 3 mL of nitric acid, and 2 mL of perchloric acid in a sealed pressure decomposition vessel made of Teflon in a boiling water bath for 3 h. The mixture was then transferred to a beaker made of Teflon and evaporated to fumes of perchloric acid. Two further digestions were performed by adding 1-mL portions of hydrofluoric acid and perchloric acid and evaporating to dryness. Concentrated nitric acid (2 mL) was then added to the residue and the mixture gently boiled. The mixture was transferred to a 50-mL flask and diluted to volume with deionized distilled water. A small amount of a light-colored undissolved residue that remained at this point slowly dissolved if the solution was left to stand for 48 h.

For the isotope dilution analyses, the isotopic spikes were added to the sediment samples prior to the first digestion. The aliquots of the isotope spike solutions were calculated to result in a ratio near 1 for each of the isotope pairs. The reference/spike isotope pairs were as follows:  $^{52}\text{Cr}/^{53}\text{Cr}$ ;  $^{60}\text{Ni}/^{61}\text{Ni}$ ;  $^{68}\text{Zn}/^{67}\text{Zn}$ ;  $^{88}\text{Sr}/^{86}\text{Sr}$ ;  $^{98}\text{Mo}/^{100}\text{Mo}$ ;  $^{114}\text{Cd}/^{111}\text{Cd}$ ;  $^{118}\text{Sn}/^{117}\text{Sn}$ ;  $^{121}\text{Sb}/^{123}\text{Sb}$ ;  $^{205}\text{Tl}/^{203}\text{Tl}$ ;  $^{208}\text{Pb}/^{207}\text{Pb}$ ;  $^{238}\text{U}/^{235}\text{U}$ .

**Isotope Ratio Measurements.** Intensity data for isotope ratio determinations were acquired by "peak-hopping" through the 22 isotopes listed above a total of 50 times. The low resolution setting of the ELAN was found to be adequate in all cases. At each peak of interest, three measurements of 0.1-s duration were made, one at the assumed peak center, and the other two at  $\pm 0.1$  u. Each isotope ratio reported was thus the mean of 50 determinations. The total analysis time was approximately 7–8 min. Corrections for known isobaric interferences were made automatically by the ELAN software where necessary.

**Mass Discrimination Corrections.** Before the results of isotope ratio measurements are applied to isotope dilution calculations, it is important to check for mass discrimination effects. If such effects are significant, a correction must of course be made to the ratios (11). In this work, checks for mass discrimination were made with 100  $\mu\text{g L}^{-1}$  natural abundance solutions of each of the elements of interest, except lead, for which a solution of the NBS SRM 981 lead isotopic standard was used, and uranium, for which a solution of the U-930 reference material was used. It was found that isotope ratios were reproducible to better than  $\pm 1\%$  from day to day provided that none of the lens voltages or plasma operating conditions were changed. With the ion lens voltages set as described in Table I, the sensitivity of the ELAN (on a molar basis) is highest, and rather uniform, in the middle of the usable mass range (i.e., 100–150 u); it decreases quite gradually toward higher mass, but somewhat more quickly in the other direction. Because of this, mass discrimination effects are

largest for the lighter elements. For example, the mean value of the  $^{61}\text{Ni}/^{60}\text{Ni}$  ratio observed over a 1 week period was  $0.0448 \pm 0.0002$ , about 3% higher than the expected value of 0.0434. The measured  $^{235}\text{U}/^{238}\text{U}$  ratio for the uranium standard was  $18.68 \pm 0.16$ , about 7.5% higher than the certified value of 17.35, corresponding to a mass discrimination of about 2.5%/u. In this work, correction factors of 2–3%/u were applied to isotope ratios for chromium, nickel, and uranium, but for the other eight elements, mass discrimination effects were found to be insignificant.

No evidence that the isotope ratios are dependent on concentration nor upon the presence of concomitant elements has been observed in measurements on unspiked solutions of the marine sediments. Even at solution concentrations as low as 10–100  $\mu\text{g L}^{-1}$ , it was possible to measure the ratios with a precision of 1% or better. In every case where isotope ratios differed significantly from the values obtained for pure solutions of the elements, the discrepancy was attributable to an isobaric interference.

**Isotope Dilution Analyses.** Each set of isotope dilution analyses involved duplicate determinations for 11 isotope pairs in four solutions. As each determination required approximately 8 min, the total analysis time was about 1 h. A continuous decrease in sensitivity for all elements was always observed, with sensitivities at the end of the run ranging from half of the original values for the heavy elements (e.g., U, Pb) to one-quarter of these values for the lighter elements (e.g., Ni, Zn). There is no doubt that most, if not all, of this sensitivity loss was caused by deposition of material on the sampler and skimmer. It was always possible to recover the original sensitivity simply by removing and cleaning these two parts. Although the rate of change of sensitivity observed in these experiments would probably be intolerable if calibration by external standardization or the method of additions were attempted, it represented only a minor inconvenience in isotope dilution analyses, in which each element has the ideal internal standard—another of its isotopes.

Analyte concentrations in the sediment samples were calculated by means of the formula

$$C = \frac{M_s K (A_s - B_s R)}{W(BR - A)}$$

where  $C$  is the analyte concentration in micrograms per gram,  $M_s$  is the mass of the stable isotope spike in micrograms,  $A$  is the natural abundance of the reference isotope,  $B$  is the natural abundance of the spike isotope,  $A_s$  is the abundance of the reference isotope in the spike,  $B_s$  is the abundance of the spike isotope in the spike,  $K$  is the ratio of the natural and spike atomic weights,  $W$  is the sample weight, and  $R$  is the measured isotope ratio after spike addition.

A separate set of isotope dilution analyses was performed to determine the blanks for the dissolution procedure. The isotopic spike masses were somewhat arbitrarily chosen to be 4% of those made for the 0.5-g sediment samples. Two blanks were carried with each set of four samples. Tin was the only element for which a significant blank was observed.

## RESULTS AND DISCUSSION

### Isotope Ratio Measurements for Unspiked Solutions.

An essential requirement for an accurate stable isotope dilution analysis is that neither of the pair of isotopes chosen is subject to any significant isobaric interference for which correction cannot be easily performed. The measurement of isotope ratios for an unspiked sample provides a very sensitive diagnostic of such interferences. Corrections for known isobaric interferences (e.g.,  $^{114}\text{Sn}$  on  $^{114}\text{Cd}$ ) are made automatically by the ELAN software. Any significant deviation of the measured ratio from the value calculated from the natural abundances of the two isotopes is then diagnostic of an interference by a molecular species.

In Table II, results of isotope ratio measurements on unspiked solutions of MESS-1 and BCSS-1 are compared with the expected values. Values for the  $^{207}\text{Pb}/^{208}\text{Pb}$  and  $^{235}\text{U}/^{238}\text{U}$  ratios are not included in the table. Because lead isotopic abundances vary in nature, ratio measurements cannot be compared with a single expected value. No measurements



**Table II. Results of Isotope Ratio Measurements for Unspiked MESS-1 and BCSS-1 Solutions**

ratio	expected	MESS-1	BCSS-1
$^{53}\text{Cr}/^{52}\text{Cr}$	0.114	$0.161 \pm 0.018$	$0.155 \pm 0.020$
$^{61}\text{Ni}/^{60}\text{Ni}$	0.0434	$0.091 \pm 0.006$	$0.077 \pm 0.002$
$^{67}\text{Zn}/^{68}\text{Zn}$	0.221	$0.382 \pm 0.064$	$0.736 \pm 0.125$
$^{86}\text{Sr}/^{88}\text{Sr}$	0.119	$0.119 \pm 0.001$	$0.118 \pm 0.001$
$^{100}\text{Mo}/^{98}\text{Mo}$	0.403	$0.416 \pm 0.003$	$0.416 \pm 0.007$
$^{111}\text{Cd}/^{114}\text{Cd}$	0.446	$0.841 \pm 0.032$	$1.16 \pm 0.08$
$^{117}\text{Sn}/^{118}\text{Sn}$	0.315	$0.314 \pm 0.004$	$0.314 \pm 0.004$
$^{123}\text{Sb}/^{121}\text{Sb}$	0.747	$0.835 \pm 0.041$	$0.897 \pm 0.032$
$^{203}\text{Tl}/^{205}\text{Tl}$	0.418	$0.428 \pm 0.004$	$0.421 \pm 0.008$

were made for uranium because of the very low natural abundance of  $^{235}\text{U}$ . Values for strontium, molybdenum, thallium, and tin agree well with the expected values, but there are clearly problems for the other elements.

The  $^{53}\text{Cr}/^{52}\text{Cr}$  ratios for both MESS-1 and BCSS-1 are much higher than expected, indicating an interference on the spike isotope,  $^{53}\text{Cr}$ . The interfering species is almost certainly  $^{37}\text{Cl}^{16}\text{O}$ ; perchloric acid used in the dissolution procedure may not be completely removed in the evaporations to dryness. Chromium was successfully determined in more dilute BCSS-1 solutions by the method of standard additions (9); apparently the potential interference of  $^{35}\text{Cl}^{16}\text{O}$  on  $^{52}\text{Cr}$  was insignificant in that case. The interference at  $m/z$  53 is much more severe not only because of the lower natural abundance of  $^{53}\text{Cr}$  but also because the  $^{37}\text{Cl}^{16}\text{O}$  peak is considerably more intense than that of  $^{35}\text{Cl}^{16}\text{OH}$ .

Overlap of  $^{67}\text{Zn}$  by  $^{35}\text{Cl}^{16}\text{O}_2$  probably accounts for the much higher than expected  $^{67}\text{Zn}/^{68}\text{Zn}$  ratios observed for the sediment solutions. Because of its low natural abundance (4.11%),  $^{67}\text{Zn}$  is very susceptible to spectroscopic interferences. Zinc was also successfully determined in more dilute BCSS-1 solutions by the method of standard additions, using  $^{68}\text{Zn}$  (9). Other zinc isotopes are subject to oxide interferences by either titanium oxides (for  $^{64}\text{Zn}$  and  $^{66}\text{Zn}$ ) or iron oxide (for  $^{70}\text{Zn}$ ). Thus, a successful isotope dilution method for zinc in marine sediments will require either a significant reduction in the chloride concentrations in the final solutions (perhaps by reducing or eliminating the use of perchloric acid) or a reduction of oxide levels, or at least an accurate correction procedure for oxide overlaps.

Overlap of  $^{61}\text{Ni}$  by  $^{44}\text{Ca}^{16}\text{OH}$  is believed to be responsible for the higher than expected values of the  $^{61}\text{Ni}/^{60}\text{Ni}$  ratio. The fact that the value is *higher* than expected implies that the interference by the corresponding oxide on  $^{60}\text{Ni}$  is less significant. This situation arises not because the hydroxide species is more abundant than the oxide but rather because  $^{61}\text{Ni}$ , with a natural abundance of only 1.13%, is much more

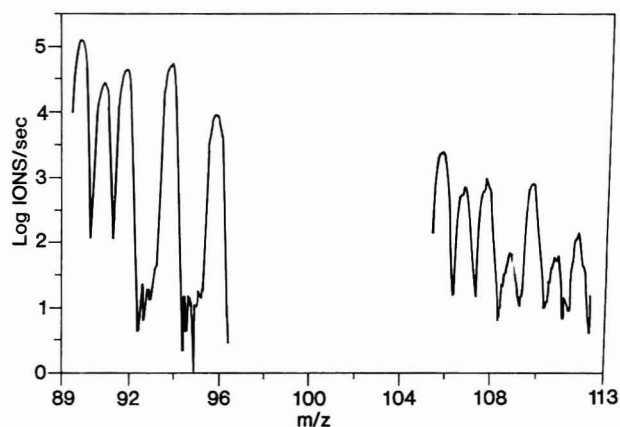
susceptible to interference than  $^{60}\text{Ni}$ , with an abundance of 26.1%. The fact that nickel was successfully determined in BCSS-1 by the method of standard additions using the latter isotope (9) suggests that interference by  $^{44}\text{Ca}^{16}\text{O}$  on  $^{60}\text{Ni}$  is small in this case. Nickel has also been determined by isotope dilution ICP-MS in a river water reference material, but only after a separation and preconcentration by adsorption on silica-immobilized 8-hydroxyquinoline (13). It was found that even after the separation,  $^{61}\text{Ni}$  was not usable because of interference by  $^{44}\text{Ca}^{16}\text{OH}$  arising from the residual calcium ( $\sim 30 \text{ mg L}^{-1}$ ) in the concentrate. This problem was circumvented by using  $^{62}\text{Ni}$  as the spike isotope and  $^{60}\text{Ni}$  as the reference. This solution is not so attractive in the case of the marine sediments because of overlap of  $^{62}\text{Ni}$  by  $^{46}\text{Ti}^{16}\text{O}$ . Despite the large discrepancies of the  $^{61}\text{Ni}/^{60}\text{Ni}$  ratios from the expected value, results of isotope dilution analyses obtained by using this isotope pair are only slightly lower than the accepted values. The interference by  $^{44}\text{Ca}^{16}\text{OH}$  is less severe in the spiked sample, in which the abundance of  $^{61}\text{Ni}$  has been adjusted to be approximately equal to that of  $^{60}\text{Ni}$ . It might be considered in this case that the isotope ratio measurement for an unspiked sample overestimates the severity of the interference problem; on the other hand, it provides a warning that there is a problem which will become increasingly severe as the calcium/nickel concentration ratio of the sample increases.

Another situation in which overlap by a hydroxide species posed a serious problem arose in the determination of cadmium. The only stable isotope available was  $^{111}\text{Cd}$ , and  $^{111}\text{Cd}/^{114}\text{Cd}$  ratios were much higher than expected for solutions of both sediments. As the molybdenum concentrations in these materials are not much higher than the cadmium concentrations, it seemed very unlikely that the discrepancy was due to an overlap of  $^{111}\text{Cd}$  by  $^{95}\text{Mo}^{16}\text{O}$ , a problem encountered by McLeod et al. (8) in the analysis of nickel-base alloys. A more likely possibility is an overlap by  $^{94}\text{Zr}^{16}\text{OH}$ . The mass spectrum of a  $3 \text{ mg L}^{-1}$  zirconium solution in the mass range from 90–96 and 106–112 u, plotted on a logarithmic intensity scale, is shown in Figure 1. While the peaks at 106, 107, 108, 110, and 112 u can be assigned as oxides of the five isotopes of zirconium, two additional peaks at 109 and 111 u are almost certainly due to  $^{92}\text{Zr}^{16}\text{OH}$  and  $^{94}\text{Zr}^{16}\text{OH}$ . (A remarkably similar set of spectra for a  $10 \text{ mg L}^{-1}$  Mo solution showing oxide and hydroxide peaks has been published by McLeod et al. (8).) Zirconium/cadmium concentration ratios for MESS-1 and BCSS-1 are approximately 850 and 1400, respectively; as would be expected from these data, the isotope ratio discrepancy is larger for BCSS-1 than for MESS-1. A possible solution to this problem would be the use of  $^{113}\text{Cd}$  as the spike isotope; while this would necessitate a correction

**Table III. Isotope Dilution Analysis of Marine Sediment Reference Materials**

element	MESS-1		BCSS-1	
	found <sup>a</sup>	accepted	found <sup>a</sup>	accepted
Cr	$55.2 \pm 0.8$	$71 \pm 11$	$95.0 \pm 1.2$	$123 \pm 14$
Ni	$26.3 \pm 0.3$	$29.5 \pm 2.7$	$53.5 \pm 0.6$	$55.3 \pm 3.6$
Zn	$171 \pm 2$	$191 \pm 17$	$85 \pm 4$	$119 \pm 12$
Sr	$94 \pm 1$	(89) <sup>b</sup>	$108 \pm 2$	(96) <sup>b</sup>
Mo	$2.2 \pm 0.1$	$(2.2 \pm 0.3)^c$	$2.03 \pm 0.04$	$(1.9 \pm 0.2)^c$
Cd	$0.40 \pm 0.03$	$0.59 \pm 0.10$		$0.25 \pm 0.04$
Sn	$3.8 \pm 0.2$	$(3.4 \pm 0.2)^d$	$1.75 \pm 0.06$	$(1.8 \pm 0.2)^d$
Sb	$0.67 \pm 0.04$	$0.73 \pm 0.08$	$0.47 \pm 0.05$	$0.59 \pm 0.06$
Tl	$0.74 \pm 0.02$	$(0.70 \pm 0.03)^c$	$0.65 \pm 0.03$	$(0.60 \pm 0.05)^c$
Pb	$33.1 \pm 0.7$	$34.0 \pm 6.1$	$22.9 \pm 0.5$	$22.7 \pm 3.4$
U	$4.1 \pm 0.4$	$(4.2 \pm 0.3)^e$	$2.7 \pm 0.2$	$(2.7 \pm 0.2)^e$

<sup>a</sup> Results in  $\mu\text{g/g}$ ; precision expressed as the standard deviation ( $n = 16$ ). <sup>b</sup> Flame atomic absorption spectrometry. <sup>c</sup> Isotope dilution spark source mass spectroscopy with preconcentration by electrodeposition. <sup>d</sup> Hydride generation graphite furnace atomic absorption spectrometry (14). <sup>e</sup> Isotope dilution spark source mass spectroscopy.



**Figure 1.** ICP mass spectrum illustrating the relative abundance of zirconium and zirconium oxide and hydroxide species at a nebulizer gas flow rate of 0.9 L min<sup>-1</sup>.

for the <sup>113</sup>In isobaric interference, the interference from <sup>96</sup>Zr<sup>16</sup>OH would be about six times less severe.

The <sup>123</sup>Sb/<sup>121</sup>Sb ratios for MESS-1 and BCSS-1 are slightly higher than expected. This may be due to an overlap of <sup>123</sup>Sb by <sup>91</sup>Zr<sup>16</sup>O<sub>2</sub>. The signal for a 3 mg L<sup>-1</sup> Zr solution at *m/z* 123 appeared to be very slightly above the background level.

**Results of Isotope Dilution Analyses.** Results of isotope dilution analyses of eight solutions each of MESS-1 and BCSS-1 are presented in Table III. These values are compared with the published accepted values for the elements for which these have been established; for the other elements, results obtained by other methods available in this laboratory are used for comparison.

Results for chromium and zinc are consistently low because of interferences by chlorine-containing molecular ions on the <sup>53</sup>Cr and <sup>67</sup>Zn spike isotopes. Values for nickel and antimony are only slightly low, indicating that the interferences discussed for these elements in the previous section are not severe. Results for strontium, molybdenum, tin, thallium, and uranium are in very good agreement with the values obtained by other methods, and the lead results are in excellent agreement with the accepted values. A striking feature of all of the results is the very high precision obtained, even for elements such as antimony and thallium at the sub-microgram-per-gram level in these materials.

## CONCLUSIONS

The use of stable isotope dilution techniques has been shown to be a very useful complement to alternative calibration strategies in ICP-MS. More concentrated solutions can be analyzed without any sacrifice of precision; in fact, precision is greatly improved because the ratioing of intensities for a pair of isotopes for each element is the ideal form of internal standardization.

## ACKNOWLEDGMENT

Spark source mass spectrographic analyses were performed by A.P. Mykytiuk of this laboratory, whom we also thank for many helpful discussions on isotope dilution techniques. R. E. Sturgeon, also of this laboratory, performed the graphite furnace atomic absorption analyses.

**Registry No.** Cr, 7440-47-3; Ni, 7440-02-0; Zn, 7440-66-6; Sr, 7440-24-6; Mo, 7439-98-7; Cd, 7440-43-9; Sn, 7440-31-5; Sb, 7440-36-0; Tl, 7440-28-0; Pb, 7439-92-1; U, 7440-61-1.

## LITERATURE CITED

- (1) Date, A. R.; Gray, A. L. *Spectrochim. Acta, Part B* **1985**, *40B*, 115-122.
- (2) Date, A. R.; Hutchison, Dawn *Spectrochim. Acta, Part B* **1986**, *41B*, 175-181.
- (3) Doherty, W.; Vander Voet, A. *Can. J. Spectrosc.* **1985**, *30*, 135-141.
- (4) Longerich, H. P.; Fryer, B. J.; Strong, D. F.; Kantipuly, C. J., submitted for publication in *Spectrochim. Acta, Part B*.
- (5) Heumann, K. G. *TrAC Trends Anal. Chem. (Pers. Ed.)* **1982**, *1*, 357-361.
- (6) Olivares, J. A.; Houk, R. S. *Anal. Chem.* **1986**, *58*, 20-25.
- (7) Pickford, C. J.; Brown, R. M. *Spectrochim. Acta, Part B* **1986**, *41B*, 183-187.
- (8) McLeod, C. W.; Date, A. R.; Cheung, Y. Y. *Spectrochim. Acta, Part B* **1986**, *41B*, 169-174.
- (9) McLaren, J. W.; Beauchemin, Diane; Berman, S. S. *J. Anal. At. Spectrom.*, in press.
- (10) McLaren, J. W.; Mykytiuk, A. P.; Willie, S. N.; Berman, S. S. *Anal. Chem.* **1985**, *57*, 2907-2911.
- (11) Ting, B. T. G.; Janghorbani, Morteza *Anal. Chem.* **1986**, *58*, 1334-1340.
- (12) Taylor, H. E.; Garbarino, J. R. Colloquium Spectroscopicum International XXIV, Garmisch-Partenkirchen, West Germany, Sept. 15-20, 1985, Abstract No. 52.
- (13) Beauchemin, Diane; McLaren, J. W.; Mykytiuk, A. P.; Berman, S. S. *Anal. Chem.*, in press.
- (14) Sturgeon, R. E.; McLaren, J. W.; Willie, S. N.; Beauchemin, D.; Berman, S. S. *Can. J. Chem.*, in press.

RECEIVED for review May 15, 1986. Accepted October 9, 1986.  
This is NRCC Publication No. 26681.



# Determination of Sites of Incorporation of Oxygen-18 Atoms in Maduramicin $\alpha$ by Fast Atom Bombardment Mass Spectrometry

Ted T. Chang\*

Chemical Research Division, American Cyanamid Company, Stamford, Connecticut 06904

Hwei-Ru Tsou and Marshall M. Siegel

Medical Research Division, American Cyanamid Company, Pearl River, New York 10965

**Elucidation of the bioorigin of the molecular structure is important for the understanding of biosynthetic mechanisms. To investigate the function of molecular oxygen, an  $^{18}\text{O}$ -labeled maduramicin  $\alpha$  was biosynthesized under  $^{18}\text{O}$  gas and analyzed by fast atom bombardment mass spectrometry. Five  $^{18}\text{O}$  atoms were found to be incorporated in the biosynthesized maduramicin  $\alpha$  structure. The exact locations of these five  $^{18}\text{O}$  atoms were determined from fragmentation patterns as O(5), O(10), O(11), O(12), and O(13) positions.**

Maduramicin  $\alpha$  is a potent coccidiostat, poultry antibiotic, effective at a level of 5 ppm. It is a polyether ionophore antibiotic possessing a polyoxygenated carbon backbone and a 2,6-dideoxysugar (1, 2) with the structure shown in Figure 1.

Elucidation of the bioorigin of carbon atoms and oxygen atoms of maduramicin  $\alpha$  (simplified as maduramicin in the following text) has been a major research subject of our laboratories. It is important not only for the understanding of the biosynthetic mechanism but also for the optimization of the fermentation processes. With  $^{13}\text{C}$  labeled precursors fed to cultures of *Actinomadura yumaensis* and a subsequent assignment of  $^{13}\text{C}$  NMR spectrum, it was recently established that the basic aglycone carbon skeleton of maduramicin (excluding the G ring) is derived from eight acetate and seven propionate units and that the methoxy carbons are derived from methionine (3, 4).

The investigations on the bioorigin of some oxygen atoms were also carried out with isotope labeled maduramicin. They were studied by incorporating [ $1\text{-}^{13}\text{C},^{18}\text{O}$ ]acetate and [ $1\text{-}^{13}\text{C},^{18}\text{O}$ ]propionate in the fermentation cultures. From the  $^{13}\text{C}$  NMR spectra of carbon atoms adjacent to the oxygen atoms, it was concluded that five oxygen atoms, O(1), O(6), O(8), O(9), and O(14), are derived from acetate while three oxygen atoms, O(3), O(4), and O(7), originated from propionate (3).

Our current objective is to understand the contribution of molecular oxygen in the biosynthesis of maduramicin. In the past, biosynthesis of antibiotics in  $^{18}\text{O}$  gas has usually resulted in poor yields. We have, therefore, designed a special closed fermentation system which is capable of producing highly enriched  $^{18}\text{O}$ -labeled maduramicin. This fermentation system and the purification procedures will be reported elsewhere (5).

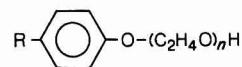
Mass spectrometry has been a major analytical tool for the structural studies of polyether ionophores (6, 7). Unfortunately, in many cases, its application was limited by the volatility and thermal stability of ionophores. This limitation was considerably minimized after the introduction of fast atom bombardment (FAB) (8). FAB was found to be very suitable

for the analysis of ionophores because ionophores produce intense and steady FAB spectra (9, 10). For this report, we have applied FAB to determine the number of molecular oxygen atoms incorporated in the structure of maduramicin. Furthermore, we successfully located the exact positions of these five oxygen atoms from the fragmentation patterns of maduramicin.

## EXPERIMENTAL SECTION

The mass spectrometer used for this study was a Kratos MS-50 high-resolution mass spectrometer, Kratos Analytical, Manchester, England. The instrument was equipped with a FAB source and gun supplied by M-Scan, Ltd., Ascot, Berkshire, England. Xenon gas was used as the gas of the FAB gun and thioglycerol as the FAB matrix liquid. The primary beam energy was 8 keV.

The instrumental resolution was set at 3000 for the low-resolution studies and 10 000 for the high-resolution studies. Exact masses were obtained by the peak matching technique. The molecular ion of maduramicin was peak matched against the molecular ion of septamycin, a known ionophore, where  $\text{MNa}^+$  ion is 937.5500,  $\text{C}_{48}\text{H}_{82}\text{O}_{18}\text{Na}$ . The fragment ions were either peak matched against two other known ionophores, monensin,  $\text{MNa}^+ = 693.4190$  ( $\text{C}_{36}\text{H}_{62}\text{O}_{11}\text{Na}$ ), and lasaloid,  $\text{MNa}^+ = 613.3716$  ( $\text{C}_{34}\text{H}_{54}\text{O}_8\text{Na}$ ), or against fragment ions whose exact masses have been determined. Correction for instrumental deviation was made for each measurement by using a correction factor established from known compounds in the mass range similar to that of the unknown mass. Ethoxylated alkylphenols



were found to be convenient for establishing the correction factor, because they have a repeating unit of 44.0262 ( $\text{C}_2\text{H}_4\text{O}$ ), cover the mass range of 400-1000, and produce steady signals.

## RESULTS AND DISCUSSIONS

Maduramicin produces intense and steady FAB mass spectra especially in the presence of alkali salts. In the presence of sodium ion, the FAB mass spectrum consists of  $\text{MNa}^+$ , ( $\text{MNa}^+ - \text{CO}_2$ ), and the base peak ( $\text{MNa}^+ - \text{H}_2\text{O} - \text{CO}_2$ ) ions as shown in Figure 2. It also consists of many other fragment ions of lesser abundance as listed in Table II, which will be discussed later.

Analysis of the biosynthesized  $^{18}\text{O}$ -labeled maduramicin by FAB showed that the cationized molecular ion ( $\text{MNa}^+$ ) of the unlabeled maduramicin was shifted from  $m/z$  939 to  $m/z$  949 as illustrated in Figure 2, indicating that the major enriched product molecule contained five  $^{18}\text{O}$  atoms in the structure. By use of the high-resolution peak-matching technique, the  $\text{MNa}^+$  ion of the  $^{18}\text{O}$ -labeled maduramicin sodium adduct ion,  $m/z$  949, was determined as 949.5467, which again confirmed the incorporation of five  $^{18}\text{O}$  atoms in the structure. (Calculated value of  $\text{C}_{47}\text{H}_{80}\text{O}_{12}^{18}\text{O}_5\text{Na} = 949.5502$ ; deviation of measured value was 3.7 ppm.) Two major fragment ions of

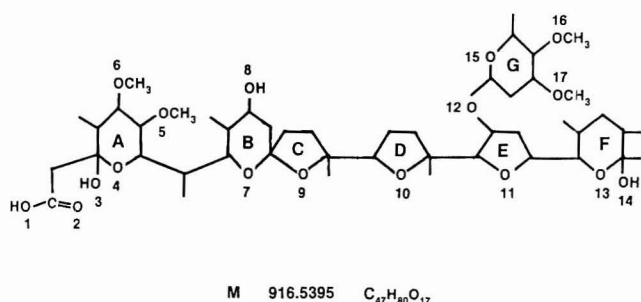


Figure 1. Structure of maduramicin  $\alpha$  as free acid.

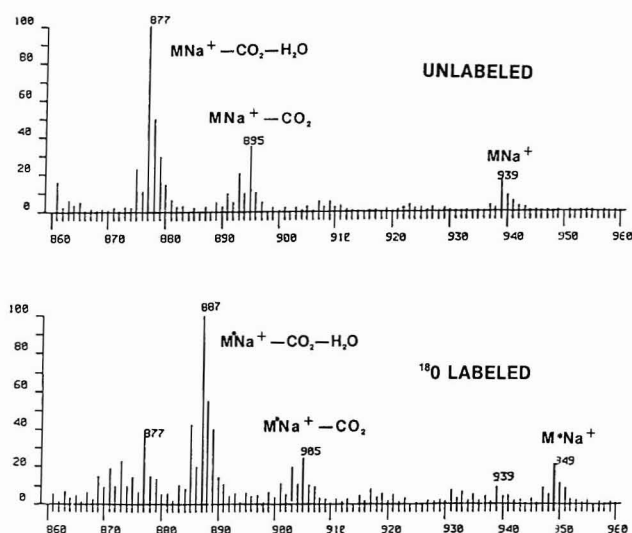


Figure 2. FAB mass spectra of unlabeled and  $^{18}\text{O}$ -labeled maduramicins.

unlabeled maduramicin were  $m/z$  895 ( $\text{MNa}^+ - \text{CO}_2$ ) and  $m/z$  877 ( $\text{MNa}^+ - \text{CO}_2 - \text{H}_2\text{O}$ ), as shown in Figure 2. The  $m/z$  877 was formed by simultaneous losses of  $\text{CO}_2$  [including O(1) and O(2)] and  $\text{H}_2\text{O}$  [including O(3)] via a McLafferty-type rearrangement. This hypothesis was substantiated by MS/MS investigations (10, 11) and the observation of an intense metastable ion at  $m/z$  819.1. In the FAB spectra of  $^{18}\text{O}$ -labeled maduramicin,  $m/z$  895 and  $m/z$  877 also shifted 10 Da to  $m/z$  905 and  $m/z$  887, showing O(1), O(2), and O(3) are not  $^{18}\text{O}$  labeled. The biosynthesized  $^{18}\text{O}$ -labeled maduramicin also contains some four and six  $^{18}\text{O}$  compounds in addition to the predominant five  $^{18}\text{O}$  compounds. The relative concentration of these  $^{18}\text{O}$ -labeled compounds was established by careful comparison of the fragment pattern around the ( $\text{MNa}^+ - \text{CO}_2 - \text{H}_2\text{O}$ ) ion, i.e.,  $m/z$  877 for the control and  $m/z$  887 for the labeled sample. The ( $\text{MNa}^+ - \text{CO}_2 - \text{H}_2\text{O}$ ) ions were selected over the molecular ion species for this study because of their intensities and better signal to noise ratios. Twenty FAB spectra were recorded and averaged under the same operational conditions for both the control and labeled samples. By comparing their ion intensity patterns, we have estimated that among the  $^{18}\text{O}$ -labeled molecules, about 77% of the molecules contain five  $^{18}\text{O}$  atoms, while almost 15% and 8% of the molecules contain four and six  $^{18}\text{O}$  atoms, respectively (see Table I).

The exact locations of the five  $^{18}\text{O}$  atoms were determined by studying the fragment ions of both control and  $^{18}\text{O}$ -labeled maduramicins. Table II lists the major fragment ions of unlabeled maduramicin in the presence of sodium and potassium ions, the major fragment ions of  $^{18}\text{O}$ -labeled maduramicin in the presence of sodium ions, the mass difference between the labeled and unlabeled fragment ions, the number of  $^{18}\text{O}$  atoms incorporated in the fragment ions, and the elemental composition of the unlabeled fragment ions. These

Table I. Relative Contribution of Peak Intensities from Various  $^{18}\text{O}$ -Labeled Maduramicins

$m/z^a$	total rel peak intens	peak intens contributed from <sup>b</sup>		
		$^{18}\text{O}_4$	$^{18}\text{O}_5$	$^{18}\text{O}_6$
883	10.7	4.2	4.3	
885	40.0	17.5	22.1	0.4
887	100.0	5.1	92.1	2.2
889	37.0	1.0	26.1	9.4
891	10.5		5.0	2.7

<sup>a</sup> The most intense high-mass fragment ion ( $\text{MH}^+ - \text{CO}_2 - \text{H}_2\text{O}$ ) of  $^{18}\text{O}_4$ ,  $^{18}\text{O}_5$ , and  $^{18}\text{O}_6$  maduramicins are  $m/z$  885, 887, and 889, respectively. <sup>b</sup> The fragment pattern around the ( $\text{MNa}^+ - \text{CO}_2 - \text{H}_2\text{O}$ ) ions are estimated according to the fragment pattern around the  $m/z$  887 of the unlabeled maduramicin ( $^{18}\text{O}_5$ ). In the unlabeled maduramicin, the relative peak intensities of  $m/z$  873, 875, 877, 879, and 881 are 4.7, 24, 100, 29, and 5.4, respectively.

Table II. Major Fragment Ions in Maduramicin and [ $^{18}\text{O}$ ]Maduramicin

madura- micin with NaCl	madura- micin with KCl	$^{18}\text{O}$ - labeled madura- micin with NaCl	no. of $^{18}\text{O}$ atoms	elemental composition of Na maduramicin <sup>a</sup>
939	955	949	5	C <sub>47</sub> H <sub>80</sub> O <sub>17</sub> Na
895	911	905	5	C <sub>46</sub> H <sub>80</sub> O <sub>15</sub> Na
877	893	887	5	C <sub>46</sub> H <sub>78</sub> O <sub>14</sub> Na
763	779	773	5	C <sub>40</sub> H <sub>68</sub> O <sub>12</sub> Na
735	751	743	4	C <sub>38</sub> H <sub>64</sub> O <sub>12</sub> Na
701	717	709	4	C <sub>38</sub> H <sub>62</sub> O <sub>10</sub> Na
593	609	601	4	C <sub>30</sub> H <sub>50</sub> O <sub>10</sub> Na
591	607	599	4	C <sub>31</sub> H <sub>52</sub> O <sub>9</sub> Na
559	575	565	3	C <sub>30</sub> H <sub>48</sub> O <sub>8</sub> Na
537	553	545	4	C <sub>27</sub> H <sub>46</sub> O <sub>9</sub> Na
535	551	543	4	C <sub>28</sub> H <sub>48</sub> O <sub>8</sub> Na
519	535	525	3	C <sub>27</sub> H <sub>44</sub> O <sub>8</sub> Na
493	509	501	4	C <sub>25</sub> H <sub>42</sub> O <sub>8</sub> Na
489	505	493	2	C <sub>26</sub> H <sub>42</sub> O <sub>7</sub> Na
453	469	461	4	C <sub>22</sub> H <sub>38</sub> O <sub>8</sub> Na
451	467	457	3	C <sub>23</sub> H <sub>40</sub> O <sub>7</sub> Na
433	449	435	1	C <sub>23</sub> H <sub>38</sub> O <sub>6</sub> Na
159	159	159	0	C <sub>8</sub> H <sub>15</sub> O <sub>3</sub>

<sup>a</sup> These elemental compositions were confirmed by exact mass measurement at 10K resolution.

elemental compositions were confirmed by high-resolution peak matching.

In the following discussions, the fragment ions are identified based on the observed masses from the unlabeled maduramicin in NaCl matrix, the first column of the Table II.

When the maduramicin was examined in the presence of KCl, all ions except the  $m/z$  159 shifted 16 Da higher (replacing the Na atom with a K atom), indicating the presence of a sodium atom in all ions except  $m/z$  159. It is also interesting to note that  $m/z$  159 originates from the G ring which does not belong to the basic aglycone skeleton.

Since the  $^{18}\text{O}$  atoms are dispersed throughout the maduramicin structure, it is possible to locate the labeled oxygen atoms from the favorable fragmentation. Most fragment ions of maduramicin can be categorized into two series, namely, A series and F series. The A series are those fragment ions retaining the A ring and the F series are fragment ions retaining the F ring. The fragmentation schemes of these fragment ions listed in Table II are shown in Figure 3. The A series fragment ions originated from the ( $\text{MNa}^+ - \text{CO}_2 - \text{H}_2\text{O}$ ) ion,  $m/z$  877 for the control and  $m/z$  887 for the labeled sample. The F series fragment ions probably also originated from the ( $\text{MNa}^+ - \text{CO}_2 - \text{H}_2\text{O}$ ) ion but could also be derived



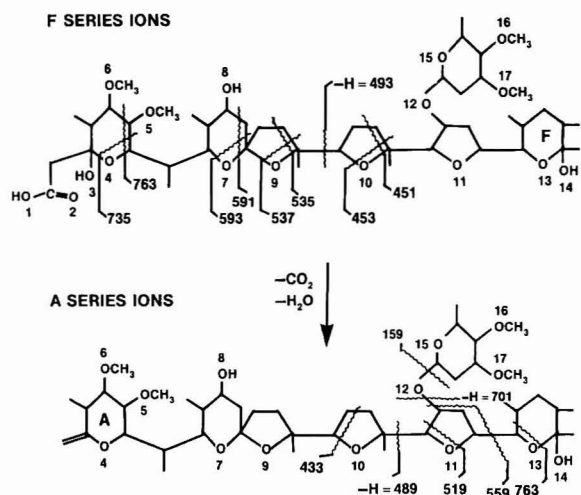


Figure 3. Fragmentation schemes of maduramicin.

directly from the MNa<sup>+</sup> ion. No attempt was made to investigate the contribution from these two pathways.

It was found that most oxygen atoms in the aglycone skeleton can be singled out by the combination of two or three fragment ions listed in Table II. The exact locations of the <sup>18</sup>O atoms, therefore, were determined from the change of <sup>18</sup>O atoms in neighboring fragment ions. Accordingly, the locations of five <sup>18</sup>O atoms were determined as O(5), O(10), O(11), O(12), and O(13) positions.

The confirmation of the O(5) position was based on two F series ions, *m/z* 763 and *m/z* 735. The *m/z* 763 has five <sup>18</sup>O, indicating O(4) and O(6) to be <sup>16</sup>O atoms as are O(1), O(2), and O(3). However, the *m/z* 735, which excluded the O(5), had only four <sup>18</sup>O atoms, thus proving the O(5) position to be <sup>18</sup>O labeled. By the same argument, the <sup>18</sup>O-labeled atom at the O(10) position was established based on the observation of two F series ions, *m/z* 451 and 453; the O(11) position was established based on the observation of two A series ions, *m/z* 519 and *m/z* 489.

The O(12) position was confirmed by two ions, *m/z* 701 of the A series and *m/z* 159 (ring G). Since the *m/z* 701 contained four <sup>18</sup>O atoms, it suggested that there was one <sup>18</sup>O atom in the excluded part, the G ring or the O(12) position. No isotope shifts were observed for the *m/z* 159 ion, indicating no <sup>18</sup>O atom in the G ring. Therefore, the <sup>18</sup>O atom had to be located at the O(12) position.

Although high-resolution results were used to confirm the proposed fragmentation schemes, the effective utilization of the high-resolution experiment was best demonstrated by the simultaneous confirmation of <sup>18</sup>O atoms at the O(5) and O(13) positions. The *m/z* 763 could have originated by either the cleavage of the A ring to form an F series ion or by the cleavage of the F ring to form an A series ion as exhibited in Figure 3. The exact origin of this fragment ion is difficult to establish based solely on the low-resolution results. A speculative assignment could only establish the location of an <sup>18</sup>O atom in one ring, for instance, the A ring, and leave the assignment of the <sup>18</sup>O atom in the other ring ambiguous, for instance, the F ring. The high-resolution results eliminated this ambiguity and clearly established the presence of <sup>18</sup>O atoms at both the O(5) and O(13) positions. Figure 4 exhibits the peak shapes of *m/z* 763 of unlabeled maduramicin, *m/z* 773 of <sup>18</sup>O-labeled maduramicin, and a normal peak shape acquired at the instrumental resolution of 10000. It shows that the *m/z* 735 is an unresolved doublet of *m/z* 763.4244, C<sub>39</sub>H<sub>64</sub>O<sub>13</sub>Na, and *m/z* 763.4608, C<sub>40</sub>H<sub>68</sub>O<sub>12</sub>Na. Similarly, the *m/z* 773 is the unresolved doublet of *m/z* 773.4457, C<sub>39</sub>H<sub>64</sub>O<sub>8</sub><sup>18</sup>O<sub>5</sub>Na, and *m/z* 773.4820, C<sub>40</sub>H<sub>68</sub>O<sub>7</sub><sup>18</sup>O<sub>5</sub>Na. The first peak is an A series ion which confirms the O(13) position and the latter peak is an

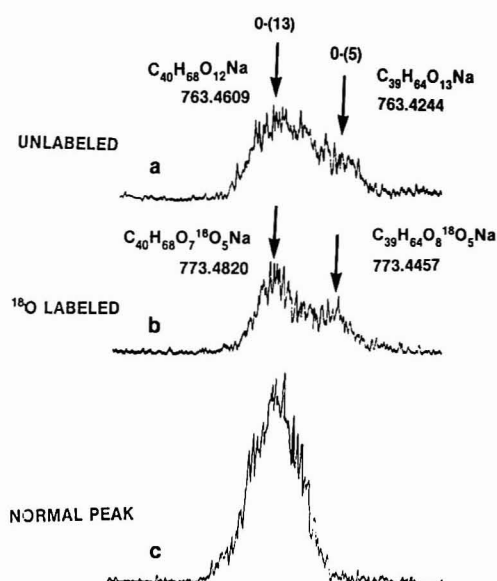


Figure 4. Peak shapes at 10K resolution: (a) *m/z* 763 of maduramicin; (b) *m/z* 773 of <sup>18</sup>O-labeled maduramicin; (c) a normal peak shape.

Table III. Summary of the Oxygen Isotope in [<sup>18</sup>O]Maduramicin

position of O atom	type of atom		significant fragment ion ( <sup>18</sup> O <sub>0</sub> - <sup>18</sup> O <sub>5</sub> )	series	no. of <sup>18</sup> O atoms in significant ions
	<sup>16</sup> O	<sup>18</sup> O			
1	X		895-995	F	5
2	X		895-995	F	5
3	X		877-887	F	5
4	X		763-773	F	5
5		X	735-743	F	4
6	X		763-773	F	5
7	X		591-599	F	4
8	X		593-601	F	4
9	X		535-543	F	4
10		X	451-457	F	3
10		X	489-492	A	2
11	X		519-525	A	3
12	X		159-159		0
12	X		701-709	A	4
13		X	763-773	A	5

F series ion which confirms the O(5) position.

Table III summarizes the above findings. It tabulates the type of oxygen isotopes for all oxygen atoms in the aglycone structure from O(1) to O(13) positions, the most significant fragment ion used for the assignment in the unlabeled and labeled maduramicin, the series that this fragment belongs to, and the number of <sup>18</sup>O atoms incorporated in this particular fragment ion.

In conclusion, FAB-MS has proven to be a powerful tool for the structural elucidation of maduramicin. This study further demonstrates that, with a highly enriched isotope-labeled sample, it is possible not only to determine the number of isotope atoms but also to establish their exact locations.

Registry No. O<sub>2</sub>, 7782-44-7; maduramicin α, 79356-08-4.

#### LITERATURE CITED

- (1) Liu, C. M.; Hermann, T. E.; Downey, A.; Prosser, B. La T.; Schildknecht, E.; Palleroni, N. J.; Westley, J. W.; Miller, P. A. *J. Antibiot.* **1983**, *36*, 343.
- (2) Labeda, D. P.; Martin, J. H.; Goodman, J. J. U.S. Patent, 4 407 946, 1983.
- (3) Tsou, H.-R.; Rajan, S.; Fiala, R.; Mowery, P. C.; Bullock, M. W.; Borders, D. B.; James, J. C.; Martin, J. H.; Morton, G. O. *J. Antibiot.* **1984**, *37*, 1000.
- (4) Rajan, S.; Tsou, H.-R.; Mowery, P. C.; Bullock, M. W.; Stockton, G. W. *J. Antibiot.* **1984**, *37*, 1495.
- (5) Tsou, H.-R.; Chang, T. T., submitted for publication in *J. Antibiot.*

- (6) Occolowitz, J. L.; Hamill, R. L. *Polyether Antibiotics*; Wiley: New York, 1982.
- (7) Tabet, J. C.; Fraisse, D.; David, L. *Int. J. Mass Spectrom. Ion Processes* 1985, 63, 29.
- (8) Barber, M.; Bordoli, R. S.; Elliot, G. J.; Sedgwich, R. D.; Tyler, A. N. *Anal. Chem.* 1982, 54, 645A.
- (9) Chang, T. T.; Lay, J. O., Jr.; Francel, R. J. *Anal. Chem.* 1984, 56, 109.
- (10) Siegel, M. M.; McGahren, W. J.; Tomer, K. B.; Chang, T. T. The 33rd Annual Conference on Mass Spectrometry, San Diego, CA, 1985.
- (11) Siegel, M. M.; Tomer, K. B.; Chang, T. T. *J. Biomed. Environ. Mass Spectrom.*, in press.

RECEIVED for review July 23, 1986. Accepted October 15, 1986.

## Comprehensive Trace Level Determination of Organotin Compounds in Environmental Samples Using High-Resolution Gas Chromatography with Flame Photometric Detection

Markus D. Müller

Swiss Federal Research Station, CH-8820 Wädenswil, Switzerland

**A comprehensive method for trace analysis of mono-, di-, tri-, and some tetrasubstituted organotin compounds is presented. The ionic compounds are extracted from diluted aqueous solutions as chlorides by using a Tropolon-C<sub>18</sub> silica cartridge and from sediment and sewage sludge by using an ethereal tropolon solution. The extracted organotin compounds are ethylated by a Grignard reagent and analyzed by using high-resolution gas chromatography with flame photometric detection (HRGC/FPD). Gas chromatography/mass spectrometry (GC/MS) was used for confirmation. The extraction behavior, gas chromatographic retention, and photometric response of a series of organotin compounds are described, and the identification via electron impact (EI) and chemical ionization (CI) mass spectrometry is discussed. The main organotin compounds detected in various samples are butyltins; cyclohexyl- and phenyltins were identified in some of the sediment and sewage sludge samples. Methylbutyltins and tetrabutyltin were not detected. Concentrations were found to range from low ng/L (parts per trillion) in surface water to low mg/kg (parts per million) in sewage sludge.**

Organotin compounds have found applications in many fields, such as stabilizers for PVC, fungicides and miticides in agriculture, and biocides (1-4), because their properties can be tailored by the variation of the type and the number of substituents to meet widely different requirements. Annual world production was estimated to be 33 000 tons in 1983, most of it dioctyltin maleate (2, 5). The toxicity and degradation in the environment depend strongly on the number and nature of the substituents (1, 5). Organotin compounds with short alkyl chains or phenyl substituents generally exhibit considerable toxicity toward both aquatic organisms and mammals. Alkyltins with small alkyl chains degrade slowly in the environment (6, 7); phenyltins are less stable and may, under certain conditions, rapidly lose the phenyl substituents (3). Organotin compounds may accumulate in sediments and aquatic organisms (6).

Trace determination of organotin compounds in environmental samples is complicated by the fact that organotins with one to three substituents are polar, involatile substances due to their ionic character. In the last few years, a series of publications dealing with different approaches for trace

analysis of organotin compounds appeared, marking a growing concern over the fate of these persistent and toxic compounds in the environment and their impact especially on aquatic organisms.

Trace level determination of these compounds can be carried out either by nonchromatographic methods (e.g., electrochemical or fluorometric assays (8, 9)) or by chromatography with an appropriate detection method. High-performance liquid chromatography (HPLC) coupled with fluorescence detection (10, 11) or ion-exchange HPLC with detection by graphite furnace atomic absorption spectroscopy (GF/AAS) (12) proved to be sensitive methods, but may lack from limitations in separation power and ease of identification of unknown products.

The preparation of volatile derivatives makes the ionic organotin compounds amenable to evaporative separation techniques (purge and trap or gas chromatography (GC)). Hydride formation in dilute aqueous solutions is becoming a routine method for determination of methyltins (13-16), methyl- and butyltins (17-19), and phenyl- and various other organotin compounds (20-22) to form the volatile hydrides (stannanes), which are analyzed either by purging and AAS or flame photometric detection (FPD) or by liquid-liquid extraction with subsequent GC analysis.

Unfortunately, stannanes are rather labile thus preventing further cleanup steps (2). Therefore, alkylation is often preferred over hydride formation, as the resulting tetrasubstituted organotin compounds can easily be purified and concentrated, which is necessary for low-level samples and complex matrices such as animal tissue or sewage sludge. A Grignard reagent or an alkyllithium compound is used to convert the ionic mono-, di-, or triorganotin compounds into the corresponding nonpolar tetrasubstituted compound. The reaction has to be carried out in aprotic solvents and thus requires extraction of aqueous samples prior to derivatization. Procedures have been described for the analysis of methyltins (23), butyltins (24, 25), mixed methylbutyltins (26), various alkyltins (27), cyclohexyltins (28), and phenyltins (29). Alkylation also offers the possibility for selection of the volatility range of the derivatives, which are in most cases analyzed by GC. However, there are few methods for the sensitive determination of a broad range of organotin compounds in environmental samples. Recently, the sensitive determination of butyltin residues in sediment and surface water was described on the basis of extraction/methylation and high-



resolution GC/FPD (30). A revised procedure is now presented allowing sensitive, rapid, and simultaneous detection of a series of organotin compounds, including their degradation and conversion products. After extraction as chlorides, the organotins are ethylated with a Grignard reagent and analyzed by using HRGC/FPD. Combined HRGC/mass spectrometry (GC/MS) in the electron impact (EI) and chemical ionization (CI) mode was used for identification and confirmation. A series of alkyltin standard compounds was synthesized as reference materials. The method was applied to surface water, sewage sludge, and sediment samples and showed the presence of various organotins at concentrations ranging from ng/kg (parts per trillion, ppt) (water) to mg/kg (parts per million, ppm) in sewage sludge.

For brevity, the chemical names of organotins are given as follows: The abbreviated names for the side chains together with the sign for tin designate a certain organotin compound; e.g., HexBu<sub>2</sub>SnEt denotes hexyldibutylethyltin. Substituents placed on the right side of the tin sign originate from derivatization. (Me, methyl; Et, ethyl; Pr, propyl; Bu, *n*-butyl; Hex, *n*-hexyl; Cyhex, cyclohexyl; Oc, *n*-octyl; Phe, phenyl.) Charges of ionic species are indicated but do not imply the presence of true ionized organotin compounds in the environment.

## EXPERIMENTAL SECTION

**Materials and Solvents.** All solvents were purchased either from Merck (Darmstadt, FRG) or Fluka AG (Buchs, Switzerland) and were at least of purissimum grade. Hydrochloric acid and silica gel (Silica Gel 60) was from Merck, Alumina (Alox basisch) from Woelm, Eschwege (FRG), and ascorbic acid (drug quality) from Siegfried (Zofingen, Switzerland). Sep-PAK C<sub>18</sub> cartridges were from Waters (Milford, MA), organotin reference compounds (cf. section "standard material"), SnCl<sub>4</sub> and 2-hydroxy-2,4,6-cycloheptatrien-1-one (tropolone) were obtained from Fluka; Grignard reagents were synthesized from Mg chips and alkyl bromides (methyl, ethyl, butyl, hexyl, octyl, and phenyl bromide) from Fluka. Triphenyltin chloride and tricyclohexyltin hydroxide were obtained from Merck and R. Maag, AG, Dielsdorf, Switzerland, respectively. Stock solutions of 1 mg/mL in toluene were prepared and kept in the dark; fresh dilutions of appropriately derivatized standards were prepared weekly.

The stationary phases for preparing the capillary columns were obtained from Fluka (Pluronic L 64, an analogue of Ucon 50 HB 5100, produced by Wyandotte Chemicals Corp.) and from Petrarch Systems, Inc., Bristol, PA (PS 255, a SE 54 analogue).

**Preparation of Grignard Reagents.** These reagents were prepared according to standard synthetic methods (31) by reacting 6.1 g of Mg (0.25 Mol) in tetrahydrofuran (THF) with equimolar quantities of the corresponding alkyl or aryl bromides, respectively. The Grignard reagent solutions were diluted with THF to give approximately 2 M solutions and were stored in the dark. *Caution:* Alkyl bromides are very toxic—use good ventilation. Grignard reagents are extremely reactive and should be handled with great care.

**Standard Material.** The following types of standard reference materials were used:

- A quantitative standard, Bu<sub>2</sub>Sn, was prepared by weighing and diluting the material with specified purity (99%).
- Quantitative standards were prepared by weighing and diluting of material of known purity with subsequent ethylation.
- Qualitative standards were prepared by reacting dilute solutions of SnCl<sub>4</sub> with controlled amounts of the corresponding Grignard reagents. In this way, complex mixtures, e.g., mixed MeBuSnEt compounds, can easily be obtained for GC retention time studies and as reference compounds for GC/MS.
- An internal standard, HexBu<sub>2</sub>SnCl, was used as described earlier (30). A solution containing 2 ng/ $\mu$ L acetone was used and added to the samples prior to extraction. The compound was added at various levels: about 10 ng/L (10 ppt) in surface water samples, 100  $\mu$ g/kg (100 ppb) in sediment samples, and 1 mg/kg (1 ppm) in sewage sludge samples.

**Extraction Procedure.** For surface water, 100–500 mL of water is acidified to pH 2–3. Internal standard, HexBu<sub>2</sub>SnCl, in acetone, tropolone (0.5 mL of a 1% solution in methanol), and

about 100 mg of ascorbic acid are added and, after mixing, the water is slowly passed through a Tropolon-Sep-PAK C<sub>18</sub> cartridge. This cartridge is prepared by elution of a Sep-PAK C<sub>18</sub> cartridge with methanol (1.5 mL) and 0.5 mL methanol containing 1% tropolone; after being dried for 1 min (vacuum), the cartridge is ready for use. When all water has passed, the cartridge is eluted with 3 mL of diethyl ether; the extract is dried with anhydrous CaCl<sub>2</sub> and is ready for derivatization.

**Sewage Sludge and Sediment.** The sample (1–20 g) is weighed in a large-mouthed flask, internal standard is added, and the sample acidified with HCl to pH 2–3. (*Caution:* H<sub>2</sub>S and CO<sub>2</sub> are evolved, use a hood.) When the evolution of gas has ceased, the slurry is extracted with three portions (10, 5, and 5 mL) of a 0.25% ethereal tropolone solution. After being shaken vigorously and centrifuged, the organic phases are combined, filtered through anhydrous CaCl<sub>2</sub>, and reduced in volume to about 2 mL at room temperature by a rotary evaporator. The extract is then ready for derivatization.

**Derivatization and Cleanup.** Small portions (0.5 mL) of the Grignard reagent, ethylmagnesium bromide (2 M in THF), are carefully added to the extracts prepared as described above. Reagent is dropwise and carefully added until an excess (indicated by a steady evolution of ethane) is present. The mixture is allowed to stand at least for 10 min and the excess of reagent is destroyed by careful, dropwise addition of about 3 mL of 2 M HCl. The organic layer, containing the compounds of interest, is dried over anhydrous sodium sulfate, reduced in volume to about 0.5 mL, and purified by adsorption chromatography on silica gel (0.5 g of silica gel in a Pasteur pipet, elution with 10 mL of 10% diethyl ether/hexane).

**Analysis by GC/FPD.** A Carlo Erba 2101 gas chromatograph fitted with a split/splitless injector, glass capillary column (30 m in length, 0.3 mm i.d., coated with either a 0.15- $\mu$ m film of Pluronic L 64 or a 0.5- $\mu$ m film of PS 255) and a Carlo Erba flame photometric detector SSD 250 were used. The detector was operated without a filter and with a hydrogen-rich flame (32). Injector and detector temperature were set at 250 °C and 225 °C, respectively. Hydrogen (0.6 bar) served as carrier gas. Sample aliquots of 2  $\mu$ L were injected at room temperature in the splitless mode (45 s); the compounds of interest were eluted with a temperature program of 4 °C/min.

**GC/MS.** A Finnigan 4000 GC/MS system with a combined EI/CI ion source and a Finnigan 6000 data system were used. The source temperature was 200 °C for EI and 120 °C for CI. Methane (source pressure of 0.6 mbar) served as reagent gas for CI. A mass range of 100–500 u was recorded. The capillary columns were coupled via an open split fused silica interface to the ion source and the same conditions were applied as for GC/FPD to elute the compounds of interest.

## RESULTS AND DISCUSSION

**General Remarks.** The procedure for trace determination of organotin compounds includes four steps: (a) acid digestion of the sample; (b) extraction; (c) derivatization; (d) analysis.

Though these steps have been described at least partially by several authors, they had to be checked and modified to meet the requirements discussed later on.

**Acid Digestion and Extraction.** Treatment with hydrochloric acid has two purposes:

(a) Inorganic particles (carbonates, sulfides) should be dissolved to release eventual inclusions of organotin compounds.

(b) The different forms of mono-, di-, and trisubstituted organotin compounds (hydroxides, sulfides (33)) present in the environment are converted into the respective chlorides, which are suited for extraction into an organic solvent. On the other hand, organotin compounds may undergo nucleophilic attack by hydrochloric acid resulting in cleavage of side groups (2). This would mimic environmental degradation.

Therefore, acid digestion was checked for eventual degrading effects on tributyl-, tricyclohexyl-, and triphenyltin chloride. Diluted aqueous solutions of these compounds were acidified to pH 2, allowed to stand 1 h at ambient temperature and extracted, derivatized, and analyzed as described above.

**Table I. Recoveries for Selected Tin Species from Tap Water**

tin species	level spiked, <sup>a</sup> ppb or µg/L	recovery, <sup>b</sup> % (SD)	recovery, <sup>c</sup> %	blank, ppb
Sn(IV)	2.5	71 (±10)	10	0.25
BuSn <sup>3+</sup>	0.55	98 (±8)	2	0.001
Bu <sub>2</sub> Sn <sup>2+</sup>	0.475	97 (±8)	24	0.002
Bu <sub>3</sub> Sn <sup>+</sup>	0.225	91 (±7)	75	0.002

<sup>a</sup> Calculated as the respective chlorides. <sup>b</sup> Four samples analyzed in parallel by using tropolone, ascorbic acid, and HCl (cf. Experimental Section). <sup>c</sup> One sample analyzed by using only HCl.

Comparison with a standard solution of the pure, unhydrolyzed product and with a standard containing all possible degradation products gave the following results: (a) Bu<sub>3</sub>SnCl showed no detectable degradation products (<0.5% Bu<sub>2</sub>Sn<sup>2+</sup> and BuSn<sup>3+</sup>, respectively); (b) Cyhex<sub>3</sub>SnCl gave rise to minor degradation products (about 2% for Cyhex<sub>2</sub>Sn<sup>2+</sup> and CyhexSn<sup>3+</sup>); (c) Phe<sub>3</sub>SnCl was most affected under these conditions and yielded about 10% and 5% of Phe<sub>2</sub>Sn<sup>2+</sup> and PheSn<sup>3+</sup>, respectively. These findings are in good agreement with the stabilities of these compounds in the environment: Phe<sub>3</sub>Sn<sup>+</sup> is a fungicide (as hydroxide or acetate) with a half-life of several days (3) depending on environmental conditions, whereas the degradation of Cyhex<sub>3</sub>SnOH is much slower (half-life about 50 days in soil (7, 28) for the degradation to Cyhex<sub>2</sub>Sn<sup>2+</sup>) and Bu<sub>3</sub>Sn<sup>+</sup> was found to have a half-life of months in surface water (6).

In order to discuss the extraction step, one has to consider the physicochemical properties of all compounds involved. There is a clearcut tendency for higher polarity and water solubility of organotin compounds with fewer and shorter alkyl chains attached to the tin atom (2). BuSn<sup>3+</sup> is therefore not extracted by an organic solvent alone and a complexing agent, tropolone, has to be used in a solvent of suitable polarity (24). Otherwise, a low and irreproducible recovery of this compound is observed (34). Tropolone was used in a solution of either benzene, chloroform, or dichloromethane (23, 24, 27). As these solvents are highly toxic (benzene and chloroform) and react with the Grignard reagent (chloroform and dichloromethane), the recovery of organotin compounds out of dilute aqueous solutions by means of a Tropolon-Sep-PAK C<sub>18</sub> cartridge was studied. Thus, handling large amounts of hazardous solvents can be circumvented. The extraction recovery was checked by addition of a synthetic mixture of BuSn<sup>3+</sup>, Bu<sub>2</sub>Sn<sup>2+</sup>, Bu<sub>3</sub>Sn<sup>+</sup>, Cyhex<sub>3</sub>Sn<sup>+</sup>, and Phe<sub>3</sub>Sn<sup>+</sup> to tap water and sediment followed by extraction and analyses as described above. The results for the recovery of butyltin compounds from tap water are given in Table I.

The recoveries were between 90 and 100% for all mono- to triorganotin compounds analyzed with the Tropolon-Sep-PAK procedure and were in good agreement with those determined by the addition of an internal standard, Bu<sub>2</sub>HexSnCl, as described earlier (30). For the phenyltins, the total recovery was used instead of single components due

to some degradation. This could be circumvented by using an acetate buffer described by Wright et al. (29), which on the other hand would possibly not recover the other alkyltin compounds. Tetraalkyltin compounds would also be recovered (34), but the more volatile compounds (e.g., Me<sub>3</sub>BuSn) would be partially lost in the concentration steps.

Though inorganic tin(IV) is also recovered (cf. Table I and ref 22), tin contents in the environmental samples were not determined as the blanks are rather high (presumably due to inorganic tin in the hydrochloric acid, magnesium, and tap water). The recovery of organotin compounds out of lake sediment samples was studied in a single experiment only and was found to be in good agreement with that described by Maguire et al. (27).

Methyltin compounds are highly solvated and are extracted only out of aqueous solutions of high ionic strength (22). No attempt was made to include this group of organotin compounds into the recovery studies. Mixed methylbutyltins however are supposed to behave as butyltins and were therefore included in the investigations.

**Derivatization.** Ethylation obtained by using the Grignard reagent EtMgBr was chosen for conversion of the various mono-, di-, and trisubstituted organotin compounds into tetrasubstituted ones. Ethylation was preferred over other methylation or alkylation using a larger alkyl group for the following reasons: Methylation of tin(IV) and butyltin species seems to occur in the marine environment leading to methyltins and mixed methylalkyltins (25, 35, 36). Further methylation of these environmental metabolites in the derivatization step would exclude the possibility of determining these conversion and degradation products. The ethylation reaction of these compounds leads to a series of tetraalkyltin compounds listed in Table II. Environmental methylation is easily recognized, as the methylated products show typical relative retention time shifts compared to their ethylbutyltin analogues (cf. section GC/FPD and Figure 3). Furthermore, ethylation facilitates identification of organotin derivatives in the GC (cf. Figure 2 and 4), as the order of elution follows increasing degree of substitution, which is not the case for hexylated products (34). The ethyl derivatives have a somewhat higher boiling point compared to the methylated compounds, which reduces evaporative losses during concentration steps.

The ethylation reaction was carefully checked for completion by means of reaction condition variation. A 10-min reaction time was found to be completely sufficient. The reagent, EtMgBr, was analyzed for being free of MeMgBr, which leads to methylated organotin compounds. Bu<sub>3</sub>SnCl was ethylated and gave less than 0.5% of the methylated relative to the ethylated product.

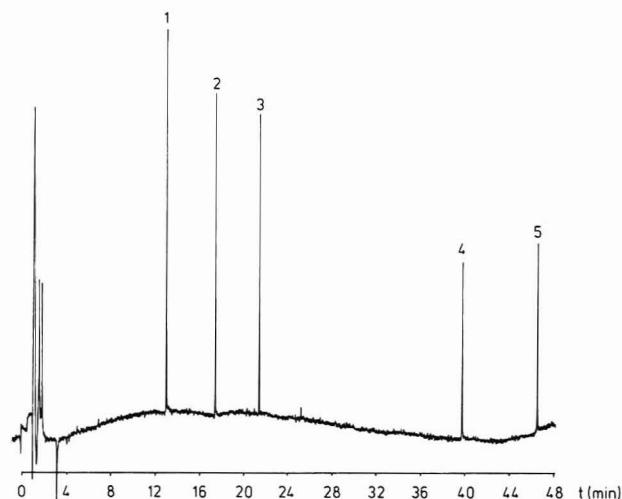
**FPD.** The photometric detection mechanism is attributed to light emission of the excited organotin species in the detector flame (32). Two different wavelengths are related to excited Sn–O and Sn–H bonds at 485 and 611 nm, respectively. The response is strongly dependent on the flame conditions, and the hydrogen-rich flame was found to enhance

**Table II. Composition of Mixed Methylbutyltin Compounds<sup>a</sup>**

methyl groups	butyl groups				
	0	1	2	3	4
0	Et <sub>4</sub> (8)	BuEt <sub>3</sub> (10)	Bu <sub>2</sub> Et <sub>2</sub> (12)	Bu <sub>3</sub> Et (14)	Bu <sub>4</sub> (16)
1	MeEt <sub>3</sub> (7)	MeEt <sub>2</sub> Bu (9)	MeEtBu <sub>2</sub> (11)	MeBu <sub>3</sub> (13)	
2	Me <sub>2</sub> Et <sub>2</sub> (6)	Me <sub>2</sub> EtBu (8)	Me <sub>2</sub> Bu <sub>2</sub> (10)		
3	Me <sub>3</sub> Et (5)	Me <sub>3</sub> Bu (7)			
4	Me <sub>4</sub> (4)				

<sup>a</sup> The molecular formulas of all tetrasubstituted organotin compounds containing Me, Et, and Bu groups are presented with the total number of carbons present in the molecule (in parentheses). The sign for tin is omitted.





**Figure 1.** GC/FPD trace of a standard solution containing five organotin compounds: amount injected, 100 pg each; column, Pluronic L 64 (column A); peak identification (1)  $\text{Bu}_2\text{SnEt}_2$ , (2)  $\text{Bu}_3\text{SnEt}$ , (3)  $\text{Bu}_4\text{Sn}$ , (4)  $\text{Cyhex}_3\text{SnEt}$ , (5)  $\text{Phe}_3\text{SnEt}$ . For details see text.

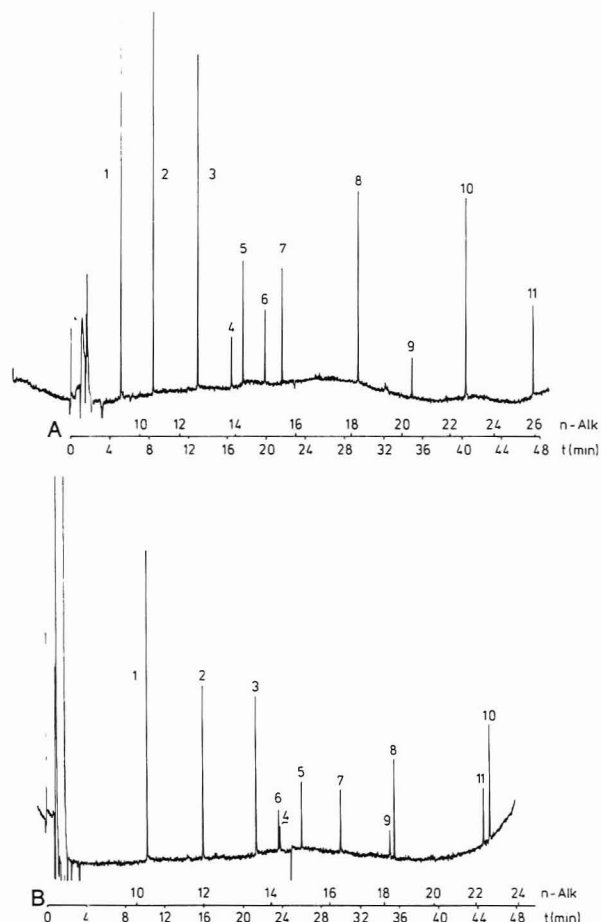
selectivity and sensitivity as well as the shape of the gas chromatographic signals. This may be due to the preferred formation of the volatile tin hydrides in the flame, which are readily removed out of the detector cell. The FPD used in this work does not possess a quartz cuvette of the type described earlier (32), which may explain the less favorable limit of detection (3 pg of  $\text{Bu}_3\text{SnEt}$  instead of 0.2 pg of  $\text{Bu}_3\text{SnMe}$  for a signal-to-noise ratio of 2:1 (32), cf. Figure 1) but also the symmetrical peak shapes as shown in the chromatograms. The detector response was found to be linear in the range of 5–10 000 pg of  $\text{Bu}_4\text{Sn}$ .

The specific response of the FPD was investigated by injecting 100 pg of a series of organotin compounds ( $\text{Bu}_2\text{SnEt}_2$ ,  $\text{Bu}_3\text{SnEt}$ ,  $\text{Bu}_4\text{Sn}$ ). The response signal area/pg of tin was found to be constant for the three compounds within the normal GC quantitation error (<5% standard deviation), which is in good agreement with other work (32).

Coextracted material in environmental samples may interfere in the GC/FPD analyses in two ways: (1) negative peaks arise from hydrocarbons and related material (32) and (2) certain compounds yield a strongly positive response such as alkyl or aryl phosphates. Cleanup of environmental sample extracts as described in the Experimental Section reduces these interferences and prolongs the cleaning intervals for the detector. The performance of the FPD is strongly affected by dirt accumulating in the detector inlet section and injection of large amounts of organotin compounds, leading to broadening and tailing peaks. Occasional cleaning completely restores the detector performance.

**Capillary GC/FPD.** The simultaneous determination of a broad range of organotin compounds including their degradation and conversion products calls for good chromatographic resolution. Two columns were used, a compromise between resolution of critical pairs of organotin compounds (Pluronic L 64, column A) and sufficient retention for the low-boiling compounds (e.g., mixed methylbutyltins, as described later on) together with elution of high-boiling compounds (PS 255, column B).

The sensitivity and resolving power of the system used are illustrated by a chromatogram of a quantitative standard solution of five organotin compounds (cf. Figure 1, column A). Due to careful optimization of the gas flows of the FPD and column end position, peak broadening can be minimized and the performance of the glass capillary column is maintained. Therefore, even closely related organotin compounds are well separated on the two columns used, as shown and discussed later on.



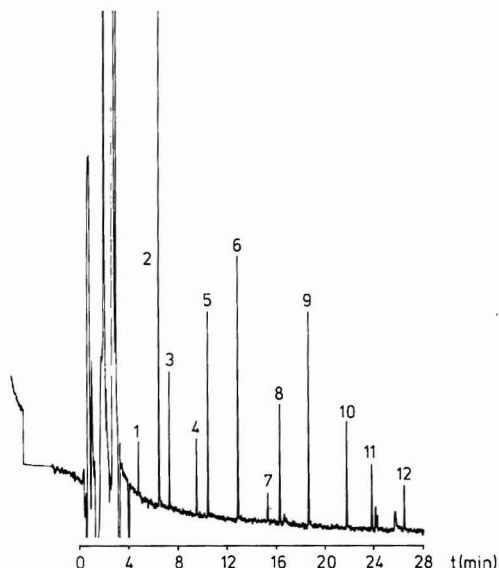
**Figure 2.** GC/FPD (column A) of a qualitative standard solution containing 11 organotin compounds with retention of linear alkanes indicated (*n*-Alk). Peak identification: 1,  $\text{SnEt}_4$ ; 2,  $\text{BuSnEt}_3$ ; 3,  $\text{Bu}_2\text{SnEt}_2$ ; 4,  $\text{CyhexSnEt}_3$ ; 5,  $\text{Bu}_3\text{SnEt}$ ; 6,  $\text{PheSnEt}_3$ ; 7,  $\text{Bu}_4\text{Sn}$ ; 8,  $\text{Cyhex}_2\text{SnEt}_2$ ; 9,  $\text{Phe}_2\text{SnEt}_2$ ; 10,  $\text{Cyhex}_3\text{SnEt}$ ; 11,  $\text{Phe}_3\text{SnEt}$ . For details see text. (B) GC/FPD (PS 255, column B) of the same mixture as in part A with retention of linear alkanes indicated (*n*-Alk); peak identification same as in part A.

The FPD chromatograms of a qualitative standard mixture containing 11 organotin compounds are shown in Figure 2, part A (column A) and part B (column B), with retention of linear alkanes indicated. Whereas column A shows better separation of the cyclohexyl- and phenyltin compounds, column B provides sufficient resolution and retention for the low-boiling methyltin compounds (cf. Figure 3). Furthermore, high-boiling compounds (e.g.,  $\text{Phe}_4\text{Sn}$ ) do not elute from column A and have therefore to be analyzed on column B.

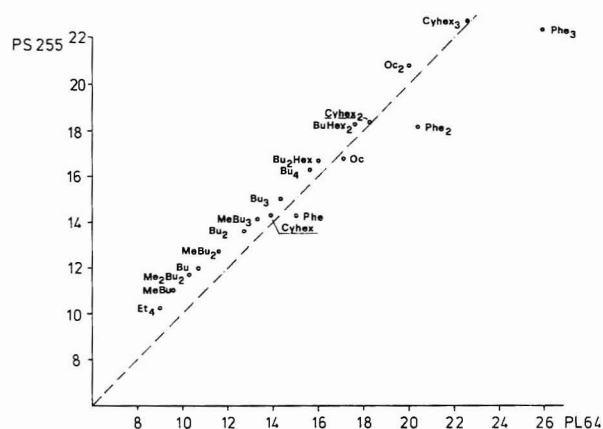
The relative retention of the organotin compounds is presented in Figure 4 in synoptical form (retention of 19 compounds on column A vs. retention on column B). The dotted line indicates the retention of *n*-alkanes. The figure clearly shows the steady increase in relative retention for the alkyltin compounds together with an increase in polarity for cyclohexyl- and phenyltins, respectively, indicated by a shift into the polar region. As expected, this shift increases from  $\text{PheSnEt}_3$  to  $\text{Phe}_3\text{SnEt}$  due to the polar contribution of the increasing number of phenyl groups.

Compounds which may be difficult to separate are easily recognized (e.g., the phenyl- and cyclohexyltin pairs on column B). The lower relative retention of the organotin compounds on column B together with the higher maximum working temperature makes this column especially useful for routine work.

Figure 3 shows the GC/FPD chromatogram of a standard solution containing all methylethylbutyltin compounds listed in Table II obtained by using column B. With exception of



**Figure 3.** GC/FPD (column B) of a solution containing all methyl-ethylbutyltin compounds. Peak identification: 1,  $\text{Me}_2\text{Et}_2\text{Sn}$ ; 2,  $\text{Me}_3\text{BuSn}$ ; 3,  $\text{MeEt}_3\text{Sn}$ ; 4,  $\text{Me}_2\text{EtBuSn}$ ; 5,  $\text{Et}_4\text{Sn}$ ; 6,  $\text{MeEt}_2\text{BuSn}$ ; 7,  $\text{Me}_2\text{Bu}_2\text{Sn}$ ; 8,  $\text{BuEt}_3\text{Sn}$ ; 9,  $\text{MeEtBu}_2\text{Sn}$ ; 10,  $\text{Bu}_2\text{Et}_2\text{Sn}$ ; 11,  $\text{MeBu}_3\text{Sn}$ ; 12,  $\text{Bu}_3\text{EtSn}$ . For details see text and Table II.

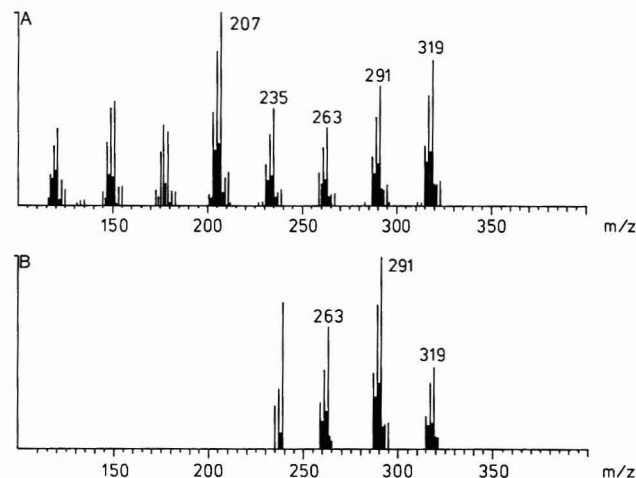


**Figure 4.** Retention of 19 ethylated organotin compounds (signs for ethyl groups and for tin omitted) relative to the retention of *n*-alkanes on column A (Pluronic L 64) vs. column B (PS 255). The broken line indicates the retention of the *n*-alkanes.

the signals for  $\text{Me}_4\text{Sn}$  and  $\text{Me}_3\text{EtSn}$ , which are hidden by solvent peaks as they elute very early, all compounds yield well separated signals. A comparison of retention times for compounds with the same number of carbons and same molecular mass shows a lower retention for compounds with higher numbers of methyl groups (e.g.,  $\text{Me}_3\text{BuSn}$  elutes before  $\text{MeEt}_3\text{Sn}$ , both have a molecular mass of 218 and contain seven C atoms).

**GC/MS.** This technique was used for identification and confirmation purposes rather than for routine detection of organotin compounds. As levels of these compounds found in environmental samples generally are low, multiple ion detection (MID) is required to detect low picogram amounts of the compounds of interest. When EI is used, coextracted interfering material calls for monitoring of the typical tin isotopic signal cluster, which, on the other hand, reduces the sensitivity and number of compounds that can be monitored. PCI was found to be a sensitive and selective ionization technique facilitating the assignment of molecular structures (26). As expected, organotin compounds yield no detectable negative ions under chemical ionization conditions when using methane.

**EI-MS.** EI mass spectra have been described for butyl-, methyl-, and phenylmethyltins (37) and cyclohexyltins (38).



**Figure 5.** EI mass spectrum (part A) and CI mass spectrum (part B) of the main component of the internal standard,  $\text{HexBu}_2\text{SnEt}$ . The signal cluster around  $m/z$  237 in part B is an impurity (the spectrum originates from a GC/MS run of an environmental sample extract).

In general, the molecular ion cluster is not observed (butyl-, methyl-, or ethyltins) or is weak (cyclohexylethyl- or phenylethyltins). The fragmentation is initiated with a homolytic cleavage of a side chain (preferably the largest), followed by cleavage of further substituents as rearrangement type reaction producing a complex fragmentation pattern showing the typical isotopic pattern for tin and intensities which depend both on number and type of side chains. The distorted tin cluster around  $m/z$  120 is due to tin and tin hydride, the final tin containing breakdown products of organotin compounds.

**PCI-MS.** Mass spectra obtained by using PCI have been reported for  $\text{Bu}_3\text{SnHex}$  (34) and cyclohexylmethyltins (39). PCI mass spectra show reduced fragmentation compared to EI. Though the quasi-molecular ion cluster of the compounds investigated is not observed under the conditions applied, the structure of the organotin compound can easily be deduced, as the main fragments are directly related to the molecular ion in two ways: (a) The relative intensities of the fragment clusters are related to the number of side chains of the same type present in the molecule. (b) Each main fragment cluster represents cleavage of a side chain.

As an example, the EI and PCI mass spectra of  $\text{HexBu}_2\text{SnEt}$  are given in Figure 5, parts A and B, respectively. In EI, a complex fragmentation pattern shows the strong dependence of the rearrangement reactions from the chain length of substituent: cleavage of larger chains (e.g., the hexyl group) leads to much more intense fragment ions than cleavage of a butyl or even ethyl moiety. In contrast, the PCI-MS shows three major fragment clusters indicating three types of side chains (the signal cluster around  $m/z$  239 is an impurity). The relative intensities of the fragment clusters are about 1:2:1, giving the indication for a  $\text{AB}_2\text{CSn}$ -type organotin compound (A, B, and C are presently unknown substituents). Solving a simple equation with three unknowns yields  $m/z$  29 (ethyl), two times 57 (butyl), and 85 (hexyl) for the three substituents and as correct structure  $\text{HexBu}_2\text{EtSn}$ .

As limits of detection in mass spectrometry may vary considerably with the ionization technique used, a comparison was made by using EI and PCI for 5 ng of  $\text{Bu}_3\text{SnEt}$ . Though the total ion current is lower in CI, the comparison of the intensities of the  $(\text{M}^+ - \text{butyl})$  ions showed a 100% increase in signal-to-noise (S/N) ratio after switching from EI to PCI. This is due to a higher yield of the key fragment ions in PCI as compared to EI.

**Residues of Organotin Compounds in Environmental Samples.** *Surface Water.* Rainwater collected at Wädenswil and surface water from various locations in Switzerland were



**Table III. Residues of Butyltin Compounds in Rainwater and Surface Water Samples from Switzerland (Concentrations in ng/L or pptr<sup>a</sup> Calculated as Chlorides; Limit of Detection 1 ng/L)**

sample, <sup>b</sup> location	BuSn <sup>3+</sup>	Bu <sub>2</sub> Sn <sup>2+</sup>	Bu <sub>3</sub> Sn <sup>+</sup>	sum
rainwater <sup>c</sup>	n.a. <sup>d</sup>	<1	<1	—
Lake Zürich, lower basin	12	6	7	25
River Aare, Lauffohr	50	10	5	65
River Limmat, Turgi	35	40	15	90
effluent, sewage treatment plant	20	25	15	60

<sup>a</sup>Corrected for recovery (typically 80%) by internal standard.  
<sup>b</sup>Surface water taken in February 1985. <sup>c</sup>Two rain events sampled in summer/autumn 1984 at Wädenswil. <sup>d</sup>n.a., not analysed.

analyzed for residues of organotin compounds. The results are given in Table III.

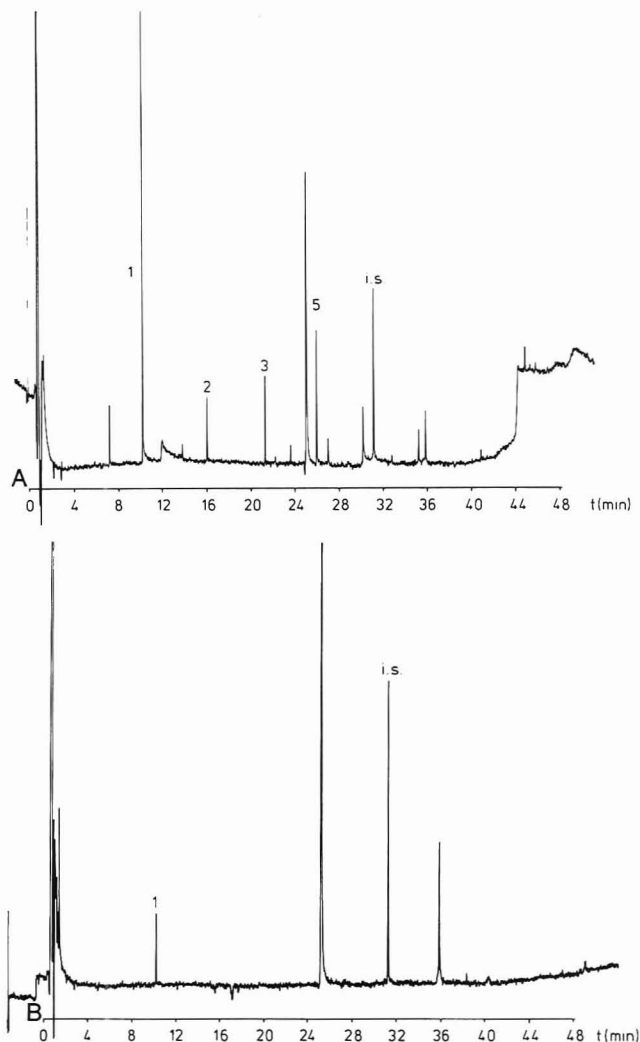
No di- and tributyltin was detected in rainwater from two rainfalls with a detection limit of 1 ng/L of water. These ionic compounds are rather involatile and the release into the environment is expected to occur via sewage. Therefore, lower levels for these compounds are expected to occur in rainwater as compared to alkyllead compounds, which were identified at the low pptr level (40) and originate from automobile exhaust, a direct input into the atmosphere.

In contrast to rainwater, all surface water samples analyzed were found to contain butyltin compounds at the low ng/L level. In some samples, tributyltin is only a minor component compared to the concentrations of di- and monobutyltin, which make up to 80% of the organotin compounds detected. Tetrabutyltin, assumed to be formed in a disproportionation reaction (19), could not be detected, although it would also be recovered.

The concentration levels for all three butyltin species detected are higher in river water samples than in lake water. This may reflect both use and disposal of Bu<sub>2</sub>Sn<sup>2+</sup> and Bu<sub>3</sub>Sn<sup>+</sup> in Switzerland. These compounds are technical products (catalysts, biocides (41)) and may enter surface water via sewage treatment plant effluents. Antifouling paints on boats containing bis(tributyltin) oxide (TBTO) are assumed to be another important source for Bu<sub>3</sub>Sn<sup>+</sup> in water (19, 27), which is in good agreement with recent observations on seasonal variations of Bu<sub>3</sub>Sn<sup>+</sup> concentration in surface water in Switzerland (42).

Figure 6 shows a GC/FPD of an extract of a water sample of Lake Zurich collected in the spring of 1986. Bu<sub>3</sub>Sn<sup>+</sup> is present at a concentration of 15 pptr, and the smaller concentrations for Bu<sub>2</sub>Sn<sup>2+</sup> and BuSn<sup>3+</sup> are typical for low-level pollution with input of Bu<sub>3</sub>Sn<sup>+</sup>. The degradation described for surface water (6) leads to this typical butyltin distribution, whereas the residues identified, e.g., in River Aare, indicate both input of Bu<sub>2</sub>Sn<sup>2+</sup> and Bu<sub>3</sub>Sn<sup>+</sup>.

**Sewage Sludge.** Samples from five treatment plants in Switzerland collected in 1984 and 1985 were analyzed for their organotin content. The results are shown in Table IV. The



**Figure 6.** GC/FPD chromatogram of a surface water sample (Lake Zurich) spiked with 15 ng/L internal standard (A) with corresponding blank (B) obtained by using column B. Aliquots injected correspond to 4 mL of water. Peak numbering is according to Figure 2. The peak with a retention of 25 min is an interference from the solvent, the peak at 36 min is a minor component (BuHex<sub>2</sub>SnEt) of the internal standard (i.s.).

total tin content in the samples was determined by an independent method (inductively coupled plasma spectroscopy, ICP) courtesy of A. Esenwein, Federal Laboratory for Materials and Testing, EMPA, Dübendorf, Switzerland). The considerable concentrations of organotin compounds in the samples illustrate the frequent use and accumulative power of these compounds. The butyltin compounds were detected in all samples investigated. Sample D was found to contain also phenyltins. Cyclohexyltin or mixed methylbutyltin compounds however could not be detected with the average limit of detection indicated. The ethylated extract of sludge of plant D was analyzed by PCI-GC/MS, confirming the GC/FPD results.

**Table IV. Organotin Residues in Sewage Sludge Samples from Four Treatment Plants in Switzerland<sup>a</sup>**

plant	BuSn <sup>3+</sup>	Bu <sub>2</sub> Sn <sup>2+</sup>	Bu <sub>3</sub> Sn <sup>+</sup>	Phe <sub>2</sub> Sn <sup>2+</sup>	Phe <sub>3</sub> Sn <sup>+</sup>	Sn, <sup>a</sup> inorg.
A (urban industrial)	2	5	2.5	n.d.	n.d.	140
B (suburban small industry)	0.2	0.5	0.3	n.d.	n.d.	200
C (urban/industrial)	5	7.5	5	n.d.	n.d.	n.a.
D (urban/industrial)	6	7	6	2	9	180

<sup>a</sup>All concentrations in mg/kg dry matter (ppm) calculated as the respective chlorides. All results are corrected for recovery typically 70%.  
<sup>b</sup>As determined by wet ashing and ICP; n.d. not detected (<0.01 ppm for butyltin, <0.02 ppm for phenyltin). n.a. not analyzed.

**Table V. Butyl- and Cyclohexyltin Residues in Sediment Samples from Lake Zürich<sup>a</sup>**

data of sediment	BuSn <sup>3+</sup>	Bu <sub>2</sub> Sn <sup>2+</sup>	Bu <sub>3</sub> Sn <sup>+</sup>	Cyhex <sub>2</sub> - Sn <sup>2+</sup>	Cyhex <sub>3</sub> - Sn <sup>+</sup>
1880-1985	n.d. <sup>b</sup>	n.d.	n.d.	n.d.	n.d.
1980-1984	55	140	280	10	75

<sup>a</sup> All results are given in µg/kg dry matter or ppb, calculated as the respective chlorides, and corrected for recovery (typically 70%). <sup>b</sup> n.d., not detected (<0.01 ppb).

**Sediment.** Samples from Lake Zurich were collected by using a gravity corer at a depth of 120 m, 1000 m off Thalwil by and dated at the Geology Institute, Swiss Federal Institute of Technology, ETH, Zürich (43). A recent sediment (period 1980-1984) and a sediment from the late 19th century (1880-1885) were investigated. The results are given in Table V. No organotin compounds could be detected in the 1880 sediment, but a series of organotin compounds are present in the recent sediment. The main components are again the butyltin compounds, indicating their frequent use, persistence, and bioaccumulative power. Cyhex<sub>2</sub>Sn<sup>2+</sup> and Cyhex<sub>3</sub>Sn<sup>+</sup> are also identified, reflecting the use of the parent compound, tricyclohexyltin, as a miticide in the region around Lake Zürich that has intense fruit growing activity. The absence of organotin residues in the 1880 sediment is explained by the fact that technical use of these compounds started after 1936 (2). The residues found in the recent sediment are considerably higher than those detected in surface sediment from the lower basin (30). As the sedimentation near the effluent of Lake Zurich in the shallow and oxygen-saturated water is dominated by processes leading to resuspension and oxidation of the fine, carbon-containing particles, the sediment taken at the deepest (and anoxic) part of the lake accumulates higher organotin residues and is therefore more representative for the overall situation in the lake sediment (44).

#### ACKNOWLEDGMENT

I wish to thank H. R. Buser (Federal Research Station, Wädenswil) for many fruitful discussions throughout the work and for carrying out the GC/MS analyses. K. Keltz, F. Niessen, and C. Siegenthaler (Geology Institute, Swiss Federal Institute of Technology (ETH), Zürich) collected and dated the sediment samples investigated. P. Schmid (Institute of Toxicology, University of Zürich and ETH) read the manuscript. Their contributions are gratefully acknowledged.

#### LITERATURE CITED

- (1) WHO Task Group: Sharrat, M. (Chairman); Vouk, V. B. (Secretary) *Environ. Health Criter.* **1980**, *15*, 1-109.
- (2) Zuckerman, J. J.; Reisdorf, P. R.; Ellis, H. V. III; Wilkinson, R. R. In *Organometals and Organometalloids, Occurrence and Fate in the Environment*; Brinckman, F. E., Bellama, J. M., Eds.; ACS Symposium Series No. 28; American Chemical Society: Washington, DC, 1978; pp 388-422.
- (3) Bock, R. *Residue Rev.* **1981**, *79*, 216-222.
- (4) Gächter, R.; Müller, H. *Handbuch der Kunststoff-Additive*; Hanser: München, 1979.
- (5) Laughlin, R. B., Jr.; French, W.; Johannesen, R. B.; Guard, H. E.; Brinckman, F. E. *Chemosphere* **1984**, *13*, 575-584.

- (6) Maguire, R. J.; Carey, J. H.; Hale, E. J. *J. Agric. Food Chem.* **1983**, *31*, 1060-1065.
- (7) Getzendanner, M. F.; Corbin, H. B. *J. Agric. Food Chem.* **1972**, *20*, 881-885.
- (8) Kenis, P.; Zirino, A. *Anal. Chim. Acta* **1983**, *149*, 157-166.
- (9) Arakawa, Y.; Wada, O.; Manabe, M. *Anal. Chem.* **1983**, *55*, 1901-1904.
- (10) Langseth, W. *Talanta* **1984**, *31*, 975-978.
- (11) Yu, T.-H.; Arakawa, Y. *J. Chromatogr.* **1983**, *258*, 189-194.
- (12) Jewett, K. L.; Brinckman, F. E. *J. Chromatogr. Sci.* **1981**, *19*, 583-593.
- (13) Andreae, M. O.; Byrd, J. T. *Anal. Chim. Acta* **1984**, *156*, 147-157.
- (14) Braman, R. S.; Tompkins, M. A. *Anal. Chem.* **1979**, *51*, 12-16.
- (15) Tugrul, S.; Balkas, T. I.; Goldberg, E. G. *Mar. Pollut. Bull.* **1983**, *14*, 297-303.
- (16) Jackson, J.-A. A.; Blair, W. R.; Brinckman, F. E.; Iverson, W. P. *Environ. Sci. Technol.* **1982**, *16*, 110-119.
- (17) Donard, O. F. X.; Rapsomanikis, S.; Weber, J. H. *Anal. Chem.* **1986**, *58*, 772-777.
- (18) Hodge, V. F.; Seidel, S. L.; Goldberg, E. D. *Anal. Chem.* **1979**, *51*, 1256-1259.
- (19) Matthias, C. L.; Bellama, J. M.; Olson, G. J.; Brinckman, F. E. *Environ. Sci. Technol.* **1986**, *20*, 609-615.
- (20) Woollins, A.; Cullen, W. R. *Analyst (London)* **1984**, *109*, 1527-1529.
- (21) Soderquist, C. J.; Crosby, D. G. *Anal. Chem.* **1978**, *50*, 1435-1439.
- (22) Hattori, Y.; Kobayashi, A.; Takemoto, S.; Takami, K.; Kuge, Y.; Sugimae, A.; Nakamoto, M. *J. Chromatogr.* **1984**, *315*, 341-349.
- (23) Chau, Y. K.; Wong, P. T. S.; Bengert, G. A. *Anal. Chem.* **1982**, *54*, 246-249.
- (24) Meinema, H. A.; Burger-Wiersma, T.; Versluis-de Haan, G.; Gevers, E. G. *Environ. Sci. Technol.* **1978**, *12*, 288-293.
- (25) Zimmerli, B.; Zimmermann, H. *Fresenius' Z. Anal. Chem.* **1980**, *304*, 23-27.
- (26) Maguire, R. J. *Environ. Sci. Technol.* **1984**, *18*, 291-294.
- (27) Maguire, R. J.; Tkacz, R. J.; Chau, Y. K.; Bengert, G. A.; Wong, P. T. S. *Chemosphere* **1986**, *15*, 253-274.
- (28) Möllhoff, E. *Pflanzenschutz-Nachr.* **1977**, *30*, 249-263.
- (29) Wright, W. B.; Lee, M. L.; Booth, G. M. *HRC CC, J. High Resolut. Chromatogr.* **1979**, *1*, 189-190.
- (30) Müller, M. D. *Fresenius' Z. Anal. Chem.* **1984**, *317*, 32-36.
- (31) *Organic Syntheses*; Gilman, H., Ed.; Wiley: New York, 1941; Collective Vol. I, p 188.
- (32) Aue, W. A.; Flinn, C. G. *J. Chromatogr.* **1977**, *142*, 145-154.
- (33) Laughlin, K.; French, W.; Guard, H. E. *Water, Air, Soil Pollut.* **1983**, *20*, 69-79.
- (34) Unger, M. A.; MacIntyre, W. G.; Greaves, J.; Huggett, R. J. *Chemosphere* **1986**, *15*, 461-470.
- (35) Guard, H. E.; Cobet, A. B.; Coleman, W. M., III *Science (Washington, D.C.)* **1981**, *213*, 770-771.
- (36) Hallas, L. E.; Means, J. C.; Cooney, J. J. *Science (Washington, D.C.)* **1982**, *215*, 1505-1506.
- (37) Gielen, M.; Mayence, G. J. *Organomet. Chem.* **1972**, *46*, 281-288.
- (38) Stewart, T. E.; Cannizzaro, R. D. *Pesticides Analytical Methodology*; ACS Symposium Series 136; American Chemical Society: Washington, DC, 1980; pp 367-388.
- (39) Fish, R. H.; Holmstead, R. L.; Casida, J. E. *Tetrahedron Lett.* **1974**, *13*, 1303-1306.
- (40) Van Cleuvenbergen, R. J. A.; Chakraborti, D.; Adams, F. C. *Environ. Sci. Technol.* **1986**, *20*, 589-593.
- (41) *Gifftliste 1*; EDMZ (Swiss Federal Printing Office): Bern, Switzerland, 1986.
- (42) Zingg, M. *Belastung der Schweizerischen Gewässer mit Tributylzinn*; BUS: Bern, Switzerland 1985.
- (43) Kelts, K.; Hsü, K. J. In *Lakes, Chemistry, Geology, Physics*; Lerman, A., Ed.; Springer: New York, 1978; p 295.
- (44) Sturm, M., Swiss Federal Institute for Water Resources and Water Pollution Control, EAWAG, Dübendorf, Switzerland, personal communication, 1986.

RECEIVED for review August 19, 1986. Accepted October 27, 1986. This work is part of a research program of the Swiss Federal Office for Environmental Protection (BUS) for the study of the occurrence and fate of toxic organic compounds in the environment. The support and encouraging discussions with Ch. Rentsch (BUS) are gratefully acknowledged.



# Determination of Alkaline-Earth Metals in Samples Containing a Large Excess of Alkali by Ion Chromatography

Dennis Jenke

Travenol Laboratories, Inc., 6301 Lincoln Avenue, Morton Grove, Illinois 60053

The presence of a 10-fold excess of alkali metals in pharmaceutical samples represents a situation in which most available silica- and polymer-based exchange columns for ion chromatography could not effectively separate these interferants from alkaline-earth analytes. However, a heart-cutting process that involves automated switching of identical tandem columns so as to direct the interferants to waste and the analytes to the detection system can be used to eliminate the problem. When coupled with regenerant flow-controlled eluent suppression/conductivity detection, the methodology is characterized by excellent performance. Area response is linear in the range of 10–120 mg/L for  $\text{Mg}^{2+}$  and 20–200 mg/L for  $\text{Ca}^{2+}$ . Accuracies for five pharmaceutical matrices routinely fell in the range of  $100 \pm 2\%$  recovery. For over 120 samples analyzed, mean and median precisions were 0.64% and 0.45% for  $\text{Mg}^{2+}$  and 0.59% and 0.46% for  $\text{Ca}^{2+}$ . After more than 1200 injections, the system is still capable of meeting rigorous suitability criteria for chromatographic performance and calibration suitability. Instrumental response is constant over periods of operation in excess of 48 h. Total analysis time is 9 min.

A large number of pharmaceutical products contain calcium and magnesium. These elements are present either as the counterion for anions, which act as preservatives, buffers, and diluents, or as electrolyte balance mediators. While ion chromatography represents a potentially viable approach for quantitating these ions in pharmaceutical samples, its universal application to these products is limited by the nature of the product's matrix. An overwhelming majority of solutions containing the alkaline earths also contain  $\text{Na}^+$  (or less commonly  $\text{K}^+$ ). The nature of these samples is such that the concentration of the alkali metals is an order of magnitude (or more) greater than that of the alkaline-earth analytes. The net result of this concentration mismatch is that under typical elution conditions the alkali metals cause chromatographic interference, especially with the  $\text{Mg}^{2+}$  peak, on most commercially available columns packed with either silica- or polymer-based resins. Even though the alkalis have little or no affinity for the resin under these conditions, the duration of what is essentially the void response is sufficiently large that complete resolution between this peak and the  $\text{Mg}^{2+}$  response is not achieved (for example, Figure 1). Even in situations where the overlap is relatively small, accurate integration of the  $\text{Mg}^{2+}$  response is hampered and analytical accuracy and precision suffer. Given the limited selectivity of these resins for  $\text{Mg}^{2+}$ , there is little the analyst can do to improve the chromatographic behavior. While mobile-phase modification may improve the difference in apparent retention times between the alkalis and  $\text{Mg}^{2+}$ , absolute resolution remains nearly constant as the increase in retention difference is nullified by an increasing peak width.

Another way of handling the coelution problem would be to remove the alkalis from the sample before they reach the detector. Such removal prior to sample introduction would

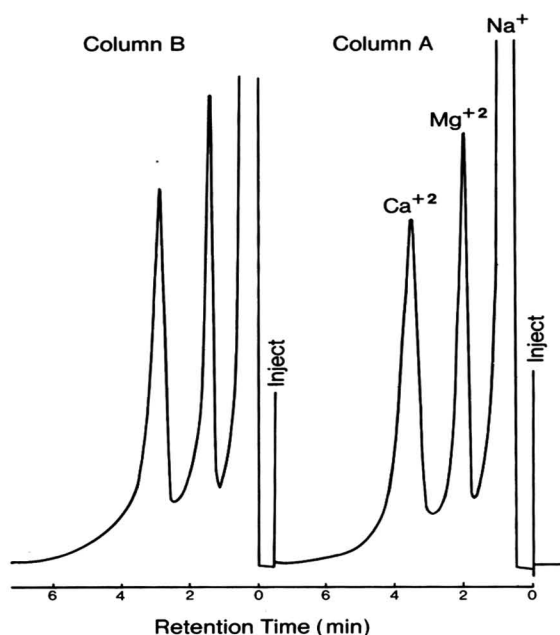
involve a lengthy process, as the alkaline earths would have to be removed from the matrix by precipitation or adsorption and then remobilized in an alternate matrix. A more effective approach, which has the advantages of being accomplished on-line and in an automated manner, involves the process known as heart cutting. In this approach, two chromatographic columns are coupled in tandem with a switching valve serving as the connection. The nature of the connection is such that the effluent from the first column is directed either to the second column or to waste. Interferants and analytes are physically separated from one another by timing the column switching event in such a way that the differing selectivity of these species is exploited. The procedure used is essentially that introduced by Deans for gas chromatography (1). It differs from the heart-cutting approaches called "recycle" or "reinjection" chromatography (2–6) in that the sample is not actually returned to the chromatographic system. In this paper, the ability of such an approach to provide accurate and precise determinations of the  $\text{Ca}^{2+}/\text{Mg}^{2+}$  content of pharmaceutical samples is documented and its overall performance is compared to that of a single column approach.

## EXPERIMENTAL SECTION

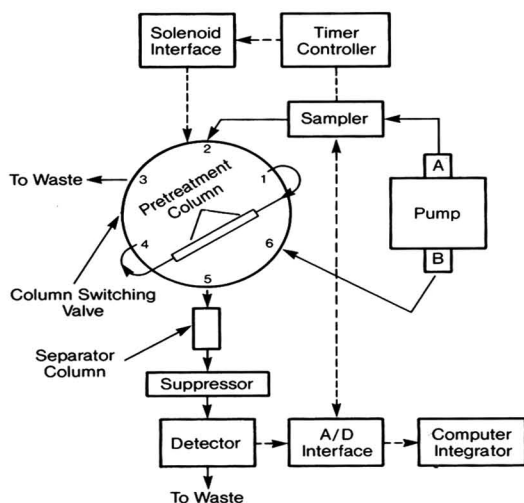
**Apparatus.** The basic chromatographic system employed included a Perkin-Elmer (Norfolk, CT) Series 3B pump, a Biorad (Richmond, CA) conductivity monitor, a strip chart recorder, and a Hewlett-Packard HP 3357 computer integrator. An analog to digital (A/D) converter with a sampling rate of 2 Hz was used as the interface between the detector and integrator. A Perkin-Elmer LC 600 autosampler equipped with a 20- $\mu\text{L}$  sample loop was used for sample introduction. Eluent suppression was accomplished with a Dionex (Sunnyvale, CA) CFS-1 fiber suppressor; regenerant to this device was provided via a peristaltic pump. The chromatographic columns were Wescan (Santa Clara, CA) Model 269-024 high-speed cation columns. Depending upon application, the column configuration includes a single column, two columns in tandem connected with a 2 cm length of 0.09 in. stainless steel tubing, or two columns connected in tandem with a switching valve. The mobile phase, supplied at a rate of 2 mL/min, was  $1 \times 10^{-3}$  M ethylenediamine at pH 6; the regenerant was a 0.05 M solution of tetramethylammonium hydroxide, supplied at a rate of 1.5 mL/min.

The apparatus used to produce the heart-cutting process is shown in Figure 2. In addition to the components mentioned above, this system utilized Autochron (Millford, MA) Model 201 solenoid interface and Model 401 valve module and a Lindberg Enterprises (San Diego, CA) Model CD45N ChronTrol timer/controller. Compressed air at a pressure at 75 psi was delivered to both the autosampler and valve module.

**Sample Preparation.** Five electrolyte solutions were chosen to analyze the system's performance, providing a representative cross section of pharmaceutical matrices as well as a sufficiently strict analytical challenge. A detailed description of these matrices is given in Table I. These solutions were prepared in the following manner. Analytic stocks were prepared at the 1000 mg/L level by dissolving the appropriate weight of the  $\text{Cl}^-$  salts of  $\text{Mg}^{2+}$  and  $\text{Ca}^{2+}$  in deionized, distilled (DD) water. Stock solutions containing the non-alkaline-earth components of each formulation (e.g., dextrose, amino acids, NaCl) were prepared by adding the stoichiometric equivalent of each reagent to deionized water and adjusting the pH where necessary. Aliquots of these stocks were heated at 65 °C for a period of 45 h to simulate a degraded



**Figure 1.** Chromatographic behavior of two Wescan high-speed columns used as single systems. The eluent was  $1 \times 10^{-2}$  M ethylenediamine at a flow rate of 2 mL/min. The sample is matrix C at 100% of the product code and contains approximately 2000 ppm  $\text{Na}^+$ , 40 ppm  $\text{Mg}^{2+}$ , and 90 ppm  $\text{Ca}^{2+}$ .



**Figure 2.** Instrumental configuration of the heart-cut apparatus: solid lines represent tubing connections; dashed lines represent electrical connections.

product. Working samples were prepared by adding the appropriate volumes of the matrix and analyte stock solutions to a volumetric flask and diluting to volume with DD water. These samples thus represent formulations that have been diluted enough for their alkaline-earth content to fall in the linear range of instrumental response. Matrix blank solutions were prepared in a similar manner, except that no aliquots of the  $\text{Ca}^{2+}/\text{Mg}^{2+}$  stocks were added prior to dilution. Standard solutions were prepared in the range of 10–120 mg/L for  $\text{Mg}^{2+}$  and 20–200 mg/L for  $\text{Ca}^{2+}$  by dilution of the analyte stocks with DD water. All working samples and standards were analyzed by direct injection into the chromatographic system and were refrigerated between uses.

**Table I. Description of Matrices Studied**

matrix code	component	concn, g/L
A	dextrose	45.45
	KCl	3.28
	NaCl	8.60
	Ca gluconate	3.02
	$\text{MgSO}_4 \cdot 7\text{H}_2\text{O}$	6.49
B	dextrose	25.0
	NaCl	5.84
	Ca gluconate	1.08
	KCl	0.37
	$\text{MgCl}_2$	0.16
	$\text{NaH}_2\text{PO}_4$	0.15
	$\text{Na}_2\text{HPO}_4$	0.04
C	amino acids	10.00
	NaCl	5.38
	Na lactate	4.48
	$\text{CaCl}_2$	0.26
	$\text{MgCl}_2$	0.05
D	$\text{NaHSO}_3$	0.30
	amino acids	85.00
	Na acetate	5.44
	$\text{K}_2\text{HPO}_4$	5.22
	NaCl	1.54
E	$\text{MgCl}_2$	1.02
	NaCl	6.00
	Na lactate	3.10
	KCl	0.30
	$\text{CaCl}_2$	0.26

**Reagents.** The mobile phase was prepared by sequential dilution of an ethylenediamine stock with DD water; the final solution was adjusted to pH 6 with 1 N  $\text{HNO}_3$ . The mobile phase was filtered through 0.2- $\mu\text{m}$  media prior to use. The regenerant was prepared by dissolving tetramethylammonium hydroxide hydrate in vacuum degassed DD water; after dissolution, the mixture was also degassed under vacuum. All materials used in this study were reagent grade. DD water was obtained from a Millipore (Bedford, MA) Milli-Q cartridge system.

## RESULTS AND DISCUSSION

Two basic types of columns exist for use in inorganic cation chromatography (conductometric detection); those containing resins based on a polymeric or divinylbenzene backbone and those with a silica-type backbone. In most cases, the relative selectivities and total capacities of either type of column are very similar and therefore their chromatographic performance with respect to this application is similar. That is, they are prone to the type of alkali metal interference illustrated in Figure 1. While the magnitude of the interference problems is affected by specific column identity, no commercially available column could be found that allows the analyst to couple interference-free operation with reasonably short analysis times and good analytical precision.

With most performance criteria being roughly equivalent for the columns whose capabilities were surveyed, the silica-based high-speed column was chosen for continued study by virtue of its ability to produce short analysis time separations. Again as shown in Figure 1, the net result of the large concentration imbalance between  $\text{Na}^+$  and the alkaline earths, which exist in many pharmaceutical products, is the formation of a large interference peak when such a column is used as recommended. Even though  $\text{Na}^+$  has only a small affinity for the column under the elution conditions employed, the peak is sufficiently large that it effectively overlaps both the  $\text{Mg}^{2+}$  and, to a lesser extent, the  $\text{Ca}^{2+}$  responses. While in most cases this overlap is not so great so as to completely mask either response, the interference, being  $\text{Na}^+$  concentration dependent, hampers the accurate integration of the analyte response, thus resulting in poor accuracy and precision. While the  $\text{Ca}^{2+}$  is affected to a lesser extent due to its longer elution time, in most instances the ability to effectively quantitate this species



**Table II. Summary of Performances of Various Chromatographic Systems**

matrix	level <sup>a</sup>	target <sup>b</sup>	concentration found, mg/L		
			single	tandem	tandem/cut
Mg <sup>2+</sup>					
A	0.8	10	9.55 (1.31)	10.1 (0.57)	10.0 (1.44)
	1.0	15	13.9 (2.07)	15.1 (0.63)	15.0 (0.74)
	1.2	20	16.3 (3.15)	19.0 (0.54)	20.1 (0.63)
B	0.8	10	9.95 (1.60)	10.2 (1.85)	10.0 (1.17)
	1.0	20	17.1 (1.22)	19.2 (1.08)	19.9 (0.67)
	1.2	30	25.9 (3.43)	28.7 (0.77)	29.6 (0.52)
C	0.8	30	27.0 (3.24)	27.3 (1.73)	29.5 (0.61)
	1.0	40	35.2 (1.78)	36.8 (1.34)	39.5 (0.49)
	1.2	50	45.1 (1.44)	47.0 (0.61)	49.5 (0.27)
D	0.8	50	53.7 (1.32)	49.8 (1.69)	49.0 (2.05)
	1.0	60	61.9 (1.56)	58.4 (0.57)	59.6 (0.20)
	1.2	70	74.9 (0.50)	69.6 (1.88)	68.7 (1.38)
Ca <sup>2+</sup>					
A	0.8	100	110.3 (5.38)	101.9 (2.69)	100.2 (0.93)
	1.0	150	167.6 (1.32)	152.5 (1.85)	150.4 (0.96)
	1.2	200	221.2 (1.05)	205.0 (1.63)	203.0 (0.54)
B	0.8	100	110.0 (2.36)	100.2 (1.42)	100.2 (0.69)
	1.0	150	163.4 (3.25)	152.7 (0.31)	149.7 (0.42)
	1.2	200	227.0 (2.92)	204.4 (1.19)	201.9 (0.46)
C	0.8	70	65.6 (3.94)	67.9 (0.66)	69.4 (0.89)
	1.0	90	83.3 (3.62)	86.9 (0.34)	88.9 (0.61)
	1.2	100	92.1 (3.64)	96.5 (0.52)	98.2 (0.79)
E	0.8	30	31.7 (7.02)	30.0 (5.45)	29.5 (2.46)
	1.0	40	43.1 (2.81)	37.6 (0.97)	39.8 (1.93)
	1.2	50	54.4 (2.21)	48.6 (0.89)	49.5 (1.47)

<sup>a</sup>Level corresponding to 0.8, 1.0, or 1.2 times the normal product concentration. <sup>b</sup>Target concentration in mg/L.

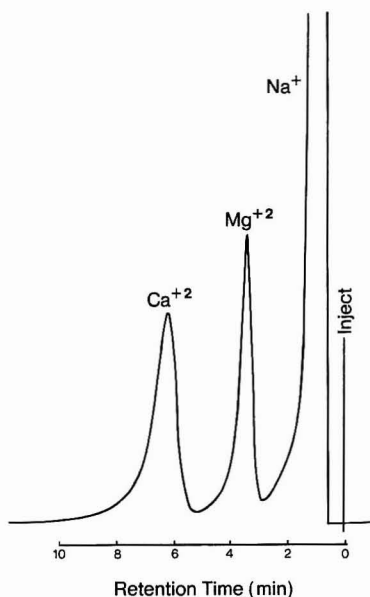
is also compromised by the excess alkalis. Results of recovery studies performed by using the single column methodology, shown in the first column of Table II, clearly identify the magnitude of the quantitation problem exhibited by this system. Even when optimized (in terms of accuracy and precision) integration parameters are used, recoveries obtained by using either peak areas or heights are extremely poor, and precisions of replicate injections are rarely better than 1.5% RSD. This behavior is contrasted to that exhibited for aqueous standards containing only the analytes, where recoveries of 100 ± 2% and precision of less than 1% RSD can be routinely obtained.

Essentially there are only three ways in which to address the alkali metal interference problem. One way to deal with the problem would be to remove the Na<sup>+</sup> from the sample before it reaches the analytical system. However, given the high solubility of most sodium salts and the fact that most extraction media have a higher affinity for Ca<sup>2+</sup>/Mg<sup>2+</sup> than for Na<sup>+</sup>, this approach in its purest form is unlikely to succeed. A derivative of this approach, automated heart-cutting chromatography, is discussed in some detail later in this paper. The converse of this approach, isolating Ca<sup>2+</sup>/Mg<sup>2+</sup> from the Na<sup>+</sup> by removal of these analytes from the aqueous sample, followed by remobilization, is theoretically possible, but in a practical sense extremely time inefficient. A second way to counteract the chromatographic interference would be to adopt a detection strategy that is insensitive to the alkali metals but highly sensitive to the alkaline earths. Unfortunately, conductivity possesses exactly the opposite behavior due to the high mobility of Na<sup>+</sup>, and is thus not necessarily a good choice for use with pharmaceutical solutions. Since none of the analytes themselves are strong chromophores, direct spectroscopy is not a viable option. While indirect detection (photometric or otherwise) represents a potential improvement over conductivity because it will normalize the molar response of the analytes, a suitable mobile phase ex-

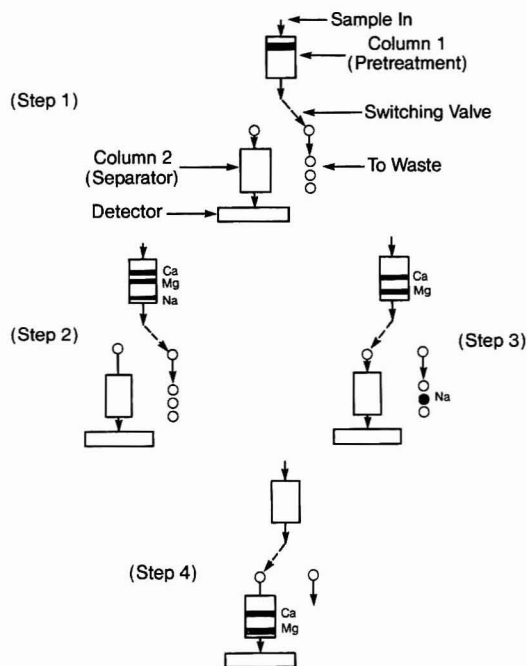
plotting this approach could not be identified. Electrochemical means of detection offer no real advantages when compared with conductivity. While atomic emission/absorption spectroscopy can distinguish between the analytes and interferants, coupling such a detector to an IC system would involve a large capital expense and in any event such a system might not be capable of adequate sensitivity. The only remaining alternative is to take advantage of differences in solution-phase chemistry between the monovalent interferants and the divalent analytes. Of specific interest is the ability of Ca<sup>2+</sup> and Mg<sup>2+</sup> to form colored complexes with organic indicator anions. In such a scenario, the indicator anion could be added to the mobile phase either pre- or postcolumn and the concentration of the resultant complex monitored spectrophotometrically. While such an approach has been documented in the literature (7, 8), and is indeed capable of a high degree of a selectivity between the analytes and interferants, in this study the sensitivity to both Ca<sup>2+</sup> and Mg<sup>2+</sup> was found to be insufficient to produce adequate precision. It was observed that pH was a major stumbling block in developing an assay that was sensitive for both Mg<sup>2+</sup> and Ca<sup>2+</sup>. While the pH of the mobile phase/derivatizing solution mixture must be high (≈9) so that the Ca<sup>2+</sup>/indicator complexation is favored, if the pH is too high (much greater than 10), Mg<sup>2+</sup> sensitivity is decreased as this analyte begins to precipitate as its hydroxide salt.

A final way to eliminate the Ca<sup>2+</sup>/Mg<sup>2+</sup> overlap would be to improve the chromatographic performance of the systems used. However, since selectivity is primarily controlled by the resin and most resins are similar with respect to this property, there is little the analyst can do in terms of nullifying performance by changing the mobile phase. Utilization of conductometric detection limits the choice of eluents available. Any improvement one could obtain in terms of increasing the difference between Mg<sup>2+</sup> and Na<sup>+</sup> retention times would be lost as both peaks would be broadened by the same process (i.e., no improvement in absolute resolution is obtained). One can improve performance somewhat by increasing the number of theoretical plates in the system; this is of course achieved essentially by increasing column length. Since the high-speed columns have a low operating back pressure, and can be operated at relatively high flow rates, one can double plate count without similarly increasing analysis time by coupling two such columns in tandem. For routine applications involving a large number of samples this is a more effective approach than using the longer columns that are commercially available. As shown in Figure 3, the use of two high-speed columns in tandem improves performance considerably. However, while this system is clearly superior to the single column approach, as shown in the second column of Table II, it is still not capable of conforming to the strict performance criteria (accuracy of 100 ± 1.5%, precision ±1% RSD or better) required for pharmaceutical applications. As was the case with the single column system, the poor performance of the tandem system can be directly linked to the presence of the alkali metals, since in their absence accuracy and precision improve dramatically. It is observed that while carrying this trend further to include a third tandem column would ultimately provide adequate resolution between the species of interest, such a methodology would involve a fairly large column cost and would be characterized by a long total analysis time. Additionally, the gain in chromatographic performance would not be additive due to the extracolumn void volume added as a result of the column coupling process.

As mentioned earlier, the term "heart cutting" refers to an on-line, automated method of sample pretreatment. Such a process, embodied in the apparatus shown in Figure 2, is shown in Figure 4. The methodology involves coupling two columns in tandem; however, it differs from the previous

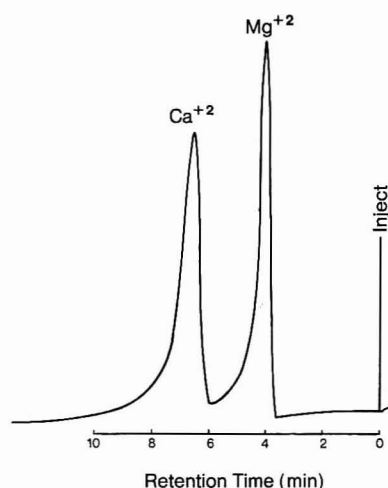


**Figure 3.** Chromatographic behavior of the two Wescan columns used in Figure 1 when placed in tandem. Experimental conditions and sample identification are the same as in Figure 1.



**Figure 4.** Operation of the heart-cutting procedure.

approach in that the columns are joined by a switching valve. Mechanistically, the system works as follows: The sample is injected into the first (pretreatment) column whose effluent is directed to waste (step 1). As the mobile phase flows through this column, the analytes are marginally separated from the interferant (step 2). Eventually, the interferant elutes from the column and is directed toward waste. At a point just prior to the elution of the first analyte ( $\text{Mg}^{2+}$ ), the switching valve is activated and the pretreatment column effluent is directed to the second (analytical) column which has been, to this point, equilibrating with the mobile phase (step 3). The separation between  $\text{Mg}^{2+}$ ,  $\text{Ca}^{2+}$ , and any residual interferant improves as the species move through the analytical column and eventually pass through the detector (step 4). After elution of the  $\text{Ca}^{2+}$ , the system is switched back to its initial configuration and the process is repeated. The working components of the system are two pumps (both of which deliver mobile phase) and a switching valve. Thus the entire heart-cutting process can be accomplished by switching be-



**Figure 5.** Chromatographic behavior of the two Wescan columns in tandem with the heart cut. The eluent was  $1 \times 10^{-3}$  M ethylenediamine at a flow rate of 2 mL/min with each pump. The sample used was the same as that for Figures 1 and 3.

**Table III.** Effect of Switching Timing on Efficiency of Heart Cut

autosampler flush time, s	peak areas <sup>a</sup>	
	$\text{Na}^+$	$\text{Mg}^{2+}$
5		611 469
10		622 420
20		620 328
30	12 289	623 775
40	1 699 333	610 206

<sup>a</sup> Average of three injections.

tween two valve rotor configurations.

In theory, a vast majority of the interferant is removed from the system during the pretreatment step, and any that gets through the first step is further separated from the analytes in the analytical column. As shown in Figure 5, excellent removal of the  $\text{Na}^+$  interference in pharmaceutical matrices can be achieved. In the case shown, the  $\text{Na}^+$  response exhibited in both the single and tandem column approaches is completely removed, resulting in excellent base line stability both before and after the analyte peaks. Of course, this type of performance is dependent on the correct timing of the switching event; if the column switch occurs too quickly, some of the interferant will get through to the detector. If the cutting event occurs too late, some of the early eluting analyte will be lost to the drain. Identification of the correct cutting time represents an optimization process, the results of which are shown in Table III. In the system employed in this study, the cutting (column switching) event was timed to occur 1 min after the autosampler sampling cycle is initiated. The amount of time the system is switched to drain (i.e., while the sample is in the first column) is 1 min minus the cycle time of the autosampler. For the autosampler used in this study, this last quantity has two components; the amount of time the sample flushes through the loop prior to injection (which is analyst controlled) and the amount of time it takes the sampler to perform the injection process (constant). Thus, in the experiment summarized in Table III, the timing of the cutting event was changed by changing the autosampler flush time. The amount of time the sample stays on the first column prior to cutting is 1 min minus the sum of the flush time and the injection time. As flush time increases, the time the sample stays on the pretreatment column prior to cutting decreases. As this occurs, one would eventually expect that  $\text{Na}^+$  would break through to the detector. As flush time decreases, eventually some  $\text{Mg}^{2+}$  would be lost to the drain prior to



Table IV. System Suitability Criteria

quantity	suitability limit	
	Mg <sup>2+</sup>	Ca <sup>2+</sup>
capacity factor	>4.0	>8.5
peak asymmetry	<2.0	<2.5
plate count	>350	>350
resolution	>2.5 <sup>b</sup>	>2.5 <sup>b</sup>
correlation coefficient	>0.9990	>0.9990
precision <sup>a</sup>	<1.5 <sup>c</sup>	<1.5 <sup>c</sup>

<sup>a</sup>For a sample containing 40 ppm Mg<sup>2+</sup>, 60 ppm Ca<sup>2+</sup> with a 20  $\mu$ L sample loop. <sup>b</sup>Greater than 2.5 between both. <sup>c</sup>Percent RSD.

switching. The former behavior is shown once the flush time increases past 30 s with observable quantities of Na<sup>+</sup> coming through at this time. The latter behavior is shown once flush time is lowered past 10 s with a clear loss of Mg<sup>2+</sup> being observed at 5 s. The apparent loss of Mg<sup>2+</sup> signal at 40 s is a reflection of incorrect peak integration as it becomes masked by the high Na<sup>+</sup> response. Thus, 20  $\pm$  10 s has been identified as the effective flush window for the particular pretreatment column employed. While this is a broad range, and might be applicable to any column of this type, clearly each pretreatment column used would need to be characterized with a similar experimental sequence. Given the effectiveness of the heart-cutting procedure, one concludes that this methodology is potentially more accurate and precise than the other approaches described herein. This improvement is apparent from the data contained in Table II; for both Mg<sup>2+</sup> and Ca<sup>2+</sup> the heart-cutting methodology is characterized by an accuracy of 100  $\pm$  2% and a precision routinely better than 1.5% RSD. For this method, the data represents an average of at least nine replicate injections of each sample made during the course of two separate analytical runs. More reflective of the short-term precision of the system is the variation in triplicate injections made of a given sample within a single analytical sequence. In this event, the mean precision of both Mg<sup>2+</sup> and Ca<sup>2+</sup> determinations for over 120 triplicate injections (of both samples and standards) approaches 0.6% with the median precision in both cases being 0.4%. For the Ca<sup>2+</sup> determination, 84.1% of the samples assayed had a precision of less than 1% RSD; 94% had a precision better than 1.5%. Similarly for Mg<sup>2+</sup>, 78.9% of the samples assayed had a precision of better than 1% RSD, while 91.4% of the samples had a precision better than 1.5%. In no case was a triplicate injection set made where the precision was worse than 2% RSD.

A major concern, even with a system that requires no automated switching, is long-term ruggedness. As used here, long-term ruggedness has two components: chromatographic

and quantitation performance. On one hand, the system must perform in a chromatographically acceptable manner for a long period of time (large number of injections) for it to be of any use in routine applications. Similarly, the method must retain its precision and calibration linearity over the course of an extended period of use. In order to confirm that a given system is operating effectively, a set of system suitability criteria are established as part of the method development/evaluation process. The criteria for the Ca<sup>2+</sup>/Mg<sup>2+</sup> assay are defined in Table IV and include both chromatographic (capacity factor, peak asymmetry, plate count, and resolution) and quantitation (correlation coefficient of standard curve and precision) criteria. These criteria must be met by a particular system being prepared for use prior to the analysis of any samples. The criteria as outline in Table IV are sufficiently strict so as to readily identify a poorly operating system; thus one way to assess the ruggedness of the heart-cutting procedure is to determine system's performance at various times over the lifetime of the system and compare them to the suitability criteria. For all the criteria except plate count, the original research system is capable of meeting these requirements after more than 1200 injections have been made. While plate count for Ca<sup>2+</sup> falls slightly below the suitability criteria after 1000 injections, clearly the system is still capable of effective (precise and accurate) operation after this point.

The heart-cutting technology is thus capable of generating highly accurate and precise data over long periods of extended operation. However, as a practical note, this analyst observed that the fiber suppressor used in the study was prone to a steadily decreasing flow rate for the basic regenerant used. This steady decrease in flow rate of the gravity-fed regenerant, clearly a manifestation of a clogging exit system, was reflected in a changing base line and sensitivity. This problem was circumvented by using a peristaltic pump to supply the caustic regenerant at a constant rate. With this control of regenerant flow rate, it was possible to produce calibration plots at the beginning and end of a continuous 48-h analysis sequence that were superimposable within the experimental precision.

#### LITERATURE CITED

- (1) Deans, O. R. *Chromatographia* **1968**, *1*, 18-22.
- (2) Bombaugh, K. J., Levangle, R. F. *J. Chromatogr. Sci.* **1970**, *8*, 560-566.
- (3) Porath, J., Bennich, H. *Arch. Biochem. Biophys., Suppl.* **1962**, *1*, 152-156.
- (4) Bombaugh, K. J. *J. Chromatogr.* **1970**, *53*, 27-35.
- (5) Hoover, T. B., Yager, G. D. *J. Chromatogr. Sci.* **1984**, *22*, 435-437.
- (6) Hoover, T. B., Yager, G. D. *Anal. Chem.* **1984**, *54*, 1206-1208.
- (7) Zenki, M. *Anal. Chem.* **1981**, *53*, 968-971.
- (8) Matsushita, S. *J. Chromatogr.* **1984**, *312*, 327-363.

RECEIVED for review July 8, 1986. Accepted November 3, 1986.

# Fluorescence Properties of Metal Complexes of 8-Hydroxyquinoline-5-sulfonic Acid and Chromatographic Applications

Krystyna Soroka, Rathnapala S. Vithanage, Denise A. Phillips, Brian Walker, and Purnendu K. Dasgupta\*

Department of Chemistry and Biochemistry, Texas Tech University, Lubbock, Texas 79409-4260

**Seventy-eight metal species are examined for fluorescence properties of their chelates with 8-hydroxyquinoline-5-sulfonic acid (HQS); 42 of these fluoresce, many intensely. The optimum pH, determined by ligand ionization vs. hydroxo complex formation, lies between 5 and 8. Cadmium forms the most fluorescent complex in a purely aqueous solution. Fluorescence is enhanced for many metals in surfactant (hexadecyltrimethylammonium ion, HTA<sup>+</sup>) containing media and in a water:dimethylformamide solvent. A number of metal ions quench the fluorescence of other metal-HQS chelates, Fe(III) being by far the most effective, and such quenching is accentuated in media containing HTA<sup>+</sup>. The fluorescence properties can be exploited by introducing the ligand through a postcolumn reactor or by incorporating it in the eluent in a chromatographic system. Subpicomole detection limits are attainable for Cd, Mg, and Zn.**

Oxine (8-hydroxyquinoline, HQ) and its derivatives occupy a uniquely important place in analytical chemistry, perhaps second only to EDTA and its analogues. Indeed, few analytical reagents have merited multivolume monographs solely devoted to them (1) and new applications of oxine and its derivatives in modern analytical chemistry are continually being developed (2, 3). Of special interest to us is the intense fluorescence exhibited by many metal complexes of oxine and its derivatives which are themselves nonfluorescent except in concentrated sulfuric and perchloric acids or anhydrous fluoroalcohols (4, 5). In a series of papers Rogers and co-workers (4, 6-8) and Stevens (9) have given an excellent account of the fluorescence or the lack thereof of oxine and its metal complexes and the effects of substituents and solvent media upon such fluorescence.

A comprehensive review of fluorometric methods for the determination of inorganic species containing more than 1400 literature citations has appeared (10). For obvious reasons, essentially all previous efforts have been directed to developing specific reagents (and conditions) for the determination of given analytes. However, a generally applicable fluorogenic complexing agent which undergoes a nonfluorescent  $\rightarrow$  fluorescent transition upon complexation with a large number of metal ions (i.e., a nonspecific fluorogenic reagent) will be of particular utility in ultratrace metal ion chromatography, of interest to us. In this regard, oxine and its derivatives are unparalleled in the large number of fluorescent metal complexes formed. Unfortunately, oxine and most of its analogues form complexes that are insoluble in water. Although it is possible to carry out metal ion chromatography involving oxine chelates with hydroorganic (11, 12) or micellar (13) solvents, it would be desirable to conduct such separations with purely aqueous eluents. From this standpoint, 8-hydroxyquinoline-5-sulfonic acid (HQS) is the ligand of choice—the complexation properties are analogous to those of HQ with essentially the same complexation constants (14, 15) but with

greatly enhanced aqueous solubility (16, 17), sufficient to preclude problems arising from precipitation, at least in neutral and alkaline solutions (18).

While there is a substantial amount of literature on the metal complexes of HQS, these largely do not deal with the fluorescence properties. Fluorescence properties of metal-HQS chelates have been exploited in a pioneering work in paper chromatography by Feigl and Heisig (19) and later in a series of 10 papers by Bishop, involving general studies on complexation or titrimetric applications; the last of these papers appeared in 1976 (20). The fluorescent indicator properties have been used by others as well (21, 22). Fluorometric determination procedures have been described for Mg (23-26) and Cd (27). A kinetic fluorometric procedure was developed for the determination of Al at low pH (28) and several oxidizing agents ( $\text{Ag}^+$ /persulfate,  $\text{MnO}_4^-$  and Ce(IV)) have been determined by their ability to oxidize HQS into an unidentified fluorescent product (29-31). The difference in fluorescence lifetimes has been exploited for the individual determination of six group II and group III (group 2 and group 3 in 1985 notation) metals from a mixture (32). The enhancement of the metal-HQS fluorescence by a cationic micelle, especially hexadecyltrimethylammonium ion, has been reported by a number of workers (33-39). A fiber-optic probe designed to sense several metals based on the fluorescence induced on immobilized HQS has recently been described (40).

However, there is a remarkable lack of quantitative data on the relative fluorescence intensities of the various metal chelates in aqueous or mixed aqueous solution. In the few cases where more than one metal has been studied, the reported orders of fluorescence intensity vary (see, for example, ref 6 and 41). For cases where the reports are less quantitative in nature, the observations are even diametrically opposite as to whether a certain metal-HQS chelate fluoresces or not (see, for example, ref 27 and 42). In order to fully assess the potential of HQS as a fluorogenic reagent in metal ion chromatography, we have carried out a systematic investigation of the fluorescence properties of HQS chelates of metal ions across the periodic table up to uranium, in regard to optimal excitation and emission wavelengths, pH, and oxidation state, and have also studied the enhancement of fluorescence intensity in micellar (hexadecyltrimethylammonium) and in water/*N,N*-dimethylformamide (DMF) solvents.

## EXPERIMENTAL SECTION

All fluorescence measurements were conducted on a Perkin-Elmer LS-5 spectrofluorometer with both excitation and emission slits set at 10 nm and an integration time of 4 s (except in peak determining scans which employed a response time of 0.5 s). Measurements of pH were made with an Altex PHI 71 pH meter equipped with an Orion Ross combination electrode calibrated by the two point method.

8-Hydroxyquinoline-5-sulfonic acid (Aldrich) was twice recrystallized (as the monohydrate) from large volumes of hot water. The majority of the metal salts used were analytical reagent grade and were typically nitrates, sulfates, or chlorides. In a few cases



as noted, fluoride complexes were used as well. The rare metal salts used were of the purest grade available; however, details of the extent and nature of any metallic impurities present were not available. While explicit attempts were not made to standardize the solutions of individual metal salts, it is unlikely that the worst case error in the target concentration is greater than 10%. For the majority of metals, this error is likely less than 1%. Hexadecyltrimethylammonium chloride (HTAC) was obtained as a 25% (w/v) concentrate (Fisher, HPLC grade). Dimethylformamide and other solvents used were reagent grade and KOH/HCl used for pH adjustment were of ultrapure quality. Water used in this work is distilled and then deionized; it meets all the specifications of ASTM type I reference reagent water, but no explicit efforts were made to determine the nature and concentrations of residual metal ions in the water.

The purity of reagents is particularly important in this work because some metals form very intensely fluorescent HQS chelates while some others appear to act as powerful quenchers (*vide infra*). Presence of these metals in the original reagents as impurities even in concentrations as low as 0.1% can completely nullify observations. For this reason, experiments were conducted in relatively dilute solutions, containing 20  $\mu$ M of the metal ion. Initial experiments were conducted at a fixed pH of  $9.05 \pm 0.03$  (unbuffered), because the published  $pK$  values of HQS indicate that the ligand is essentially completely ionized by this pH. To 50 mL of a 1 mM solution of HQS at pH 9.05, 200  $\mu$ L of a 5 mM solution of the metal was added. The pH was readjusted to 9.05 by the addition of microaliquots of dilute KOH or HCl if it altered by more than 0.03 units. The optimum  $\lambda_{ex}$  and  $\lambda_{em}$  values cited pertain to this pH. The fluorescence intensity as a function of pH (integer pH units between 4 and 10) was determined in an analogous manner at the  $\lambda_{ex}$  and  $\lambda_{em}$  values found to be optimum for pH 9; in a few preliminary studies it was determined that the shifts of the optimal  $\lambda_{ex}$  and  $\lambda_{em}$  values as a function of pH are minimal. The addition of HTAC to an unbuffered HQS solution causes a drop in pH because of deprotonation of HQS to form the  $HTA^+-QS^-$  ion pair. In HTAC media, the maximal excitation and emission wavelengths are slightly red-shifted ( $\sim 5$  nm). The emission was measured at the optimum wavelengths after adjusting the pH to the specified optimum value. For water-DMF solvent studies, (10 -  $x$ ) mL of DMF were added to  $x$  mL of the aqueous metal-HQS chelate (100  $\mu$ M metal ion, 1 mM HQS, except for Cd for which a 10  $\mu$ M concentration was used) prepared at the optimum pH for the fluorescence of the metal chelate. The fluorescence intensity was measured at the optimum wavelengths for the purely aqueous medium. Wavelengths of maximum emission in water/DMF media are slightly red-shifted (5–10 nm) compared to purely aqueous solutions; the optimal excitation wavelength does not shift noticeably. To calculate the enhancement factor, the dilution by DMF was taken into account.

In all cases, fluorescence intensities were also measured at least at one other metal concentration lower than the concentration specified above, to ensure that the operational range is in the linear domain of fluorescence intensity-concentration relationship. Except for cadmium as indicated, no significant departure from linearity was noted at 20  $\mu$ M metal concentration in aqueous solutions; more dilute solutions were used for cadmium to avoid the inner filter effect.

Chromatographic experiments were conducted on a Gilson 2-pump HPLC system equipped with a pressure monitor/pulse dampener (Gilson Medical Electronics, Middleton, WI), a low dead volume high pressure dynamic mixer (Knauer, W. Germany), a Rheodyne 7010 loop injector (Rheodyne, Inc., Cotati, CA), and a variable wavelength fluorescence detector (FS970, Kratos Instruments, Ramsey, NJ). This detector uses a  $D_2$  lamp as excitation source. The excitation monochromator was set at 362 nm and the emission filter was high pass type, the 50% cutoff point being 470 nm. Although the optimal (energy corrected) excitation wavelength for most metal-HQS complexes is around 390 nm, the lamp output characteristics result in greater detector response when the excitation wavelength is chosen as cited. A 50- $\mu$ L sample volume was used in all work to maximize concentration sensitivity.

For HQS-bearing eluents, the stationary phase was a surface-sulfonated poly(styrene-divinylbenzene) cation exchanger of unspecified particle size (likely  $\geq 15 \mu$ m) and an ion exchange

capacity of  $\sim 40 \mu$ equiv/g, (column type HS, 50  $\times$  4.2 mm Wescan Instruments, Santa Clara, CA). For use of HQS as a postcolumn reagent, a glass-lined column (250  $\times$  4 mm, Scientific Glass Engineering, Austin, TX) packed with 5- $\mu$ m  $C_{18}$ -silica was initially coated with 100 mL of 5 mM sodium octanesulfonate (Eastman Kodak) and then used with an eluent containing 50 mM sodium potassium tartrate and 0.4 mM sodium octanesulfonate, adjusted to pH 3.4 with NaOH, after Cassidy and Elchuk (43). The postcolumn reactor was a filament-filled porous membrane type of  $\sim 10 \mu$ L volume that has been described earlier (44). Stainless steel screen-T reactors (44) lead to an undesirable degree of iron contamination and fluorescence quenching. The reactor was operated under nitrogen pressure and was adjusted to obtain an eluent:reagent mixing ratio of 5:3. Buffering agents used in the eluents or reagent (Tris, Bicine, MOPS, MOPSO) were used without further purification (Serva Fine Biochemicals, Westbury, NY).

## RESULTS AND DISCUSSION

The data for purely aqueous solutions are presented according to the periodic groups (see Table I).

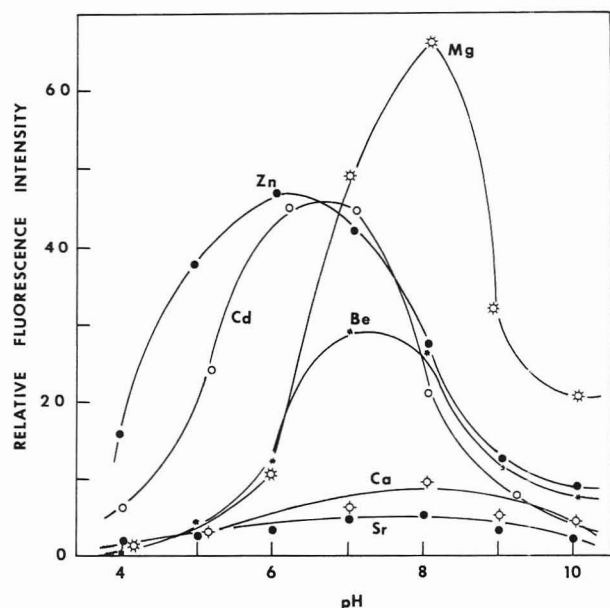
**Group I.** The alkali metals are not expected to associate strongly with HQS and this is generally observed. However, solutions containing Rb and Cs decidedly show perceptibly increased fluorescence compared to the K-containing (KOH is used for pH adjustment) blank. The purity specifications on the Rb and Cs salts used are excellent and suggest that the fluorescence is not due to impurities. It is difficult to distinguish with certainty if blank values are lower if the pH is adjusted with LiOH and NaOH compared with KOH because of the greater amount of impurities present in the first two compounds. The blank value, however, is perceptibly lower if tetra-*n*-propylammonium hydroxide is used for pH adjustment.

It is interesting to note that alkali-metal salts of HQ in neat DMF have been reported to exhibit more intense fluorescence than almost any other metal (45). Regardless of whether significant complexation occurs with the heavier alkali metals in aqueous media, it appears certain that a significant amount of the "blank" fluorescence is due to association with residual metals in reagents and solvent; the blank is significantly reduced upon the addition of ethylenediaminetetraacetate (EDTA). Group IB metals do not form fluorescent chelates with HQS. Chelates are formed nevertheless, as indicated by UV spectroscopy; a number of these efficiently quench the fluorescence of other metal chelates. If oxidized to the trivalent state (for example with persulfate), Ag oxidizes HQS to an unidentified fluorescent product (29), the same as that formed with Ce(IV) or Sb(V).

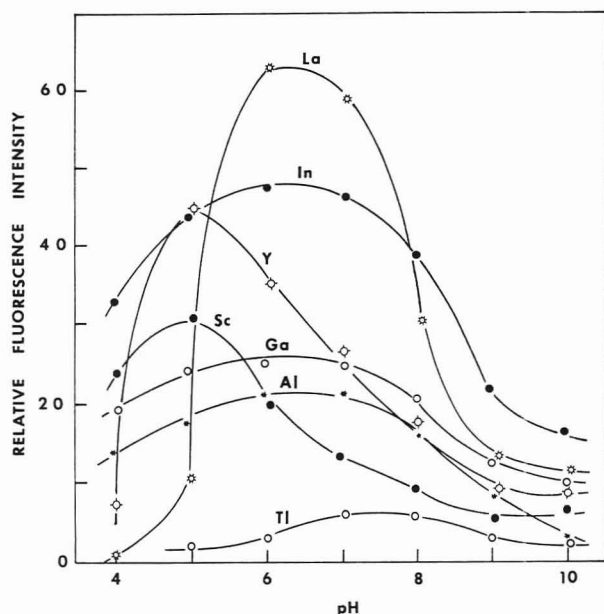
**Group II.** All of the metals belonging to group IIA (radium was not studied) produce fluorescent chelates with HQS with the optimal pH being around 8, except for Be which optimally fluoresces at pH 7. At high pH and in the presence of excess HQS, polymeric complexes are reportedly formed with Be (20). The fluorescence intensities decrease from Mg to Ba, with Ba being only marginally fluorescent. While the trend is expected due to both the internal "heavy atom effect" (45) as well as the decreasing complexation constant (14, 15), the drop in fluorescence is rather steep along the series. The fluorescence of the heavier metal chelates is more susceptible to quenching by adventitious quenchers present as impurities (*vide infra*) and the observed low fluorescence may actually be partially due to quenching.

Among group IIB metals, Hg forms nonfluorescent chelates in either of its oxidation states. In contrast, both Cd and Zn form strongly fluorescent chelates. The Cd chelate is a factor of 5 to 10 more fluorescent than virtually all other fluorescent HQS chelates. The pH dependence of the fluorescence of group II metal-HQS chelates is shown in Figure 1.

**Group III.** Among group IIIA metals, trivalent Al, Ga, and In are strongly fluorescent, all optimally at pH 6, with in-



**Figure 1.** pH dependence of the fluorescence intensities of group II metal-HQS chelates: Cd, 2  $\mu$ M; all other metals in this and following figures, 20  $\mu$ M; HQS, 1 mM.

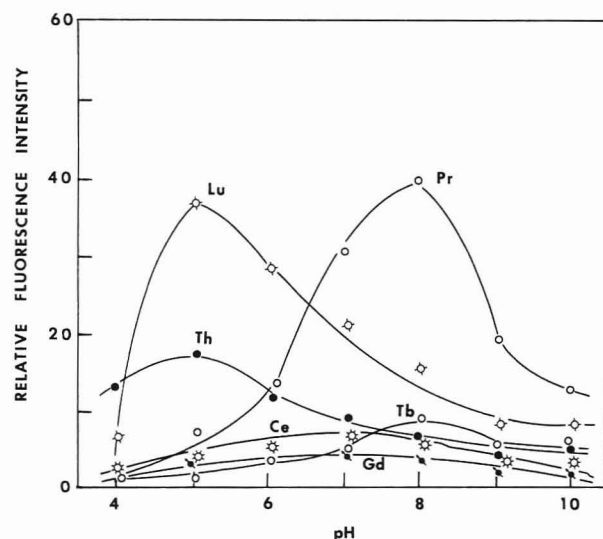


**Figure 2.** pH dependence of the fluorescence intensities of group III metal-HQS chelates.

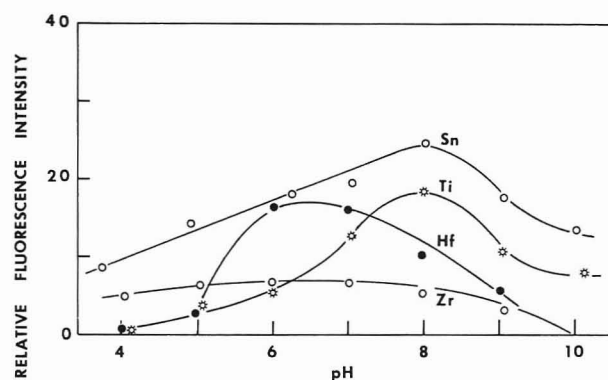
creasing fluorescence intensity along the series. Boron as the borate anion is nonfluorescent. Trivalent Tl is nonfluorescent and is a powerful quencher, but univalent Tl is moderately fluorescent. The fluorescence of the Tl(I) chelate, which fluoresces optimally at pH 7, indicates that caution should be exercised with the adage that metals with more than one commonly occurring oxidation state do not form fluorescent chelates (see ref 4, other notable examples being Ti(IV) and Sn(IV)).

Among group IIIB metals, Sc, Y, and La all form strongly fluorescent chelates at optimal pH values of 5 to 6 and the fluorescence increases along the series. The pH dependence of the fluorescence of group III metal-HQS complexes is shown in Figure 2.

**Lanthanides and Actinides.** The only two strongly fluorescent HQS chelates among the lanthanides are those of Pr and Lu. Eu and Dy chelates are marginally fluorescent at best; the data for the two oxidation states of Ce indicate that the complexes are nonfluorescent; however, Ce(IV) ox-



**Figure 3.** pH dependence of the fluorescence intensities of some lanthanide and actinide metal-HQS reaction products.



**Figure 4.** pH dependence of the fluorescence intensities of some group IV metal-HQS chelates.

idizes HQS to some unidentified fluorescent product. Among the actinides, only the naturally occurring elements, Th and U, were studied. Th(IV) forms a moderately fluorescent chelate, the  $\text{UO}_2^{2+}$  chelate is nonfluorescent. The pH dependence of the fluorescence intensities of the metal-HQS reaction product for several lanthanides and actinides is shown in Figure 3. For the case of Ce(IV), the reaction was allowed to proceed for 30 min at pH 8; the pH was then adjusted.

**Group IV.** Among group IVA metals, Sn(IV) forms a strongly fluorescent chelate whereas the Sn(II) chelate is nonfluorescent. The Pb(II) chelate is marginally fluorescent and also appears to be the least soluble among the HQS chelates in that precipitation occurs at concentrations of 1 mM and above. The Pb(IV) chelate of HQ has been reported to be nonfluorescent in DMF (45). In group IVB, quadrivalent Ti, Zr, and Hf chelates are all moderately fluorescent; Ti(III) is nonfluorescent. the pH dependence of the fluorescence intensities of the metals in group IV is shown in Figure 4.

**Group V.** Among group VA elements, As(III), As(V), or Bi(V) all as the oxo anions, and Sb(III) or Bi(III) as the oxo cations, do not form fluorescent HQS chelates. The fluorescent product formed with Sb(V) appears to be an oxidation product, because both the development of fluorescence is slow and the fluorescence behavior is identical with that of the product formed with Ce(IV). Among group VB metals, V(V) as the metavanadate and V(IV) as the  $\text{VO}^{2+}$  cation did not form fluorescent HQS chelates. Although intense fluorescence was observed from pentavalent Nb and Ta chelates, the purity specifications on the compounds used were rather poor and the data should be regarded as tentative.



Table I. Fluorescence Properties of Metal-HQS Chelates

metal (oxidation state)	$\lambda_{\text{ex,max}}^{a,b}$ nm	$\lambda_{\text{em,max}}^{a,b}$ nm	pH <sub>max</sub> <sup>c</sup>	rel fluorescence intens <sup>d</sup>	metal (oxidation state)	$\lambda_{\text{ex,max}}^{a,b}$ nm	$\lambda_{\text{em,max}}^{a,b}$ nm	pH <sub>max</sub> <sup>c</sup>	rel fluorescence intens <sup>d</sup>
Group IA					Actinides				
Li(I) <sup>e</sup>				nfl <sup>f</sup>	Th(IV) <sup>i</sup>	395	506	5	17.3
Na(I) <sup>e</sup>				nfl	U(VI) <sup>n</sup>				nfl
K(I) <sup>e</sup>				nfl					
Rb(I) <sup>e</sup>	393	506	8	3.9	Group IVA				
Cs(I) <sup>e</sup>	393	506	8	4.1	Sn(II) <sup>i</sup>				nfl
Group IB					Sn(IV) <sup>o</sup>	397	516	8	24.3
Cu(I) <sup>g</sup>				nfl	Pb(III) <sup>e</sup>	396	514	8	4.3
Cu(II) <sup>h</sup>				nfl	Group IVB				
Ag(I) <sup>e</sup>				nfl	Ti(III) <sup>i</sup>				nfl <sup>j</sup>
Au(III) <sup>i</sup>				nfl <sup>j</sup>	Ti(IV) <sup>o</sup>	394	505	8	18.3
Group IIA					Zr(IV) <sup>q</sup>	396	508	6	6.5
Be(II) <sup>h</sup>	392	507	7	29.2	Hf(IV) <sup>r</sup>	393	507	6	16.7
Mg(II) <sup>e</sup>	393	506	8	66.4	Group VA				
Ca(II) <sup>e</sup>	394	512	8	9.6	As(III) <sup>s</sup>				nfl
Sr(II) <sup>e</sup>	395	506	8	5.4	As(V) <sup>t</sup>				nfl
Ba(II) <sup>e</sup>	394	512	8	2.9	Sb(III) <sup>u</sup>				nfl
Group IIB					Sb(V) <sup>v</sup>	396	507	7	6.3
Zn(II) <sup>i</sup>	393	506	6	46.9	Bi(III) <sup>e</sup>				nfl
Cd(II) <sup>h</sup>	387	522	7	450 <sup>k</sup>	Bi(V) <sup>w</sup>				nfl
Hg(I) <sup>e</sup>				nfl	Group VB				
Hg(II) <sup>e</sup>				nfl	V(IV) <sup>x</sup>				nfl
Group IIIA					V(V) <sup>y</sup>				nfl
Al(III) <sup>h</sup>	395	500	6	21.4	Nb(V) <sup>z</sup>	394	506	7	60.3
Ga(III) <sup>e</sup>	397	512	6	24.9	Ta(V) <sup>z</sup>	395	502	7	76.6
In(III) <sup>e</sup>	398	517	6	47.5	Group VIB				
Tl(I) <sup>e</sup>	393	511	7	6.0	Cr(III) <sup>e</sup>				nfl <sup>j</sup>
Tl(III) <sup>e</sup>				nfl <sup>j</sup>	Cr(VI) <sup>aa</sup>				nfl
Group IIIB					Mo(II) <sup>i</sup>				nfl <sup>j</sup>
Sc(III) <sup>e</sup>	394	511	5	30.7	Mo(VI) <sup>ab</sup>				nfl
Y(III) <sup>e</sup>	394	508	5	45.1	W(VI) <sup>ac</sup>	394	522	7	17.3
La(III) <sup>e</sup>	393	511	6	63.0	Group VIIIB				
Lanthanides					Mn(II) <sup>e</sup>				nfl
Ce(IV) <sup>h</sup>	396	507	7	6.7 <sup>l</sup>	Mn(VII) <sup>ad</sup>				nfl
Ce(III) <sup>h</sup>				nfl <sup>m</sup>	Re(III) <sup>i</sup>				nfl
Pr(III) <sup>e</sup>	395	503	8	40.0	Group VIIIB				
Nd(III) <sup>e</sup>	396	509	8	3.7	Fe(II) <sup>h</sup>				nfl
Sm(III) <sup>e</sup>	394	510	7	3.2	Fe(III) <sup>e</sup>				nfl <sup>ae</sup>
Eu(III) <sup>e</sup>	392	506	8	2.3	Co(II) <sup>e</sup>				nfl <sup>j</sup>
Gd(III) <sup>e</sup>	396	509	8	8.8	Ni(II) <sup>e</sup>				nfl
Tb(III) <sup>e</sup>	394	509	6	4.9	Ru(III) <sup>i</sup>				nfl
Dy(III) <sup>e</sup>	394	508	8	2.3	Rh(III) <sup>i</sup>				nfl
Ho(III) <sup>e</sup>	397	510	7	3.2	Pd(III) <sup>i</sup>				nfl
Er(III) <sup>e</sup>	394	508	8	4.2	Os(III) <sup>i</sup>	393	504	7	8.9
Tm(III) <sup>e</sup>	395	505	8	4.2	Ir(IV) <sup>i</sup>	394	508	8	28.5
Yb(III) <sup>e</sup>	394	509	8	4.4	Pt(II) <sup>af</sup>	395	518	8	5.7
Lu(III) <sup>e</sup>	394	508	5	37.1	Pt(IV) <sup>i</sup>				nfl

<sup>a</sup> At pH 9 but does not shift markedly with pH. <sup>b</sup> Because of the relatively large slit widths (10 nm) employed and the natural width of both the absorption and emission bands, these values should be regarded accurate to only within  $\pm 2$  nm. The values are corrected for lamp output and phototube response. <sup>c</sup> The pH at which highest fluorescence is observed, to the nearest integer unit. <sup>d</sup> At the optimum pH, at the cited values of  $\lambda_{\text{ex,max}}$  and  $\lambda_{\text{em,max}}$ . The blank value reaches a maximum at pH 8 and is 1.8 at that pH ( $\lambda_{\text{ex}}$  393,  $\lambda_{\text{em}}$  506). <sup>e</sup> Nitrate salt. <sup>f</sup> Nonfluorescent, the fluorescence is equal to or below blank value. <sup>g</sup> Solid CuCl dissolved in deoxygenated 1 mM sulfoxine at pH 9 to reach a concentration of 20  $\mu\text{M}$  Cu(I). <sup>h</sup> Sulfate salt. <sup>i</sup> Chloride or chloro complex. <sup>j</sup> This metal ion exerts a significant quenching action on the fluorescence of other metal-sulfoxine chelates. <sup>k</sup> A value of fluorescence intensity of 45 in relative units was obtained at 2  $\mu\text{M}$  Cd<sup>2+</sup>. The experiment was carried out at this concentration to avoid the inner filter effect. The value has been multiplied by 10 to correspond to the concentration of other metal ions. At 20  $\mu\text{M}$  Cd<sup>2+</sup>, the relative fluorescence intensity is somewhat less than 450. <sup>l</sup> A transient red-violet species is formed immediately on Ce(IV) addition and slowly disappears. The decreasing visible absorption is accompanied by increasing fluorescence. The value quoted is taken after 30 min, at which point the fluorescence intensity is stable. <sup>m</sup> Ce(III) is itself intensely fluorescent ( $\lambda_{\text{ex}}$  253,  $\lambda_{\text{em}}$  358); however, the sulfoxine chelate is not, either at wavelengths characteristic of uncomplexed Ce(III) or at wavelengths typical of other sulfoxine chelates. <sup>n</sup> As uranyl nitrate. <sup>o</sup> As sodium stannate. <sup>p</sup> As titanium sulfate. <sup>q</sup> As zirconium nitrate. <sup>r</sup> As hafnium nitrate. <sup>s</sup> As sodium arsenite. <sup>t</sup> As sodium arsenate. <sup>u</sup> As antimony sulfate. <sup>v</sup> Liquid SbCl<sub>5</sub> directly added to 1 mM sulfoxine to reach a concentration of 20  $\mu\text{M}$  Sb(V). <sup>w</sup> As sodium bismuthate. <sup>x</sup> As vanadyl sulfate. <sup>y</sup> As sodium metavanadate. <sup>z</sup> As fluoride, HF digest of the metal pentoxide. <sup>aa</sup> As sodium chromate. <sup>ab</sup> As sodium molybdate. <sup>ac</sup> As sodium tungstate. <sup>ad</sup> As potassium permanganate. <sup>ae</sup> The only stable sulfoxine complex that displays an intense visible absorption, visually the color is dark green. <sup>af</sup> As the *cis*-diamine dichloride.

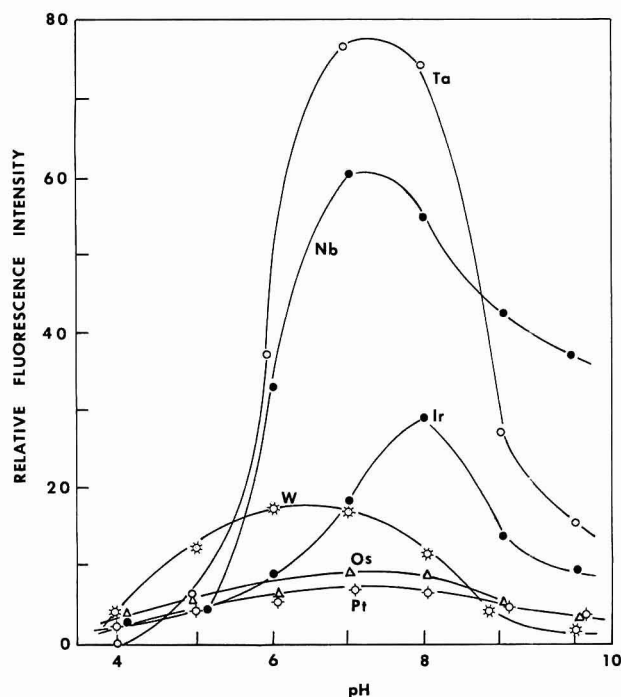


Figure 5. pH dependence of the fluorescence intensities of some group V–VIII metal–HQS chelates.

**Group VI.** Among the metals in group VIB, only W(VI) forms a fluorescent chelate, whether added as a salt of the tungstic cation or as a tungstate. Neither hexavalent Mo nor Cr as the anions react with HQS, both cationic Mo(II) and Cr(III) form nonfluorescent chelates and act as effective quenchers.

**Groups VII and VIII.** The majority of the metals belonging to these groups do not form markedly fluorescent chelates. Indeed, a number of these nonfluorescent chelates are highly efficient quenchers, Fe(III) being the most notable (vide infra). Mn as  $\text{MnO}_4^-$  has been reported to oxidize HQS to a fluorescent product (30); however in the present experiments ( $\text{pH} \geq 4$ ), oxidation was not observed. Divalent Pt, trivalent Os, and quadrivalent Ir form fluorescent HQS chelates, the last being markedly so. However, Ir(IV) is a strong oxidizing agent; it is possible that the fluorescence is due to the HQS oxidation product rather than the metal chelate. The pH dependence of the fluorescence of metal–HQS complexes is shown in Figure 5.

**Enhancement of Fluorescence by HTAC.** Significant increases in fluorescence intensities were observed in the presence of HTAC for all the metals so studied, Mg, Ca, Sr, Ba, Al, Cd, and Zn. This is similar to the observations of Meshkova et al. (35) for the lanthanides. The enhancement factors (at the optimum pH) range from  $\sim 1.2$  for Sr to nearly an order of magnitude for Al; also the optimum pH is reduced by 1–2 units in the micellar system. Further, in general, the pH range for maximal fluorescence is extended. Maximum enhancement is reached in all cases in the 0.25–1.0 mM HTAC concentration range. For any given metal, this optimum HTAC concentration does not change upon a 2-fold change in the metal concentration. A summary of these results is given in Table II; details of the fluorescence intensity dependence upon pH and HTAC concentration will be reported elsewhere.

**Fluorescence Intensities of Metal–HQS Chelates in Water/DMF Media.** Because significant enhancement was reported for DMF (neat) as solvent for the Mg–HQS chelate compared to water (8), it was of interest to us to investigate the effect of mixed water/DMF solvents on the HQS chelates of some representative metals, Al, Cd, Zn, and Ca. The results are shown in Table III. Although the degree of enhancement,

Table II. Enhancement of Fluorescence by a Cationic Micelle<sup>a</sup>

metal	optimum HTAC concn, mM	optimum pH range	enhancement factor over pure aqueous solution (at optimum pH)
Mg	0.5–1	6.8–7.2	1.6
Sr	0.25	6.7–7.5	1.2
Ba	0.5	6.6–6.9	2.6
Al	0.5	5.4–7	10.2
Zn	0.5–1	4–7.5	1.8
Cd	0.25	6.2–6.8	1.6

<sup>a</sup> All of the systems studied contain 1 mM HQS, the metal concentrations used were 500  $\mu\text{M}$  (Ba, Sr), 100  $\mu\text{M}$  (Mg, Al, Zn), and 10  $\mu\text{M}$  (Cd).

Table III. Enhancement of Fluorescence in Water/DMF Media

vol % DMF	rel fluorescence intens enhancement factor <sup>a</sup>			
	Al	Cd	Zn	Ca
10	2.65	1.71	1.33	1.24
20	5.80	1.91	1.31	0.60
30	9.14	1.74	1.39	0.59
40	14.9	1.65	1.62	0.59
50	22.3	1.81	2.02	0.82
60	31.4	2.22	2.77	1.13
70	41.6	2.79	3.86	1.55
80	48.1	3.09	5.20	3.10
90	82.5	2.96	7.05	7.98

<sup>a</sup> For each metal, the relative fluorescence intensity is normalized to unity for a purely aqueous solution. The absolute value can be estimated from the data in Table I.

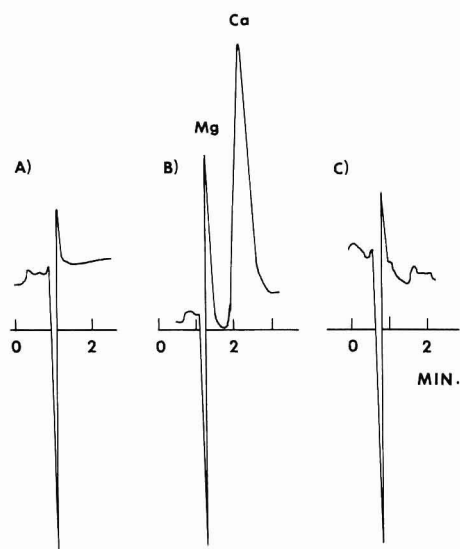
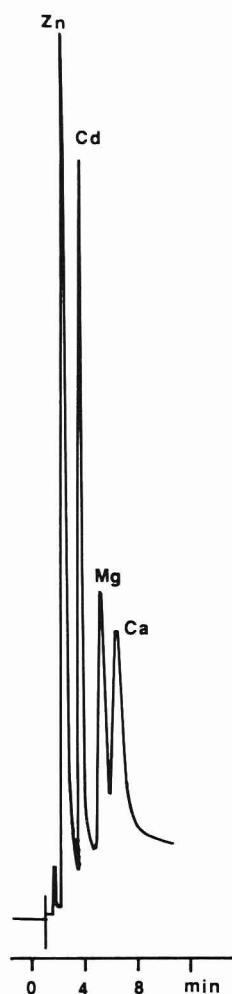


Figure 6. Ultratrace detection of magnesium: eluent, 1 mM HQS, 10 mM Tris, pH 8.0, 150 mM  $\text{KNO}_3$ ; flow rate, 1 mL/min; column, Wescan HS,  $50 \times 4.2$  mm; PMT voltage, 660 V, 0.05  $\mu\text{A}$  full scale. Samples used were as follows: (a) water, (b) aqueous solution of 500 fmol of  $\text{Mg}^{2+}$  and 500 pmol of  $\text{Ca}^{2+}$ , (c) water. Note the slight increase in the water response in (c) due to cross contamination in the sample valve from injection (b).

if any, varies a great deal from metal to metal, even among the limited subset tested, the enhancement at high DMF content is remarkable, most notably for Al. It should be emphasized that throughout the entire range of solvent composition, the changes in the value of the blank are negligible, and in going from purely aqueous to 90 vol % DMF media, the optimal excitation wavelength does not shift and only a



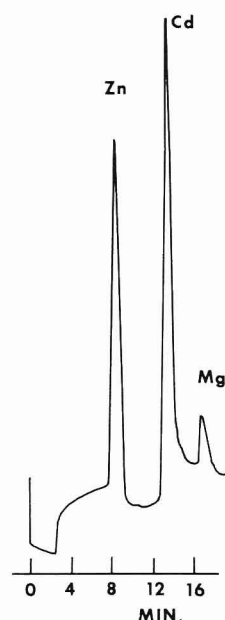


**Figure 7.** Gradient separation of Zn, Cd, Mg, and Ca: column, Wescan HS ( $50 \times 4.2$  mm); flow rate, 1 mL/min; eluent A, 250  $\mu$ M HQS, 2.5 mM MOPS, pH 7.0; eluent B, A + 500 mM  $\text{KNO}_3$ ; program, linear gradient from 0 to 65% B in 0–2.35 min; sample injected electropneumatically at 1 min into the program, 65–100% B in 2.35–4.80 min, hold at 100% B; samples, 135 pmol of Zn, 33 pmol of Cd, 135 pmol of Mg, 20 nmol of Ca; PMT voltage, 375 V, 0.02  $\mu$ A full scale.

slight red shift (5–10 nm) is observed for the emission maximum.

**Quenching of the Fluorescence of Metal-HQS Chelates.** Some quantitative data on the quenching action of a few metal ions, which were observed to act as quenchers upon the fluorescence of the Mg-HQS chelate, are presented in Table IV. These experiments were conducted in the presence of excess HQS with the quencher concentration significantly lower than the fluorescing metal chelate concentration. This is in contrast to the study of Meshkova et al. (35) on the quenching of the fluorescence of the La-HQS chelate by quencher ions present in an order of magnitude greater concentration. The very powerful quenching action exhibited by Fe(III) on the fluorescence of HQS chelates has not been reported previously and is particularly important in view of its wide occurrence in real samples and may indeed limit the usefulness of the recently reported innovative fiber-optic sensors which employ immobilized HQS (40).

Quenching by iron clearly has important consequences on the use of HQS in trace metal ion chromatography. Modern high-performance liquid chromatographic hardware makes extensive use of stainless steel as fluid contact parts. Iron is inevitably leached off in trace amounts as complexing ligands are commonly incorporated in aqueous eluents (which contain significant amounts of dissolved oxygen even after ordinary degassing) for metal ion chromatography. While details of the quenching effects of iron will be reported elsewhere, we



**Figure 8.** Detection of Zn, Cd, and Mg by postcolumn reaction with HQS: column, SGE-C18 5  $\mu$ m ( $250 \times 4$  mm), coated with octane-sulfonate; eluent, 50 mM sodium potassium tartrate, 0.4 mM octane-sulfonate, pH 3.4; flow rate, 0.5 mL/min; postcolumn reagent, 1 mM HQS, 300 mM bicine, pH 9.3, 0.3 mL/min; reactor effluent, pH  $\sim$ 8.0; sample, 25 pmol of Zn, 6 pmol of Cd, 500 pmol of Mg; PMT voltage, 590 V, 0.02  $\mu$ A full scale.

wish to note a few salient points here. Among the HQS chelates of Ca, Mg, Cd, and Al in purely aqueous medium, the quenching effect decreases in the order  $\text{Ca} > \text{Mg} > \text{Cd} > \text{Al}$ ; this may very well simply be mirroring the corresponding increase in the respective complexation constants (ref 14 and 15; the complexation constant for the Al-HQS system has not been reported; however, we estimate it to be the highest among the four metals above on the basis of the reported complexation constants with HQ).

The presence of HTAC greatly accentuates the quenching effect; the anionic Fe-HQS complex is likely concentrated at the micellar interface and thus exhibits greater quenching ability. The quenching effect is sufficiently large so as to wipe out all gains of the surfactant enhancement of the original fluorescence at all but very low quencher concentrations. Indeed, it is possible that the rapid drop of fluorescence intensity at high HTAC concentrations for some metals may partly be due to the presence of adventitious quenchers that are present in the HTAC reagent itself. These factors limit the usefulness of HTAC enhancement of the fluorescence intensity of HQS chelates. In contrast, the DMF/water medium does not appear to be nearly as susceptible to quenching; the enhancement factor is still sufficiently large for most quencher concentrations so as to outweigh the greater susceptibility to quenching.

**Chromatographic Applications.** HQS can be used successfully as an integral component of the eluent similar to the use of dithiocarbamates (46) or diazo dyes (47) in metal ion chromatography. However, careful optimization of column-eluent combinations are often necessary to achieve a desired separation. A chromatogram of  $10^{-8}$  M  $\text{Mg}^{2+}$  and  $10^{-5}$  M  $\text{Ca}^{2+}$  on a short column (50 mm) is shown in Figure 6, with preceding and succeeding injections of water. The water dip is not noticeable at lower detector sensitivity and may be completely separated from the Mg peak on a 100-mm column; however, the attainable limit of detection will deteriorate. This example constitutes the first demonstration, to our knowledge, of subpicomole detection of Mg. If ultratrace determinations are not essential, HQS-bearing eluents easily permit gradient elution. An example separation of Zn, Cd, Mg, and Ca is

**Table IV. Effect of Selected Quenching Metal Ions upon the Fluorescence of the Mg-HQS Complex<sup>a,b</sup>**

quenching ion	% original fluorescence remaining	quenching ion	% original fluorescence remaining
Cr(III)	94.1	Au(III)	59.4
Ag(I)	91.0	Tl(III)	17.7
Ti(III)	62.4	Fe(III)	1.0

<sup>a</sup> At a quencher concentration of 50  $\mu$ M. <sup>b</sup> 100  $\mu$ M Mg, 1 mM HQS, pH 8,  $\lambda_{ex}$  390 nm,  $\lambda_{em}$  510 nm.

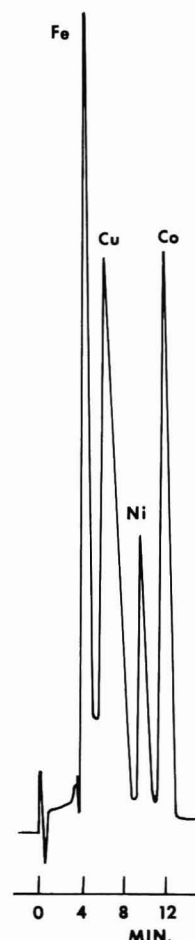
shown in Figure 7.

By and large, however, introducing HQS postcolumn is a more versatile approach, for much the same reasons that the vast majority of metal ion chromatography is currently carried out by introducing chromogenic reagents in a postcolumn mode. The chromatogram in Figure 8 showing the separation of Zn, Cd, and Mg was obtained with a porous membrane postcolumn reactor (PCR). Detection limits for both Zn and Cd in this mode are routinely well below  $10^{-8}$  M and approaches  $10^{-9}$  M under optimum conditions. Another example of a postcolumn application involving HQS is the detection of metals such as iron which act as quenchers by introducing a fluorescent HQS metal complex in a micellar solvent through the PCR and monitoring the decrease in fluorescence. An example is shown in Figure 9. Detection limits in this mode are not nearly as good as in direct fluorescence detection, as may be expected.

## CONCLUSIONS

HQS appears to be an unusually promising reagent for postcolumn addition or other applications in metal ion chromatography—an ideal fluorometric complement to (pyridylazo)resorcinol (PAR), which is in wide use in metal ion chromatography today. Indeed, PAR works best with those metals which form nonfluorescent or very weakly fluorescent chelates with HQS. HQS cannot compete with PAR as an absorptiometric reagent, since the molar absorptivities of the chelates ( $\lambda_{max}$  360–400 nm) are uniformly below  $10^4$ , at least a factor of 4 lower than the corresponding PAR chelates. Although the effects of further substitution, specifically at the 2 and 7 positions in HQS, on metal chelation selectivity and stability, have been studied (18, 48), there is no evidence to believe that any advantage is to be gained over HQS in regard to fluorescence properties. Further, except for the 7-iodo derivative (Ferron), they are not commercially available and must be synthesized. For the 7-iodo derivative, our preliminary studies confirm what may be expected on the basis of the internal heavy atom effect: the fluorescence intensities obtained with this compound are uniformly lower than those obtained with HQS itself, typically by a factor of 8 to 10.

Meaningful further improvements along this line should involve the development of a ligand that forms complexes with much greater molar absorptivities, without sacrificing the fluorescence properties, such that tandem or even same cell (49) absorptiometric detection can be sensitively performed for metals that do not form fluorescent chelates. Most of the more intensely absorbing azo derivatives (azoxines) do not form fluorescent complexes, however. The sole exception are derivatives in which 1-amino-2-naphthol or its sulfonated derivatives are diazotized and coupled to the 7 position in HQS or HQ, as originally reported by Badrinan (50). These form metal complexes that fluoresce an intense pink and may be worthy of further studies.



**Figure 9.** Detection of Fe, Cu, Ni, and Co by fluorescence quenching, postcolumn reaction with the Al-HQS complex: column and eluent conditions, as given in Figure 8; postcolumn reagent, 300  $\mu$ M Al, 900  $\mu$ M HQS, 500  $\mu$ M HTAC, 300 mM MOPSO, pH 7.9, 0.3 mL/min; reactor effluent pH  $\sim$ 7.0; sample, 500 pmol each of Fe and Cu, 2 nmol of Co, 5 nmol of Ni.

## ACKNOWLEDGMENT

We are grateful to Philip W. West, Louisiana State University, for valuable suggestions. We thank Scientific Glass Engineering (Austin, TX) and Wescan Instruments (Santa Clara, CA) for the gift of the columns used.

## LITERATURE CITED

- Hollingshead, R. G. W. *Oxine and Its Derivatives*; Butterworths: London, 1954–1956; Vol. I–IV.
- Marshall, M. A.; Mottola, H. A. *Anal. Chem.* **1985**, *57*, 375–376.
- McLaren, J. W.; Myktiuk, A. P.; Willie, S. N.; Berman, S. S. *Anal. Chem.* **1985**, *57*, 2907–2911.
- Popovych, O.; Rogers, L. B. *Spectrochim. Acta* **1959**, *15*, 584–592.
- Bratzel, M. P.; Aaron, J. J.; Winefordner, J. D.; Schulman, S. G.; Gershon, H. *Anal. Chem.* **1972**, *44*, 1240–1245.
- Ohnesorge, W. E.; Rogers, L. B. *Spectrochim. Acta* **1959**, *15*, 27–40.
- Ohnesorge, W. E.; Rogers, L. B. *Spectrochim. Acta* **1959**, *15*, 41–48.
- Popovych, O.; Rogers, L. B. *Spectrochim. Acta* **1960**, *16*, 49–57.
- Stevens, H. M. *Anal. Chim. Acta* **1959**, *20*, 389–396.
- Fernandez-Gutierrez, A.; Munoz de la Pena, A. In *Molecular Luminescence Spectroscopy. Methods and Application: Part I*; Schulman, S. G., Ed.; Wiley: New York, 1985; pp 371–546.
- Berthod, A.; Kolosky, M.; Rocca, J.-L.; Vittori, O. *Analyst* **1979**, *7*, 395–400.
- Hoffmann, B. W.; Schwedt, G. *HRC CC, J. High Resolut. Chromatogr. Chromatogr. Commun.* **1982**, *5*, 439–440.
- Hoshino, H.; Yotsuyanagi, T. *Bunseki Kagaku* **1980**, *29*, 807–808.
- Smith, R. M.; Martell, A. E. *Critical Stability Constants*; Plenum: New York, 1975; Vol. 2, pp 227–229.
- Martell, A. E.; Smith, R. M. *Critical Stability Constants*; Plenum: New York, 1982; Vol. 5, Supplement No. 1, p 245.
- Berg, R. Z. *Anorg. Allg. Chem.* **1932**, *204*, 208–212.
- Näsänen, R.; Uusitalo, E. *Acta Chem. Scand.* **1954**, *8*, 835–841.
- Hollingshead, R. G. W. *Anal. Chim. Acta* **1958**, *19*, 447–457.
- Fiegl, F.; Heisig, G. B. *Anal. Chim. Acta* **1949**, *3*, 561–566.
- Bishop, J. A. *Anal. Chim. Acta* **1976**, *87*, 255–257.
- Badrinas, A. *Publ. Inst. Biol. Apl. (Barcelona)* **1958**, *28*, 75–80.
- Van Slageren, R.; Den Boef, G.; Van der Linden, W. E. *Talanta* **1973**, *20*, 739–748.



- (23) Schachter, D. J. *Lab. Clin. Med.* **1961**, *58*, 495-498.
- (24) Patrovsky, V. *Fresenius' Z. Anal. Chem.* **1967**, *230*, 355-356.
- (25) Patrovsky, V. *Collect. Czech Chem. Commun.* **1967**, *32*, 2656-2660.
- (26) Pelczar, T.; Siedlanowska-Krowczynska, H. *Diagn. Lab.* **1973**, *9*, 257-262.
- (27) Ryan, D. E.; Pitts, A. E.; Cassidy, R. M. *Anal. Chim. Acta* **1966**, *34*, 491-494.
- (28) Wilson, R. L.; Ingle, J. D., Jr. *Anal. Chim. Acta* **1977**, *92*, 417-421.
- (29) Ryan, D. E.; Pal, B. K. *Anal. Chim. Acta* **1969**, *44*, 385-389.
- (30) Pal, B. K.; Ryan, D. E. *Anal. Chim. Acta* **1969**, *47*, 35-39.
- (31) Pal, B. K.; Toneguzzo, F.; Corsini, A.; Ryan, D. E. *Anal. Chim. Acta* **1977**, *88*, 353-361.
- (32) Nishikawa, Y.; Hiraki, K.; Morishige, K.; Katagi, T. *Bunseki Kagaku* **1977**, *26*, 365-370.
- (33) Kina, K.; Tamura, K.; Ishibashi, N. *Bunseki Kagaku* **1974**, *23*, 1404-1406.
- (34) Shi, H.; Cui, W.; Wang, R. *Gaodeng Xuexiao Huaxue Xuebao* **1982**, *46*-52.
- (35) Meshkova, S. B.; Rusakova, N. B.; Pouletkov, N. S. *Zh. Anal. Khim.* **1982**, *37*, 1988-1990.
- (36) Shi, H.; Cui, W.; Wang, R. *Huaxue Xuebao* **1983**, *41*, 1029-1037.
- (37) Cui, W.; Shi, H. *Fenxi Huaxue* **1983**, *11*, 778-781.
- (38) Cui, W.; Wang, J.; Shi, H. *Fenxi Huaxue* **1983**, *11*, 900-904.
- (39) Cui, W.; Mi, L.; Shi, W. *Huaxue Shiji* **1985**, *7*, 125-128.
- (40) ZhuJun, Z.; Seitz, W. R. *Anal. Chim. Acta* **1985**, *171*, 251-258.
- (41) Onoue, Y.; Hiraki, K.; Morishige, K.; Nishikawa, Y. *Nippon Kagaku Kaishi* **1973**, 1237-1243.
- (42) Bishop, J. A. *Anal. Chim. Acta* **1963**, *29*, 172-177.
- (43) Cassidy, R. M.; Elchuk, S. *Anal. Chem.* **1982**, *54*, 1558-1563.
- (44) Cassidy, R. M.; Elchuk, S.; Dasgupta, P. K. *Anal. Chem.* **1987**, *59*, 85-90.
- (45) Lytle, F. E.; Storey, D. R.; Juricich, M. E. *Spectrochim. Acta, Sect. A* **1973**, *29*, 1357-1369.
- (46) Bond, A. M.; Wallace, G. G. *Anal. Chem.* **1984**, *56*, 2085-2090.
- (47) Zenki, M. *Anal. Chem.* **1981**, *53*, 968-971.
- (48) Fresco, J.; Freiser, H. *Inorg. Chem.* **1963**, *2*, 82-85.
- (49) Gant, J. R.; Perrone, P. A. *Am. Lab. (Fairfield, Conn.)* **1985**, *17*(3), 104-111.
- (50) Badrin, A. *Talanta* **1963**, *10*, 704-708.

RECEIVED for review July 29, 1986. Accepted October 27, 1986. This research was supported by the U.S. Department of Energy, Division of Chemical Sciences, Office of Basic Energy Sciences, through Grant No. DE-FG-05-84ER-13281. However this report has not been subject to review by the DOE and no official endorsement should be inferred.

## Artifacts Arising from the Improper Preparation and Use of Nonaqueous Ion Exchange Resins

Michael G. Strachan<sup>1</sup> and R. B. Johns\*

Department of Organic Chemistry, University of Melbourne, Parkville, Victoria 3052, Australia

**This paper reports on the consequences of inadequate conditioning of nonaqueous macroporous ion-exchange resins in the separation of coal-derived liquids and/or petroleum substitutes. In such cases any residual resin decomposition products will be incorporated into the fractions eluted from the resins. These contaminants have certain spectral and analytical characteristics similar to the complex fossil fuel derived fractions from the resin separation procedure which make their presence less obvious. Indeed, some characteristic features, such as  $f(a)$  values, pyrogram data, very high H/C and O/C ratios, and high  $H_{Ar}/H_{Al}$  ratios from the Brown-Ladner equation are different enough to bias the quantitative data and lead to incorrect structural compositional conclusions. The data suggest that it is an essential step, in such a fractionation procedure, to adequately precondition the resins.**

The increasing use of nonaqueous ion exchange resins for the separation of complex mixtures such as coal-derived liquids (1-5) and petroleum (6-10) raises the issue of the extent to which contaminants released from the resins may bias the analytical data eventually obtained. Current resins in use have much improved resistance to mechanical attrition and do not show the fragmentation in either polar or nonpolar organic solvents characteristic of conventional exchange resins. Accordingly they are open to a wider application in analytical separations. The more widely used resins are the Rohm and Haas Amberlyst series, A-21 and A-27 (weak and strong anion exchangers, respectively) and A-15 (strong cation exchanger). Previously A-29 was used (6-8) but in the literature it has been

replaced by Amberlite IRA-904, also a macroporous resin with exchange characteristics and properties similar to A-27.

Much time is required to activate and condition these resins into their particular functionalized form and to remove resin decomposition products. The literature reports developments in understanding the methods of conditioning and packing and the use of these resins, but characteristically the reasons for the changes recommended are not elaborated upon (7, 8, 10). In a previous paper the use of resins A-21, A-27, and A-15 was described (4) for the separation of a coal-derived liquid on the basis of functionality. Since A-27 had not previously been reportedly used for such a purpose, the introduction of the combination as described (4) raised the need to know the potential bias which may be introduced into the range of physicochemical analyses of the product fractions from contaminants derived from improperly prepared resin columns. This paper reports our assessments.

### EXPERIMENTAL SECTION

**Resins and Chemicals.** The Amberlyst anion (A-21 and A-27) and cation (A-15) exchange resins were obtained from Rohm and Haas. Methanol (May and Baker, Ltd., Sydney, Australia) and methylene dichloride (Ajax Chemicals, Sydney, Australia) were both analytical reagent grade and redistilled prior to use.

**Extraction and Preparation of Resin Samples.** The only modifications to the procedures published (4) for the activation and conditioning of the resins was that fresh conditioning solvent (i.e., methanol or methylene dichloride) was used every 50 h rather than after the 200-h washing cycle used for each solvent. Coloration was observed until the third batch of methanol for all three resins, the fourth batch was colorless in each case. Methylene dichloride extracted little material from all resins, coloration only being observed in the first 50-h washing. However, washing was continued for the 200-h period. The resins were washed for a total of 400 h each. The methanol and methylene dichloride washings of each resin were combined, and the solvent was removed by rotary evaporation under high vacuum. They were then concentrated in vials. The residual solvent was removed by a nitrogen

<sup>1</sup> Present address: Petroleum Geochemistry Group, School of Applied Chemistry, W.A.I.T., Kent St., Bently 6102, W.A., Australia.

Table I. Percentage Yields of Washings from Resins

	yield, <sup>a</sup> % (w/w)		
	A-21	A-27	A-15
"as received" dry resin	1.03	0.76	1.19
CDL charged <sup>b</sup>	20.60	15.20	23.80

<sup>a</sup> Average of duplicate 200-g resin extractions. <sup>b</sup> Based on 5 g of CDL charged to ion-exchange column, containing 100 g of resin. This amount of CDL is that used in our reported separation procedure (4).

gas purge, and the vial and contents were dried to constant weight in a desiccator (vacuum, P<sub>2</sub>O<sub>5</sub>). The three resin washings were characterized by the same chemical and spectroscopic techniques as reported for the total oil and separated fractions of the coal-derived liquid from the hydrogenative liquefaction in tetralin of Loy Yang brown coal (bore 1277, medium-light lithotype) (4).

**Instrumental and Elemental Analyses.** <sup>1</sup>H and <sup>13</sup>C NMR spectra were obtained on a JEOL FX-100 NMR spectrometer operated at 100 and 25 MHz, respectively. The <sup>13</sup>C NMR spectra are not quantitative, as they were obtained without the use of either chromium acetyl acetonate or inverse gated decoupling. The infrared spectra were recorded in the absorbance mode on a Pye-Unicam SP-300 spectrophotometer as either smears or cast films on NaCl plates. Pyrolysis gas chromatography (Py-GC) was performed by use of a CDS 190 pyroprobe, operating at 700 °C/20 s, interfaced to a Perkin-Elmer 900 gas chromatograph, fitted with a 25-m BP-5 bonded polar phase silica column and FID detection. Molecular weight (MW) profiles were obtained by gel permeation chromatography-high-performance liquid chromatography (GPC-HPLC) using 1000-Å, 500-Å, and 100-Å  $\mu$ -Styragel columns in series with both UV and refractive index detection. The lack of appropriate calibration standards prevented absolute data from being obtained by GPC-HPLC. Elemental analyses were performed by the Australian Microanalytical Service Division of AMDEL (Melbourne, Australia).

## RESULTS AND DISCUSSION

The resins are normally activated by acid and base washing with KOH and HCl, for strong anion and cation exchangers, respectively, and then, in the majority of cases, conditioned by Soxhlet extraction for 24 h with the solvents with which they are to be used. Final preparation typically involved drying the resin at a low temperature (40 °C) in a vacuum oven prior to dry packing into a recycling chromatography column. The sample to be separated was then applied as a solution in either pentane or cyclohexane. The unentrained material was removed by continuous elution with the solvent of application. More recently Cogswell and Latham (3) and McKay and co-workers (10) have recommended wet packing their anion and cation exchange resins in the columns, stressing (10) that the resins should not be allowed to dry out or become exposed to heat. These procedural changes contrast with earlier recommendations of dry packing followed by 24 h only of Soxhlet extraction in the solvents of use. Recently, Green and co-workers (5) have reported storing conditioned anion and cation exchange resins as cyclohexane slurries in airtight amber-colored containers. They observed that even these precautions did not entirely prevent the formation of resin decomposition products upon prolonged storage. Hence these developments in procedure point to the need for low conditioning temperatures and the prevention of oxidation. To

these criteria must be added adequate solvent preextraction, as data in this paper will highlight.

In this study, resin decomposition material was still extracted after 100 h of conditioning in methanol, in fact, sequential 50-h extractions show that conditioning for only 24 h in each of the solvents of use is not sufficient to remove all contaminants. On an as received basis (i.e., unwashed) the percentage yield of the washings are small, typically 1% (w/w) (Table I). However, as these contaminants are soluble in the solvents used for applying the coal-derived liquid (CDL) sample to the resins and removing the resultant fractions from them, it is more appropriate to express the yields in terms of the amount of CDL charged to and eluted from the resins. When the data are expressed in this form, the percentage yields of the washings are considerable, ranging from 15 to 24% (w/w) of the CDL sample (Table I). These percentage values are based on 5 g of CDL charged to 100 g of ion-exchanged resin, this being the amount of sample used in our earlier reported separation procedure (4). (We have found that this quantity of CDL (5 g) (i) does not overload the exchange capacity of the resin and (ii) provides sufficient yields of the respective fractions for their further characterization.) Indeed, if a smaller quantity of CDL is charged to the resins, then the percentage yields of the washings would be correspondingly greater. This effect is even more significantly pronounced if the resin washings are expressed as a weight percentage of the corresponding resins' fractions. The possibility that a fraction eluted from a resin may contain a substantial amount of contamination is therefore a real problem. Hence the effect of incomplete resin extraction may perturb not only the physicochemical characteristics of the fractions separated by the resins but also the CDL composition via an overestimation of the gross acid and base yields.

The compositional complexity of the CDL fractions favors resin washings being considered as genuine components unless they contain specific diagnostic features permitting their differentiation. Hence we report both the spectral and analytical characterization of the washings to the level of compound types. A direct comparison can then be made with the appropriate fractions separated by the same scheme from a CDL. In this case, the fractions used as comparative standards were from a CDL produced by the liquefaction of a medium-light lithotype Loy Yang brown coal (4).

Table II reports the elemental analyses of the three resin washings and Table III the <sup>1</sup>H NMR data and related average structural parameters derived by using modified Brown-Ladner equations (11). When the data in these tables are compared with those for fractions A1-A3, A4-A6, and B1-B2, respectively, and reported earlier (4), three features emerge, viz., (i) a large aliphatic bias in the resin washings, (ii) a high heteroatom content, either nitrogen or oxygen, and (iii) increased alkyl carbons bonded to heteroatoms.

The H/C ratios of all three washings are greater than 1.5, whereas the CDL fractions range from 0.86 to 1.35, reflecting the lower absolute percentage values for carbon in the washings. In contrast, the percentage of hydrogen and oxygen contents are higher in the washings than in the CDL fractions. The IR spectra (Figure 1), although complex and showing much heteroatom functionality, are not dissimilar to those from the CDL fractions. Indeed, that for resin A-27 with its

Table II. Elemental Analyses (%) of Resin Washings<sup>a</sup>

sample	C	H	O <sup>b</sup>	N	S	H/C	O/C	N/C	O/H
A-21	60.1	9.1	28.3	2.5	N.D. <sup>c</sup>	1.74	0.37	0.04	0.20
A-27	62.4	8.3	25.2	4.1	N.D. <sup>c</sup>	1.59	0.29	0.06	0.18
A-15	38.6	5.3	54.3	0.5	1.31	1.65	1.06	0.01	0.64

<sup>a</sup> Dry ash-free basis. <sup>b</sup> Oxygen by difference. <sup>c</sup> N.D., not determined.



Table III.  $^1\text{H}$  NMR Distribution and Structural Parameter Data<sup>a</sup>

sample	$H_0$	$H_\alpha$	$H_{Ar}$	$H_{exch}$	$H_{Ali}/H_{Ar}$	$f(a)^b$	$\sigma^b$	$n = (H_0/H_\alpha) + 1$
A-21	2.1	29.6	7.8	60.5	4.04	0.72	0.82	1.07
A-27	19.2	53.1	8.6	19.2	8.38	0.57	0.84	1.36
A-15	75.0	9.1	11.6	4.4	7.28	0.19	0.91	9.26

<sup>a</sup>  $H_0$ , percentage of protons on carbons  $\beta$  and further from an aromatic ring;  $H_\alpha$ , percentage of protons on carbons  $\alpha$  to an aromatic ring;  $H_{Ar}$ , percentage of protons on aromatic rings;  $H_{exch}$ , percentage of protons exchangeable upon  $\text{D}_2\text{O}$  addition;  $H_{Ali}/H_{Ar}$ , aliphatic to aromatic proton ratio;  $f(a)$ , aromatic carbon to total carbon ratio;  $\sigma$ , degree of aromatic substitution;  $n$ , averaged chain length of alkyl substituents.  
<sup>b</sup> Derived using modified Brown-Ladner equations (11).

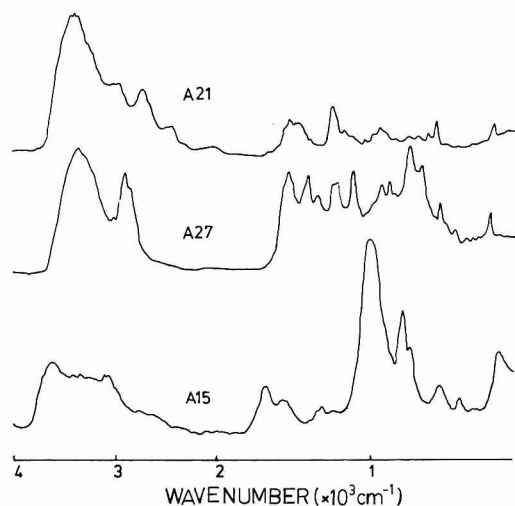


Figure 1. IR spectra of resin washings.

moderately well-resolved aliphatic C-H stretching absorption closely resembles fraction A1 in particular. The IR spectra, therefore, are not useful as a diagnostic tool in distinguishing resin washings from CDL fractions. The  $^1\text{H}$  NMR spectra of the washings are all broad, with very little resolved fine structure, but they do consistently show reduced amounts of aromatic, relative to aliphatic, protons reflected in the much higher  $H_{Ali}/H_{Ar}$  ratios. Interestingly, the aliphatic carbon bias in the A-21 and A-27 washings is not due to longer side chains, unlike the A-15 washings where 75% of the protons present are in the  $H_0$  spectral region and  $n$  has a very high value of 9.26. In fact, the A-21 and A-27 washings give lower values for these parameters than the corresponding CDL fractions. The aliphatic bias here stems from increased aryl methyl groups (for example, with the A-27 washings,  $H_\alpha$  at 53.1% is at least twice that for the corresponding CDL fractions) and alkyl carbons bonded to heteroatoms (cf. Figure 2, 50–70 ppm region). These last carbons are typically only 3–4% of the total carbon in the  $^{13}\text{C}$  NMR spectra of the CDL acid fractions.

The functionality of the resins accounts for the very high oxygen and nitrogen contents of the washings, relative to the respective CDL fractions. The high elemental nitrogen contents of A-21 and A-27 washings must arise from decomposition of their respective tertiary (12) and quaternary (13) amine functionalities.  $H_{exch}$  is a measure of the exchangeable protons on both oxygen and nitrogen and is significantly higher for the resin washings from A-21 and A-27 (Table III) than is found for the respective CDL acid fractions (14–34% and 7–14% respectively (4)); the value for the A-15 resin washing, however, is comparable with those observed for the CDL base fractions.

The  $f(a)$  values calculated for the resin washings are also consistent with their increased aliphatic structural features as outlined above. The differences in  $f(a)$  values between A-27 and A-15 washings and the respective CDL fractions are significant; the  $H_{Ar}$  values are markedly lower for all washings and suggest, together with the high  $\sigma$  values, a high level of substitution into the aromatic rings of the resin polymers.

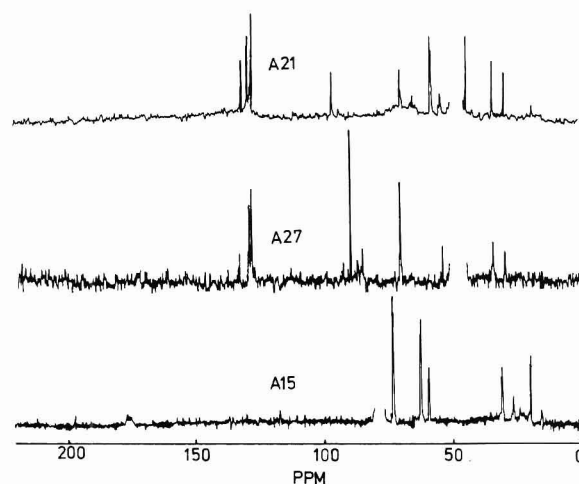
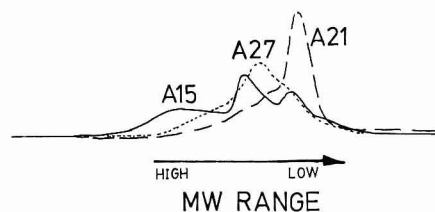
Figure 2.  $^{13}\text{C}$  NMR spectra of resin washings.

Figure 3. GPC-HPLC derived molecular weight profiles of resin washings.

The overview above shows that contaminants from the resins can be significant in quantity and hence can unduly affect quantitation through a range of parameters commonly used for the characterization of fossil fuel related materials. This results in a biased interpretation at the gross structural level of characterization of the separated acid and base fractions and thus a misrepresentation of the true situation.

The GPC-HPLC chromatograms (Figure 3) of the three washings, although not giving absolute values of the number ( $M_n$ ) and weight average ( $M_w$ ) molecular weights (MW) due to the lack of suitable calibration curves (14), at least give a reliable MW profile. These profiles can be compared with those obtained for the respective CDL resin fractions and the variation in elution volume and hence MW determined. The MW profiles of the three washings, although broad in range, differ greatly in intensities in the three regions. The A-15 washing has three discrete maxima at high, medium, and low MW regions and the A-21 washing, one maximum in the low MW region. The maxima in all cases are easily discernible; however they cannot be regarded as *diagnostic* for contamination in a CDL fraction MW profile as elution volumes, and hence profile range, are very similar to those observed for these resin fractions (14, 15).

The pyrolysis gas chromatograms (Py-GC) of the washed resins and their washings (Figures 4 and 5) differ substantially. The former are predominantly pyrolysis products from the solid resin polymer, while in the latter they are actual components of the washings (which are liquids). The conditions

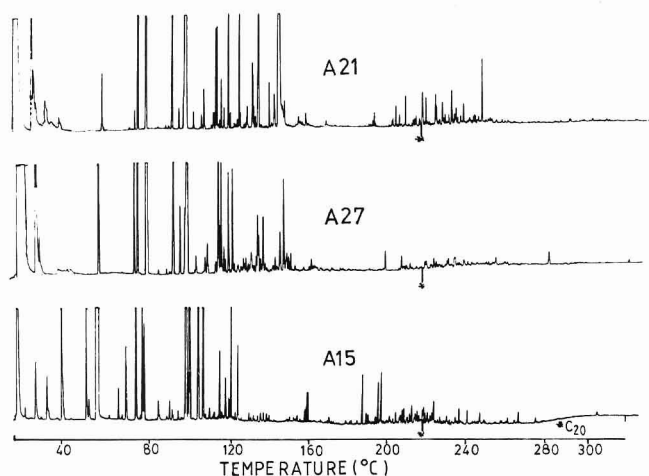


Figure 4. Pyrolysis gas chromatograms of washed resin.

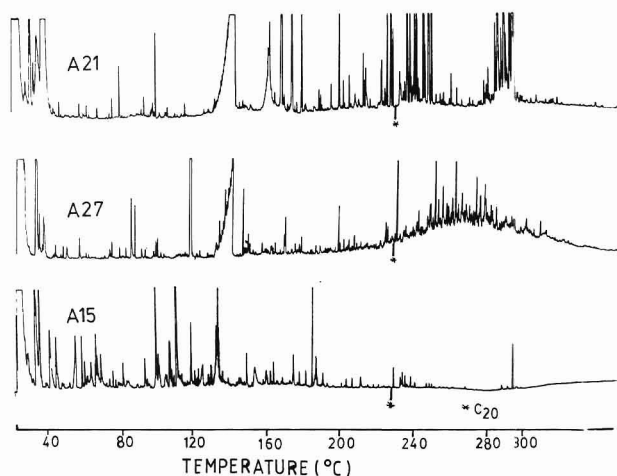


Figure 5. Pyrolysis gas chromatograms of resin washings.

were chosen to vaporize the sample of the washings and hence produce a distillation profile of the mixture. All three resins gave pyrograms consisting mainly of lower molecular weight components, with negligible material above  $n\text{-C}_{20}$ . The washings, however, could be separated into two groups, A-21 and A-27 against A-15. The former both contained a very large amount of one component, as shown by the characteristic long rise and short drop time of the GC peak, and had little lower molecular weight components, with the majority of the components in the chromatogram above  $n\text{-C}_{20}$ . This is unlike the pyrograms of the corresponding resin CDL fractions A1 and A4 where the majority of the acidic components elute before this region (4). The A-15 washing is similar to its parent resin, although there are observable differences. It contains most of the components in the low molecular weight region, with

an insignificant proportion eluting above  $n\text{-C}_{20}$ . The pyrograms of the CDL base fractions B1 and B2 have most of their components eluting at a slightly higher molecular weight range than those from the washings. The significant differences between the pyrograms of the resins and their respective washings, especially the proportions of material greater than  $n\text{-C}_{20}$  in the A-21 and A-27 washings, indicate that the latter originate in the decomposition of the polymeric skeleton of the resins. This explanation cannot fully account for the washings from the A-15 resin, which have predominantly lower molecular weight material and would appear to be a function of smaller molecular weight components comprising the resin.

Py-GC data, unlike much of the preceding physicochemical data, can be used as a diagnostic test for resin contamination in the corresponding CDL fractions, because the regions of elution of the majority of components are quite different between washings and these fractions.

The consequences of inadequate resin conditioning prior to CDL separation have been clearly illustrated in this paper (1) on actual yields of acidic and basic fractions, (2) on incorrect chemical-class compositional assignment, and (3) in bias in assessing structural characteristics. There would, however, be real difficulty in easily differentiating components of the washings from any specific CDL fraction separated. This conclusion points up the practical need to initially eliminate resin artifacts before material is fractionated by this (and other) resin separation procedures.

**Registry No.** Amberlyst A-21, 9049-93-8; Amberlyst A-27, 9074-22-0; Amberlyst A-15, 9037-24-5.

#### LITERATURE CITED

- (1) Schweighardt, F. K.; White, C. M.; Friedman, S.; Schultz, J. F. In *Organic Chemistry of Coal*; Larsen, J. W., Ed.; ACS Symposium Series 71, American Chemical Society: Washington, DC, 1978; pp 240-251.
- (2) Charlesworth, J. M. *Fuel* **1981**, *60*, 167-169.
- (3) Cogswell, T. E.; Latham, D. R. *Prepr. Pap.—Am. Chem. Soc., Div. Fuel Chem.* **1978**, *23*, 58-66.
- (4) Strachan, M. G.; Johns, R. B. *Anal. Chem.* **1986**, *58*, 312-319.
- (5) Green, J. B.; Hoff, R. J.; Woodward, P. W.; Stevens, L. L. *Fuel* **1984**, *63*, 1290-1301.
- (6) Jewell, D. M.; Weber, J. H.; Plancher, H.; Latham, D. R. *Anal. Chem.* **1972**, *44*, 1391-1395.
- (7) McKay, J. F.; Jewell, D. M.; Latham, D. R. *Sep. Sci.* **1972**, *7*, 361-370.
- (8) Jewell, D. M.; Albough, E. W.; Davis, B. E.; Ruberto, R. G. *Ind. Eng. Chem. Fundam.* **1974**, *13*, 278-282.
- (9) Boduszynski, M.; Chadha, B. R.; Szkuta-Pochopien, T. *Fuel* **1977**, *56*, 432-436.
- (10) McKay, J. F.; Amend, P. J.; Harnsberger, P. M.; Cogswell, T. E. A.; Latham, D. R. *Fuel* **1981**, *60*, 14-16.
- (11) Schwager, I.; Farmanian, P. A.; Yen, T. F. *Adv. Chem. Ser.* **1978**, No. 170, 66-77.
- (12) Rohm and Haas, Technical Bulletin **1967**, IE92.
- (13) Rohm and Haas, Technical Bulletin **1976**, IE-94-65/72.
- (14) Strachan, M. G.; Johns, R. B. *J. Chromatogr.* **1985**, *329* 65-80.
- (15) Strachan, M. G. Ph.D. Thesis, University of Melbourne, 1985.

RECEIVED for review May 5, 1986. Accepted October 21, 1986. M. G. Strachan acknowledges the financial support of a Melbourne University Postgraduate Scholarship.



# On-Line Supercritical Fluid Extraction-Capillary Gas Chromatography

Bob W. Wright,\* Stephen R. Frye, Dennis G. McMinn,<sup>1</sup> and Richard D. Smith

Chemical Methods and Separations Group, Chemical Sciences Department, Pacific Northwest Laboratory,<sup>2</sup>  
Richland, Washington 99352

**A new analytical methodology combining on-line supercritical fluid extraction with high-resolution capillary gas chromatography for automated sample preparation and analysis is described. Analytical-scale supercritical fluid extraction utilizes the variable solvating power of a supercritical fluid to selectively extract and isolate discrete fractions from a sample matrix. The supercritical fluid extract is decompressed through a restrictor to deposit and concentrate the analytes at the inlet of a standard capillary gas chromatography column for subsequent analysis. This methodology allows several modes of operation including quantitative extraction of all analytes from a sample matrix, quantitative extraction and concentration of trace analytes, selective extractions at various solvating powers to obtain specific fractions, or multiple-step extractions at various pressures for qualitative characterizations. This initial report describes the later two modes of operation and demonstrates the potential usefulness of this methodology for sample extraction and selective fractionation using a standard polycyclic aromatic hydrocarbon mixture and two complex sample matrices.**

Until recently the use of supercritical fluid extraction (SFE) has been generally confined to relatively large-scale chemical processing applications (1-3). However, the use of SFE methods for analytical applications is attracting increased attention (4-8). The potential advantages of SFE accrue from the physical properties of supercritical fluids. The compressibility of supercritical fluids is large above the critical temperature, and small changes in pressure result in large changes in the density (and solvating power) of the fluid (2). At higher densities molecular interactions increase due to shorter intermolecular distances and solvating characteristics approaching that of a liquid are imparted. However, the viscosity and solute diffusivity can remain similar to those of a gas (2), thus allowing more rapid mass transfer of solutes than feasible with liquids. Many fluids have comparatively low critical temperatures that allow extractions to be conducted at relatively mild temperatures, e.g., 31 °C for carbon dioxide. In addition to using pressure and/or temperature to control the density or solvating power, various fluids or fluid mixtures that exhibit different specific chemical interactions can be used to obtain the desired selectivity.

Recent studies have shown that analytical SFE provides comparable or better extraction efficiencies than conventional Soxhlet extraction and with over an order of magnitude increase in the rate of extraction (6). Other important potential advantages of SFE include the capability of selective extraction as a function of fluid solvating power, fractionation during collection (9), and the compatibility with on-line analysis of the extraction effluent. Various modes of on-line

analyses have been reported and include continuous monitoring of the total SFE effluent by mass spectrometry (10, 11), combined SFE-high performance liquid chromatography (4), combined SFE-packed column supercritical fluid chromatography (5), and preliminary descriptions of SFE-gas chromatography (7, 12). A logical extension of supercritical fluid extraction is to combine the process with a chromatographic analysis method. The variable solvating power of a supercritical fluid provides the mechanism for the selective extraction of the components of interest from the sample matrix and provides the basis for an automated method where sample preparation and analysis can be instrumentally linked. The on-line extraction-analysis approach is particularly attractive for small sample sizes and/or trace analysis where low levels of analytes are present.

The instrumentation and methodology developed for the automated on-line combination of SFE with high-resolution capillary column gas chromatography and its application to sample preparation and analysis are described in this report. Capillary gas chromatography (GC) was utilized for the analysis method in this study since the types of components of interest were amenable to this technique. However, other chromatographic methods, including capillary supercritical fluid chromatography (SFC), would also be compatible with this concept. The use of SFC would allow application to a wider range of compounds than is possible with GC including thermally labile and less volatile (polar and/or high molecular weight) species (13, 14). Gas chromatography, however, provides simpler operation and higher efficiencies than feasible with SFC or HPLC and is amenable to the vast majority of compounds extractable with nonpolar fluids such as carbon dioxide. Several modes of operation are possible utilizing the on-line SFE-GC approach including quantitative extraction and analysis, selective extraction or fractionation, and periodic sampling (and analysis) of the extraction effluent at various pressures for qualitative characterization of a sample matrix. The present work focuses on the development of the instrumentation and a qualitative demonstration of the applicability of this methodology for sample fractionation and compound isolation with the supercritical carbon dioxide extraction of two complex mixture samples and a standard mixture of polycyclic aromatic hydrocarbons (PAH). The utilization of this methodology for quantitative extraction analyses will be described in a subsequent report.

## EXPERIMENTAL SECTION

The samples utilized in this investigation included a complex polycyclic aromatic compound (PAC) material that was adsorbed on deactivated glass beads, a polycyclic aromatic hydrocarbon (PAH) standard mixture that was also adsorbed on deactivated glass beads, and a National Bureau of Standards air particulate sample, Urban Dust SRM 1649. Glass beads (45-150- $\mu$ m i.d.) were deactivated by refluxing in a 1:1 mixture of chlorotrimethylsilane and hexamethyldisilazane for 16 h and provided an inert support for the PAC material and the PAH standard mixture. The complex PAC material was a mixture of coal tar containing predominately parent ring structures ranging from two to six rings

<sup>1</sup> On leave from Gonzaga University Chemistry Department, Spokane, WA.

<sup>2</sup> Operated by Battelle Memorial Institute.

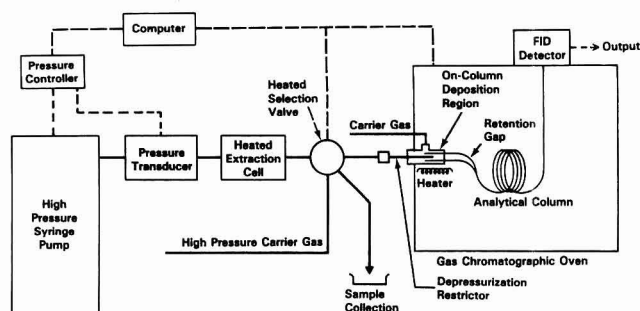


Figure 1. Schematic illustration of the on-line supercritical fluid extraction-capillary gas chromatography instrumentation.

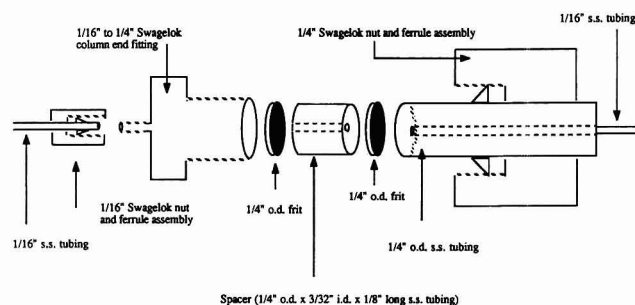


Figure 2. Schematic illustration of the microextraction cells.

with lower concentrations of alkylated homologues (15) and the PAH fraction (16) of a coal liquid containing relatively higher concentrations of alkylated species. The components of the PAH standard mixture were chosen to cover a relatively wide molecular weight range and included naphthalene, fluorene, phenanthrene, pyrene, chrysene, and benzo[e]pyrene and were spiked on the glass beads at either 25 or 0.5 ppm. Small sample sizes of approximately 10 mg were utilized in these studies.

The automated on-line SFE-gas chromatography instrumentation consisted primarily of four sections that included a high pressure pump and extraction cell, a switching valve and interface region, a gas chromatograph with a flame ionization detector, and a minicomputer and its associated interface circuitry. A schematic diagram of this instrumentation is shown in Figure 1.

A modified Varian 8500 syringe pump provided a high-pressure supply of carbon dioxide to the extraction cell. The carbon dioxide was purified by distilling through activated charcoal while filling the syringe pump. The microextraction cells (see Figure 2) were constructed from Swagelok stainless-steel zero volume  $\frac{1}{4}$  to  $\frac{1}{16}$  in. column end fittings (SS-400-6-1ZV) containing two  $\frac{1}{4}$  in. o.d. sintered stainless steel frits with 2.0- $\mu$ m mean pore size separated by a  $\frac{1}{8}$  in. long  $\times$   $\frac{1}{4}$  in. o.d.  $\times$   $\frac{3}{32}$  in. i.d. stainless steel insert. The  $\frac{1}{4}$  in. o.d. inlet to the extraction cell was made by cutting and silver soldering the smoothed end from standard  $\frac{1}{16}$  in. o.d. stainless steel tubing that was inserted through a short length (1–2 in.) of  $\frac{1}{4}$  in. o.d.  $\times$   $\frac{5}{64}$  in. i.d. stainless steel tubing. This design provided an entirely stainless steel extraction cell with a total volume of approximately 15  $\mu$ L (excluding internal frit volumes). Larger cell volumes could be obtained by using larger inside diameter and/or longer inserts. The extraction cell and several inches of inlet tubing were placed inside a thermostatically regulated heating block to control the fluid and extraction cell temperature. Extraction temperatures in the range of 40–50 °C were generally used.

An air-actuated Rheodyne 7010 six-port switching valve was used to direct the extraction cell effluent either to an exterior collection reservoir or to the gas chromatographic column for on-column deposition and concentration of the extract. Short lengths (2–4 cm) of nominally 5- $\mu$ m i.d. fused silica were used as depressurization restrictors to maintain supercritical pressures up to the point of on-column deposition or sample collection. The decompressed gas flow rate of the extraction fluid was typically 5 mL/min ( $\sim$ 5  $\mu$ L/min fluid flow). The restrictor for the on-column deposition was mounted through a  $\frac{1}{8}$ -in. tee to allow the gas chromatograph carrier gas to enter coaxially along the restrictor. This connection was also mounted in a heated block to

control the temperature of the restrictor and expansion region. Typically, this region was maintained near the upper operating temperature of the chromatographic oven which was between 250 and 280 °C. High-pressure carrier gas (300 psi) was also connected to the six-port valve that was alternately switched with the extraction effluent between the chromatographic column and the collection vent to purge any remaining extract from the system.

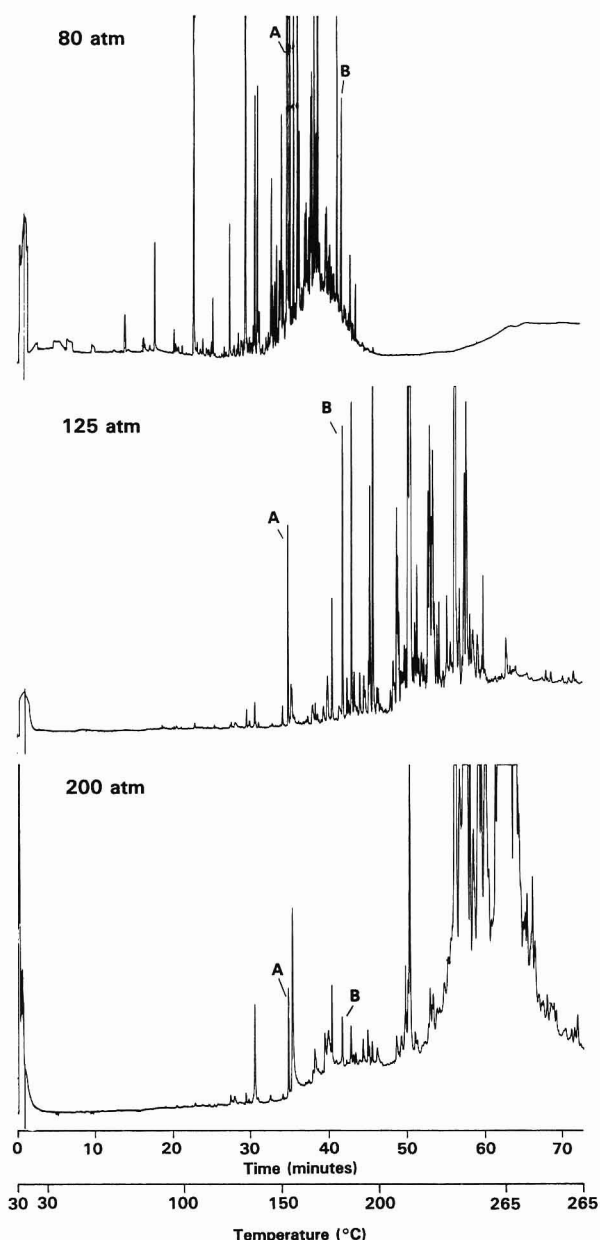
A Hewlett-Packard 5890 gas chromatograph equipped with a single flame ionization detector was used to perform chromatographic analyses. Typically, 15 m  $\times$  0.25 mm i.d. fused silica capillary columns coated with a 0.25- $\mu$ m film thickness of cross-linked 5% phenylpolymethylphenylsiloxane (SE-54) were utilized. A short retention gap of deactivated fused silica tubing (30 cm  $\times$  0.53 mm i.d.) was connected to the inlet of the chromatographic column to aid solute focusing and concentration of the extraction effluent. The fused silica retention gap was deactivated by simple silylation with hexamethyldisilazane at 350 °C. An all polyimide connection was made between the retention gap and the analytical column to prevent thermal drag during temperature programming. The chromatographic oven temperature was lowered to 30 °C during on-column deposition and concentration of the extraction effluent. Subsequent analyses were performed by temperature programming at 4 °C/min to 265–280 °C. Helium was used for the carrier gas at linear velocities of approximately 40 cm/s. Detector sensitivity was adjusted to give full-scale peak response for approximately 5 ng/component. Signal output was acquired on a strip chart recorder or with a Nelson Analytical 4416 chromatographic data system.

The instrumentation was automated by using an Apple IIe minicomputer with an Adalab interface card (Interactive Microwave Inc, State College, PA) and other in-house designed control circuitry. System automation included computer operation of the syringe pump to control pressure, switching of the six-port valve, start-up of the gas chromatograph temperature program cycle, and initiation and termination of data acquisition. A Fourth computer program allowed automated operation in which a sample could be subjected to numerous extractions at selected pressures for defined time intervals. In addition, the computer checked if fluid was still available in the pump, if the correct extraction pressure was reached, and if the oven temperature was ready for another cycle to begin.

## RESULTS AND DISCUSSION

Typically, sample preparation and fractionation requires several procedures that may be more time consuming than the actual analysis. The selective solvating power of a supercritical fluid can be used to fractionate a sample during the extraction process. An example of on-line sample fractionation and analysis is shown in Figure 3. In this example, the PAC material adsorbed on glass beads was extracted for 1-min at three progressively higher pressures with the effluent from each extraction being analyzed by temperature programmed capillary GC prior to the next extraction. During each GC analysis, the extraction process was continued ( $\sim$ 75 min) with the effluent being vented to the collection reservoir. In this way, essentially all of the material which was soluble at each pressure was extracted from the matrix prior to the next higher extraction pressure. After the GC analysis of a specific extract was completed, the fluid pressure was raised to a new setpoint, and after a 5-min equilibration period the effluent was again directed to the chromatographic column. Carbon dioxide, which has a critical temperature of approximately 31 °C and a critical pressure of 73 atm, was used as the extraction fluid. The extractions were all conducted at 50 °C and at pressures of 80, 125, and 200 atm that corresponded to densities (proportional to the solvating power) of 0.23, 0.62, and 0.78 g/mL, respectively (17, 18). The extraction effluent was collected and concentrated on-column at 30 °C that proved adequate to focus the solute injection band. Collection at higher temperatures or without the retention gap resulted in broadened peaks and lower resolution separations. After an extraction step was completed the oven





**Figure 3.** Capillary gas chromatograms of polycyclic aromatic compound fractions obtained from the supercritical carbon dioxide extraction at various pressures of a complex matrix. See text for detailed extraction and chromatographic conditions. Compounds A and B were arbitrarily marked in each fraction to facilitate comparison.

temperature was maintained at 30 °C for 2 min before the GC analysis was accomplished by temperature programming at 4 °C/min to a final temperature of 265 °C.

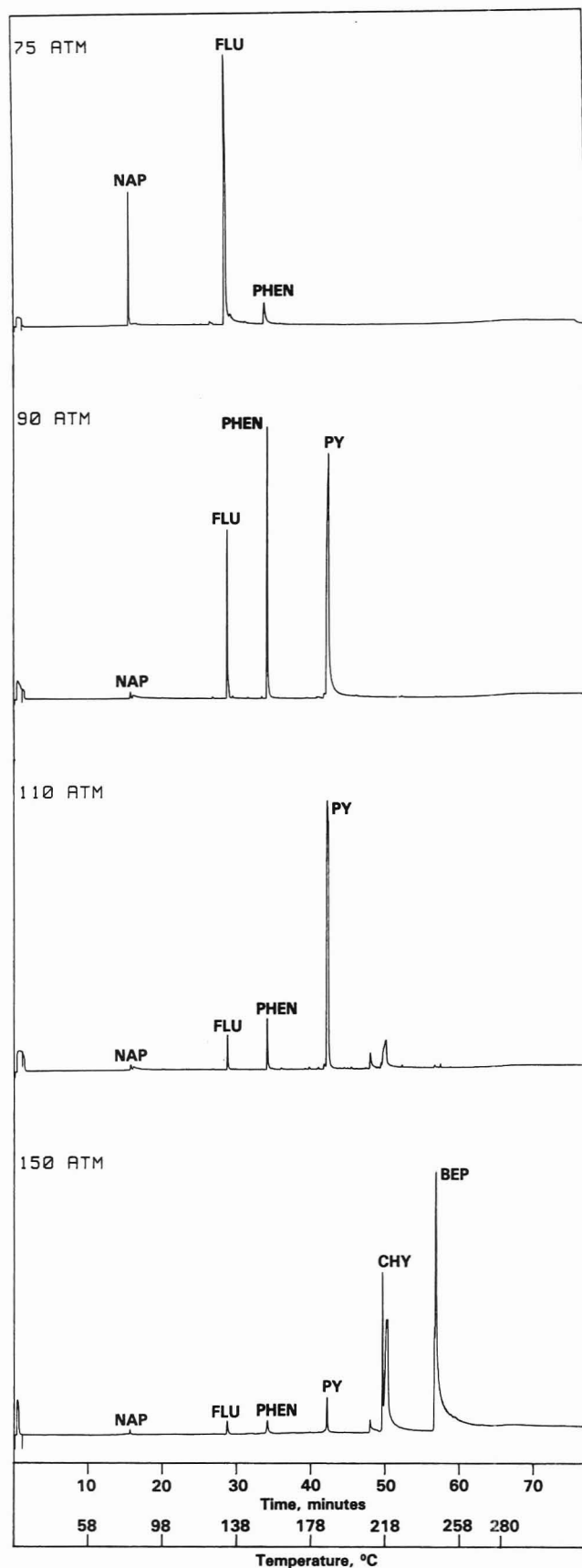
Examination of the chromatograms in Figure 3 indicates that high-resolution separations of three essentially unique fractions of the material were obtained. As expected, progressively higher molecular weight material was extracted with the higher density extraction fluid. Since this material was essentially all polycyclic aromatic hydrocarbons, a separation based on molecular weight would be expected rather than a distribution characteristic of a class-selective fractionation. The peaks labeled "A" and "B" refer to the same respective components in each fraction and were arbitrarily chosen to serve as reference points to facilitate comparison. Although some overlap of components occurred in the different fractions, this example clearly demonstrates the potential of this method for reasonably efficient on-line fractionations and analyses. The components in the 80-atm fraction consisted primarily of two-ring, alkylated two-ring, three-ring, and some lower alkylated three-ring compounds. The 125-atm fraction

consisted predominately of alkylated three-ring, four-ring, and some alkylated four-ring structures, and the 200-atm fraction consisted primarily of alkylated four-ring and larger structures. More distinct fractions could have been obtained with longer (or faster fluid flow) extractions at each pressure. The rate of extraction is limited by the solubility of the compounds in the fluid and the volume of fluid used in the extraction. Thus, samples with higher component concentrations require longer extraction times (or larger fluid volumes) or a more solvating fluid for complete extraction. Very slow fluid flows were purposely used in these extractions, but faster flow rates could have been used to obtain more rapid extraction rates.

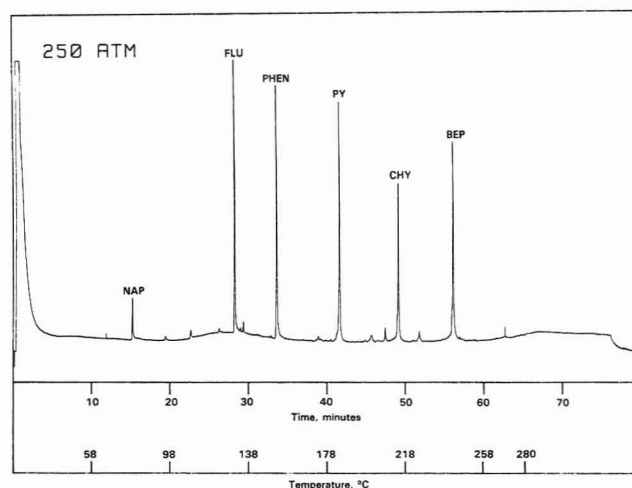
The selective extraction capability that can be achieved as a function of fluid pressure is further illustrated with the analyses shown in Figure 4 of PAH from the glass beads. In this example, each chromatogram was obtained from the progressively higher pressure extraction of the glass beads that were spiked with 25 ppm of each PAH. Carbon dioxide at 50 °C was used as the extraction fluid. As in the previous example, the extraction effluent was directed into the GC column for 1 min and then to the collection reservoir at the specified pressure for the duration of the GC analysis. The oven temperature was held at 30 °C during the extraction and for an additional 2 min before the temperature programmed GC analysis was initiated. The temperature was programmed at 4 °C/min to 280 °C. When the extraction was conducted at 75 atm (density = 0.20 g/mL), essentially only the naphthalene and the fluorene were extracted. (A smaller than expected naphthalene peak was obtained due to volatility losses that presumably occurred during sample preparation.) At the next extraction pressure of 90 atm (density = 0.30 g/mL) essentially all of the naphthalene was exhausted and phenanthrene was the major component along with a significant quantity of pyrene. At 110 atm (density = 0.52 g/mL), pyrene was the only major component that was extracted, although low levels of the previous components were also still present. At 150 atm (density = 0.71 g/mL), chrysene and benzo[e]pyrene were the major components extracted. The tailing peaks adjoining the chrysene and benzo[e]pyrene peaks are contaminants that were extracted from rubber O-ring material that inadvertently entered the extraction cell.

These extractions obtained under arbitrarily chosen conditions illustrate that very selective extraction of specific components could be obtained by optimizing the extraction conditions. Extraction at low density could be used to remove unwanted components, and then extraction at the minimum density necessary to obtain the desired analytes would produce a simplified fraction. Trace levels of the desired analytes could also be concentrated in this specific fraction since the bulk of the material would not be subjected to chromatographic analysis. In addition to pressure to control the density, temperature could also be manipulated to take advantage of both density and volatility effects. The use of other supercritical fluids with a range of solvating properties could also be used to obtain the specific selectivity desired. Finally, different polarity chromatographic columns could be used to further enhance the selectivity of the separation in a similar manner as is used in two-dimensional chromatography.

Exhaustive extraction of a matrix at higher pressures where all of the components are soluble provides the potential for a quantitative analysis. This is illustrated by the example shown in Figure 5 in which glass beads spiked with a low level (0.5 ppm) of the PAH compounds were subjected to exhaustive extraction with the entire effluent being deposited on-column for analysis. The extraction was conducted for 2 min with carbon dioxide at 50 °C and 250 atm (density = 0.83 g/mL). After extraction, the fluid flow was stopped rather than being switched to the collection port. Due to the small sample cell



**Figure 4.** Capillary gas chromatograms obtained from the supercritical carbon dioxide extraction at various pressures of a polycyclic aromatic hydrocarbon standard adsorbed on deactivated glass beads. See text for detailed extraction and chromatographic conditions. Peak identifications: NAP = naphthalene, FLU = fluorene, PHEN = phenanthrene, PY = pyrene, CHY = chrysene, and BEP = benzo[*e*]pyrene.

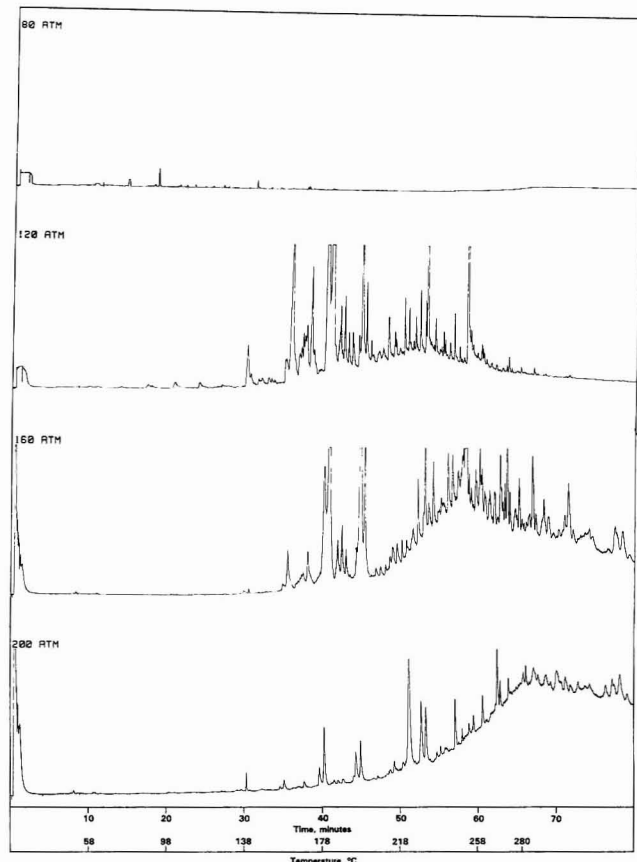


**Figure 5.** Capillary gas chromatogram obtained from the supercritical carbon dioxide extraction at 250 atm of the polycyclic aromatic hydrocarbon standard. See text for detailed extraction and chromatographic conditions. Peak identifications are the same as in Figure 4.

size (15  $\mu$ L), the low analyte levels ( $\sim 4$  ng), and a relatively higher fluid flow rate ( $\times 10$ ), an exhaustive extraction was obtained very rapidly. Longer extraction times would have been necessary for larger samples. The oven temperature was held at 30  $^{\circ}$ C during extraction, and then the GC analysis was accomplished by temperature programming at 4  $^{\circ}$ C/min to a final temperature of 280  $^{\circ}$ C. Except for the naphthalene, all of the components in the mixture were found at similar concentration levels. Significant losses of naphthalene probably occurred through volatility during sample preparation. Since the detector response was not rigorously calibrated, quantification of the sample components could not be performed. However, since no detectable levels of PAH were recovered when a second extraction was applied, complete removal of the PAH components likely occurred with the first extraction.

The application of on-line extraction-gas chromatography for sample preparation and analysis of air particulate matter is illustrated in Figure 6. The chromatograms shown in this example were obtained from the progressively higher pressure supercritical fluid extraction steps of NBS Urban Dust. Similar extraction and chromatography parameters as described in Figure 4 were utilized. At an extraction pressure of 80 atm (density = 0.23 g/mL) essentially no compounds were extracted from the dust particles. It is interesting to note that extraction of the glass beads spiked with the PAC material at similar solvating power conditions removed a significant amount of material (see Figure 3). This probably illustrates the stronger matrix effect on extraction efficiency of the dust particles. At 120 atm (density = 0.60 g/mL) where much higher solvating conditions were obtained, a complex fraction of material was extracted. Going to 160 atm where somewhat higher solvating power was obtained (density = 0.72 g/mL), a significantly greater amount of material was further extracted which illustrates the overall complexity of the matrix. Extraction at 200 atm (density = 0.78 g/mL) removed additional higher molecular weight material that is particularly evident in the unresolved "hump" near the end of the chromatogram. However, the lower molecular weight material was nearly exhausted, and the overall complexity of the resolved components in the chromatogram was significantly reduced. Due to the complexity of the sample matrix and the method of extraction used, exhaustive extractions were not obtained between the individual analyses. A smaller sample size, increased extraction times between GC analyses, or increased flow through the collection reservoir restrictor would have allowed more exhaustive extraction. However, in many in-





**Figure 6.** Capillary gas chromatograms of various fractions obtained from the supercritical carbon dioxide extraction at various pressures of Urban Dust particles. See text for detailed extraction and chromatographic conditions.

stances, exhaustive extraction is not necessary for qualitative sample fractionation.

### CONCLUSIONS

On-line supercritical fluid extraction-gas chromatography provides the potential for combined sample preparation and analysis. In addition to completely automated operation, rapid analyses and high sensitivities can be achieved with this methodology. The selectivity obtainable with the wide range of solvent powers available with supercritical fluid extraction provides the potential for fractionation of complex samples

and isolation of specific analytes from a matrix. The present work demonstrates the viability of the on-line SFE-GC concept and demonstrates its qualitative operation for sample extraction from adsorbent matrices and the potential for fractionation and isolation of specific components from more complex matrices. For the full importance of this methodology to be recognized it will be necessary to demonstrate that quantitative extraction and transfer of analytes from a sample matrix to the GC column can be achieved. This and other aspects of the quantitative operation of this methodology will be addressed in a subsequent report.

### LITERATURE CITED

- (1) Schneider, G. M.; Stahl, E.; Wilke, G., Eds. *Extraction with Supercritical Gases*; Verlag Chemie: Deerfield Beach, FL, 1980.
- (2) McHugh, M. A.; Krukonis, V. J. *Supercritical Fluid Extraction, Principles and Practice*; Butterworths: Boston, MA, 1986.
- (3) Paulaitis, M. E.; Krukonis, V. J.; Kurnik, R. T.; Reid, R. C. *Rev. Chem. Eng.* **1983**, *1*, 179-250.
- (4) Unger, K. K.; Roumeliotis, P. J. *Chromatogr.* **1983**, *282*, 519-526.
- (5) Sugiyama, K.; Saito, M.; Hondo, T.; Senda, A. *J. Chromatogr.* **1985**, *332*, 107-116.
- (6) Wright, B. W.; Wright, C. W.; Gale, R. W.; Smith, R. D. *Anal. Chem.* **1987**, *59*, 38-44.
- (7) Hawthorne, S. B.; Miller, D. J. *Chromatogr. Sci.* **1986**, *24*, 258-264.
- (8) Schantz, M. M.; Chestler, S. N. *J. Chromatogr.* **1986**, *363*, 397-401.
- (9) Campbell, R. M.; Lee, M. L. *Am. Chem. Soc., Div. Fuel Chem. Prepr.* **1985**, *30*, 189-194.
- (10) Smith, R. D.; Udseth, H. R. *Fuel* **1983**, *62*, 466-469.
- (11) Kalinoski, H. T.; Udseth, H. R.; Wright, B. W.; Smith, R. D. *Anal. Chem.* **1986**, *58*, 2124-2129.
- (12) Smith, R. D.; Udseth, H. R.; Wright, B. W. In *Supercritical Fluid Technology*; Penninger, J. M. L., Radosz, M., McHugh, M. A., Krukonis, V. J., Eds. Elsevier: Amsterdam, The Netherlands, 1985; pp 191-223.
- (13) Wright, B. W.; Smith, R. D. *J. High Resolut. Chromatogr.* **1985**, *8*, 8-11.
- (14) Chester, T. L. *J. Chromatogr.* **1984**, *299*, 424-431.
- (15) Vassilaros, D. L.; Kong, R. C.; Later, D. W.; Lee, M. L. *J. Chromatogr.* **1982**, *252*, 1-20.
- (16) Later, D. W.; Lee, M. L.; Bartle, K. D.; Kong, R. C.; Vassilaros, D. L. *Anal. Chem.* **1981**, *53*, 1612-1620.
- (17) Michels, A.; Botzen, A.; Schuurman, W. *Physica* **1957**, *23*, 95-102.
- (18) Michels, A.; Michels, C. *Proc. R. Soc.* **1935**, *A153*, 201-222.

RECEIVED for review July 21, 1986. Accepted October 30, 1986. Although the research described in this article has been funded wholly or in part by the United States Environmental Protection Agency through Interagency Agreement DW 899930650-01-1 through a Related Services Contract with the U.S. Department of Energy under Contract DE-AC06-76RLO-1830, it has not been subjected to Agency review and therefore does not necessarily reflect the views of the Agency and no official endorsement should be inferred. Mention of trade names or commercial products does not constitute endorsement or recommendation for use.

# Theory and Experimental Verification of Catalytic Determinations by Continuous Addition of Catalyst to a Reference Solution

Guillermo López-Cueto\* and A. F. Cueto-Rejón

Department of Analytical Chemistry, University of Alicante, 03080 Alicante, Spain

**A new method of catalytic determination is described. The method involves the comparison of the kinetic curve for the sample solution with the one for a reference solution to which a standard solution of catalyst is added at a constant rate, and in this way a so-called "intersection time" may be measured. From the value of the mentioned "intersection time", the concentration of catalyst may be obtained either by a direct calculation (pseudostoichiometric approach) or by a calibration plot (comparative approach). Theoretical equations are derived and experimental assessment is made by examining the behavior of the iodide-catalyzed Ce(IV)-As(III) reaction. Amperometric monitoring is used.**

Kinetic (or dynamic) methods of analysis have been progressively introduced into the analytical methodology together with the equilibrium (or static) methods. Although the coverage of kinetic methods of analysis is not yet as extensive as the coverage of equilibrium methods, some of the kinetic methods characteristics, for example, low cost, simplicity of application (facilitated by the possibility of computer use and automatic or semiautomatic devices), and the sensitivity and selectivity, have caused a notable increase in their popularity as routine methods in some analytical fields. Kinetic catalytic methods of analysis are distinguished by their high sensitivity and, therefore, they are useful in trace determinations. Many kinetic methods have been developed for the determination of species with catalytic properties. In the conventional modes, the initial rate, or the rate constant or some other kinetic parameter (as the time required to achieve a fixed concentration or the concentration achieved in a fixed time) are measured, and then the concentration of the analyte (catalyst) is determined by comparison with a calibration plot obtained by operating with standard solutions of the catalyst under the same conditions. Accordingly, catalytic methods of analysis are comparative methods, as are most of the physicochemical ones, since they are based on empirical relations between the measured signal and the concentration of analyte.

The application of stoichiometric analytical methods (sometimes called absolute methods), contrary to empirical ones, does not involve calibration plots, because the amount or the concentration of analyte may be calculated by means of generally simple calculations, applied to a single measurement (mass, volume, quantity of electricity), and based on the stoichiometry of a compound or a chemical reaction. Gravimetric, titrimetric, and coulometric methods are stoichiometric in the sense mentioned.

In this paper a new approach to catalytic determinations is reported in which two kinetic curves are recorded. The first one being obtained from the *sample solution* (which contains the analyte to be determined) and the second one from the so-called *reference solution*. This solution contains initially a zero concentration of catalyst, but a standard solution of catalyst is added to them at a constant rate. The resulting

kinetic curve has an unconventional sigmoidal shape. Both the sample and the reference curves must cross at a certain time. This *intersection time* is the only experimental measurement that needs to be taken, and so this may be considered as a single-point method. From here, two different choices may be followed to determine the catalyst concentration in the sample solution: either the use of a calibration plot prepared from standard solutions of catalyst or the direct calculation from a nonempirical equation, without the need of a calibration curve. This last option seems to be the most interesting, as its methodology approaches the stoichiometric methods.

The new catalytic method has been tested by means of the iodide-catalyzed cerium(IV)-arsenic(III) reaction (1, 2) with amperometric monitoring of reaction rate.

## THEORY

For a catalyzed reaction



pseudo-first-order conditions may frequently be attained as long as one of reactants (e.g., X) is present in a great excess. So the rate of reaction will be (including the rate of the uncatalyzed reaction)

$$v = -d[R]/dt = k[R] = (k_u + k_c[C]_x)[R] \quad (2)$$

where  $k_u$  and  $k_c$  are, respectively, the pseudo-first-order and pseudo-second-order rate constants for the uncatalyzed and catalyzed reactions,  $[R]$  is the concentration of the monitored species, and  $[C]_x$  is the unknown concentration of catalyst (the analyte) in the sample solution. Integration of eq 2 yields

$$[R] = [R]_0 \exp(-k_u t) \exp(-k_c [C]_x t) \quad (3)$$

Let us consider a second solution (the *reference solution*) with the same composition of the *sample solution*, catalyst excepted. If a standard solution of catalyst with a concentration  $[C]_s$  is added at a constant rate  $m$  to a volume  $V_0$  of reference solution, the concentration of catalyst will increase with time according to the equation

$$[C] = \frac{m[C]_s}{V_0 + mt} t \quad (4)$$

For a  $[C]_s$  sufficiently high, the addition rate of catalyst to the reference solution may be low enough for  $mt \ll V_0$ , and then

$$[C] = \frac{m[C]_s}{V_0} t \quad (5)$$

As the reference solution contains the same reactants as the sample solution and also the same experimental conditions (pH, temperature, ionic strength, etc.), then  $k_u$  and  $k_c$  will also be the rate constants, and the reaction rate in the reference solution will follow the law



$$-\frac{d[R]}{dt} = \left( k_u + k_c \frac{m[C]_s}{V_0} t \right) [R] \quad (6)$$

which, by integration, gives

$$[R] = [R]_0 \exp(-k_u t) \exp\left(-k_c \frac{m[C]_s}{2V_0} t^2\right) \quad (7)$$

Equations 3 and 7 have been plotted in Figure 1 for equal initial concentrations of the monitored species [R] and for simulated kinetic parameters and conditions. Both sample and reference curves start from a common point and they intersect after the reaction has proceeded to some extent. Let  $t_x$  be the *intersection time* (time elapsed from the start of reaction until the monitored species has again attained equal concentration in the sample and in the reference curves) and let  $[C]_x$  be the catalyst concentration in the sample solution.

By equating eq 3 and 7, the following expression can be derived for  $[C]_x$ :

$$[C]_x = \frac{m[C]_s}{2V_0} t_x \quad (8)$$

Two alternative analytical procedures arise from the above-described behavior. The first option is a *comparative procedure*, based on a linear calibration plot. Indeed, eq 8 shows how the intersection time is linearly related to the catalyst concentration as long as dilution of the reference solution may be considered negligible before the intersection point is reached. Two interesting properties of this calibration graph must be pointed out. First, and although this is a kinetic method, the slope is not a function of the rate constant but is only a function of parameters  $m$ ,  $[C]_s$ , and  $V_0$ . It is appropriate to underline the relevance of this fact, since the *analytical sensitivity* is defined as the slope of the calibration curve, then any kinetic analytical procedure based on this calibration plot will theoretically have the same sensitivity, irrespective of the value of the rate constant for the indicator reaction. Second, the calibration plot must always have a zero intercept, regardless of the rate of the uncatalyzed reaction. As the *statistical detection limit* is involved in the intercept of the calibration plot (more exactly, it does in its stability) (3), it may be concluded that, theoretically, the rate of the uncatalyzed reaction will no longer exert a troublesome background effect when this procedure is applied. Despite these theoretical predictions, in practice it can be expected that results will be more precise when the rate of the uncatalyzed reaction is small.

The second option to catalyst determination is a *noncomparative procedure* (in the sense that no use is made of a calibration plot), which may be available whether dilution of the reference solution is negligible or not. In the first case (dilution may be considered negligible) the procedure consists in a simple direct calculation of the analyte concentration from eq 8. This is not an empirical equation, as it contains only the constants  $m$ ,  $[C]_s$ , and  $V_0$  as parameters. Knowledge of the rate constants  $k_u$  and  $k_c$  (whose values would be obtained empirically) is therefore not needed to make the calculations. Hence, this catalytic procedure shows, from a formal viewpoint, a certain similarity with stoichiometric methods of analysis. Thus, the intersection of the sample and the reference curves may be considered as the "end point" for the catalyst determination (Figure 1). From eq 5, the amount of catalyst added to the reference solution at the "end point" will be  $V_0[C]_x = m[C]_s t_x$ , whereas the amount of catalyst present in the sample solution is  $V_0[C]_x = m[C]_s t_x/2$ , according to eq 8. The number of moles of reagent "added" is twice the number of moles of analyte "taken", which apparently leads to a "stoichiometric" 2:1, reagent:analyte, ratio. Of course,

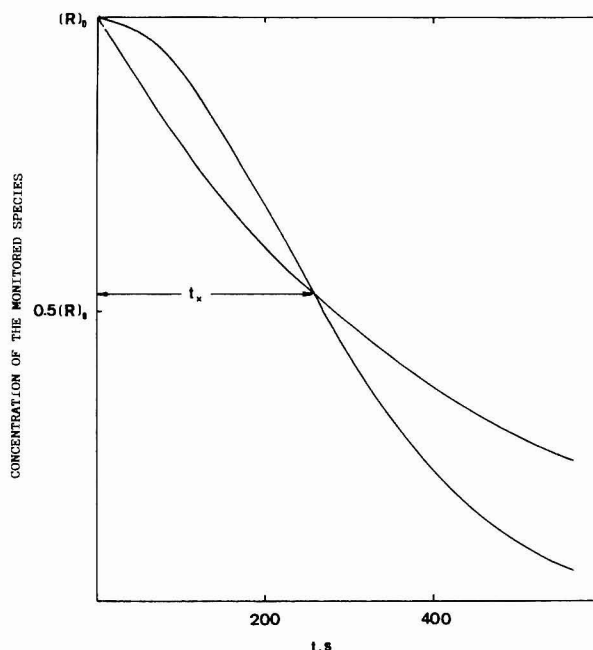


Figure 1. Reference and sample curves simulated for the following conditions:  $m$ ,  $10^{-2}$  mL s $^{-1}$ ;  $[C]_s$ ,  $10^{-4}$ ;  $V_0$ , 50 mL;  $k_u$ ,  $10^{-6}$  s $^{-1}$ ;  $k_c$ ,  $10^3$  M $^{-1}$  s $^{-1}$ ;  $[C]_x$ ,  $2.5 \times 10^{-6}$ .

the reported kinetic method is not stoichiometric in nature, because it is not based on the reaction stoichiometry, but, because of the apparent equivalence between reagent and analyte, it may be considered as a nonempirical *pseudostoichiometric* procedure.

In the second case (dilution is not negligible), the overall rate concentration change of monitored species R will be given by the sum of both the *reaction* and the *dilution* rates

$$-\frac{d[R]}{dt} = -\left(\frac{d[R]}{dt}\right)_{\text{reaction}} - \left(\frac{d[R]}{dt}\right)_{\text{dilution}} \quad (9)$$

According to eq 6, the reaction rate will be

$$-\left(\frac{d[R]}{dt}\right)_{\text{reaction}} = \left(k_u + k_c \frac{m[C]_s}{V_0 + mt}\right) [R] \quad (10)$$

On the other hand, dilution of the reagent R takes place according to the equation

$$[R] = [R]_0 \frac{V_0}{V_0 + mt} \quad (11)$$

and derivation leads to the *dilution* rate

$$-\left(\frac{d[R]}{dt}\right)_{\text{dilution}} = \frac{m}{V_0 + mt} [R] \quad (12)$$

then the overall rate will be

$$-\frac{d[R]}{dt} = \left(k_u + k_c \frac{m[C]_s}{V_0 + mt} t + \frac{m}{V_0 + mt}\right) [R] \quad (13)$$

and, by integration, the following equation is obtained for the kinetic curve in the reference solution:

$$[R] = [R]_0 \left(\frac{V_0 + mt}{V_0}\right)^{k_c[C]_s V_0/m} \exp(-k_u t) \times \exp(-k_c[C]_s t) \frac{V_0}{V_0 + mt} \quad (14)$$

Finally the catalyst concentration in the sample solution,  $[C]_x$ , is obtained by equating eq 3 and 14 at the intersection time,  $t_x$

$$[C]_x = [C]_s \left( 1 - \frac{V_0}{mt_x} \ln \frac{V_0 + mt_x}{V_0} \right) + \frac{1}{k_c t_x} \ln \frac{V_0 + mt_x}{V_0} \quad (15)$$

By comparison of eq 8 and 15, it can be seen that  $k_c$ , the rate constant for the catalyzed reaction, appears only when dilution is not negligible. A drawback arises from the appearance of  $k_c$  in eq 15, since its value should be determined empirically in order to apply the analytical method, and so this procedure would no longer be nonempirical. An approach to overcome this problem consists in not using the experimental values of the concentration of the monitored species R, but the corrected ones. From eq 14

$$[R]_{\text{corr}} = [R] \frac{V_0 + mt}{V_0} = [R]_0 \left( \frac{V_0 + mt}{V_0} \right)^{k_c [C]_s V_0 / m} \exp(-k_u t) \exp(-k_c [C]_s t) \quad (16)$$

and, by equating eq 3 and 16 for  $t = t_x$

$$[C]_x = [C]_s \left( 1 - \frac{V_0}{mt_x} \ln \frac{V_0 + mt_x}{V_0} \right) \quad (17)$$

we obtain an equation that does not contain the rate constant  $k_c$ , and therefore the analytical procedure is nonempirical. The procedure may be considered *pseudostoichiometric*, although its "stoichiometry" will be slightly different from that described when dilution is negligible.

The concentration of R vs. time can be continuously monitored by analytical techniques as photometry or amperometry. As the continuously measured property is proportional to R concentration, the absorbance-time curves as well as the current-time ones will follow equations as the ones derived for the concentration-time curves.

### EXPERIMENTAL SECTION

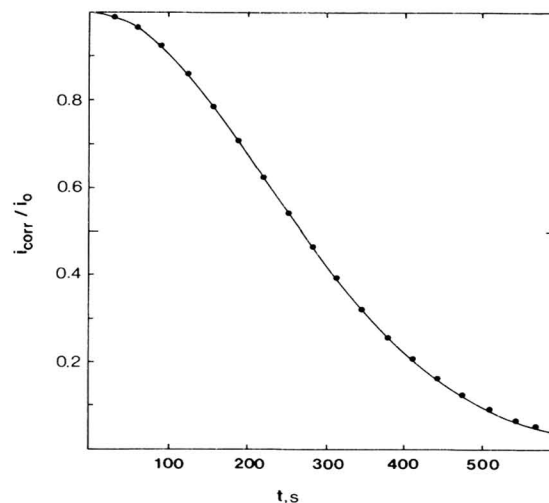
**Reagents and Solutions.** All the chemicals used were reagent grade. Deionized water was used throughout for preparation of stock solutions which included 0.0100 M ceric sulfate in 1.8 M sulfuric acid, 0.1000 M sodium arsenite, 1.8 M sulfuric acid, and  $1.21 \times 10^{-2}$  M potassium iodide standardized by titration with  $\text{AgNO}_3$ .

**Apparatus.** Current-time curves were obtained by a Metrohm Polarecord E-506 polarograph with a Metrohm 628-50 rotating disk platinum electrode as indicator electrode. Platinum wire and Ag/AgCl were used as the auxiliary and the reference electrodes, respectively. A Metrohm EA 876-20 thermostated titration vessel was the reaction cell. The catalyst solution was added by a E-655 Metrohm Dosimat electronic buret. The temperature was kept constant at  $25.0 \pm 0.1^\circ\text{C}$  by using a Haake K circulation bath.

**Procedure.** The composition of the sample solution (50 mL) was  $1.00 \times 10^{-3}$  M Ce(IV), 0.0100 M As(III), 0.5 M  $\text{H}_2\text{SO}_4$ , and  $6.9 \times 10^{-8}$  to  $4.6 \times 10^{-7}$  M I $^-$ . The reaction may be started by addition of either the iodide or the Ce(IV) solution. The reference solution had both the same volume and composition as the sample solution with the difference that the catalyst was initially absent. The catalyst was continuously added from a  $1.9 \times 10^{-6}$  to  $3.0 \times 10^{-5}$  M standard solution at a rate of  $7.74 \times 10^{-3}$  to  $2.5 \times 10^{-2}$  mL  $\text{s}^{-1}$ . The reaction rate was monitored amperometrically by measuring the cerium(IV) cathodic current at 0.500 V. The measured currents in the reference solutions were corrected by using the dilution factor,  $(V_0 + mt)/V_0$ . Both the  $i/i_0$  values for the sample solutions and the  $i_{\text{corr}}/i_0$  values for the reference ones were plotted vs. time, and then the time until their crossing was measured. The concentration of catalyst in the sample solution may be determined either from a calibration plot or directly by the use of eq 17.

### RESULTS AND DISCUSSION

Because of the well-known poor reproducibility of surface area in solid electrodes and therefore in the measured currents,



**Figure 2.** Experimental (●) and simulated (—) normalized reference curves for the iodide-catalyzed Ce(IV)-As(III) reaction with amperometric monitoring: Ce(IV),  $10^{-3}$  M; As(III),  $10^{-2}$  M;  $\text{H}_2\text{SO}_4$ , 0.5 M;  $m$ ,  $7.8 \times 10^{-3}$  mL  $\text{s}^{-1}$ ;  $[C]_s$ ,  $10^{-5}$ ;  $V_0$ , 50 mL;  $T$ ,  $25^\circ\text{C}$ .

the values of current obtained at zero time are not exactly coincident. Therefore, if the intersection times are used for calculating the concentration of catalyst, random errors would arise. In order to avoid this, both the sample and the reference curves must be normalized by plotting the ratios  $i/i_0$  and  $i_{\text{corr}}/i_0$ , respectively, rather than the  $i$  values, vs. time. From eq 3 and 16, and taking into account that current intensities are proportional to R concentrations

$$i/i_0 = \exp(-k_u t) \exp(-k_c [C]_s t) \quad (18)$$

$$\frac{i_{\text{corr}}}{i_0} = \left( \frac{V_0 + mt}{V_0} \right)^{k_c [C]_s V_0 / m} \exp(-k_u t) \exp(-k_c [C]_s t) \quad (19)$$

The rate of the Ce(IV)-As(III) uncatalyzed reaction is negligible (1, 2) and eq 19 can be written as

$$\frac{i_{\text{corr}}}{i_0} = \left( \frac{V_0 + mt}{V_0} \right)^{k_c [C]_s V_0 / m} \exp(-k_c [C]_s t) \quad (20)$$

and

$$\ln \frac{i_{\text{corr}}}{i_0} = -\frac{k_c [C]_s}{m} F(t) \quad (21)$$

where

$$F(t) = mt - V_0 \ln \frac{V_0 + mt}{V_0} \quad (22)$$

A straight line must be obtained when plotting  $\ln(i_{\text{corr}}/i_0)$  vs.  $F(t)$  with a slope

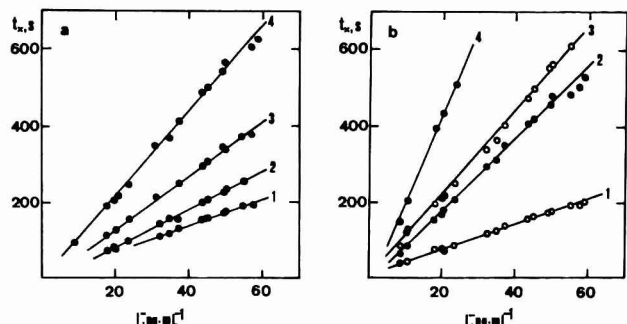
$$\text{slope} = -k_c [C]_s / m \quad (23)$$

In Figure 2, experimental and simulated normalized reference curves are shown. The reference curve has an inflection point at the time

$$t_{\text{infl}} = \left( \frac{V_0}{k_c m [C]_s} \right)^{1/2} \quad (24)$$

Reference curves for different values of  $m$  and  $[C]_s$  were obtained and, after being linearized, their slopes were plotted vs.  $m^{-1}$  and  $[C]_s$ , respectively. According to eq 23, straight lines are obtained, from whose slopes the pseudo-second-order constant for the catalyzed reaction,  $k_c$ , may be calculated.





**Figure 3.** Intersection time,  $t_x$ , as a function of iodide concentration in the sample solution. Effect of (a) addition rate of catalyst to the reference solution,  $m$ , and (b) catalyst concentration in the standard solution,  $[C]_s$ : Ce(IV),  $10^{-3}$  M; As(III),  $10^{-2}$  M;  $H_2SO_4$ , 0.5 M;  $V_0$ , 50 mL;  $T$ , 25 °C; (a)  $[C]_s$ ,  $10^{-5}$  M;  $m$ , mL s $^{-1}$ , (1)  $2.5 \times 10^{-2}$  M, (2)  $1.9 \times 10^{-2}$ , (3)  $1.3 \times 10^{-2}$ , (4)  $7.74 \times 10^{-3}$ ; (b)  $m$ ,  $7.92 \times 10^{-3}$  mL s $^{-1}$ ;  $[C]_s$ , (1)  $3.05 \times 10^{-5}$  M; (2)  $1.13 \times 10^{-5}$ , (3)  $9.54 \times 10^{-6}$ , (4)  $4.98 \times 10^{-6}$ .

Values of  $1.19 \times 10^4$  and  $1.17 \times 10^4$  M $^{-1}$  s $^{-1}$  are obtained, in good agreement both with those obtained by the conventional method and with those reported in the literature (4).

**Approaches to Catalyst Determination.** Straight lines are obtained by plotting  $t_x$  against the catalyst concentration when dilution produced by the addition of catalyst is negligible as predicted by eq 8. Slopes of these linear calibration plots decrease as  $m$  as well as  $[C]_s$  increases (Figure 3).

Extrapolation of the calibration plots to zero catalyst concentration gives slightly negative intercepts. This is probably because the catalyzed reaction is not first-order dependent at very low iodide concentrations, as reported by Lein and Swartz (5). The intersection time can be used, however, as the analytical property for determining traces of iodide by use of a calibration plot (*comparative procedure*).

The second approach (*pseudostoichiometric procedure*) consists of the determination of the catalyst concentration by measuring  $t_x$  and then applying, directly, eq 17. The determination of trace amounts of iodide between 8.8 and 58.9 ng mL $^{-1}$  has been carried out by using a reference curve obtained at  $m = 7.8 \times 10^{-3}$  mL s $^{-1}$  and  $[C]_s = 10^{-5}$ . Results of these determinations are shown in Table I. Relative standard deviations of 4.4% and 2.7% were obtained for 16 and 32 ng mL $^{-1}$ , respectively (10 determinations). The range of amounts of catalyst to be determined may be extended to either higher or lower concentrations if reference curves with adequate  $m$  and  $[C]_s$  values are used. Interferences from Cl $^{-}$ , Br $^{-}$ , SCN $^{-}$ , Ag(I), Hg(II), and Os(VIII) have been studied at 32 ng mL $^{-1}$  iodide level. Maximum tolerable concentrations are  $2 \times 10^{-4}$  M for both Cl $^{-}$  and Br $^{-}$ ,  $2 \times 10^{-6}$  M for SCN $^{-}$ ,  $2 \times 10^{-8}$  M for both Ag(I) and Hg(II), and  $7 \times 10^{-10}$  M for Os(VIII).

It can be expected that both accuracy and precision of results as well as speed of the determinations will be improved

**Table I. Iodide Determination by the Pseudostoichiometric Procedure:**  $[C]_s = 10^{-5}$ ;  $m = 7.8 \times 10^{-3}$  mL s $^{-1}$ ;  $V_0 = 50$  mL

amt of I $^{-}$ added, ng mL $^{-1}$	$t_x$ , s	amt of I $^{-}$ found, ng mL $^{-1}$	difference, ng mL $^{-1}$	error, %
8.8	83	8.1	-0.7	-8.0
10.8	107	10.5	-0.3	-2.8
18.0	185	18.0		
20.1	204	19.8	-0.3	-1.5
20.8	213	20.6	-0.2	-1.0
23.6	242	23.4	-0.2	-0.9
32.1	337	32.2	0.1	0.3
34.8	359	34.3	-0.5	-1.4
37.3	394	37.5	0.2	0.5
43.7	463	43.7		
45.2	484	45.6	0.4	0.9
49.2	522	49.0	-0.2	-0.4
50.0	537	50.5	0.5	1.0
55.0	585	54.6	-0.4	-0.7
57.5	589	55.0	-2.5	-4.3
58.9	608	56.6	-2.3	-3.9

by using a microcomputer with a data acquisition system.

#### GLOSSARY

$[C]$	concentration of catalyst in the reference solution
$[C]_s$	concentration of catalyst in the standard solution
$[C]_x$	concentration of catalyst in the sample solution
$F(t)$	$mt - V_0 \ln(V_0 + mt)/V_0$
$i$	current
$i_{\text{corr}}$	"corrected" current
$i_0$	initial current
$k_c$	rate constant of the catalyzed reaction
$k_u$	rate constant of the uncatalyzed reaction
$m$	rate of addition of catalyst
$[R]$	concentration of the monitored species
$[R]_{\text{corr}}$	"corrected" concentration of the monitored species
$[R]_0$	initial concentration of the monitored species
$t$	time
$t_{\text{infl}}$	inflection time
$t_x$	intersection time
$v$	reaction rate
$V_0$	initial volume of the reference solution
$[X]$	concentration of the reactant in excess

#### LITERATURE CITED

- (1) Sandell, E. B.; Kolthoff, I. M. *J. Am. Chem. Soc.* **1934**, *56*, 1426.
- (2) Sandell, E. B.; Kolthoff, I. M. *Mikrochim. Acta* **1937**, 9-25.
- (3) Kaiser, H. *Guiding Concepts Relating to Trace Analysis*; Senda, M., Ed.; International Congress on Analytical Chemistry, IUPAC: Kyoto, 1972; pp 35-61.
- (4) Rodriguez, P. A.; Pardue, H. L. *Anal. Chem.* **1951**, *41*, 1376-1380.
- (5) Lein, A.; Schwartz, N. *Anal. Chem.* **1969**, *23*, 1507-1510.

RECEIVED for review July 22, 1986. Accepted October 23, 1986. This work was supported by CAICYT (Spain), Grant No. 955/84. Part of the reported material has been presented at the First International Symposium on Kinetics in Analytical Chemistry, Córdoba, Spain, 1983, Paper No. P.I.3.

# Time-Warping Algorithm Applied to Chromatographic Peak Matching Gas Chromatography/Fourier Transform Infrared/Mass Spectrometry

Ching Po Wang<sup>1</sup> and Thomas L. Isenhour<sup>\*2</sup>

Department of Chemistry, University of North Carolina, Chapel Hill, North Carolina 27514

**Before combined gas chromatography/Fourier transform infrared (GC/FT-IR) and gas chromatography/mass spectrometry (GC/MS) data can be used, the paired spectral information has to be matched. A time-warping algorithm has been used to eliminate the time axis stretch and squeeze in the chromatograms so that the peaks can be matched. Various techniques have been used on the chromatographic intensities to find the best match by the time-warping algorithm.**

Data collected from gas chromatography/Fourier transform infrared/mass spectrometry (GC/FT-IR/MS) experiments or from two separate GC/FT-IR and GC/MS experiments with similar chromatographic conditions should supply complementary information. A search system utilizing combined FT-IR and MS data collected in one GC/FT-IR/MS run has been developed (1). However, one basic problem still has not been satisfactorily solved. In order to use data from both detection devices, one has to be sure that the FT-IR interferograms are matched to the right mass spectrograms; i.e., the peaks from the two chromatograms that came from FT-IR and MS data, respectively, must be matched before one can use the combined information. This problem exists whether the combined data are searched or separate library searches are performed before the results are combined.

A simple unknown does not present too much of a problem in matching the chromatographic peaks. However, for a complex unknown mixture the problem is more difficult and too many misleading results may arise from using a simplistic match algorithm.

Several methods have been suggested or tried to solve the chromatographic matching problem. A cross correlation technique was suggested as a possible method for determining the concordance of the chromatograms (2). This method treats the chromatograms as two separate functions with the highest cross correlation point indicating the best overlap. It is found in real GC/FT-IR/MS data that small differences in the starting and ending point in the chromatograms make a large difference in the correlation result (3). Manual matching followed by a polynomial fit also has been reported (3, 4), but the deviation from the linear relationship cannot easily be described by a simple polynomial function.

The following factors make the chromatogram matching a difficult task: (1) FT-IR and MS have different sensitivities and detection limits for different chemical compounds. The relative intensities obtained from these two different detection devices do not follow a simple relationship. (2) Variation in environmental parameters such as temperature, dead volume,

and flow rate differences in transfer tubes etc. cause a wide variation in the time axis.

Even with these variations, the chromatograms should still follow certain rules: (1) The peak elution sequence is not altered by the factors mentioned above. (2) Under similar separation conditions, the variation from a linear relationship in the time axis should be small in comparison to the total chromatographic time. (3) Concentrations of compound and peak intensity in the chromatograms should still follow a rough relationship, especially for chemically similar compounds.

Similar problems exist in speech recognition. The variation from one speech pattern to another lies mainly on the time-axis expansion or compression. The method used by the speech scientists to recognize vocabularies or words is called a time-warping algorithm that minimizes the distance between the test sample and the reference sample by stretching or squeezing the time axis within some reasonable restrictions (5-7).

The possible utilization of a time-warping algorithm to match chromatograms that were reconstructed from FT-IR and MS data after the elution from a GC is examined. The peak matching results of the time-warping algorithm are much superior to other methods that have been reported.

## THEORY

Time warping, an application of a dynamic programming algorithm, is almost the exclusive method of comparing speech sequences today. Dynamic programming is an optimization method that decomposes a multivariable optimization problem into a series of stages (8, 9). Optimization is done at each stage with respect to one variable only.

Several time-axis constraints are applied in addition to using the dynamic programming algorithm in time warping. The optimization of the comparison of the time sequence results in the need to stretch or squeeze the time axis locally, which explains the term "time warping".

In the time-warping algorithm, two time series records are treated as multidimensional vectors **A** (give in eq 1, a vector with *M* elements) and **B** (given in eq 2, a vector with *N* elements).

$$\mathbf{A} = a_m \quad 1 \leq m \leq M, m \quad (1)$$

$$\mathbf{A} = a_1, a_2, \dots, a_m, \dots, a_M$$

$$\mathbf{B} = b_n \quad 1 \leq n \leq N, n \quad (2)$$

$$\mathbf{B} = b_1, b_2, \dots, b_n, \dots, b_N$$

The purpose of the time-warping algorithm is to provide a mapping between the indices *m* and *n* such that the minimal distance between **A** and **B** is obtained. The warping is defined in eq 3, where  $f(k) = (m(k), n(k))$ .

$$\mathbf{F} = f(1), f(2), f(3), \dots, f(K) \quad (3)$$

The simplest warping function is a linear function, **F<sub>L</sub>** (as defined in eq 4), which would be adequate if the two chro-

<sup>1</sup>Present address: Analytical Chemistry Department, General Motors Research Lab, Warren, MI 48090.

<sup>2</sup>Present address: Department of Chemistry and Biochemistry, Utah State University, Logan, UT 84322-0300.



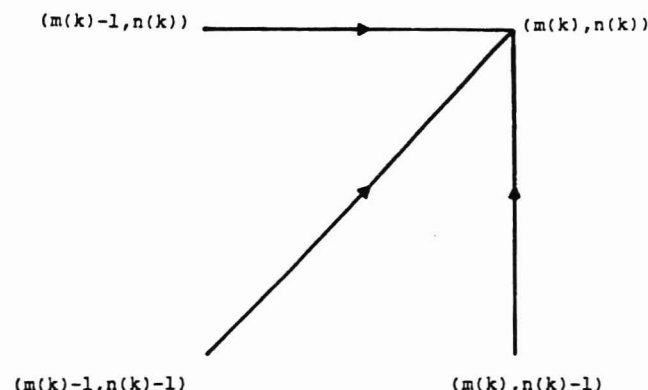


Figure 1. Possible routes to point  $(m(k), n(k))$ .

matograms were obtained under the identical environmental conditions.

$$\mathbf{F}_L(k) = (m_L(k), n_L(k)) \quad (4)$$

$$m_L(k) = k$$

$$n_L(k) = [(N-1)/(M-1)]/(k-1) + 1$$

Variations in temperature, transfer pipe conditions, and gas-transfer rates in separate pipes all contribute to make the function nonlinear. Such nonlinear variations are not easily estimated. One of the best methods of handling such time-axis variations is the time-warping algorithm.

Whatever the effects of the variations, the elution sequence of the two chromatograms should not be altered. This fact makes the warping function a monotonic and nondecreasing function as shown in eq 5.

$$m(k-1) \leq m(k) \quad (5)$$

$$n(k-1) \leq n(k)$$

Besides the monotonic condition, the warping function must obey a continuity condition such that every data point in one vector should be mapped onto and by at least one point from the other vector. The continuity condition is expressed in eq 6.

$$m(k) - m(k-1) \leq 1 \quad (6)$$

$$n(k) - n(k-1) \leq 1$$

The combination of these two restrictions yields the relationship (eq 7) that holds between two consecutive points. Figure 1 illustrates this relationship.

$$f(k-1) = (m(k), n(k)-1), (m(k)-1, n(k)-1), \text{ or } (m(k)-1, n(k)) \quad (7)$$

Although the warping function is not a linear function, it is often found that the deviation of  $\mathbf{F}$  from a linear function,  $\mathbf{F}_L$ , should be small. Thus a constraint could be applied to  $\mathbf{F}$  such that the deviation of  $\mathbf{F}$  from the linear function  $\mathbf{F}_L$  is limited:

$$m(k) = 1 \quad (8)$$

$$n_L(1) - C \leq n(k) \leq n_L(1) + C$$

where  $C$  is a constant. The restriction in equation 8 is called the window constraint that is an overall boundary condition. In addition to the window constraint, a local constraint (the slope limit or a number of one directional consecutive move restriction) can be imposed on the warping function. The slope limit is defined as the allowed number of consecutive moves in one direction of either time axis. This restriction is adopted because a local stretch or squeeze in time axis

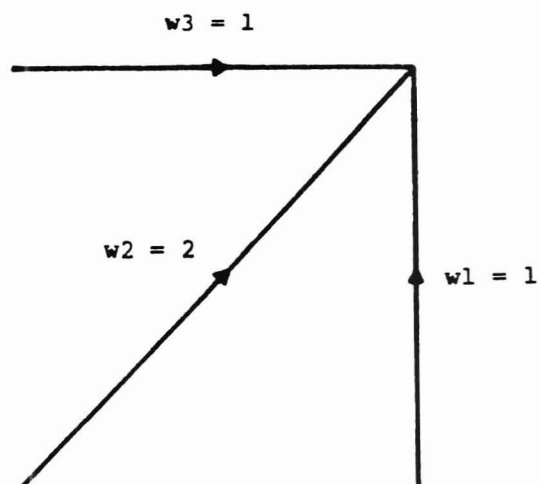


Figure 2. Symmetric weighting coefficients of the time-warping function.

should be a limited scope operation.

The elimination of the time-axis deviation by the warping function should be applied to the whole vector including the first point and the last point. Allowing flexible starting and ending can help the warping function achieve this goal. To count the variation effects from both vectors, symmetric weighting coefficients  $w_1$ ,  $w_2$ , and  $w_3$  are used as illustrated in Figure 2.

The method of dynamic programming was developed by Bellman for sequentially solving minimization problems that can be formulated as multistage decision processes. An optimal decision sequence has the property that whatever the past states and decisions, the remaining decision forms an optimal decision sequence with respect to the state resulting from the past decision.

The distance between two elements  $a_m$  of  $\mathbf{A}$  and  $b_n$  of  $\mathbf{B}$  is defined as

$$d(a_m, b_n) = \|a_m, b_n\| = (a_m - b_n)^2 \quad (9)$$

The distance of the first point (1,1) is defined as  $2(a_1 - b_1)^2$ .

The minimal residual distance between  $\mathbf{A}$  and  $\mathbf{B}$  can be found by calculating all the possible combinations of mappings. This directly enumerates all allowable sequences but requires a huge storage space and an enormous number of calculation steps for large dimensional problems. Time warping decomposes the calculation into several smaller steps. A problem is decomposable if it can be solved by recursive optimization. Numerically, time-warping optimization is an attempt to find the closest matched number sequence that is subject to an elastic operation.

The recursive calculation is carried out as follows: referring to Figures 1 and 2, let  $D(m-1, n-1)$  be the minimal distance from the starting point to  $(m-1, n-1)$ ,  $D(m-1, n)$  be the minimal distance from the starting point to  $(m-1, n)$ , and  $D(m, n-1)$  be the minimal distance from the starting point to  $(m, n-1)$ , then

$$D(m, n) = \min \begin{matrix} D(m, n-1) + w_1 d(m, n) \\ D(m-1, n-1) + w_2 d(m, n) \\ D(m-1, n) + w_3 d(m, n) \end{matrix}$$

Recursive computations calculate the minimal distance  $D(m, n)$  of every possible grid point within the boundary. The overall minimal residual distance  $D_{AB}$  is then obtained by using eq 10, where  $K$  in eq 10 is the length of the warping

$$D_{AB} = \min \frac{\sum_{k=1}^K d(f(k))w(k)}{\sum_{k=1}^K w(k)} \quad (10)$$

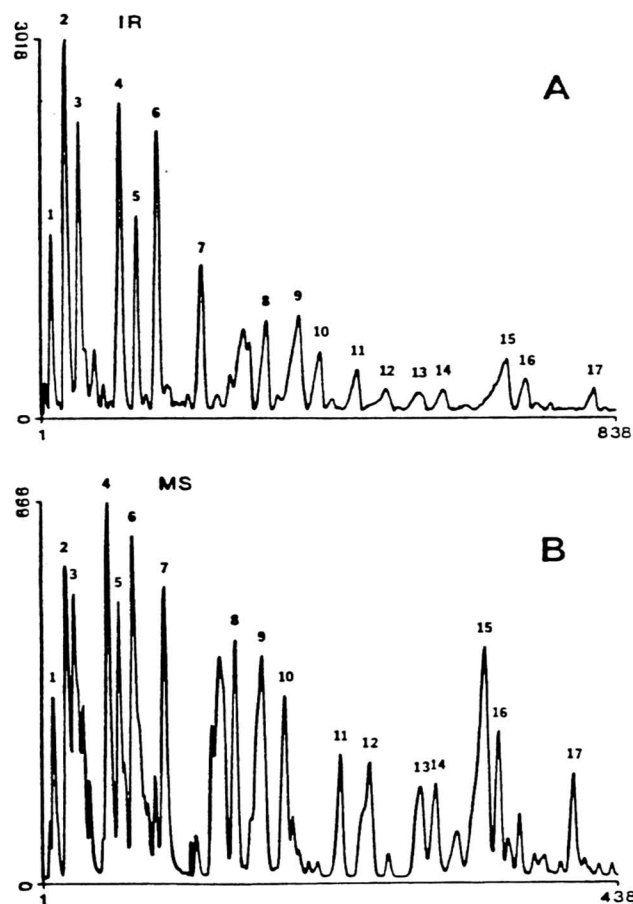


Figure 3. Chromatograms: (A) reconstructed from FT-IR interferograms; (B) total ion intensities from MS.

function. The denominator is included to compensate for the variable length of the warping route that is due to the allowed flexible starting and ending points of the warping function.

### EXPERIMENTAL SECTION

The chromatograms were reconstructed from data collected from a GC/FT-IR/MS experiment of a gasoline sample (3). The GC/FT-IR/MS consists of a Varian 3700 gas chromatograph, equipped for direct injection capillary chromatography, an IBM Instruments IR-85, with a 1 mm × 54 cm gold-coated light pipe, and a quadrupole mass spectrometer, taken from a Finnigan 3300 GC/MS system after the gas chromatograph portion was removed, in series mode. The data were collected by using a 30 m × 0.27 mm fused silica capillary DB-5 column with a carrier flow of 2.0 mL/min and a temperature program of 40 °C/min. The injector was packed with 3% SE-30 and heated to 180 °C. The FT-IR interferograms were collected at a rate approximately 2 scans/s, and a rate of approximately 1 scan/s was used to collect mass spectra.

All the calculations were done on a DEC VAX 11/780 computer. The polynomial regression program was written in Basic; all other programs were written in Fortran.

### RESULTS AND DISCUSSION

The chromatograms reconstructed from data collected by FT-IR and MS are shown in Figure 3. Figure 3A is the chromatogram reconstructed from FT-IR data (the FT-IR chromatogram) by using the Gram-Schmidt method (10). Figure 3B is the chromatographic trace of total ion intensity of mass spectra (the MS chromatogram). The peak maxima

Table I. Equations Obtained from Linear Regression Results

Second Order		
$x = A0 + A1y + A2y^2$		
A0 = 7.519 81		
A1 = 2.203 75	(1.066 66)	
A2 = -0.677 414E-03	(-0.087 296 7)	
$y = B0 + B1x + B2x^2$		
B0 = -2.582 52		
B1 = 0.444 985	(0.919 35)	
B2 = 0.870 926E-04	(0.095 289 5)	
Third Order		
$x = C0 + C1y + C2y^2 + C3y^3$		
C0 = -17.417 3		
C1 = 3.052 72	(1.477 58)	
C2 = -0.600 994E-02	(-0.774 486)	
C3 = 0.874 07E-05	(0.344 691)	
$y = D0 + D1x + D2x^2 + D3x^3$		
D0 = 9.110 52		
D1 = 0.242 87	(0.501 776)	
D2 = 0.723 392E-03	(0.791 475)	
D3 = -0.522 108E-06	(-0.344 894)	

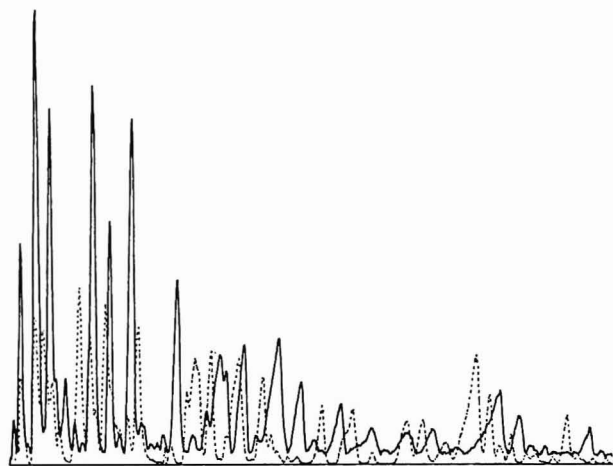
Table II. Observed and Predicted Values from Least-Squares Fit

peak no.	x			y		
	observn	2nd	3rd	observn	2nd	3rd
1	16	27	10	9	5	13
2	37	49	38	19	14	19
3	57	64	58	26	23	25
4	117	120	126	52	51	46
5	141	137	145	60	62	56
6	172	161	172	71	77	70
7	235	211	226	95	107	99
8	328	319	331	148	153	148
9	376	359	367	168	177	175
10	407	392	397	185	193	193
11	463	475	470	228	222	225
12	505	518	508	251	244	249
13	555	590	576	290	271	277
14	589	609	595	301	290	296
15	682	678	669	340	341	346
16	709	696	690	350	357	359
17	807	791	816	406	413	402

labeled from 1 to 17 in both chromatograms were used to test the matching ability of the linear regression and time-warping algorithms. Because of the uncertainty of the peak maximum, those peaks that overlapped were not included in testing the match results.

The linear regression results are presented in Table I. Both second-order and third-order linear regressions were applied. The  $x$  axis represents the FT-IR chromatographic time-axis value, and the  $Y$  axis represents the MS chromatographic time-axis value. This expression will be used through the rest of the text. Each  $x$  and  $y$  have been used as the independent variable with the other as a dependent variable to obtain the linear regression results. From the coefficients obtained, it is apparent that these two time-axis values closely follow a linear relationship. The standardized coefficients (the ones in parentheses) do not give any strong positive evidence about the importance of the higher order coefficients. The predicted values of  $x$  and  $y$ 's using the regression functions are shown in Table II. The observed values are taken directly from the reconstructed chromatographic data. The observed  $x$  and  $y$  values are the paired data used in the linear regression. The predicted values of  $x$  and  $y$  were obtained from the linear





**Figure 4.** Overlay of the two chromatograms from Figures 5 and 6 with the same intensity ( $y$ -axis) scale: solid line from FT-IR (Figure 3A) and dashed line from MS (Figure 3B).

regression equations using  $y$  and  $x$  as the independent variable, respectively. A comparison between the observed values and the predicted values reveals that the deviation of the predicted values from the observed values cannot precisely be expressed by simple polynomial functions. To achieve a better match between these two chromatograms, other methods than polynomial methods must be applied. Figure 4 demonstrates very clearly the need of another method. The  $x$  axis is the time axis, and the  $y$  axis is the intensity value ranging from 0 to 3018; the solid line is the FT-IR chromatogram, and the dashed line is the MS chromatogram.

This set of chromatographic intensity data were subject to various manipulations and then treated with the time-warping algorithm. Time warping results of using the raw or the manipulated chromatographic data were obtained with the following calculation conditions: (1) flexible starting point,  $x = 6$  and  $y = 6$ ; (2) flexible ending point,  $x = 20$  and  $y = 20$ ; (3) window width, 50; (4) one-direction consecutive move allowed, 3.

The symmetric calculation was used in the algorithm and two matching results were obtained at the same time. One treats the FT-IR chromatogram ( $x$ ) as the reference vector and the MS chromatogram ( $y$ ) as a test vector. The reverse match is also found. In the following tables of matching results, the time-warping results of  $x$  were obtained from the matching results using  $x$  as the test vector and the results of  $y$  were obtained from the matching results of using  $y$  as the test vector. In a correct matching, the two results should complement each other.

Although close matches were obtained, there is no guarantee that it should always work. One important reason is that the units of the intensity in these two chromatograms are not the same which makes the intensity value less meaningful. To eliminate the disagreement between the two chromatographic intensity units, several manipulation schemes were applied to the chromatographic intensity data and then treated with the time-warping algorithm.

Both chromatograms were base line corrected to eliminate any possible offset. A zeroth-order base line fits the MS chromatogram well, so a constant 18 was subtracted from every intensity value in MS chromatogram. The FT-IR chromatogram has a slightly sloping base line that commonly exists in the chromatograms reconstructed by using the Gram-Schmidt reconstruction method from GC/FT-IR data. For this particular FT-IR chromatogram, the seventh smallest points from two base line regions were used to construct a straight base line. If any value in these two chromatograms is negative after base line correction, the value is set to zero in order to eliminate negative-valued spikes. The results of

**Table III.** Time-Warping Results Using Base Line Corrected Data

peak no.	$x$		$y$	
	observn	TW result	observn	TW result
1	16	13-16	9	9
2	37	33-36	19	20
33	57	57-60	26	26
4	117	120-121	52	51
5	141	140-143	60	60
6	172	167-170	71	72
7	235	235-237	95	95
8	328	325-328	148	148
9	376	370-372	168	169
10	407	406	185	186
11	463	461-463	228	228
12	505	506	251	246-249
13	555	555	290	287-290
14	589	589	301	299-302
15	682	683	340	336-339
16	709	709	350	349-350
17	807	807	406	404-406

**Table IV.** Time-Warping Results Using the Base Line Corrected and Maximum Adjusted to 10 000 Data

peak no.	$x$		$y$	
	observn	TW result	observn	TW result
1	16	8	9	22
2	37	15	19	52
3	57	17	26	70
4	117	36-38	52	95
5	141	42	60	119
6	172	57	71	136
7	235	116-119	95	168
8	328	189	148	211
9	376	235	168	229
10	407	275	185	248
11	463	374	228	274
12	505	407	251	296
13	555	502	290	319
14	589	508	301	339
15	682	589	340	384
16	709	592	350	396
17	807	728	406	430

the time-warping matching of these two base line corrected chromatograms is presented in Table III. Because the corrections of the base line in both chromatograms were so small, the matching result is very similar to the one obtained by using the raw chromatographic data.

To remove the inconsistency of the two chromatographic units, a spanning of the intensity values from 1 to 10000 was carried out on both base line corrected chromatograms. The time-warping matching result of these two unitless chromatograms is presented in Table IV. Peaks shifted by one to three peaks and some nonmatches were observed. These are caused by the different sensitivity between FT-IR and MS. The comparatively lower intensity values in FT-IR chromatogram of the compounds eluted later in separation make the matching of the MS shift to peaks with higher chromatographic numbers and lower chromatographic intensities. The incorrect matching is easy to detect by cross-referencing the matching results.

In an attempt to improve the matching result by making the peaks more distinguishable from the base line and also putting more weight on the smaller intensity value peaks, all the intensity values from both the unitless chromatographic spectra that were greater than 100 were recalculated as their square root multiplied by 100. The resulting two square root treated chromatograms were time-warped; the results are presented in Table V. Some improvements are observed, but

**Table V. Time-Warping Results Using the Base Line Corrected, Maximum Adjusted, and Square Root Treated Peaks Data**

peak no.	<i>x</i>		<i>y</i>	
	observn	TW result	observn	TW result
1	16	14-15	9	10
2	37	34-37	19	19
3	57	42	26	32
4	117	117	52	51-52
5	141	121	60	70-73
6	172	141	71	94
7	235	172-173	95	117
8	328	302	148	166-169
9	376	328	168	187
10	407	374	185	205
11	463	462	228	229
12	505	506	251	247-250
13	555	588	290	265
14	589	591	301	292-295
15	682	681	340	344-346
16	709	683	350	364-366
17	807	807	406	403-406

**Table VI. Time-Warping Results Using Base Line Corrected, Maximum Adjusted, and Segmented Adjusted Data**

peak no.	<i>x</i>		<i>y</i>	
	observn	TW result	observn	TW result
1	16	15-16	9	9
2	37	34-37	19	19
3	57	42	26	32
4	117	119-122	52	51
5	141	139	60	61
6	172	170	71	72
7	235	234-236	95	95
8	328	328	148	147-148
9	376	376	168	167-168
10	407	407	185	183-186
11	463	457-459	228	229
12	505	505	251	249-251
13	555	557-558	290	288
14	589	591	301	300
15	682	682-684	340	339
16	709	709-712	350	350
17	807	807-809	406	406

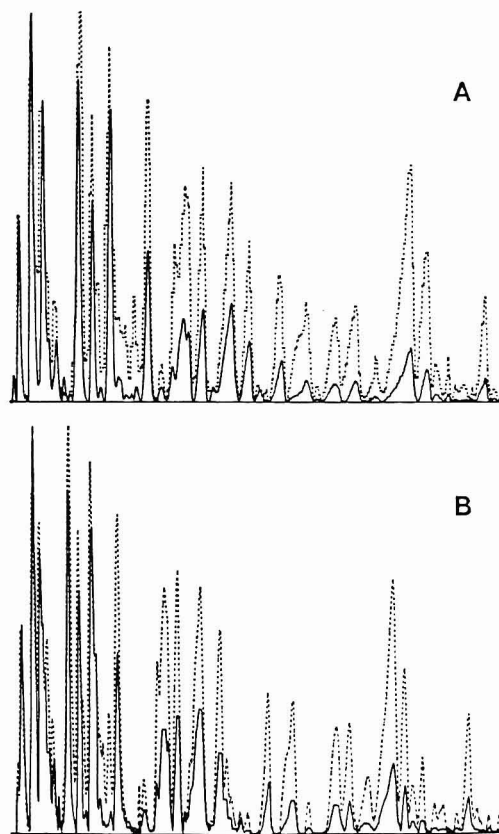
the match is still unsatisfactory.

Because the problem was caused by the different sensitivity of these two instruments, a mathematical treatment was applied to the data to minimize the intensity difference. The unitless chromatograms were divided into four segments, and the intensity values in the FT-IR chromatogram were adjusted to make the average value of the most intense three or four peaks' maxima in every segment be the same as the average of the most intense three or four peaks' maxima in the same segment of the MS chromatogram. The segmented adjusted FT-IR chromatograms were time-warped with the unitless MS chromatograms. The time-warping results are presented in Table VI. All the peaks except peak 3 were matched. A significant improvement is achieved by this segmented adjustment of the chromatographic intensity values.

A combination of the last two treatments was also applied to the unitless FT-IR chromatograms. All the intensity values that were greater than 100 in the segmented adjusted FT-IR chromatogram were recalculated as their square root multiplied by 100. The resulting FT-IR chromatogram was then time-warped with the square root treated MS chromatogram. The matching result is presented in Table VII. All the peaks matched the corresponding peak in the other chromatogram. Figure 5 contain these final matched results. Figure 5A is the

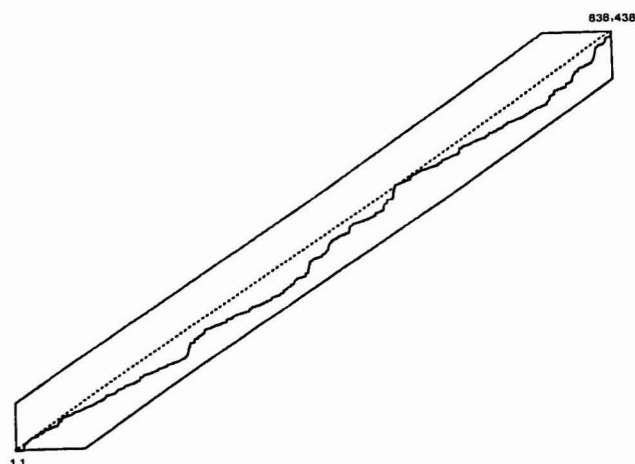
**Table VII. Time-Warping Results Using Base Line Corrected, Maximum Adjusted, Segmented Adjusted, and Square Root Treated Peaks Data**

peak no.	<i>x</i>		<i>y</i>	
	observn	TW result	observn	TW result
1	16	14-16	9	9
2	37	34-37	19	19
3	57	55-58	26	26
4	117	119-122	52	51
5	141	140	60	61
6	172	170	71	72
7	235	234-236	95	95
8	328	328	148	147-148
9	376	376	168	167-168
10	407	407	185	184-186
11	463	457-459	228	229
12	505	505	251	249-251
13	555	555	290	288-290
14	589	588-591	301	301
15	682	682-684	340	339
16	709	709	350	350
17	807	807-809	406	406

**Figure 5.** Final time-warping results with solid line from FT-IR and dashed line from MS: (A) solid line as the reference; (B) dashed line as the reference.

result of the FT-IR chromatogram that is depicted by the solid line as the reference vector and the dashed line as the matched MS chromatogram. The dashed line in Figure 5B is the MS chromatogram that was used as the reference vector, and the matched FT-IR chromatogram is shown by the solid line. Not only were the major peaks matched to the corresponding peaks, but also the smaller peaks also matched. The warping path of the last matching is shown in Figure 6. It is clear that the path is not represented by any simple function, which makes the time-warping algorithm the best choice to solve this kind of problem. One may wonder why the raw data work much better than most of the matching results that were obtained by time warping of various data treatments. Examining Figure 4 carefully, one can see the closeness of the





**Figure 6.** Final time-warping function plotted in solid line and the linear function  $F_L$  plotted in dashed line with the window constraint surrounded.

intensity values between the last two-thirds of the two chromatograms. This agreement, which is the goal of the segmented adjustment, greatly enhances the matching. However, as has been mentioned earlier, there is no reason to believe that the intensity values from two different instruments should agree. The results show that the intensities should be made similar in order to achieve a good match by the time-warping algorithm.

### CONCLUSIONS

Time warping using chromatographic intensity information to correct the time-axis mismatching has been shown to provide a better match of two related chromatograms than the match using a linear regression method. Two-dimensional

information is utilized instead of one in the linear regression of the peak positions. To make the time warping work, the intensity values in the two chromatograms should agree. If the intensity values vary too greatly, it is probably better to use the retention time information only, as a match using retention time markers would give a better result. The restrictions in time axis should be carefully chosen to meet the experimental conditions. Too restricted conditions will not leave enough room for the time axis to expand or contract. Too broad conditions will not allow convergence at all.

The applications of the time-warping algorithm certainly are not limited to the chromatogram matching. As long as an elastic operation is preferred in one axis, time warping can be applied.

### LITERATURE CITED

- (1) Williams, S. S.; Lam, R. B.; Isenhour, T. L. *Anal. Chem.* **1983**, *55*, 1117-1121.
- (2) Williams, S. S.; Lam, R. B.; Sparks, D. T.; Isenhour, T. L.; Hass, J. R. *Anal. Chim. Acta* **1982**, *138*, 1.
- (3) Williams, S. S. Ph.D. Dissertation, 1984.
- (4) Greene, W. E.; Williams, S. S.; Isenhour, T. L. Pittsburgh Conference Paper No. 193, 1984.
- (5) Schmoff, D.; Kruskal, J. B., Eds. *Time Warps, String Edits, and Macro-molecules: The Theory and Practice of Sequence Comparison*; Addison-Wesley: Reading, 1983.
- (6) Sakoe, H.; Chiba, S. *IEEE Trans. Acoust., Speech, Signal Process.* **1978**, *ASSP-26*, 43-49.
- (7) Rabiner, L. R.; Rosenberg, A. E.; Levinson, S. E. *IEEE Trans. Acoust., Speech, Signal Process.* **1978**, *ASSP-26*, 575-582.
- (8) Mital, K. V. *Optimization Methods*; Wiley Eastern Limited: New Delhi, 1976.
- (9) Wismer, D. A.; Chattergy, R. *Introduction to Nonlinear Optimization*; North-Holland: Amsterdam, 1978.
- (10) de Haseth, J. A.; Isenhour, T. L. *Anal. Chem.* **1977**, *49*, 1977.

RECEIVED for review February 4, 1985. Resubmitted August 8, 1986. Accepted October 27, 1986.

## Problems of Smoothing and Differentiation of Data by Least-Squares Procedures and Possible Solutions

Arshad Khan

Chemistry Department, The Pennsylvania State University, DuBois, Pennsylvania 15801

Smoothing and differentiation of experimental data sometimes necessitate least-squares polynomial fitting of a large number of data points at a time (17, 19, or 21 points) rather than 3, 5, or 7 points with repetition of the procedure for several iterations. For a 5- or 7-point fit, one loses smoothing of only 2 or 3 points, respectively, at each end, and for a 19- or 21-point fit one loses 9 or 10 points, respectively, at each end. No other smoothing procedure is known today to handle the edge point smoothing and differentiation. In this paper a procedure is suggested for smoothing and differentiating essentially every data point. In addition, different orders of polynomial fits have been tried for the same data set. It is noticed that the parabolic fit gives the best smoothing of the noisy data set.

In some experiments it is difficult to achieve a satisfactory signal-to-noise ratio because of the superimposition of random noise in experimental data. In order to retrieve information

from the experimental data, it is necessary to remove as much of this noise as possible without degrading any underlying information. Several numerical techniques are known today and have been applied for data analysis (1-4). In this paper a smoothing and differentiation of experimental data by a least-squares procedure is described. Special reference is made to the analysis of the molecular beam experimental data which is used to obtain energy distributions (5, 7) of Penning ions (e.g.,  $H_2^+$ ) coming from the  $He(2^1s)/H_2$  reaction. Here  $He(2^1s)$  represents a metastable state of He generated by electronic excitation of the ground state He (6, 7). The energy of the metastable He (20.6 eV) is large enough to ionize almost any atom or molecule. The following reaction takes place in the "reaction chamber", with  $H_2^+$  ions scattered at different angles with respect to  $H_2$  beam direction:



The detector was set at a certain angle with respect to the ground-state beam (here  $H_2$  beam). Data were collected for a certain interval of time ranging from 5 min to 1 h depending

upon the counting rate at that angle. In the energy analysis experiments, the scattered ions ( $H_2^+$ ) experience a retarding ramp voltage ( $E'$ ) before being detected and recorded by a 100-channel multiscalar (Honeywell SAI-42 A). The detection system, which consists of a mass spectrometer and a spiraltron electron multiplier, has been elaborately discussed elsewhere (5-7). Each channel (bin) number of the multiscalar is related to the energy of the scattered ions. For  $H_2^+$  scattering experiments, the energy expression is given by

$$E = (\text{bin number} - 17.5) \times 0.708 \text{ kcal/mol}$$

Counts (signal) at bin numbers from 18 to 98 provided the whole spectrum. The signal recorded at each channel is related to the intensity  $I(E)$  of the scattered ions by the following expression:

$$\text{signal} = - \int_{E'}^{\infty} I(E) dE$$

Differentiation of the above equation (i.e., data recorded at different channels) provided the energy distribution  $I(E)$  of the Penning ions. Differentiation without smoothing or after smoothing by a five- or seven-point least-squares fit generated spurious and unacceptable peaks on the distribution plot (i.e.,  $I(E)$  vs.  $E$  plot). To get the best distribution, a larger point fit (19 or 21) was necessary. To recover the loss of information from the edge points, which provided the low and the high energy part of distribution, a smoothing procedure was developed and is described in this paper.

### THEORY AND DISCUSSIONS

Let the fitting function be defined by the following polynomial equation of order  $m$ :

$$y(x) = a_0 + a_1x + a_2x^2 + \dots + a_mx^m \quad (1)$$

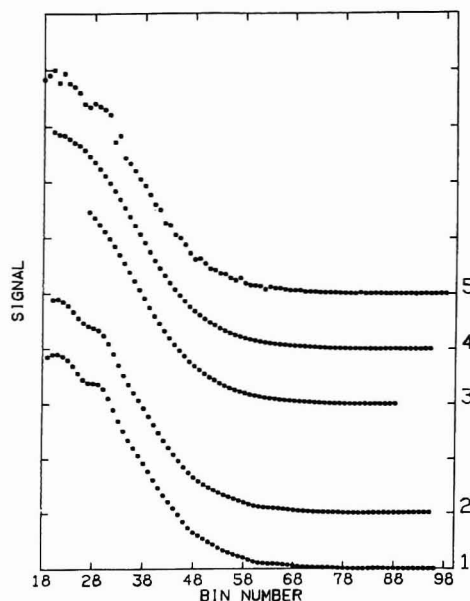
The coefficients of the polynomial,  $a_0, a_1, \dots, a_m$ , are determined by minimizing the weighted residual function

$$R = \sum \omega_i [y_i - y(x_i)]^2 \quad (2)$$

Here  $x_i$  and  $y_i$  represent the coordinates (here bin number and signal counts, respectively) of the  $i$ th data point, and  $\omega_i = 1/\sigma_i^2$  is the weighting factor that weights each term of the sum in  $R$  according to how large or small a deviation is expected. The summation ranges from  $N$  to  $NPT$ , where  $N$  and  $NPT$  are the indexes of the data points between which the fitting is done.  $NPT = N + NFT - 1$ , where  $NFT$  is the number of data points used on polynomial fitting. By minimization of the residual function with respect to each coefficient of the polynomial, i.e., by setting  $\delta R / \delta a_i = 0$  ( $i = 1, 2, \dots, m$ ), one obtains a system of  $m$  simultaneous equations. This can be written in the form  $CA = B$ , where  $C$ ,  $A$ , and  $B$  are the following matrices:

$$\begin{aligned} C &= \begin{bmatrix} \sum \omega_i & \sum \omega_i x_i & \dots & \sum \omega_i x_i^m \\ \sum \omega_i x_i & \sum \omega_i x_i^2 & \dots & \sum \omega_i x_i^{m+1} \\ \dots & \dots & \dots & \dots \\ \sum \omega_i x_i^m & \sum \omega_i x_i^{m+1} & \dots & \sum \omega_i x_i^{2m} \end{bmatrix} \\ B &= \begin{bmatrix} \sum \omega_i y_i \\ \sum \omega_i x_i y_i \\ \dots \\ \sum \omega_i x_i^m y_i \end{bmatrix} \\ A &= \begin{bmatrix} a_0 \\ a_1 \\ \dots \\ a_m \end{bmatrix} \end{aligned} \quad (3)$$

As before, the summations are taken over the range from  $N$  to  $NPT$ . In order to determine  $A$ , and hence the coefficients



**Figure 1.** Effect of increased NFT on the quality of smoothing. The curves are separated from each other by arbitrary amounts for clarity of viewing. The curves 1 and 2 are obtained by using NFT = 5, ITERATION = 5 and NFT = 7, ITERATION = 3, respectively. It is quite noticeable that an appreciable amount of information toward each end is lost by the conventional procedure as in curve 3, where NFT = 21, ITERATION = 1. Curve 4, generated by the new procedure, recovers most of the edge point information. Curve 5 represents the original data collected by multiscalar.

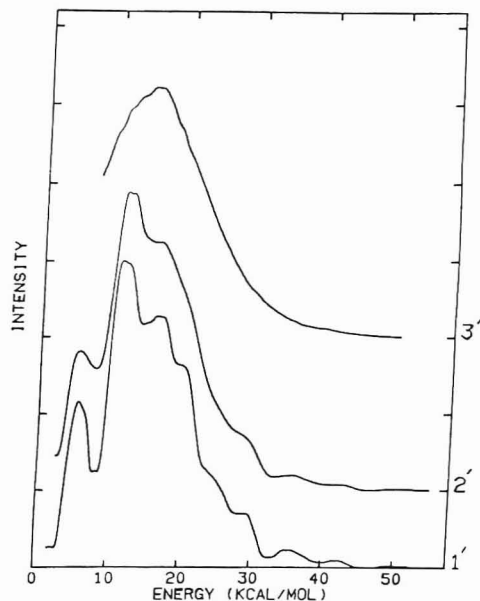
of the polynomial ( $a_i$ 's), it is necessary to invert the matrix  $C$  followed by its multiplication with the matrix  $B$ . That is

$$A = C^{-1}B \quad (4)$$

In the present analysis  $\omega_i$  is considered to be equal to  $1/y_i$  because of the statistical fluctuations in collections of a finite number of counts (by the multiscalar) in a certain interval of time (8). In the curve-smoothing procedure a segment consisting of a few data points is taken beginning at  $N = N\text{BEGIN}$ , the index of the very first data point from which the polynomial fitting starts. As mentioned above, by inversion of matrix  $C$  and multiplication by matrix  $B$ , one gets the coefficients ( $a_0, a_1$ , etc.) of the polynomial used in fitting the segment. At the midpoint of the segment a value of  $y$  is calculated by using eq 1, which represents the first smoothed value. Then  $N$  as well as  $NPT$  are increased by 1. A new polynomial function is obtained by fitting the data points between the new values of  $N$  and  $NPT$  followed by inversion and multiplication of matrices as before. This would provide the second smoothed value. This procedure is continued until  $NPT$  becomes equal to  $N\text{END}$ , the index of the very last point used in smoothing. The whole procedure can be repeated several times (iterations) by using the smoothed values ( $y$ ) from the previous fits to obtain greater smoothing. In this procedure of smoothing, a few points at the beginning and a few points at the end are not smoothed. For a five-, seven-, or nine-point segment ( $NFT = 5, 7$ , or  $9$ ) only two, three, or four points at each end (this will be termed edge points) are left out and not smoothed. However, for  $NFT = 19$  or  $21$ , 9 or 10 points at each end are not smoothed and hence would involve a significant loss of information.

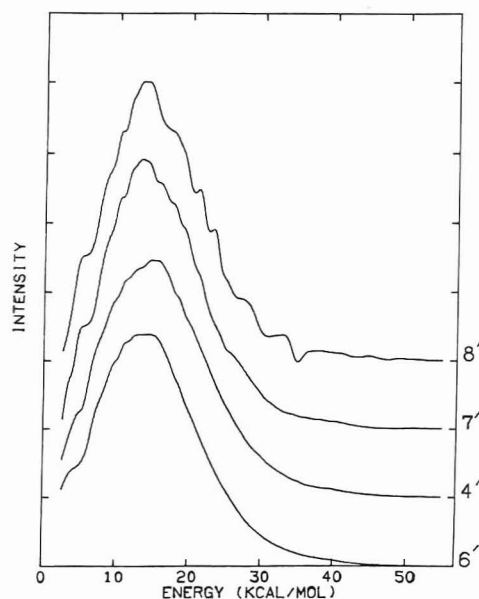
In smoothing and differentiation of data points with large errors, a relatively large NFT value (19 or 21) and one iteration is favored over a small NFT (5 or 7) and a larger number of iterations for two reasons. First, a larger NFT provides better smoothing. This has been shown in Figure 1. Curve 5 represents the raw data collected by a 100-channel multiscalar (Honeywell SAI-42 A) for  $H_2^+$  ions scattered at a certain angle ( $0^\circ$ ). Curve 1 represents the smoothed values obtained by





**Figure 2.** Differentiation (or energy distribution) curves obtained from curves 1, 2, and 3 of Figure 1 are shown. These are also separated by arbitrary amounts. Undesirable structures are noticeable for NFT = 5 or 7 in energy distribution curves (1' and 2'). Low- and high-energy distribution values are missing in curve 3', obtained by conventional procedure.

using five point segments of the original data (curve 5) at a time and repeating the whole procedure 5 times (NFT = 5 and iterations = 5). Curve 2 represents the smoothed values obtained by using NFT = 7 and iterations = 3 and curve 3 represents the smoothed values for NFT = 21 and iterations = 1. 1', 2', and 3' in Figure 2 are obtained by differentiating 1, 2, and 3 of Figure 1, respectively, and plotting their negative values. This gives the energy distribution of  $H_2^+$  ions with intensity of ions along the ordinate and energy along the abscissa. These curves are separated from each other for clarity of viewing. While in 1, 1' and 2, 2' only a few points are missing (which can be ignored); in 3, 3' a significant amount of information is lost. In order to identify which of the plots 1, 2, 3 (or 1', 2', 3') represents the best smoothed values (or best distribution), the energy distributions 1', 2', and 3' are compared with the distribution obtained from a different experiment (5, 6), i.e., a time-of-flight (TOF) experiment which was carried out under the same experimental conditions as that of the multichannel analysis. The TOF velocity (or energy) distribution shows only one peak at about 15 kcal/mol without other structures at low or high energies. This clearly indicates that the low and the high energy structures on 1' and 2' are not real but come from noise. Hence 1 and 2, from which 1' and 2' are derived, do not represent well smoothed data sets. On the other hand, 3' represents a distribution which most closely resembles the TOF distribution and hence 3 represents the most acceptable smoothed values among 1, 2, and 3. Therefore, a large NFT and 1 iteration does a better smoothing job than a small NFT and a larger number of iterations. One can explain these findings by considering the fact that the noise is reduced approximately as the square root of the number of points used at a time (1). The second reason for which a larger NFT and 1 iteration is favored is the CPU time required for various computations. More iterations involve a larger number of matrix inversion and matrix multiplication steps and hence a larger CPU time. For comparison, the ratio of CPU time for NFT = 5, ITERATION = 5 to NFT = 21 and ITERATION = 1 is about 3:2 when polynomials of the same order are used. In choosing a large value of NFT, one should be very careful not to lose finer structures which may be present together with more

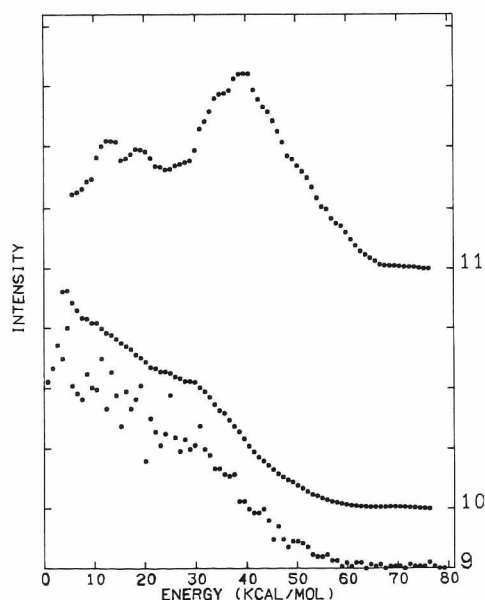


**Figure 3.** Effects of different polynomial orders on the differentiation (distribution) values are presented. All such curves are obtained by the new procedure of smoothing and differentiation using NFT = 21, ITERATION = 1. Curve 4' may be compared with 3' of Figure 2. In curve 4', most of the low- as well as the high-energy information is recovered. Most of the curves presented in Figures 1 through 3, except 6' (straight line), 7' (cubical), and 8' (quartic), are generated by the parabolic fit.

pronounced structures. This undoubtedly limits the optimum value of NFT. It has been noticed that any structure arising in differentiation curves (here energy distribution curves in Figures 2 and 3) from noise is fairly sensitive to even a small increment of NFT. Hence, by gradually increasing NFT one can come up with the best value of NFT to get the best smoothing of the data sets. In the analysis of the kind of data presented here, NFT = 19 or 21 and ITERATION = 1 has been found to give the best smoothing (5, 7).

In order to obtain a quantitative estimate of errors involved in the smoothing and differentiating procedure, smoothed data sets were generated by taking points from a parabolic function. Smoothing and differentiation of these data by NFT = 21, ITERATION = 1 provided slope values which were then compared with the true values. This provided a systematic error, which was found to be less than 2% in every case. Then errors were superimposed on the original data sets and smoothing and differentiation were done as before. The slope values, thus obtained, were compared with the true values. This provided errors in slope values due to errors on the data sets and systematic error involved in the differentiation procedure. When the superimposed error on data was between 10% and 12%, the error in slope was about 5% and when error on data was fairly large 40% to 60%, the error in slope ranged from 15% to 20%. The same tests were carried out with a smaller NFT value (NFT = 7, ITERATIONS = 3). For a small error (less than 4%) on the data it provided an excellent result (error in slope < 4%). However, as error on data was increased from 20% to 60%, percent error in slope value increased from 30% to 70%. These tests also suggest the use of a large NFT and 1 iteration when data points have large errors.

Even though NFT = 21 gives a better smoothing than NFT = 5 or 7, a significant amount of information at each end (plots 3, 3') is lost. Several procedures have been tried to carry out smoothing of most of these edge points so as to retrieve information from them. First, smoothing has been tried by using the same polynomial fit and calculating from it the smoothed values ( $y_i$ ) at different abscissa values ( $x_i$ ) of the edge points. This, however, did not yield good smoothing, since this forces



**Figure 4.** Differentiation curve (11) with finer structures, obtained from curve 9, is presented here. Curve 10 is obtained by smoothing of noisy data set (curve 9) and using NFT = 21 and ITERATION = 1.

all the smoothed values at the end to obey the polynomial function used in fitting. As an example, if the smoothed values at the edge are calculated from the same straight-line fit (polynomial of order 1), the slope values for all these points will then be the same, which obviously will give a wrong distribution.

The procedure that yielded the best smoothing is described below. Smoothing of the first few edge points begins by lowering the NFT value by 2 and fitting the points from NBEGIN to NPT (defined by the new value of NFT) and using a polynomial of the same order. Since the NFT value is reduced, one would expect a poorer smoothing compared to the other smoothed values. To compensate for the loss of the original data points from the segments, a smoothed value from the previous fit replaces the original data at the middle to be used by the next fit of lower NFT. Hence each reduction of NFT is compensated by an additional replacement of a smoothed value. By maintaining the same starting point (NBEGIN) and gradually reducing NFT and calculating the smoothed and the slope values in the middle, one can get a reasonably good smoothing. For smoothing of the edge points at the end, the same technique has been applied. This was done by maintaining the same last point (NEND) in each of these fits of gradually reducing NFT and compensating the loss of data points by the inclusion of smoothed values from previous fits into the segment of data points to be used by

succeeding fits. It is found that this procedure gives a fairly good smoothing of edge points down to a segment length of around 7. Curves 4 and 4' are obtained by using this procedure for NFT = 21 and ITERATION = 1. Comparing them with 3 and 3', where NFT = 21 and no edge points are smoothed, one sees that most of the edge point information had been retrieved by this procedure. Figure 3 represents the effect of polynomial fits of different orders on the smoothing and the differentiation of data. Curve 6' represents the slope values obtained by a straight line fit (polynomial of order 1); 4', 7', and 8' are, respectively, the values obtained by using polynomials of orders 2 (parabolic), 3 (cubic), and 4 (quartic), respectively. Even though straight-line and parabolic functions give similar distributions (slope values), the straight-line fit slightly distorts the peak of the distribution by making it flat. Curves 7' and 8' on the other hand show several low- and high-energy structures. Hence, curve 4', obtained by the parabolic fit, most closely resembles the true distribution (5).

In the  $\text{He}(2^1s)/\text{H}_2$  system, the energy distribution (presented here) had no finer structures. However, in the  $\text{Ne}(^3P_{2,0})/\text{H}$  and  $\text{Ne}(^3P_{2,0})/\text{D}$  systems there were finer structures (5) in the distributions. Interestingly, such finer structures were retained even after smoothing by NFT = 21 and ITERATION = 1. Curve 11, in Figure 4, represents the energy distribution of  $\text{H}^+$  ions with several structures, obtained by smoothing and differentiating the data (curve 9) collected at  $0^\circ$  with respect to the H beam in the  $\text{Ne}(^3P_{2,0})/\text{H}$  system. Curve 10 is the smoothed data obtained from curve 9.

This new procedure of edge point smoothing and differentiation, which has been applied here for the analysis of molecular beam experimental data, may be useful for the other kinds of data sets where one needs to use a large window size (NFT) for smoothing and differentiation of almost every data point.

#### ACKNOWLEDGMENT

The author acknowledges helpful discussions with P. E. Siska and C. A. Hollingsworth of the University of Pittsburgh and R. W. Gregor of Bell Labs.

#### LITERATURE CITED

- (1) Savitzky, A.; Golay, M. J. E. *Anal. Chem.* **1964**, *36*, 1627.
- (2) Bush, C. A. *Anal. Chem.* **1974**, *46*, 890.
- (3) Hayas, J. W.; et al. *Anal. Chem.* **1972**, *44*, 943.
- (4) Johnson, K. J. *Numerical Methods in Chemistry*; Marcel Dekker: New York, 1980; p 273.
- (5) Khan, A. Ph.D. Dissertation, University of Pittsburgh, 1983.
- (6) Gregor, R. W. Ph.D. Dissertation, University of Pittsburgh, 1981.
- (7) Siska, P. E.; et al. *Chem. Phys. Lett.* **1981**, *84*, 280.
- (8) Bevington, P. R. *Data Reduction and Error Analysis for the Physical Sciences*; McGraw-Hill: New York, 1969; p 108.

RECEIVED for review August 8, 1985. Resubmitted October 28, 1986. Accepted October 28, 1986.



# Rigorous Convergence Algorithm for Fitting a Monoexponential Function with a Background Term Using the Least-Squares Method

Željko Jeričević,<sup>1</sup> Douglas M. Benson, Joseph Bryan, and Louis C. Smith\*

Department of Medicine and Department of Cell Biology, Baylor College of Medicine, Houston, Texas 77030

**An algorithm has been developed to analyze data that contain a single exponential function plus a background term, as described by the equation  $y = b + ae^{-kt}$ . Since  $k$  is the only nonlinear parameter, the linear parameters  $a$  and  $b$  can be eliminated from the normal equations. This transforms the least-squares problem to one of finding the root of a transcendental equation. This can be approximated by applying the Newton-Raphson method inside an interval located by the Fibonacci order search. The features of the algorithm are that (a) close initial guesses for the parameters are not required from the user, (b) convergence to a global minimum is guaranteed, (c) there is a rigorous test to establish that a global minimum has been reached, and (d) the algorithm is numerically stable.**

Reliable data processing methods and procedures are fundamentally important in physical and biological sciences (1-3). Linear systems, because they have a principal solution, have been studied extensively. Unfortunately, many systems of interest are nonlinear. Solutions for such systems are approximate and usually based either on transformations from a nonlinear to a linear system or on a local Taylor series expansion in which the higher terms are neglected (1). Other procedures for nonlinear problems have been developed (4, 5), such as search methods for finding a minimum (maximum) on the least-squares surface. However, an intrinsic feature of nonlinear systems is the existence of multiple solutions which can cause search methods to find a local minimum instead of the global minimum being sought. Convergence to a local minimum is more common with increasing complexity of the system. One method to avoid this difficulty is to approach the solution from different directions in the parameter space and compare results. When all these strategies are combined, the processing of large data sets requires unacceptable amounts of computer time. For this reason, it is worthwhile to develop a specific procedure for the nonlinear problem of interest. One such example is the separation of multiexponential terms which appear in some relaxation processes, in chemical kinetics, and in the decay of a mixture of radionuclides. The best solution methods to date include those developed by Provencher (6), Wiscombe and Evans (7), and Knutson, Beechnet, and Brandt (8). A very elegant and efficient procedure has been developed by Gampp et al. (9), but unfortunately it uses numerical differentiation, which can be susceptible to errors for experimentally sampled functions (10).

In this paper we present a method for analyzing data that contain a single exponential function plus a background term or, expressed in another way, a biexponential function in which one of the two rate constants is equal to zero. The method

is valid only for this system and is not equivalent to methods (6-9) which deal with multiexponentials. However, the method has some features that are not common in nonlinear methods, which makes it attractive for certain applications.

We have used the method described here to analyze photobleaching processes in single cell using a fluorescence microscope and digital imaging equipment. With this instrument (11), we have documented the spatial heterogeneity of rates of photobleaching sampled at different  $0.065 \mu\text{m}^2$  areas within a single fluorescently labeled cell. Rate constants were calculated on a pixel by pixel basis, using at least 20 images, acquired successively at different times (11). Each image contains 61 440 pixels. With such large data sets, manual control of the calculation process is nearly impossible and effectively prevents the calculations.

Our objective was to construct an algorithm, based on the least-squares method, with the following features:

- A. The user is required to make only one nonzero initial guess for the value of the rate constant and that guess does not need to be close to the true value. For convenience, the initial guess is usually a characteristic of the image acquisition system and is appropriate for each of the 61 440 rate constants reported in this paper.
- B. Convergence to the global minimum is guaranteed.
- C. There is a rigorous test to establish that a global minimum has been reached.
- D. The algorithm is numerically stable.

## THEORY

The algorithm is designed to find the unknown parameters,  $a$ ,  $b$ , and  $k$ , of the model expressed by the following equation:

$$y = b + ae^{-kt} \quad (1)$$

Parameter  $a$  is the photobleachable component at the initial time, parameter  $b$  is the background plus the nonfading components which comprise the fluorescence intensity at infinite time, and  $k$  is the rate constant for the reaction. The dependent variable,  $y$ , is the fluorescence intensity at time  $t$ .

Equation 1 is a special case of the biexponential equation

$$y = be^{-k_0t} + ae^{-kt} \quad (2)$$

where  $k_0$  is zero and the first exponential factor shown in eq 2 is 1.

The expression for the sum of the squared residuals ( $\sum \delta_i^2$ ) is

$$\sum_{i=1}^n \delta_i^2 = \sum_{i=1}^n w_i (y_i - b - ae^{-kt_i})^2 \quad (3)$$

where  $n$  is the number of experimental  $y_i$ ,  $t_i$  pairs and  $w_i$  is the weight. Taking the derivative of eq 3 with respect to every parameter we want to optimize, we obtain the following normal equations:

$$0 = -\sum_{i=1}^n w_i y_i e^{-kt_i} + b \sum_{i=1}^n w_i e^{-kt_i} + a \sum_{i=1}^n w_i e^{-2kt_i} \quad (4)$$

<sup>1</sup> Permanent address: Rugjer Bošković Institute, Zagreb, Croatia, Yugoslavia.

$$0 = -\sum_{i=1}^n w_i y_i t_i e^{-kt_i} + b \sum_{i=1}^n w_i t_i e^{-kt_i} + a \sum_{i=1}^n w_i t_i e^{-2kt_i} \quad (5)$$

$$0 = -\sum_{i=1}^n w_i y_i + b \sum_{i=1}^n w_i + a \sum_{i=1}^n w_i e^{-kt_i} \quad (6)$$

$$0 = -\sum_{i=1}^n w_i y_i t_i + b \sum_{i=1}^n w_i t_i + a \sum_{i=1}^n w_i t_i e^{-kt_i} \quad (7)$$

Equations 4-6 are derivatives of eq 3 with respect to parameters,  $a$ ,  $k$ , and  $b$ . Equation 7 is the derivative with respect to the rate constant  $k_0$  in eq 2. The use of eq 7 reduces the number of some computations, as described later.

For a typical least-squares fit, the normal equations are usually constructed in a matrix form and solved simultaneously. The order of the Jacobi matrix is equal to the number of parameters. We have adopted a different approach. In eq 3, the only nonlinear parameter is the rate constant  $k$ . Therefore it is unnecessary to search in three dimensional parameter space by solving the normal equations simultaneously. It is faster and more accurate to eliminate the linear parameters,  $a$  and  $b$ , and search a one dimensional parameter space for the optimum value of the nonlinear parameter  $k$ . This approach transforms the least-squares problem to one of finding the root of a transcendental equation.

The development of the algorithm itself is straightforward algebra. Of the four equations (eq 4-7), we use the simplest ones (eq 4, 6, and 7) to reduce computing time. Combining eq 4 and 6 gives the following equation:

$$\frac{\sum w y e^{-kt} - a \sum w e^{-2kt}}{\sum w e^{-kt}} = \frac{\sum w y - a \sum w e^{-kt}}{\sum w} \quad (8)$$

All of the subscripts in eq 8 and later equations have been omitted for simplicity. Combining eq 6 and 7 gives the following expression for  $a$ :

$$\frac{\sum w y - a \sum w e^{-kt}}{\sum w} = \frac{\sum w y t - a \sum w t e^{-kt}}{\sum w t} \quad (9)$$

In eq 8 and 9, parameter  $b$  has been eliminated. Combining eq 8 and 9 gives a function which depends only on  $k$

$$f(k) = (\sum w \sum w y t - \sum w y \sum w t) \times (\sum w e^{-kt} \sum w e^{-kt} - \sum w \sum w e^{-2kt}) - (\sum w y \sum w e^{-kt} - \sum w \sum w y e^{-kt})(\sum w \sum w t e^{-kt} - \sum w t \sum w e^{-kt}) = 0 \quad (10)$$

The root of eq 10 is the optimal value for the parameter  $k$ . The Newton-Raphson method can be applied to approximate the root of  $f(k)$ . In this case

$$k_n = k - f(k)/f'(k) \quad (11)$$

where  $k_n$  and  $k$  are the improved and the previous values of  $k$ , respectively, and  $f'(k)$  is the first derivative of function  $f(k)$  with respect to  $k$ .  $f'(k)$  can be written as

$$f'(k) = -2(\sum w \sum w y t - \sum w y \sum w t) \times (\sum w e^{-kt} \sum w t e^{-kt} - \sum w \sum w t e^{-2kt}) + (\sum w y \sum w t e^{-kt} - \sum w \sum w y t e^{-kt})(\sum w \sum w t e^{-kt} - \sum w t \sum w e^{-kt}) + (\sum w y \sum w e^{-kt} - \sum w \sum w y e^{-kt})(\sum w \sum w t^2 e^{-kt} - \sum w t e^{-kt} \sum w t) \quad (12)$$

An initial guess is required for the Newton-Raphson method. In our algorithm, this is supplied by the Fibonacci order search (5), moving in a positive direction, i.e., for values of  $k$  greater than 0. The Fibonacci order search requires two initial values from the user. We have used 0.0, a trivial value, and one other value, which can be in the range from 0.0 to the noise level in the system. The only requirement for the second value of  $k$  is that it should be less than the true value of  $k$ . The value  $\ln 0.99/t_{\max}$  is certainly smaller than the true value of the rate constant, since we have shown in a previous

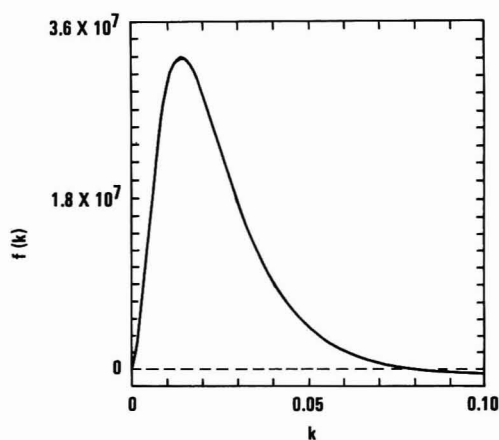


Figure 1. Plot of function  $f(k)$  for typical data set.

paper (11) that the noise level is less than 1% and it is reasonable to suppose that the overall decrease in fluorescence intensity since the last sampling time is greater than the noise level. If it is not, it would be more appropriate to repeat the experiment. With these two initial values, the Fibonacci order search,  $k_n = k_{n-1} + k_{n-2}$ , is iterated until the sign of the function  $f(k)$  changes. A sign change for the value of  $f(k)$  characterizes the interval in which the root of eq 10 is located and defines the areas of the search by the Newton-Raphson method. Inside the interval located by the Fibonacci search (Figure 1), convergence is always achieved by using the Newton-Raphson method.

We tested for convergence of the Newton-Raphson method by evaluating the first and second derivative at successive points within the interval, found by the Fibonacci search, in which the root is located. It is well-known that the Newton-Raphson method will converge if  $f(k)$  is positive and we are approaching the root from the left side and if  $f'(k) < 0$  and the product  $f(k) \cdot f''(k) > 0$ . However, because the Fibonacci method does not use derivatives, this evaluation requires extra calculations and is not used routinely. We have found that a heuristic approach can be used to save computing time. The general shape of the function  $f(k)$ , illustrated in Figure 1, implies that the interval over which the search for the root is done can be narrowed until a predetermined tolerance or interval width is achieved. We have been using a relative tolerance of 10% for the value of  $k$ , i.e., the root was always located between  $k$  and  $1.1k$ , before this initial guess was supplied to the Newton-Raphson method. For our data, this approach has been a completely satisfactory procedure with respect to convergence and is much faster than evaluating the first and second derivatives.

After completion of the calculations for  $k$ , the values of  $a$  and  $b$  can be evaluated by using eq 8 and 9 for  $a$  and eq 13 and 14 for  $b$ . A comparison of values for parameter  $a$  cal-

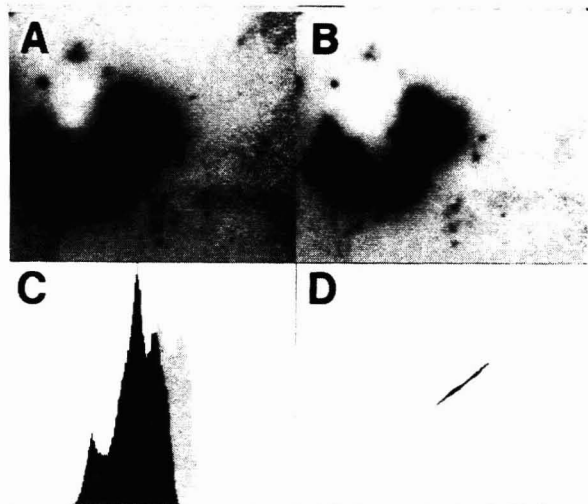
$$b = \frac{\sum w y \sum w e^{-2kt} - \sum w e^{-kt} \sum w y e^{-kt}}{\sum w \sum w e^{-2kt} - \sum w e^{-kt} \sum w e^{-kt}} \quad (13)$$

$$b = \frac{\sum w y \sum w t e^{-kt} - \sum w y t \sum w e^{-kt}}{\sum w \sum w t e^{-kt} - \sum w t \sum w e^{-kt}} \quad (14)$$

culated from eq 8 and 9 and for parameter  $b$  with values from eq 13 and 14 allows us to determine if the true value of  $k$  has been obtained. If the true value of  $k$  has been reached, the values for  $a$  and  $b$  should give differences at least an order of magnitude smaller than the corresponding standard errors of the parameters.

The rigorous test that a global minimum has been reached comes from evaluation of linear parameters by the two different substitutional schemes from the normal equations. After  $k$  has been approximated by the Newton-Raphson





**Figure 2.** Comparison of rate constant maps. The same data set, which consists of a timed series of 20 images of  $240 \times 256$  pixels, was used for all calculations. (A) Rate constant map using our method. (B) Rate constant map using the Wentworth method. (C) Frequency distributions for A (black) and B (gray). The range of the vertical scale is from 0 to 1513 pixels; the horizontal scale is from 0.0 to  $0.255 \text{ s}^{-1}$ . (D) Two-dimensional histogram of A (vertical axis) vs. B (horizontal axis). The vertical scale ranges from 0.0 to  $0.240 \text{ s}^{-1}$ ; the horizontal scale is from 0.0 to  $0.255 \text{ s}^{-1}$ .

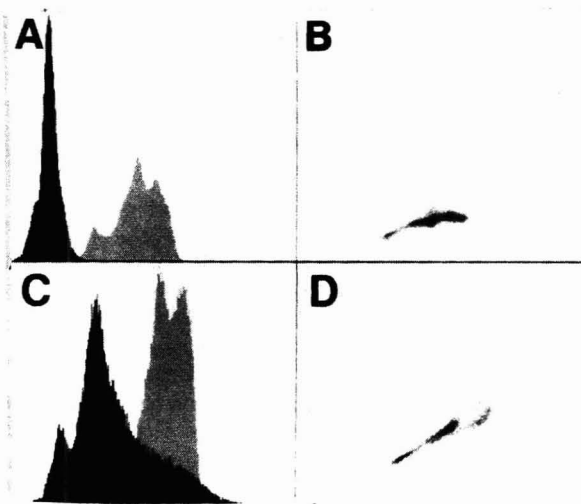
method with sufficient accuracy, all exponential sums can be evaluated and substituted into the normal equations. This substitution transforms the system of nonlinear normal equations to a linear system. It is well-known that the solution of such a system, if it exists, is unique. The uniqueness of a solution represents not only a necessary but also a sufficient condition for establishing that a global minimum has been reached. If the root of eq 10 corresponds to a global minimum on the least-squares surface, the two different substitutional schemes must give the same value for the respective parameters  $a$  and  $b$ .

## RESULTS AND DISCUSSION

The algorithm was used to calculate 61 440 rate constants for the photobleaching of acridine orange in rat hepatocytes (11). The values obtained from a data set of 20 different images are displayed as a rate constant map (Figure 2A) and compared to values obtained with an algorithm described by Wentworth (12) in which all parameters were updated simultaneously (Figure 2B). The algorithm was also tested successfully using synthetic data sets with different ranges of input data, errors, and convergence criteria.

The initial guesses for the Wentworth algorithm were obtained by scanning the data. Parameter  $b$  was the last sampled value of fluorescence intensity, parameter  $a$  was the difference between the first and last values, and  $k$  was the rate constant calculated on the preceding pixel. For the first pixel, an initial guess for  $k$  was provided by the user. Calculations using the Wentworth method required about 48 h. With our method, only 4 h was needed with the same data set, using the same convergence criteria and the same number of iterations.

The difference between the two algorithms is easily visible by comparing areas in Figure 2A vs. Figure 2B. A more quantitative comparison of the two algorithms, a histogram analysis of the rate constant maps, is given in Figure 2C,D. The two-dimensional histogram of the two images is a two-dimensional table,  $h(r,c)$ , containing the number of pixels having an intensity value  $r$  in the first image and an intensity value  $c$  in the second image. If the two images are identical and have an intensity range greater than one, the two-dimensional histogram of these two images will be straight line with a slope of  $45^\circ$ . The two-dimensional histogram in (Figure 2D) has a slope less than  $45^\circ$  because of systematic differences



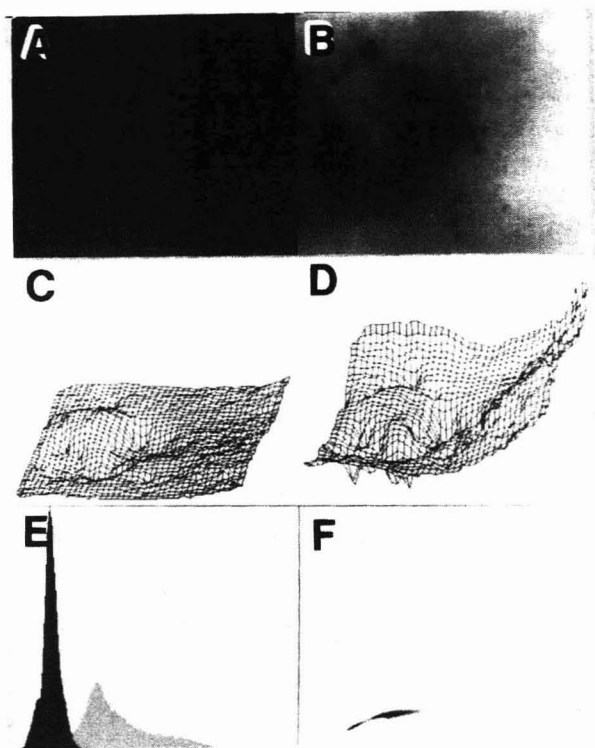
**Figure 3.** Dependence of the rate constant error on the rate constant. (A) Rate constant error (black) and rate constant (gray) frequency distributions using our method. The range of the vertical scale is from 0 to 3507 pixels. Horizontal scale ranges from 0.0 to  $0.255 \text{ s}^{-1}$  for the rate constant and from 0.002 to  $0.051 \text{ s}^{-1}$  for the error. (B) Two-dimensional histogram of the rate constant error (vertical axis) vs. the rate constant (horizontal axis) using our method. The vertical scale is from 0.002 to 0.0481; the horizontal scale is from 0.0 to  $0.255 \text{ s}^{-1}$ . (C) Rate constant error (black) the rate constant (gray) frequency distributions using the Wentworth method. The range of the vertical scale is from 0 to 1239 pixels; the horizontal scale is from 0.0 to  $0.255 \text{ s}^{-1}$  for the rate constant and from 0.002 to  $0.051 \text{ s}^{-1}$  for the error. (D) Two-dimensional histogram of rate constant error (vertical axis) vs. rate constant (horizontal axis) using the Wentworth method. The vertical scale is from 0.002 to 0.0481; the horizontal scale is from 0.0 to  $0.255 \text{ s}^{-1}$ .

between the two rate constant maps (Figure 2A,B).

The relationship between rate constants from the same data set calculated by the two algorithms is shown in Figure 2D. Our values are generally lower, although frequency distributions are similar in shape (Figure 2C). The relationship between the rate constant and the rate constant error is shown in Figure 3. Error analysis was performed in the manner described by Bard (4), using the sum of squares and the partial derivatives of the function given in eq 1. We can see that, for the algorithm developed in this paper, the shape of the frequency distribution for error is largely independent of the frequency distribution of the rate constant (Figure 3A). Further, the magnitude of error is independent of rate constant values (Figure 3B). By comparison, Figure 3, parts C and D, shows the relationship of the same parameters for the Wentworth algorithm (11). It is interesting to note the similarity of distributions for the rate constant and for the rate constant error (compare also Figures 2B and 4B), but with a greater dispersion of values for the larger rate constants.

The comparison of the error analysis of the rate constants for the two algorithms is presented in Figure 4. From the magnitude of the rate constant error and the shape of the frequency distribution curve, the better performance of our algorithm is obvious. The same analysis was performed for the other parameters, with essentially the same result as for the rate constant. The differences between the rate constant values are the most significant, by comparison with the other parameters.

The correlation index comparison presented in Figure 5 is informative. Not only are there differences in the magnitude and the shape of the correlation index map, but we see two completely separated frequency distributions. This means that the results of calculations by the two algorithms differ at every pixel. Thus, the difference between the performance of the two algorithms is more significant than can be observed by a simple comparison of the rate constant maps (Figure



**Figure 4.** Rate constant error. (A) Rate constant error map using our method. (B) Rate constant error map using the Wentworth. (C) Isometric projection of A. (D) Isometric projection of B. (E) Frequency distributions for A (black) and B (gray). The range of the vertical scale is from 0 to 3507 pixels; the horizontal scale is from 0.002 to 0.051  $s^{-1}$ . (F) Two-dimensional histogram of A (vertical axis) vs. B (horizontal axis). The vertical scale ranges from 0.002 to 0.0481  $s^{-1}$ ; the horizontal scale ranges from 0.002 to 0.051  $s^{-1}$ .

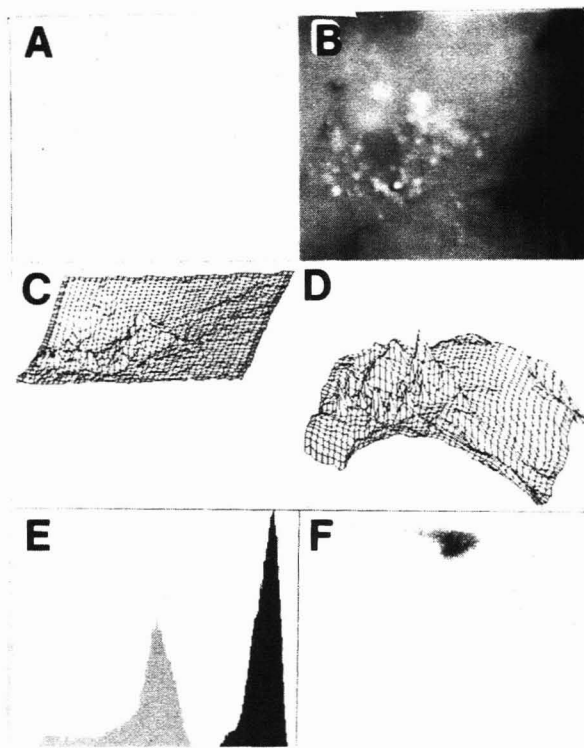
2A,B). Finally, plotting the correlation index vs. the rate constants, shown in Figure 6, emphasizes the superiority of the present algorithm in all cases and illustrates the failure of the Wentworth algorithm when estimating the higher values of the rate constants (compare Figure 6, parts B and D).

Some interesting conclusions can be made from the histogram analysis. As shown above, with increasing values of the rate constants, the difference between the performance of the two algorithms becomes more pronounced. The reason for this difference is that with increasing  $k$  values, the least-squares surface in three-dimensional space exhibits stronger nonlinearity. The least-squares surface looks like a deep narrow valley (13) and the sum of the squares will be more sensitive to changes in  $k$  than to changes in  $a$  or  $b$ .

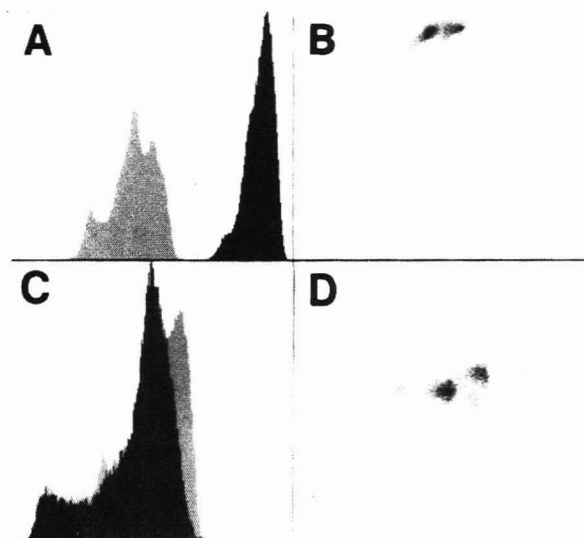
For a more general application of this algorithm, the only requirement is that the initial nonzero guess for the Fibonacci order search should be positive and less than the true value.

It is possible that some specific applications of this algorithm may require different criteria for the initial guess; however, the experimenter should be able to give a reasonable estimate. The advantage of the algorithm for our particular application is that 61 440 different rate constants are optimized with a single nonzero initial guess. We emphasize that this is not typical performance for optimization of nonlinear models. For most other methods, the usual recommendation is that the initial guess for each individual parameter should be as close as possible to the true value.

In general, because the solution of the three-dimensional least-squares problem is a domain in three-dimensional space, the calculation may terminate anywhere inside that domain or, in the worse case, in some local minimum. Elimination of the linear parameters from the normal equations gives the nonlinear equation (10), which is a continuous function in form  $f(k) = 0$  and is suitable for approximating the root with the Newton-Raphson method. The problem of finding a mini-



**Figure 5.** Correlation index. (A) Correlation index map using our method. (B) Correlation index map using the Wentworth method. (C) Isometric projection of A. (D) Isometric projection of B. (E) Frequency distributions for A (black) and B (gray). The range of the vertical scale is from 0 to 2368 pixels; the horizontal scale is from 0.97 to 1.0. (F) Two-dimensional histogram of A (vertical axis) vs. B (horizontal axis). The vertical scale ranges from 0.9718 to 1.0; the horizontal scale ranges from 0.97 to 1.0.



**Figure 6.** Dependence of the correlation index on the rate constant. (A) Correlation index (black) and rate constant (gray) frequency distributions using our method. The range of the vertical scale is from 0 to 2368 pixels; the horizontal scale is from 0.0 to 0.255  $s^{-1}$  for the rate constant and from 0.97 to 1.0 for the correlation index. (B) Two-dimensional histogram of correlation index (vertical axis) vs. rate constant (horizontal axis) using our method. Vertical scale ranges from 0.9718 to 1.0; the horizontal scale ranges from 0.0 to 0.255  $s^{-1}$ . (C) Correlation index (black) and rate constant (gray) frequency distributions using the Wentworth method. The range of the vertical scale is from 0 to 1370 pixels; the horizontal scale is from 0.255  $s^{-1}$  for the rate constant and from 0.97 to 1.0 for the correlation index. (D) Two-dimensional histogram of correlation index (vertical axis) vs. rate constant (horizontal axis) using the Wentworth method. The range of the vertical scale is from 0.9718 to 1.0; the horizontal scale is from 0.0 to 0.255  $s^{-1}$ .

mum on the least-squares surface is avoided because one of the roots of eq 10 corresponds to a global minimum. For that particular root, the derivative of  $f'(k)$  is not zero; therefore



the root can be approximated by using the Newton-Raphson method. There are two other roots, one at  $k = 0$  and another asymptotic root at  $k = +\infty$ . These roots do not have interesting physical meanings in our model. The first corresponds to a static system; the second corresponds to an infinitely fast reaction. The algorithm developed in this paper provides, as a solution a single point in one-dimensional space, the optimum value of the rate constant.

In our experience, the numerical stability of the algorithm is very good. Although we have not developed a formal proof that the algorithm is numerically stable, our reasoning in support of this statement is the following. In principle, the only dangerous point is when  $f'(k)$  is equal to zero, but this is not inside the interval defined and constricted by the Fibonacci search. Furthermore, we know that all exponentials have values between 0 and 1 and that the input data values for the time and intensity are nonnegative numbers within a controllable range (i.e., they can be rescaled if necessary) so there is no possibility of overflow. The parameter  $k$  has physical meaning and its range falls within the interval defined as  $0 < k \leq k_{\max}$ . Also  $f(k)$  is constructed in such a way that there is no division. Finally, we have calculated about 10-12 million rate constants to date using data sets containing from 20 to 30 images, each of which was contained either 61 440 or 245 760 pixels.

### CONCLUSION

The development and use of a stable algorithm that always converges have been presented. The algorithm does the least-squares fitting of a monoexponential function with a background to a large data set. The procedure is self-contained and requires only one nonzero value in order for each

individual kinetic process to be optimized. We find systematic differences between the specific algorithm and a general nonlinear least-squares program. It is worthwhile to point out that, in some applications, these differences could be crucial. One such example would be the calculation of rate constants in studies of isotope effects because the difference between constants for a labeled and a nonlabeled compound is usually only a few percent of the rate constant values.

### LITERATURE CITED

- (1) Bevington, P. R. *Data Reduction and Error Analysis for the Physical Sciences*; McGraw-Hill: New York, 1969; 336p.
- (2) Lawson, C. L.; Hanson, R. J. *Solving Least Squares Problems*; Prentice-Hall: Englewood Cliffs, NJ, 1974; 384p.
- (3) Longley, J. W. *Least Squares Computations Using Orthogonalization Methods*; Marcel Dekker: New York, 1984; 288p.
- (4) Bard, Y. *Nonlinear Parameter Estimation*; Academic: New York, 1974; 341p.
- (5) Scales, L. E. *Introduction to Non-Linear Optimization*; Springer-Verlag: New York, 1985; 243p.
- (6) Provencher, S. W. *Biophys. J.* **1976**, *16*, 27-41.
- (7) Wiscombe, W. J.; Evans, J. W. *J. Comput. Phys.* **1976**, *24*, 416-444.
- (8) Knutson, J. R.; Beechem, J. M.; Brand, L. *Chem. Phys. Lett.* **1983**, *102*, 501-507.
- (9) Gampp, H.; Maeder, M.; Meyer, C. J.; Zuberbühler, A. D. *Talanta* **1985**, *32*, 95-101.
- (10) Zeldovich, Y. B.; Myskis, A. D. *Elements of Applied Mathematics*; Mir Publishers: Moscow, 1976; pp 39-64.
- (11) Benson, D. M.; Bryan, J.; Plant, A. L.; Gotto, A. M., Jr.; Smith, L. C. *J. Cell Biol.* **1985**, *100*, 1309-1323.
- (12) Wentworth, W. E. *J. Chem. Educ.* **1965**, *42*, 96-103.
- (13) Lawton, W. H.; Sylvestre, E. A. *Technometrics* **1971**, *13*, 461-467.

RECEIVED for review May 27, 1986. Accepted October 6, 1986. This work was supported by Robert A. Welch Foundation Q-343, HL-15648, HL-23741, HL-26973, HL-33750, GM-26091, and GM-27468. D.M.B. was an NCI postdoctoral fellow (CA-07090).

## Rapid Anodic Stripping Analysis with Ultramicroelectrodes

Andrzej S. Baranski

Department of Chemistry, University of Saskatchewan, Saskatoon, Saskatchewan, Canada S7N 0W0

**Mercury-film microelectrodes (7-10  $\mu\text{m}$  in diameter) prepared by the electrodeposition of mercury on a carbon fiber or a thin platinum wire were used in rapid-multicomponent-trace determinations of heavy metals in very small (5- $\mu\text{L}$ ) samples. Stripping experiments were carried out under linear sweep voltammetry conditions with sweep rates in the range of 1-100 V/s. The preconcentration time was varied from 10 to 640 s. Background currents were determined in a separate sweep cycle, conducted without preconcentration after each stripping experiment, and they were numerically subtracted from the stripping curves. The unique properties of ultramicroelectrodes enable determinations of heavy metals without time-consuming deoxygenation of samples. The detection limit was about  $5 \times 10^{-9}$  M for a 10-s preconcentration time.**

Anodic stripping voltammetry with hanging-mercury-drop or mercury-film electrodes is recognized as one of the most sensitive techniques of heavy metal analysis. The main disadvantages of this technique include the length of time re-

quired for deoxygenation of a sample and preconcentration of analytes (typically 10-30 min), the requirement of a relatively large sample (typically >5 mL), and poor precision (5-20%). In recent years some efforts have been made to develop a method allowing trace determination of heavy metals in air-saturated solutions by employing potentiometric oxidation (1), square-wave voltammetry (2), or subtractive voltammetry (3).

The use of mercury-film ultramicroelectrodes opens new, more effective ways of improving performance of stripping analysis. It was suggested (4) and demonstrated (5) that ultramicroelectrodes can be used in analysis of very small (5- $\mu\text{L}$ ) samples. This is possible because a fast, steady-state diffusion to microelectrodes makes stirring of a solution unnecessary. Wehmeyer and Wightman (6) developed a mercury microelectrode (a mercury droplet deposited on a platinum microelectrode) and used it for the determination of lead under stripping voltammetry conditions. The relative standard deviation of 0.5-1.5% was reported for  $\text{Pb}^{2+}$  concentrations of  $10^{-7}$ - $7 \times 10^{-10}$  M. Again the improvement can be attributed to the elimination of stirring in the preconcentration cycle.

In our previous paper (5), the possibility of developing a super-fast potentiometric stripping technique that does not require deoxygenation of a sample was suggested. Very brief studies revealed, however, that a contamination of electrodes significantly affects the rate of oxygen reduction and, thus, the length of transition time observed in the potentiometric stripping mode. This, of course, introduces an additional error to the determinations. At the same time, it was realized that determinations of metals with microelectrodes in the presence of oxygen can be carried out without problems under subtractive voltammetry conditions.

## EXPERIMENTAL SECTION

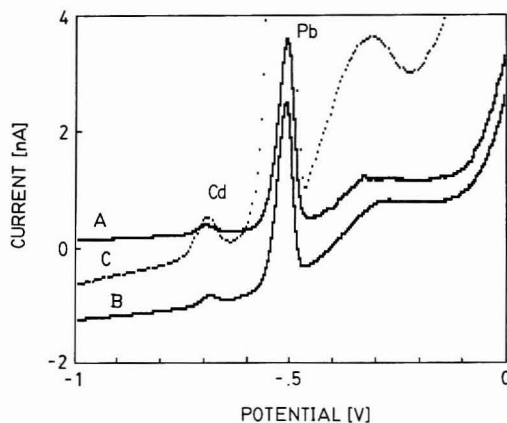
**Reagents.** Analytical grade chemicals,  $\text{Hg}(\text{CH}_3\text{COO})_2$ ,  $\text{Pb}(\text{CH}_3\text{COO})_2$ ,  $\text{Cd}(\text{CH}_3\text{COO})_2$ ,  $\text{HCl}$ ,  $\text{CH}_3\text{COOH}$ , and  $\text{CH}_3\text{COONa}$ , were used to prepare stock solutions. Two types of supporting electrolytes were used: (i) a 0.01 M  $\text{HCl}$  solution prepared by diluting concentrated  $\text{HCl}$  (AnalaR) with Millipore water (this solution contained impurities, such as  $\text{Cu}$ ,  $\text{Pb}$ , and  $\text{Cd}$  at concentrations lower than  $10^{-9}$  M); (ii) a 0.01 M  $\text{CH}_3\text{COONa}/0.01$  M  $\text{CH}_3\text{COOH}/0.01$  M  $\text{NaCl}$  buffer solution.

A 1 M stock solution of the second buffer was electrolyzed for 24 h at a large mercury cathode at  $-1$  V vs. a standard calomel electrode (SCE), to remove heavy metal impurities. All solutions were prepared with Millipore water.

**Electrodes.** Carbon fibers,  $(7.0 \pm 0.3) \times 10^{-4}$  cm in diameter (Union Carbide, Thornell 300, grade WYP 30 1/0), were washed with 1 M  $\text{HCl}$  and distilled water, dried, and heated for 30 min in a quartz tube under argon at  $600^\circ\text{C}$  to remove organic impurities. A single fiber (2–3 cm long) was inserted into a glass tube. The tube was sealed at one end and the other end was connected to a vacuum pump. The part of the tube containing the fiber was heated in a gas burner flame to melt the glass and seal the fiber. Finally, the glass tube was cut perpendicular to its length to expose the carbon surrounded by glass. Before use the electrodes surface was polished with an extrafine carborundum sandpaper and  $0.3\text{-}\mu\text{m}$  alumina. Unless otherwise specified, a mercury film was prepared by the electrodeposition of  $\text{Hg}$  on the carbon-fiber electrode (5 min) from a solution containing  $5 \times 10^{-3}$  M  $\text{HCl}$  and  $10^{-4}$  M  $\text{HgCl}_2$  at  $-1$  V vs. SCE. The volume of  $\text{Hg}$  in the film estimated on the basis of eq 1 was about 5 fL. The electrode was carefully washed by immersing in distilled water before placing it in the cell.

Platinum microelectrodes were prepared in a similar way with a  $10\text{-}\mu\text{m}$  diameter platinum wire (Goodfellow Metals). The reference electrode was made of an amalgamated gold wire (5 mm long,  $50\text{-}\mu\text{m}$  in diameter) electrochemically coated with a thin layer of  $\text{Hg}_2\text{Cl}_2$ . In solutions containing 0.01 M  $\text{Cl}^-$ , this electrode had a potential of 0.153 V vs. SCE.

**Electrochemical Measurements.** Stripping experiments were carried out with a computer-controlled system consisting of an Apple IIe computer, a PAR Model 273 potentiostat, and a PAR Model 181 current preamplifier. All experiments were done in a two-electrode configuration; the potentiostat was used only as a convenient data acquisition interface. All potential programs were numerically generated; this means that the ramp program assembled by the potentiostat for use in the stripping cycle had the form of a staircase function with the step width always equal to 100  $\mu\text{s}$  and the step height determined by the sweep rate. However, before being applied to the reference electrode the potential output of the potentiostat was passed through a 1-kHz low-pass filter ( $R = 100\ \Omega$ ,  $C = 10\ \mu\text{F}$ ) in order to obtain an almost linear ramp. The current flow was monitored by the current preamplifier. The output of this preamplifier was connected through a 10-kHz low-pass filter to the auxiliary analog to digital (A/D) input of the potentiostat. Both filters significantly reduced the noise level; the distortion of the signal of interest acquired at sweep rates lower than 10 V/s was negligible. However, at higher sweep rates, the low-pass filter at the potentiostat output caused a parallel shift of the potential ramp by a value  $E_s = aT$  (where  $a$  is the sweep rate and  $T = 1.02 \times 10^{-3}$  s is the time constant of the filter). All plots shown in this paper were corrected for this shift (linearized staircase function  $-E_s$ ). Data acquisition was carried out at the fastest rate available on the Model 273 potentiostat, i.e., 10 000 points/s. All points were plotted as



**Figure 1.** Stripping voltammograms of  $10^{-7}$  M  $\text{Pb}^{2+}$  and  $5 \times 10^{-9}$  M  $\text{Cd}^{2+}$  in 0.01 M  $\text{HCl}$  obtained with a Hg-coated carbon-fiber microelectrode: (A) deoxygenated solution, sweep rate 10 V/s; (B) air-saturated solution, sweep rate 10 V/s; (C) air-saturated solution, sweep rate 50 V/s. Preconcentration was carried out for 60 s at  $-1.2$  V.

acquired without any smoothing or averaging.

The previously described microelectrochemical cell (5) was used in all experiments, unless otherwise specified. In microanalysis, a small drop of the analyzed solution has to be placed on the top of the working electrode. This can be easily accomplished only if the walls of the working electrode are hydrophobic. For this application a jacket made of Teflon was formed around the electrodes by using a heat-shrinkable tubing made of Teflon (Mandel Scientific). The cell was located in a faraday cage. All electrical connections outside the cage were made with coaxial cables. All measurements were carried out without deoxygenation of solutions, unless otherwise specified.

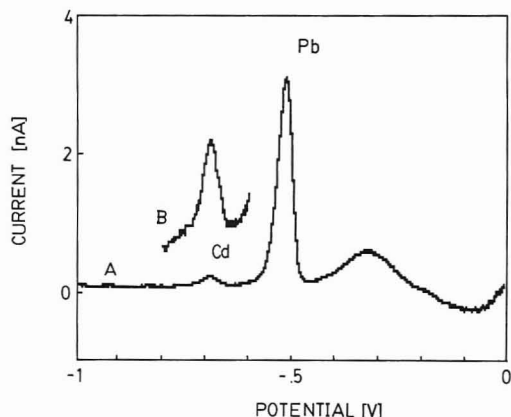
## RESULTS AND DISCUSSION

**Effect of Dissolved Oxygen.** The removal of dissolved oxygen required by most well-established electroanalytical methods is a time-consuming procedure. In addition, particularly when working with microsamples, deoxygenation may lead to errors caused by the evaporation of solvent and/or the loss of volatile components. Reduction of oxygen has two major effects on electrochemical determination: (i) the change of the pH in the vicinity of the electrode resulting from the reactions  $\text{O}_2 + 2\text{H}_2\text{O} + 2e^- \rightarrow \text{H}_2\text{O}_2 + 2\text{OH}^-$  and  $\text{H}_2\text{O}_2 + 2e^- \rightarrow 2\text{OH}^-$ , and (ii) a significant current, which in a case of standard size, stationary electrodes is a complex function of time and potential.

The increase of the pH may cause a precipitation of heavy metal hydroxides, leading to negative errors in anodic stripping analysis. However, this effect of oxygen reduction is easy to overcome by using a buffer as the supporting electrolyte. The current associated with oxygen reduction processes interferes with the signal of interest, making anodic stripping determinations very difficult or impossible to carry out. These interferences can be minimized by using techniques in the stripping cycle that have relatively low sensitivity toward irreversible processes (e.g., square-wave voltammetry or ac voltammetry).

A unique mass transport characteristic of ultramicroelectrodes (7–11) makes it possible to resolve this problem differently. One can notice that, with the exception of very short times, current associated with diffusion-controlled processes occurring at ultramicroelectrodes is time independent. Therefore, current caused by reduction of oxygen is only a function of the potential that can be easily determined and subtracted from the signal of interest. This idea in relation to anodic stripping analysis was verified experimentally. Experiments were carried out in a standard electrochemical cell containing 20 mL of 0.01 M  $\text{HCl}$ ,  $10^{-7}$  M  $\text{Pb}^{2+}$ , and  $5 \times 10^{-9}$  M  $\text{Cd}^{2+}$ . Preconcentration of the metals was carried out for 1 min at  $-1.2$  V on a carbon-fiber electrode with prede-





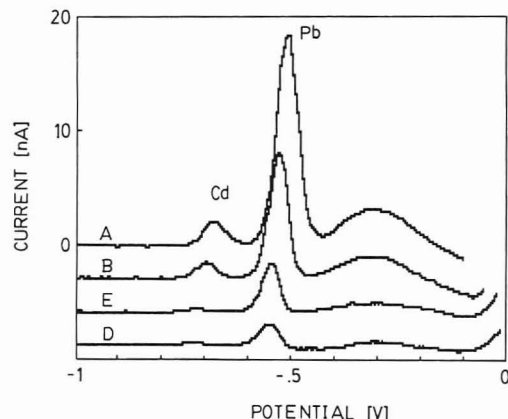
**Figure 2.** (A) Subtractive stripping voltammogram of  $10^{-7}$  M  $\text{Pb}^{2+}$  and  $5 \times 10^{-9}$  M  $\text{Cd}^{2+}$  in 0.01 M HCl. (B) Cd peak plotted at a 10 $\times$  expanded scale. All experimental conditions were the same as for curve B in Figure 1.

posited Hg film; then the stripping cycle was performed at a 10 V/s sweep rate. In Figure 1 the stripping curves obtained for the deaerated (curve A) and air-saturated (curve B) solutions are shown. Curve A has a small positive offset current caused by the capacitance current. Curve B has a larger negative offset current resulting from the difference between the current associated with reduction of oxygen and the capacitance current. The capacitance current and the oxygen reduction current have opposite signs, and in favorable conditions these currents may compensate each other. This is the case at sweep rates between 50 and 100 V/s (Figure 1C).

Alternatively, the background current can be subtracted from the data. To do this the following procedure was developed. Metal ions were preconcentrated at potential  $E_p$  for a precisely defined time  $t_p$ ; then potentials were swept from  $E_p$  to a more positive final value ( $E_f$ ) and values of the resulting current were stored in memory as curve C1. Then the working electrode was disconnected from the circuit for 5 s to allow diffusion of oxidation products away from the electrode. After that,  $E_p$  was applied to the working electrode for 1 s to obtain steady-state mass transport conditions for reduction of oxygen, and again potentials were swept from  $E_p$  to  $E_f$  in exactly the same way as in the first sweep cycle. The results were stored in memory as curve C2. Finally, curve C2 was subtracted from curve C1, the currents were plotted as a function of potential, and peak currents, peak potentials, and electrical charge associated with the peaks were determined.

The results of such an experiment are shown in Figure 2 (the solution composition and other experimental conditions were the same as in Figure 1). The smaller Cd peak is quite well developed (Figure 2B, 10 $\times$  expanded scale). A broad peak at potential  $-0.33$  V (seen also in Figures 1, 3, and 4) is caused by an unknown impurity present in the solution or on the electrode surface. As long as the offset current caused by reduction of oxygen does not exceed the dynamic range of a current preamplifier, the results obtained by this method for air-saturated solutions are indistinguishable from ones obtained for deaerated solutions. The remainder of the experiments in this paper were done in air-saturated solutions, and the background currents were subtracted as described above.

**Effect of Analyte Concentration.** The concentration dependence of the current response of mercury-film microelectrodes was studied varying the concentration of  $\text{Pb}^{2+}$  from  $5 \times 10^{-9}$  to  $10^{-6}$  M (a 2-fold increase for each new solution) in 0.01 M HCl containing  $2 \times 10^{-4}$  M  $\text{HgCl}_2$ . For each concentration five replicate measurements were recorded. Mercury film was formed in situ on the carbon-fiber microelectrodes. The working microelectrode was washed with three 10- $\mu\text{L}$  portions of the solution to be analyzed; then a



**Figure 3.** Effect of the sweep rate on subtractive stripping voltammetry at a Hg-coated carbon-fiber microelectrode. The analyzed solution contained  $5 \times 10^{-8}$  M  $\text{Pb}^{2+}$  and  $5 \times 10^{-9}$  M  $\text{Cd}^{2+}$  in 0.01 M HCl. Preconcentration was carried out for 60 s at  $-1.2$  V. Sweep rates were (A) 100 V/s, (B) 50 V/s, (C) 20 V/s, and (D) 10 V/s. (Curves B, C, and D were shifted down by 3, 6, and 9 nA, respectively.)

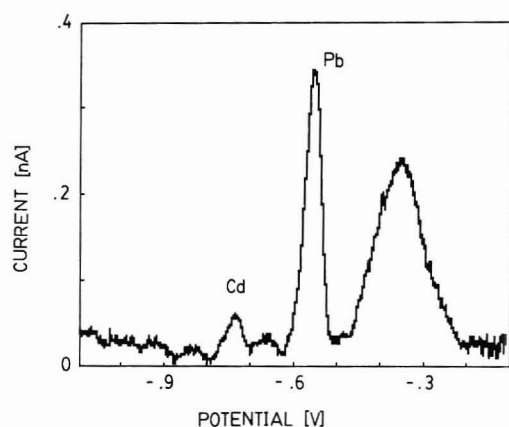
5- $\mu\text{L}$  sample was placed on the top of the electrode and the reference electrode was immersed in the sample. Preconcentration of lead was carried out for 1 min at  $-1.1$  V. The sweep rate in the stripping cycle was 10 V/s. The relation between peak currents and  $\text{Pb}^{2+}$  concentrations was linear (slope =  $(29 \pm 1.2)$  A  $\text{cm}^3/\text{mol}$ , correlation coefficient = 0.995). The electrical charge associated with the peaks agreed within 20% with that predicted by

$$Q = 4nFD_0C_0rt_p \quad (1)$$

where  $t_p$  is the preconcentration time,  $r$  is the radius of the electrode,  $D_0$  and  $C_0$  are the diffusion coefficient and concentration of  $\text{Pb}^{2+}$ , respectively, and other symbols have their usual meaning. The relative standard deviation for replicate measurements will be discussed in the last section of this paper.

**Effect of Sweep Rate.** A 0.01 M HCl solution containing  $5 \times 10^{-9}$  M  $\text{Cd}^{2+}$  and  $5 \times 10^{-8}$  M  $\text{Pb}^{2+}$  was used to study the effect of the sweep rate on stripping voltammograms. The sweep rate was varied from 1 to 100 V/s (a 2- or 2.5-fold increase for each new experiment). Preconcentration of metals were carried out for 1 min at  $-1.2$  V. Other experimental conditions were the same as described in the preceding section. The peak current was found to increase almost linearly with sweep rate. Plots of the logarithm of the peak current vs. the logarithm of the sweep rate had slopes of  $0.84 \pm 0.04$  for Cd and  $0.86 \pm 0.01$  for Pb. Correlation coefficients were 0.995 and 0.999 for Cd and Pb, respectively. Slopes lower than 1 are associated with the increase in peak width measured at higher sweep rates (half-height widths of 38 mV at 1 V/s and 53 mV at 100 V/s). At least 75% of this increase can be explained by the action of the low-pass filter at the output of the current preamplifier. In contrast, the electrical charge associated with the peaks was independent of sweep rate:  $(1.2 \pm 0.3)$  pC for Cd and  $(11.6 \pm 1.2)$  pC for Pb. The peak potentials for both metals moved in a positive direction with an increase in the sweep rate (29 mV per decade for both Pb and Cd). In Figure 3, stripping voltammograms recorded at sweep rates 10, 20, 50, and 100 V/s are shown.

Thus, the data show that an increase in sweep rate increases the sensitivity of the technique. A similar improvement of sensitivity with large mercury-film electrodes was recently reported by Stojek and Kublik (12). However, such an improvement has some limits and some negative consequences. First, one can encounter instrumental limitations. The electronic system used in this work was not designed to operate at sweep rates greater than 10 V/s. Experiments at higher



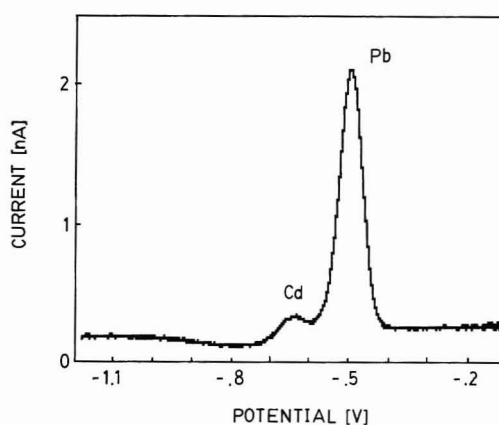
**Figure 4.** Subtractive stripping voltammogram of  $5 \times 10^{-8}$  M  $\text{Pb}^{2+}$  and  $5 \times 10^{-9}$  M  $\text{Cd}^{2+}$  in 0.01 M HCl obtained with a Hg-coated carbon-fiber microelectrode. Preconcentration was carried out for 10 s at  $-1.2$  V. Sweep rate was 10 V/s.

sweep rates were done at a cost of severe reduction in the number of points acquired in the stripping cycle (from 1000 points/V at 10 V/s to 100 points/V at 100 V/s). Secondly, at higher sweep rates, an increase in the peak's width and a consequent decrease in selectivity of the technique are observed. This phenomenon may be caused by a change in mass transport conditions for reactants and products of the electrode reaction (11), slow charge-transfer kinetics (not observed in the described experiment), and a slow response of the current monitoring circuit. Finally, at higher sweep rates, the peak height will be more affected by the kinetics of preceding chemical reactions occurring in amalgams (e.g., slow dissociation of intermetallic compounds).

**Effect of Preconcentration Time.** A 5- $\mu\text{L}$  sample containing 0.01 M HCl,  $5 \times 10^{-9}$  M  $\text{Cd}^{2+}$ , and  $5 \times 10^{-8}$  M  $\text{Pb}^{2+}$  was measured by using a carbon-fiber microelectrode with a predeposited Hg film (Hg was deposited for 3 min from a  $10^{-4}$  M  $\text{HgCl}_2$  solution). Preconcentration of Cd and Pb was carried out at  $-1.2$  V. The preconcentration time was varied from 10 to 640 s (a 2-fold increase for each new experiment). The sweep rate in the stripping cycle was 10 V/s. As expected, the height of both peaks observed in the stripping cycle was proportional to the preconcentration time. A plot of the logarithm of the peak current vs. the logarithm of the preconcentration time had a slope of  $1.02 \pm 0.01$  for lead and  $0.87 \pm 0.09$  for cadmium. Correlation coefficients were 0.9996 and 0.980 for Pb and Cd, respectively. The stripping curve recorded after a 10-s preconcentration time is shown in Figure 4.

**Detection Limit.** The size of the cadmium peak in Figure 4 was very close to its detection limit. The electrical charge associated with this peak was about 0.18 pC, which corresponds to the oxidation of  $10^{-16}$  g of cadmium (570 000 atoms). The peak current was about 43 pA. The chief component of the background noise seen in Figure 4 was a power line interference with an amplitude of 15 pA. On the basis of this information and the relations between the peak current and experimental parameters described in preceding sections, one can estimate the detection limit for various sweep rates and preconcentration times. For example, if  $v = 100$  V/s and  $t_p = 10$  min, the approximate detection limit of the technique is  $1.2 \times 10^{-11}$  M.

**Precision.** The relative standard deviation (RSD) for the determination carried out with in situ prepared carbon-fiber microelectrodes was established on the basis of five replicate measurements. Eight solutions containing  $5 \times 10^{-9}$ – $10^{-6}$  M  $\text{Pb}^{2+}$  were analyzed. The RSDs varied from 8.5 to 15.2% for the highest and the lowest analyte concentration, respectively.



**Figure 5.** Subtractive stripping voltammogram of  $5 \times 10^{-7}$  M  $\text{Pb}^{2+}$  and  $5 \times 10^{-7}$  M  $\text{Cd}^{2+}$  in a (1:1) 0.01 M acetic buffer obtained with a Hg-coated platinum microelectrode. Preconcentration was carried out for 60 s at  $-1.4$  V. Sweep rate was 2 V/s.

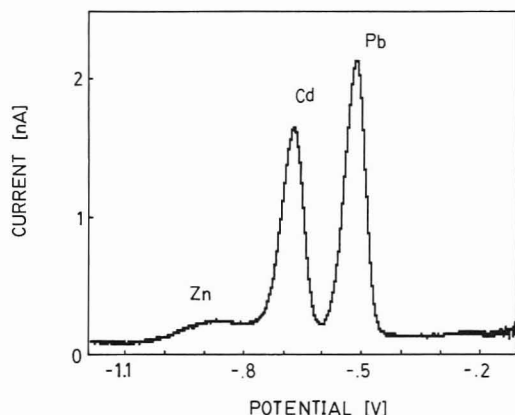
for similar electrodes under potentiometric stripping conditions (5) and have the same possible causes. The reproducibility of results obtained by using carbon-fiber microelectrodes with predeposited films is difficult to assess. In some series of measurements RSDs as low as 3% were found, whereas in others a significant drop of the electrode sensitivity during replicate measurements was observed. This decrease in sensitivity is most likely caused by a partial loss of the mercury coating. Since carbon is not wetted by mercury, mercury deposits on carbon fiber are very unstable. Mercury-film-carbon-fiber electrodes, formed in situ, are more reliable. The precision of determinations at such electrodes can probably be increased by using a multimicrodisk electrode made of several carbon fibers. Application of such electrodes for anodic stripping analysis was recently studied by Ciszewska and Stojek (13). In an ideal case the RSDs should be proportional to  $1/N^{1/2}$  (where  $N$  is the number of electrodes in the array). In practice however, the improvement may be much smaller because a possible, randomly occurring major malfunction of a single electrode (or electrodes) in the array could contribute significantly to the overall error. The use of multidisk electrodes having separate contacts for each disk, multichannel data acquisition, and adequate data processing routines ( $Q$  test) could solve these problems; however, such a solution would be both costly and technically difficult.

A significant improvement of precision can be achieved in a simple way by using microelectrodes prepared by a deposition of mercury on noble metals. Since most noble metals are wettable by Hg, such films are uniform and relatively stable. A high reproducibility of stripping voltammograms obtained by using such electrodes has been demonstrated (6).

A disadvantage of this approach is that noble metals dissolved

in mercury may interfere with the determination of many analytes. Platinum microelectrodes (10  $\mu\text{m}$  in diameter) coated with a 2- $\mu\text{m}$ -thick layer of mercury were briefly tested in this work. The RSD for replicate determination of  $\text{Pb}^{2+}$  and  $\text{Tl}^+$  at concentration  $10^{-7}$  M was 1.5% (set of seven measurements). However, the stripping peak of cadmium was poorly reproducible. Despite random variation in the peak height, the following trends were observed: (i) the Cd peak was always smaller at new electrodes than at electrodes used extensively in stripping experiments and (ii) simultaneous preconcentration of  $\text{Cd}^{2+}$  and  $\text{Zn}^{2+}$  always caused an increase of the Cd peak (Figures 5 and 6). Probably Cd reacts with platinum (or with impurities present in platinum) in the Hg layer or at the interface between the support metal and mercury. Zinc and possibly other metals inhibit this reaction. This is quite likely because Zn, Cu, In, and Sn inhibit disso-





**Figure 6.** Subtractive stripping voltammogram of Cd and Pb obtained with a Hg-coated platinum microelectrode. Conditions are the same as in Figure 5 except that  $5 \times 10^{-6}$  M  $\text{Zn}^{2+}$  was added to the analyzed solution.

Pt/Hg microelectrodes may become an important tool in stripping analysis. This, however, will require more fundamental studies in the area of thermodynamics and kinetics of processes occurring in amalgams.

## LITERATURE CITED

- (1) Granell, A.; Jagner, D.; Josefson, M. *Anal. Chem.* **1980**, *52*, 2220-2223.
- (2) Wojciechowski, M.; Go, W.; Osteryoung, J. *Anal. Chem.* **1985**, *57*, 155-158.
- (3) Wang, J.; Dewald, D. H. *Anal. Chem.* **1984**, *56*, 156-159.
- (4) Schulze, G.; Frenzel, W. *Anal. Chim. Acta* **1984**, *159*, 95-103.
- (5) Baranski, A. S.; Quon, H. *Anal. Chem.* **1986**, *58*, 407-412.
- (6) Wehmeyer, K. R.; Wightman, R. M. *Anal. Chem.* **1985**, *57*, 1989-1993.
- (7) Shoup, D.; Szabo, A. J. *Electroanal. Chem. Interfacial Electrochem.* **1982**, *140*, 237-245.
- (8) Aoki, K.; Osteryoung, J. J. *Electroanal. Chem. Interfacial Electrochem.* **1984**, *160*, 335-339.
- (9) Aoki, K.; Koji, A.; Koichi, T.; Hiroaki, M.; Osteryoung, J. J. *Electroanal. Chem. Interfacial Electrochem.* **1984**, *171*, 219-230.
- (10) Baranski, A. S. *J. Electrochem. Soc.* **1986**, *133*, 93-97.
- (11) Penczek, M.; Stojek, Z. J. *Electroanal. Chem. Interfacial Electrochem.* **1985**, *191*, 91-100.
- (12) Stojek, Z.; Kublik, Z. *Chem. Anal. (Warsaw)* **1985**, *30*, 363-368.
- (13) Ciszowska, M.; Stojek, Z. J. *Electroanal. Chem. Interfacial Electrochem.* **1985**, *191*, 101-110.
- (14) Galus, Z. *CRC Crit. Rev. Anal. Chem.* **1974**, *4*, 359-422.

RECEIVED for review June 18, 1986. Accepted October 1, 1986. This work was supported by the Natural Sciences and Engineering Research Council of Canada (NSERC) through the operating grant.

# Electrochemical Determination of Sulfur Dioxide in Air Samples in a Closed-Loop Flow Injection System

Angel Ríos, M. D. Luque de Castro, and Miguel Valcárcel\*

Departamento de Química Analítica, Facultad de Ciencias, Universidad de Córdoba, Córdoba, Spain

Horacio A. Mottola\*

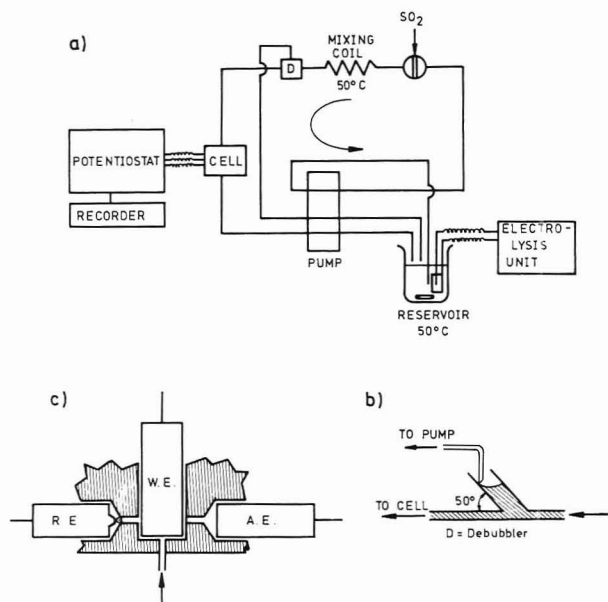
Department of Chemistry, Oklahoma State University, Stillwater, Oklahoma 74078-0447

$\text{SO}_2(\text{g})$  in air samples is amperometrically determined in a closed-loop flow injection system by direct intercalation of the air sample into a carrier solution containing the binuclear form of the iron(III) complex with 1,10-phenanthroline acting as a regenerable chemical probe. The extent of reduction to the mononuclear iron(II) complex, ferroin, by reaction at the gas/liquid interface is amperometrically monitored with a three-electrode system at an applied potential of 0.964 V vs. Ag/AgCl reference electrode (working electrode, carbon paste). The ferroin produced in the reduction process is electrochemically oxidized back to the binuclear iron(III) complex permitting the implementation of a closed-loop system with regeneration of the main reagent. By application of a continuous-flow/stopped-flow operation,  $\text{SO}_2(\text{g})$  can be determined in the range of 0.3-14.0 ppm (v/v) with relative standard deviations of about 3% (11 replicas) and at a rate of 25 samples per hour. By pretreatment of the carbon paste electrode with a surfactant solution, the same limit of detection can be achieved without need for stopping the sample plug, thus increasing the number of samples that can be determined per hour to 35.

Analytical methodologies applied to environmental problems requiring the manipulation of gaseous samples are

marred by the requirement of complicated procedures and complex instrumentation (1). Unsegmented continuous-flow sample processing (e.g., flow injection analysis) has permitted the implementation of simplified procedures and sample handling situations of interest in environmental analysis of water and soil samples (2) as well as the determination of gaseous species taking advantage of chemical reactions at gas/solid and gas/liquid interfaces (3, 4).

The work reported here was aimed at evaluating electrochemical detection using a configuration similar to one reported earlier (4). The redox couple constituted by the mononuclear complex of iron(II) and the binuclear complex of iron(III) with 1,10-phenanthroline is used as a reversible chemical probe. The gaseous species reduces the iron(III) complex to iron(II) [the organic moiety remaining unaffected] and the extent of conversion, proportional to the concentration of  $\text{SO}_2$  in the sample, is amperometrically monitored at a carbon paste working electrode. A closed-loop continuous-flow system is used for sample/reagent transport; this system incorporates an electrolysis unit in the loop for the conversion of the ferroin form to the binuclear iron(III) form. Electrochemical detection affords competitive limits of detection without the need for preconcentration (e.g., by a microinjector (4)) for direct determination in samples of power plant plume and for industrial hygiene measurements. Direct measurement in ambient air samples is not possible since limits of detection at the parts-per-billion (v/v) level are



**Figure 1.** (a) Closed-loop configuration for amperometric determination of  $\text{SO}_2(\text{aq})$  and  $\text{SO}_2(\text{g})$ : peristaltic pump, Minipuls-2 (Gilson Medical Electronics, Inc., Middleton, WI); injection valve, Tecator L100-1 (Tecator, Inc., Herndon, VA). (b) Debubbler. (c) Details of amperometric flow cell.

required. It should be mentioned here that continuous coulometric analyzers for  $\text{SO}_2$  in ambient air samples have been described (5). The sensitivity of the method proposed here can be improved by a stopped-flow/continuous-flow operation in which the reacting sample plug is stopped in a mixing/reaction coil located between the points of sample intercalation and reaction product detection. The same effect, and an increase in the number of samples processed per hour, is achieved by a surfactant (Triton X-100) pretreatment of the carbon paste surface used for detection.

## EXPERIMENTAL SECTION

**Reagents and Solutions.** The recirculated carrier solution (100 mL in total volume) of di- $\mu$ -hydroxy-bis[bis(1,10-phenanthroline)]iron(III), i.e., the binuclear complex of iron(III), was prepared by electrolytic oxidation of a ferroin solution composed of 4.0 mL of a 0.025 M solution of ferroin (G. F. Smith Chemical Co., Columbus, OH) and 0.337 g of 1,10-phenanthroline (Merck, AR grade), in about 96 mL of acetate buffer of pH 4.50 and 0.20 total acetate molarity and 1.0 M in KCl. Electrolytic conversion was accomplished as reported earlier (4).

The solutions of  $\text{SO}_2(\text{g})$  in air were prepared from compressed  $\text{SO}_2(\text{g})$  and were standardized by reaction with iodine (6). Aqueous solutions of sodium sulfite (Merck, AR grade) were prepared in acetate buffer solutions of pH 4.50.

**Apparatus.** A Metrohm E-506 potentiostat with built-in recording system was used through this work. The amperometric detection was accomplished at a Metrohm E 1096 cell with carbon paste electrode as working electrode, a silver/silver chloride reference electrode, and a glassy carbon electrode as counter (auxiliary) electrode.

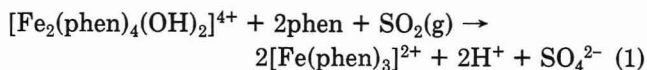
The carbon pastes were prepared by thorough mixing of UCP-1-M graphite powder from Ultra Carbon (Bay City, MI) with hexadecane (Aldrich Chemical Co., Milwaukee, WI) and/or high-vacuum grease from Dow Corning Corp. (Midland, MI).

**Operational Characteristics of the Hydrodynamic System.** Details of the closed-loop configuration adopted in this work are given in Figure 1. Once the binuclear species has been electrochemically generated, and during the operation of the instrumental setup, the electrolysis unit is kept in operation in order to effect the regeneration of the main reagent. Controlled-potential electrolysis in the reservoir solution was carried out maintaining the anode potential at +1.10 V with respect to a saturated calomel electrode and a MP-1026 potentiostat-regulated power supply operated in the potentiostat mode (Pacific Precision Instruments, Concord, CA). The anode was a platinum gauze cylinder 3.2 cm

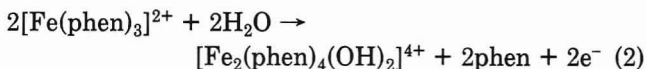
in diameter and 9.5 cm tall. A thin platinum wire (6 cm in length and 1 mm in diameter) was used as cathode. Return of the carrier solution to the reservoir was aided by a peristaltic pump to overcome the resistance to flow caused by the flow cell. Figure 1 shows a detailed sketch of the debubbler, a key component in the system. Flow conditions are adjusted such that the bulk of carrier solution flows through the closed-loop path and a minimal portion is allowed to partially fill the upper arm of the debubbler ("gas collecting arm", 6 mm i.d.) (4). A small tube connected to the peristaltic pump and located at a fixed position in the side arm of the debubbler removes any excess solution that "invades" this arm and returns it to the reservoir container. This detail is critical for a correct functioning of the system since the aim is an efficient elimination of gas bubbles and a minimization of dispersion. The flow rates for entering and leaving the debubbler were  $1.3\text{--}1.4\text{ mL}\cdot\text{min}^{-1}$  and  $1.2\text{ mL}\cdot\text{min}^{-1}$ , respectively.

## RESULTS AND DISCUSSION

The chemical basis for  $\text{SO}_2$  determination is an exploitation of the reversible redox couple of the complexes of mononuclear iron(II) and binuclear iron(III) with 1,10-phenanthroline. The binuclear iron(III) complex (7) acts as the main reagent and is reduced to the mononuclear ferroin by the  $\text{SO}_2$



Oxidative electrochemical regeneration occurs according to



The first of these two reactions takes place at the gas/liquid interface of the intercalated sample plug and carrier solution during transport to the detection unit; the second takes place at the anode of the electrolysis unit.

The electrochemical behavior of the complexes of iron(II) and iron(III) with 1,10-phenanthroline has been recently studied in detail (8). Hydrodynamic voltammograms indicated that a potential of +0.964 V vs. the silver/silver chloride electrode provides a satisfactory difference between the currents for reagent and product species. This potential does not permit, however, the use of sulfate or nitrate as supporting electrolyte.

**Determination of Aqueous  $\text{SO}_2$  Solutions.** Aqueous sulfur dioxide was determined by injection as  $\text{SO}_3^{2-}$  under the following optimum experimental conditions: flow rate,  $0.3\text{ mL}\cdot\text{min}^{-1}$ , length of reacting coil, 30 cm; sample volume,  $184\text{ }\mu\text{L}$ . Under these conditions,  $\text{SO}_2(\text{aq})$  can be determined by use of calibration curves obeying the following equation:

$$i(\mu\text{A}) = 0.314C_{\text{SO}_2(\text{aq})} - 0.087 \quad (3)$$

with  $C_{\text{SO}_2(\text{aq})}$  expressing the concentration in parts per million (v/v) of  $\text{SO}_2$ . A correlation coefficient of 0.9998 was observed. Good sensitivity ( $0.314\text{ }\mu\text{A}/\text{ppm}$ ) and a wide concentration range (2–80 ppm) were also observed. The detection limit (defined as the average of the blank signal plus three times its standard deviation) was found to be 1.6 ppm, and a typical standard deviation value (for 11 replicas) was  $\pm 1.9\%$  for 8.0 ppm  $\text{SO}_2(\text{aq})$ . The number of determinations per hour is limited to 25 because of the low flow rate required, which results in relatively large dispersion (e.g., the time for return to base line for 8.0 ppm is almost 1 min).

**Determinations with  $\text{SO}_2(\text{g})$ .** Injection of the gaseous sample was accomplished by adapting a septum to the injection valve allowing a syringe injection of the gaseous sample into the sample loop. Optimum conditions were found to be as follows: flow rate,  $1.2\text{ mL}\cdot\text{min}^{-1}$ ; length of reacting coil, 125 cm; sample volume,  $198\text{ }\mu\text{L}$ . The volume of sample injected is related to the amount of liquid in the side arm of the debubbler. In this case, a volume of 0.22 mL was chosen, which assured that the plug formed with the ferroin produced



**Table I. Dependence of Signal Height on the Sample Volume of SO<sub>2</sub>(g)-Containing Sample**

sample volume, $\mu\text{L}$	peak height, $\mu\text{A}$	sample volume, $\mu\text{L}$	peak height, $\mu\text{A}$
41.0	0.064	152.7	0.665
68.3	0.192	198.1	0.710
98.2	0.380	219.4	a

<sup>a</sup> Introduction of bubbles into the detection area was observed.

in the reaction is all transported to the detection point after elimination of the unreacted gas plug. Table I illustrates this point. Although the reaction coil is considerably larger than that used in the determination of SO<sub>2</sub>(aq), the higher flow rate compensates for the effect that such length has on dispersion. Under the reported conditions, SO<sub>2</sub>(g) can be determined from calibration curves with the following equation:

$$i(\mu\text{A}) = 0.369C_{\text{SO}_2(\text{g})} + 0.32 \quad (4)$$

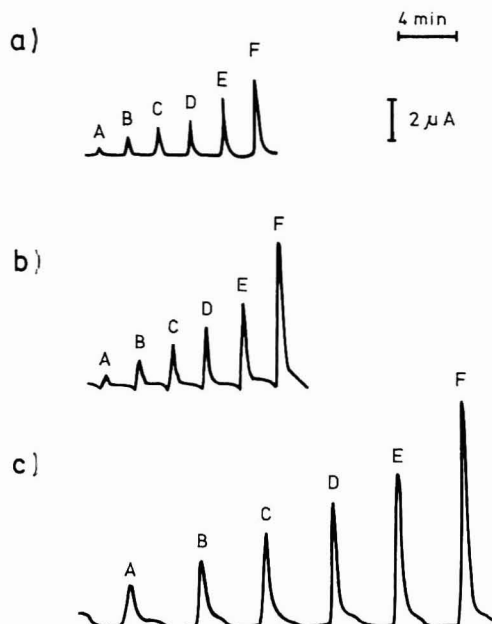
A correlation coefficient of 0.9988 was observed. The concentration of gas is given in parts per million (v/v). The method can be applied in the 0.5–16 ppm concentration range with a detection limit of 0.38 ppm and relative standard deviations of 2–3%. As many as 35 determinations can be made in 1 h with a sensitivity comparable to the one reported for SO<sub>2</sub>(aq). Better sensitivity can be obtained if a stopped-flow approach is adopted. Interruption of the flow is recommended when the reacting sample plug reaches the reaction coil. The effect of the length of time elapsed until the flow is reinitiated is illustrated in Figure 2. As this time increases, allowing more time for diffusion of SO<sub>2</sub> into the reacting layer, the signal height increases without detrimental effect on the dispersion. This effect is illustrated in a more quantitative manner in Table II. Stopping the flow for 60 s lowers the limit of detection to 0.3 ppm although the sample rate is decreased. After a stopping time of 30 s the working curves cross each other at about the same point (4.5 ppm) indicating that below about 4.5 ppm the optimum value for the stop time is 1 min but above such a concentration the optimum value is obtained at longer stop times (see Figure 4). This would indicate that proportionally the same extent of reaction requires shorter reaction times at low concentrations of SO<sub>2</sub>(g). The curves illustrated in Figure 3 resemble kinetic signals vs. time profiles. In actuality, the initial rate, defined as  $\Delta i(\mu\text{A})/\Delta t(\text{min})$ , follows the relationship

$$\text{initial rate} = 0.591C_{\text{SO}_2(\text{g})} + 0.572 \quad (5)$$

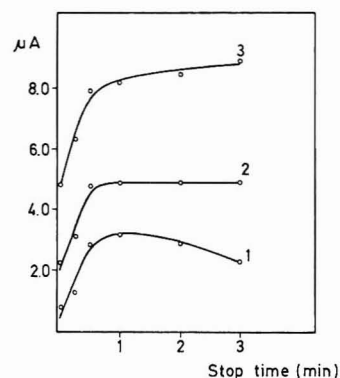
and the practical order with respect to analyte is 1.

The relative standard deviation for 11 replicas containing 5.0 ppm (v/v) of SO<sub>2</sub>(g) was found to be 3.2% with a stop time of 30 s allowing a sample rate of 25 injections per hour.

**Detection with Pretreated Graphite Surfaces of Different Paste Composition.** The resistance (conductivity) of carbon paste electrodes greatly depends on the paste composition and on the nature of the pasting oil. Treatment of



**Figure 2.** Typical flow injection profiles obtained at different concentrations of SO<sub>2</sub>(g) in ppm (v/v), (A) blank injection, (B) 1.2, (C) 2.3, (D) 4.2, (E) 6.9, and (F) 8.0, and at different stop times in the mixing/reaction coil, (a)  $t = 0$ , (b)  $t = 15$  s, and (c)  $t = 3$  min.



**Figure 3.** Current-stop time curves obtained with different concentrations of SO<sub>2</sub>(g) in ppm (v/v): (1) 1.2; (2) 4.5; (3) 10.5.

the surface after the smoothing process with a solution of a surfactant has been shown to considerably decrease such resistance and an increase in current is realized (9). In order to improve the limit of detection, sensitivity, and sample rate, a study of different paste compositions and the effect of surfactant treatment was made. The surfactant used was Triton X-100 (Sigma Chemical Co., St. Louis, MO) in 0.1% (w/v) aqueous solution. The pretreatment consisted of immersing the carbon paste surface in the surfactant solution for 15 or 45 min under stirring conditions.

Table III summarizes the observations collected with different pastes before and after treatment; comparison is based

**Table II. Typical Parameters in the Determination of SO<sub>2</sub>(g) Using the Stopped-Flow Approach and the Closed-Loop Continuous Flow System Described Here**

stop time, s	working curve equation $i(\mu\text{A}), [\text{SO}_2]$ in ppm (v/v)	corr coeff	limit of detection, ppm (v/v)	determination range, ppm (v/v)	sensitivity, $\mu\text{A}/\text{ppm}$
0	$i = 0.369[\text{SO}_2] + 0.32$	0.9988	0.38	0.5–16	0.369
15	$i = 0.553[\text{SO}_2] + 0.54$	0.9989	0.30	0.4–15	0.553
30	$i = 0.554[\text{SO}_2] + 2.25$	0.9990	0.36	0.4–15	0.554
60	$i = 0.557[\text{SO}_2] + 2.42$	0.9993	0.28	0.3–14	0.557
120	$i = 0.619[\text{SO}_2] + 2.03$	0.9986	0.28	0.3–14	0.619
180	$i = 0.698[\text{SO}_2] + 1.62$	0.9984	0.26	0.3–14	0.698

Table III. Performance of Carbon Paste Electrodes of Different Composition with and without Treatment with Surfactant<sup>a</sup>

paste	composition	treatment	calibration curve	limit of detection, ppm	determination range, ppm	sensitivity, $\mu\text{A/ppm}$
A	40% graphite	without treatment	$i = 0.032x + 0.3$	2.5	2.5–50	0.032
	30% hexadecane	15 min with Triton	$i = 0.043x + 0.4$	2.5	2.5–50	0.043
	30% grease	45 min with Triton	$i = 0.058x + 0.7$	2.5	2.5–45	0.058
B	50% graphite	without treatment	$i = 0.370x + 0.3$	0.4	0.5–16	0.370
	25% hexadecane	15 min with Triton	$i = 2.944x + 1.1$	0.4	0.8–14	2.944
	25% grease	45 min with Triton	$i = 5.763x - 1.5$	0.2	0.3–7	5.763
C	67% graphite	without treatment	$i = 1.454x - 4.5$	3.5	4–25	1.454
	16.5% hexadecane	15 min with Triton	$i = 3.114x - 3.4$	1.3	1.4–22	3.114
	16.5% grease	45 min with Triton	$i = 4.542x - 10.8$	2.6	2.7–18	4.542
D	67% graphite	without treatment	$i = 1.210x - 0.6$	1.2	1.5–50	1.210
	33% grease	15 min with Triton	$i = 2.110x - 2.1$	1.2	1.4–50	2.110
		45 min with Triton	$i = 0.556x + 3.2$	0.3	0.5–32	0.556
E	67% graphite	without treatment	$i = 0.867x - 2.5$	3.5	3.5–22	0.867
	33% hexadecane	15 min with Triton	$i = 8.800x - 14.8$	1.8	2.0–15	8.800
		45 min with Triton	$i = 3.984x - 8.2$	2.2	2.5–15	3.984

<sup>a</sup>Data extracted from calibration curves for  $\text{SO}_2(\text{g})$  determination.  $x = [\text{SO}_2(\text{g})]$ , in ppm. 67% graphite is the maximum that can be used and still have reasonable paste consistency.

on the values of detection limits, sensitivity, and determination range extracted from calibration curves. All the results correspond to determinations under continuous-flow conditions without stopping the reacting sample plug in the mixing/reaction coil.

The method sensitivity, as would be expected, improves with an increase in the percentage of carbon in the paste. Use of more than 67% carbon powder, however, becomes impractical because the resulting mixture is difficult to handle as a paste. Carbon percentages of 40% or less give calibration curves with very small slopes (low sensitivity).

Determination ranges are wide in general but slightly larger as the percent of graphite increases. The surfactant treatment considerably improves the detection limit and sensitivity for all paste compositions. Pastes A, B, and C (Table III) containing the three ingredients with a longer time of contact with the Triton X-100 solution improve the electrochemical performance of the surface. Such an effect can be clearly seen for paste B but is only slightly noticeable with paste A. Paste compositions D and E, with maximum percentage of carbon and a single pasting component, show maximum sensitivity with 15-min treatment; longer treatment times produced surfaces of lesser efficiency for electrochemical detection. Pastes D and E contain the minimum percent of pasting components. Since Triton X-100 decreased the percent of pasting component at the electrode/solution interface, alteration of the "optimum" percentage may be responsible for the deterioration of electrochemical detection.

From an analytical viewpoint it is of interest to achieve low limits of detection, high sensitivity, and wide calibration ranges. For comparative purpose, a parameter combining these three factors is defined here as

$$S' = [\text{sensitivity}] \frac{[\text{linear range of calibration curve}]}{[\text{limit of detection}]} \quad (6)$$

with units of  $\mu\text{A/ppm}$ , that is, the same units as sensitivity. Figure 4 shows how  $S'$  varies with paste composition and treatment procedure. Paste B after 45 min of treatment with surfactant seems to be the formulation to prefer for the electrochemical detection proposed here. This paste allows realizing good sensitivity ( $5.76 \mu\text{A/ppm}$ ), very competitive limit of detection (0.2 ppm of  $\text{SO}_2(\text{g})$ ), and an acceptable determination range (0.3–7 ppm). Since pretreatment allows operation at low limits of detection without stopped-flow operation, the number of samples per hour that can be pro-

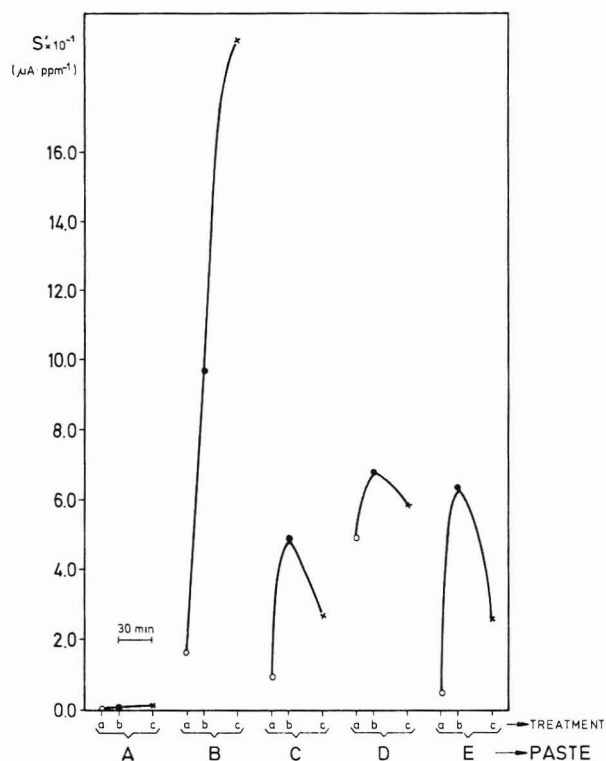


Figure 4. Plot of parameter  $S'$  (see text for definition) as a function of paste composition and electrode surface pretreatment: (a) untreated surface; (b) surface treated for 15 min with 0.1% (w/v) Triton X-100 aqueous solution; (c) surface treated for 45 min with 0.1% (w/v) Triton X-100 aqueous solution. As  $S'$  increases, sensitivity, limit of detection, and determination range are better from an analytical viewpoint. For paste composition see Table III.

cessed is improved to at least 35.

**Registry No.**  $\text{SO}_2$ , 7446-09-5;  $\text{H}_3\text{C}(\text{CH}_2)_{14}\text{CH}_3$ , 544-76-3; graphite, 7782-42-5; triton, 9083-53-8;  $[\text{Fe}_2(\text{phen})_4(\text{OH})_2]^{4+}$ , 21360-98-5.

#### LITERATURE CITED

- (1) Fox, D. L. *Anal. Chem.* **1985**, *57*, 223R–238R.
- (2) Lázaro, F.; Luque de Castro, M. D.; Valcárcel, M. *Analisis* **1985**, *13*, 147–159.
- (3) Ramasamy, S. M.; Jabbar, M. S. A.; Mottola, H. A. *Anal. Chem.* **1980**, *52*, 2062–2066.
- (4) Ramasamy, S. M.; Mottola, H. A. *Anal. Chem.* **1982**, *54*, 283–286.
- (5) *Sulfur in the Environment*; Nriagu, J., Ed.; Wiley: New York, 1978; Part I, Chapter 10.
- (6) Jacobs, M. B. *Analytical Chemistry of Industrial Poisons, Hazards and Solvents*, 2nd. ed.; Interscience: New York, 1949; pp 166–168.
- (7) Anderegg, G. *Helv. Chim. Acta* **1962**, *45*, 1643–1657.



- (8) Luque de Castro, M. D.; Valcárcel, M.; Albadilly, F. N.; Mottola, H. A. *J. Electroanal. Chem.*, in press.  
(9) Albadilly, F. N.; Mottola, H. A., *Anal. Chem.*, in press.

RECEIVED for review June 30, 1986. Accepted October 27,

1986. This work was part of Project No. 84-063 supported by the US-Spain Joint Committee for Scientific and Technological Cooperation. Such a support is gratefully acknowledged here.

## Characterization of Electrode Heterogeneity with Electrogenenerated Chemiluminescence

Royce C. Engstrom,\* Kirk W. Johnson,<sup>1</sup> and Scott DesJarlais

Department of Chemistry, University of South Dakota, Vermillion, South Dakota 57069

**Electrogenenerated chemiluminescence (ECL) was used to form images showing the distribution of electrochemical activity at microheterogeneous electrode surfaces. ECL was generated by the reaction of luminol, rubrene, or Ru(bpy)<sub>3</sub><sup>2+</sup> at carbon electrodes. Images of the luminescence patterns were recorded photographically after sufficient magnification to show the location, size, and shape of individual active regions. Epoxy-impregnated reticulated vitreous carbon electrodes served as test electrodes, since they possess active regions that are visible under magnification and external illumination. Quantitative information obtained from the photographs included the percent active area of the electrode surface and histograms showing the distribution of active site dimensions. Those parameters were also evaluated on a carbon paste electrode.**

Electrodes with microscopically heterogeneous surfaces are frequently used by electroanalytical chemists in the form of composite electrodes. For example, the carbon paste electrode, prepared by mixing graphite powder with an organic binder such as mineral oil, has been used for years (1, 2). More recently, carbon composites have been prepared with epoxy (3-6) or Kel-F (7-10) as the binder. The surfaces of electrodes prepared from composite materials contain regions of electrochemically active graphite as well as regions of the inactive binder, creating a heterogeneous surface with regard to electron transfer. A heterogeneous electrode with well-defined and visible active regions has been prepared from reticulated vitreous carbon with the void spaces filled with epoxy, and the surface sanded and polished to a smooth finish (11). Besides deliberate electrode design, microscopic heterogeneity has been reported as a result of adsorption processes (12, 13) and the anodization of graphite (14). Microscopic heterogeneity has several implications to electroanalytical chemistry. First, the active area of a heterogeneous electrode is obviously less than that of a uniformly active electrode of the same geometric area. Second, the dimensional relationships between the active and inactive regions may result in significant nonlinear diffusion. Third, a signal-to-noise advantage has been demonstrated (9, 10).

Information about heterogeneity on electrode surfaces has come from two general categories of techniques, those based on measurement of the total current through an electrode with the application of mathematical modeling, and those based

on microscopic probing of the electrode surface or the solution immediately adjacent to the electrode surface. In the first category, a number of theoretical treatments have appeared that attempt to relate the degree of coverage and dimensions of active and inactive regions to the results of various electrochemical experiments (15-22). Those theories have been used to estimate the dimensions of active and inactive regions on carbon paste electrodes (15) anodized graphite electrodes (14) and Kel-F graphite electrodes (9, 10). The theories generally rely on the assumption that active regions have uniform size, shape, and distribution. As a result, the information obtained from the use of those theories presents an average description of the electrode surface, without information regarding the distribution of active site dimensions or geometry. In the second category of techniques, "maps" of electrode surface activity have been generated with the use of various types of microprobes. Isaacs and co-workers have located centers of corrosion on metal surfaces with the use of scanning microreference electrodes or microreference-auxiliary combinations (23-25). We have adapted a physiological technique known as iontophoresis to the spatial resolution of electrode activity and have applied it to studying the distribution of activity on graphite-epoxy surfaces (26, 27). We have also used carbon fiber or platinum ultramicroelectrodes to detect species generated at microscopically localized regions of another electrode surface, with the two electrodes being part of a bipotentiostat circuit (28). In all of these microprobe-based techniques, the spatial resolution that has been achieved has been of the order of tens of micrometers. Lui and co-workers have obtained substantially better resolution in an adaptation of scanning electron-tunneling microscopy, carried out in solution with the probe being a microelectrode that was electropolished to submicrometer dimensions (29). Butler has reported on a photoelectrochemical imaging technique, in which photocurrents were induced on microscopically localized regions of semiconductor electrode surfaces with a focused laser (30). The position of the electrode surface with respect to the laser beam was controlled with a stepper-motor driven stage in 1- $\mu$ m increments, so that photocurrents were plotted as a function of position or displayed as a video image (31) with a resolution of 3  $\mu$ m. Rubinstein located nonconducting inclusions on metal surfaces by electrodeposition of a polymer film on the surface. Inclusions of at least 30  $\mu$ m diameter showed up as regions devoid of the polymer coating (32).

We report here a technique for obtaining an image of surface electrochemical activity based on the observation of electrogenerated chemiluminescence (ECL), a phenomenon that has been described extensively in the literature (33, 34,

<sup>1</sup> Present address: Eli Lilly Co., Indianapolis, IN.

and references therein). In this experiment, the potential of the electrode being studied is stepped to a value that initiates the ECL reaction sequence. The light generated by the reaction originates at the electrochemically active regions of the electrode only, forming an image of activity distribution with the location, size, and geometry of individual active regions clearly visible. After magnification the image is recorded photographically. This technique has several important features: information gained is related directly to electrochemical activity and not structure; by careful choice of the ECL system, spatial resolution can be high since it is determined by the distance the excited species diffuses before releasing a photon; a relatively large fraction of the electrode or the entire electrode can be observed in a single experiment; the results are largely unaffected by surface topography. In this paper, the ECL imaging technique was characterized with model heterogeneous electrodes prepared from reticulated vitreous carbon and then used to image a carbon-paste surface.

## EXPERIMENTAL SECTION

**Apparatus.** In experiments where photographic images of the ECL reactions were recorded, the electrode being studied was mounted in a cell machined from cast acrylic so that the electrode surface faced upward. The surface was covered to a depth of approximately 2 mm with a solution containing the compounds required for the ECL reaction (see Results). The tip of a silver-silver chloride reference electrode and a platinum wire auxiliary electrode were immersed in the solution. The cell potential was applied with a conventional three-electrode potentiostat, usually a Bioanalytical Systems Model CVIA (West Lafayette, IN). Photographic images were recorded with a Nikon N2000 camera attached to a bellows and a 55-mm "micro" lens. The entire apparatus was kept in a darkroom, so that only the light generated by the ECL reaction reached the film. The equipment was mounted on a vibrationally isolated table so the pictures were not blurred by room vibrations.

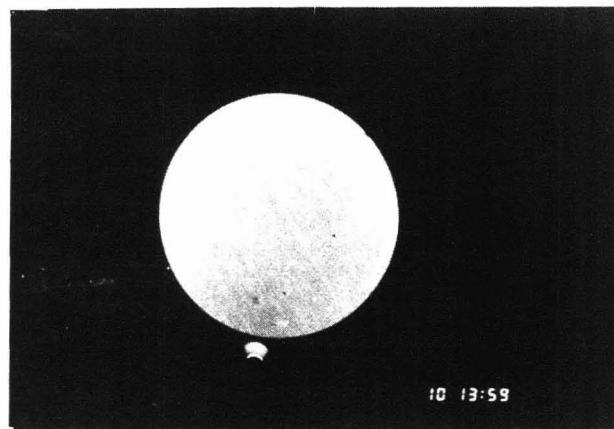
**Electrodes.** Glassy carbon electrodes were used as examples of uniformly active surfaces and were obtained from Bicanalytical Systems. The epoxy-impregnated reticulated vitreous carbon electrode (RVC-epoxy) used as a model heterogeneous electrode was prepared as described in the literature (11, 26). Carbon paste electrodes were prepared by mixing graphite powder with squalane in a 2:1 weight ratio, packing some of the paste into a length of 5 mm diameter glass tubing, and inserting a piece of copper wire to make electrical contact with the paste. The surfaces of the carbon paste electrodes were made smooth by rubbing on a manila folder.

**Reagents.** Luminol (5-amino-2,3-dihydro-1,4-phthalazinedione) was obtained from Eastman Kodak (Rochester, NY); rubrene (5,6,11,12-tetraphenylnaphthacene) was obtained from Aldrich (Milwaukee, WI); tris(2,2'-bipyridyl)ruthenium(II) chloride was obtained from Strem Chemicals, Inc. (Newburyport, MA). All of the above were used as received. All supporting electrolytes and buffers were prepared from reagent grade chemicals without further purification.

**Procedure.** Based on the initial investigations of the three ECL systems, the luminol system was used to obtain the images presented here. A solution containing 0.20 mM luminol, 0.10 mM hydrogen peroxide, and 0.05 M sodium borate, adjusted to pH 10.0, was placed in the cell. The lights were turned off in the darkroom, and the camera shutter was opened. A potential of 0.6 V vs. SCE was then applied to the working electrode, resulting in visible luminescence. After a predetermined length of time, the potential to the cell was turned off and the camera shutter closed. Usually, several exposure durations were taken for each experiment in the range of 5–15 min.

## RESULTS AND DISCUSSION

**Initial Characterization of ECL Systems.** Three ECL systems were evaluated by use of glassy carbon electrodes to determine which was most suitable for the characterization of electrode heterogeneity. The important criterion was to find a system that gave an emission intensity under nonconvective conditions that would be strong enough to photograph.



**Figure 1.** ECL image of 3 mm diameter glassy carbon electrode at 0.6 V vs. SCE in a luminol solution (see text for details); magnification, approximately 10X.

A solution of 1.0 mM  $\text{Ru}(\text{bpy})_3^{2+}$ , 0.10 M sodium oxalate, and 0.1 M acetate buffer at pH 6.0 yielded a faint orange luminescence at an applied potential of 0.95 V. The luminescence in this system has been reported to result from the oxidation of  $\text{Ru}(\text{bpy})_3^{2+}$  to  $\text{Ru}(\text{bpy})_3^{3+}$  at the electrode, followed by chemical reduction of  $\text{Ru}(\text{bpy})_3^{3+}$  to  $\text{Ru}(\text{bpy})_3^{2+}$  by the radical anion,  $\text{CO}_2^{\cdot-}$ , and the subsequent annihilation reaction between  $\text{Ru}(\text{bpy})_3^{3+}$  and  $\text{Ru}(\text{bpy})_3^{2+}$  to produce  $\text{Ru}(\text{bpy})_3^{2+}$  in the excited state (35–37). In our hands, the intensity generated by this system faded rapidly to a level that was not usable, possibly due to fouling of the electrode.

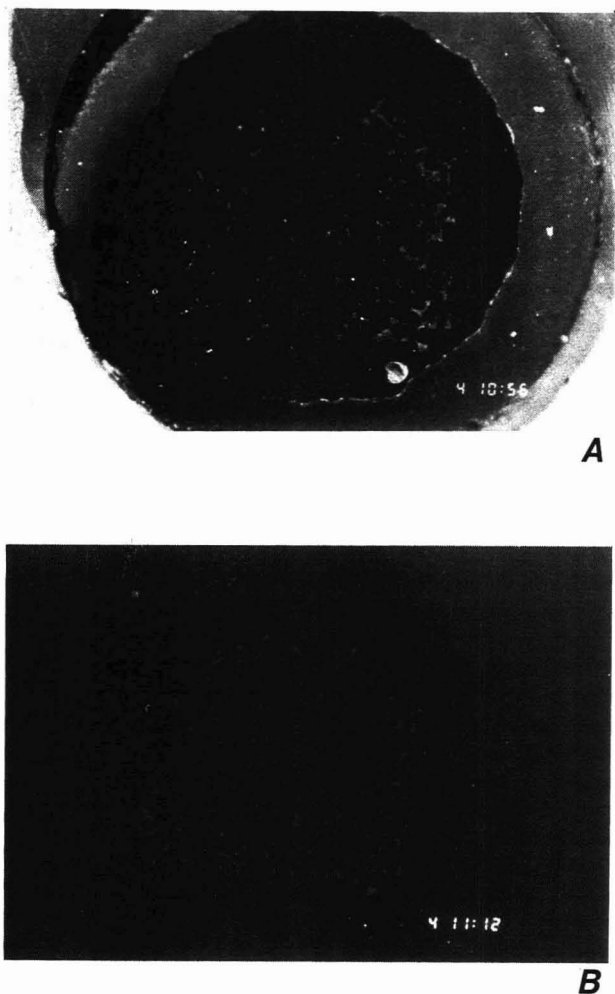
A solution of 0.43 mM rubrene, 0.41 mM benzoyl peroxide, and 0.1 M tetraethylammonium perchlorate, in dimethylformamide emitted a yellow light intense enough to be seen with the room lights on at an applied potential of -1.4 V. Deaeration of the solution was necessary to observe the emission. In this system, luminescence arises from the cathodic production of the anion radical of rubrene, which is then chemically oxidized by the presence of benzoyl peroxide, producing an excited state of rubrene (38). While the rubrene system gave satisfactory results, it was not used for the work reported here since the nonaqueous solvent was not compatible with carbon paste electrodes.

The solution of luminol described in the Experimental Section yielded a moderately intense blue luminescence at an applied potential of 0.6 V. The luminol reaction has been studied fairly extensively (39–42) and the luminescence is thought to result from the oxidation of luminol to a radical, which reacts with a superoxide radical to form 3-amino-phthalate in an excited state. Of the three systems, the luminol system was chosen for the work reported here.

Figure 1 shows a photograph of an ECL image generated at a 3 mm diameter glassy carbon electrode. The electrode was bathed in a solution containing the ingredients of the luminol ECL system, at an applied potential of 0.6 V vs. SCE. As seen in the figure, the light intensity was quite uniform over the entire surface, indicating a uniformly active electrode as expected for highly polished glassy carbon. The small region of light below the large circle is a reflection from a bubble next to the electrode.

**Reticulated Vitreous Carbon Electrodes.** To characterize the ability of ECL to provide information about electrode heterogeneity, a model electrode system was needed that had well-defined active and inactive regions that were visible under magnification. Figure 2A shows a photograph of an RVC-epoxy electrode under external illumination. In that photograph, the light-colored regions are the active regions of carbon in the darker epoxy matrix. As pointed out by Sleszynski et al. (11), the RVC-epoxy surface contains an array of irregularly shaped and sized active regions which tend to

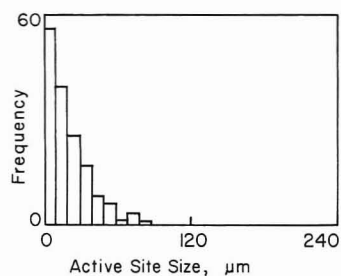




**Figure 2.** Epoxy-impregnated reticulated vitreous carbon electrode: (a) external illumination of surface, (b) ECL image. Conditions are given in Figure 1.

have a greater length than width, the former typically measuring in the hundreds of micrometers and the latter in tens of micrometers. In the presence of the luminol solution and at an applied potential of 0.6 V vs. SCE, the active regions generated chemiluminescence. Figure 2B shows a photograph of the ECL pattern of the same electrode as in Figure 2A and under the same magnification. Upon careful inspection, it can be seen that the luminescence image faithfully reproduces the pattern of active regions of the externally illuminated surface. Each active region on the electrode surface is represented in the ECL image by a region of exposure having the same size, shape, and relative position as the active region. The ECL photograph was taken with a 5-min exposure, over which time the products of the electrochemical reaction would diffuse a considerable distance. However, at the magnification level used here the light originates only at the active regions, indicating that either the duration of the ECL reaction sequence is short compared to the time needed for diffusion to occur over a detectable distance or that the emitting species is surface bound to the carbon. The latter was ruled out by gently agitating the solution and observing that the image blurred as the emitting species was convectively removed from the active regions.

Of interest in an electroanalytical sense is the fraction of the geometric electrode area that is electrochemically active. On the RVC electrode, that fraction was evaluated by enlarging the image through projection onto a sheet of graph paper. Each point of intersection of the graph paper was inspected to see if it fell within or outside a region of activity. The percent active area was calculated by dividing the number



**Figure 3.** Histogram of active region dimensions for an RVC-epoxy electrode taken from ECL image.

of intersections within active regions by the total number of intersections inspected. The total number of intersections used was 600, and the areas obtained by this method agreed within 1% of areas determined by a more tedious "cut-and-weigh" method. (In the latter, regions of exposure on the enlarged image were traced onto a sheet of preweighed paper and cut out with a scalpel. The residual paper was weighed and the percent active area calculated from the weight difference.) The active area of the RVC electrode as determined from the externally illuminated picture (Figure 2A) was 26.7% of the total area. From the ECL picture (Figure 2B) the active area was found to be 21.3%. The discrepancy suggests that not all of the carbon that is visible on the RVC surface is electrochemically active. Perhaps during fabrication or polishing the edges of the carbon regions become covered with a thin layer of epoxy that blocks the surface.

Another quantitative descriptor of the electrode surface is concerned with the dimensions of the active regions. Indeed, one of the primary reasons for development of the technique was to provide detailed information about heterogeneous surfaces to replace the assumptions about active region size and shape used in existing theories of heterogeneous surfaces. While there could be several descriptors of active site size (linear dimension, area, "boundary density"), it is not certain which is the most appropriate with respect to electrochemical behavior. We have chosen to use a linear dimension to characterize the surface. A transparent grid was placed over the projected ECL image, with 12 evenly spaced vertical and horizontal lines. The distances between the point where a line entered a region of ECL exposure and where it left the same region was measured. Every line was used, and each line intersected a number of exposed regions. The distances were plotted in the form of a histogram which is shown in Figure 3 for an RVC-epoxy electrode.

**Carbon-Paste Electrodes.** Electrodes prepared by mixing graphite powder with an inert binder possess electrochemically active regions of graphite and inactive regions of binder. Visual observation of the composite electrode surface, even with a microscope, does not allow the identification of active and inactive regions as with the RVC-epoxy electrodes. The ECL technique provides a visual image of the surface activity on a carbon paste electrode as shown in Figure 4. The active regions comprise 46.9% of the geometric area, determined by using the procedure described above for the RVC-epoxy electrode. The histogram of active region dimensions is shown in Figure 5, which shows that most active region dimensions fall under 100  $\mu\text{m}$ , with a few larger than that. A detailed study of the relationship between bulk composition, surface activity distribution, and electrochemical behavior of carbon-paste electrodes is in progress.

Detailed information about heterogeneity such as that generated by the ECL technique should help describe the behavior of composite (and other heterogeneous) electrodes in electroanalytical situations. For example, histograms of active region size combined with histograms of distance between active regions should make it possible to define the time

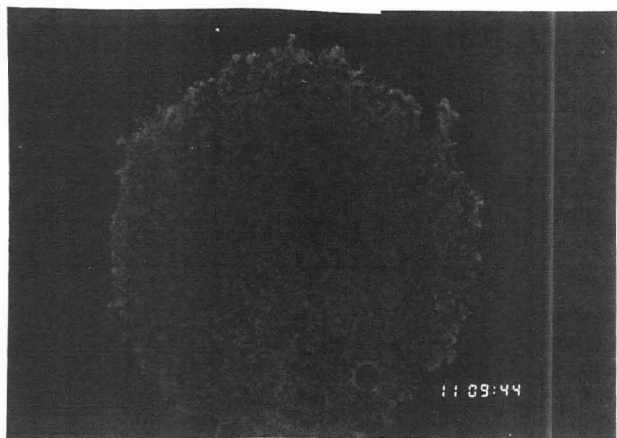


Figure 4. ECL image of a carbon paste electrode. Conditions are given in Figure 1.

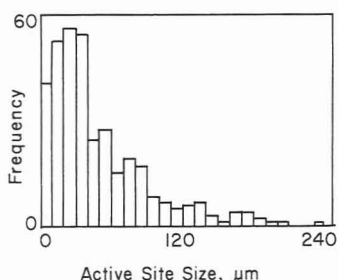


Figure 5. Histogram of active region dimensions for a carbon-paste electrode.

at which the electrode makes the transition from behaving as an array of independent microelectrodes to an electrode that appears to be uniformly active.

#### ACKNOWLEDGMENT

We wish to thank Simon Spicer and Elise Sudbeck for help with the photography and Timothy Nieman for his helpful discussions in the initial phases of the work.

#### LITERATURE CITED

- (1) Adams, R. N. *Anal. Chem.* **1958**, *30*, 1576.
- (2) Adams, R. N. *Electrochemistry at Solid Electrodes*; Marcel Dekker: New York, 1969; pp 26, 280.
- (3) Swofford, H. S.; Carman, R. L. *Anal. Chem.* **1966**, *38*, 966.
- (4) Anderson, J. E.; Tallman, D. E. *Anal. Chem.* **1976**, *48*, 209.

- (5) Cheng, H. Y.; Falat, L. *Anal. Chem.* **1982**, *54*, 2111.
- (6) Cheng, H. Y.; Falat, L. *J. Electroanal. Chem.* **1983**, *157*, 393.
- (7) Anderson, J. E.; Tallman, D. E.; Chesney, D. J.; Anderson, J. L. *Anal. Chem.* **1978**, *50*, 1051.
- (8) Weisshaar, D. E.; Tallman, D. E.; Anderson, J. L. *Anal. Chem.* **1981**, *53*, 1809.
- (9) Weisshaar, D. E.; Tallman, D. E. *Anal. Chem.* **1983**, *55*, 1146.
- (10) Tallman, D. E.; Weisshaar, D. E. *J. Liq. Chromatogr.* **1983**, *6*, 2157.
- (11) Sleszynski, N.; Osteryoung, J.; Carter, M. *Anal. Chem.* **1984**, *56*, 130.
- (12) Lindemann, J.; Landsberg, R. *J. Electroanal. Chem.* **1971**, *31*, 107.
- (13) Povarov, Y.; Lukovstev, P. *Electrochim. Acta* **1973**, *18*, 13.
- (14) Scheller, F.; Landsberg, R.; Wolf, H. *Electrochim. Acta* **1970**, *15*, 525.
- (15) Landsberg, R.; Thiele, R. *Electrochim. Acta* **1966**, *11*, 1243.
- (16) Scheller, F.; Muller, S.; Landsberg, R.; Spitzer, H. *J. Electroanal. Chem.* **1968**, *19*, 187.
- (17) Levart, E.; Schumann, D.; Contamin, O.; Etman, M. *J. Electroanal. Chem.* **1976**, *70*, 117.
- (18) Gueshi, T.; Tokuda, K.; Matsuda, H. *J. Electroanal. Chem.* **1978**, *89*, 747.
- (19) Gueshi, T.; Tokuda, K.; Matsuda, H. *J. Electroanal. Chem.* **1979**, *101*, 29.
- (20) Reller, H.; Kirowa-Eisner, E.; Gileadi, E. *J. Electroanal. Chem.* **1982**, *138*, 65.
- (21) Amatore, C.; Saveant, J. M.; Tessier, D. *J. Electroanal. Chem.* **1983**, *147*, 39.
- (22) Contamin, O.; Levart, E. *J. Electroanal. Chem.* **1982**, *136*, 259.
- (23) Isaacs, H. S.; Kissel, G. *J. Electrochem. Soc.* **1972**, *119*, 1628.
- (24) Isaacs, H. S.; Kendig, M. W. *Corrosion* **1980**, *36*, 269.
- (25) Isaacs, H. S. *ASTM Spec. Tech. Publ.* **1972**, No. 516, 158.
- (26) Engstrom, R. C. *Anal. Chem.* **1984**, *56*, 890.
- (27) Engstrom, R. C.; Weber, M.; Werth, J. *Anal. Chem.* **1985**, *57*, 933.
- (28) Engstrom, R. C.; Weber, M.; Wunder, D. J.; Burgess, R.; Winkvist, S. *Anal. Chem.* **1986**, *58*, 844.
- (29) Lui, H.-Y.; Fan, F.-R. F.; Lin, C. W.; Bard, A. J. *J. Am. Chem. Soc.* **1986**, *108*, 3838.
- (30) Butler, M. A. *J. Electrochem. Soc.* **1983**, *130*, 2358.
- (31) Butler, M. A. *J. Electrochem. Soc.* **1984**, *131*, 2185.
- (32) Rubinstein, I. *J. Appl. Electrochem.* **1983**, *13*, 689.
- (33) Bard, A. J.; Faulkner, L. R. *Electrochemical Methods*; Wiley: New York, 1980; p 621.
- (34) Tachikawa, H.; Faulkner, L. R. *Laboratory Techniques in Electroanalytical Chemistry*; Kissinger, P. T., Heineman, W. R., Eds.; Marcel Dekker: New York, 1984; p 660.
- (35) Rubinstein, I.; Martin, C. R.; Bard, A. J. *Anal. Chem.* **1983**, *55*, 1580.
- (36) Ege, D.; Becker, W. G.; Bard, A. J. *Anal. Chem.* **1984**, *56*, 2413.
- (37) Rubinstein, I.; Bard, A. J. *J. Am. Chem. Soc.* **1981**, *103*, 512.
- (38) Akins, D. L.; Birke, R. L. *Chem. Phys. Lett.* **1974**, *29*, 428.
- (39) Haapakka, K. E.; Kankare, J. J. *Anal. Chim. Acta* **1982**, *138*, 263.
- (40) Merenyi, G.; Lind, J. S. *J. Am. Chem. Soc.* **1980**, *102*, 5830.
- (41) Epstein, B.; Kuwana, T. *Photochem. Photobiol.* **1967**, *6*, 605.
- (42) Kuwana, T.; Epstein, B.; Seo, E. T. *J. Am. Chem. Soc.* **1964**, *67*, 2243.

RECEIVED for review August 25, 1986. Accepted October 27, 1986. This work was supported in part by the National Science Foundation, Grant No. CHE-8411000. K.W.J. received a Grant-in-Aid of Research from Sigma Xi, the Scientific Research Society.



# Dielectric Characterization of Binary Solvents Containing Acetonitrile

Orland W. Kolling

Chemistry Department, Southwestern College, Winfield, Kansas 67156

**For electrochemical solvents containing acetonitrile (AN) paired with a cosolvent having either a lower or higher dielectric constant ( $\epsilon$ ), the trend in  $\epsilon_m$  vs. mole fraction is usually nonlinear at 25 °C. Maxima or minima occur in the excess function ( $\Delta\epsilon$ ) among representative systems and the magnitude of that deviation with respect to pure AN is governed by the dipolarity, polarizability, and any hydrogen bonding tendency from the added cosolvent. The empirical patterns in dielectric behavior for 10 solvent systems including AN-polar aprotic and AN-hydrogen bond donor pairs conform to rational correlation functions for  $\epsilon_m = f(X_1)$  over the complete mole fraction range.**

Even though acetonitrile (AN) has been explored as a nonaqueous solvent during only the past 35 years, it is now as important in analytical chemistry as other common Lewis-base solvents including dimethyl sulfoxide ( $\text{Me}_2\text{SO}$ ) and dimethylformamide. Although AN differs from the latter by a very weak hydrogen bond donor (HBD) tendency, the HBD acidity of acetonitrile is largely overshadowed by its dipolar and aprotic characteristics as exemplified by its extremely low autoionization ( $K_i \approx 10^{-33}$ ) and its dipole moment of 3.92 D (1). Contemporary applications that are representative of acetonitrile as a solvent include the evaluation of medium effects on the kinetics of solvent assisted nucleophilic substitution reactions (2) and the voltammetric behavior of alkanes at ultramicroelectrodes (3). Although ion pair association by electrolytes in AN is the norm because of an intermediate value for the dielectric constant of the solvent, several investigators have demonstrated that associative complications involving the supporting electrolyte and the electrogenerated ionic intermediates can be eliminated by the use of the ultramicroelectrodes in the presence of little or no added supporting electrolyte (4, 5). Thus, there may well be potentially significant extensions of such electrochemical techniques to cosolvents containing AN that are "tunable" in terms of continuously increasing or decreasing the dielectric constant from 36.0 (pure AN) upon adding a more or less dipolar cosolvent.

The static dielectric constant ( $\epsilon$ ) remains a key descriptor of polarity in all solvent continuum models for medium effects upon electrolytic equilibria, ionic solvation and solubility, and ionic mechanisms of reaction. However, as one reviews the literature data on binary solvents, clearly the trend in  $\epsilon$  with changing composition of the mixture is rarely an exact linear function for most cosolvent systems (6, 7), and AN-cosolvent systems do not seem to be exceptions to that pattern (8-11). On the other hand, the earlier dielectric constant data sets for acetonitrile-containing solvent pairs (8-11) are typified by too restricted a mole fraction range for their mixtures and by being too limited in the types of cosolvents represented. Within these limitations it is not possible to identify with any certainty the sources of specific solvent-solvent interactions which give rise to such nonideal dielectric behavior for the AN mixtures.

In the present report the dielectric characteristics are examined for 15 binary solvents containing acetonitrile which

cover a total  $\epsilon$  interval from 2 to 43 (at 25 °C). A full range of solvent types was included as the second component, i.e., nonpolar and polar aprotic solvents as well as strong hydrogen bond donors (HBD). As a consequence, it is now possible to estimate the magnitude of the deviation from ideal dielectric behavior for the mixed solvent by applying a general linear regression in dipolarity and HBD acidity parameters for the added component. Likewise, nonlinear correlation functions of the form reported previously (6, 7) were devised to represent the empirical trend in  $\epsilon_m$  vs. solvent composition for the ten more important cosolvent systems containing acetonitrile.

## EXPERIMENTAL SECTION

**Solvents.** Spectroscopic (ACS) grade acetonitrile was dried initially for 3 weeks over anhydrous calcium sulfate. This was followed by fractional distillation through a 52-cm Raschig column from which center 75% cut was retained (corrected boiling range 81.3-81.6 °C). Just prior to preparation of the solvent mixtures, the distilled AN was passed through a column of activated alumina to remove traces of acetic acid and water. The latter did not exceed 0.0005% in the final product, based on Karl Fischer titration, and is well below the limit of a detectable effect upon the measured dielectric constant.

All other spectroscopic (ACS) grade solvents were redried and redistilled as reported previously (6), following standard procedures (12).

**Instrumentation.** Experimental values for dielectric constants were determined from changes in dielectric cell capacitance with a Sargent Model 5 cathode-coupled oscillator. Standard values at 25 °C from the literature (12) for several of the pure liquids were used to calibrate the instrument; i.e., acetonitrile, benzene, *o*-dichlorobenzene, ethanol, ethyl acetate, methanol, and tetrahydrofuran.

Experimental procedures have been given in detail elsewhere (13). The precision in the  $\epsilon$  values of the mixed solvents is  $\pm 0.06$ -0.14 (standard deviation) for the lower dielectric constant range (2-36) and  $\pm 0.10$ -0.15 for the upper range (32-43). A minimum of five replicate measurements were made for each cosolvent mixture and mean values for the more important solvent systems are summarized in Table I.

## RESULTS AND DISCUSSION

The initial phase of this study centered on the comparison of the empirical trends in  $\epsilon$  vs. mole fraction plots for representative AN-cosolvent systems in order to identify common patterns of dielectric behavior as well as those solvent characteristics modifying such patterns.

**Dielectric Constants for Mixed Solvents.** A suitable measure of the departure of the dielectric constant for the solvent mixture from ideal behavior has been defined by Payne and Theodorou (14) using eq 1. Here,  $\epsilon_m$  is the measured

$$\Delta\epsilon_m = \epsilon_m - \epsilon_{\text{calcd}} = \epsilon_m - (X_1\epsilon_1 + X_2\epsilon_2) \quad (1)$$

dielectric constant of the mixture,  $\epsilon_1$  and  $\epsilon_2$  are the values for the pure components, and  $X_1$  and  $X_2$  are their respective mole fractions. Although this excess function will be zero for the ideal binary mixture, real mixtures have finite values which are most often negative in sign (6, 7).

Dielectric constant data from Table I were used to calculate the excess function ( $\Delta\epsilon_m$ ), and the plots of those deviations as a function of  $X_2$  for the specific binary systems are shown in Figure 1. The hydrogen bond donor-acceptor pair, eth-

**Table I. Dielectric Constants (at 25 °C) for Binary Solvents**

AN/acetic anhydride		AN/benzene		AN/ <i>o</i> -dichlorobenzene	
$X_2^a$	$\epsilon_m$	$X_2$	$\epsilon_m$	$X_2$	$\epsilon_m$
0.000	22.00	0.000	2.28 <sup>b</sup>	0.000	10.12 <sup>b</sup>
0.102	23.01	0.158	5.34	0.084	11.23
0.209	24.48	0.297	8.18	0.191	12.80
0.325	26.02	0.421	11.47	0.304	14.36
0.411	27.20	0.530	14.55	0.445	17.01
0.527	28.80	0.629	18.03	0.530	19.22
0.644	30.37	0.717	21.54	0.616	21.41
0.752	32.02	0.798	25.10	0.742	25.05
0.876	33.91	0.878	28.51	0.828	28.27
0.928	34.77	0.938	32.22	0.912	31.62
1.000	36.01 <sup>b</sup>				

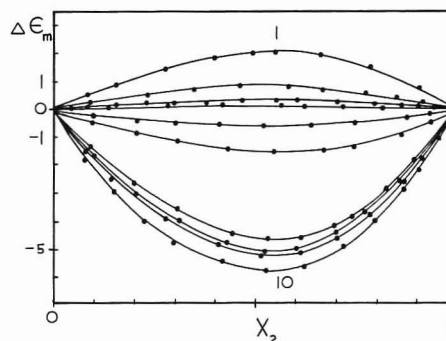
AN/ethyl acetate		AN/dimethylacetamide		AN/sulfolane	
$X_2$	$\epsilon_m$	$X_2$	$\epsilon_m$	$X_2$	$\epsilon_m$
0.000	6.02 <sup>b</sup>	0.000	37.79 <sup>c</sup>	0.000	43.32 <sup>c</sup>
0.105	7.81	0.087	37.72	0.069	43.15
0.208	9.79	0.159	37.65	0.158	42.90
0.313	11.86	0.301	37.48	0.280	42.58
0.430	14.42	0.470	37.21	0.395	42.21
0.522	16.48	0.558	37.05	0.499	41.75
0.605	19.26	0.631	36.88	0.550	41.35
0.776	25.50	0.708	36.76	0.676	40.26
0.860	29.24	0.798	36.54	0.788	39.03
0.912	31.58	0.860	36.33	0.909	37.46
0.970	34.47	0.948	36.10	0.952	36.75

AN/tetrahydrofuran		AN/ethanol		AN/methanol	
$X_2$	$\epsilon_m$	$X_2$	$\epsilon_m$	$X_2$	$\epsilon_m$
0.000	7.54 <sup>b</sup>	0.000	24.34 <sup>b</sup>	0.000	32.63 <sup>b</sup>
0.076	8.71	0.090	25.45	0.092	33.30
0.166	10.23	0.175	26.60	0.230	34.08
0.248	11.61	0.262	27.66	0.352	34.59
0.327	13.21	0.348	28.59	0.465	34.98
0.439	15.72	0.477	30.07	0.582	35.26
0.524	18.02	0.683	32.51	0.660	35.42
0.613	20.58	0.770	33.46	0.776	35.63
0.706	23.77	0.855	34.34	0.848	35.76
0.820	28.00	0.921	35.18	0.913	35.85
0.903	31.44	0.974	35.78	0.963	35.97
0.961	34.08				

<sup>a</sup> Mole fraction of acetonitrile. <sup>b</sup> Reliable literature values used as standards (12). <sup>c</sup> Redetermined value for the pure solvent.

anol:AN, is the only case that approximates ideal dielectric behavior. Most of the nonpolar to moderately polar aprotic cosolvents paired with AN yield deviations that are negative and their curves are similar in the magnitude of the curvature and general shape to those for aprotic pairs reported previously (6). The greatest differences in the  $\Delta\epsilon_m$  vs.  $X_2$  graphs are found for the cases of AN/sulfolane, AN/Me<sub>2</sub>SO, and AN/acetic acid (not included in Figure 1) in which clear maxima occur. For purposes of concise comparison, the values of the excess function at the minimum or maximum ( $\Delta\epsilon_{mm}$ ) are listed in Table II for the 15 AN-containing solvent pairs considered in this study. In general  $\Delta\epsilon_{mm}$  lies in the mole fraction range of 0.50–0.55 in all instances, including those pairs containing a strong HBD component.

Adequate  $\epsilon_m$  data are now available for a sufficient number of AN-solvent pairs to permit useful general rules of correspondence to be developed as a substitute for only qualitative rationalizations about particular solvent systems (14). For a starting point, one anticipates that primary interactions between two aprotic components will be dipole-dipole orientation and dipole-induced dipole interactions governed



**Figure 1.** Trend in the excess function ( $\Delta\epsilon_m$ ) with changing mole fraction  $X_2$  (AN) for representative binary solvents containing acetonitrile. Cosolvents are (1) sulfolane, (2) methanol, (3) dimethylacetamide, (4) ethanol, (5) acetic anhydride, (6) acetone, (7) *o*-dichlorobenzene, (8) ethyl acetate, (9) 1,4-dioxane, and (10) benzene.

**Table II. Solvent Parameters and Dielectric Constant Deviations ( $\Delta\epsilon_{mm}$ ) for Binary Solvents Containing Acetonitrile**

	$\pi^*$ (cosolv) <sup>a</sup>	$\alpha$ (cosolv)	$\Delta\epsilon_{mm}$ (exptl)	$\Delta\epsilon_{mm}^b$ (calcd)
aprotic cosolvent				
acetic anhydride	0.76		-0.80	-1.45
benzene	0.59		-5.80	-5.90
<i>o</i> -dichlorobenzene	0.67		-4.62	-4.50
dimethylacetamide	0.88		0.38	0.65
dimethyl formamide	0.88		0.60	0.65
dimethyl sulfoxide	1.00		2.80	2.80
1,4-dioxane	0.55		-5.23	-5.12
ethyl acetate	0.55		-5.20	-5.12
sulfolane	0.98		2.28	2.40
tetrahydrofuran	0.58		-4.51	-4.59
hydrogen bonding cosolvent				
acetic acid	0.64	1.12	3.55	3.65
acetone	0.71	0.08	-1.63	-1.80
acetonitrile	0.75	0.19	0.00	-0.10
ethanol	0.54	0.83	0.05	0.03
methanol	0.60	0.93	0.73	1.70
			1.38 <sup>c</sup>	
1-propanol	0.52	0.78	-0.70	-0.65

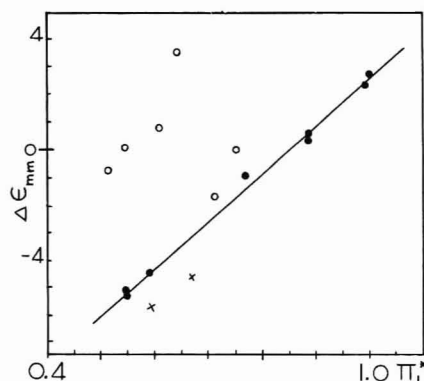
<sup>a</sup> Kamlet-Taft parameters from the recent comprehensive summary (18). <sup>b</sup> Values computed from eq 4. <sup>c</sup> Second value based on literature data (8).

largely by the molecular structure of the added component compared to acetonitrile. As was pointed out initially by Abboud, Kamlet, and Taft (15) and expanded by Brady and Carr (16), the dipolar effect of a given pure solvent is approximately proportional to its molecular dipole moment and for "select solvents" the dipole moment correlates well with the semiempirical Kamlet-Taft  $\pi^*$  (dipolarity) parameter.

When a dipolar but non-hydrogen-bonding component is mixed with the moderately polar acetonitrile, two structure-making and structure-breaking processes will give rise to nonideal dielectric behavior for the mixed solvent: (a) a more polar additive may interact with AN to form a new dipolar pair or higher aggregate while simultaneously disrupting any dipole-dipole structure for the pure component 1 and/or AN; and (b) a less polar additive may promote the dipolar self-aggregation of AN to form species of lower dipole moment through the effect of decreasing  $\epsilon$  alone. For a strong HBD additive solvent, specific donor-acceptor (AN) interactions may approximate stable stoichiometric complexes which form in competition with the simultaneous disruption of the solvent structure for the HBD component (14).

By using the above solvent-solvent processes, one may construct a simple semiquantitative model for the various interactive factors influencing the magnitude of the deviation  $\Delta\epsilon_{mm}$  corresponding to that condition of the maximum or





**Figure 2.** Scatter diagram comparing  $\Delta\epsilon_{mm}$  at the maximum or minimum with the dipolarity value ( $\pi_1^*$ ) of the added solvent in binary solvents containing acetonitrile. Points refer to (●) the polar aprotic, (○) hydrogen bonding, and (×) aromatic solvents.

minimum. As an approximation, one may assume an additivity for the contributions of the major perturbing influences, i.e., simple dipolar  $\Delta\epsilon_p$ , induced dipolar  $\Delta\epsilon_i$ , and hydrogen bonding  $\Delta\epsilon_h$ . Then, eq 2 follows with the expectation that the

$$\Delta\epsilon_{mm} = \Delta\epsilon_p + \Delta\epsilon_i + \Delta\epsilon_h + \Delta\epsilon_0 \quad (2)$$

real signs for each of the terms will not necessarily be positive and that the net deviation is relative to AN as component 2. Since the deviation  $\Delta\epsilon_{mm}$  is expressed in terms of the static bulk dielectric constant, the individual contributions to that sum can be substituted by specific solvent parameters measuring those particular effects. The Kamlet-Taft parameters conform to the requirements for the isolated terms (17):  $\pi_1^*$  dipolarity ( $\Delta\epsilon_p$ );  $\delta_1$  polarizability effect ( $\Delta\epsilon_i$ ); and  $\alpha_1$  HBD acidity ( $\Delta\epsilon_h$ ). The resulting general form of a linear regression in  $\Delta\epsilon_{mm}$  is given by eq 3 in which the weighting

$$\Delta\epsilon_{mm} = s\pi_1^* + d\delta_1 + a\alpha_1 + \Delta\epsilon_0 \quad (3)$$

coefficients and intercept  $\Delta\epsilon_0$  are included. The scatter diagram in Figure 2 showing the pattern of  $\Delta\epsilon_{mm}$  (exptl) vs.  $\pi_1^*$  clearly indicates that separate polarizability and HBD acidity influences coming from component 1 are present in these cosolvent systems.

The final regression expressed in the Kamlet-Taft parameters is given by eq 4 and is based on the data summary in

$$\Delta\epsilon_{mm} = 17.5(\pi_1^* - 0.085\delta_1) + 6.42\alpha_1 - 14.74 \quad (4)$$

Table II and the most recent literature values for the parameters (18). Here, the small negative  $d\delta$  term is actually zero ( $\delta_1 = 0$ ) for all cases except the aromatic and polyhalide solvents for which  $\delta_1$  is unity, and the ratio  $s/a = 2.7$  indicates that dipolarity is the dominant effect for even the stronger HBD solvents (ROH and HOAc). The uncertainties in the coefficients are  $s \pm 0.1$ ,  $d \pm 0.005$ ,  $a \pm 0.02$ , and intercept  $\Delta\epsilon_0 \pm 0.01$ .

Calculated values for  $\Delta\epsilon_{mm}$  listed in Table II have an overall precision of  $\pm 0.22$  (SD) and the correlation coefficient ( $r$ ) is 0.961 when all values are included. Since this  $r$  value is lower than usual for such regressions, it must be emphasized that eq 4 is suitable for only approximate estimates of the deviation in dielectric constant at  $\epsilon_{mm}$  and has been verified for an interval of 0.5–1.0 in  $\pi_1^*$ . Nevertheless, the relationship is useful in that it allows one to predict whether a given or unknown AN-cosolvent pair will exhibit a positive or negative deviation from ideal behavior for  $\epsilon_m$  vs.  $X_2$  plots. Among "select solvents", the condition of  $\Delta\epsilon_{mm} = 0$  corresponds to a  $\pi_1^* \approx 0.84$  which is close to the values for propylene carbonate (PC) and tetramethylurea (18).

When eq 4 is applied to pure acetonitrile itself (see Table II), an assumed HBD acidity of 0.25 is necessary for  $\Delta\epsilon_{mm}$  to be zero; however, even though the literature mean  $\alpha$  value is

**Table III.** Constants for the Rational Regression Functions for the Calculations of  $\epsilon_m^a$

cosolvent with AN	$a_1$	$b_1$	$\epsilon$ (calcd) SD ( $n = 10-14$ )
acetic anhydride	-0.259	0.0059	$\pm 0.08$
acetone <sup>b</sup>	-0.122	0.0146	$\pm 0.02$
benzene <sup>c</sup>	-0.879	0.0254	$\pm 0.12$
<i>o</i> -dichlorobenzene	-0.408	0.0307	$\pm 0.13$
dimethylacetamide	0.540	0.0128	$\pm 0.03$
1,4-dioxane <sup>b</sup>	-0.885	0.0244	$\pm 0.13$
ethyl acetate	-0.689	0.0239	$\pm 0.15$
methanol	-0.664	-0.0175	$\pm 0.03$
sulfolane	2.34	0.0493	$\pm 0.15$
tetrahydrofuran	-0.607	0.0243	$\pm 0.16$
overall uncertainties	$\pm 0.001$	$\pm 0.0001$	

<sup>a</sup> Fixed values of  $a_0 = 1$  and  $b_0 = 0.0278$  apply to all binary systems containing acetonitrile. <sup>b</sup> Reported previously (6, 7). <sup>c</sup> Revised values based on more complete data.

0.19 (18), its range of values appears to be 0.15–0.27 and uncertainties of  $\pm 20\%$  are not uncommon for the  $\alpha$  numbers of weak HBD liquids. Because of such uncertainties and the limited number of solvent pairs used to establish the function, no claim of *exact* linearity for eq 4 should be made. Likewise, an assumed equivalence between  $\Delta\epsilon_0$  and the  $\Delta\epsilon_{mm}$  for cyclohexane may well be incorrect since eq 2–4 are deviation statements rather than integral and are untested in the 0–0.5 $\pi_1^*$  range.

**Correlation Equations for  $\epsilon_m$ .** For any given AN-cosolvent system, dielectric constants for a minimum of 9–12 solvent mixtures were obtained before data processing was initiated, and graphic distributions of the points for  $\epsilon_m$  vs.  $X_2$  were checked for internal consistency prior to compiling the composite sets. Among important cases which repeat the work of earlier investigators (i.e., AN/sulfolane and AN/methanol (10)), it was found that the quality and quantity of the published data were not adequate for correlation analysis. Surprisingly, this was especially so for AN:methanol as was noted some time ago by Cunningham, Vidulich, and Kay (8), and therefore, the redetermination of  $\epsilon_m$  values was necessary for this solvent pair having a very narrow dielectric constant range (32.6–36.0).

Because of the apparent role of the common descriptors,  $\pi_1^*$  and  $\alpha$ , as cofactors influencing nonideal dielectric behavior in the AN cosolvent systems, it was expected that the  $\epsilon_m$  vs.  $X_1$  curves should again conform to a single type of correlation function. The rational function in the form of the reciprocal of the Padé approximant (19) which has been used previously with some success on purely aprotic solvent pairs (6) was applied to the AN binary solvents in the form of eq 5. Here,

$$\epsilon_m = \frac{a_0 + a_1 X_1}{b_0 + b_1 X_1} \quad (5)$$

$a_0 = 1$  by assignment and  $X_1$  is the mole fraction of the component added to AN, and, since  $b_0$  is  $1/\epsilon_2$  (AN), only the two empirical coefficients  $a_1$  and  $b_1$  must be determined. The numerical values for the latter constants are listed in Table III for 10 AN solvent pairs along with the uncertainties in the calculated results. The precisions with which the computed  $\epsilon_m$  vs.  $X_1$  curves reproduce the corresponding experimental trends are comparable to results obtained for the previous cases (6, 7) and justify the application of the simple first-power rational function given as eq 5.

Correlation equations for the acetonitrile cosolvent systems exhibit two important differences from similar functions developed for other aprotic and HBD binaries examined earlier (6, 7). Firstly, all of the previous polar-nonpolar aprotic and HBD-polar aprotic pairs showed only negative deviations

as  $\Delta\epsilon_m$ . On the other hand, AN cosolvent systems include the total range of possible systems from  $-\Delta\epsilon_m$  to 0 to  $\Delta\epsilon_m$  (Figure 1), and thus, the rational function in eq 5 has now been found to be adequate for representing data sets having either positive or negative deviations from ideal dielectric behavior. Secondly, with AN serving as a moderately polar Lewis base in those nonideal binary solvents which are hydrogen bond donor-hydrogen bond acceptor pairs (AN-alkanols), no exceptional behavior for the correlation function is observed over the total composition range. This contrasts with some other aprotic-HBD systems containing the lower alkanols reported earlier which were fitted by the simple rational function for only about half of the mole fraction range (7). However, the AN-strong HBD cases have moderately positive deviations from ideal dielectric behavior (Table II) for which the magnitude of  $\Delta\epsilon_{mm}$  decreases with the decreasing HBD acidity. The AN-alkanol systems resemble the cyclic carbonate-methanol pairs in this respect, and even though the carbonates have much larger dielectric constants (14) than AN, their  $\pi^*$  dipolarities and  $\pi^*/\beta$  ratios are similar to AN (18).

As one reconsiders the electrochemical characteristics of AN cosolvent systems, there is good evidence that ionic conductance and ion pair association conform to regular behavior in AN-aperotic pairs over the broad dielectric constant interval from 2 to 43 (10); however, there are slight departures from the exact linearity for  $\ln K_A$  vs.  $1/\epsilon_m$  predicted by the Fuoss-Onsager theory of ion pair association. Such minor departures from linearity as well as the slight but general asymmetry in the excess function curves as  $X_1 \rightarrow 0$  (Figure 1) are consistent with an argument for a changing degree of dipole-dipole self-association by AN as small amounts of a polar cosolvent are added. These effects are not significant enough (10) to preclude the application of such solvent pairs to electroanalytical studies if the trend in  $\epsilon_m$  as a function of solvent composition shows only minor deviation from ideal behavior and follows a correlation like that in eq 5.

On the other hand, if one may generalize from cases like AN:methanol and PC:methanol, ion pair association and acid-base ionization equilibria appear to be irregular in those

AN mixed solvents containing a strong HBD solvent (10, 20). For the latter, electrolytic equilibria become more complex through the preferential solvation of solute species by the separate aprotic and HBD cosolvents (20) as well as by specific structure-breaking processes within the mixed solvent itself. Thus, because of the shifting degree of hydrogen bonded self-association by the lower alcohols in mixed solvents, AN/ROH systems do not appear to be solvents of choice for electrochemical studies even though their trends in dielectric constants are adequately represented by the rational regression functions.

Registry No. AN, 75-05-8.

## LITERATURE CITED

- (1) Serjeant, E. *Potentiometry and Potentiometric Titrations*; Wiley-Interscience: New York, 1984; p 366.
- (2) Bunton, C.; Mhala, M.; Moffatt, J. *J. Org. Chem.* **1984**, *49*, 3637.
- (3) Cassidy, J.; et al. *J. Phys. Chem.* **1985**, *89*, 3933.
- (4) Bond, A.; Fleischmann, M.; Robinson, J. *J. Electroanal. Chem.* **1984**, *168*, 299.
- (5) Howell, J.; Wightmann, R. *Anal. Chem.* **1984**, *56*, 524.
- (6) Kolling, O. W. *Anal. Chem.* **1985**, *57*, 1721.
- (7) Kolling, O. W. *Anal. Chem.* **1986**, *58*, 870.
- (8) Cunningham, G.; Vidulich, G.; Kay, R. *J. Chem. Eng. Data* **1967**, *12*, 336.
- (9) D'Aprano, A.; Fuoss, R. *J. Phys. Chem.* **1969**, *73*, 400.
- (10) D'Aprano, A.; Donato, I. *J. Chem. Soc., Faraday Trans. 1* **1973**, 1685.
- (11) D'Aprano, A.; Goffedi, M.; Triolo, R. *J. Chem. Soc., Faraday Trans. 1* **1976**, 79.
- (12) Riddick, J.; Bunger, W. *Organic Solvents*, 3rd ed.; Wiley-Interscience: New York, 1970; Chapter, 5 pp 638, 704-706, 720, 749, 836, 844, 857, 860.
- (13) Kolling, O. W. *Trans. Kans. Acad. Sci.* **1979**, *82*, 218.
- (14) Payne, R.; Theodorou, I. *J. Phys. Chem.* **1972**, *76*, 2892.
- (15) Abboud, J.; Kamlet, M.; Taft, R. *J. Am. Chem. Soc.* **1977**, *99*, 8325.
- (16) Brady, J.; Carr, P. *J. Phys. Chem.* **1984**, *88*, 5796.
- (17) Taft, R.; Abboud, J.; Kamlet, M. *J. Am. Chem. Soc.* **1981**, *103*, 1080.
- (18) Kamlet, M.; et al. *J. Org. Chem.* **1983**, *48*, 2877.
- (19) King, M.; Queen, N. *J. Chem. Eng. Data* **1979**, *24*, 178.
- (20) Lesniewski, B.; Przybyszewski, B. *J. Chem. Soc., Faraday Trans. 1* **1984**, *80*, 1769.

RECEIVED for review August 4, 1986. Accepted November 3, 1986.



## CORRESPONDENCE

### Characterization of a Microinjector for Capillary Zone Electrophoresis

*Sir:* Recent advances have stimulated interest concerning the development of microcolumn liquid-phase separation methods, including capillary liquid chromatography in various forms, and capillary zone electrophoresis. It has become increasingly evident that microcolumn techniques, especially those employing capillary columns ( $<100\ \mu\text{m}$  i.d.), offer several advantages over conventional liquid-phase techniques (1). One significant advantage of microcolumn methods is the suitability for determining solutes from extremely small-volume samples. This prospect is exceedingly important for many biological analyses.

A major problem associated with the application of microcolumn techniques to ultrasmall sample analysis is that of acquiring and injecting subnanoliter samples. Currently, microcolumn LC injections are performed by use of either static or dynamic splitting techniques (2-4). Splitting techniques have allowed extremely small samples to be placed onto capillary columns with very little band broadening due to the injection. However, splitting methods suffer from the need to use initially large samples of which only about 1% or less is actually injected. Jorgenson and co-workers (5) have recently introduced an extremely small, pressure-based injector for injecting very small samples onto capillary LC columns. This injector utilizes a single-barreled micropipet with a tip diameter on the order of  $10\ \mu\text{m}$ , which is inserted into the end of the capillary column.

A recently introduced alternative to microcolumn LC is capillary zone electrophoresis (6-10). Capillary zone electrophoresis is an extremely efficient ultrasmall volume separation method suitable for the analysis of ionizable species. Capillary zone electrophoresis does not use a stationary phase or pressure-driven flow. Hence, this technique is amenable to ultrasmall sample analysis, while avoiding problems associated with coating stationary phases and the high pressures necessary to cause flow through ultrasmall capillaries.

Sample injection in capillary zone electrophoresis is usually performed through electromigration—a term collectively recognizing the effects of electrophoresis and electroosmosis (6, 7). One end of the capillary and the electrophoresis anode are placed into the sample and a voltage is briefly applied, causing a small band of sample to electromigrate into the capillary. Attempts to physically inject samples in capillary zone electrophoresis have been reported to cause band broadening, apparently due to the laminar flow profile introduced during the injection (7). Other less-common injection methods include gravity flow (11) and an electronic sample splitter (12). All of these injection methods are capable of placing subnanoliter volumes of sample onto the electrophoresis column with a minimum of band broadening; however, all suffer from the need to start with sample volumes large enough to receive the end of the column and the electrode. This usually results in the use of milliliters of solution, although with care one could possibly use sample volumes in the microliter domain.

By use of technology from electrophysiologists, an injector for capillary electrophoresis has been developed that operates on the principles of microiontophoresis (13) and can be constructed small enough to remove samples from extremely small volumes. Microiontophoresis concerns the ejection of ex-

ogenous substances into specific regions in biological systems. This technique employs micropipets ( $<1\ \mu\text{m}$  outer tip diameter) filled with the substance of interest (ionized) through which a suitable current is passed to cause ejection of the ions out of the micropipet tip. Neutral compounds can also be ejected using microiontophoresis due to the presence of electroosmosis within the pipet tip (13).

The injector presented here is similar in nature to microiontophoresis pipets, except that we are injecting into the micropipet rather than ejecting substances out of the tip. This injector is constructed from a dual-barreled micropipet ( $15\text{--}70\ \mu\text{m}$  outer tip diameter) with a carbon fiber in one barrel and the electrophoresis capillary inserted into the other buffer-filled barrel (Figure 1). The carbon fiber serves as the anode in order to cause electromigration of the analyte into the injector barrel and subsequently into the electrophoresis capillary with the application of a potential. The electroosmotic flow along with iontophoretic effects cause migration of the analyte into the injector tip, and subsequently onto the electrophoresis column.

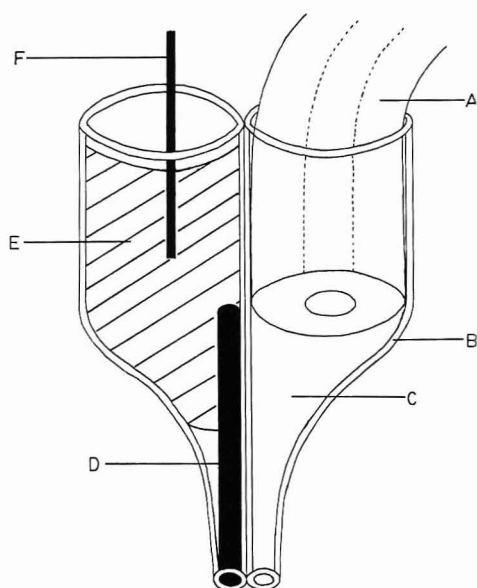
This paper details fabrication procedures and presents initial data showing the feasibility of this system. Some insights into the principles of operation and the band broadening factors present are offered.

#### EXPERIMENTAL SECTION

**Apparatus.** The electrophoresis apparatus used was similar to that described by Jorgenson and Lukacs (7). Fused silica capillaries with inner diameters of  $50$  and  $75\ \mu\text{m}$  were obtained from Scientific Glass Engineering. The capillaries were filled with either  $0.025\ \text{M}$  bicarbonate buffer with  $10\%$  (v/v) 2-propanol at pH 10,  $0.025\ \text{M}$  bicarbonate buffer with  $12\%$  (v/v) 2-propanol at pH 10.35, or  $0.05\ \text{M}$  bicarbonate buffer at pH 10. A Spellman high-voltage dc power supply delivering  $0\text{--}30\ \text{kV}$  was used to provide the electric field for the electrophoresis. The operator was protected from accidental contact with the high-voltage electrode by housing the high-voltage end in a Plexiglas box equipped with an interlock system. In the case of normal capillary electrophoresis experiments, graphite rods or platinum wires were used as the electrodes.

Detection was performed with a locally constructed on-column fluorescence detector similar to that of Green and Jorgenson (14). The detector used a  $200\text{-W}$  mercury arc lamp (Oriel Corp.) as the ultraviolet light source. The  $365\text{-nm}$  mercury line was isolated using a single monochromator (Jarrell-Ash, Minichromator) and a line filter (35-3045, Ealing Corp.). Fluorescent light was collected at  $90^\circ$  to the excitation beam and was isolated by using two identical glass filters with a cutoff of  $420\ \text{nm}$  (52170, Oriel Corp.). Fluorescence was detected with an end-on photomultiplier tube (R1104 Hamamatsu Corp.) operated at a bias of  $1000\ \text{V}$ . The photomultiplier current was amplified with a Keithly Model 427 current amplifier, the output of which was sent to a locally constructed noise-suppression circuit. The fluorescence signal was followed as a function of time on a Fisher Recordall series 5000 strip-chart recorder. The on-column detector cell was created by burning off a small section of the polymer coating on the capillary.

**Chemicals.** Histamine,  $\gamma$ -aminobutyric acid (GABA), taurine, and glycine were obtained from Aldrich Chemical Co. Fluorescamine was obtained from Sigma Chemical Co. and was used as an acetone solution. CAPS buffer (3-(cyclohexylamino)-1-propanesulfonic acid) was obtained from Sigma Chemical Co. All chemicals were used as received.



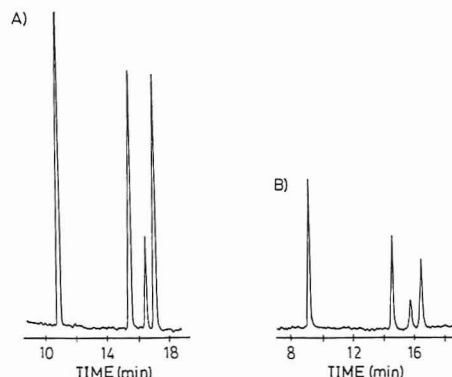
**Figure 1.** Schematic of dual-barreled microinjector: (A) fused silica capillary column; (B) glass dual-barreled micropipet; (C) buffered solution; (D) carbon fiber; (E) mercury; (F) platinum wire.

**Dual-Barreled Microinjector Construction.** Carbon fibers with an outside diameter of 10  $\mu\text{m}$  were aspirated into one barrel of a dual-barreled glass capillary (microfilament glass 6070, A-M Systems). The dual-barreled capillary was pulled down around the carbon fiber with a vertical microelectrode puller (Harvard Bioscience). The tip of the structure was then cut under a microscope to outer diameters in the 15–70  $\mu\text{m}$  range. The barrel containing the carbon fiber was filled with mercury, and a piece of platinum wire was inserted in the end in order to make electrical contact to the fiber (see Figure 1). The tip of the injector was placed into a vial containing the operating buffer allowing capillary action to partially fill the open barrel. Filling the open barrel with buffer was completed by using a syringe with a small piece of 100  $\mu\text{m}$  i.d. capillary attached to it. The anodic end of the electrophoresis capillary was placed into the buffer-filled barrel prior to injection. During injection with the microinjector, a potential was briefly (5–50 s) applied to the carbon fiber causing solutes to electromigrate into the capillary. After injection, the microinjector was removed from the capillary and the capillary end with sample was placed into a buffer reservoir for electrophoresis. Injections without the microinjector (direct injections) were performed as discussed by Jorgenson (6). All injections used for comparisons of efficiency were timed to produce equivalent peak areas (solute amount injected) with the fluorescence detector.

**Single-Barreled Injector Test System (Not Shown).** Injectors made with single-barreled micropipets and using an external platinum wire as the anode were fabricated. Single-barreled glass capillaries were obtained from A-M Systems (standard capillary glass, 6270). The capillaries were pulled down to sub-micrometer tip diameters and then cut under an optical microscope to the desired tip diameter. The micropipets were filled with operating buffer in the manner described above. For injection, the anode end of the capillary column was placed into the microinjector, the tip of which was placed into the sample reservoir. A voltage was briefly applied via a platinum wire anode placed in the reservoir in order to cause electromigration of the solute into the injector and subsequently onto the column. After injection, the microinjector was removed, the column end placed into a buffer reservoir, and a voltage applied. The operating buffer used was 0.1 M CAPS, adjusted to pH 10 with sodium hydroxide. The test solute was  $1 \times 10^{-3}$  M histamine derivatized with fluorescamine and diluted in 0.05 M CAPS at pH 10.1.

## RESULTS AND DISCUSSION

Figure 2 compares electropherograms of four fluorescamine-derivatized amino acids (histamine,  $\gamma$ -aminobutyric acid, taurine, glycine) injected directly (10 s at 30 kV) and via a dual-barreled microinjector with an outer diameter of ca. 50  $\mu\text{m}$  (15 s at 30 kV). Both electropherograms were run at an



**Figure 2.** Electropherograms of fluorescamine-derivatized amino acids comparing direct injection (A) and injection through a 50  $\mu\text{m}$  o.d. dual-barreled microinjector (B).

applied voltage of 30 kV on a 100 cm length of 75  $\mu\text{m}$  i.d. fused silica capillary, filled with 0.025 M  $\text{NaHCO}_3$  + 10% 2-propanol at pH 10.16. The statistical efficiencies obtained by the direct injection ranged from 60 000 to 134 000 theoretical plates for the various components. Injecting through the microinjector caused a decrease in efficiency for all four components, with values ranging from 35 000 to 60 000 theoretical plates. This represents an average decrease in efficiency of approximately 49% when employing a dual-barreled injector of these dimensions.

To obtain an estimate of the sample volume injected, one needs to know the rate of electroosmosis in the capillary. In the absence of a neutral solute, the best estimates are from anions with the shortest migration times or cations with the longest migration times, since these solutes must necessarily have a large component of their column transit time due to electroosmosis. Using the histamine peak in Figure 2 as a rough indicator of the electroosmotic flow rate, we estimate that approximately 24 nL of sample is injected under the conditions presented here. Since histamine (anion) was used as our marker for electroosmotic flow, this estimate is expected to be slightly lower than the actual injection volume. Although this is a small injection volume, injections of picoliter volumes should be possible with this method if extreme care is maintained in matching column and injector diameters (*vide infra*) and if detection methods can be improved.

Although this dual-barreled injector shows tremendous promise, some technical problems still exist at present. The rate of successful injection with the dual-barreled injectors is approximately 10%. This low success rate can be attributed to electrical coupling between the two barrels in some injectors. Electrical coupling occurs when current passes through the glass walls separating the two pipet barrels. This creates a current path which does not enter the capillary column from the injector orifice and thus does not introduce sample onto the column. Although electrical coupling is a concern at present, work is being done employing theta capillary glass to eliminate this problem (13).

In order to address the band broadening characteristics of this injector, it was necessary to design an alternate test system which eliminates problems associated with electrical coupling between pipet barrels (13). This was most easily accomplished by placing the anode end of the capillary column into a buffer-filled single-barreled pipet with a representative tip diameter. Details of this system are presented in the Experimental Section. With this system, electrical coupling was eliminated as the current was forced to flow from the anode through solution and into the injector tip, thereby causing electromigration of sample into the injector tip and subsequently onto the column. With this method, the success rate of injections approached 90%. While obviously not suitable for most microenvironment sampling applications, this con-



**Table I. Comparison of Statistical Efficiencies<sup>a</sup> Obtained with Two Different Size Single-Barrel Injectors and with Direct Injections<sup>b</sup>**

injector tip diameter, $\mu\text{m}$	$N_{\text{injector}}^c$	$N_{\text{direct}}^d$	$N_{\text{injector}}/N_{\text{direct}}$
85	210 000	220 000	0.95
45	132 000	220 000	0.60

<sup>a</sup>Computed using the formula  $N = 5.54 (t_m/W_h)^2$ , where  $t_m$  is the migration time and  $W_h$  is the peak width at half maximum.

<sup>b</sup>Data are for  $10^{-3}$  M histamine derivatized with fluorescamine and run on a  $75\text{-}\mu\text{m}$  i.d. fused silica column at a potential of 30 kV.

<sup>c</sup>Based on injection times of 36–41 s at 30 kV. <sup>d</sup>Based on 4-s injections at 30 kV.

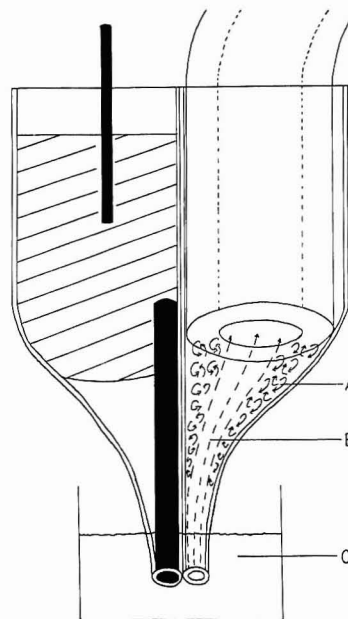
figuration represents a reliable test system through which to evaluate band-broadening characteristics of injecting through small orifices. The single-barreled injector configuration was tested by using a  $10^{-3}$  M fluorescamine-derivatized histamine sample. The efficiency of two single-barrel injectors with differing tip diameters was examined with a  $75\text{-}\mu\text{m}$  i.d. capillary column. Variation in efficiency due to different amounts injected (15, 16) was minimized by timing the microinjector injections to produce similar peak areas to those of the 4-s direct injections. The pertinent data from these experiments are summarized in Table I. These data indicate that as the injector tip diameter decreases relative to the inner diameter of the separation capillary, a loss of efficiency is observed. In this case, decreasing the injector tip diameter by 47% caused the efficiency to decrease by 37%. These initial data imply that in order to use this type of microinjector for sample removal from microenvironments without introducing considerable band broadening, correspondingly small separation capillaries will be necessary. The use of such small capillaries requires more sensitive detectors than presently described.

The introduction of significant band broadening with injectors whose diameter is much smaller than the inside diameter of the separation column can be understood by examining the paths and behavior of the sample as it flows through the injector and onto the column. The flow present in this system is a combination of electroosmotic flow and electrophoretic migration, with electroosmotic flow usually dominating. Electroosmotic flow is unique in that, unlike pressure-based flow, a flat flow profile is created (17). Because of this flat flow profile, differential migration of solutes from resistance to mass transfer in the mobile phase occurs only in a very small region near the solution/glass interface. With the direct electromigration injection technique, this behavior results in a well-defined sample plug being placed onto the column.

On comparison of two injectors, one with a barrel inside diameter approximately equal to the inside diameter of the capillary column and one whose inside diameter is much smaller than the column inside diameter, differences in the behavior of the solute flow are expected. For an injector of small inside diameter, there exists a lateral expansion of the sample plug as it follows the current path through the injector tip and into the column (Figure 3). In passing through the injector orifice and into the column, two band broadening processes can occur: (1) molecular diffusion and (2) generation of turbulence or eddy currents. The contribution of molecular diffusion to band broadening can be given by Einstein's law of diffusion which implies that the spatial variance of a zone after time,  $t$ , is represented as

$$\sigma^2 = 2Dt \quad (1)$$

where  $D$  is the molecular diffusion coefficient of the solute in the zone. A greater amount of time is needed for a band



**Figure 3.** Model of sample solution flow through a dual-barreled microinjector showing possible mechanism for creation of eddy currents when injector and column bores are mismatched: (A) eddy currents; (B) sample flux; (C) sample reservoir.

of solute to migrate from the tip of the injector to the end of the column than is needed with direct injection. Thus, the solute band is expected to be slightly more diffuse by the time it reaches the column than it would be during a direct injection where the sample band migrates directly onto the column. With direct injections of short duration, the contribution of molecular diffusion to band broadening is negligible. However, in the case of the microinjector, this diffusional contribution is considered to be more significant due to the larger cross-sectional area of the injector barrel and the longer time involved for injection.

The generation of turbulence or eddy currents during injection through a small diameter injector can be understood through the analogous fluid dynamics problem of flow at an abrupt enlargement (18). This problem describes the effects on a sample plug flowing through a small diameter pipe when the pipe is at some point, sharply enlarged to a much larger cross-sectional area. With the microinjector, sample is drawn through the small tip of the injector and flows into the much larger cross-sectional area near the entrance to the column. Fluid emerging from the small tip of the injector is unable to follow the large deviation of the boundary and, consequently, pockets of turbulent eddies form and result in dissipation of energy as heat. This heat along with the turbulence created can contribute significantly to band broadening of the sample plug introduced onto the column. The largest turbulent effects will be encountered when there is a large difference between the injector tip and column inside diameters. Lukacs and Jorgenson (9) have shown that at pH 10 electroosmotic flow is greater in silica capillaries than in glass. Therefore, in the system presented here, the stronger electroosmotic flow in the silica column is thought to create a negative pressure which tends to pull sample through the injector tip. When the inner diameters of the injector tip and the column are closely matched, the flow is expected to be smooth since there will then be a negligible boundary deviation and since the dominant force on the flow is that of negative pressure set up by electroosmosis in the fused silica capillary.

Jorgenson and Lukacs (6) have derived an equation describing the spatial variance of a zone in capillary zone electrophoresis ( $\sigma_L^2$ ). This equation ignores the effects of injection and is given by

$$\sigma_L^2 = 2Dt = \frac{2DL_c^2}{(\mu_{ep} + \mu_0)V} \quad (2)$$

where  $\mu_{ep}$  is the electrophoretic mobility,  $\mu_0$  is the electrophoretic mobility of the buffer,  $L_c$  is the length of the column,  $D$  is the diffusion coefficient, and  $V$  is the applied voltage. Since two band broadening factors are introduced with the microinjector, the spatial variance due to the injector ( $\sigma_i^2$ ) can be represented as

$$\sigma_i^2 = 2Dt_i + B_{turb} = \frac{2DL_i^2}{(\mu_{ep} + \mu_0)V_i} + B_{turb} \quad (3)$$

where  $t_i$  is the injection time,  $L_i$  is the distance from the tip of the injector to the column,  $V_i$  is the injection voltage, and  $B_{turb}$  is a term describing the contribution due to the presence of turbulence within the injector. The injector turbulence term is experimentally related to the difference between the column and injector tip inside diameters ( $d_c - d_i$ ), and is also expected to be related to the distance from the tip of the injector to the column ( $L_i$ ), the electroosmotic mobility of the buffer ( $\mu_0$ ), the injection time ( $t_i$ ), the length of the column ( $L_c$ ), the applied voltage during injection ( $V_i$ ), and the electrophoretic mobility of the species ( $\mu_{ep}$ ). Work is currently being done to correlate the relationship of these parameters to the band broadening contribution observed. The total spatial variance ( $\sigma_T^2$ ) expected when a microinjector is used is the sum of the individual spatial variances

$$\sigma_T^2 = \sigma_L^2 + \sigma_i^2 = \frac{2DL_c^2}{(\mu_{ep} + \mu_0)V} + \frac{2DL_i^2}{(\mu_{ep} + \mu_0)V_i} + B_{turb} \quad (4)$$

The separation efficiency in capillary zone electrophoresis has been borrowed from chromatography (6) as suggested by Giddings (19). The number of theoretical plates,  $N$ , is defined as

$$N = L_c / \sigma_T^2 \quad (5)$$

Substituting eq 4 into this expression results in

$$N = \frac{L_c^2}{\frac{2D}{(\mu_{ep} + \mu_0)} \left( \frac{L_c^2}{V} + \frac{L_i^2}{V_i} \right) + B_{turb}} \quad (6)$$

Our results suggest that the major parameter involved in determining  $B_{turb}$  is apparently the difference between the

inside diameters of the injector tip and the column. This suggestion is in agreement with the data shown in Table I where an injector tip more closely matching the diameter of the separation capillary shows a loss in efficiency of only about 5%. Thus, by minimization of the orifice diameter difference, the  $B_{turb}$  term appears to approach a negligible value. If this behavior is consistent with a wide range of capillary diameters, then efficiencies approaching those obtained with direct injection should be attainable with ultrasmall injectors as long as similarly small capillary bores are applied.

#### ACKNOWLEDGMENT

The authors are grateful to James Jorgenson and John Green of the University of North Carolina at Chapel Hill for their assistance in constructing the capillary electrophoresis apparatus.

#### LITERATURE CITED

- (1) *Microcolumn Separations*; Novotny, M., Ishii, D., Eds.; Elsevier: New York, 1985, Preface.
- (2) Yang, F. J. *J. HRC CC, J. High Resolut. Chromatogr. Chromatogr. Commun.* **1980**, *3*, 589-590.
- (3) Yang, F. J. *J. Chromatogr.* **1982**, *236*, 265-277.
- (4) Jorgenson, J. W.; Guthrie, E. J. *J. Chromatogr.* **1983**, *255*, 335-348.
- (5) Kennedy, R.; St. Claire, R. L., III; White, J. G.; Jorgenson, J. W. Pittsburgh Conference; Atlantic City, NJ, March 12, 1986; No. 538.
- (6) Jorgenson, J. W.; Lukacs, K. D. *J. Chromatogr.* **1981**, *218*, 209-216.
- (7) Jorgenson, J. W.; Lukacs, K. D. *Science* **1983**, *222*, 266-272.
- (8) Gebauer, P.; Deml, M.; Bocek, P.; Junak, J. *J. Chromatogr.* **1983**, *267*, 455-457.
- (9) Jorgenson, J. W.; Lukacs, K. D. *J. HRC CC, J. High Resolut. Chromatogr. Chromatogr. Commun.* **1985**, *8*, 407-411.
- (10) Lauer, H. H.; McManigill, D. *Anal. Chem.* **1986**, *58*, 165-170.
- (11) Tsuda, A.; Norura, K.; Nakagawa, G. *J. Chromatogr.* **1983**, *264*, 385-392.
- (12) Deml, M.; Foret, F.; Bocek, P. *J. Chromatogr.* **1985**, *320*, 159-165.
- (13) Stone, T. W. *Microiontophoresis and Pressure Injection*; Wiley: New York, 1985; Chapters 1-3.
- (14) Guthrie, E. J.; Jorgenson, J. W. *Anal. Chem.* **1984**, *56*, 483-486.
- (15) Tsuda, A.; Nomura, K.; Nakagawa, G. *J. Chromatogr.* **1983**, *264*, 385-392.
- (16) Fujiwara, S.; Honda, S. *Anal. Chem.* **1986**, *58*, 1811-1814.
- (17) Pretorius, V.; Hopkins, B. J.; Shieke, J. D. *J. Chromatogr.* **1974**, *132*, 23-30.
- (18) Massey, B. S. *Mechanics of Fluids*, 4th ed.; Van Nostrand Reinhold: New York, 1979; pp 197-200.
- (19) Giddings, J. C. *Sep. Sci.* **1969**, *4*, 181-189.

Ross A. Wallingford  
Andrew G. Ewing\*

Department of Chemistry  
The Pennsylvania State University  
University Park, Pennsylvania 16802

RECEIVED for review July 29, 1986. Accepted October 20, 1986.  
This material is based upon work supported by the National Science Foundation under Grant No. BNS-8504292.

## Application of a Modulated Magnetic Field to a Flame Photometric Detection Burner in the Detection of Phosphorus

Sir: Phosphorus is one of the important elements that needs to be detected in the semiconductor industry and in environmental, biological, and geochemical scientific work (1-3). Analytical techniques commonly used for phosphorus determinations include the colorimetry of phosphomolybdenum heteropoly blue, N/P thermionic detection, and flame photometric detection (FPD). FPD has seen widespread use in gas chromatography as a specific detector for sulfur- and phosphorus-bearing compounds. This detector operates on the principle that phosphorus and sulfur compounds emit characteristic green and blue colorations, respectively, in

hydrogen-air flames. In the case of phosphorus, the green emission is due to the HPO molecules and the intensity of this emission is known to vary linearly with P atom flow into the flame (4).

Recently, we found that the emission intensity of some excited species in hydrogen-oxygen flames changed under the effect of a static magnetic field; for example, the emission intensity of HPO was partially magnetically quenched, taking minimum value at 0.45, 0.81, and 1.58 T (5). The emission intensity from HPO decreased about 20% at 0.45 T. This phenomenon cannot be explained by the Zeeman effect, be-



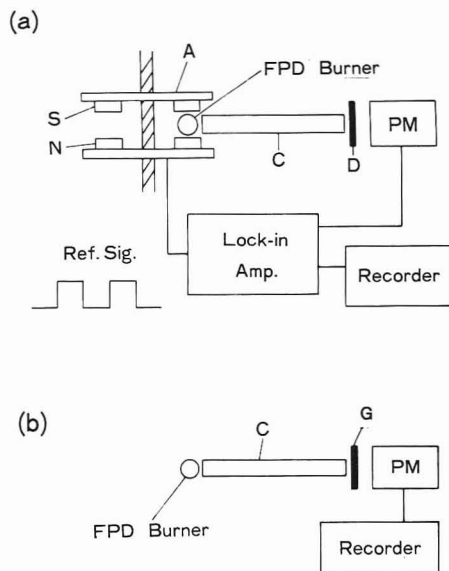


Figure 1. Outline of the experimental arrangement of the new background correction system (a) and the conventional FPD (b).

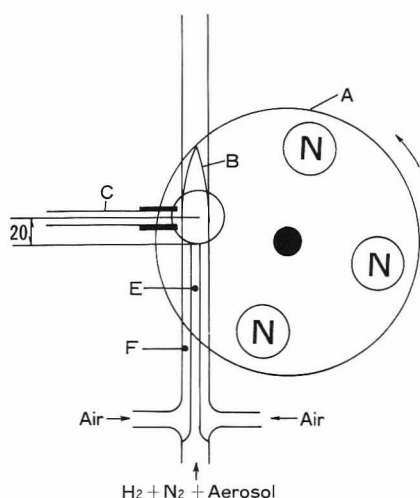


Figure 2. Experimental arrangement of the burner, rotating magnetic system, and optical guide.

cause relative spectral distributions did not change. In this report, we propose a new background correction system for FPD detection of phosphorus (6) that uses the magnetic field effect found in HPO. In the present system, a modulated magnetic field, the strength of which varied from 0 to 0.45 T at 98 Hz, was applied to the FPD burner in order to modulate the emission from HPO selectively. Associated noises, i.e., flame noises and PM dark current noises, were not modulated. The output of PM was fed to a tuned band-pass amplifier (98 Hz) and a phase sensitive detector to reject associated noises and extract the signal of phosphorus from high noise levels. This new technique will be compared with a conventional FPD.

## EXPERIMENTAL SECTION

**Outline of Experimental Arrangement.** The outline of the experimental apparatus is shown in Figure 1a. Figure 2 illustrates the arrangement of the FPD burner, rotating magnetic system, and optical guide. A modulated magnetic field was applied to the FPD burner by using a rotating magnetic system (A). The magnetic field, flame (B), and optical guide (C) were perpendicular to each other. The flame emission was guided by a Pyrex glass rod (10 mm in diameter, 300 mm in length, covered by aluminum foil) through broad band-pass glass filters (D) to a photomultiplier (PM) (HTV, R453). The PM supply voltage was 800 V. The outputs of PM and reference signals from the rotating magnetic

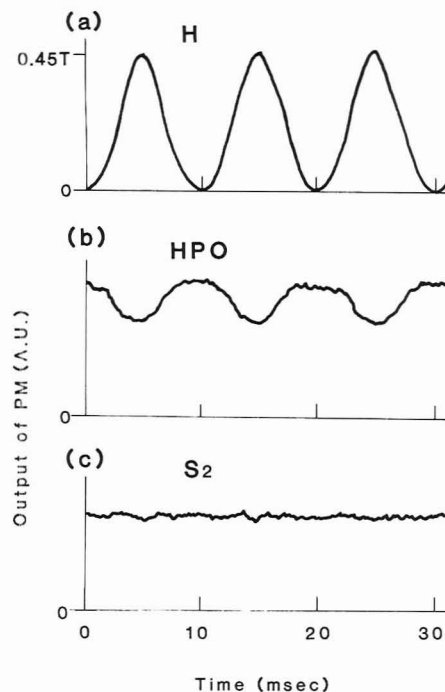


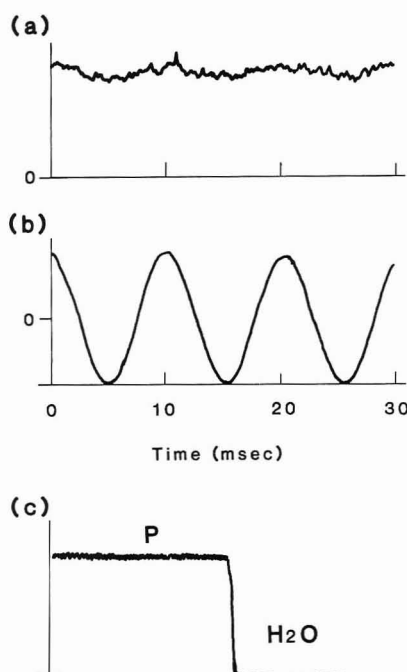
Figure 3. Transient behaviors of a modulated magnetic field (a) and the PM outputs in the aspiration of the  $(\text{NH}_4)_2\text{HPO}_4$  solution (P, 10  $\mu\text{g/mL}$ ), the aerosol of an aqueous solution of  $(\text{NH}_4)_2\text{HPO}_4$  (0.16 mL/min), and nitrogen (820 mL/min) flowed through the central nozzle (E), the diameter of which was 3 mm. Air (300 mL/min) passed through the outer ring (F), the inner and outer diameters of which were 5 and 8 mm, respectively. The aerosol of the phosphorus solution was produced by an ICP nebulizer (Shimadzu), which was operated by flowing nitrogen. The ICP nebulizer introduced a trace amount of phosphorus into the flame in these experiment. Of course, it is possible to use the present system as a detector for phosphorus in gas chromatographic effluents.

system were fed to a lock-in amplifier (PAR 124A).

**Burner.** A schematic illustration of the FPD burner is shown in Figure 2. It was made of Pyrex glass. Premixed hydrogen (540 mL/min), the aerosol of an aqueous solution of  $(\text{NH}_4)_2\text{HPO}_4$  (0.16 mL/min), and nitrogen (820 mL/min) flowed through the central nozzle (E), the diameter of which was 3 mm. Air (300 mL/min) passed through the outer ring (F), the inner and outer diameters of which were 5 and 8 mm, respectively. The aerosol of the phosphorus solution was produced by an ICP nebulizer (Shimadzu), which was operated by flowing nitrogen. The ICP nebulizer introduced a trace amount of phosphorus into the flame in these experiment. Of course, it is possible to use the present system as a detector for phosphorus in gas chromatographic effluents.

**Rotating Magnetic System.** A modulated magnetic field was obtained by rotating a pair of soft iron disks to which four pairs of magnets (Sumitomo Special Metals Co., NEOMAX-30, 25 mm in diameter, 9.5 mm in thickness) were attached. The disk in front was omitted in this figure. The pole gap was 13 mm. The direction of the magnetic field was from back to front. This system delivered a modulated magnetic field, the strength of which varied from 0 to 0.45 T at 98 Hz, as shown in Figure 3a. The reference signals were synchronized to coincide with peak and zero field. Of course, it is possible to use an electromagnet instead of the rotating magnetic system.

**Measuring System.** A modulated magnetic field was applied to the spot 20 mm above the nozzle head of the burner. The flame emission from the part where a modulated magnetic field was applied was guided by the glass rod through broad band-pass glass filters (D) (Toshiba VY-50, Corning 4-96) to a PM. The output of the PM was fed to a lock-in amplifier, which consisted of a tuned band-pass amplifier and a phase-sensitive detector. First, the former amplified a narrow band of frequency (98 Hz,  $Q = 12.34$ ), i.e., the modulated signal from phosphorus compounds, rejecting associated noises. Then the latter provided the means to extract low-amplitude signals from high noise levels. In this report, the present background correction technique was compared with a conventional FPD (Figure 1b). In the latter case, the flame emission was observed through a narrow band-pass interference filter (G) ( $\lambda_{\text{max}}$ , 528 nm;  $\Delta\lambda_{1/2}$ , 8.5 nm;  $T_{\text{max}}$ , 42.5%), and the output of the PM was directly traced by a recorder. Other experimental conditions were similar to those described previously. The transient behaviors of the emission from HPO and  $\text{S}_2$  were recorded by a signal averager (TN-1505).



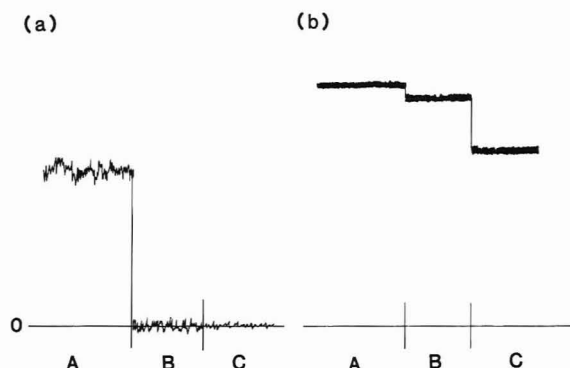
**Figure 4.** Transient behaviors of the PM output (a), the signal from a tuned band pass amplifier (b), and the output of a lock-in amplifier (c) in the aspiration of the  $(\text{NH}_4)_2\text{HPO}_4$  solution (P,  $0.5 \mu\text{g/mL}$ ).

**Reagents.** The standard solutions of phosphorus (P,  $1000 \mu\text{g/mL}$ ), sulfur (S,  $1000 \mu\text{g/mL}$ ), and carbon (C,  $100 \mu\text{g/mL}$ ) were prepared by dissolving ammonium phosphate, diabasic  $(\text{NH}_4)_2\text{HPO}_4$ , ammonium sulfate  $(\text{NH}_4)_2\text{SO}_4$ , and ethanol in distilled water, respectively. Other concentrations used were prepared fresh from the standard solutions for every experiment. All of the reagents were special grades (Wako Chem. Ind., Ltd.).

## RESULTS AND DISCUSSION

**Effects of a Modulated Magnetic Field.** The output of the PM was composed of the signal from phosphorus compounds (HPO) and associated noises. The latter were due to flame noise and PM dark current noise. When the concentration of the phosphorus solution was high, the signal from HPO was much larger than the background noises. Figure 3b shows the transient behavior of the emission intensity from HPO at a P concentration of  $10 \mu\text{g/mL}$ . Magnetically induced quenching (about 30%) was observed around the peak of a magnetic field. On the other hand, associated noises, i.e., flame emissions (OH,  $\text{C}_2$ , CH,  $\text{S}_2$ , etc.) and PM dark currents, were observed not to be affected by a modulated magnetic field. Figure 3c shows the transient behavior of the emission intensity from  $\text{S}_2$  molecules at a S concentration of  $50 \mu\text{g/mL}$ . These experimental results indicate that the signal from phosphorus can be selectively modulated by applying a modulated magnetic field. As the sample concentration decreased, the signal from phosphorus decreased relative to the associated noise. At the low sample concentration (P,  $0.5 \mu\text{g/mL}$ ), a modulated HPO signal was not observed, as shown in Figure 4a. When the output of the PM was filtered by a tuned band-pass filter, a modulated signal from phosphorus was observed, with most of the associated noises being rejected (Figure 4b). The output of a lock-in amplifier is shown in Figure 4c. The signal from P was clearly observed, as compared with the blank signal obtained with distilled water.

**Detectability.** Most prior FPDs have used a narrow band-pass interference filter in order to cut off the associated flame emissions (OH,  $\text{S}_2$ ,  $\text{C}_2$ , CH, etc.). In the present system, a modulated magnetic field, a tuned band-pass amplifier, and a phase sensitive detector were used to select the emissions from HPO. Therefore, only broad band-pass glass filters were used since the emission intensity of HPO observed through



**Figure 5.** Comparison of the new background correction technique (a) with the conventional FPD (b): (A) aspiration of  $0.1 \mu\text{g/mL}$  phosphorus solution, (B) aspiration of distilled water, and (C) flame off.

these glass filters was about 12 times as large as through a narrow band-pass interference filter. The increase of the signal obtained by using broad band-pass glass filters was expected to be larger than the decrease obtained by using only magnetically modulated signals in the present system. The contributions from associated flame emissions were observed to be negligible in the present system. For example, the signal from sulfur compounds,  $\text{S}_2$ , was observed to be negligible in comparison with that from phosphorus ( $1 \mu\text{g/mL}$ ), when the aqueous solution of  $(\text{NH}_4)_2\text{SO}_4$  (S,  $50 \mu\text{g/mL}$ ) was nebulized into the flame. Similarly, the sensitivity of the present method to hydrocarbons was less than 0.01% of its sensitivity to phosphorus.

One of the major features of the present system is the potential for increase in sensitivity. This is demonstrated in Figure 5a, which shows the analysis of the phosphorus solution ( $0.1 \mu\text{g/mL}$ ). The signal produced by P was clearly recorded, compared with the blank signal which was obtained in the aspiration of distilled water. As a comparison, a measurement was performed by the conventional FPD. Direct tracing of PM output is shown in Figure 5b. The signal from P was about twice as large as the peak-to-peak noise level of the blank signal. Comparison of these figures shows that the ratio of the P signal to the peak-to-peak noise level (distilled water) of the present system is larger than that of the conventional FPD.

**Static Background Correction.** Accurate background correction of the present system is demonstrated in Figure 5a. The background intensities were measured in the aspiration of distilled water and in the absence of the flame. Both of these cases caused no base-line shifts. On the other hand, large base-line shifts were observed both in the absence of the flame and in the aspiration of distilled water in the case of the conventional FPD (Figure 5b). The former base-line shift is considered to be caused by the PM dark currents, while the difference between these two kinds of base-line shifts is due to the flame emissivity. The signal intensity from phosphorus was observed to be much smaller than the blank signal (distilled water), the ratio of the former to the latter being about 0.05. Comparison of parts a and b of Figure 5 shows the ability of the present system to correct for static backgrounds completely.

**Calibration Curve and Detection Limit.** The calibration curves were linear in the range from 0.02 to  $200 \mu\text{g/mL}$  in the present system, as shown by the equation

$$\log I(\text{mV}) = 1.086 \log C(\mu\text{g/mL}) + 0.139$$

The standard deviations for the slope and intercept are 0.009 and 0.008, respectively. The detection limit of the present system was about  $0.008 \mu\text{g/mL}$  defined as the concentration corresponding to twice the standard deviation in the blank signal (distilled water). The present system was about 5 times



as sensitive as the conventional FPD, the detection limit of which was about 0.04  $\mu\text{g/mL}$ .

In conclusion, the major advantages of the present technique are the improvement of the sensitivity by about a factor of 5 as well as the accurate correction for static backgrounds. Nevertheless, the improvement of the sensitivity by the present method is not as good as expected. This may be due to the incompleteness of the modulated magnetic field used, because the accuracy of the period and peak strength is estimated to be about  $\pm 1\%$ . The purpose of this work is to compare the performance of this new technique relative to that of conventional FPD. In order to get performance higher than that presented here, it will be necessary to use an improved modulated magnetic field (higher modulation frequency, a more completely modulated magnetic field), a burner, optical system, sample introduction system, combustion conditions, etc.

#### ACKNOWLEDGMENT

The authors thank T. Katayama of the Electro Technical Laboratory for sharing his knowledge of magnets and S. Nishi

and K. Fukuda of the National Chemical Laboratory for Industry for useful discussions.

#### LITERATURE CITED

- (1) Nczoze, H.; Someno, K. *Bunseki Kagaku* **1985**, *8*, 508-509.
- (2) Hashimoto, S.; Fujiwara, K.; Fuwa, K. *Anal. Chem.* **1985**, *57*, 1305-1309.
- (3) Murphy, J.; Riley, J. P. *Anal. Chim. Acta* **1962**, *27*, 31-36.
- (4) Brody, S. S.; Chaney, J. E. *J. Gas Chromatogr.* **1966**, *4*, 42-46.
- (5) Wakayama, N. I.; Ogasawara, I.; Nishikawa, T.; Ohyagi, T.; Hayashi, H. *Chem. Phys. Lett.* **1984**, *107*, 207-211.
- (6) Wakayama, N. I.; Nozoye, H.; Ogasawara, I.; Fukuda, K. Japanese Patent 60-43516.

Nobuko I. Wakayama\*  
Hisakazu Nozoye  
Ichiro Ogasawara

National Chemical Laboratory for Industry  
Tsukuba Research Center  
Yatabe, Ibaraki 305, Japan

RECEIVED for review July 22, 1986. Accepted November 12, 1986.

## AIDS FOR ANALYTICAL CHEMISTS

### Purge Gas Enhancement of Peak Resolution in Differential Scanning Calorimetry

Guang-Way Jang, Ranjana Segal, and Krishnan Rajeshwar\*

Department of Chemistry, The University of Texas at Arlington, Arlington, Texas 76019-0065

Overlapping peaks are a nuisance in the analyses by differential scanning calorimetry (DSC) of mixtures and compounds that undergo more than one thermal event. The strategy for enhancing peak resolution in DSC usually is based on a reduction in heating rate or sample mass. This method, however, suffers from the handicap associated with prolonged analysis times and lowered sensitivity, respectively. This paper describes an alternative method based on the use of a thermally conductive purge gas (e.g., He) to enhance peak resolution in DSC. The theory is verified through use of computer simulations and experiments on model compounds and mixtures.

#### THEORY

The equivalent-circuit model previously developed for DSC cells of the heat-flux type (1) is shown in Figure 1. The slope,  $d(dq/dt)/dT_{SH}$ , of the leading edge of a DSC peak may be written as

$$\frac{d(dq/dt)}{dT_{SH}} = \frac{1}{R_S} - \frac{1}{R_D'} + \frac{1}{KR_D'} + \frac{1}{KR_G} + \frac{2}{KR_G'} \quad (1)$$

In eq 1 and as before (1),  $dq/dt$  is the heat-flow rate,  $T_{SH}$  is the sample-holder temperature,  $R_S$  is the thermal resistance between sensor and sample,  $R_D'$  is the thermal resistance of the disk between the sample and reference platforms,  $R_G$  is the thermal resistance of the gas phase separating the heater block from the sample and reference,  $R_G'$  is the gas thermal resistance between sample and reference, and  $K$  is the thermal lag term containing sample and instrumental contributions. It is important to emphasize that  $R_S$  also contains contributions from the thermal resistance of the *interfacial region* between the sample pan and the sample platform. Narrowing of the peak width and thus better separation of overlapped DSC signals can be achieved by minimizing the magnitudes

of  $R_S$  and the other component resistances (cf. eq 1) through the use of a purge gas with facile heat conduction characteristics.

#### EXPERIMENTAL PROCEDURES

All experiments were performed on a Du Pont Model 1090 thermal analysis system fitted with the Model 910 DSC accessory module. Fusion endotherms were recorded usually after one or two initial "conditioning" heat-cooled cycles through the transition. Commercial samples of In and adipic acid (99.99% purity or better) were used as received. The purge gas (either Ar or He) was flushed through the DSC cell at the rate of ca. 80 mL/min. Sealed Al sample pans were used in all the cases.

Computer simulations of DSC thermograms were carried out on an IBM PC-XT fitted with a Hewlett-Packard Model 9575A graphics plotter. These simulations were facilitated by decomposing the overall thermograms into pretransition, transition, and posttransition regimes. Input parameters comprised the scanning temperature limits, resolution element size, transition enthalpy, transition temperature, and the heat capacities of sample plus container. Multiple transitions were individually simulated prior to summation. Parameters such as sample mass, heating rate, and the component thermal resistances in eq 1 were then systematically varied to assess their influence on DSC peak shapes and resolution. Further details of the simulation protocol will be published elsewhere (2).

#### RESULTS AND DISCUSSION

For initial investigations on purge gas enhancement of DSC peak resolution, we chose the melting transitions of indium (mp 153.6  $^{\circ}\text{C}$ ; heat of fusion,  $\Delta H_f = 28.4 \text{ J/g}$ ) and adipic acid (mp 152.0  $^{\circ}\text{C}$ ,  $\Delta H_f = 253 \text{ J/g}$ ) as model systems. The simulated thermograms in Figure 2 parts a and b, for In and In/adipic acid mixtures, respectively, confirm our expectations (vide supra) on (a) increase of the slope of the leading edge of the DSC endotherm, (b) narrowing of the endotherm, and (c) enhancement of peak resolution when the purge gas is

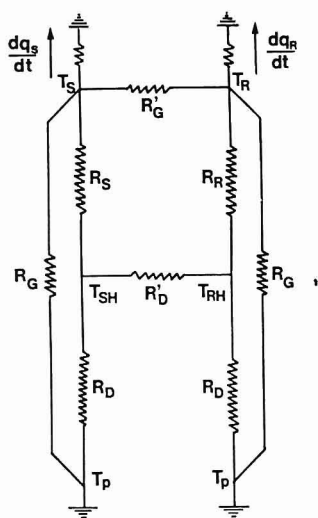


Figure 1. Equivalent circuit of a heat-flux DSC system.

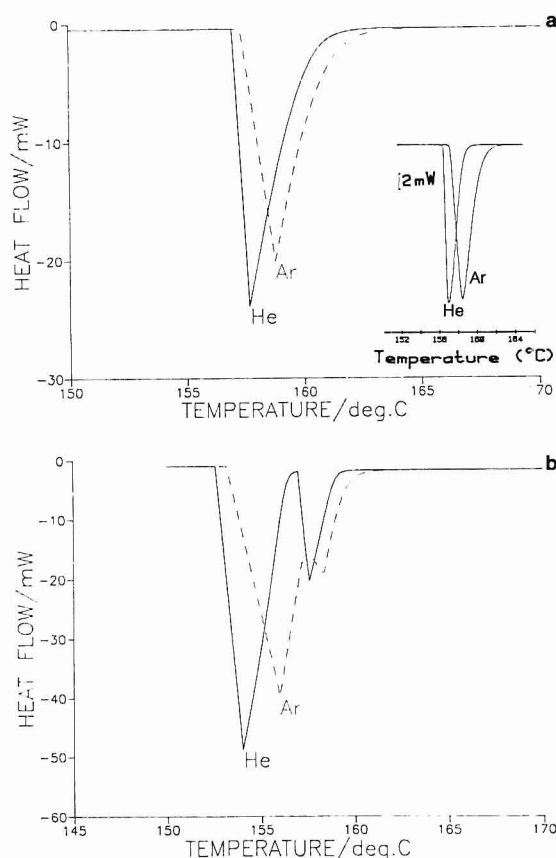


Figure 2. Computer-simulated DSC thermograms illustrating (a) the enhanced slope of the leading-edge and peak-narrowing in He vs. Ar for the In melting transition and (b) the enhanced peak resolution for an In/adipic acid mixture in He vs. Ar. The inset in Figure 2a contains a set of DSC thermograms for In in He and Ar atmospheres. The sample mass was 10.16 mg and the heating rate was 10 °C/min.

switched from Ar to He. Figure 3 contains experimental data, attesting to the positive influence of He on peak resolution.

Figure 4 contains experimental thermograms of In/adipic acid mixtures, wherein the purge gas peak resolution technique is compared with the usual method of reducing sample mass or heating rate. We have employed the peak resolution parameter,  $P$ , defined by previous authors for chromatogram analyses (3) for quantitative comparisons. With reference to Figure 5, this parameter is given by

$$P = f/g \quad (2)$$

. Base line resolution ( $P = 1.00$ ) is achieved at identical heating rate and comparable sample mass when the purge gas

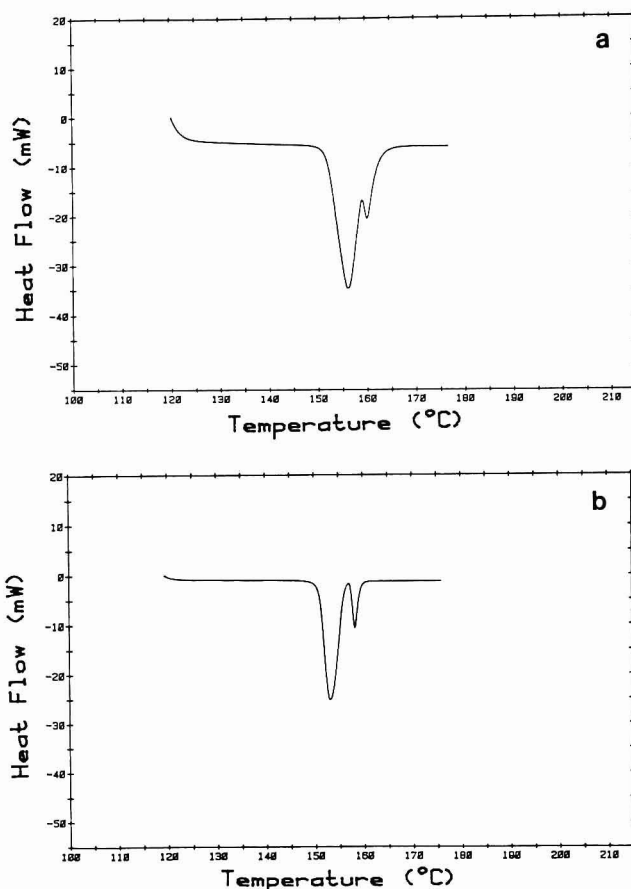


Figure 3. Experimental DSC thermograms (heating rate, 10 °C/min) for In/adipic acid mixtures in Ar (a) and He (b) atmospheres. The mixture contained in each case 4.95 mg of In and 3.91 mg of adipic acid.

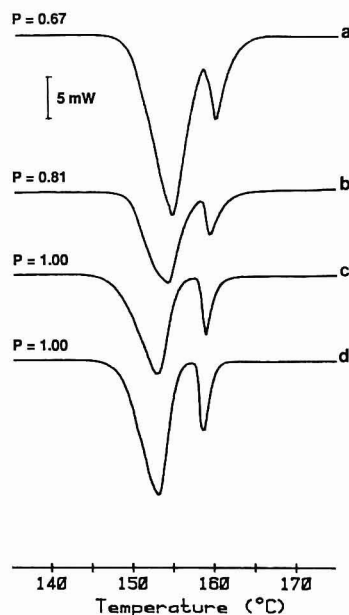


Figure 4. Influence of varying sample mass, heating rate, and purge gas atmosphere on peak resolution in DSC thermograms for In/adipic acid mixtures. Parts a–c pertain to Ar atmosphere and part d shows data in He atmosphere. The heating rate was 10 °C/min for parts a, b, and d, whereas the thermogram in Figure 4c was run at 5 °C/min. The sample masses were (a) 8.00 mg, (b) 4.00 mg, (c) 7.93 mg, and (d) 8.02 mg.

atmosphere is switched from Ar to He (compare Figure 4 parts a and d). On the other hand, peak resolution is incomplete (cf. Figure 4b,  $P = 0.81$ ) for a 50% reduction in sample mass. Complete resolution can be achieved, however, by halving the heating rate (cf. Figure 4c,  $P = 1.00$ ), but at the cost of ap-



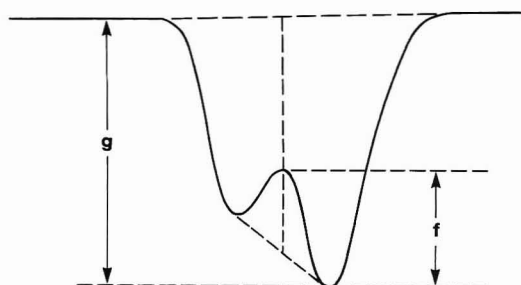


Figure 5. Definition of peak resolution parameter,  $P$  (cf. ref 3 and eq 2 in the text).

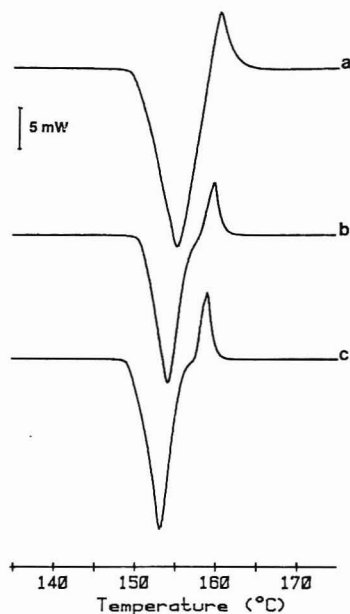


Figure 6. Comparison of DSC thermograms in Ar (a and b) and He (c) with In and adipic acid samples contained in separate Al pans. The heating rates were 10 °C/min in parts a and c, and 5 °C/min in part b. The sample masses were maintained constant for In and adipic acid at 4.94 mg and  $3.04 \pm 0.04$  mg, respectively.

proximately double the analysis time and ca. 50% reduction in analytical sensitivity. Different samples were utilized for the data in Figure 4 parts a–d, to preclude complications from slow volatilization of adipic acid. The relative weight fraction of adipic acid/In in the mixture was maintained constant at a ratio of 38:62 in all the cases.

A subtle feature of purge gas effects is that the enhancement of the endotherm slope does depend on the sample thermal conductivity (cf. eq 1). Thus, the influence of He on the endotherm slope may be expected to be more pronounced for In than for a sample with lower thermal conductivity such as adipic acid. This was verified experimentally. In fact, when this happens, the diminution in time to peak maximum that always results when He is used (cf. eq 14, ref 1), may have an overriding influence on analytical sensitivity. This effect is actually seen in a careful examination of the thermograms in Figure 4a and Figure 4d, wherein the adipic acid peak amplitude is attenuated in He, contrasting the In case. It should also be noted that ordinate recalibration is necessary when the purge gas is switched from Ar to He.

The dramatic effect of He on peak resolution is better revealed in an experimental format wherein the two samples (e.g., In and adipic acid) are stationed in different pans (i.e., reference and sample pans, respectively). Complications arising from chemical reactions between the mixture components are also thereby avoided. Figure 6 illustrates representative data utilizing this "twin-pan" strategy.

After extensive evaluation of this purge gas resolution technique using model compounds and mixtures, we have

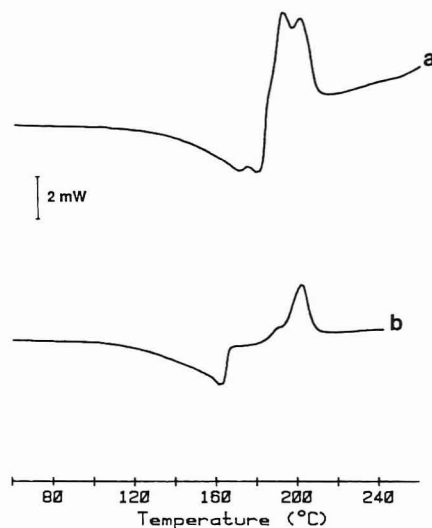


Figure 7. Comparison of DSC thermograms for **1a** in Ar (a) and He (b), respectively. The sample mass was 2.60 mg and the heating rate was 10 °C/min.

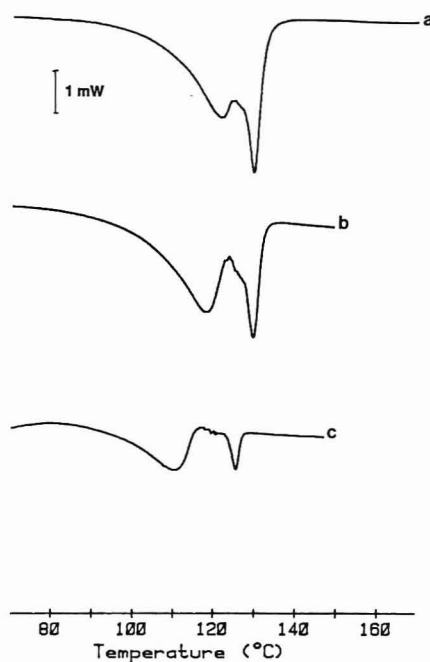
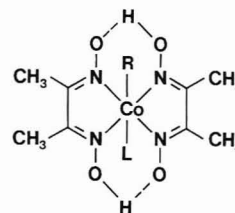


Figure 8. Comparison of DSC thermograms for **1b** in Ar (a) and He (b and c). The heating rates were 10 °C/min in parts a and b and 5 °C/min in part c. The sample masses were 1.15, 1.72, and 1.49 mg, respectively, in parts a, b, and c.

begun to utilize it for the analyses of "real-world" samples. For example, this technique has proved to be useful for the study of deaquation and dealkylation reactions of cobalt complexes, **1**, containing the bis(dimethylglyoximate) equatorial ligand.



**1a**:  $R = \text{CH}_3\text{CHCH}_2$ ;  $L = \text{H}_2\text{O}$   
**1b**:  $R = \text{C}_6\text{H}_5\text{OCH}_2\text{CH}_2$

As illustrated by the thermograms in Figure 7 for compound **1a**, use of He (instead of Ar) alone suffices to completely separate the dealkylation exotherm from the deaquation en-

The authors thank the Du Pont Co. for instrumental sup-

RECEIVED for review August 11, 1986. Accepted October 6, 1986. This research was supported by the Texas Advanced Technology and Research Program and the Strategic Defense Initiative Office, Innovative Science and Technology Branch, through the Defense Nuclear Agency, Contract No. DNA 001-85-6-0181.

## 0003-2700/87/0359-0687\$01.50/0 © 1987 American Chemical Society



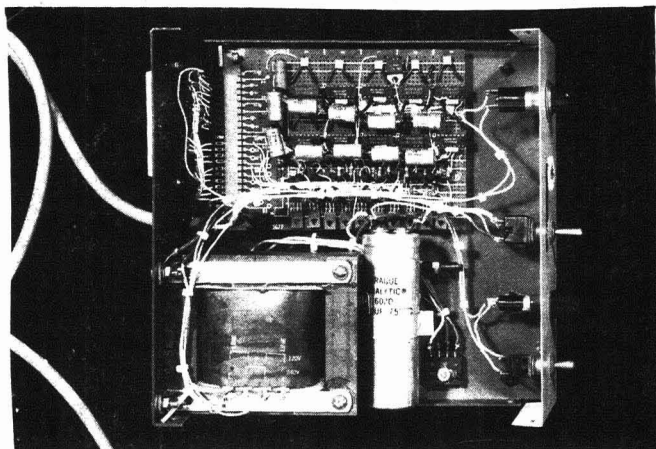


Figure 2. Assembled circuit.

voltage, and 500- $\mu$ A threshold current. Since the signal used is ac, the ac ripple component should be minimized before the signal reaches the solenoid driver stage; therefore a filter capacitor was connected between pin 9 of IC LM1830 and common ground.

### DISCUSSION

The IC LM1830 prevents the deposits of electrolytes or any charged organic compounds on the platinum probes because of the ac current. When a strong electrolytic solution is used, traces of the solution on the walls act as a conductor, but the

IC LM1830 overcomes this residual current. Commercial solenoids need modification on their tips.

The device is simple in design and inexpensive to set up. The cost of all the components together was less than \$200. It allowed us to increase our efficiency significantly by enabling us to handle a greater number of columns at any one time. We increased the number of columns from four to ten, and in addition, we can expand the system to 24 columns or more if needed. The device has a simple purpose, which to our knowledge is not being used in any other laboratory for ion-exchange columns or column chromatography. It can also be used in gel filtration.

### ACKNOWLEDGMENT

The authors are greatly indebted to B. K. Lee, for designing and assembling all of the electronic circuitry and for his many valuable suggestions.

### LITERATURE CITED

- (1) Glerum, C.; Balatinecz, J. J. *Can. J. Bot.* **1980** *58*, 40-54.
- (2) Zweig, G.; Sherma, J. *Handbook of Chromatography*; CRC Press: Cleveland, OH, 1972; Vol. 2, p 70.
- (3) Zweig, G.; Sherma, J. *Handbook of Chromatography*; CRC Press: Cleveland, OH, 1972; Vol. 2, pp 195-254.
- (4) Blackburn, S. *Handbook of Chromatography: Amino Acids and Amines*; Zweig, G., Sherma, J., Eds.; CRC Press: Boca Raton, FL, 1983; Vol. 1, p 201.
- (5) Dickson, R. E. *Physiol. Plant.* **1979**, *45*, 480-488.

RECEIVED for review August 25, 1986. Accepted October 27, 1986.

### CORRECTION

#### Elemental Characterization of the National Bureau of Standards Milk Powder Standard Reference Material by Instrumental and Radiochemical Neutron Activation Analysis

Robert R. Greenberg (*Anal. Chem.* **1986**, *58*, 1986).

An error was introduced into this paper in the final stages of the production cycle, after author review of the galley proof. On page 2511 the correct spelling of the name of the author is Robert R. Greenberg.



Available on  
STN International

**The only  
online database  
in the  
entire world  
which offers  
chemists the  
capability  
to find**

- **experimental procedures**
  - **experimental data, and to**
  - **crossover from Chemical Abstracts**
- in seconds.***



CHEMICAL JOURNALS ONLINE is the new powerful information search system that permits you to quickly search 40,000 journal articles and display • complete and comprehensive experimental data • verbatim experimental procedures from every journal article, and allows you to • instantaneously crossover from searches in Chemical Abstracts to appropriate journal articles.

Use CHEMICAL JOURNALS ONLINE in your library or in your lab. Just turn on the computer or terminal. In minutes you can save yourself days of manual searching.

CHEMICAL JOURNALS ONLINE is not only precise in its searching but also cost effective.

To put CHEMICAL JOURNALS ONLINE to work for you, call an American Chemical Society sales representative today at 800-424-6747. The call is free.

Or write: Sales Office, American Chemical Society, 1155 Sixteenth Street, N.W., Washington, D.C. 20036.

Search CHEMICAL JOURNALS ONLINE.

CHEMICAL JOURNALS ONLINE contains: Accounts of Chemical Research, Analytical Chemistry, Biochemistry, Chemical Reviews, Environmental Science & Technology, Industrial & Engineering Chemistry Research (Fundamentals—Process Design & Development—Product Research & Development), Inorganic Chemistry, Journal of Agricultural and Food Chemistry, Journal of Chemical and Engineering Data, Journal of American Chemical Society, Journal of Chemical Information and Computer Sciences, Journal of Medicinal Chemistry, The Journal of Organic Chemistry, The Journal of Physical Chemistry, Langmuir, Macromolecules, Organometallics, Energy and Fuels (available January 1987).



**The Computer-Powered  
Full-Text Search System  
From The American  
Chemical Society**

**CHEMICAL JOURNALS  
ONLINE**



The people in your lab want systems from a company they know and respect in the world of analytical chemistry.

The people in your MIS department want systems from a company they know and respect in the world of computing. With HP you can satisfy both.

We're the only top 10 computer company that is also a leading manufacturer of analytical instrumentation. And we have a long-standing reputation for quality, reliability, service and support in both worlds.

Ask your lab people and your computer people to make a list of their top three choices for a LIMS supplier. Chances are, Hewlett-

Packard will be the only name to appear on both lists.

Before you make your LIMS decision, talk to HP. The lab people in the computer business.

Write Hewlett-Packard Operations Center, P.O. Box 17910, Milwaukee, WI 53217. Or call 800-558-3077, ext. 100.



**HEWLETT  
PACKARD**

Visit HP at the Pittsburgh  
Conference • West Hall Boardwalk  
Level and Street Level Hall

## THE COMPUTER SYSTEM FOR LAB PEOPLE.

## THE LAB SYSTEM FOR COMPUTER PEOPLE.

